Cornel Stan

Alternative Propulsion for Automobiles

Springer

Alternative Propulsion for Automobiles

Cornel Stan

Alternative Propulsion for Automobiles

Springer

Cornel Stan
West Saxon University
Zwickau, Germany

ISBN 978-3-319-31929-2 ISBN 978-3-319-31930-8 (eBook)
DOI 10.1007/978-3-319-31930-8

Library of Congress Control Number: 2016947733

Printed on acid-free paper

This Springer imprint is published by Springer Nature
The registered company is Springer International Publishing AG Switzerland

Preface

A fourth edition of this book was recently published in German. The preface of the first edition 10 years ago asserted that, like an all-purpose automobile, an all-purpose propulsion system was impossible. A modular distribution of functions within the propulsion system was considered the most viable concept for the next generation of vehicles. In the second edition, explicit tendencies in this direction were highlighted: full hybrids for urban areas, diesel engines for rural areas and motorways, and micro- and mild hybrids for a variety of purposes were introduced into production or developed as concept cars.

The third edition was published at a time when a book about alternative propulsion systems for automobiles was in danger of extinction: the electric car had appeared as a knight in shining armor, the savior of general mobility. In May 2010, the National Platform of Electrical Mobility was founded in Germany with the aim of establishing 1 million electric cars in the German traffic system by 2020. Nevertheless, the third edition of the book collected, presented, and analyzed numerous propulsion systems with a variety of modular configurations.

In the preface of the fourth edition, we note that, in 2015—halfway to the deadline of establishing 1 million electric cars in Germany—only 19,000 are in place, whereas we have 44.4 million cars with gasoline and diesel engines.

With all due respect to, and appreciation for, the goal of electric mobility, and for the very complex, intensive and extensive activities in this domain, the continuing variety of automobiles and propulsion systems appears completely necessary: the wide range of geographic economic, or egolocical conditions worldwide allows no other option.

Therefore, in this fourth edition, we present scores of new concepts, prototypes, and series systems—beginning, of course, with electric cars, from light vehicles with compact batteries through to 2-ton luxury cars in which the battery is responsible for half this weight. However, we also present plug-ins as 2-in-1 solutions: electric propulsion in cities, and electrically assisted internal combustion engines for rural areas and motorways.

However, the main scope of this book continues to be the evaluation and analysis of conception and optimization of alternative propulsion systems for automobiles, such as combinations of on-board propulsion modules, energy sources, energy storage, and energy conversion devices that can be adapted according to the functions required. The evaluation and analysis criteria includes specific power,

torque, and acceleration behavior; specific energy consumption; and emission of chemical substances and continues through to available energy, ecological impact, on-board storage, technically complex systems, costs, safety, and infrastructure.

The combination of theoretical background, analysis of potential and limitations, and numerous concrete examples offers not only engineers but also automotive engineering students a basis for critical reflection and, possibly, the development of new concepts.

Zwickau, Germany Cornel Stan

Contents

List of Formula Symbols

A	$[m^2]$	Surface
b_e, bsfc	$\left[\frac{g}{kWh}\right]$	Brake specific fuel consumption
c	$\left[\frac{m}{s}\right]$	Velocity
c	$\left[\frac{kg\,C}{kg\,Kst}\right]$	Carbon fraction in hydrocarbon
c_p	$\left[\frac{kJ}{kgK}\right]$	Specific heat capacity at constant pressure
c_V	$\left[\frac{kJ}{kgK}\right]$	Specific heat capacity at constant volume
d	[m]	Diameter
E	[J, kJ]	Energy
F	[N]	Force
f	[Hz]	Frequency
G	[J, kJ]	Free enthalpy of combustion
H	[J, kJ]	Enthalpy
H^*	[J, kJ]	Dynamic enthalpy
H_U	$\left[\frac{kJ}{kg}\right]$	Lower heating value
H_G	$\left[\frac{kJ}{kg}\right]$	Mixture heating value—mass related
H_g	$\left[\frac{kJ}{m^3}\right]$	Mixture heating value—volume related
h	$\left[\frac{J}{kg}, \frac{kJ}{kg}\right]$	Specific enthalpy
h^*	$\left[\frac{J}{kg}, \frac{kJ}{kg}\right]$	Specific dynamic enthalpy
I_λ	$\left[\frac{W}{m^3}\right]$	Intensity of radiation
k	[−]	Isentropic exponent
$\left(\frac{L}{K}\right)_{st}$	$\left[\frac{kg\,Luft}{kg\,Kst}\right]$	Stoichiometric air/fuel ratio

(continued)

l	[m]	Length
$\overline{M}$	$\left[\frac{\text{kg}}{\text{kmol}}\right]$	Molar mass
n	$\left[\text{s}^{-1}, \text{min}^{-1}\right]$	Rotation speed
P	[W, kW]	Power
p	$\left[\frac{\text{N}}{\text{m}^2}\right]$	Pressure
Q	[J, kJ]	Heat
$\dot{Q}$	[W, kW]	Heat flow
q	$\left[\frac{\text{J}}{\text{kg}}, \frac{\text{kJ}}{\text{kg}}\right]$	Specific heat
$\overline{R}$	$\left[\frac{\text{J}}{\text{kmolK}}\right]$	Molar gas constant
R	$\left[\frac{\text{J}}{\text{kgK}}\right]$	Specific gas constant
r	[m]	Radius
r	$\left[\frac{\text{J}}{\text{kg}}, \frac{\text{kJ}}{\text{kg}}\right]$	Specific vaporization
S	$\left[\frac{\text{J}}{\text{K}}, \frac{\text{kJ}}{\text{K}}\right]$	Entropy
s	$\left[\frac{\text{J}}{\text{kgK}}, \frac{\text{kJ}}{\text{kgK}}\right]$	Specific entropy
T	[K]	Temperature
t	[°C]	Temperature
t	[s]	Time
U	[J, kJ]	Internal energy
u	$\left[\frac{\text{J}}{\text{kg}}, \frac{\text{kJ}}{\text{kg}}\right]$	Specific internal energy
V	[m^3]	Volume
V_H	[m]	Swept volume
v	$\left[\frac{\text{m}^3}{\text{kg}}\right]$	Specific volume
W	[J, kJ]	Work
w	$\left[\frac{\text{J}}{\text{kg}}, \frac{\text{kJ}}{\text{kg}}\right]$	Specific work
α	[rad]	Angle, angle of rotation
α	[−]	Stirling type
β	[−]	Stirling type
γ	[−]	Stirling type
ε	[−]	Compression ratio
η	[−]	Efficiency
η_{th}	[−]	Thermal efficiency
λ	$\left[\frac{\text{kg Luft}}{\text{kg Kst}}\right]$	Air ratio of combustion

(continued)

λ	[m, µm]	Wave length at radiation
λ	$\left[\frac{\mathrm{W}}{\mathrm{mK}}\right]$	Conductivity at heat conduction
π	[−]	Pressure ratio
ρ	$\left[\frac{\mathrm{kg}}{\mathrm{m}^3}\right]$	Density
ω	$[\mathrm{s}^{-1}]$	Angular velocity

Mobility: Conditions, Requirements, and Scenarios

1

1.1 Development Conditions

In 2013 there were more than 7.3 billion human beings and 1.18 billion automobiles on the planet. Although most people live in urban areas, the number of megacities (cities with >10 million residents) is rapidly increasing. Figure 1.1 illustrates the situation as of January 2015.

The consequent polarization of mobility leads to dangerous increases not only in traffic density but also in the local concentration of exhaust gases from internal combustion engines—carbon dioxide, pollutants, particulates—as well as noise pollution. As such, transport in silent and compact electric vehicles that do not produce emissions would be ideal. Moreover, wheel-integrated motors (see Fig. 1.2) were first successfully applied in a prototype by Ferdinand Porsche in 1899 and are now being developed in actual projects; they could revolutionize driving dynamics and kinematics, with enormous benefits for city-based traffic.

If each wheel operates as an intelligent android with a large degree of freedom, new movement forms become possible for the automobile. Figure 1.3 shows some interesting examples: lateral parking, cornering with adaptive four-wheel steering, and turning on its own axis.

These scenarios have two fundamental problems: the availability of sufficient on-board electric energy and the source of this energy. Electric propulsion with energy stored in batteries and supercaps, as well as with energy converted on board from hydrogen via fuel cells, is being developed in national and international programs.

However, when calculated in kilowatt hours per kilogram, the density of energy achievable with such systems is far less than that available via gasoline or diesel fuel, which strongly reduces the operational range of the vehicle. Furthermore, these systems are complex and obtaining a good level of reliability involves high costs and very large and/or heavy accumulators or conversion systems. For example, to create 10 kW h of electric energy would require a 100-kg lithium-ion battery

C. Stan, *Alternative Propulsion for Automobiles*,
DOI 10.1007/978-3-319-31930-8_1

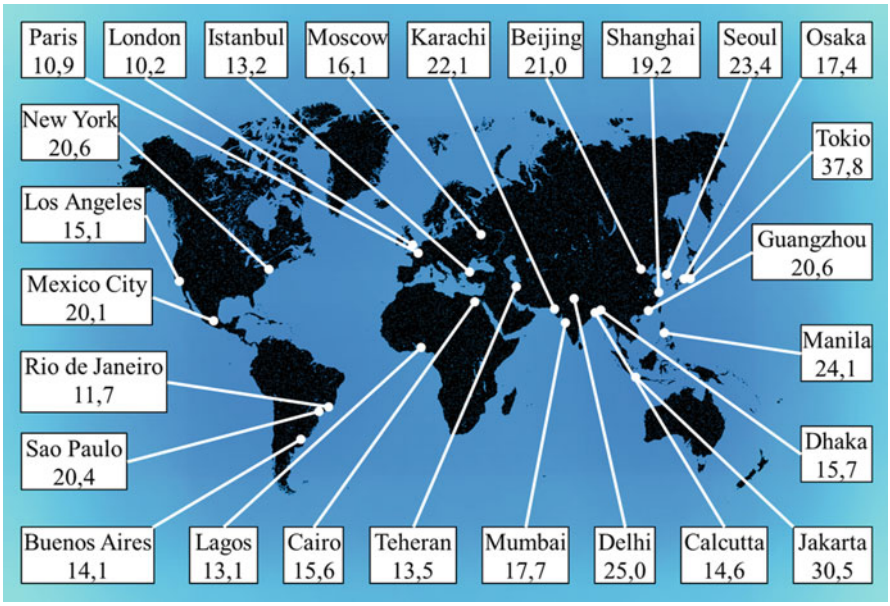

Fig. 1.1 Megacities of the world: number of inhabitants (millions)

versus only 1 l or 0.84 kg of diesel fuel. This ratio of 1:100 is impossible to overcome only by technical progress.

From another perspective, the problem of carbon dioxide emission is not solved by on-board storage of electric energy or hydrogen—it is simply displaced: worldwide, electric energy is produced primarily in coal-burning power plants, and hydrogen is produced almost solely from natural gas, heavy oil, and gasoline. Both cases result in carbon dioxide emissions at the place of production.

Figure 1.4 shows the main energy sources for electricity production in 2011 in representative industrialized countries. For example, Norway sources 98.5 % of its electric energy from natural water forces, which is, of course, ideal; however, Norway has specific geographical conditions that are not necessarily available in other countries.

China obtains 78 % of its electric energy from coal. Although Germany currently obtains only 43 % from coal, this will increase as its nuclear power plants have been decommissioned. The USA and Russia sit somewhere between China and Germany; Italy and the UK use natural gas to produce electric energy; France sources 76.5 % of its electricity via nuclear power plants. The worldwide use of natural gas, water, and nuclear energy is more or less equal at 15–20 %, whereas coal continues to provide 40 % of energy resources in the production of electric energy.

A comparison of the yearly carbon dioxide emissions of five currently available electric cars (Mitsubishi IMiEV, Mercedes AClass, E-CELL Smart For Two

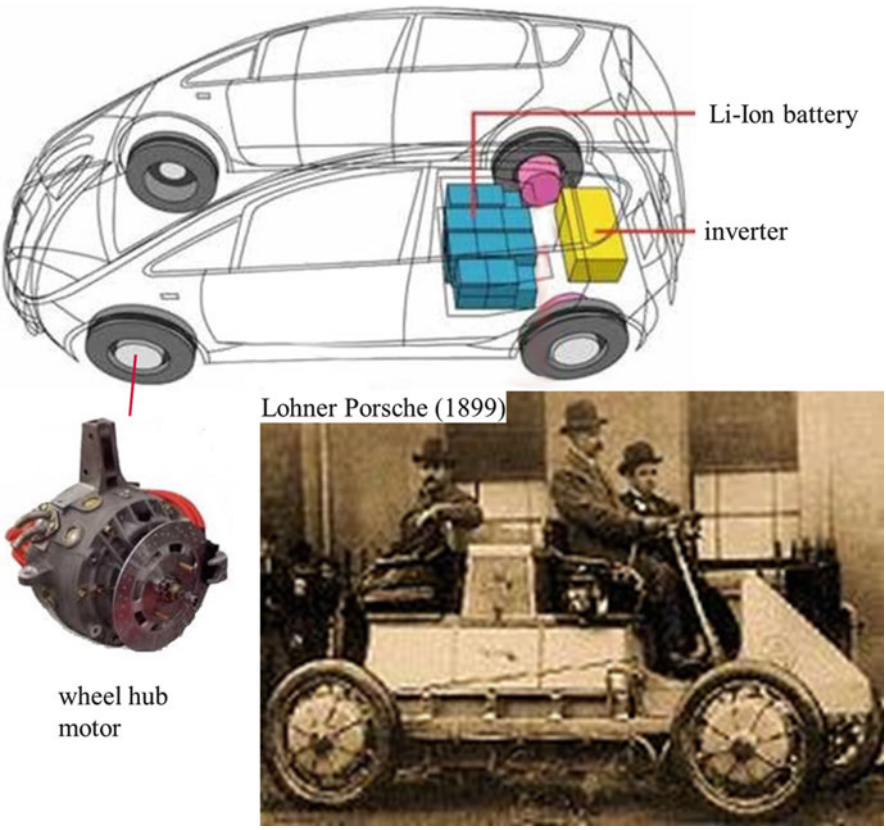

Fig. 1.2 Electric automobile with wheel hub motors

Electric Drive, Nissan Leaf, Citroen Berlingo) and a car with a diesel engine (VW Polo Blue Motion), while also accounting for both the production (EU mix) and the consumption of the respective energy, highlights the following points [35] (Table 1.1).

When used in cities, the electric cars produce 17 % less carbon dioxide emissions than the car with the diesel engine. In rural areas, this difference decreases to only 11 %. In the production of electric energy, the EU mix leads to lower carbon dioxide emissions than does lignite and anthracite.

The polarization of many ideal scenarios around electric propulsion involving motors and batteries often leads to the perception of an automobile as a structure around the propulsion system itself. Thus, the automobile must be adapted to the motor/battery unit (small, light, compact) because of the limited amount of energy on board. Figure 1.5 illustrates such a scenario.

A limited energy amount, E (kilowatt hours), in a large battery, m_{BATT} (kilograms), for an established range, s (kilometers), constrains the car to a smaller mass, m (kilograms), sacrificing safety and comfort. On the other hand, motor

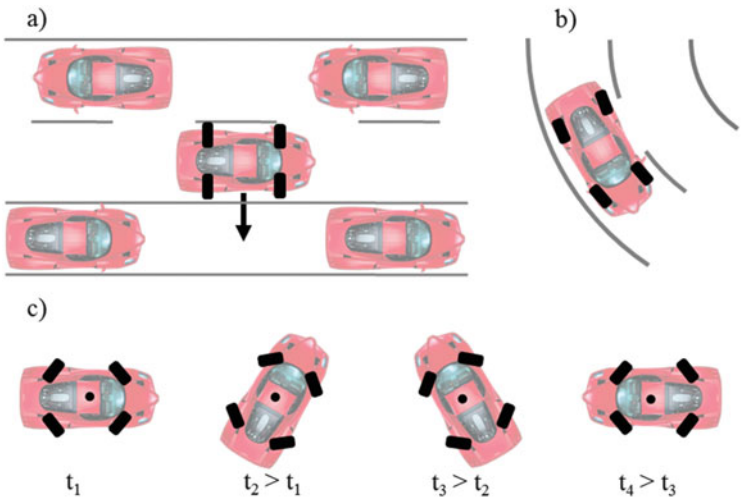

Fig. 1.3 Degrees of freedom with intelligent propulsion wheels: (**a**) lateral parking, (**b**) cornering with adaptive four-wheel steering, (**c**) turning around its own axis

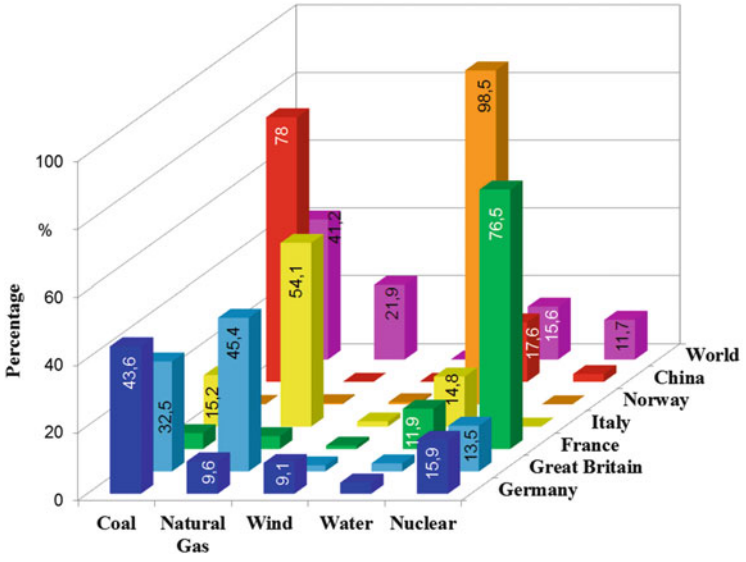

Fig. 1.4 Share of the main energy sources for electricity production worldwide

power and therefore acceleration, *a* (meters per second squared), must decrease, negatively influencing traffic flow. Even with such measures, the mass and dimensions of the battery mean the range remains limited, which is far less acceptable to the customer, even though statistics show that cars in cities are used for very short distances every day. Furthermore, issues around heating and climate

Table 1.1 CO_2 emissions

		Energy production	Car propulsion
City (7500 km/year)			
	E-car	820 kg CO_2	–
	Diesel car	194 kg CO_2	794 kg CO_2
Country (15,000 km/year)			
	E-car	1739 kg CO_2	–
	Diesel car	381 kg CO_2	1561 kg CO_2

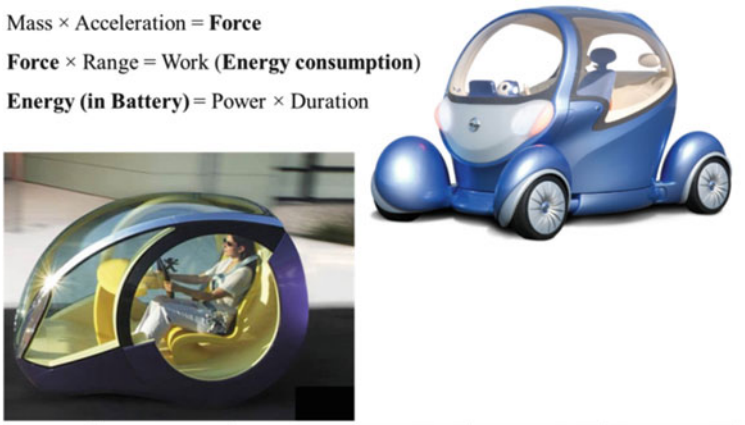

	Energy in Battery [kWh]	Car mass [kg]	Power motor [kW]	Energy consumption [kW/100km]	Range [km]
Toyota COMS	3,7	400	5	7,4	50
BMW i3	18,8	1270	125	16	190

Fig. 1.5 Automobiles with electric propulsion: relationship between car mass and stored electric energy

remain: a compact electric car handling a temperature difference of 30° between the environment (−10°) and the cabin (+20°) will consume approximately 10 (Mitsubishi iMiEV) to 20 kW h/100 km (Mercedes AClass E Cell).

This use of energy for heating leads to a decrease of approximately 37 % in an eco test and approximately 44–51 % under real operating conditions for the two cars. To avoid such problems, some series cars with a motor and battery are equipped with a gasoline heating circuit, consuming some 0.7 l/h of gasoline. Obviously, this form of electrical mobility is undesirable in cities.

An advanced automobile must meet requirements regarding not only propulsion but also active and passive safety, autonomous driving, connectivity, climate control, and comfort (as illustrated in Fig. 1.6).

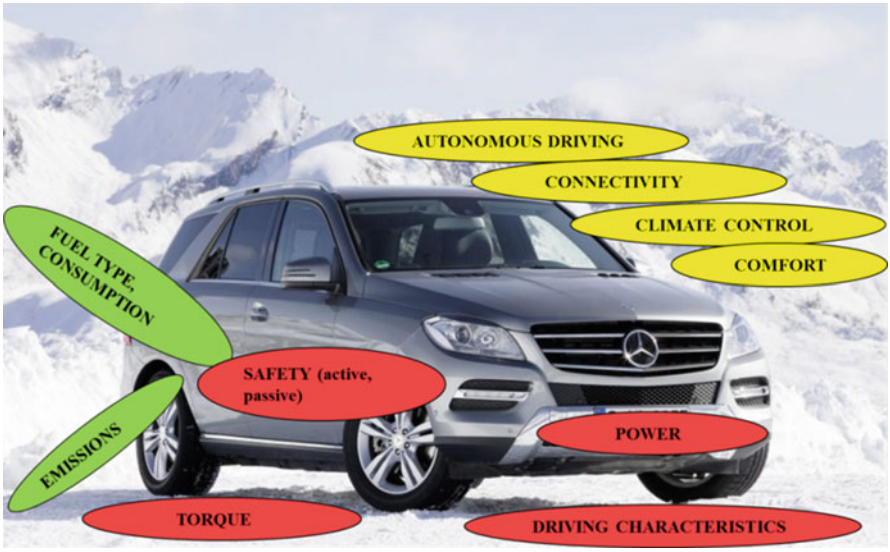

Fig. 1.6 The automobile is more than a structure around the method of (electric) propulsion

A universal car and propulsion system would be a contradiction in terms of the natural, economic, technical, and social environments. A mobile future means diversity with a modular base, from compact car to upper class, from cheap pick-up in India to luxury electric car for zero emission zones in Berlin and London, through to the sport utility vehicle (SUV), sedan, coupe, and station wagon to the cabriolet. As shown in Fig. 1.7, different geographic, economic, or ecological conditions—from difficult terrain to agglomerated cities and family transport—require different types of automobiles.

It seems unrealistic that the current range of social structures could be uniformly represented by a single transport vehicle. Upper-class cars, middle-class cars, and cheap all-rounders will continue to mark transport between villas, town houses, and block houses. Additionally, the customer's objective or subjective physical and mental criteria determine the final purchase: everyone has a dream car. For example, the worldwide market share of SUVs increased from 9.55 % in 2000 to 13.5 % in 2010; the forecast for 2020 is 16 million SUVs, representing 15 % of annual car production. The percentage of upper and luxury class vehicles in the same period is estimated at 10 %. The characteristics of currently available automobiles can be categorized as follows:

- Car classes: mini, small, compact, middle class, upper middle class, upper class, van, SUV
- Car types: off-road, pick-up, sedan, convertible, coupé, and roadster
- Engine position: front, middle, rear; along or across the vehicle length axle
- Driving axle: front, rear, front and rear

Fig. 1.7 Diversity of current and future automobile types

Power and torque are usually a requirement in all categories. Criteria such as power-to-class or power-to-car dimension can be objective, but the customer viewpoint is often subjective. There is a fundamental trade-off between power/torque and fuel consumption/pollutant emission; however, car developers are continually decreasing this trade-off. For example, a VW Golf II built in 1983 had a mass of 790 kg and a power of 70 hp, with diesel fuel consumption of 5.5 l/100 km. A new-generation VW Golf equipped with an anti-lock braking system (ABS), electronic stability program (ESP), airbags, and a climate control system has a mass of 1314 kg (an increase of 524 kg), requiring a power increase to 105 hp, but diesel fuel consumption decreased to 4.5 l/100 km.

A notable recent development is the complex management between the function modules of the car based on standard electronic platforms, where propulsion plays a very important role. This is beneficial in the exploitation of the potential that remains in engines and motors when working together in hybrid configurations. Nevertheless, the increasing demand for mobility, power, and torque is at odds with the rapidly decreasing limits for pollutant emissions, as shown in Tables 1.2 and 1.3. For example, the USA has introduced classifications for passenger vehicle emissions, including low emissions vehicle (LEV), ultralow emissions vehicle (ULEV), and super ultralow emissions vehicle (SULEV), whereas European limits refer to "Euro 1 to 6."

Over the last three decades, pollutant emissions have reduced drastically, as a result of process improvements in piston engines: unburned hydrocarbons (HC) and oxides of nitrogen (NO_x) have decreased by 86 %, carbon monoxide (CO) by 84 %, and soot by 97 %. However, limits are becoming increasingly severe.

Table 1.2 Dynamic evolution of the limits for pollutant emissions of internal combustion engines for automobiles in Europe

Norm valid from	CO [g/km]		$HC + NO_x$ [g/km]		Particles [g/km]	
	Gasoline	Diesel	Gasoline	Diesel	Gasoline	Diesel
Euro 1 1992	3.16	3.16	1.13	1.13	–	0.18
Euro 2 1997	2.2	1	0.5	0.7 (0.9[a])	–	0.08 (0.1[a])
Euro 3 2000	2.3	0.64	0.2 + 0.15	0.56 (x + 0.5)	–	0.05
Euro 4 2005	1	0.5	0.1 + 0.08	0.3 (x + 0.25)	–	0.025
Euro 5 2009	1	0.5	0.1 + 0.06	0.23 (x + 0.18)	0.005[a]	0.005
Euro 6 2014	1	0.5	0.1 + 0.06	0.17 (x + 0.08)	0.0045[a]	0.0045

Sources: EU directives 91/441/EWG, 94/12/EC, 98/69/EC, 2002/80/EC, 2007/715/EC
[a]For direct injection engines

Table 1.3 Limits for pollutant emissions of internal combustion engines for automobiles in California, USA

Norm USA[a]	Yearly range [km/year]	CO [g/km]	HCHO [g/km]	NO_x [g/km]	Particles [g/km]	NMOG [g/km]
LEV II	80,467/5	2.113	0.009	0.031	–	0.047
	160,934/10	2.610	0.011	0.043	0.006	0.056
ULEV II	80,467/5	1.056	0.005	0.031	–	0.025
	160,934/10	1.305	0.007	0.043	0.006	0.034
SULEV II	80,467/5	–	–	–	–	–
	160,934/10	0.621	0.002	0.012	0.006	0.006

HCHO formaldehyde, *LEV* low emissions vehicle, *NMOG* non-methane organic gasses, *SULEV* super ultralow emissions vehicle, *ULEV* ultralow emissions vehicle
Sources: Environmental Pollution Agency, Air Resources Board of California
[a]Values for vehicles with spark-injection and compression-injection engines

On the other hand, the detectable climate change provoked by carbon dioxide emissions from industrial processes have also resulted in limits being determined, including for the automobile industry. The European Automobile Manufacturers' Association (Association des Constructeurs Européens d'Automobiles) initially committed to reducing carbon dioxide emissions to an average of 140 g CO_2/km for each brand. This limit was subsequently decreased to 130 g CO_2/km for 2012–2015, European Commission directive for 2020 provides for 95 g CO_2/km. With a target of warming of the earth's atmosphere by no more than 2 °C until 2050, the G8 council agreed on a limit of 20 g CO_2/km.

Given this, it should be taken into account that a direct relationship exists between fuel consumption and carbon dioxide emission. For ideal combustion in a piston engine using, for example, gasoline and oxygen from the air in a

stoichiometric ratio, without a mass-significant emission of CO or HC, 20 g CO_2/km corresponds to a gasoline consumption of 0.88 l/100 km, with the gasoline structure as follows:

Carbon: $c = 0.847$ kg C/kg gasoline
Hydrogen: $h = 0.153$ kg H_2/kg gasoline

The stoichiometric complete reaction of combustion leads to [1]:

$$\frac{c}{12} \cdot \mathrm{C} + \frac{c}{12} \cdot \mathrm{O_2} \rightarrow \frac{c}{12}\mathrm{CO_2}$$
$$\frac{h}{2} \cdot \mathrm{H_2} + \frac{h}{4} \cdot \mathrm{O_2} \rightarrow \frac{h}{2}\mathrm{H_2O}$$

The parts of carbon and hydrogen (c, h) have been transformed for the chemical balance equation from kilograms to kilomoles, by dividing by the molar mass (c/12 kmol C/kg fuel and h/2 kmol H_2/kg fuel).

In the mass balance of substances in the combustion reaction, the pollutants such as CO, C_mH_n, and NO_x remain together at a level under 2 %, which is not significant for the relationship between fuel consumption and carbon dioxide emission.

The exact recording of the CO, C_mH_n, and NO_x emission is important in relation to their toxic effects. The relationship between carbon dioxide and fuel consumption is based on the substances resulting from combustion:

$$\mathrm{CO_2}: \quad \underset{\left[\frac{\mathrm{kmol\,CO_2}}{\mathrm{kg\ \ fuel}}\right]}{\frac{0.847}{12}} \cdot \underbrace{(1 \cdot 12 + 2 \cdot 16)}_{\left[\frac{\mathrm{kg\ \ CO_2}}{\mathrm{kmol\ \ CO_2}}\right]} = \underbrace{3.1}_{\left[\frac{\mathrm{kg\,CO_2}}{\mathrm{kg\,fuel}}\right]}$$
$$(Molmass\,CO_2)$$
$$\mathrm{H_2O}: \quad \underset{\left[\frac{\mathrm{kmol\,H_2O}}{\mathrm{kg\ \ fuel}}\right]}{\frac{0.153}{2}} \cdot \underbrace{(2 \cdot 1 + 1 \cdot 16)}_{\left[\frac{\mathrm{kg\ \ H_2O}}{\mathrm{kmol\ \ H_2O}}\right]} = \underbrace{1.38}_{\left[\frac{\mathrm{kg\,H_2O}}{\mathrm{kg\,fuel}}\right]}$$
$$(\mathrm{Molmass\,H_2O})$$

Considering the stoichiometric air-to-fuel ratio [1]:

$$\left(\frac{L}{K}\right)_{st} = 4.31(2.664c + 7.937h)$$

and the oxygen content of the atmosphere, the air demand presents as:

$$\left(\frac{L}{K}\right)_{st} = 14.96 \ \left[\frac{kg\,air}{kg\,fuel}\right]$$

The remaining nitrogen after the combustion reaction (the NO_X mass is not significant, as already mentioned) is:

$$N_2 = 0.768 \left(\frac{L}{K}\right)_{st} = 11.48 \left[\frac{kg N_2}{kg fuel}\right]$$

The mass-related balance of products before and after combustion is:

Fuel: 1 kg	CO_2: 3.1 kg
Air: 14.96 kg	H_2O: 1.38 kg N_2: 11.48 kg
15.96 kg	15.96 kg

Considering the usual density of gasoline (0.736 kg/l), the carbon dioxide emissions from 1 l of gasoline are:

$$\underset{\left[\frac{kg\,CO_2}{kg\ fuel}\right]}{3.1} \cdot \underset{\left[\frac{kg\ fuel}{liter\ fuel}\right]}{0.736} = \underset{\left[\frac{kg\,CO_2}{liter\,fuel}\right]}{2.28}$$

Thus, a fuel consumption of 5.7 l/100 km or 0.057 l/km leads to:

$$\underset{\left[\frac{kg\,CO_2}{liter\ fuel}\right]}{2.28} \cdot \underset{\left[\frac{liter\ fuel}{km}\right]}{0.057} = \underset{\left[\frac{kg\,CO_2}{km}\right]}{0.13} \rightarrow \underset{\left[\frac{g\ CO_2}{km}\right]}{130}$$

A successful car with a swept volume of 3 l, consuming 12 l gasoline/100 km has an emission of 274 g CO_2/km. Consequently, to compensate and achieve the required average carbon dioxide emission for the whole brand, the manufacturer must produce in the next generation (2020) double the number of automobiles without any hydro-carbon combustion—either in combustion engines or in motors receiving sourcing power from coal plants. The limit for carbon dioxide emission can be calculated as applied to stationary operating engines; however, the situation is more complex for engines in on-road vehicles, as demonstrated in the following examples:

– The operational profile of the new European driving cycle (NEDC) is shown in Fig. 1.8.

This cycle was established based on statistical data, but it corresponds to an engine operation field with a very low speed and torque, far from the minimum brake-specific fuel consumption (BSFC) or maximum torque, which is an effect of the maximum temperature of combustion. The adjustment of consumption for a test such as new European driving cycle or federal test procedure (FTP) is not a problem for a manufacturer—as shown by the recently discovered manipulations of

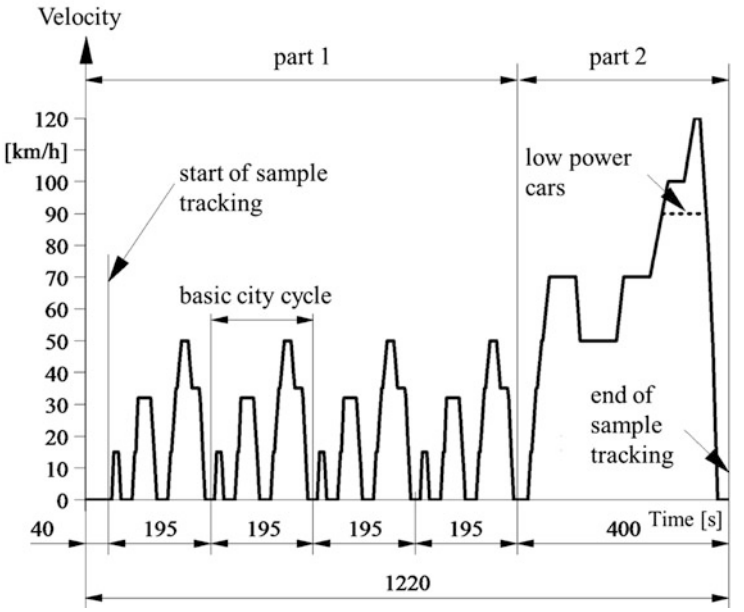

Fig. 1.8 New European driving cycle (Source: EU directive 91/441/EWG)

pollutant emissions—but in this case, the values in the other means the major parts of the operating fields are impaired.

This unreliable situation leads us to expect the introduction of real driving tests in the very near future, in which carbon dioxide and pollutant emission limits will certainly be re-evaluated.

Another aspect must also be considered: a luxury car travels an average of some 8000 km/year, whereas a family car travels some 30,000 km/year. The luxury car is generally operated at a higher load, leading to greater fuel consumption and thus to higher carbon dioxide emissions. However, this is partially compensated for by the improved thermal efficiency at higher loads. Considering both the yearly driving distance and the load range, the absolute value of the yearly carbon dioxide emission is lower for the luxury car than for the family car.

The challenge of achieving high power and torque but low fuel consumption and pollutant emission provides the motivation to generate new propulsion configurations. Figure 1.9 presents a summary of the mentioned development conditions.

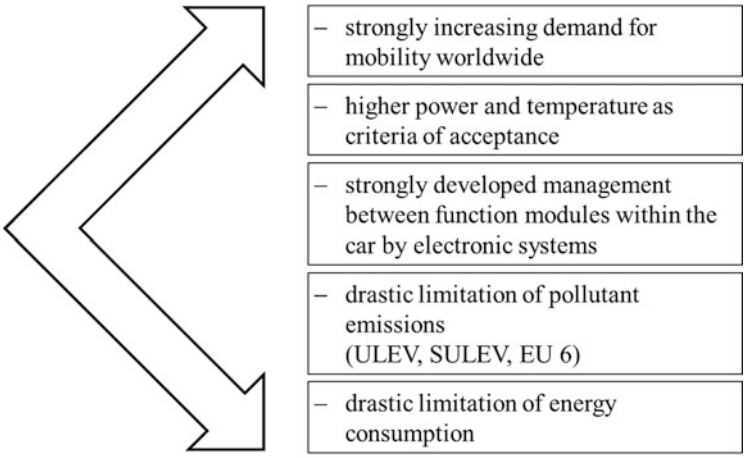

Fig. 1.9 Development conditions for automobile propulsion systems

1.2 Development Requirements

Development scenarios for automobile manufacturers worldwide are somewhat controversial: hybrid systems (engine and motor) based on gasoline engines (because of market acceptance in the USA and Japan) have no advantage over advanced diesel engines; diesel is actually superior in vehicles driven on the motorway. Diesel and motor is possible, as two-stage turbocharging of the diesel seems more efficient; however, for short trips in city centers, the combination of diesel and a small motor is an interesting solution because of its emission-free nature.

Hydrogen in fuel cells, as well as hydrogen in piston and Wankel engines is a very interesting subject at this time, as is the use of alcohol, vegetable oils, and liquefied petroleum gas (LPG). This is not a sign of lack of concept or of doubt, but testimony that the propulsion system and its on-board management must adapt to the diversity of automobiles in the future.

The main requirements are as follows:

- Available energy sources
- Minimal ecological impact from energy conversion
- Technical implementation—conditional on technical complexity, dimensions, weight, costs, safety, infrastructure
- Active and passive safety
- Traffic characteristics
- Recycling of used cars.

1.2.1 Energy Availability

Last century, transport was a primary criterion in the development of civilization. Transport systems required dynamic development of techniques, which activated a multitude of domains, from technology and economic structures through to politics.

The worldwide increase in automobile production between 2002 and 2015, from 57 million to 76 million cars per year (source: VDI Germany) led to an increase in value, from €645 to €903 billion respectively, whereas participation of the original equipment manufacturer (OEM) in this process decreased from 35 to 23 % in favor of suppliers and service providers.

In 2002, value creation was €227.1 billion in the North American Free Trade Agreement (NAFTA) zone, €204 billion in Europe, and €115.4 billion in Japan. In 2015, the increase in value creation was expected to reach 56 % (€318.1 billion) in Europe and 17 % (€266.6 billion) in the USA. However, the structural change generated by the development and production of automobiles can be better deduced from the increase in value creation in China (+260 %), South America (+109 %), and India (+328 %) (source: Verein Der Automobilindustrie Germany).

The increasing participation of suppliers and service providers in this process generates a transfer of techniques and technologies from products for automobiles to products in many other industries. On the other hand, any job in the automobile industry generated at least three closely related jobs.

The dynamics of this progress are accelerated by research and development (R&D) in the automobile industry, which is considerably higher than in other industries. In the year 2010, more than 30 % of total R&D expenditure in Germany (€61.5 billion, or 2.46 % gross product) was directed toward the automobile industry, totaling three times more than all government support for R&D in benefit of German industry. The automobile industry R&D budget equals that of the machine construction, chemical, electrotechnics, informatics, and optics industries combined.

These research priorities and structures in Germany show a clear relationship with global innovation: worldwide, 36 % of patents for inventions are from Germany, 19 % are from Japan, 17 % from the USA, 8 % from France, and 20 % are from all the other countries of the world combined.

This creativity and innovation combined with a wide distribution of production locations has the potential to create a true export champion and has considerable influence on global energy demand. As illustrated in Fig. 1.10, worldwide, the average total energy consumption per person is 21,600 kJ/h · person. This corresponds to a perpetual power demand of 6 kW/person, from house and road construction through to food and transportation. In this contest, the demand for food seems poor, as it is 35 times less than the total value.

From this perspective, the expected increase in global population of 1.8 % per year—estimated to reach 9 billion inhabitants in the year 2020—is an important but not decisive criterion for the future global demand for energy. The mobility scenarios and structures in the industry states play a more significant role.

The usual case, of one person per car, with a mean power demand of 30 kW, generally driving 20,000 km/year, implies a power demand of 1.368 kW, which is

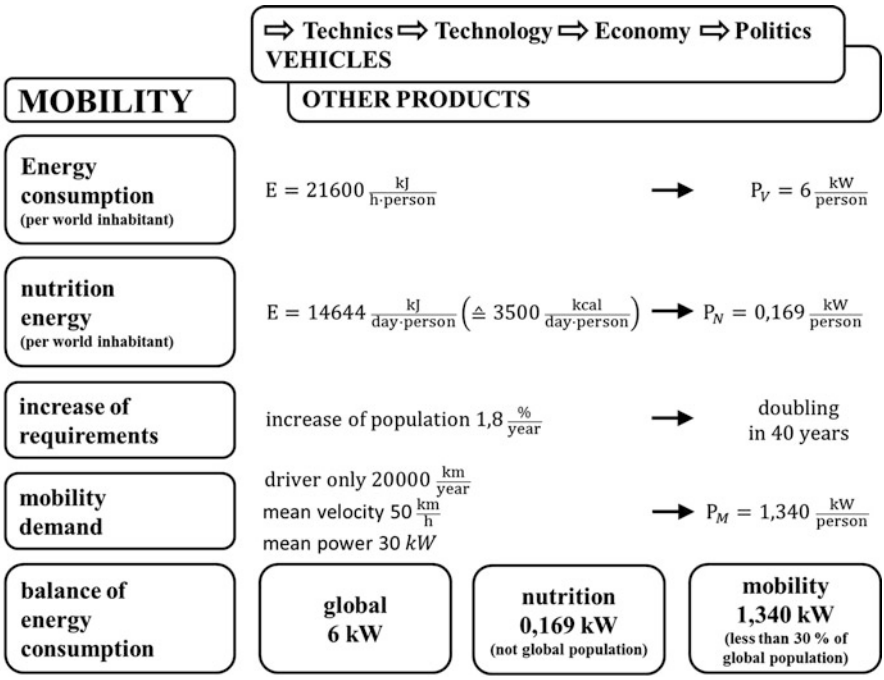

Fig. 1.10 Mobility: tendencies and requirements

available for only one-fifth of the world's inhabitants. However, this model is now very popular everywhere, with the friendly encouragement by the car manufacturers. Figure 1.11 shows this tendency in terms of car inventory increase worldwide.

The number of vehicles worldwide (currently 1.18 billion, accumulated over a century) is expected to double in the next 30 years (Source: Ward's Automotive Group, R.L. Polle Marketing Systems). The number of vehicles per inhabitants is reported to be 700/1000 in the USA (Source: US Dept. of Transportation), in 27/1000 in China, and 10/1000 in India. It is no coincidence that the development strategies of most automobile manufacturers are concentrated in Brazil, Russia, India, and China (BRIC). Figure 1.12 illustrates the dynamics of automobile production per country for the last 15 years; not only the number but also the barycenter is changing comprehensively.

In this context, the availability of energy resources is therefore decisive.

Crude oil: Calculated from current consumption levels without accounting for the expected strong increase, at least for automobile transport (from Fig. 1.12), the estimated reserves could be sufficient for the next 80 years. Based on current known reserves, this period reduces to 30 years. Optimistic predictions, such as those from BP are 36 years. Alternative sources and their availability are shown in Fig. 1.13.

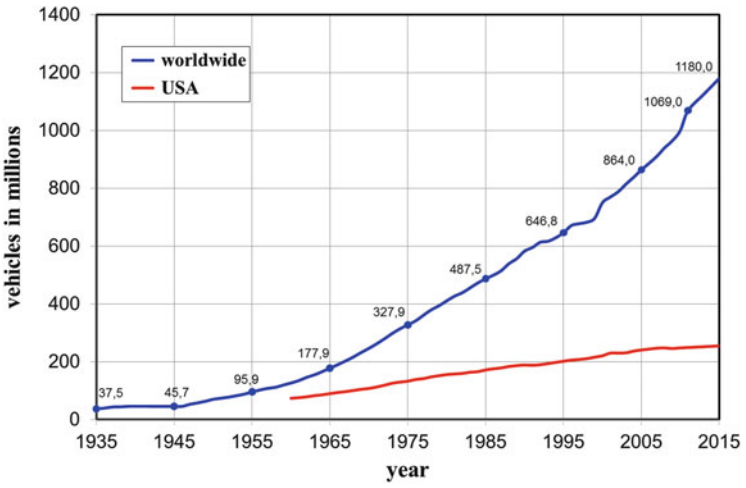

Fig. 1.11 Inventory of cars and trucks worldwide and in the USA (Source: worldwide 1935–2009 Ward's Automotive Group, worldwide 2015 R.L. Polk Marketing Systems, USA U.S. Department of Transportation, Federal Highway Administration)

Fig. 1.12 Automobile production per year and country

Natural gas: This is a fossil energy resource that will be available for 60 years. The increasing number of cars with gas engines is, at present, a meaningful measure because of the use of a complementary source. However, the limited availability of both crude oil and natural gas remains an unavoidable problem.

Coal: The coal reserves are estimated to last 500 years. Coal hydrogenation and its subsequent transformation to water gas leads to hydrogen; the catalytic conversion leads to hydrocarbon structures, such as gasoline and diesel fuel, with

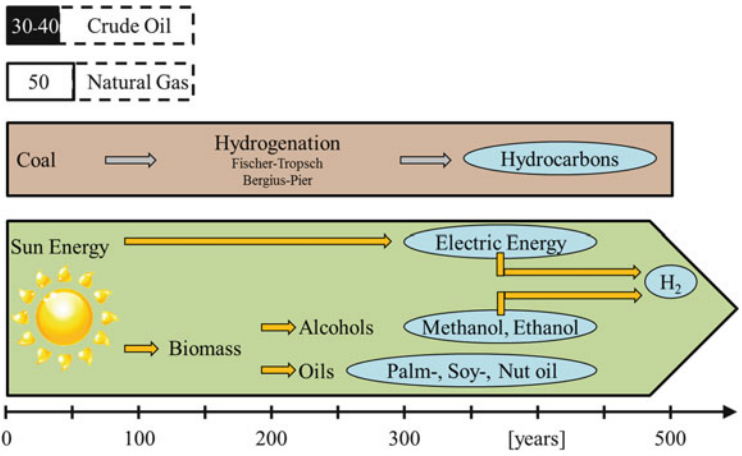

Fig. 1.13 Available energy sources for car propulsion

secondary products (liquid gas and white wax). The disadvantages of transforming coal to fuel include the high price and the carbon dioxide emissions, as well as the infrastructural, geopolitical, and social problems of large-scale coal exploitation.

Plants, biomass: The availability of plants or biomass, as recipients and transformers of solar energy has practically no limits. Use in piston engines is technically feasible—alcohols such as methanol and ethanol in gasoline engines, dimethyl ether, oils, oil-esters, and bio-fuels with diesel fuel structure. The yearly global biomass potential is, as an energy equivalent, 22 times higher than the energy equivalent of the early extracted crude oil.

Geothermal energy: The flux density of the geothermal energy is too low to use in mobility systems, reaching only 0.05 W/m^2. Utilization of geothermal energy from an area of 20×10^6 km^2 worldwide, corresponding to the cultivable land of 90 countries, would result in 11.4 MW h/year. In comparison, the energy potential of the crude oil extracted annually is 38×10^6 MW h/year.

Solar energy: Energy via solar radiation to the earth corresponds to 175×10^{12} kW. In comparison, the combined annual energy from extracted gas and oil combined equals 24,000 kW. As a moderate example, in middle Europe, solar power density is 114 W/m^2. In an ideal scenario, the production of electric energy and hydrogen in the desert would require only 12 % of the deserts worldwide; 1.9×10^6 km^2 at an efficiency no higher than 3 % would cover the energy demands of the whole world.

Water, wind, and nuclear energy: Water and wind play an insignificant role in the production of electrical energy and hydrogen worldwide. The use of nuclear energy is generally very controversial; any extension into transport would be strongly contested.

The current potential of plants and biomass, and the increasing number of photovoltaic plants, for production of electric power or hydrogen are the true alternatives to fossil resources for the mobility sector.

1.2.2 Environmental Impact of Energy Conversion

Environmental impact has become a primary criterion for the assessment of energy sources for transport in recent decades. Since industrialization began, the earth's atmosphere has warmed nearly 1 °C. In the same period, the concentration of carbon dioxide in the atmosphere increased from 280 to 385 parts per million (ppm). However, the contribution of carbon dioxide to global warming is very controversial. Climate researchers from the Intergovernmental Panel for Climate Change (IPCC) believe the increasing concentration of anthropogenic substances in the atmosphere is responsible for global warming, at least in the last 5–6 decades. Other researchers believe it is the changed intensity of solar radiation and doubt the greenhouse effect theory.

The predicted warming of the earth atmosphere with increase of 5.8 °C until the end of this century at the current CO_2 emission obliges to consequent measures. Therefore, the stated intent to maintain the temperature increase at less than 2 °C until 2050 means that a drastic reduction of CO_2 emissions is crucial.

Earth's climate is regulated by complex inter-related mechanisms involving the biosphere, oceans, and cryosphere. However, the primary influence on earth's temperature can be calculated, despite the complexity of the whole process, from a basic balance: the middle temperature (15 °C) of the atmosphere is determined by tracer gases, consisting of molecules with two asymmetrical atoms and molecules with three or more atoms.

It has been calculated, that without the natural greenhouse effect brought about by these gases, the average temperature of the atmosphere would decrease by 33 °C to a value of –18 °C. The natural greenhouse effect can be explained in a simplified form for more clarity in terms of the object of this book, by the descriptions in Fig. 1.14.

Solar radiation is mostly emitted in the range of $\lambda = 0.35$–10 µm. This includes the visible light radiation between $\lambda = 0.35$ and $\lambda = 0.75$ µm. The atmospheric gases with molecules formed by one or by two symmetrically disposed atoms are generally permeable by electromagnetic beams at every wavelength. On the other hand, gases with molecules formed by two non-symmetrically disposed atoms or by three and more atoms are selective in terms of wavelength of electromagnetic radiation. The high intensity of the solar radiation to the earth is concentrated mostly in short wavelengths, in the visible domain, as illustrated in Fig. 1.15, with a small percentage in the ultraviolet and roentgen sectors. The radiation intensity I_λ (watts/square meter) at a wavelength λ (meters) leads to a density of heat flow $\dot{q}$ (watts/cubic meter) that penetrates into earth's atmosphere, as well as into bodies across their surface A (square meters) in the form of heat flow $\dot{Q}$ (watts):

$$\dot{q} = \int_0^\infty I_\lambda \cdot d\lambda \quad and \quad \dot{Q} = \dot{q} A$$

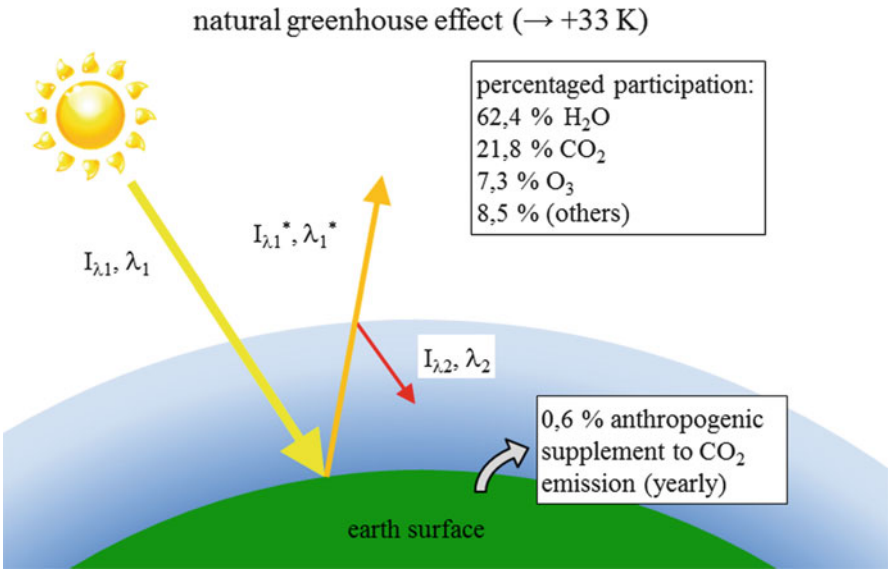

Fig. 1.14 Greenhouse effect: natural balance

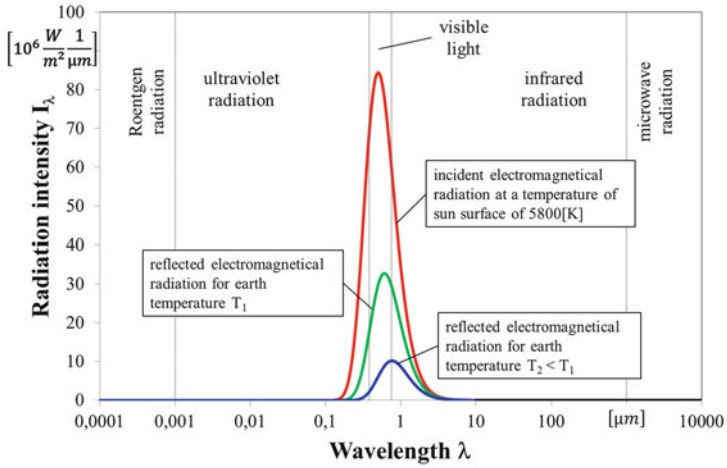

Fig. 1.15 Spectrum of incident and reflected electromagnetic radiation

The transmission of radiation energy to atmospheric gases and bodies on earth decreases the energy of the reflected beams, which provokes a displacement of the wavelength to the infrared zone. The reflection is not obstructed by one or two symmetrical atom gases; instead, gases with two non-symmetrical atoms, or with more atoms, form a barrier to lower wavelength radiation beams, provoking their

partial deviation back to the atmosphere. This generates a new heat flow, whereas the intensity and the wavelength of the beams again lower. Thus, the atmosphere's internal energy, expressed in temperature, increases to an energetic balance between the absorbed and the reflected radiation. This natural greenhouse effect in the atmosphere is mostly caused by water vapor, carbon dioxide, and ozone. Their roles are shown in Fig. 1.14.

After water vapor, which is partially redirected to earth via saturation and condensation, carbon dioxide is the primary influence. Every energy conversion via the complete combustion of a hydrocarbon generates carbon dioxide; the current yearly emission of which is 20 billion tons or 0.6 % of natural emissions, which is primarily recycled via photosynthesis. Most researchers predict that the effect of carbon dioxide accumulation in the atmosphere via combustion of fossil energy will increase the average atmospheric temperature by 5.8 °C up to 2100. Incidentally, the mean winter temperature in Europe has increased by 2.7 °C over the last 50 years. Critics of this theory state global warming over the past 150 years has been primarily provoked by the variable intensity of solar radiation and by volcanic activity. Furthermore, they believe the model of the carbon dioxide circuit in the atmosphere, biosphere, and hydrosphere; the characteristics of beam absorption by CO_2; and the defined CO_2 lifetime to be implausible. Despite such doubts, the global community pursues drastic limitations to the growing anthropogenic CO_2 emission. Transportation, and therefore road vehicles with gasoline and diesel engines, is responsible for a significant portion of carbon dioxide emission via fossil fuel combustion.

In this context, and as discussed, Europe legislated a CO_2 emission limit of 95 g/km by car fleet for every OEM in Europe by the year 2020. In the USA, efforts are being made to reduce fuel consumption to 7 l/km by 2020, which would lead to a CO_2 emission of 160 g CO_2/km. The current fleet fuel consumption in the USA is 9.7 l/100, resulting in 221 g CO_2/km. Japan planned and achieved a limit of 5.9 l/100 km, corresponding to 135 g CO_2/km, by 2015. However, the balance of energy and emissions must include the energy supply through to its work application, thus "well to wheel." As an example, in the chain from crude oil to application in a gasoline engine, considering 100 % energy of crude oil, the processes within the chain require energy as follows:

- 10 % gasoline production from crude oil—including prospecting, extraction, transport, refinery, distribution
- 10 % vehicle losses
- 2–3 % gear losses
- 70 % dissipated in the thermodynamic engine cycle, by cooling and exhaust gas enthalpy losses

The energy losses—from prospecting of the crude oil reserves through to extraction, transport, refinery, and distribution—are not significant compared with utilization of the product in the engine itself. Thus, a direct relationship exists between fuel consumption and CO_2 emission, as already discussed. Some

automobiles with diesel engines currently reach CO_2 values very close to the goal of 95 g CO_2/km for 2020. Figure 1.16 shows the CO_2 emissions of a VW Golf Diesel Blue Motion with a swept volume of 1.6 l compared with the well-to-wheel CO_2 emissions of a VW Golf Blue "e-motion," which is equipped with a motor and a lithium-ion battery. The electric energy is obtained from different sources:

- The EU current mix is obtained from coal (41.2 %), crude oil (7.9 %), natural gas (22 %), water force (15 %), uranium (11.7 %), and other (5 %) (source: Energy Information Administration, International Energy Annual). In this case, electric propulsion has an advantage over the diesel engine: 89 versus 99 g CO_2/km, respectively.
- The mix in Germany as at 2014 uses more coal, as shown in Fig. 1.4. In this case, the electric propulsion is at a disadvantage: 115 versus 99 g CO_2/km, respectively. Moreover, it should be noted that, in 2014, a significant amount (11.7 %) of electric energy was produced by nuclear plants, the use of which is now strongly reduced in favor of coal plants.

Figure 1.16 shows what would happen if electric energy were produced via lignite or anthracite: for the considered case, an increase to 188 g CO_2/km using lignite. The situation would become critical if lithium-ion batteries were replaced with lower energy density sources, for example lead-acid batteries.

The use of emission-free electric motors in the congested urban areas of the future will simply relocate CO_2 emissions to a coal plant in a lower-density population area; however, this does not solve the problem of global warming. An interesting alternative is offered by decentralized modular current-generation plants

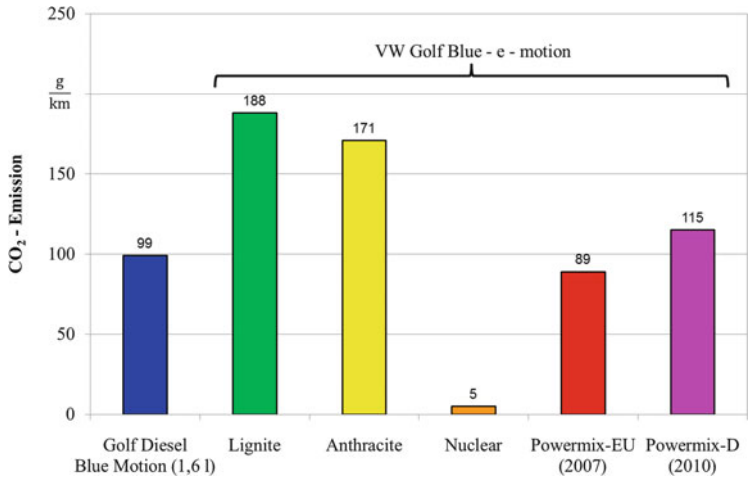

Fig. 1.16 Influence of the efficiency of well-to-wheel energy conversion on CO_2 emission (Source: Hadler, J.: Mobilität im Spannungsfeld globaler Energieketten, Int. Wiener Motorensymposium 2011, ISBN 978-3-18-373512-9)

for vehicles in agglomerated urban areas, as shown at the end of this chapter in the form of a photovoltaic station. Only 10 % of generated energy is required by all road traffic worldwide; thus, such decentralized structures seem viable.

1.2.3 Technical Implementation

The availability of energy resources and their environmental impact are important; however, they are not the only considerations in the choice of on-board fuel or energy. The accumulation or conversion of the energy also determines the application. Numerous criteria exist in the realistic valuation of tanks, accumulators, and conversion systems, such as mass volume, safety, materials, and infrastructure for distribution.

Figure 1.17 compares the mass and volume of different fuels and for a battery, including the mass and volume of the accumulator itself. The comparison is based on the energy equivalent of 37 l diesel fuel, which corresponds to a middle-class car on a usual driving cycle for a range of 500 km. With the diesel fuel, accounting for tank dimensions, the total tank volume becomes 46 l, fuel mass is 30 kg, and total tank mass is 43 kg. The values for gasoline are generally similar; the higher consumption is compensated for by mass with the lower density. LPG, a mixture of propane and butane, has a much lower density than gasoline—0.00235 kg/l versus 0.72–0.78 kg/l at the same pressure and temperature. At 0 °C/1 MPa, the density of LPG increases to 0.5 kg/l. However, tank mass also increases because of the higher fuel pressure, which requires stronger walls: for 37 kg of fuel, the tank mass becomes 72 kg.

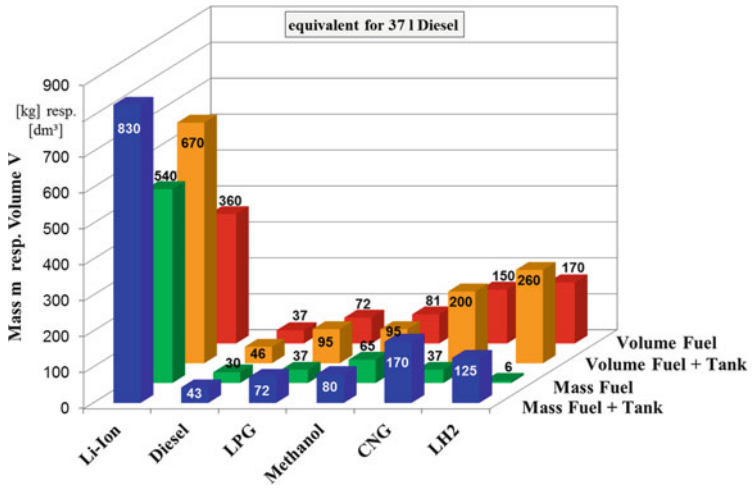

Fig. 1.17 Comparison of the stored mass and volume for different fuel types and on-board batteries for the same energetic content

Therefore, both the mass and the volume of the full tank for LPG are twice that required for diesel fuel to obtain the same energy content. Methanol has a similar density to that of diesel fuel and can also be stored under atmospheric conditions, which is a net technical benefit. The heating value (kilojoules/kilogram) of methanol is less than half of that for diesel fuel, which means more than double stored quantity is necessary to achieve the same energy and the same range. Consequently, both the mass and the volume of the whole tank system increase, as shown in Fig. 1.17.

Compressed natural gas (CNG) is stored at a higher pressure (20 MPa) at ambient temperature, but the density is no higher than 0.141 kg/l. Thus, the tank is not only heavy but also large, as shown in Fig. 1.17. Cryogenic storage (–150 °C and 0.1 MPa) has the advantage of a higher density (0.409 kg/l); however, the tank design would be more complex. Hydrogen has a comparatively lower mass than diesel fuel at the same energy content, but the density is the lowest of all fuels: 0.009 kg/l at −200 °C and 0.1 MPa. The liquid form has a density of 0.071 kg/l, which is one-tenth that of gasoline; however, it requires a storage temperature of −253 °C, with obvious technical complexities. Therefore, the volume becomes very large, as shown in Fig. 1.17. An extreme example is the use of electric energy in a battery: for the same energy content as 37 l diesel fuel, an advanced and expensive lithium-ion battery would be the weight and dimension of an entire compact car.

On-board energy storage will have a very important role in the future of alternative fuels for automobiles. The structure and design of cars, as shown in Fig. 1.18, and consequently the driving dynamics will be newly defined when using batteries (Fig. 1.19) or hydrogen tanks (Fig. 1.20). On the other hand, the integration of such energy accumulators within active and passive safety systems seems much more complex than the integration of conventional fuel tanks.

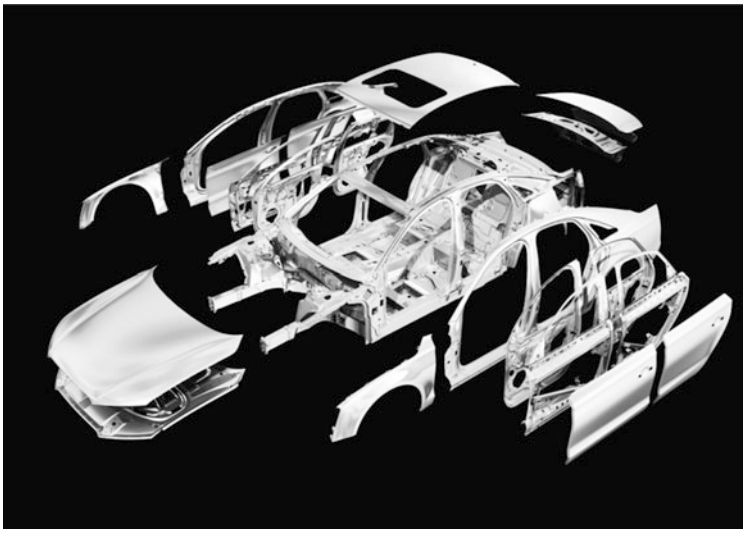

Fig. 1.18 Space frame *(*Source*:* Audi*)*

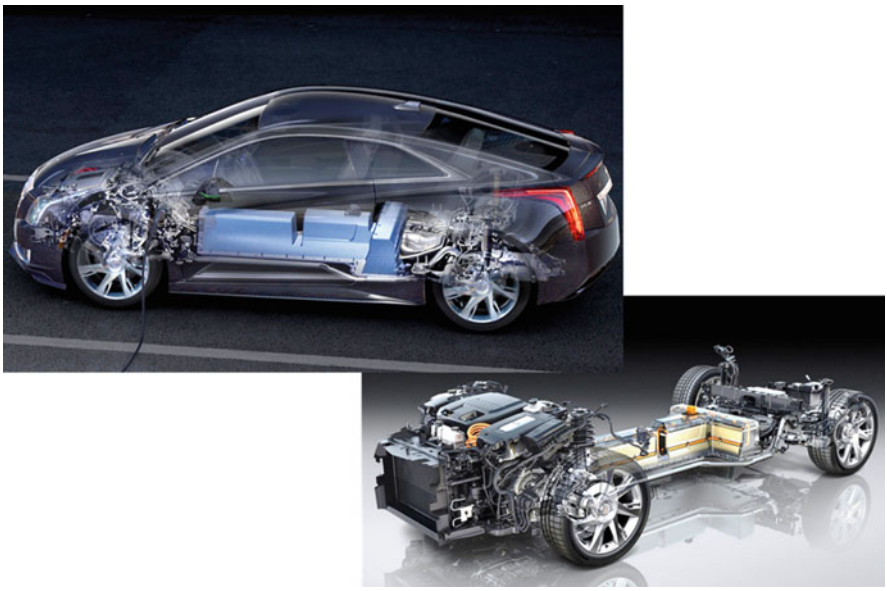

Fig. 1.19 Car with battery storage of electrical energy (Source: Cadillac)

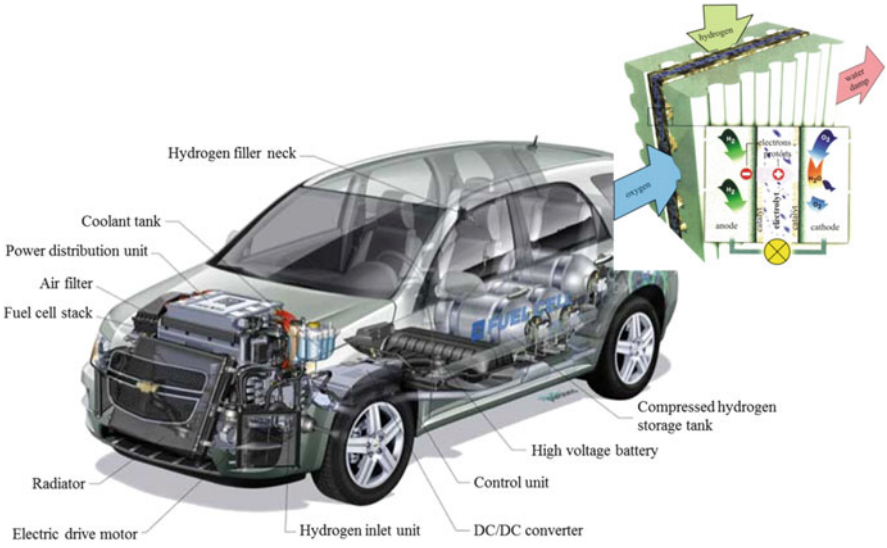

Fig. 1.20 Car with fuel cell and storage of hydrogen (Source: GM)

1.3 Development Scenarios for On-board Energy Management

Between the constraints of demand, available energy resources, environmental impact, technical complexity, typical forms of car utilization and customer acceptance, a multitude of viable propulsion system configurations are possible.

Given the above requirements, the development of any future propulsion system, including on-board energy storage and/or conversion, must consider the following criteria:

- Mass-to-power and power-to-volume ratio
- Torque characteristics, acceleration behavior
- Specific fuel/energy consumption, specific emission of chemical substances, intensity and frequency of noise
- Availability and on-board storage
- Technical complexity, costs, safety
- Infrastructure and service facilities

The propulsion of car wheels is possible using either thermal engines or motors or both forms together.

Figure 1.21 shows an example of typical torque curves for an engine (in this case, a gasoline engine) and a motor for car propulsion. The power can be calculated from the torque as follows:

$$\begin{aligned} P_e &= M_d \cdot \omega \qquad with\ \ \omega = 2\pi n \\ P_e &= M_d \cdot 2\pi n \end{aligned} \tag{2.9a}$$

Corresponding to these equations, the power curve can be represented as shown in Fig. 1.21. Another form of power display is as hyperbolas with constant power value in the (M_d, n) diagram, as illustrated in Fig. 1.21.

The most significant difference between propulsion by engine and motor is in torque characteristics:

- The maximum torque of an engine deploys with increasing engine speed. Figure 1.21 shows a maximum torque at 1300 min^{-1}, which is caused by the requirement for sufficient air flow entering the engine.
- The maximum torque of a motor is already available from a standstill, before the first rotation; this is caused by the magnetic circuit that appears when the current is switched on. As the rotor speed increases, the incremental dispersion of magnetic wires from the circuit produces the noticeable decrease in torque, as shown in Fig. 1.21.

Given the same maximum torque at a lower speed as available in a motor, the corresponding power is lower, as can be deduced with Eq. (2.9a). The instant availability of maximum torque is a net advantage for car acceleration from standing. This relationship is illustrated in Fig. 1.22.

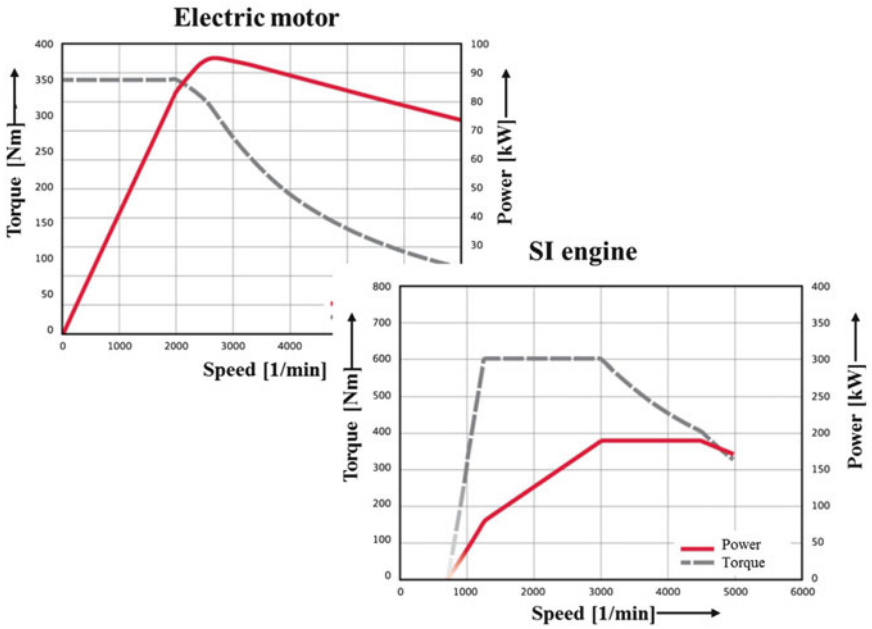

Fig. 1.21 Typical torque/power history in electric motor and spark-injection engine

Fig. 1.22 Torque on the wheel of an automobile (Source: Stan, Porsche)

Acceleration requires force. Given the wheel radius, this force determines the momentum, as described by the following equations:

$$F = m_F \cdot a \tag{1.1}$$

$$a = \frac{2s}{t^2} \tag{1.2}$$

hence

$$F = m_F \cdot \frac{2s}{t^2} \tag{1.3}$$

and consequently:

$$M_r = F \cdot r = m_F \cdot 2s \cdot r \cdot \frac{1}{t^2} \tag{1.4}$$

with:

F	propulsion force (newtons)
r	wheel radius (meters)
m_F	car weight (kilograms)
a	car acceleration (meters/second)
s	distance (meters)
t	acceleration time (seconds)

Generally, between the engine and the wheel, speed transformation takes place via gears, which have more transmission ratios for engines, because of their torque characteristics.

Figure 1.23 illustrates the relationship between engine torque, transmission ratio in gear, differential, and force at the car wheel.

During propulsion, the energy flow—the power between engine and wheel—is conserved across the transmission chain (i_G, i_T), with the afferent efficiencies (η_{GT}). The resulting force at wheel is as shown:

$$F_R = M_M \cdot \eta_{GT} \cdot \frac{i_G \cdot i_T}{r_R} \tag{1.5}$$

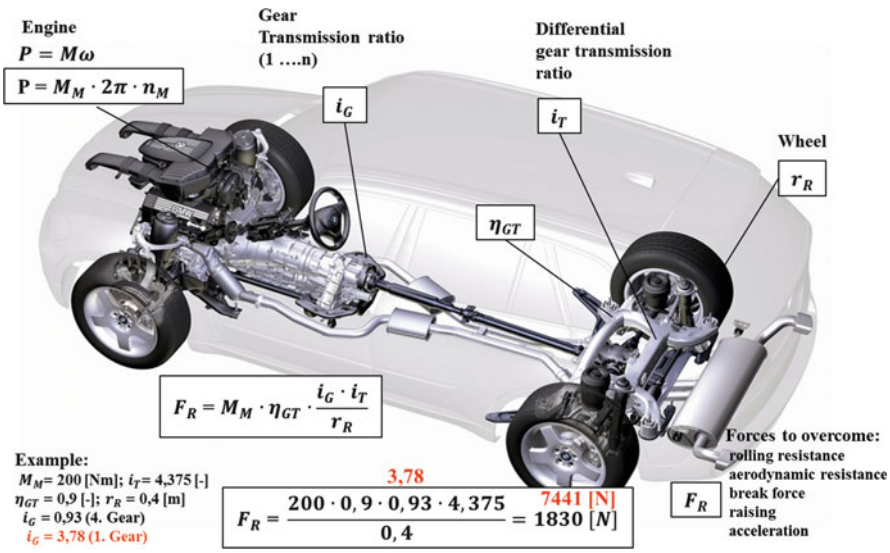

Fig. 1.23 Relationship between engine torque and force at the wheel of an automobile (Source: Stan, BMW)

The comparison of two different transmission ratios in a real car, as represented in Fig. 1.23, gives the following results:

- An engine torque of 200 N m generates along the first gear $i_G = 3.78$ a force at wheel of 7441 N. Belong the fourth gear ($i_G = 0.93$) the force is only 1830 N, but the wheel speed increases four times, even with the ratio (3.78: 0.93).

The relationship between force at wheel and car speed, resulting from wheel rotation speed and radius, can be represented as a traction force/car speed diagram, as shown in Fig. 1.24 for a real car with two gear variants, both with six transmission ratios. The implemented hyperbolas demonstrate the conservation of energy flow (power) between engine and wheel independent of transmission ratio.

An interesting comparison between propulsion with an engine with six gear ratios and a motor with a fixed transmission ratio is shown in Fig. 1.25. This diagram shows the acceleration upon speed, not the force upon speed, as in Fig. 1.24. In this mode, the different mass of each car is not considered. The motor, which has a high torque of 600 N m (Tesla), always has a higher acceleration level throughout the entire speed range of the car compared with the engine across the six gears.

Most motors in the current series of electric cars have a maximum torque in the range of 200–250 N m, imposed by the relationship between electric energy consumption and battery weight. A lower maximum torque determines a lower force at wheel. In this case, acceptable acceleration behavior is obtainable only by

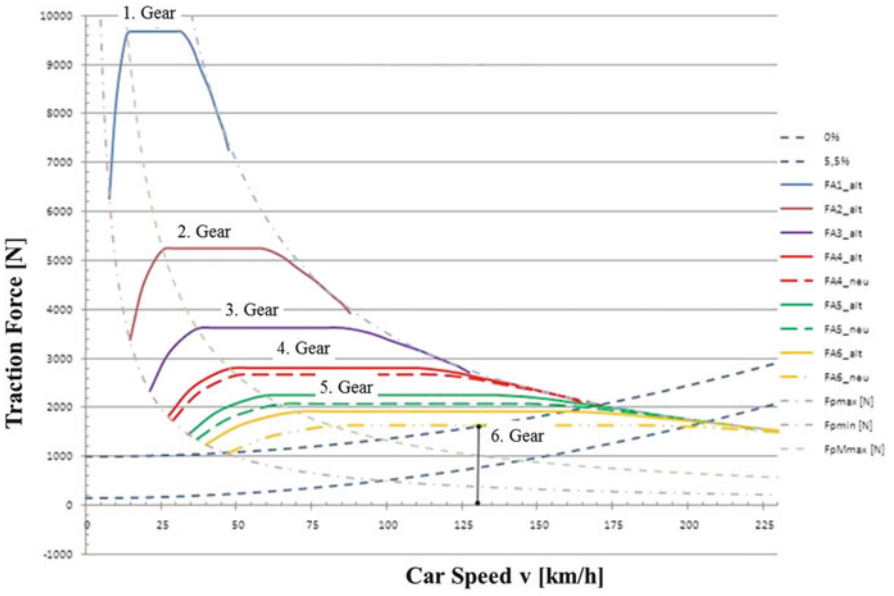

Fig. 1.24 Relationship between traction force at wheel and car speed (Source: Stan, Tesla)

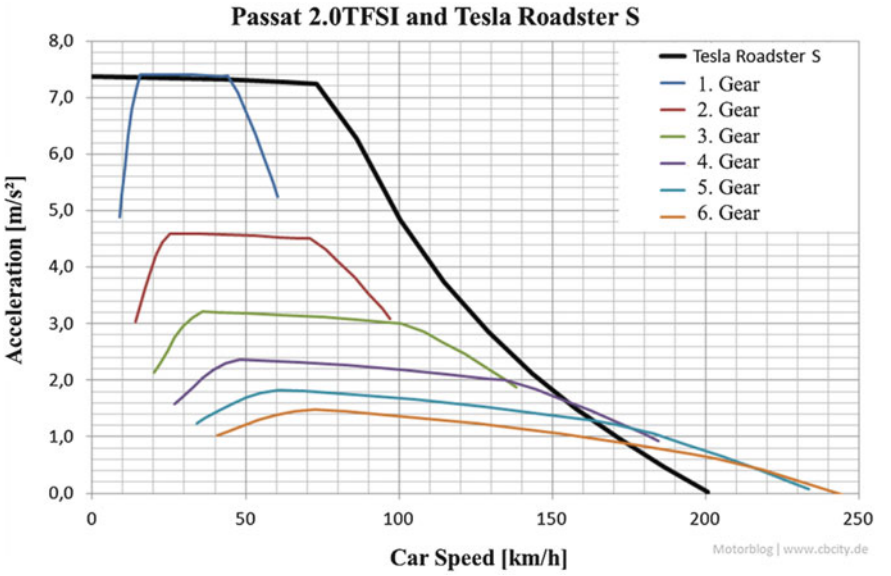

Fig. 1.25 Comparison between a motor and an engine

reducing the car mass. On the other hand, the breakpoint of motor torque, as shown in Fig. 1.21, is generally given at the same speed. Therefore, as can be deduced from Fig. 1.25, moving the horizontal motor characteristic to a lower level, with the breakpoint at the same speed, the motor can no longer achieve a higher speed without additional transmission ratios in a gear.

Figure 1.26 presents an overview of the possible processes, propulsion systems, energy sources, and on-board energy storage/conversion forms that can be combined in different forms.

Some advanced development scenarios and some classic solutions are available. The propulsion of the wheels can be ensured, as mentioned, by thermal engines and/or with motors. The chain of propulsion has, to date, produced two classic scenarios:

- Piston engine with spark or compression ignition, with liquid fuel (gasoline, diesel, LPG, oil esther) or gas (CNG)
- Direct current or three-phase-current motor with battery (lithium-ion/nickel–metal hydride battery)

The first scenario currently dominates the automobile industry; the second remains insignificant, despite continued work. The efficient management of energy from well to wheel requires reconsideration of the function modules, from the energy source and on-board energy storage and conversion through to propulsion. Some paths are particularly interesting:

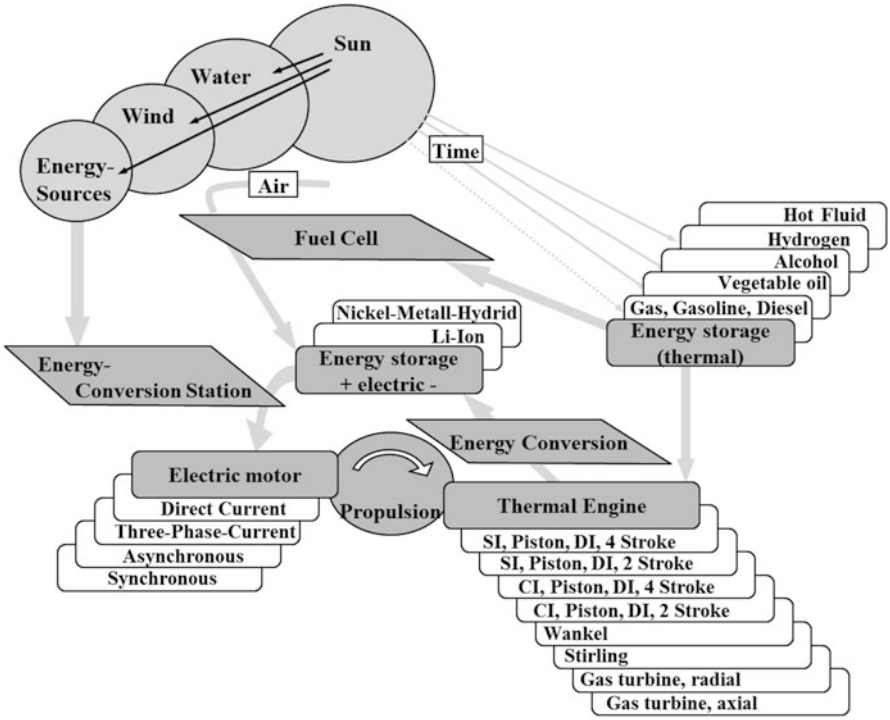

Fig. 1.26 Overview of processes, propulsion systems, and energy sources for automotive propulsion

- A motor that receives energy from a battery is generally disadvantaged by a limited range. Energy storage can be replaced by on-board conversion, for example with fuel cells and appropriate energy sources, as shown in Fig. 1.27. In this case, the fuel cell is fed with hydrogen and with oxygen from the ambient air.
- Without the propulsion by motor gains in this case on interest. However, storing hydrogen on board an automobile is disadvantaged by the low hydrogen density, despite very high pressure or cryogenic storage. From this viewpoint, use of gasoline, diesel fuel, and methanol undoubtedly has an advantage. This leads to an alternative: a tank for liquid fuel and a chemical reactor to transform liquid hydrocarbon or alcohol in hydrogen, when combined with water damp, can be added to the chain hydrogen—fuel cell—motor. In this case, a battery can serve as an energy accumulator.
- Between the motor and the hydrogen in the above scenario, an alternative solution (see Fig. 1.28) seems to have notable advantages: hydrogen (or another fuel) can be directed to a thermal engine (instead of the fuel cell) with the same role—producing current on board.

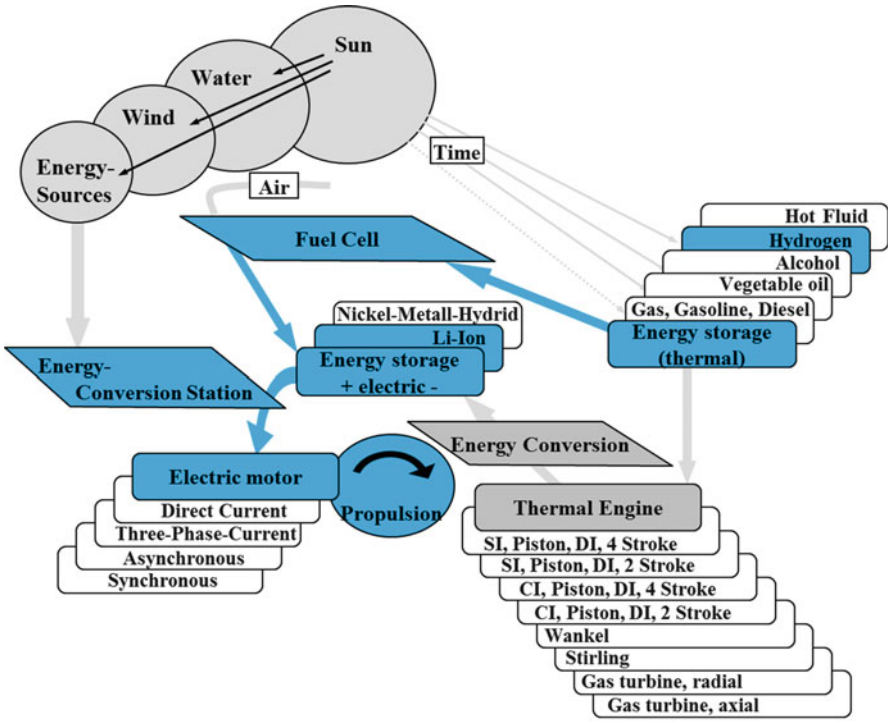

Fig. 1.27 Overview of processes, propulsion systems, and energy sources for automotive propulsion: fuel cell

In this case, it is no longer necessary for the thermal engine to cover the large range of torque and speed needed for direct propulsion of the car, but can remain in a restricted function domain. Thus, all stages of the process—from sourcing and mixing air and fuel through to combustion—can be tuned for maximum efficiency. When operating at a more or less constant speed that does not depend on the motor or the car speed, the type of thermal engine can differ from the usual four-stroke piston engines: two-stroke gasoline or diesel engines, Wankel, Stirling, diesel engines, and gas turbines can all work at high efficiency as compact current generators in the power range necessary for automobiles. A battery as an energy accumulator would also be advantageous in this case. A fuel cell in the same role can be compared with the same criteria—weight, dimension, price, and efficiency—determining future configurations.

- For a higher power demand corresponding to the type of car, propulsion can be ensured by combining engine and motors in fixed or variable couplings. In this case, electric energy for the motor can be generated in one of the above-mentioned forms. Figure 1.29 illustrates such a configuration.

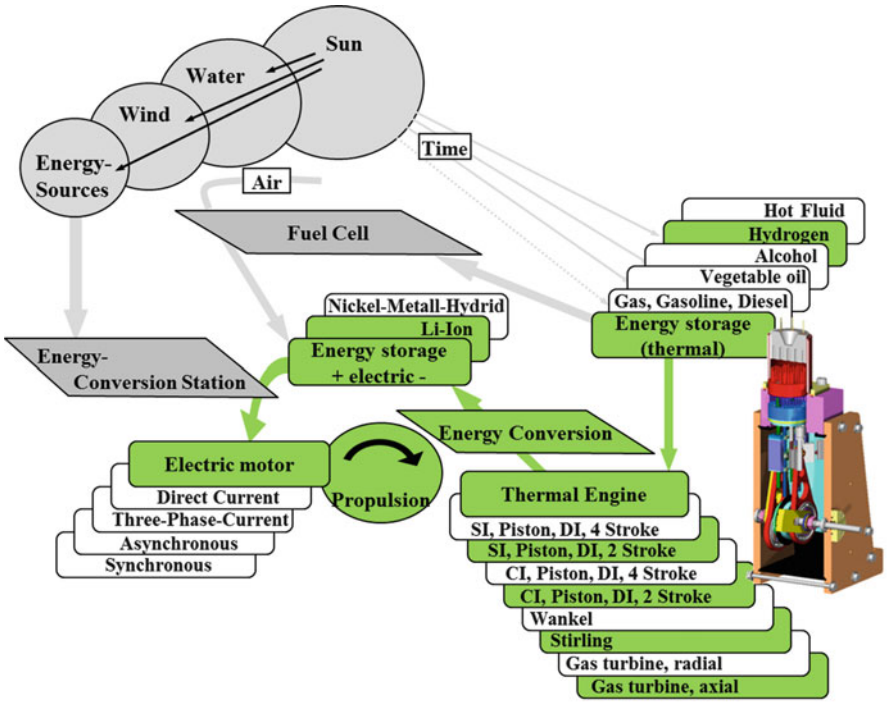

Fig. 1.28 Overview of processes, propulsion systems, and energy sources for automotive propulsion: hydrogen-range extender

- The numerous safety and comfort functions in modern automobiles require increasingly more electric power, ranging from 4 to 7 kW, which cannot be obtained from the usual generators. Independent of the propulsion form (engine or motor) the energy used for propulsion can be partially conducted to a current supplier—a fuel cell or a thermal engine with fuel cell function—operating in a fixed point. Such a configuration is illustrated in Fig. 1.30.
- Figure 1.31 shows a rational propulsion form for agglomerated urban areas and a restricted range.
- Electric energy can be produced by the sun, wind, or water and stored in small batteries for compact electric cars.

Figure 1.32 shows such an application: a photovoltaic station developed at the West Saxon University of Zwickau, Germany, with an achievable power peak of 1.5 kW, depending on the intensity of sun radiation. The electric energy generated is sufficient to run one electric car that ensures the IT service between university buildings.

Such solutions, with the advantage of real zero emissions, are suitable for administrative offices in cities. Depending on regional conditions, such a model can be extended. For example, sun radiation in Israel is very intensive, and the

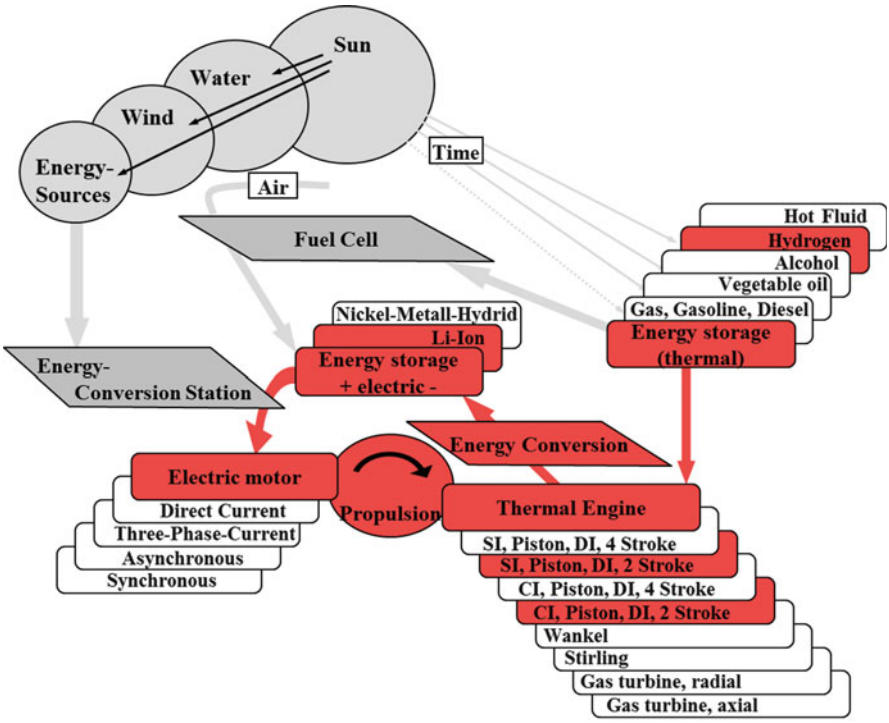

Fig. 1.29 Overview of processes, propulsion systems, and energy sources for automotive propulsion: hydrogen-hybrid

desert surfaces offer space for large photovoltaic plants. On the other hand, the driving distances are relatively short, unlike ranges in the USA or in Europe; thus, the restricted range is not a disadvantage. Given these characteristics, a project for the large-scale use of electric cars with advanced batteries charged solely with photovoltaic current was recently initiated.

Figure 1.33 provides explicit examples of the paths presented in Figs. 1.27, 1.28, 1.29, 1.30, 1.31, including the energy form, energy conversion, energy storage, and propulsion unit.

Solutions that claim zero local emissions are generally questionable when the energy chain between source and propulsion is considered. For example, engines working with compressed air or hot fluids could be envisaged based on Fig. 1.26. Although recent news reports have referred to such solutions as revolutionary, they have provided no information about the energy form and its generation, transport, and thermal isolation through to the on-board accumulator.

On the other hand, such ideas could be very interesting for niche applications, such as in road trains in Australia where solar radiation is very intense and continuous. Road trains have wide surfaces and, thus, high-pressure hot water or hot gas can be obtained easily. Such energy would not be sufficient for propulsion

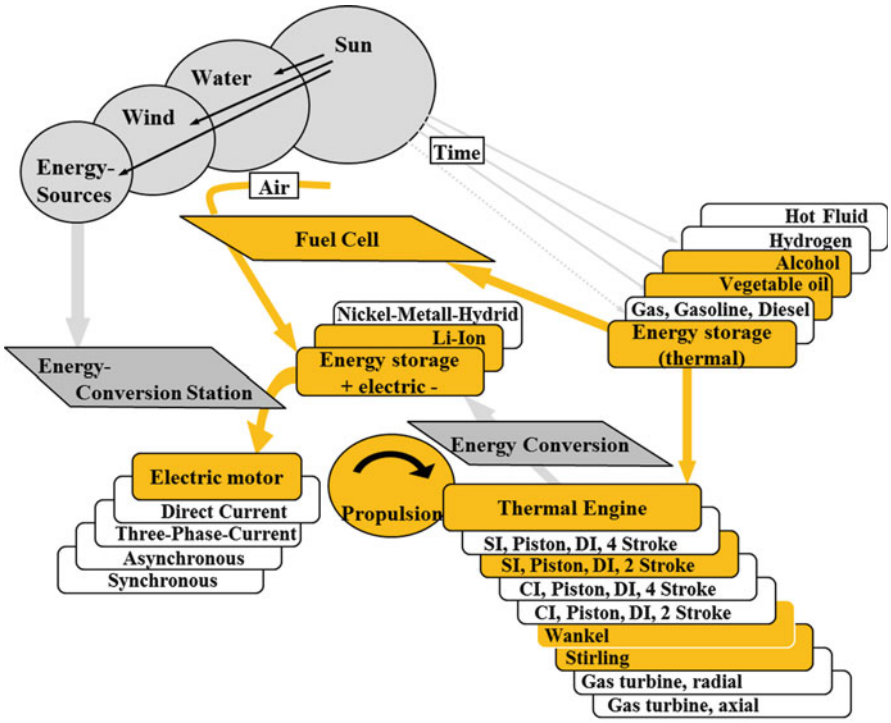

Fig. 1.30 Overview of processes, propulsion systems, and energy sources for automotive propulsion: same fuel for propulsion engine and fuel cell for current generation

but could provide efficient on-board current generation in thermodynamic cycles in circuits such as in power plants. A similar effect could be obtained using photovoltaic modules. The technical complexity, weight, dimensions, price, and amount of energy could be arguments for one or other of the solutions.

The increasing demand for diversity as well as specific regional conditions in terms of infrastructure, state of the art, available energy sources, traffic conditions, and customers' economic situations strongly indicate that future propulsion systems would contain modular adaptable configurations of energy sources, propulsion units, and on-board energy storage and conversion modules.

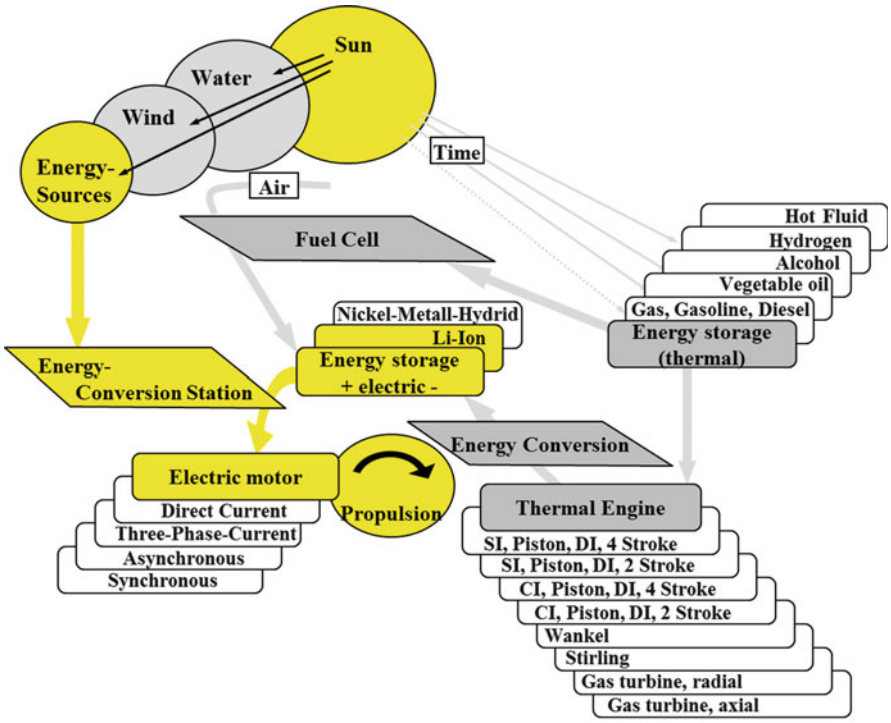

Fig. 1.31 Overview of processes, propulsion systems, and energy sources for automotive propulsion: propulsion by motor; electric power from sun, wind, or water stored in a battery

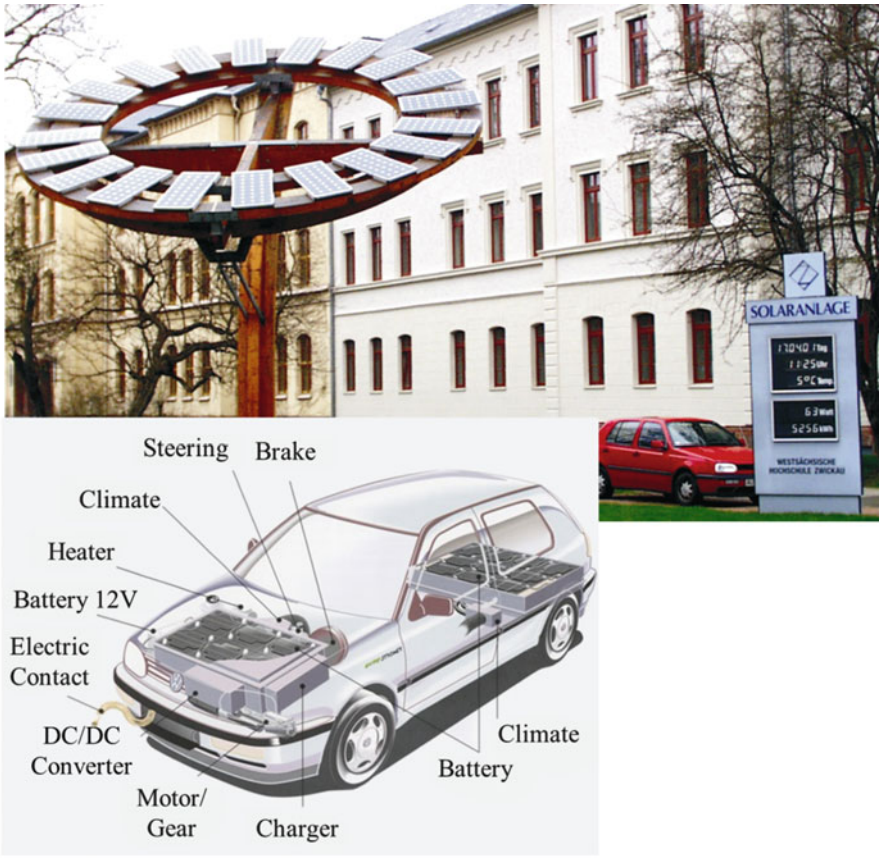

Fig. 1.32 Power station for electric cars at the West Saxon University of Zwickau, Germany

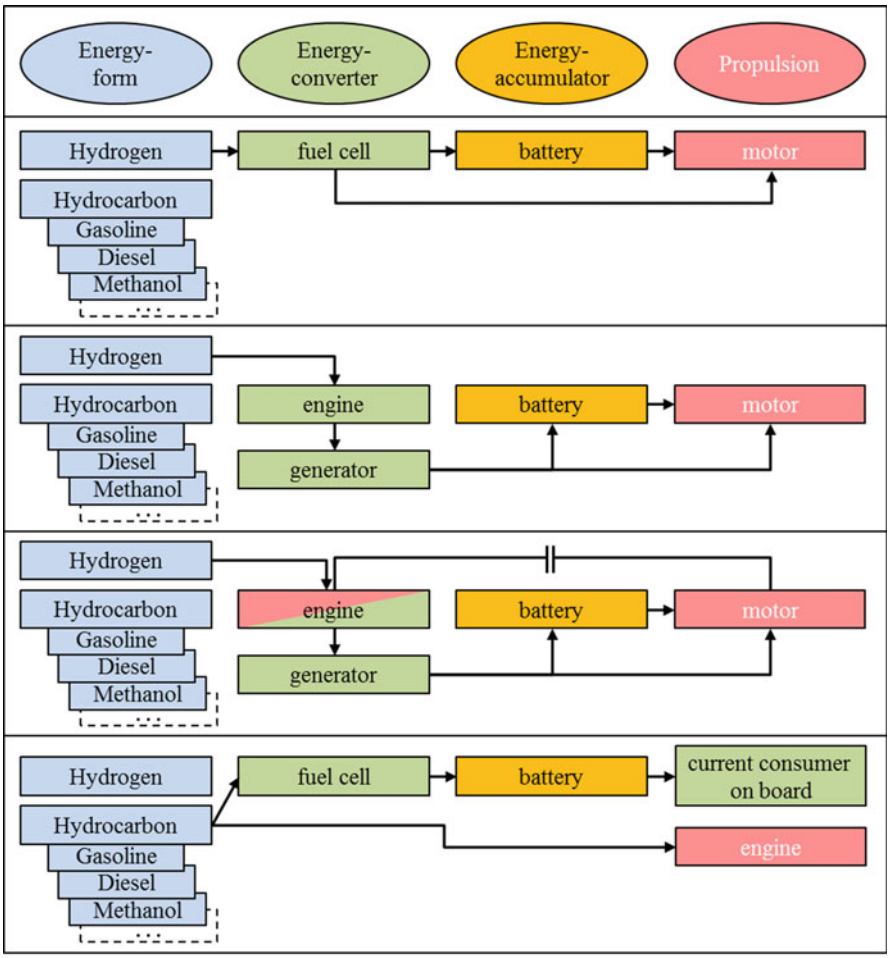

Fig. 1.33 Alternative propulsion systems, from energy form to propulsion modules

Thermal Engines

2

2.1 Thermodynamic Cycles: Potential and Limitations

The feasibility and limitations of thermodynamic cycles for the transformation of heat to work are considered in this chapter in relation to development scenarios for propulsion systems. As described in Sect. 1.3, these scenarios include thermal machines as direct propulsion systems, propulsion modules in hybrids, and on-board generators for electric energy. Thus, the efficiency of a thermal engine is considered in reference to its function as a propulsion system module, and not for a broad range of load and speed.

The transformation of heat to work in a thermal engine—if related to the quantity (obtained work) or to the quality (achieved thermal efficiency)—basically depends on the maximum and minimum temperature during heat input and heat release during the cycle [1]. For a working fluid with known specific heat values at constant pressure and constant volume, $c_p(T)$ and $c_v(T)$ (kilojoules/kilogram Kelvin), the extreme temperatures of the available heat sources (warm source and cold source) are T_{max} and T_{min} (Kelvin). Considering the utilization of a thermal engine for automobile propulsion, the cold source is given by the ambient air. The warm source within a thermodynamic cycle is generated, in most cases, by combustion of a fuel and air mixture. For comparable volumes of different types of thermal machines, the heat value of a fuel–air mixture H_u (kilojoules/kilogram mixture) is decisive, but not the heat value of the fuel itself, H_g (kilojoules/kilogram fuel). The mixture heat values for different fuels are listed in Table 3.1 in Chap. 3. It should be noted that, despite the strong differences in heat values for different fuels, the mixture heat values for all kinds of fuel–air mixtures are more or less similar (see Fig. 3.4 in Chap. 3). This fact is also determined by the strong differences between the stoichiometric air-to-fuel ratios for every fuel. The generation of a warm source by combustion of fuel with air is more efficient than any kind of heat transfer. On the other hand, the similar mixture heat values for gasoline, alcohol, oil, and hydrogen leads to the same domain of maximum temperature as a result of combustion. Therefore, the energy conversion from heat to work occurs in thermal

C. Stan, *Alternative Propulsion for Automobiles*,
DOI 10.1007/978-3-319-31930-8_2

engines between practically the same temperature limits (T_{max} and T_{min}). The quality of energy conversion is expressed by the specific work within the cycle w_k (kilojoules/kilogram), the thermal efficiency η_{th} resulting in the braked specific fuel consumption b_e (grams/kilowatt hour), and the specific emission of combustion products such as CO_2, CO, C_mH_n, H_2O, NO, NO_2, and SO_2 (grams/kilowatt hour). This quality of energy conversion between two sources with given temperatures T_{max} and T_{min} is determined by the course of the thermodynamic cycle. A comparison between different thermodynamic cycles, independent of engine features, is indispensable in this context for evaluation of the potential and limitations of the conversion of energy from heat to work.

Comparing thermodynamic cycles, there is often a trade-off between the maximum obtainable specific work and maximum achievable thermal efficiency. This trade-off becomes more complex when moving from a full load to a partial load.

The potential and limitations of energy conversion from heat to work by thermal engines are evaluated in this chapter for the following representative cycles: Carnot, Stirling, Otto, Diesel, Seiliger, Joule, and Ackeret–Keller.

For clarity, all cycles are considered ideal; that is, all transformations of state are reversible and the working fluid is an ideal gas with unchanged (at this stage of evaluation) mass and chemical structure.

Each cycle is considered as a chain of elementary transformations of state. Independent of each specific transformation (isochoric, isobaric, isothermic, isentropic), there are four basic forms of process: compression, heat input, expansion, and heat release. Ideal air is considered as the ideal working fluid. The starting point of the cycle is at ambient conditions. In this example, $p_{atm} = 0.1$ MPa and $T_{atm} = (273.15 + 10)$ K. Using the real combustion temperatures of the mentioned fuels at full load and partial load of an engine, the values for this example are fixed as follows:

For full load: $T_{max_V} = (273.\ 15 + 1900)$ K

For partial load: $T_{max_T} = (273.\ 15 + 1100)$ K

For comparison with current spark ignition (SI) and compression ignition (CI) car engines, the mass of working fluid is deduced on the basis of a swept volume of $V_H = 1.8$ dm^3. Because of the different compression ratios of the processes:

$$\varepsilon = \frac{V_{max}}{V_{min}} \tag{2.1}$$

and of the relationship:

$$V_H = V_{max} - V_{min} \tag{2.2}$$

the maximum and the minimum volumes are given by:

$$V_{max} = \frac{\varepsilon}{\varepsilon - 1} V_H \quad ; \quad V_{min} = \frac{1}{\varepsilon - 1} V_H \tag{2.3}$$

The mass of working fluid is then deduced as:

$$p_{\text{atm}} \cdot V_{max} = m \cdot R_{\text{air}} \cdot T_{\text{atm}} \quad \rightarrow \quad m = \frac{p_{\text{atm}} \cdot V_{\text{atm}}}{R_{\text{air}} \cdot T_{\text{atm}}} \tag{2.4}$$

2.1.1 Carnot Cycle

The Carnot cycle has the advantage of the highest thermal efficiency between the considered temperature limits and thus of the minimum energy consumption for a considered cycle of work (when realizable). The Carnot cycle consists of two isothermic and two isentropic processes. The ideal cycle is represented in the pressure–volume–temperature (pVT) diagram in Fig. 2.1.

Independent of the heat transfer, this cycle is a chain of two compression and two expansion sequences (CDA and ABC). Each of these is formed by one isotherm and one isotropic curve, which do not show significant differences:

- Isotherm CD: $pV^1 = \text{constant}$
- Isentropic curve DA: $pV^k = \text{constant}$
- Isotherm AB: $pV^1 = \text{constant}$
- Isentropic curve BC: $pV^{1.33\text{–}1.4} = \text{constant}$
  with $k(T)$ for ideal air being $1.33 - 1.4$.

AB	ISOTHERM	→	heat in / expansion	q_{in} / $w_{exp.}$
BC	ISENTROPIC	→	- / expansion	- / $w_{exp.}$
CD	ISOTHERM	→	heat out / compression	q_{out} / $w_{comp.}$
DA	ISENTROPIC	→	- / compression	- / $w_{comp.}$

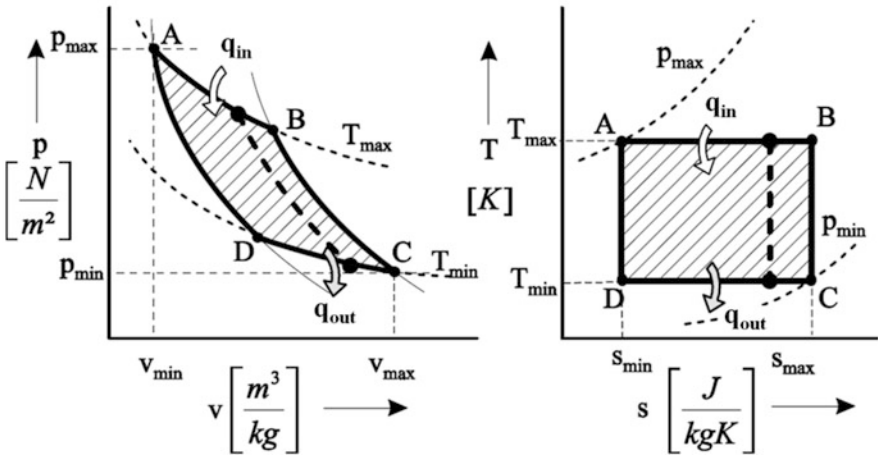

Fig. 2.1 Carnot cycle

The process was calculated for the same specific work, $w_{kV} = 783.3$ kJ/kg and $w_{kT} = 275.5$ kJ/kg, as for the Diesel process in this analysis. The resulting values for pressure, temperature, and volume in the basic points of the cycle are as follows:

	A	**B**	**C**	**D**	Full load $\eta_{th} = 0.87$
$p\ \left[10^5 \frac{N}{m^2}\right]$	5322.7	1255.8	1	4.24	
$V\ \left[10^{-3} m^3\right]$	0.00272	0.01153	1.886	0.44	
T [K]	2173.15	2173.15	283.15	283.15	

Partial load $\eta_{th} = 0.79$		**A**	**B**	**C**	**D**
	$p\ \left[10^5 \frac{N}{m^2}\right]$	607.1	251.7	1	2.41
	$V\ \left[10^{-3} m^3\right]$	0.01506	0.03634	1.886	0.78
	T [K]	1373.15	1373.15	283.15	283.15

A Carnot cycle could be realizable as a chain of compression and expansion sequences of the following forms:

- In a piston engine, as a closed system:
  - Compression CD could be realized with concomitant strong cooling and the following stage of compression DA without any heat transfer.
  - Expansion AB could be realized with strong warming. For the same course, DA–AB is realizable by connecting a heat flow around the cylinder of a piston engine. The following stage of expansion BC then occurs without any heat transfer, with a course corresponding to CD, where the cooling flow must be interrupted.
- In a fluid flow engine or thermal turbomachine, as an open system, with mass flow, using a chain of two compressors and two turbines:
  - Compression CD with strong cooling
  - Compression DA without heat transfer
  - Expansion AB in the turbine with strong heat input, using, for example, burner ramps
  - Expansion BC in the turbine without heat transfer

As shown by these examples, the Carnot cycle is technically feasible. The problem consists of the extreme (not realizable) pressure and volume differences for the given specific work, as in a diesel engine with 1.8 dm^3:

- Maximum pressure: $p = 5322.7 \times 10^5$ N/m^2
- Ratio V_{max}/V_{min}: $\varepsilon = 693.38$ full load
  $\varepsilon = 125.23$ part load

On the other hand, limiting the maximum pressure at the level of the Diesel cycle to $p = 75.77 \times 10^5$ N/m^2 the specific work becomes insignificant at $w_{kV} = 150.02$ kJ/kg and $w_{kT} = 120.27$ kJ/kg.

This means that at full load there would be only a fifth of the Diesel work. However, the pressure limitation would also lead to a decrease in maximum temperature. The thermal efficiency decreases in this case to a value under the thermal efficiency of the Diesel cycle:

$$\eta_{\mathrm{th}_V} = 0.638 \quad \text{and} \quad \eta_{\mathrm{th}_T} = 0.561 \tag{2.5}$$

2.1.2 Stirling Cycle

The Carnot cycle has maximal thermal efficiency because of complete utilization of the warm and cold sources at the given temperatures $T_{\max}$ and $T_{\min}$, as demonstrated by the lines in the T versus entropy (s) diagram:

With

$$\eta_{\mathrm{th}} = \frac{w_k}{q_{zu}} = \frac{q_{zu} - |q_{ab}|}{q_{zu}} = 1 - \frac{|q_{ab}|}{q_{zu}}$$

and

$$q = \int T ds$$

it can be deduced that a horizontal line AB corresponds to complete exploitation of the warm source at $T_{\max}$:

$$q_{zu} = q_{\max}$$

Similarly, for a horizontal line CD at $T_{\min}$:

$$q_{ab} = q_{\min}$$

Therefore

$$\eta_{\mathrm{th,\ max}} = 1 - \frac{|q_{ab}|_{\min}}{q_{zu,\ \max}}$$

It seems to be evident that maximum thermal efficiency is only given for a square process in the T–s diagram.

But what about a parallelogram? Well, every entropy variation means heat exchange. However, in a parallelogram there are two equal projection surfaces to

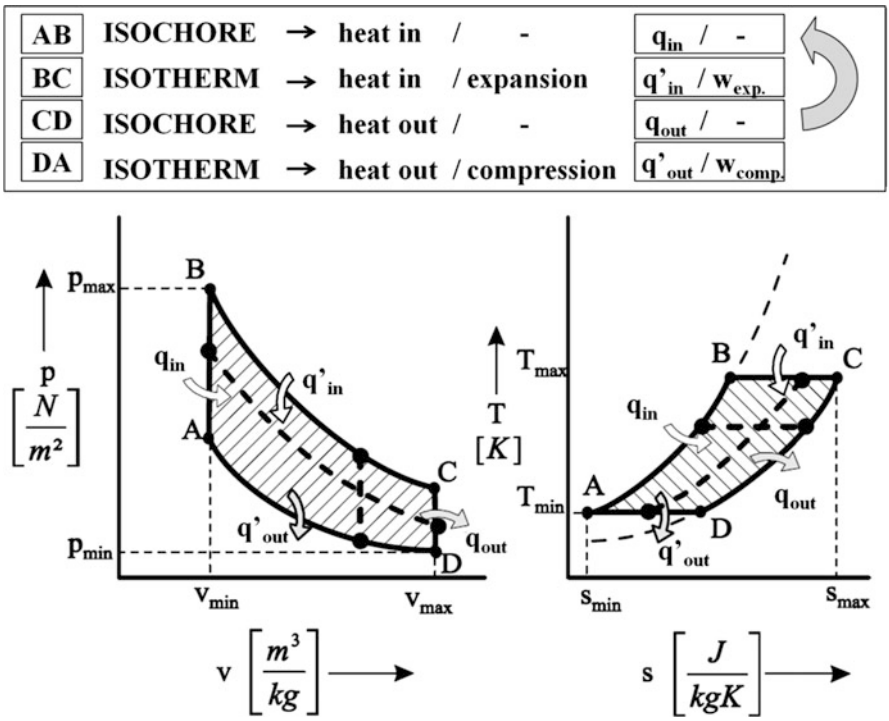

Fig. 2.2 Stirling cycle

the abscissae: one for heat release and one for heat input. If heat recuperation is possible, the result is similar to the Carnot cycle.

The Stirling cycle is formed by two isotherms and by two isochoric processes (instead of isentropic processes in the Carnot cycle), as shown in Fig. 2.2.

Stirling engines were and are developed in different forms, as presented in Sect. 2.3. Between 1960 and 1970, Stirling engines were utilized for direct propulsion in buses (General Motors, MAN, DAF) as well as in automobiles (Ford Torino, 125 kW). Comparison of the Stirling cycle with other cycles, for an engine with swept volume of 1.8 dm^3, at a compression ratio $V_{max}/V_{min} = 11$, leads to the fluid mass $m = 2.436$ g.

The maximum temperatures for full and partial loads have the same values as in the considered Carnot cycle:

$T_{max_V} = (273.\ 15 + 1900)\ \mathrm{K}$

$T_{max_T} = (273.\ 15 + 1100)\ \mathrm{K}$

The resulting values for pressure, temperature, and volume at the basic points of the cycle are as follows:

	A	B	C	D	Full load $\eta_{th} = 0.87$
$p\ \left[10^5 \frac{N}{m^2}\right]$	11	84.42	7.67	1	
$V\ \left[10^{-3} m^3\right]$	0.18	0.18	1.98	1.98	
T [K]	283.15	2173.15	2173.15	283.15	

Partial load $\eta_{th} = 0.79$		A	B	C	D
	$p\ \left[10^5 \frac{N}{m^2}\right]$	11	53.35	4.85	1
	$V\ \left[10^{-3} m^3\right]$	0.18	0.18	1.98	1.98
	T [K]	283.15	1373.15	1373.15	283.15

As mentioned, the thermal efficiency is the same as for the Carnot cycle if the heat release on the isochore CD can be recuperated as heat input on the isochore AB.

The remarkable advantage of the Stirling cycle in comparison with the Carnot cycle, at same thermal efficiency, is the increase in specific work in the cycle:

Full load $w_{kV} = 1300.9$ kJ/kg

(Carnot full load 783.3 kJ/kg)

Partial load $w_{kT} = 750.2$ kJ/kg

(Carnot partial load 275.5 kJ/kg);

Namely, for a maximum pressure and compression ratio that correspond to current gasoline engines. It must be underlined that this specific work is approximately twice the values for gasoline and diesel engines, which are presented in the following sections.

On the other hand, it should be mentioned that the heat input occurs in Stirling engines by heat transfer, whereas in gasoline and diesel engines there is direct combustion. This means that generally a lower speed is required in Stirling engines than in gasoline and diesel engines. However, this does not impair the power because the speed is compensated for by the value of the specific work.

Stirling engines with uniform heat transfer at low speed but remarkable work yield, at a swept volume and pressure and temperature values that are common for gasoline and diesel engines, could be very effective as on-board current generators for automobiles, as shown in Sect. 2.3.

2.1.3 Otto Cycle

The Otto cycle consists of isochoric heat input and heat release and isentropic compression and expansion, as shown in Fig. 2.3.

Comparison of an ideal Otto cycle with other cycles at the same swept volume of 1.8 dm^3 is based on a compression ratio of $\varepsilon = 12$, which corresponds to current development tendencies for direct fuel injection. For these conditions, a working fluid mass (ideal air) of $m = 2.416$ g was calculated. The extreme temperatures T_{max} and T_{min} have the same values as for the Carnot and Stirling cycles. The obtained values are as follows:

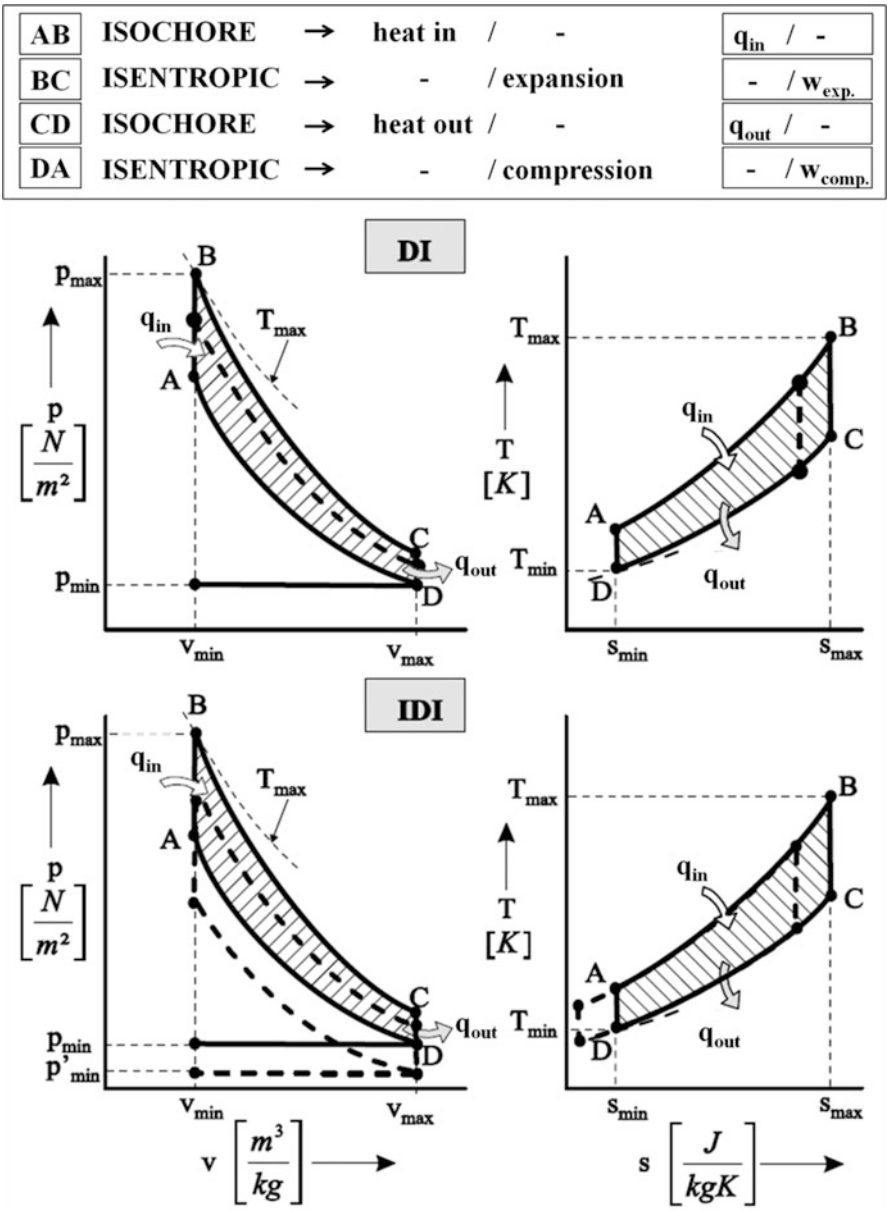

Fig. 2.3 Otto cycle

	A	B	C	D	Full load $\eta_{th} = 0.63$
$p\ \left[10^5 \frac{N}{m^2}\right]$	32.41	92.1	2.84	1	
$V\ \left[10^{-3} m^3\right]$	0.164	0.164	1.964	1.964	
T [K]	764.67	2173.15	804.7	283.15	

Partial load $\eta_{th} = 0.63$		A	B	C	D
	$p\ \left[10^5 \frac{N}{m^2}\right]$	32.41	58.19	1.8	1
	$V\ \left[10^{-3} m^3\right]$	0.164	0.164	1.964	1.964
	T [K]	764.67	1373.15	508.47	283.15

The thermal efficiency $\eta_{th} = 0.63$ is unchanged at full and partial load.

- The negative scavenging work, intensified by throttling, was not considered in this calculation. The avoidance of throttling in gasoline engines from full to partial load is the subject of new developments facilitated by internal mixture formation when applying direct fuel injection. Figure 2.3 also shows, for comparison, a cycle that includes throttling .
- On the other hand, calculation of the thermal efficiency at full and partial load was made on the basis of the mean specific heat value c_{vm} (kilojoules/kilogram) in the temperature range (T_{max} to T_{min}).

In real cases, the specific heat value increases with temperature, provoking a decrease in the isentropic exponent, as follows:

$$k = \frac{c_p(T)}{c_v(T)} = \frac{c_v(T) + R}{c_v(T)} \tag{2.6}$$

Therefore, the expansion at full and partial load should be calculated with the corresponding isentropic exponent. This gives a correction of the thermal efficiency between full and partial load. In a real cycle there are also differences in the heat input, which is not exactly isochoric, impairing the thermal efficiency from full to partial load, as discussed in Sect. 2.2. Values for the specific work remain considerably less than those in the Stirling cycle:

Full load $w_{kV} = 638.8$ kJ/kg

Partial load $w_{kT} = 275.1$ kJ/kg

However, the speed of advanced gasoline engines is much higher than the speed of Stirling engines; therefore, the effective power at comparable swept volume is higher. The difference between four-stroke and two-stroke engines here is that the specific work is generated during two rotations or one, respectively. From this aspect, two-stroke engines could have twice the power of four-stroke engines. Unfortunately, the scavenging losses in two-stroke engines are higher, which impairs the specific work, partially diminishing the advantage. Before calculating a Diesel cycle, the effect of an increase in compression ratio was calculated. The compression ratio is obtainable under the knock limit when adapting direct fuel

injection to the process. The aim of this calculation was to achieve the same thermal efficiency as in a Diesel cycle, but with a lower compression ratio. The following values have been obtained:

$$\varepsilon_{\text{Otto}} = 13.8 \;\rightarrow\; \eta_{\text{th}} = 0.65$$

$$\varepsilon_{\text{Diesel}} = 22 \;\rightarrow\; \eta_{\text{th}} = 0.65$$

The compression ratio for diesel does correspond to older engines, the actual values being limited at 15.5–16 because of the restriction on NO_x emissions. However, this further underlines the potential of the Otto cycle. The technical complexity is higher for diesel: much higher injection pressure, higher friction losses, and higher NO_x emission. A high-compression gasoline engine seems to be an alternative to the diesel engine. For the calculated variant of an Otto cycle with $\varepsilon = 13.8$, the results are as follows:

	A	**B**	**C**	**D**	Full load $\eta_{\text{th}} = 0.65$
$p\ \left[10^5 \frac{\text{N}}{\text{m}^2}\right]$	39.41	105.91	2.69	1	
$V\ \left[10^{-3}\text{m}^3\right]$	0.141	0.141	1.941	1.941	
T [K]	808.61	2173.15	760.97	283.15	

Partial load $\eta_{\text{th}} = 0.65$		**A**	**B**	**C**	**D**
	$p\ \left[10^5 \frac{\text{N}}{\text{m}^2}\right]$	39.41	66.92	2.69	1
	$V\ \left[10^{-3}\text{m}^3\right]$	0.141	0.141	1.941	1.941
	T [K]	808.61	1373.15	760.97	283.15

The specific work remains as for the initially calculated Otto cycle, $w_{kV} = 636.6$ kJ/kg and $w_{kT} = 263.4$ kJ/kg.

2.1.4 Diesel Cycle

The only difference between the Otto and Diesel cycles, independent of the compression ratio, is the form of heat input: isochoric for Otto and isobaric for Diesel. Apart from this difference, the compression and expansion in an ideal cycle are considered isentropic and the heat release as isochoric, for all kind of piston engines. The ideal Diesel cycle is represented in Fig. 2.4.

At the same starting point, under ambient conditions, with the same swept volume and also at the same compression ratio, the isochoric heat input (Otto) leads to higher thermal efficiency than isobaric heat input (Diesel). Therefore, in a real Diesel cycle the combustion process should be accelerated, as far as allowed by temperature and NO_x limits. New forms of direct injection rate modulation and new combustion concepts are promising in this sense.

AB	ISOBAR	→	heat in	/ expansion	q_{in} / $w_{exp.}$
BC	ISENTROPIC	→	-	/ expansion	- / $w_{exp.}$
CD	ISOCHORE	→	heat out	/ -	q_{out} / -
DA	ISENTROPIC	→	-	/ compression	- / $w_{comp.}$

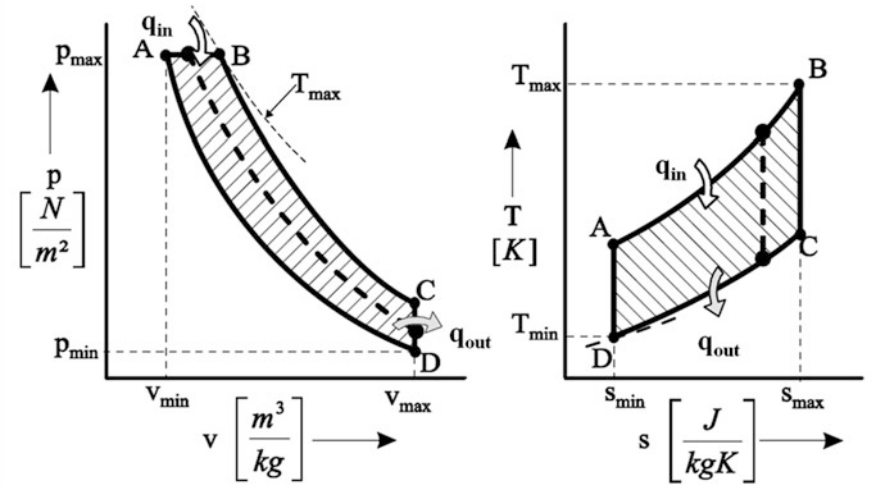

Fig. 2.4 Diesel cycle

The Diesel process was calculated, as already mentioned, using a compression ratio of $\varepsilon = 22$, resulting in the mass of working fluid (ideal air) $m = 2.33$ g. The obtained values are as follows:

	A	B	C	D	Full load $\eta_{th} = 0.65$
p $\left[10^5 \frac{N}{m^2}\right]$	75.7	75.7	3.07	1	
V $\left[10^{-3} m^3\right]$	0.086	0.191	1.886	1.886	
T [K]	974.32	2173.15	870.31	283.15	

Partial load $\eta_{th} = 0.69$		A	B	C	D
	p $\left[10^5 \frac{N}{m^2}\right]$	75.4	75.7	1.62	1
	V $\left[10^{-3} m^3\right]$	0.191	0.121	1.886	1.886
	T [K]	2173.15	1373.15	457.72	283.15

The thermal efficiency of the Diesel cycle increases from part to full load, as also explainable on the basis of the T–s diagram. The specific work values are a bit higher than for the Otto cycle, $w_{kV} = 783.3$ kJ/kg and $w_{kT} = 275.5$ kJ/kg.

It must be mentioned that, under real conditions, the maximum temperature in Diesel processes is generally higher than in Otto cycles, which influences both the thermal efficiency and the specific work. However, for a revealing comparison at different cycles, a heat source with the same maximum temperature seems to be advantageous.

2.1.5 Seiliger Cycle

As mentioned, the ideal cycle of all piston engines is characterized by three similar process sequences: isentropic compression, isentropic expansion, and isochoric heat release. The only difference is in the form of heat input: isochoric for Otto and isobaric for Diesel. In the Seiliger cycle, both forms of heat input are combined, as shown in Fig. 2.5.

At partial load, the heat transfer generally remains in the isochoric region, as shown in Fig. 2.5. Combining the isochoric and the isobaric ratio of heat input in an adequate proportion, the ideal Seiliger cycle can be used as the basis for analysis of real Otto or Diesel processes.

The isochoric/isobaric proportion can also be optimized in terms of thermal efficiency and specific work. For the present comparison, the isochoric part is 30 % and the isobaric part 70 %. The compression ratio corresponds to that of the initially calculated Otto cycle, $\varepsilon = 12$. The swept volume at the maximum temperature at full and partial load is the same as for the processes calculated previously. The mass of working fluid is the same as for the Otto process at the same compression ratio, $m = 2.416$ g. The obtained values are as follows:

	A	**B**	**C**	**D**	**E**	Full load $\eta_{th} = 0.61$
$p\ \left[10^5 \frac{\mathrm{N}}{\mathrm{m}^2}\right]$	32.41	54.79	54.79	3.5	1	
$V\ \left[10^{-3}\mathrm{m}^3\right]$	0.164	0.164	0.275	1.964	1.964	
T [K]	764.64	1292.78	2173.15	990.41	283.15	

Partial load $\eta_{th} = 0.61$		**A**	**B**	**C**	**D**	**E**
	$p\ \left[10^5 \frac{\mathrm{N}}{\mathrm{m}^2}\right]$	32.41	42.08	42.08	2.04	1
	$V\ \left[10^{-3}\mathrm{m}^3\right]$	0.164	0.164	0.226	1.964	1.964
	T [K]	764.64	992.81	1373.15	578.86	283.15

The thermal efficiency is lower than for the Otto and Diesel cycles, which is explainable as follows:

- In comparison with the Otto cycle, at the same compression ratio, there seeme to be a portion of isobaric heat input, which impairs efficiency.
- In comparison with the Diesel cycle, the compression ratio is much lower, again impairing thermal efficiency.

AB	ISOCHORE	→	heat in	/ -	q_{in1} / -
BC	ISOBAR	→	heat in	/ expansion	q_{in2} / $w_{exp.}$
CD	ISENTROPIC	→	-	/ expansion	- / $w_{exp.}$
DE	ISOCHORE	→	heat out	/ -	q_{out} / -
EA	ISENTROPIC	→	-	/ compression	- / $w_{comp.}$

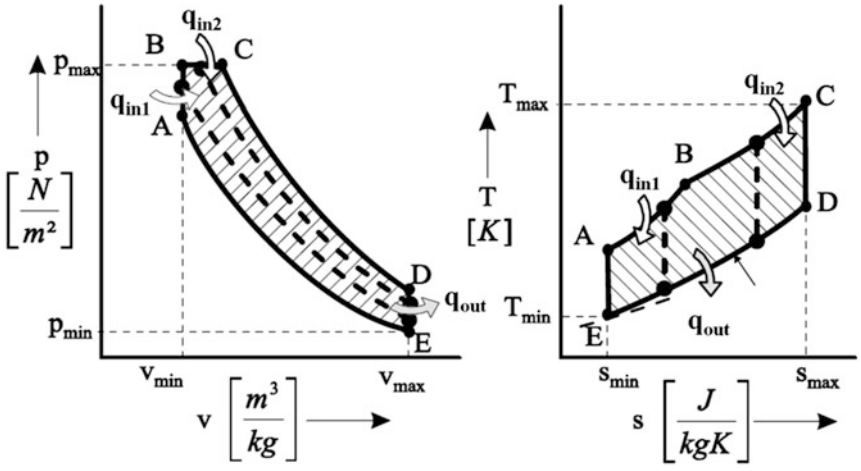

Fig. 2.5 Seiliger cycle

Values for specific work at full and partial load are between those of Otto and Diesel cycles, $w_{kV} = 756.2$ kJ/kg and $w_{kT} = 333.7$ kJ/kg.

2.1.6 Joule Cycle

The Joule cycle is implemented in turbomachines (gas turbines). Such machines were tested about 25 years ago as direct propulsion systems for automobiles. The Firebird gas turbines of General Motors were made in two variants, 147 kW and 271 kW. However, much more interesting is the use of gas turbines as on-board current generators for automobiles, providing energy for electric propulsion. Such a hybrid configuration has been successfully tested in prototypes. The Joule cycle consists of two isobaric sequences (heat input + expansion, heat release + compression) and two isentropic sequences (compression, expansion). The ideal Joule cycle is illustrated in Fig. 2.6.

The starting point of the cycle corresponds to those of the previous processes, under ambient conditions. The mass flow of the working fluid corresponds to the mass in the Diesel cycle ($m = 2.33$ g) at a diesel engine speed of $n = 3000$ min^{-1}.

AB	ISOBAR	→	heat in / expansion	q_{in} / $w_{exp.}$
BC	ISENTROPIC	→	- / expansion	- / $w_{exp.}$
CD	ISOBAR	→	heat out / compression	q_{out} / $w_{comp.}$
DA	ISENTROPIC	→	- / compression	- / $w_{comp.}$

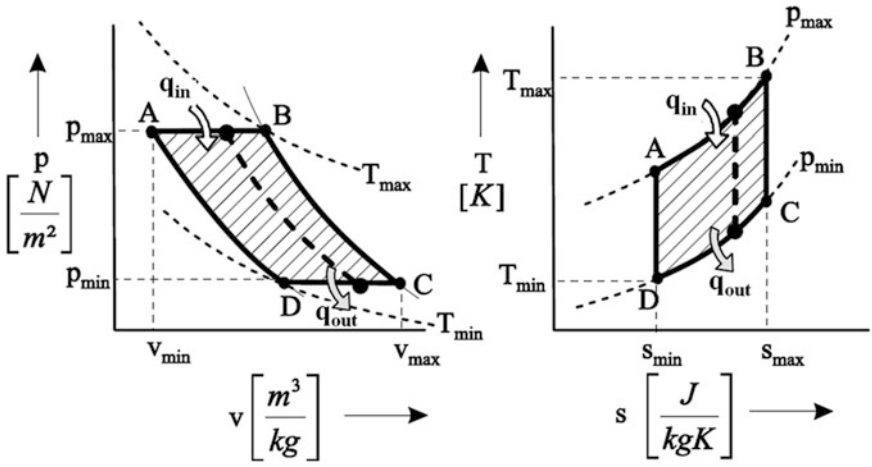

Fig. 2.6 Joule cycle

The resulting mass flow is $m = 58.25$ g/s. As in the Diesel process, the partial load is generated by reducing the isobaric heat input, as shown in Fig. 2.6.

A significant difference between the Joule cycle and the Diesel cycle, despite the similar processes of compression, heat input, and expansion, is the heat release at constant, ambient pressure. This has the essential advantage of an enlarged expansion, up to ambient pressure. In diesel and Otto engines, such a complete expansion is not possible because of the limitation imposed by the unchangeable piston course during compression and expansion. Complete expansion can be obtained when coupling a turbine after the piston engine. Such turbines are generally used for the compressor drive.

Hence, the Joule cycle has, in comparison with the Diesel cycle, the basic advantage of full expansion, resulting in an increase in specific work—when the same compression ratio is realizable. However, this does not occur in fact. The maximum pressure ratio p_A/p_D has been fixed for this calculation at a value $p_A/p_D = 7$, which is realistic for gas turbines. A corresponding compression ratio cannot be expressed because there is a mass flow, otherwise, the compression ratio in the Diesel cycle allows the calculation of a pressure ratio:

from $\varepsilon = \frac{V_A}{V_D} = 22 \rightarrow \frac{p_A}{p_D} = 75.77$

The resulting values for pressure, temperature, and specific volume at the basic points of the cycle are as follows:

	A	B	C	D	Full load $\eta_{th} = 0.427$
$p \left[10^5 \frac{N}{m^2}\right]$	7	7	1	1	
$v \left[10^{-3} \frac{m^3}{kg}\right]$	0.2025	0.891	3.564	0.8127	
T [K]	493.69	2173.15	1246.35	283.15	

Partial load $\eta_{th} = 0.427$		A	B	C	D
	$p \left[10^5 \frac{N}{m^2}\right]$	7	7	1	1
	$v \left[10^{-3} \frac{m^3}{kg}\right]$	0.2025	0.563	2.252	0.8127
	T [K]	493.69	1373.15	787.5	283.15

Values for specific work are $w_{kV} = 719.9$ kJ/kg and $w_{kT} = 275.5$ kJ/kg.

Despite the much lower compression, leading to a maximum pressure ratio of 7 (gas turbine) instead of 75.5 (diesel), the specific work in both engines has similar values at full load: 719.9 kJ/kg (gas turbine) compared with 783.3 kJ/kg (diesel), which is explainable by the better expansion in gas turbines.

On the other hand, the mass flow in a gas turbine is higher than the value obtained for a diesel engine with a swept volume of 1.8 dm^3. This is a consequence of the very high rotation speed that is realizable in gas turbines. An example is very instructive: the cited General Motors Firebird gas turbines for direct propulsion achieved a power (P) of 271 kW. The calculated ideal Joule cycle would achieve this power with a mass flow of 376 g/s.

$$\begin{aligned} P\ [\mathrm{kW}] &= m\ \left[\frac{\mathrm{kg}}{\mathrm{s}}\right] \cdot w_{KV}\ \left[\frac{\mathrm{kJ}}{\mathrm{kg}}\right] \\ 271\ \mathrm{kW} &= 0.376\ \frac{\mathrm{kg}}{\mathrm{s}} \times 19.9\ \frac{\mathrm{kJ}}{\mathrm{kg}} \end{aligned} \tag{2.7}$$

This means an induced air flow of 5.27 l/min at ambient conditions ($p = 0.1$ MPa and $T = 293.15$ K), which is realizable with compact gas turbines in their usual speed domain.

The thermal efficiency of the Joule cycle is lower than the values for the other presented cycles, as a result of the lower compression. However, at the present state of the art, higher compression is possible, promising a high potential in terms of thermal efficiency and specific work.

2.1.7 Ackeret–Keller (Ericsson) Cycle

This ideal cycle is has not been considered for the propulsion of automobiles but its potential is very interesting as a basis of comparison with the Joule cycle in gas turbines.

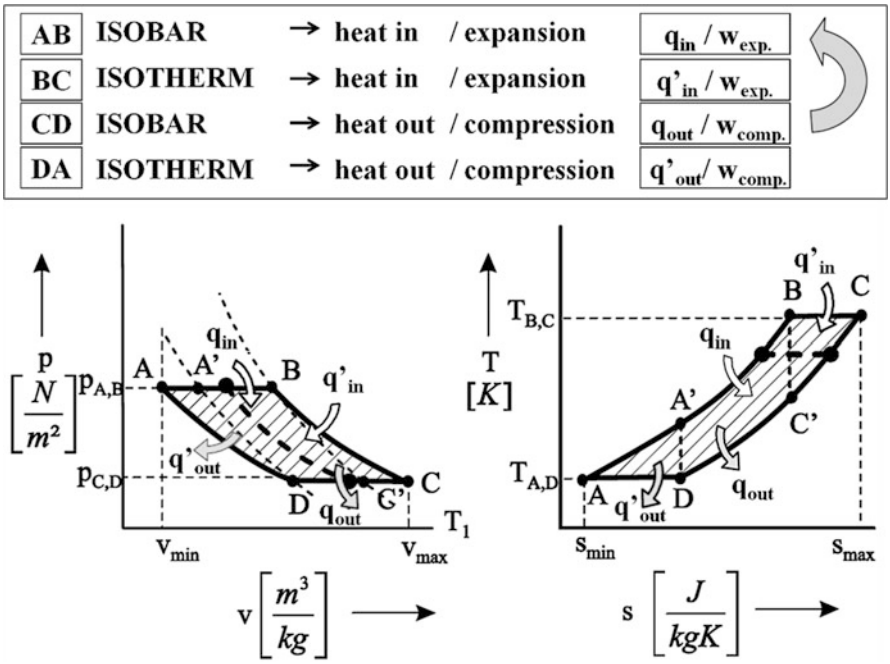

Fig. 2.7 Ackeret–Keller cycle

The main difference between the Ericsson cycle and the Joule cycle is the realization of compression and expansion at constant temperature, with strong heat exchange, instead of isentropic compression and expansion within the Joule cycle. Figure 2.7 shows the Ackeret–Keller (Ericsson) cycle in comparison with the Joule cycle (dashed curves BC′ and DA′). From the p–V diagram it can be deduced that between comparable temperatures, $T_{max} = T_B$ and $T_{min} = T_A$.

The isothermic compression and expansion lead to an increase in specific work. On the other hand, the *T*–*s* diagram demonstrates strong similarity with that of the Stirling cycle: there is only a movement of the isochores AB and CD to isobars, the difference in their courses being:

$$k = c_p/c_v \quad k = 1.33 - 1.4\,(\text{ideal air}).$$

With similar heat recuperation in the Ackeret–Keller (Ericsson) cycle as in the Stirling cycle (CD → AB), the thermal efficiency of both are identical:

$$\eta_{thCarnot} = \eta_{thStirling} = \eta_{thAckeret\text{-}Keller} \tag{2.8}$$

The resulting values for pressure, temperature, and specific volume at the basic points of the cycle are as follows:

	A	B	C	D	Full load $\eta_{th} = 0.87$
p $\left[10^5 \frac{N}{m^2}\right]$	7	7	1	1	
v $\left[10^{-3} \frac{m^3}{kg}\right]$	0.1161	0.891	6.237	0.8127	
T [K]	283.15	2173.15	2173.15	283.15	

Partial load $\eta_{th} = 0.79$		A	B	C	D
	p $\left[10^5 \frac{N}{m^2}\right]$	7	7	1	1
	v $\left[10^{-3} \frac{m^3}{kg}\right]$	0.1161	0.563	3.941	0.8127
	T [K]	283.15	1373.15	1373.15	283.15

Values for specific work are $w_{kV} = 1055.7$ kJ/kg and $w_{kT} = 608.8$ kJ/kg.

As expected, the similar heat balance results in similar specific work as in the Stirling cycle and more work than in the Joule cycle. Thus, this process has the advantages of more specific work and higher thermal efficiency with respect to the Joule cycle. Comparisons of the Stirling cycle with the cycles of all piston engines are equivalent. Nevertheless, an Ackeret–Keller (Ericsson) cycle is not applicable for direct propulsion or for on-board current generation for automobiles, because of the very extensive and intensive heat exchange. In power plants, the process is approximated by cooling and heating in stages along the isotherms.

Aircraft gas turbines work similarly, but with only one stage of intercooling and interheating. The isobaric intercooling can be realized by water injection, and the interheating by an injector ramp between two turbines. This is probably too complex for automobiles, but the principle could be interesting if the supplementary heat exchange could be realized by recuperators.

Comparison of the described ideal cycles for thermal engines within the considered temperature limits shows remarkable differences in terms of specific work and thermal efficiency, which determine the power density and energy consumption. Their realization depends on the technical complexity. However, the demonstrated potential of cycles that are different to the current Otto and Diesel cycles in piston engines can open new possibilities. Some interesting applications are presented in the following sections.

2.2 Four-Stroke Piston Engines: Potential and Trends

2.2.1 Optimization and Adaptation of Engine Processes: Future Internal Combustion Engines as Function Suppliers Around the Combustion

The required drastic reduction in fuel consumption and, consequently, in carbon dioxide and pollutant emissions will decide the future of piston engines. This aim requires the systematic analysis, improvement, and control of energy conversion

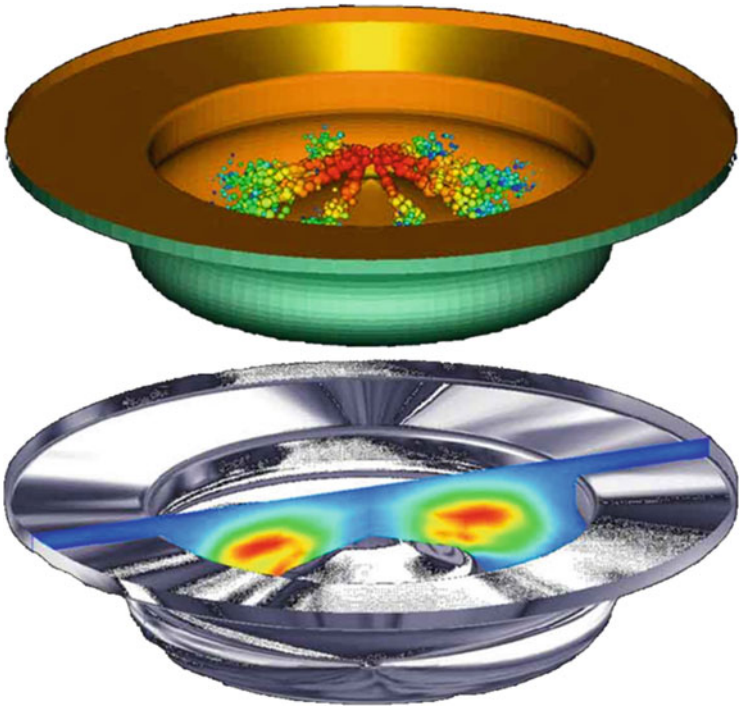

Fig. 2.8 Simulation of fuel droplet distribution and size within the combustion chamber of a piston engine with direct fuel injection

from the chemical energy of fuel to heat and, further, to work. Combustion plays a central role in this process. The distribution of fuel droplets within the air in the combustion chamber, their fast vaporization, and turbulence during mixture formation in every elementary volume of the combustion chamber are decisive for the efficiency of energy conversion, for local and momentary temperature and pressure values, and for the combustion products from CO_2, H_2O, and N_2 (complete combustion) to NO, NO_2, OH, H, and O (as a result of dissociation at high local combustion temperature). An example of fuel droplet distribution within a combustion chamber during direct fuel injection is shown in Fig. 2.8.

A major problem during the optimization of a combustion process is conservation of obtained values of configurations for every combination of load and speed, for variable ambient conditions in terms of pressure, temperature, and humidity, and for transient operating conditions.

The basic approach for solving this problem is adjustment of the air and fuel introduced into the combustion chamber in terms of the start, modulation, and duration at the given conditions. The air suppliers (charger, intake/exhaust valve control, intake and exhaust ducts) and the fuel supplier (direct injection system) directly serve the combustion process, as suggested by Fig. 2.9. A series piston engine with such function modules is shown in Fig. 2.10.

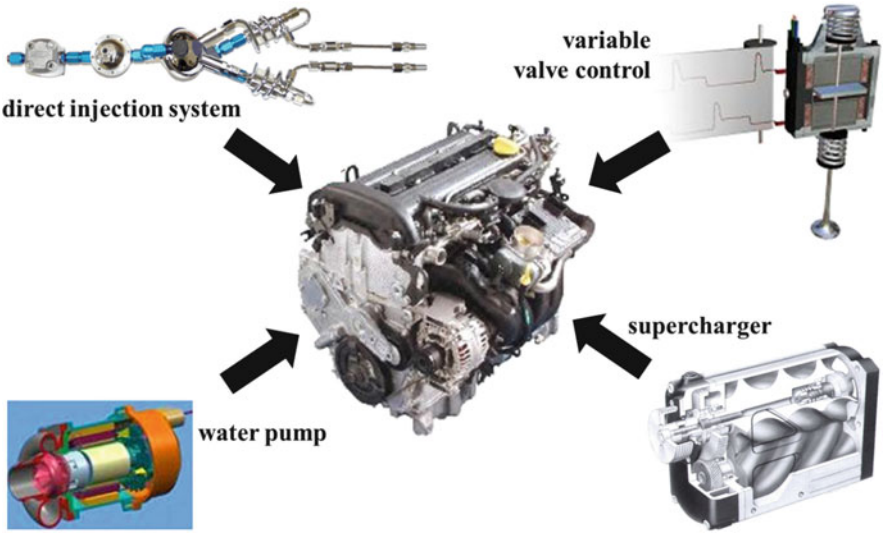

Fig. 2.9 Function modules of an internal combustion engine

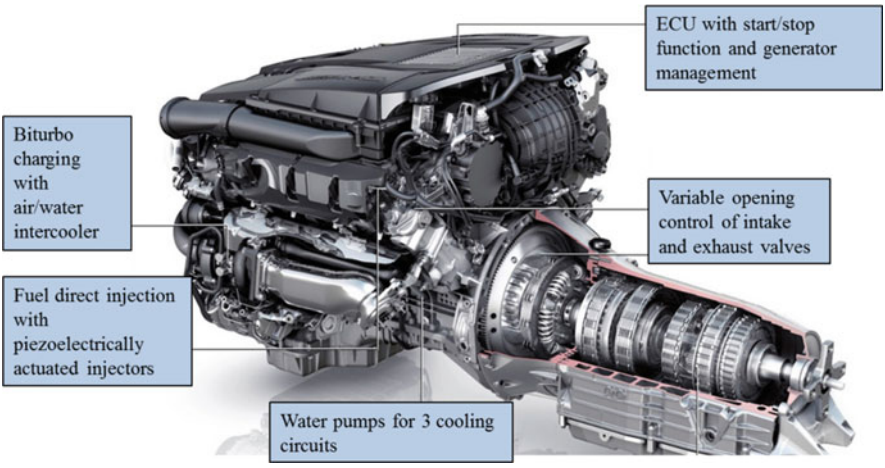

Fig. 2.10 Advanced piston engine with highly developed configuration of the functions around the working cylinders (Source: Daimler)

The control and optimization of combustion requires the actuation and regulation of the supplier's functions independent of the crankshaft rotational speed. The thermodynamic process sequences around the combustion itself, so that scavenging, mixture formation, and heat transfer become modular. The significant modules of the process in a seminal piston engine are shown in Fig. 2.11.

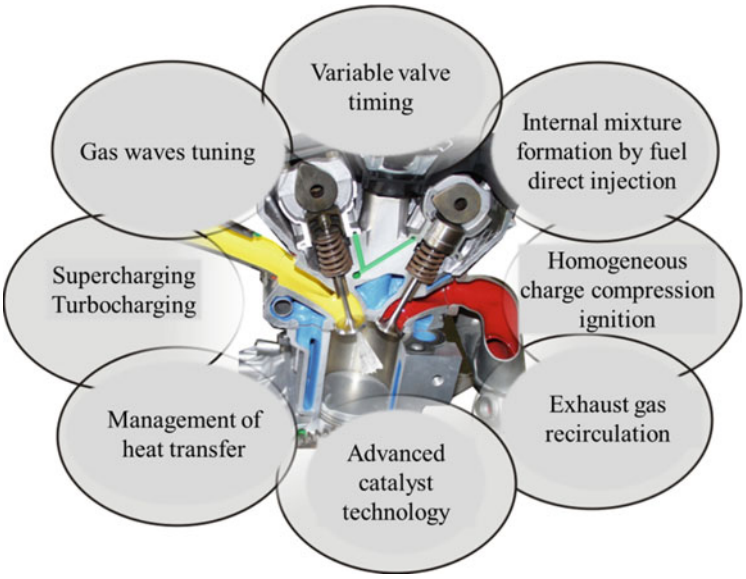

Fig. 2.11 Modular optimization of processes in internal combustion engines

There are one or more stages in supercharging/turbocharging, tuning of the pressure waves within intake and exhaust ducts, fully variable value control, internal mixture formation by direct fuel injection, controlled self-ignition, exhaust gas recirculation, management of heat transfer, and increasing the effective compression pressure of the air–fuel mixture. Further reduction in friction losses and engine weight and the further development of exhaust gas treatment are measures for process improvement.

The adaptation of all process stages to give a combustion that is as efficient as possible would enlarge the torque/speed with minimum brake-specific fuel consumption (bsfc) and pollutant emission. Constant values at minimum levels for all torque and speed combinations are not achievable in practice. Figure 2.12 shows the map with bsfc isoclines for an advanced gasoline engine. A bsfc value of 201–215 g/kW h in a power range of 20–40 kW and a speed domain of 1500–2700 min^{-1} (as usual on highways) demonstrates a very efficient process configuration and adjustment. Nevertheless, in urban traffic the power is only 5–7 kW at 1200–2000 min^{-1}. The transition to such a partial load provokes an increase in bsfc of approximately 30 %, as shown in Fig. 2.12.

The reason is process-related:

- A load-dependent decrease in injected fuel mass leads to a reduction in mixture density and, therefore, to a slower burning rate in a spark ignition engine, with lower maximum temperature. The effect is a reduction in thermal efficiency and, thus, an increase in bsfc.

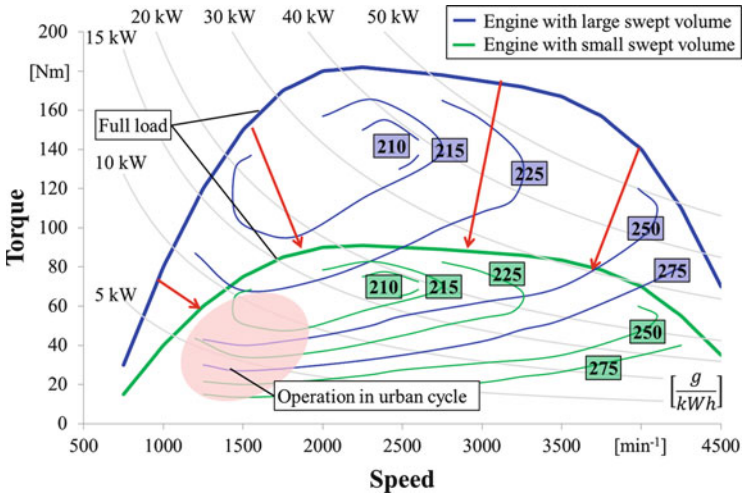

Fig. 2.12 Shifting of the operating map of an engine by down-sizing

- A reduction in speed leads to lower kinetic energy of the entering air, decreasing mixture turbulence and, therefore, the burning rate.

A promising approach is displacement of the whole operating domain of the engine to lower torque (power) or speed, as shown in Fig. 2.12 and explained by Eq. (2.9):

$$P_e = w_e \cdot V_H \cdot n \cdot \frac{T_U}{T_A} \tag{2.9}$$

P_e	[kW]	Effective power
V_H	[m^3]	Swept volume
w_e	$\left[\frac{kJ}{m^3}\right]$	Effective energy density
n	$[min^{-1}; s^{-1}]$	Engine speed
T_U	[−]	Strokes per revolution
T_A	[−]	Strokes per cycle

A lower power at high effective energy density, and thus at higher thermal efficiency, is given by reducing the swept volume ("downsizing"). One solution is to cut the heat input in a number of cylinders of a multicylinder engine by closing their intake and exhaust values, with concomitant interruption of fuel supply. A second solution is to keep the swept volume at the downsized value, but with displaceable maximum effective energy density. This is possible by intensive means (related to the specific work of the cycle) and by extensive means (related to the mixture mass within the cylinder).

2.2.1.1 Increase in the Effective Energy Density

The relationship between energy density, cycle work, and mixture mass is given by:

$$w_e = \frac{w_k}{v_H} \tag{2.10}$$

$w_k \quad \left[\frac{kJ}{kg}\right]$	Specific cycle work
$v_H \quad \left[\frac{m^3}{kg}\right]$	Specific swept volume in a piston engine
$v_H = \frac{V_H}{m_{mix}}$	

The energy density is the same as the "effective mean pressure" p_{me} (newtons/square meter):

$$\begin{aligned} p_{me} &= w_e \\ \left[\frac{kN}{m^2}\right] &= \left[\frac{kJ}{m^3}\right] \rightarrow \left[\frac{kN \cdot m}{m^3}\right] \end{aligned} \tag{2.11}$$

On the other hand, the power is given by:

$$\begin{aligned} P_e &= M_d \cdot \omega \quad \text{with } \omega = 2\pi n \\ P_e &= M_d \cdot 2\pi n \end{aligned} \tag{2.9a}$$

From Eqs. (2.9) and (2.9a) it results that:

$$w_e \cdot n \cdot \frac{T_U}{T_A} \cdot V_H = M_d \cdot 2\pi n \tag{2.11a}$$

Hence, the torque is given by:

$$M_d = w_e \cdot V_H \cdot \frac{T_U}{T_A} \cdot \frac{1}{2\pi} \tag{2.12}$$

M_d [Nm]	Torque
ω (radians)	Angular speed

Intensive ways to increase the energy density of an engine are related in general to the path of the thermodynamic cycle, as discussed in Sect. 2.1. This is not applicable for a downsized engine, which has the full load at low power. Therefore, in this case, the energy density can be increased only in extensive mode. This means an increase in heat input and, thus, more fuel and more air. With the given swept volume, this is feasible with turbo- or supercharging. For currently developed piston engines, turbo- and supercharging is generally the basis of every downsizing concept.

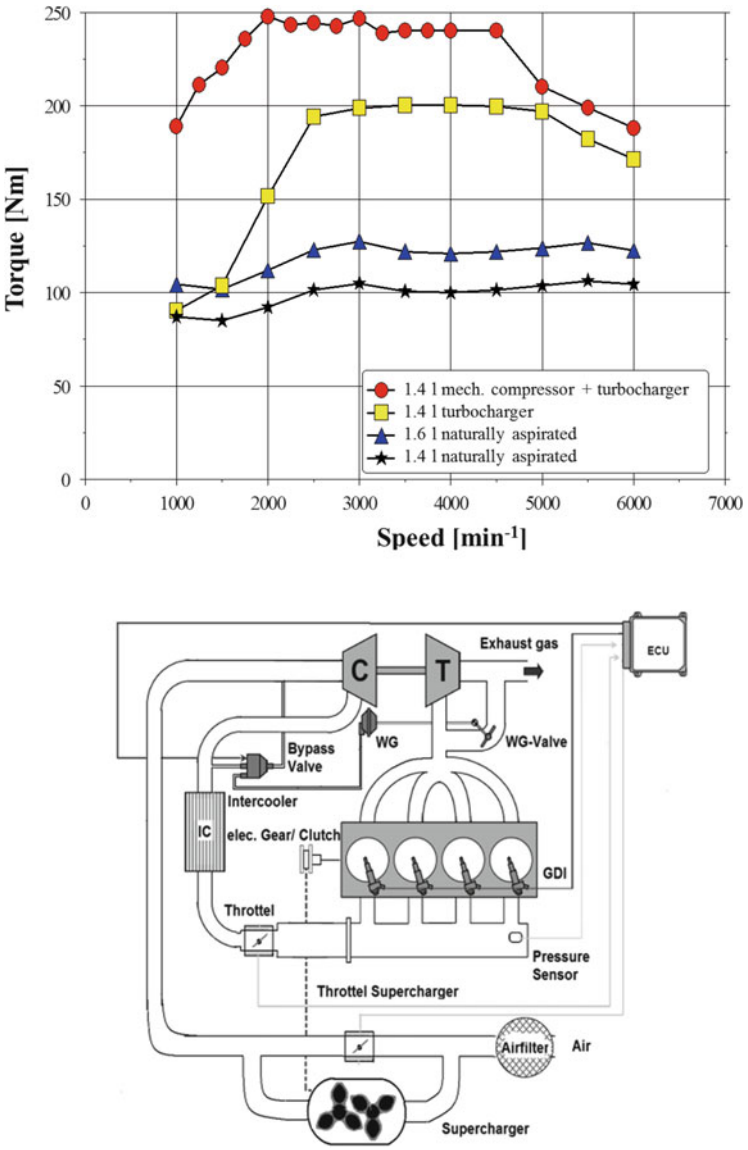

Fig. 2.13 Down-sizing compact engines with super- or turbocharging

Figure 2.13 illustrates the increase in torque for a compact gasoline engine with two charging stages, supercharging and turbocharging. In this mode, the torque becomes 2.5 times higher when operated with both charging systems than for a basically aspirated compact engine. The charging in a large torque/speed region is, however, linked to the volumetric efficiency of the engine. The high air flow as a result of charging requires a flexible range of torque and speed, meaning fully

variable control of the intake and exhaust valves in terms of opening start and duration and valve lift. However, this measure is not sufficient if extreme limitation of pollutant emission is required. In this case, the fuel must be eliminated from scavenging, being injected into the cylinder only after the scavenging (i.e., during compression).

On the other hand, direct fuel injection can allow mixture stratification within the combustion chamber and, consequently, to controlled self-ignition at partial load by well-defined burned gas zones. The main advantages of controlled self-ignition are an increase in thermal efficiency and a noticeable decrease in pollutant emission. Furthermore, direct fuel injection allows a perceptible increase in the compression ratio in SI engines under the knock limit, with similar advantages regarding thermal efficiency and pollutant emission. However, elevated energy density obtained by engine downsizing generally sharpens the problem of heat loss by cooling and exhaust gas. The management of heat transfer from the cylinder by measures within the cooling circuit is an important development target for future piston engines. Regarding exhaust heat, the general utilization of downstream turbines seems to be a necessity.

Therefore, downsizing can become the platform for causal connection of functions such as super-/turbocharging, fully variable valve control, internal mixture formation by direct fuel injection, controlled self-ignition, increased compression ratio, and management of the heat generated by combustion.

Charging, with the aim of torque increase, can be performed with or without a compressor, with exhaust gas support, or using pressure waves. A classification of the various charging methods is shown in Fig. 2.14. Mechanically driven compressors (in general screw-type) are utilized in advanced gasoline engines for increasing torque, especially at low engine speed, despite their disadvantage of

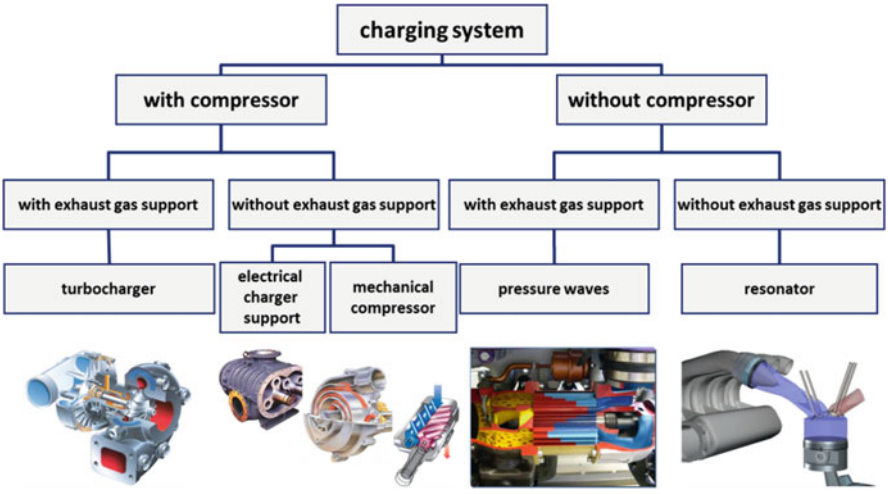

Fig. 2.14 Charging systems for piston engines

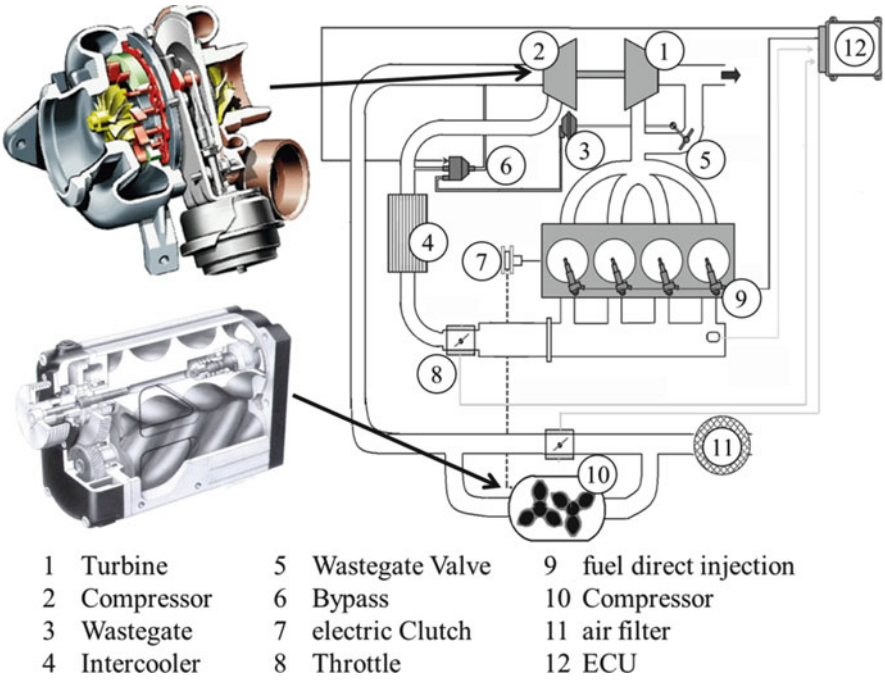

Fig. 2.15 SI engine with super- and turbocharging

consuming engine power for driving. However, the obtained torque shortens the time needed for the required power to be achieved, which partially compensates for the efficiency loss caused by compressor driving. Diesel engines have a better torque characteristic at low engine speed; therefore, a supercharger is generally not necessary in such cases.

Turbocharging shows more inertia in terms of torque response, especially for SI engines with throttling of the air mass at partial load. However, the net advantage of turbocharging is higher thermal efficiency of the whole system, because of the utilization of exhaust gas enthalpy. The avoidance of air throttling at partial load in SI engines, which is the subject of intensive development at present, together with direct fuel injection and mixture stratification will increase the utilization of turbocharging in SI engines. This aspect is described in Sect. 2.2.2. In advanced charging systems, different modules (such as supercharger and turbocharger) can be connected according to the required response characteristic and the obtainable efficiency. Such an example is illustrated in Fig. 2.15. Charging is possible using a compressor, but also without a compressor:

- A compressor can be driven by a turbine, which uses exhaust gas energy, or by a motor.
- Charging without a compressor is possible by using the exhaust gas enthalpy directly, a Roots blower, or the resonance and impulse waves of the entering fresh air column.

Figure 2.16 shows a system for impulse charging. When an intake valve opens, the intake duct is initially closed by a solenoid valve, which opens only before maximum cylinder volume: this is before bottom dead center (BDC). The generated pressure difference between intake duct and cylinder volume as the solenoid valve closes provokes, at their opening, an impulse of the air column entering the cylinder, which intensifies the filling. This process is more efficient than keeping the intake duct open for the duration of opening of the intake valve. The momentary pressure difference between intake duct and cylinder is very low, being continuously annihilated by the momentary air flow. Figure 2.17 shows the benefits of impulse charging in terms of the air charging ratio in a piston engine. The increase in air charging ratio corresponds to that achievable by a middle-sized supercharger.

The most recent charging systems for piston engines in automobiles consist of an electrically driven supercharger, in combination with one or two turbocharger

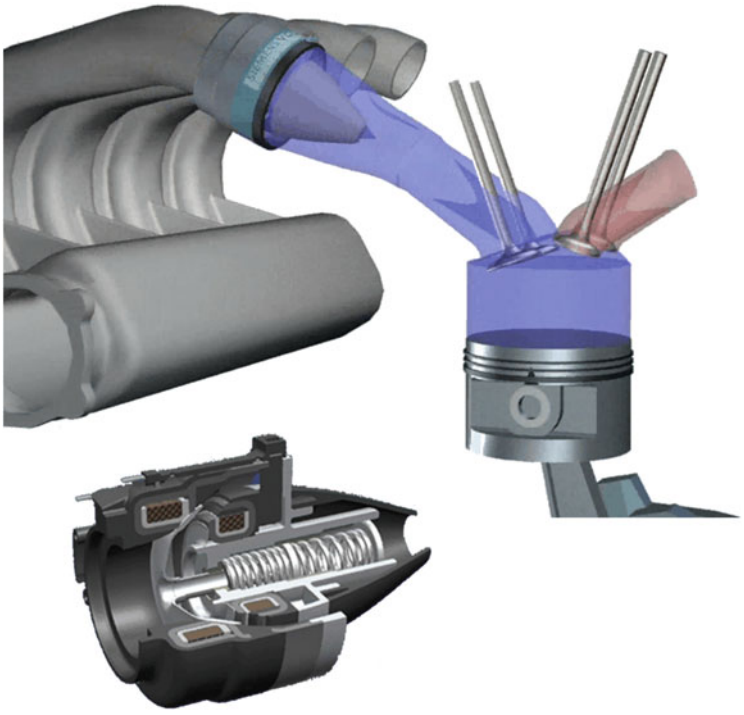

Fig. 2.16 Electromagnetically controlled impulse charging (Source: Siemens)

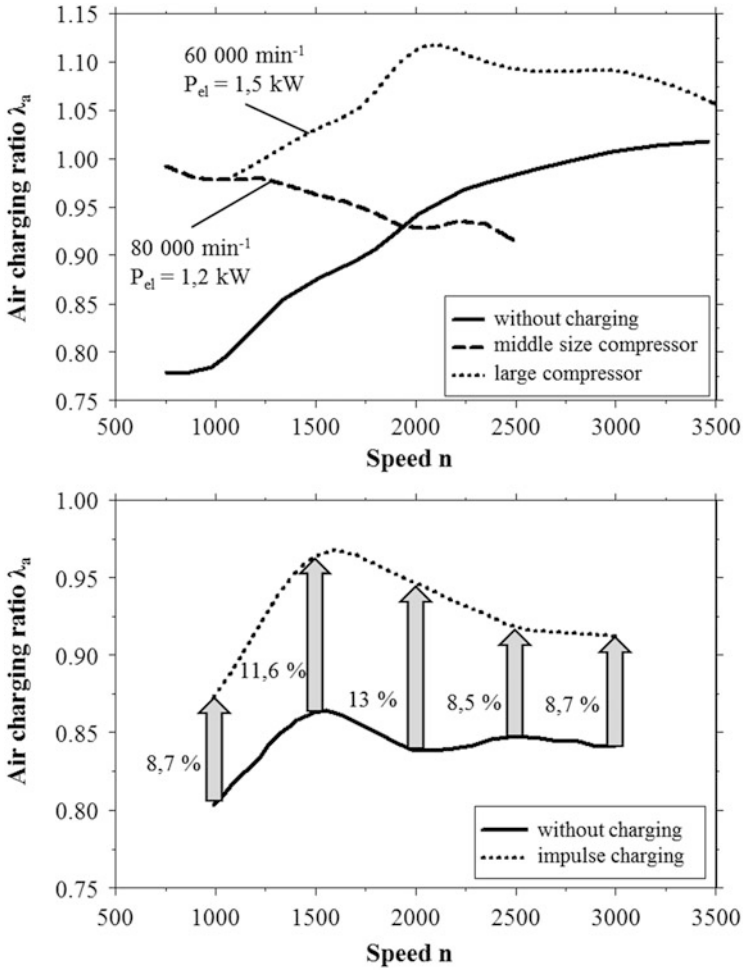

Fig. 2.17 Benefits of impulse charging

modules, which are adaptable to different load and speed situations. Adaptation of the charging system to load and speed is centered on the maximum captured fresh air mass within the cylinder at full load and on the optimum fresh air/residual gas ratio in the cylinder at partial load. For all load and speed combinations, the scavenging losses must be maintained at a very low level. On the other hand, the power required by the charging system should be minimized for all operating points. Figure 2.18 shows an example of management of a charging system with two charging stages.

Figures 2.19 and 2.20 illustrate the adaptation and management of a screw-type supercharger. The first stage of optimization is a reduction in charging pressure in relation to the transmission ratio between supercharger and piston engine.

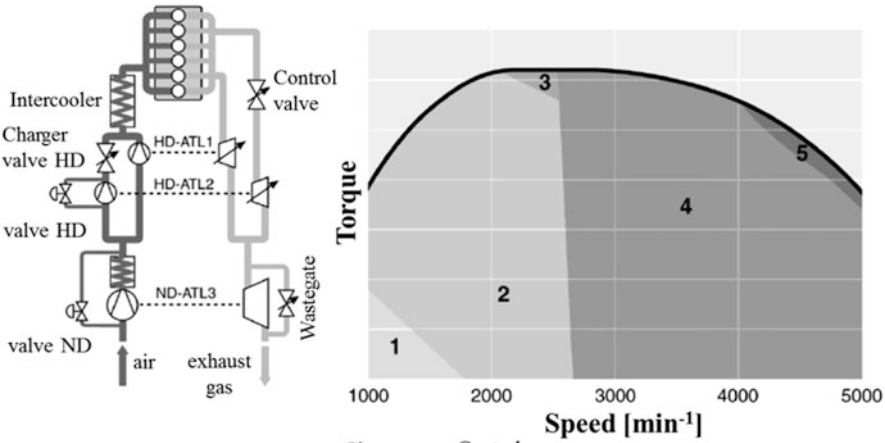

area	valve ND	valve HD	Charger valve HD	Control valve	Wastegate	HD-ATL1	HD-ATL2
1	open	open	closed	closed	closed	controlled	closed
2	closed	open	closed	closed	closed	controlled	closed
3	closed	open	closed	closed	controlled	controlled	closed
4	closed	closed	open	open	closed	controlled	controlled
5	closed	closed	open	open	controlled	controlled	controlled

Fig. 2.18 Example of the management of a two-stage turbocharging system (Source: BMW)

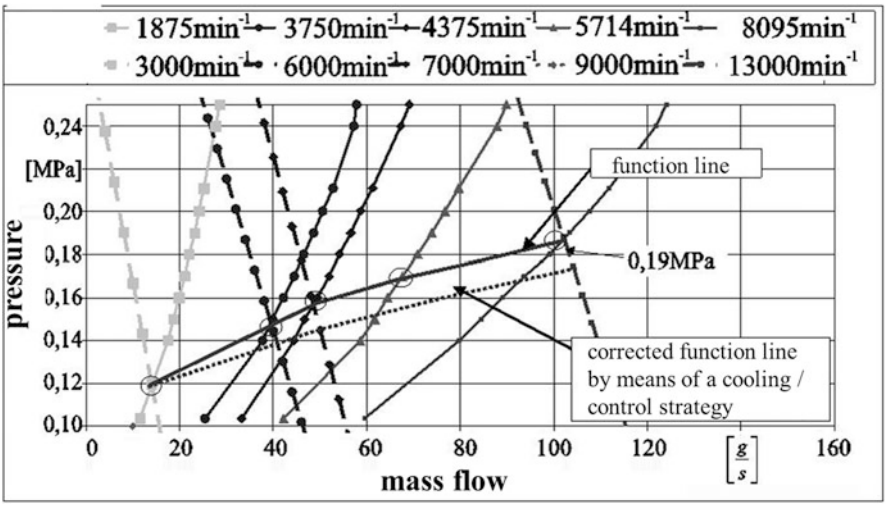

Fig. 2.19 Function line of a supercharged piston engine

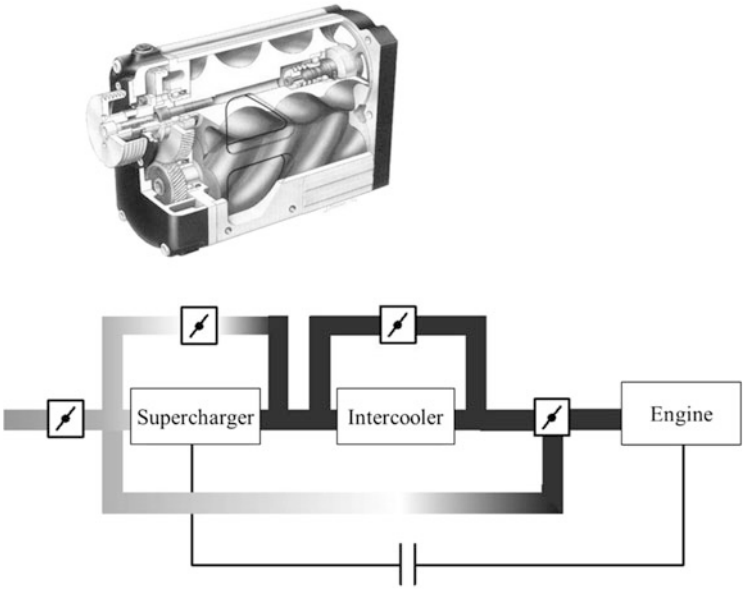

Fig. 2.20 Control strategies for supercharged engines

A pressure–mass (p, $\dot{m}$) flow map for every engine speed can be obtained by simulation or at an engine test bench. On the other hand, the p–$\dot{m}$ curves of an existing supercharger can be determined at every fixed speed by measurement. A functional point between supercharger and engine results at the crossing of the function lines of engine and supercharger at a considered speed or speed ratio, as shown in Fig. 2.19. The chain of functional points forms the operating curve of the supercharger–engine system. This curve can be displaced to higher or lower pressure by changing the transmission ratio between supercharger and engine rotation. A more complex problem in terms of fresh air mass and supercharger power is given at partial load.

Figure 2.19 shows an optimized operating curve. Figure 2.20 presents schematically the most efficient control strategies between full and partial load. Coupling of the supercharger to the engine at variable transmission ratio, with the possibility of fast connection and disconnection, would be very effective but is also very complex. Throttling of the aspirated air upstream of the supercharger and throttling after the charger (in the intake duct to the engine), combined with a backflow, are effective for the control of pressure and air mass but the efficiency is low.

A bypass in parallel to the supercharger or intercooler also has low efficiency. A pragmatic solution is optimization of a system formed by throttling and coupling using numerical simulation. However, a better solution is, as mentioned, the combination of an electrically driven and electronically controlled supercharger with one or two turbochargers. The optimization criteria are, in this case, the fresh

air pressure and the energetic efficiency of the charging system for every load and speed combination.

2.2.1.2 Engine Speed-Related Pressure Waves in Intake and Exhaust Ducts

Wave timing within intake and exhaust ducts completes the measures that contribute to generation of an adequate fresh air mass entering the cylinder, such as variable intake/exhaust valve control and super-/turbocharging, at all combinations of load and speed.

As an example, at full load, maximum air mass with minimum scavenging losses is required; at partial load, it is advantageous to keep a mass of burned gas within the combustion chamber, beside the fresh air charge, for reducing the scavenging work but, more importantly, for controlled self-ignition of the fuel–air mixture. A pressure wave, for example within the intake duct, is generated by the steep deceleration of gas flow when closing the intake valve at the end of aspiration. The gas that still streams to the now-closed intake valve is compressed by the impact with this valve. This transformation of state propagates back in the duct, against the air flow that is still directed to the valve, as shown in Fig. 2.21.

This transformation of state can be considered isentropic, which means without heat exchange from the duct to the surroundings, because of the very short time of wave propagation. The process can be described by following equations:

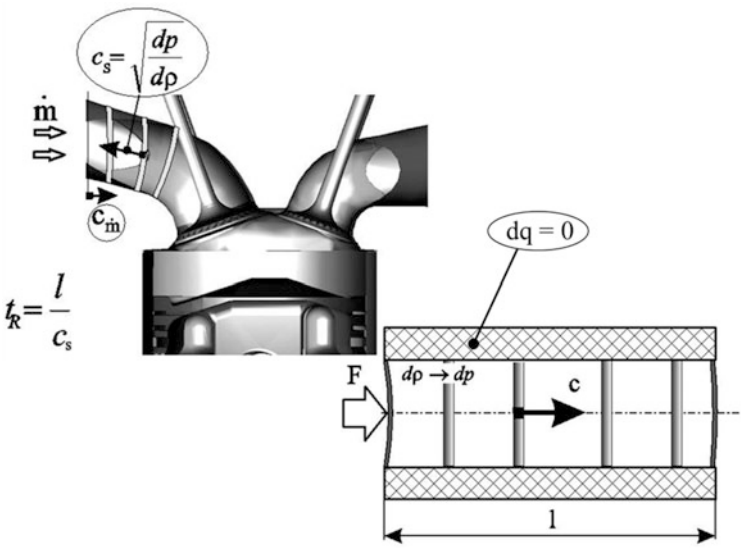

Fig. 2.21 Propagation of a pressure wave with sound velocity through the fluid in the intake and exhaust pipes of a piston engine

$$pv^k = \text{constant} = C \tag{2.13}$$

$$\text{with } v = \frac{1}{\rho} \quad \text{results} \quad \frac{p}{\rho^k} = C \rightarrow p = C \cdot \rho^k \tag{2.13a}$$

$$\text{and } \ln p = \ln\left(C \cdot \rho^k\right) \tag{2.13b}$$

$$\ln p = \ln C + k \ln \rho \tag{2.13c}$$

$$\frac{dp}{p} = k\frac{d\rho}{\rho} \tag{2.13d}$$

The local pressure transformation within the duct (dp) as a result of density change ($d\rho$), caused by the advancing air flow gives:

$$\frac{dp}{d\rho} = k\frac{p}{\rho} \tag{2.13e}$$

with $\frac{p}{\rho} = pv$ and $pv = RT$, the result is:

$$\frac{dp}{d\rho} = kRT \tag{2.13f}$$

The term $\sqrt{\frac{dp}{d\rho}}$ has the dimension of a velocity (meters/second) and describes the propagation of a pressure wave, often called the "sound velocity" (c_s):

$$c_S = \sqrt{kRT} \tag{2.14}$$

with $k = \frac{c_p(T)}{c_V(T)}$

The time of wave arrival at the duct entrance, t_R, is given by:

$$t_R = \frac{l}{c_S}$$

l	[m]	Length of intake duct
c_S	$\left[\frac{\text{m}}{\text{s}}\right]$	Sound velocity
k	$[-]$	Isentropic exponent
c_p; c_V	$\left[\frac{\text{kJ}}{\text{kgK}}\right]$	Specific heat at constant pressure/volume
ρ	$\left[\frac{\text{kg}}{\text{m}^3}\right]$	Air density

The difference between air wave and surrounding pressure at the duct entrance generates a depression wave, which propagates through the duct in the direction of the closed intake valve. This depression in the duct, which is in contact with the

atmospheric pressure at the duct entrance, provokes a new air flow to the still-closed intake valve. From this point, the impact of the air flow and, therefore, generation of a pressure wave is repeated.

It seems to be advantageous for the intake valve to open for a new scavenging sequence just at the moment when a positive wave in the duct is arriving at the valve, provoking dynamic cylinder charging. This periodic process depends (as shown in Fig. 2.21) on the duct length and sound velocity. A typical pressure wave course is shown in Fig. 2.22, with and without throttling, for two different engine speeds. It can be seen that, as expected, the engine speed has no direct influence on the wave period.

On the other hand, the opening duration of the intake valve depends on the cam profile angle, if the engine has no variable valve control. Therefore, the opening duration is a function of engine speed, as follows:

$$\alpha = 2\pi nt \tag{2.15}$$

For example, in an engine speed domain $n = 800–8000\ \text{min}^{-1}$ this difference is noticeable. Adjustment of the pressure wave to the variable opening duration of the valves is possible by varying duct length. For example, at low speed a longer wave period is required. This is usually accomplished by duct length variation, in most cases in only two steps. Another method for changing the wave period is variation of the sound velocity. A solution is to inject a cold liquid medium (which, in some circumstances, could be water) that requires enthalpy from the air for vaporization, provoking a decrease in air temperature and, consequently, in sound velocity, as deduced from Eq. (2.14). The effect is similar to a prolongation of the intake duct. The tuning of gas waves is generally known from exhaust pipes in two-stroke engines. There are interesting solutions such as reflection plates, connectable additional pipes, or water injection for changing the exhaust gas temperature and, thus, the sound velocity.

The adaptation of such a solution for four-stroke engines can contribute to control of the exhaust gas flow, in combination with variable valve control.

2.2.1.3 Variable Valve Control

The aims of variable control of the valves are:

- Maximum fresh charge for the cylinder at full load over the whole speed range of the engine
- Optimum ratio between fresh charge and burned gas within the cylinder, as required by fuel vaporization and self-ignition at partial load
- Minimum fresh charge losses at all load and speed combinations

In four-stroke piston engines, such scavenging management is feasible by the control of opening start, opening duration, and valve lift of intake and exhaust valves.

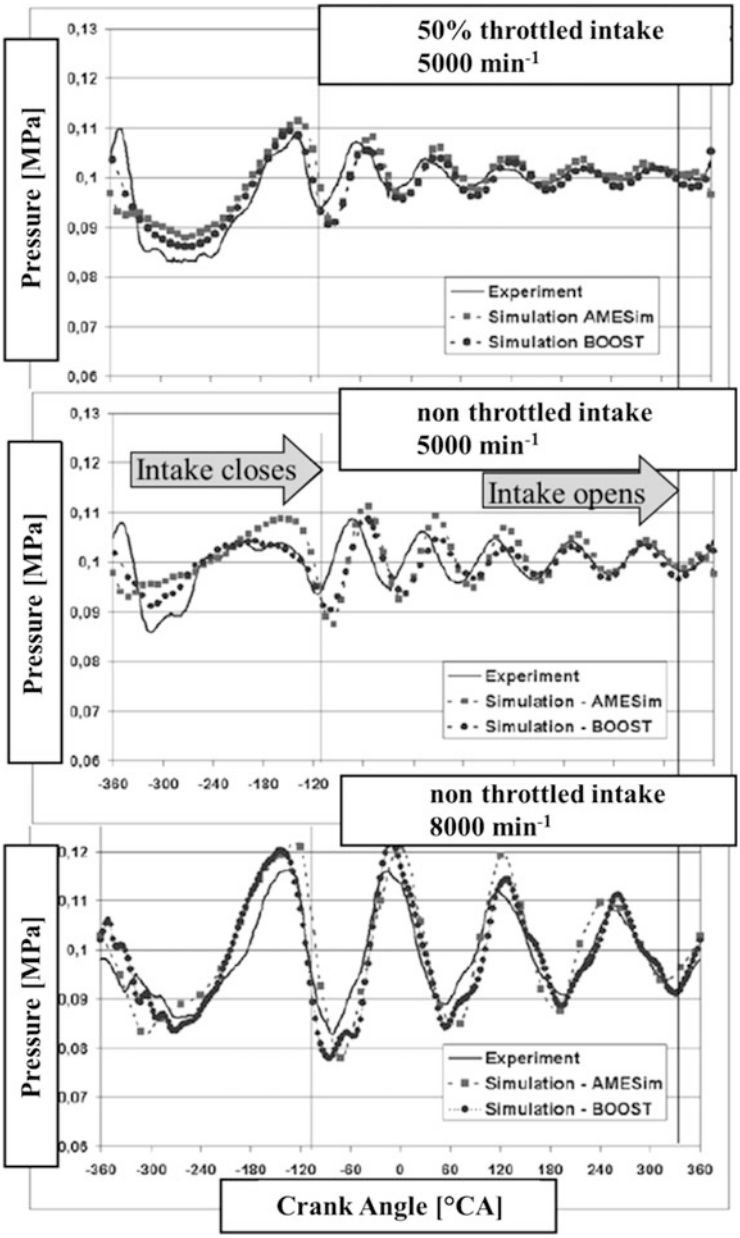

Fig. 2.22 Pressure waves through the air flow within the intake pipe of a piston engine for different load–speed combinations

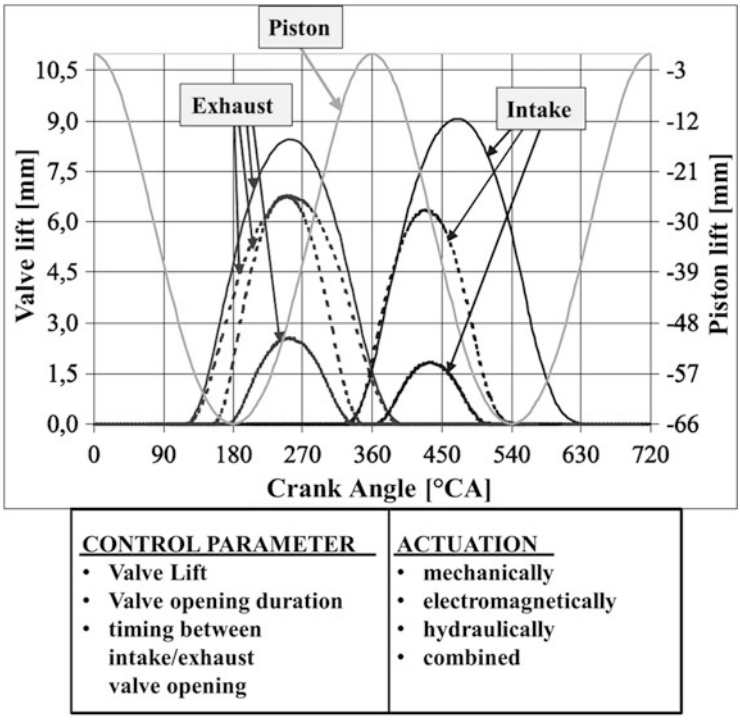

Fig. 2.23 Forms of variable valve control

Figure 2.23 presents the desirable valve lift as a function of crank angle for intake and exhaust valves, as well as the possible control parameters and actuation forms. Currently, there are several technical solutions that allow at least partial control of such functions; some are listed below.

Variocam (Porsche) is a system with mechanical variation of opening start, opening duration, and valve lift, in two distinct stages. This occurs when switching between two cam profiles by shifting a transverse pin. Inserting the pin, two parallel lateral cams with larger profile pushing a bowl are connected to the valve shaft. Retiring the pin, the bowl is disconnected from the force circuit and the valve shaft only has contact with a smaller central cam. This solution is shown in Figs. 2.24 and 2.25.

VVTLi (Toyota) is a system that also involves mechanical variation of opening duration of valves. Figure 2.26 shows the principle of its function.

VW (Volkswagen) presented a solution for cylinder deactivation, which is generally applicable for switching between different cam profiles, similar to ratiocam. The switching occurs by a movement along the cam axle, as shown in Fig. 2.27.

Valvetronic (BMW) combines both mechanical and electromagnetic activation. The concept is shown in Fig. 2.28. Between the intake valve and the cam is a rocket

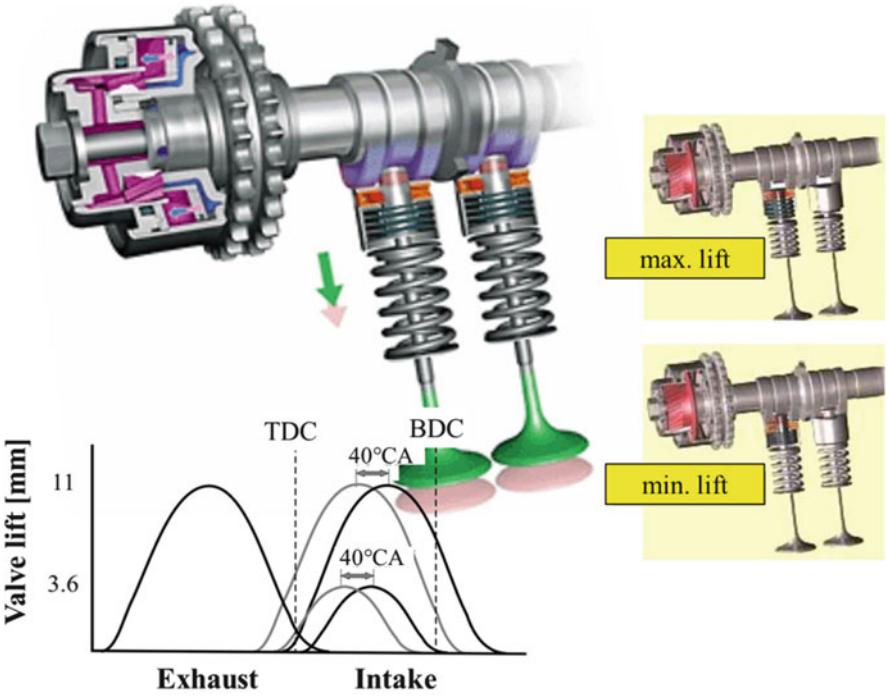

Fig. 2.24 Variocam-Plus (Porsche): mechanical control of valve lift and opening angle (Source: Porsche)

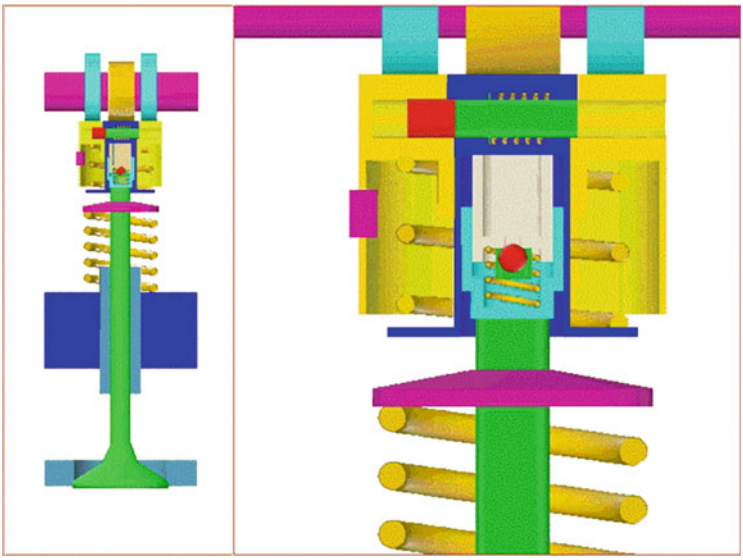

Fig. 2.25 Variocam-Plus (Porsche): changing of the cam contact with the valves (Source: Porsche)

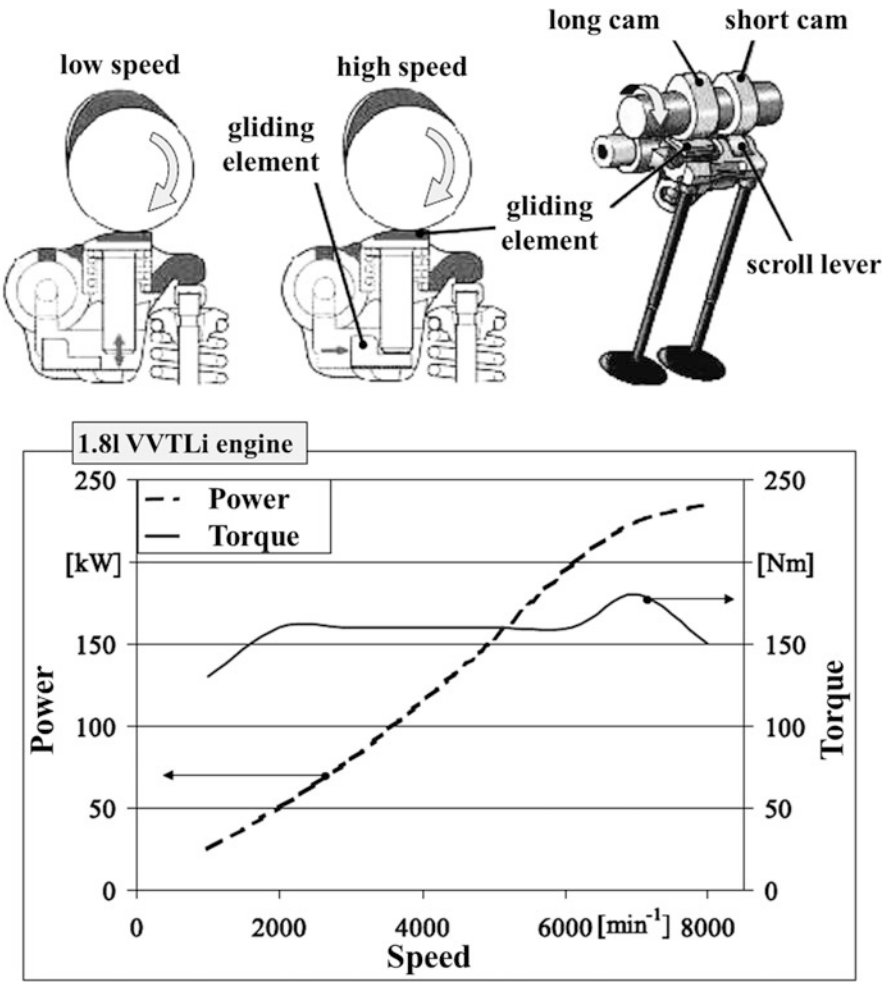

Fig. 2.26 Mechanical control of lift and angle and their influence on engine performance (Source: Toyota)

for force transmission. The rocket rotation, which is actuated by a motor, causes a displacement of the contact point between cam and rocket, as well as between rocket and valve shaft. Therefore, the lever arm length is variable, which allows modification of valve lift and opening duration. The continuously variable contact point between cam and rocket by motor actuation permits variation of valve lift and opening duration, leading to fuel economy of about 15 %, with a remarkable increase in torque. The reduction in bsfc at partial load can be explained as follows: in conventional SI engines, the load decrease is realized by diminishing both the air mass and fuel mass, for a constant air/fuel ratio, as a premise of the flame propagation using spark ignition.

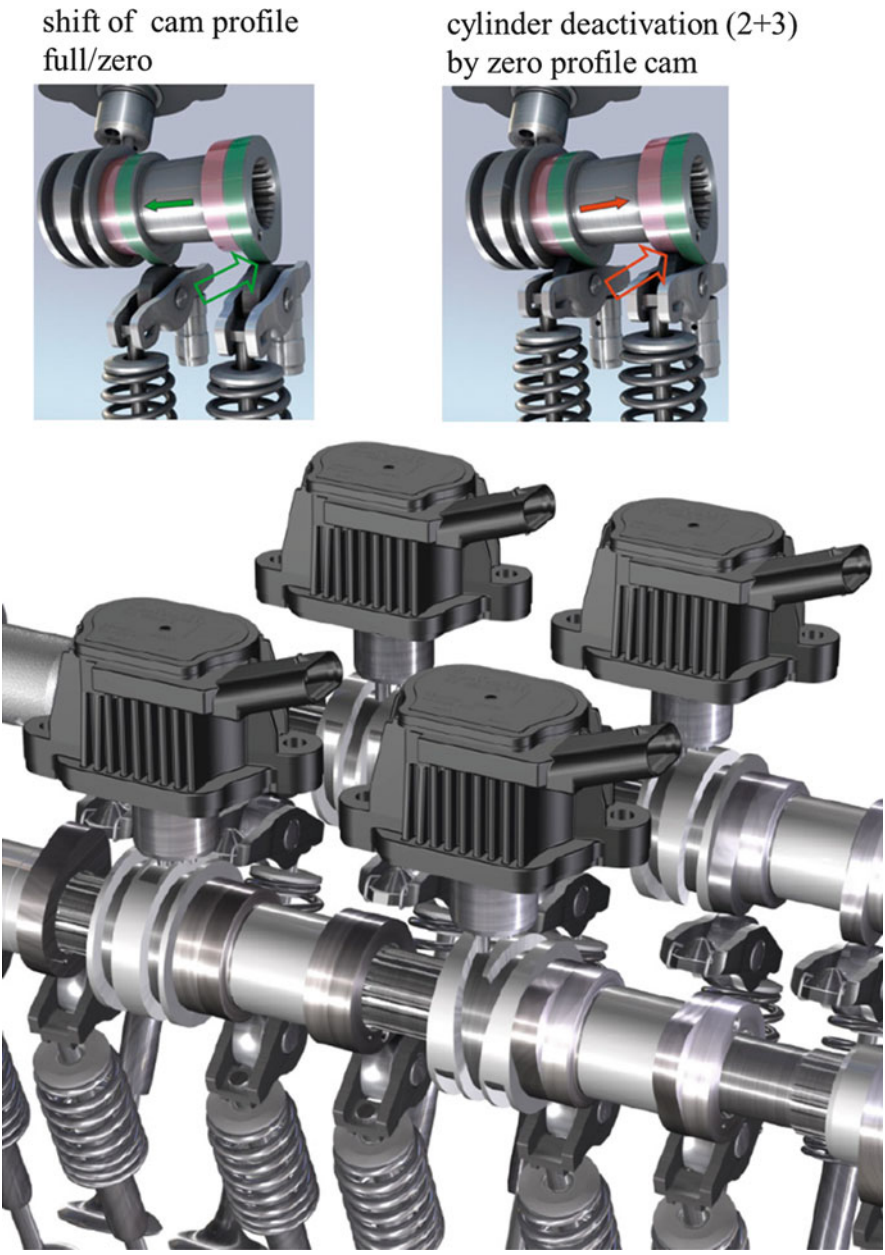

Fig. 2.27 System for shifting of cam profiles (Source: Volkswagen)

Applying Valvetronic, the air throttling occurs by reducing the valve lift; therefore, a throttle in the intake duct is no longer required. In both cases, with valve lift reduction and with throttling, the air mass variation is basically the same.

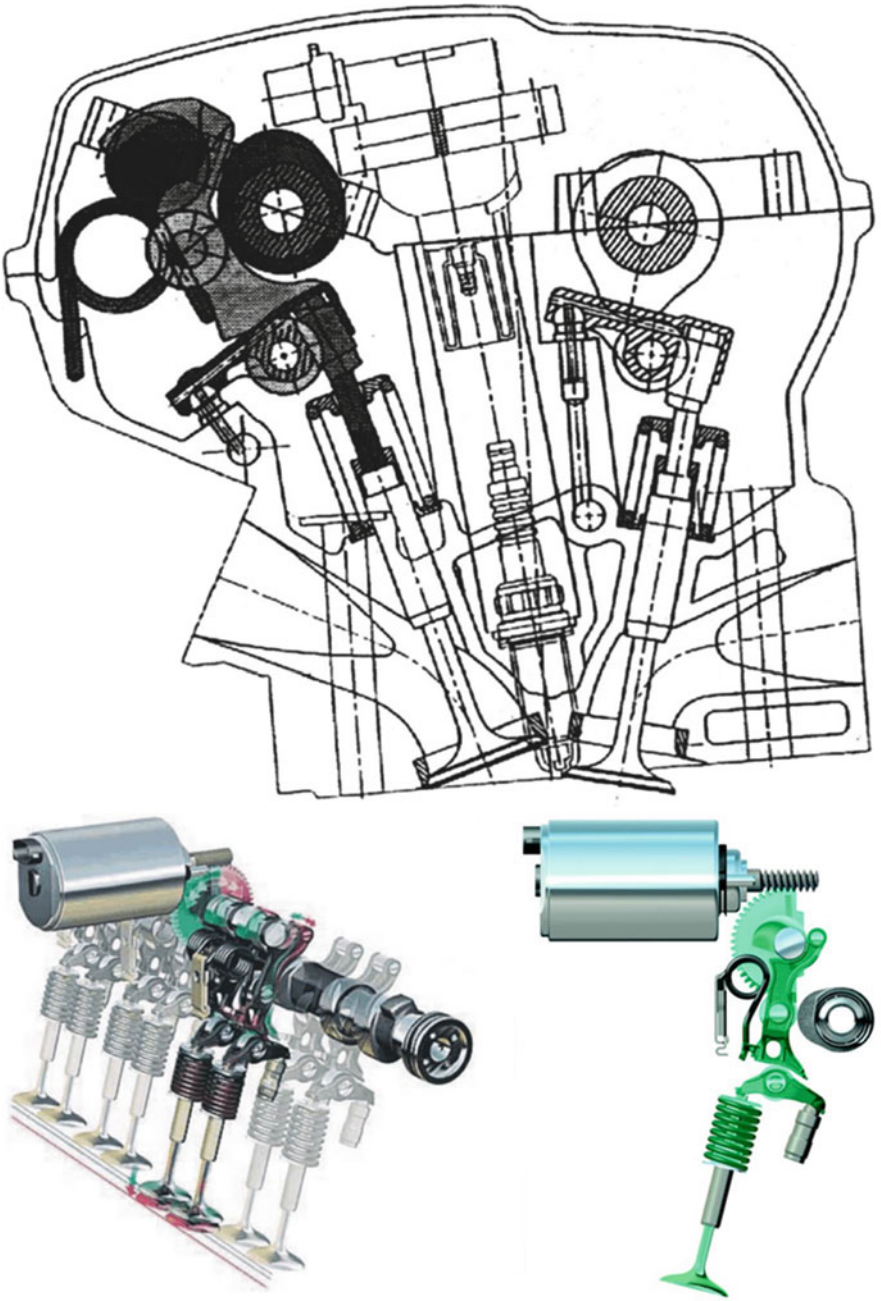

Fig. 2.28 BMW Valvetronic: mechanical control of valve lift and angle by means of electrical control (Source: BMW)

However, the air mass reduction by valve lift is given by a smaller flow cross-section, at more or less unchanged air velocity and density, whereas throttling within the intake duct causes a decrease in density of the air flow.

Flow striation by valves with reduced lift, instead of air rarefaction by throttling at unchanged valve lift, leads to mixture stratification: the homogeneous fuel–air mixture with stoichiometric ratio remains in this case at high density, which is favorable for fast combustion, resulting in high thermal efficiency.

MV2t (Mahle), as presented in Fig. 2.29, is similar to the previous solution. The cam movement is transmitted in this case to the rocket by means of three intermediate parts. Their position is controlled by a motor, which changes the lever ratios between cam and rocket. In this mode, both the valve lift and opening duration can

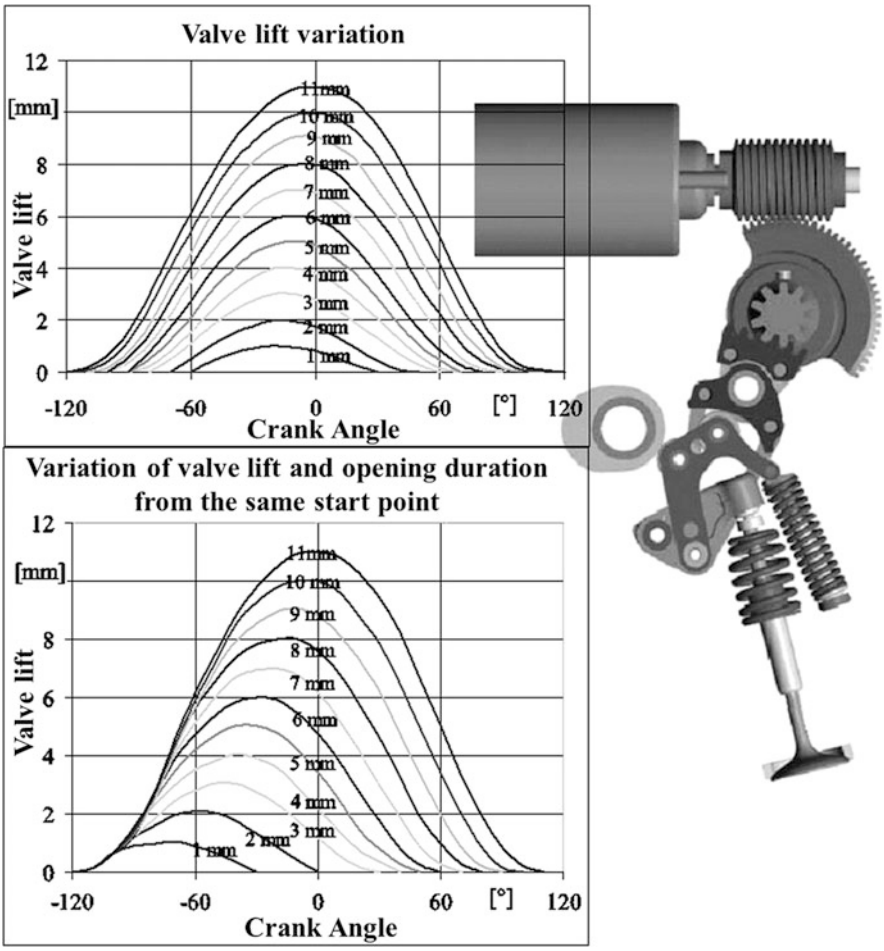

Fig. 2.29 MV^2T (Mahle): mechanical control of valve lift and angle with electric control (Source: Mahle)

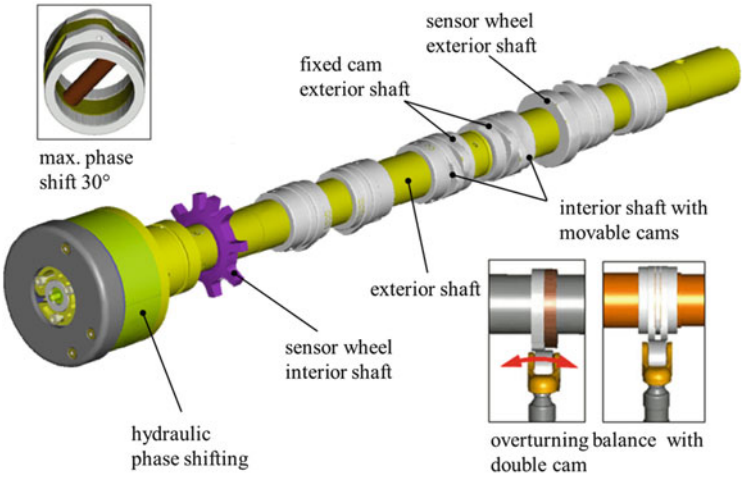

Fig. 2.30 Concentric Cam Type II (ThyssenKrupp Presta): mechanical control of valve angle (Source: ThyssenKrupp Presta)

be practically continuously varied, as shown by the upper diagram in Fig. 2.29. The start of opening can be adjusted, as shown in the lower diagram in Fig. 2.29, using a phase variator.

Concentric Cam (Thyssen Krupp Presta) is characterized by two camshafts that are concentrically interleaved and moveable into each other by means of a phase variator. Each of the shafts is provided with cams with their own different profiles. A concentric cam system is shown in Fig. 2.30.

Each intake valve is actuated by two cams, one from each shaft. To avoid turning moments, a new solution provides two lateral cams from one shaft and one central cam from the other shaft for each valve, similar to the Variocam system. Relative rotation between both shafts leads to variation of the resulting cam profile at the contact with the valve shaft. Three profiles, resulting from the relative rotation of the camshaft with 0°, 30°, and 60° CA are shown in Fig. 2.31.

Variation of the cam profile pushing the intake valves influences both the entering air mass as well as the air swirl within the combustion chambers. When the fuel is introduced by direct injection, this swirl improves the fuel droplet distribution and the duration of vaporization. The benefits of a concentric cam system applied to a car diesel engine with turbocharging and diesel fuel injection have been analyzed by 3D process simulation, with experimental calibration and validation [27]. Figure 2.32 shows some results of this analysis. The swirl within the cylinder (Fig. 2.32a) is intensified when turning the cam position from 0° to 15° and further to 30° CA. On the other hand, the longer opening duration of the valve causes a certain scavenging mass loss by backflow from the cylinder.

The intensified air swirl determines a better distribution of the fuel droplets within the combustion chamber and, consequently, faster droplet vaporization.

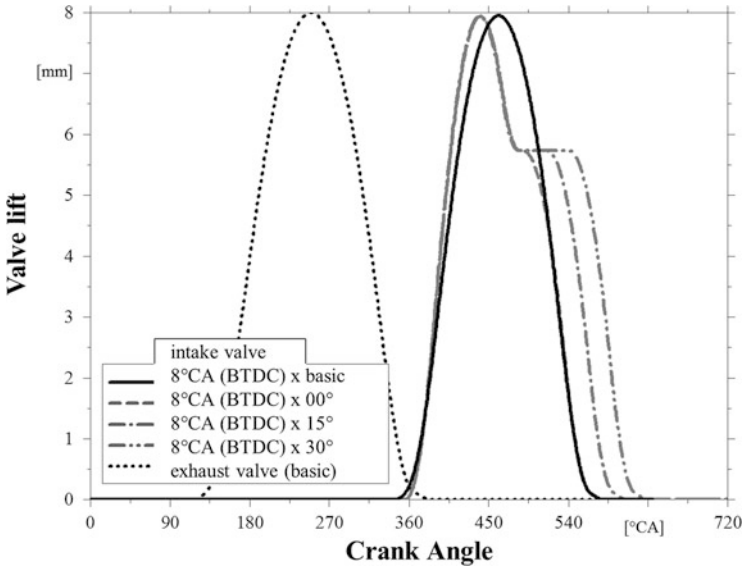

Fig. 2.31 Variability of opening duration with Concentric Cam Type II

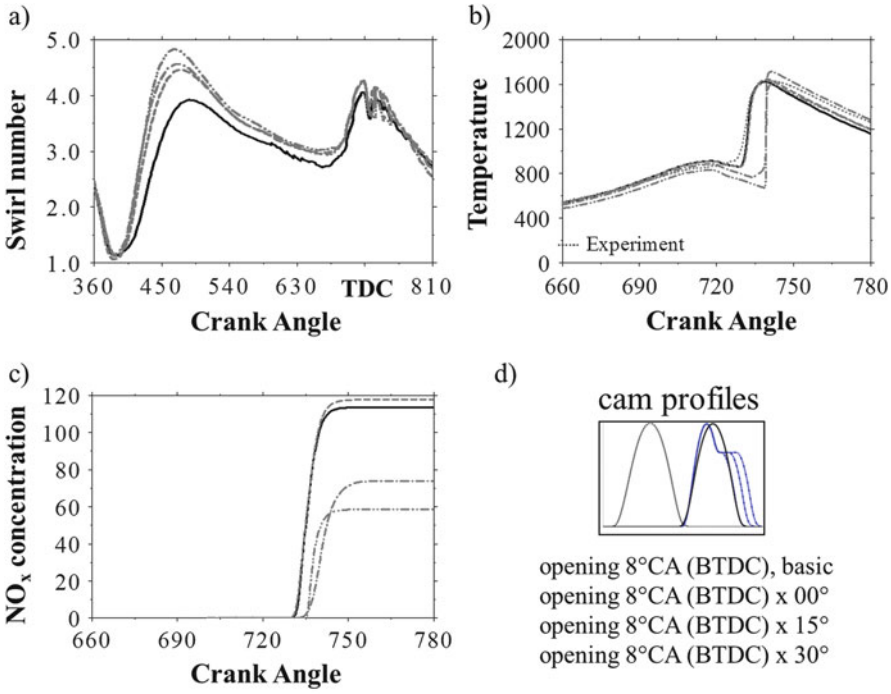

Fig. 2.32 Relationship between (**a**) swirl number, (**b**) mean combustion temperature, and (**c**) NO_x concentration for (**d**) different cam profiles

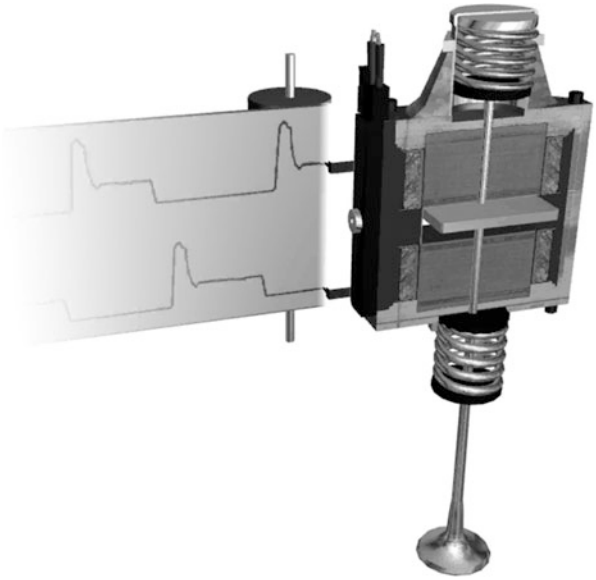

Fig. 2.33 Electromagnetic valve control

When using a classic camshaft, the fuel droplets become concentrated in the piston bowl, provoking earlier self-ignition, as deduced from the temperature–crank angle diagram in Fig. 2.32. Despite the longer delay of start of self-ignition, when the droplets are distributed homogeneously in a larger volume, faster vaporization leads to faster combustion, as shown by the steep temperature rise. The main advantage of this behavior is an improvement in thermal efficiency, expressed by a decrease in bsfc and, therefore, in CO_2 emission. Despite the fact that the steep temperature rise leads to a higher maximum temperature (as shown in Fig. 2.32), the lower air mass in the cylinder caused by the backflow at scavenging leads to a remarkable decrease in NO_x emission. On the other hand, the better fuel droplet vaporization caused by the intensified swirl should give a lower soot emission. However, this expectation is diminished by the decreased air mass in the combustion chamber. In the presented example, the optimum behavior was achieved for a camshaft rotation angle of 15°.

Continuous variation of the start and duration of opening of an intake or exhaust valve, fully independent of the engine speed, is in principle achievable only if guidance by the camshaft is eliminated. A possible method involves the utilization of magnetic forces, with a current history that should be independent of angles or camshaft speed, as shown in Fig. 2.33.

Within the electromagnetic valve, an armature is moved between two coils that generate two separate magnetic circuits. The springs assist the reverse movements of the armature. The electromagnetic valves can be designed in very compact form (as shown in Fig. 2.34), allowing their use in compact car engines, which generally

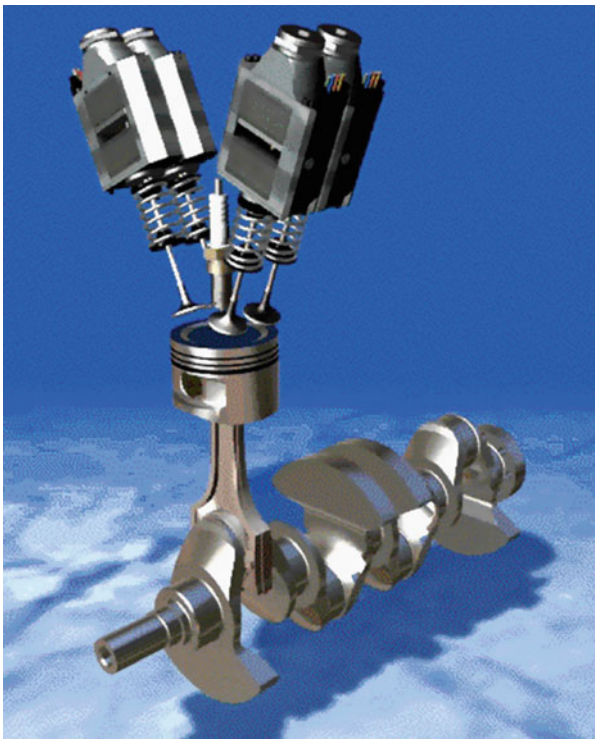

Fig. 2.34 Electromagnetic valves at intake and exhaust

require two intake and two exhaust valves. The start and duration of opening can be controlled independent of the engine speed, whereas the valve lift is generally constant. Valve lift scaling is obtainable through the use of lock mechanisms.

The benefits of limiting fresh mass via the intake valve instead of a throttle within the intake duct have been mentioned in relation to the Valvetronic system. There are additional benefits to controlling the residual gas mass within the cylinder via the exhaust valve lift. Furthermore, the possibility of opening only one of two intake or exhaust valves, (hardly feasible with mechanical systems) has the net advantage of controlling the masses of fresh air and residual gas within the cylinder at every speed and load, as well as generating swirl movements in the mixture. The introduction of electromagnetically controlled intake and exhaust valves has been impeded by the requirement for electrical energy. In this context, on-board energy management, between propulsion and auxiliary systems that consume electric energy, again seems imperative for future applications. In Sect. 1.3, Fig. 1.30 shows the configuration of such an energy management system.

Multiair (INA Schaeffler) is a solution that combines electromagnetic and hydraulic actuation. In this form, the necessary electromagnetic force to open an intake or exhaust valve is widely reduced; on the other hand, the system allows more variability in the valve lift. The system is illustrated in Figs. 2.35 and 2.36. The force for valve opening is given by the cam of a rotating camshaft, which is

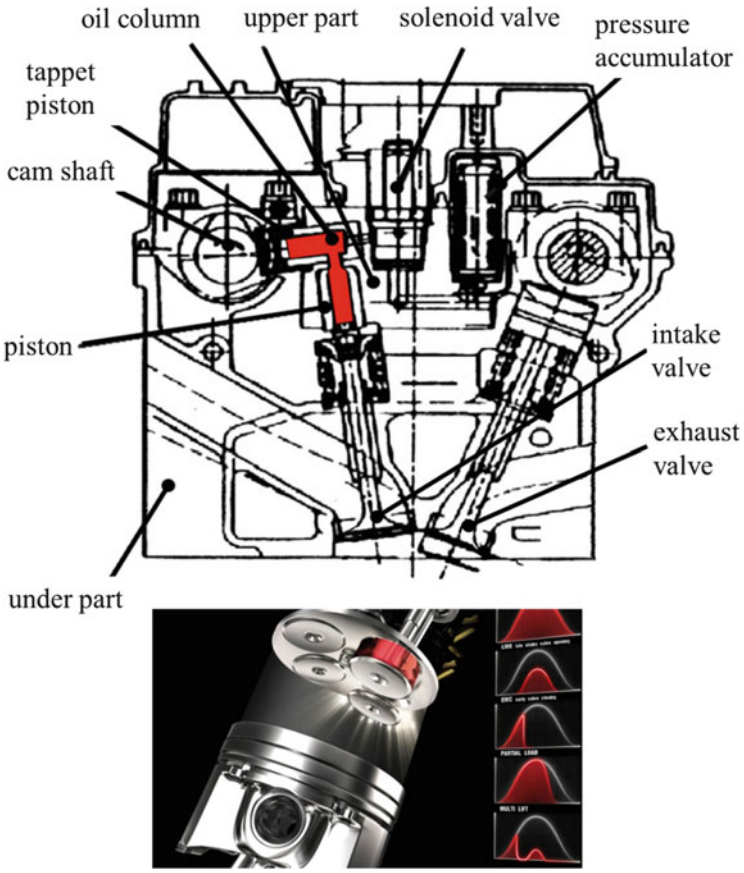

Fig. 2.35 Combined hydraulic-electromagnetic valve control

actuated by the engine crankshaft. Thus, there is a basic dependence on the engine speed, but that does not have a direct effect on valve control.

The acting force is transmitted from the cam to the valve shaft by a hydraulic oil column. The oil duct is provided with an electromagnetic valve that allows, at opening, a backflow of hydraulic oil and, thus, the force transmission between cam and valve is short-circuited. The cam profile is designed for maximum valve lift and opening duration. For reduced lift and opening duration, but also for variation of opening start, different segments of the cam profile can be activated by opening and closing of the electromagnetic valve in the oil column. This solution allows a compact design and a larger variability.

The relationship between opening start, opening duration, and valve lift at every load and speed combination, and considering the gas waves into the intake and exhaust ducts, can be established using an accurate numerical simulation for each of the presented systems. Figure 2.37 shows a chain of 1D and 3D codes for the

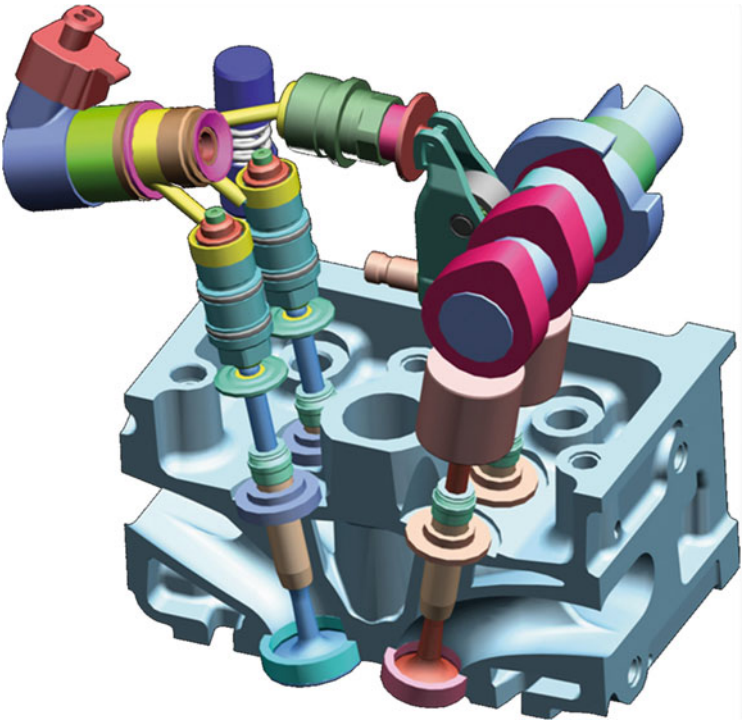

Fig. 2.36 Design of a system with hydraulic-electromagnetic valves (Source: MTZ)

simulation of scavenging, direct injection, mixture formation, and combustion within a piston engine as a basis for deduction of the optimum movement of the intake and exhaust valves. In the first step, such 1D models are efficient for approximate dimensioning, which allows fast evaluation of the whole system when combining a high number of parameters (Fig. 2.37, top left)

In the second step, the geometry of intake and exhaust ducts and valves, throttling effects at different valve cross-sections, combustion chamber design, and temperature distribution at walls must be taken into account when calculating the mass flows. Furthermore, fuel injection mainly influences mixture formation and, therefore, the flows. For calculation of the process within the direct injection system itself, an appropriate 1D code (Fig. 2.37, lower left) can be used.

However, a 3D calculation is strongly recommended for analysis of the development of the fuel spray within the combustion chamber and of the time- and space-related mixture formation and combustion (Fig. 2.37, right). In this mode, 3D simulation offers the possibility of intensive analysis of the most interesting parameter combinations derived from extensive analysis by 1D simulation.

As example, such a model for a diesel engine consists of partial models for intake and exhaust ducts and valves, filters, turbochargers, intercooler, exhaust gas

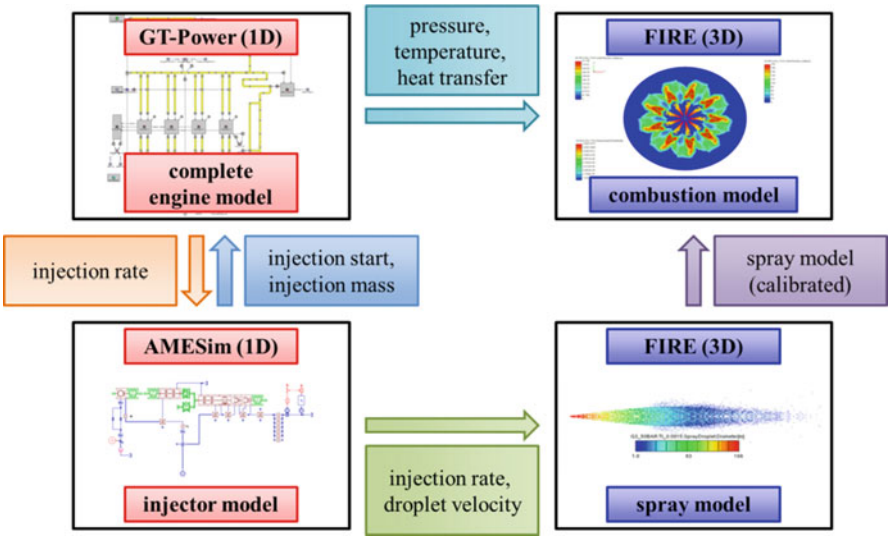

Fig. 2.37 Chain of 1D and 3D computational fluid dynamics codes for the simulation of scavenging, direct injection, mixture formation, and combustion within a piston engine [27]

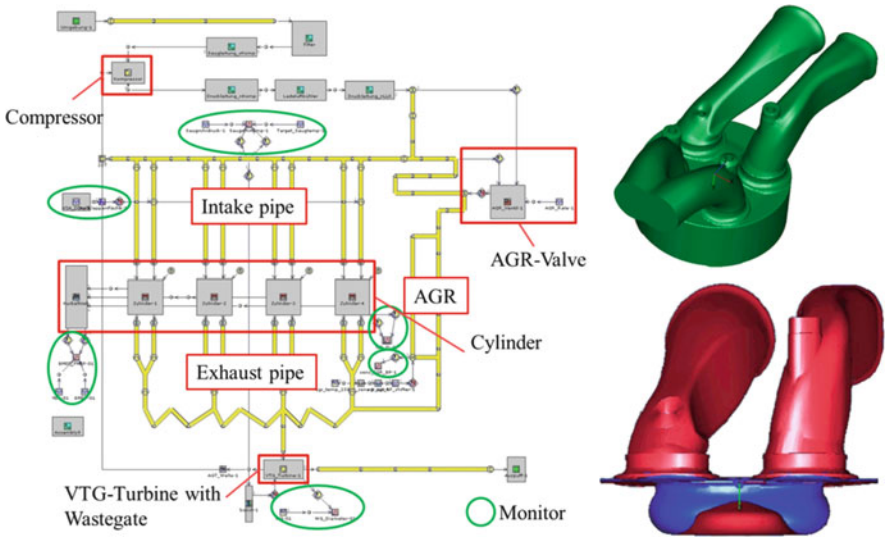

Fig. 2.38 1D (*left*) and 3D (*right*) models for coupled computational fluid dynamics analysis

recirculation module, and cylinder. The model takes into account the form of the ducts and the combustion chamber design, as shown in Fig. 2.38.

Other decisive parameters are the injector location and the spray angle. The 3D simulation of mixture formation and combustion is based on separate

phenomenological models for the formation and vaporization of fuel droplets, their interaction with turbulent air movement, the impact of droplets on combustion chamber walls, and the subsequent combustion process and formation of combustion products. These examples are given to underline the fact that the control of scavenging by variable valve movement strongly influences the whole process and requires complex analysis.

2.2.1.4 Internal Mixture Formation by Direct Fuel Injection in SI and CI Engines

Internal mixture formation by direct fuel injection is, at present, no longer only a feature of diesel engines, being increasingly used in gasoline engines as well. Direct injection in SI engines has a remarkable potential in terms of low fuel consumption and low pollutant emission, but also with respect to the specific cycle work and the power-to-volume ratio when combined with super- or turbocharging. The 1990s saw the first phase of gasoline direct injection in series applications, which was stimulated by the development of many interesting configurations for direct injection systems, but quickly damped by substantial problems with internal mixture formation. In the second phase, new mixture formation concepts were successfully applied, marking the beginning of a new era of mixture formation in SI engines, after the long supremacy of carburetors and then of low-pressure injection into the intake duct [2].

Tightly focused internal mixture formation (such as shown in Fig. 2.39 for partial load) can be used to avoid completely throttling of the fresh air mass entering the cylinders. Another advantage is the displacement of the knock limit to higher values, allowing an increase in compression ratio. Both the elimination of throttling and the increase in compression ratio lead to a noticeable increase in thermal efficiency (as best value and as torque/speed domain with very good

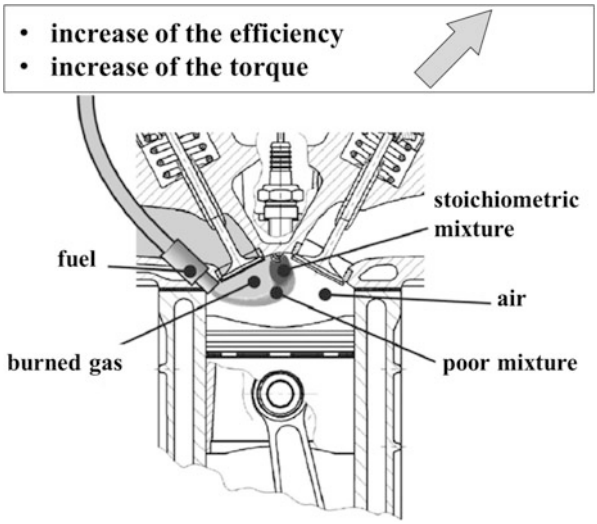

Fig. 2.39 Ideal internal mixture formation by direct injection in a SI engine at partial load

values), which is expressed by the obtained bsfc. Furthermore, direct fuel injection at high velocity into the compressed air just before combustion generates local turbulence centers, which intensify the combustion process. Considering the same air mass captured within the cylinder as in the case of intake duct injection and, therefore, the same fuel mass (e.g., at stoichiometric air/fuel ratio), the generally observed 8–10 % increase in maximum torque when changing from intake duct injection to direct injection is clearly explainable by the increase in turbulence during combustion. Faster combustion tends to an isochoric process, improving the specific cycle work and, thus, bsfc. An ideal configuration for internal mixture formation at partial load is illustrated in Fig. 2.39.

The basic condition is the formation of a homogeneous fuel–air mixture, generally at stoichiometric ratio, without discontinuities such as air bubbles, fuel droplets, or burned gas zones, which should keep direct contact with the spark source at every combination of load and speed. This mixture cloud should be partially enclosed in fresh air, which is in excess at partial load. Additionally, the mixture should have a contact surface with the rest of the burned gas in the cylinder. This last aspect is explained in the next point of Sect. 2.2, which discusses controlled self-ignition. The fresh air cover around the burning fuel–air mixture partially impedes the heat transfer from combustion to the combustion chamber walls and then to the cooling system, an effect that stimulates the transformation of internal energy of the burning mixture (temperature) into work (pressure). At full load, a fuel–air mixture that fills the entire cylinder is required, similar to mixture formation in the intake duct. However, the local turbulence provoked by the fuel droplets in the case of direct injection leads to an increase in torque at full load, as already mentioned. The described mechanism of internal mixture formation is an ideal scenario, which is more or less realizable by different measures, as illustrated in Fig. 2.40.

The reciprocal adjustment of such parameters for an operating point of the engine or for a small operating domain also seems feasible. The more complex problem is to enlarge such a reciprocal adjustment of parameters to a wide range of loads and speeds or to adapt it to transient conditions. Note that some of these parameters are not variable (variable parameters are marked in Fig. 2.40 by “k”).

Different methods for ideal internal mixture formation have been developed and are known as wall-guided, air-guided, and spray-guided mixture formation (see Fig. 2.41). It is noticeable that the combustion chamber design, especially the form of the piston bowl, plays a very important role in the variants. The main features of the three methods are described below:

- The spray-guided method has, as expected, the highest efficiency. It was applied in an initial form in the 1950s, before series application. The considerable difference between the enthalpies of fuel and air in the case of direct fuel injection results from differences in both density and velocity; therefore, fuel is the main contributor to mixture formation. For the configuration shown in Fig. 2.41a (as mostly applied at this time) sufficient droplet atomization requires a high fuel pressure during injection, which results in high droplet velocity. The

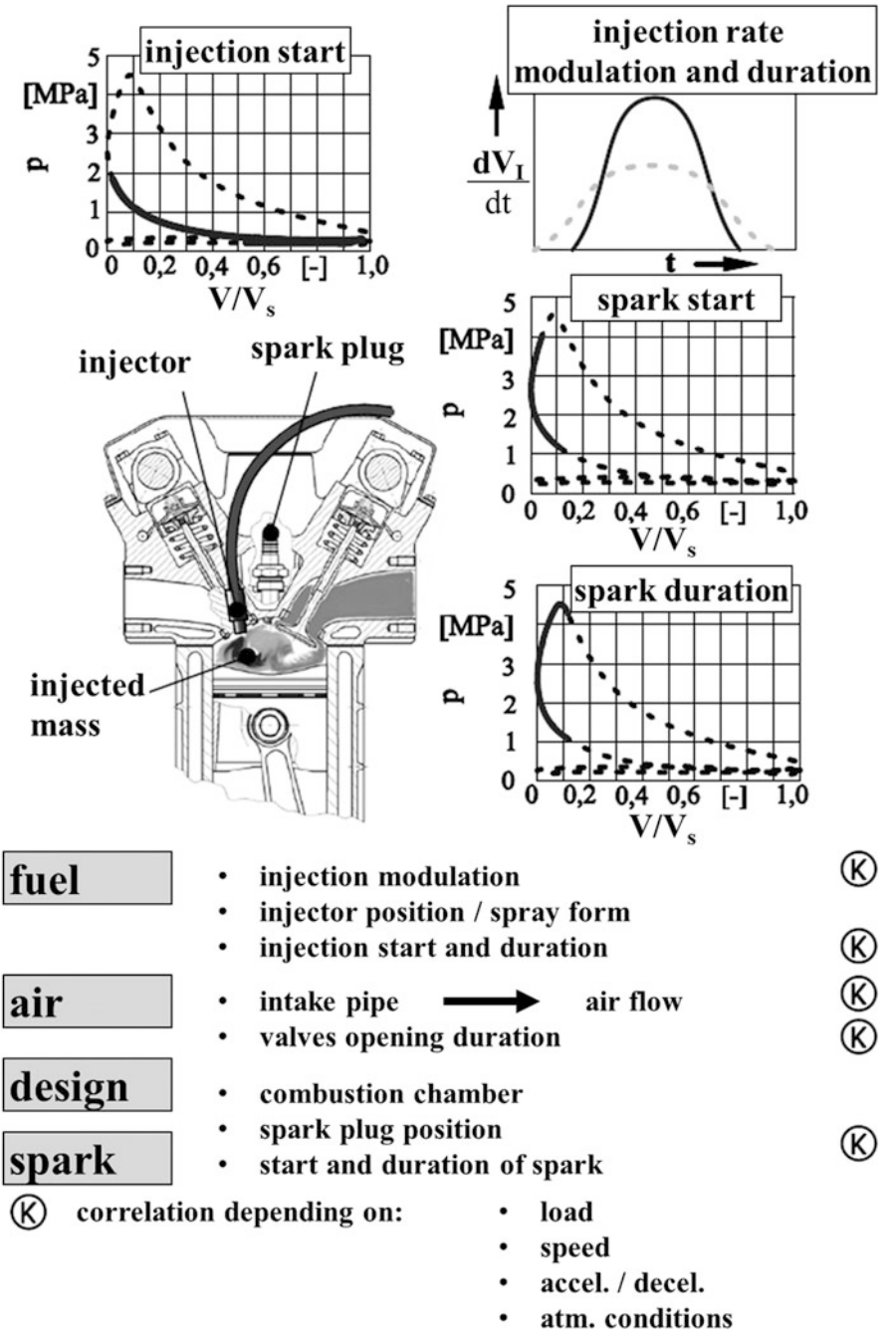

Fig. 2.40 Correlation of parameters for optimization of internal mixture formation in an SI engine. Variable parameters are indicated by *K*

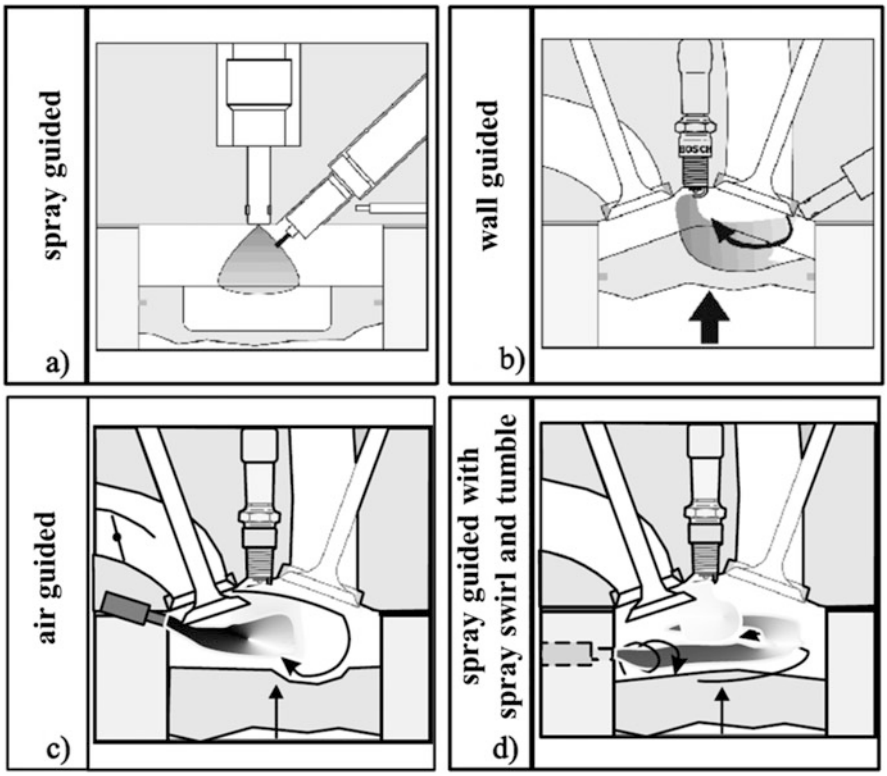

Fig. 2.41 (**a**) Spray-, (**b**) wall-, and (**c**) air-guided mixture formation by means of direct injection in SI engines. (**d**) Spray guided mixture formation with swirl and tumble

consequence is a spray penetration length of 20–80 mm. This is generally greater than the distance between injector tip and piston surface, despite the compensating piston bowl. The impact of fuel droplets that are still liquid on the piston surface causes incomplete combustion and, thus, hydrocarbon (HC) emission. The spray-guided method seems to be similar to direct fuel injection in diesel engines. However, there are several fundamental differences: the pressure difference between direct injection systems for diesel and gasoline is approximately 2000:200; therefore, there is better vaporization of diesel fuel droplets, injected through injectors with much smaller holes. On the other hand, the air temperature during compression and injection is approximately 200 °C higher in diesel engines, whereas the piston surface temperature is at least 100 °C higher. A crucial issue is the contact between the shell of the fuel spray and the spark plug, which should occur at every combination of load and speed. Deviations in the shell of the angle of fuel streaks from a multihole injector when changing the injection mass, by air flow displacement with load and speed, or by general tolerances of parts can cause the spark to occur in zones with different air/fuel

ratios, varying in zones with a thickness of under 10 µm. The propagation of flames from such an initial point with very rich or very poor mixtures impairs combustion and favors pollutant emission.

- The wall-guided method, as shown in Fig. 2.41b, ensures a stable path of the mixture cloud to the spark plug, as well as good contact to the spark plug at a passable fuel/air ratio, with geometric support by a piston bowl. The generated mixture tumble facilitates both mixture formation and combustion. This method is reminiscent of the diesel engine (in this case the M principle) if the spark plug is not considered. Nevertheless, the differences in the thermodynamic process are noticeable. The difference in injection pressure (2000:200 bar) causes not only lower vaporization but also lower relative velocity between droplets and piston bowl surface. Moreover, the temperature of the piston surface is at least 100 °C lower. This leads to the formation of a fuel film on the piston surface, provoking incomplete combustion over a relatively large area, with repercussions in terms of HC emission and bsfc.
- The air-guided method, as shown in Fig. 2.41c, is based on controlled air movement from intake duct to the piston bowl. This method is also reminiscent of the diesel M principle. However, in this case, tumble is generated only at partial load by throttling a half cross-section within the intake duct. The resulting air film takes the direct injected fuel to the spark plug. Guidance of the fuel by air is obviously more advantageous than guidance by the piston, as confirmed by bsfc and by HC emissions. However, because of the mentioned differences between the enthalpies of fuel and air, such tuning only functions for a small range of load and speed.
- A mitigation of the trade-off between fuel droplet size and spray penetration length, and a stable position of the fuel–air mixture cloud around the spark plug, is shown in Fig. 2.41d as an alternative to the classic spray-guided method. In this case, the energy of the entering fuel spray is deflected from translation to rotation by a helicoidal duct within the injector, around the needle. This rotation of the spray shortens its penetration length. Moreover, the tangential location of the injector in the cylinder and the appropriate design of the piston bowl lead to a horizontal swirl of the fuel spray around the cylinder axle. Therefore, the mixture cloud moves in a toroidal volume without wall or piston contact, the center being the spark plug. Changing the injected mass, corresponding to load, also changes the intensity of the spray swirl around its own axis and around the cylinder axis . This method is especially advantageous for very compact engines with a broad speed range.

Power increases not only as a result of an increase in energy density, but also through an increase in speed, as already mentioned and shown in Eq. (2.9.):

$$P_e = w_e \cdot n \cdot \frac{T_U}{T_A} \cdot V_H \tag{2.9}$$

An increase in engine speed is becoming very popular in new series engines. The basic problem associated with increased engine speed is the piston velocity along the cylinder, which provokes increased friction. For a given combination of materials for cylinder liner, piston, and rings, the increased friction leads to a shorter lifetime of the engine. A simple criterion for comparison is the mean piston velocity, as given by Eq. (2.16):

$$c_m = 2Hn \tag{2.16}$$

c_m	$\left[\frac{\text{m}}{\text{s}}\right]$	Mean piston velocity
H	[m]	Stroke
n	$[\text{s}^{-1}]$	Engine speed

A higher engine speed consequently imposes a shorter stroke length. For the same swept volume, the piston diameter must be enlarged:

$$V_h = \frac{\pi \cdot D^2}{4} \cdot H \tag{2.17}$$

V_h	$[\text{m}^3]$	Swept volume per cylinder
D	[m]	Piston diameter

The tendency to low stroke/bore ratios in car engines is perceptible. From the point of view of scavenging, this seems to be beneficial because of the possibility of providing larger or more valves. However, from another perspective, a high compression ratio is imposed by the thermal efficiency and favored by direct injection, which pushes the knock limit:

$$\varepsilon = \frac{V_{\max}}{V_{\min}} = \frac{V_h + V_b}{V_b} \tag{2.1}$$

ε	[−]	Compression ratio
$V_{\max}$	$[\text{m}^3]$	Maximum cylinder volume
$V_{\min}$	$[\text{m}^3]$	Minimum cylinder volume
V_b	$[\text{m}^3]$	Volume of combustion chamber

The influence of the stroke/bore ratio on the shape of combustion chamber is shown in Fig. 2.42.

The presented forms of mixture formation (spray-, wall-, and air-guided) involve more or less pronounced piston bowls (as shown in Fig. 2.41), which lead to an increase in combustion chamber volume and, thus, to a lower compression ratio for values allowed by direct injection. Consequently, a sufficient fuel droplet distribution within a controlled volume of combustion chamber, without wall contact, at

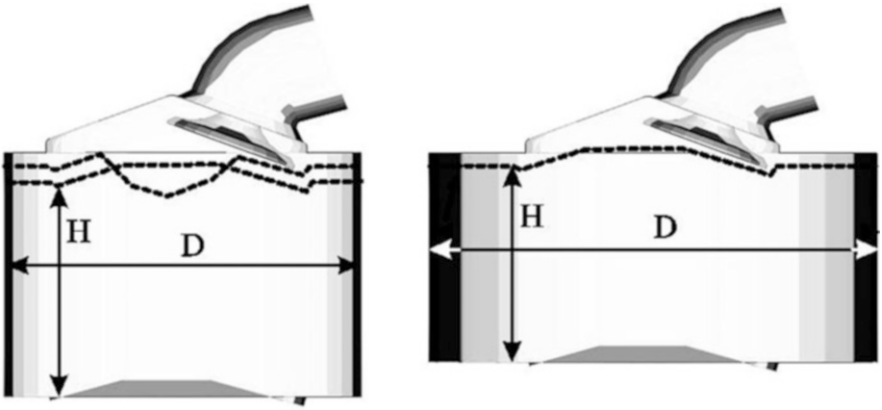

Fig. 2.42 Influence of bore/stroke ratio on the shape of the combustion chamber

every load/speed combination, must be achieved with no freedom in chamber design. On the other hand, a liquid fuel kernel must be avoided.

An advantageous approach is to shorten the spray length as much as possible but keep the high injection pressure as the basis of atomization and vaporization. This is possible by increasing the fuel passage cross-area by changing from one to two or more injectors [3]. In this way, the contact between fuel and air also increases.

Pintle-type nozzles offer a remarkable potential for such applications. The outward opening of the needle allows very small injector dimensions, which is an essential condition for use in very compact piston engines. Furthermore, a very small injector requires elimination of opening control from the injector housing it. This is possible when using an injector system with high pressure modulation, the injector opening being controlled in this case by the fuel itself and not by electromagnetic or piezoelectric devices. Figure 2.43 shows such micro-injectors and their positioning in an engine head.

Using two injectors for each combustion chamber, the mixture formation has extremely favorable conditions: the fuel sprays of the two injectors are injected as hollow cones, with a continuous surface when using pintle-type nozzles and with striations when using multi-hole injectors. Orientation of the injectors as shown in Fig. 2.43 leads to an intersection of the two hollow cones (as shown in Fig. 2.44), where contact of the droplets from both cones is given on elliptical curves.

The double intersection of each hollow cone generates a spherical, thin fuel cap with a central air kernel. The double contact of the two sprays strongly decelerates the fuel droplets and, therefore, impact of droplets on the combustion chamber walls can be avoided. On the other hand, generation of a stable, thin fuel cap can be positioned near to the spark plug by inclination of the spray axes. This form of mixture stratification allows the elimination of air throttling in the intake duct, increasing the thermal efficiency. Furthermore, the acceleration behavior is favored by the circumstance that the variation in injected fuel mass corresponding to load variation does not change the position of the fuel cap within the combustion

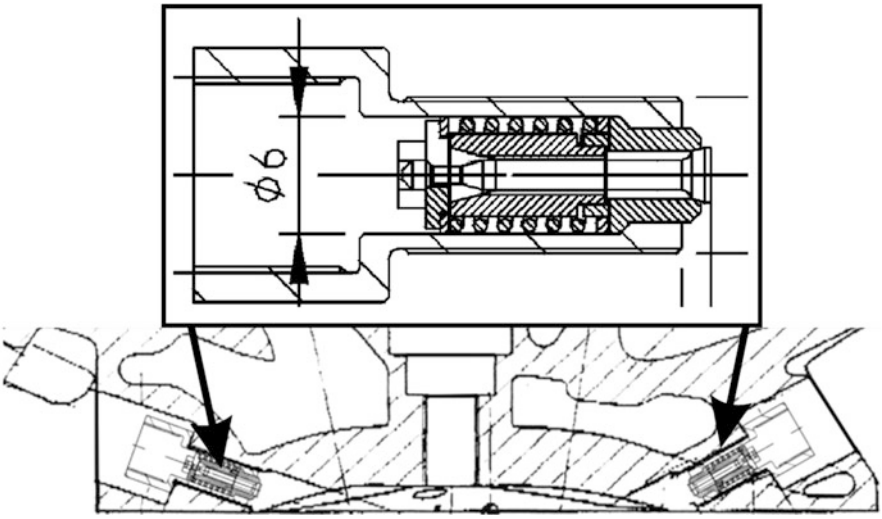

Fig. 2.43 Direct injection systems with two micro-injectors in the cylinder head

chamber. Figure 2.45 shows an experimentally determined time-related penetration of two conical sprays before and after their collision. The droplet atomization is not affected by the spray intersection and a liquid kernel cannot be detected.

This configuration remains unchanged for a wide range of injection mass. Visualization with a high-speed camera clearly shows the abrupt deceleration of droplets after the first and the second impact on a hollow cone surface, as a condition to avoid impact with the combustion chamber walls. Figure 2.46 shows the advantages of this method in comparison with direct fuel injection by means of one injector for each cylinder. The map presents the bsfc difference in a single-cylinder research engine with an extremely compact combustion chamber, with a broad speed range up to 10,000 min^{-1}. In this comparison, the air was throttled using only one injector, corresponding to an optimum air/fuel ratio; using two injectors, the air was not throttled. For both configurations (one or two injectors) the torque characteristics corresponded to those of the basic engine with external mixture formation.

This method has been successfully tested for application in high-performance engines. The required characteristics of the injected fuel spray, when used for internal mixture formation, depend on the nozzle type (as shown in Figure 2.47):

- Multi-hole nozzles are widely applied in diesel engines; in gasoline engines they offer advantages in term of fuel atomization and droplet distribution. However,

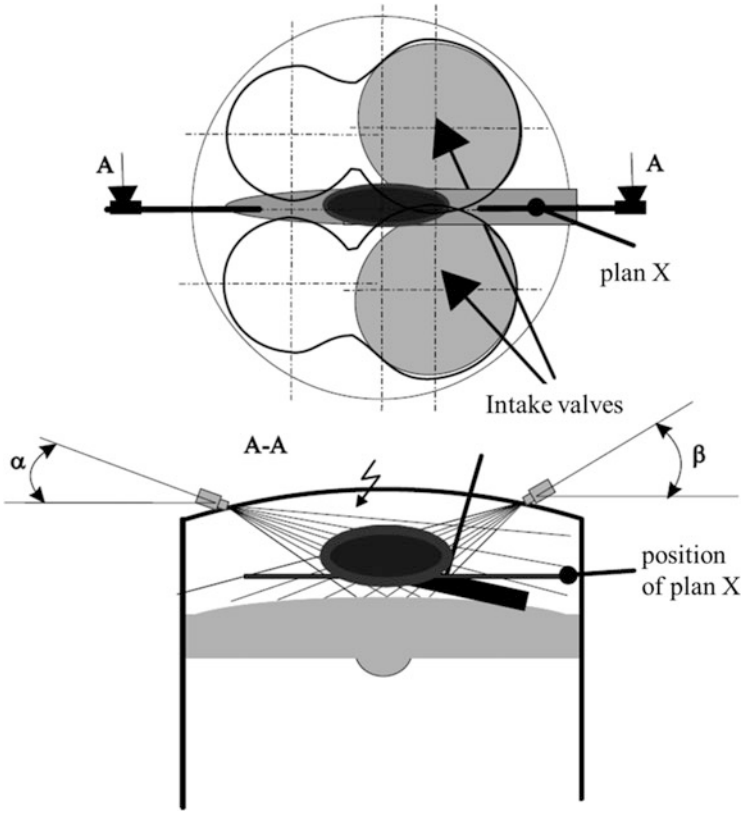

Fig. 2.44 Direct injection with two conical sprays, which generate a spherical, thin fuel cap

in general, opening of the holes requires an inward movement of the injector needle. A suitable force balance at needle opening requires a difference between the pressures on the front and rear of the needle. Therefore, an isolation surface is needed between the needle and its housing, which influences the mass of the needle and, thus, the forces for opening and closing it.

- Pintle-type nozzles are outwardly opening and, in this case, the needle opens an annular cross-section instead of holes. The fuel flow forms not more striations within the combustion chamber but a hollow cone with a very thin continuous surface. The cone angle can be determined by the geometric form at the needle tip and the thickness of the fuel surface by the needle lift. By replacing a number of striations from holes with a continuous conical surface of extreme thickness, the spray penetration length can be reduced, as a condition of good mixture formation in compact combustion chambers.
- Swirl nozzles are applied to reduce the spray penetration length. They can be based on multi-hole nozzles or pintle-type nozzles, forming helicoidal ducts around the needle.

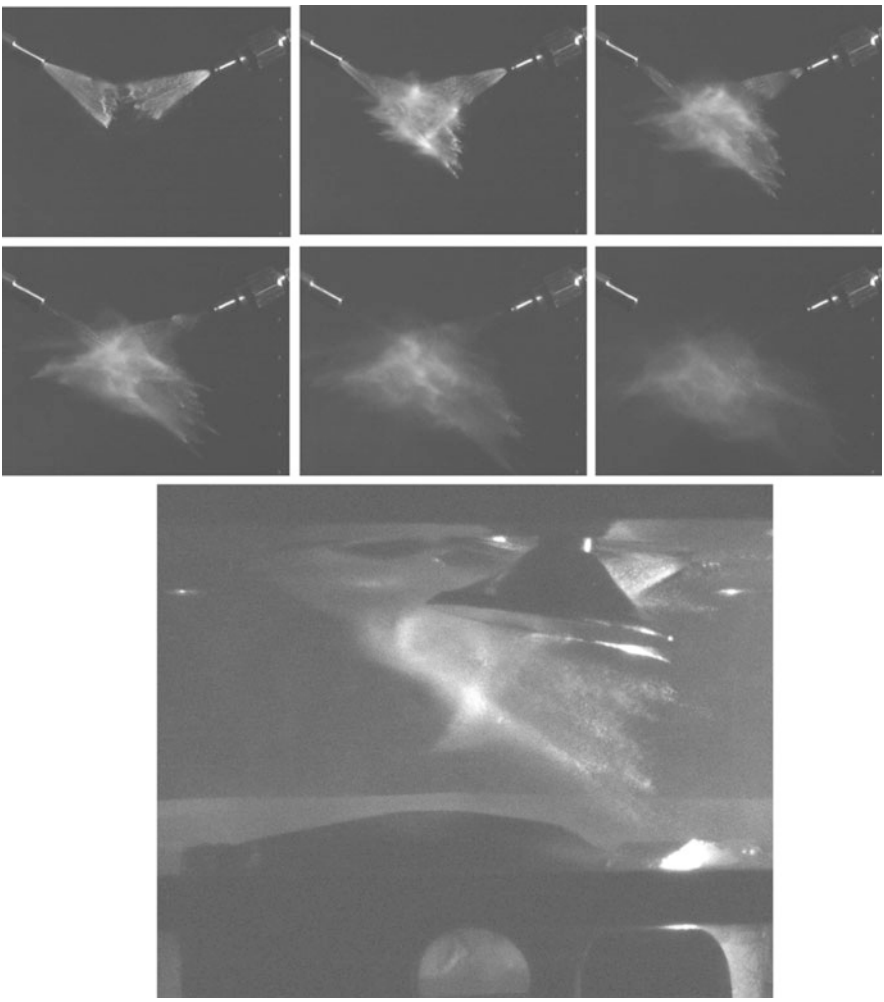

Fig. 2.45 Time-related penetration of two conical sprays, before and after their collision, and image from the combustion chamber of a high-performance SI engine

Various configurations of direct injection systems have been conceived for spark ignition engines and can be classified into two distinct categories [2]:

- Direct injection of a partially formed mixture of fuel and air (emulsion) that has been generated within the injection system
- Direct injection of liquid fuel

Each of these concepts has specific advantages, recommending their application as a function of the engine concept.

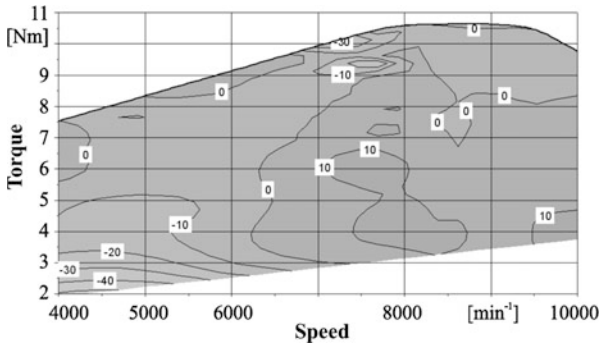

Fig. 2.46 Map of bsfc difference between direct injection with single injector and air throttling and with two injectors, without air throttling

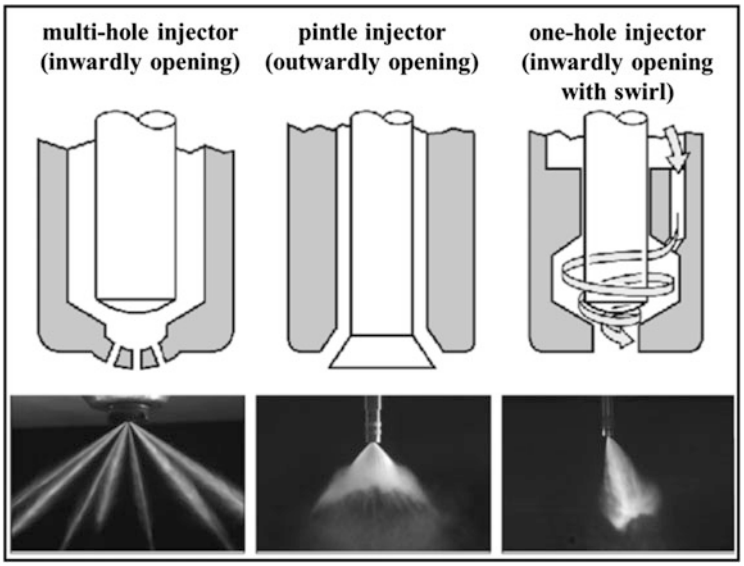

Fig. 2.47 Injectors for gasoline direct injection

Direct injection of a partially formed mixture is, in practice, displacement of part of the mixture formation from the combustion chamber to the injection system, as a means of reducing the duration of complete mixing. The pressures of the fuel and air within the injection system are realized in separate modules. Figure 2.48 shows a system of this type.

The air part is supplied by a piston compressor, whereas the fuel comes from a low pressure pump, such as provided in injection systems for intake ducts. Both the air and the fuel are guided to a mixing chamber, forming an emulsion that is then injected into the combustion chamber by opening an electromagnetically or

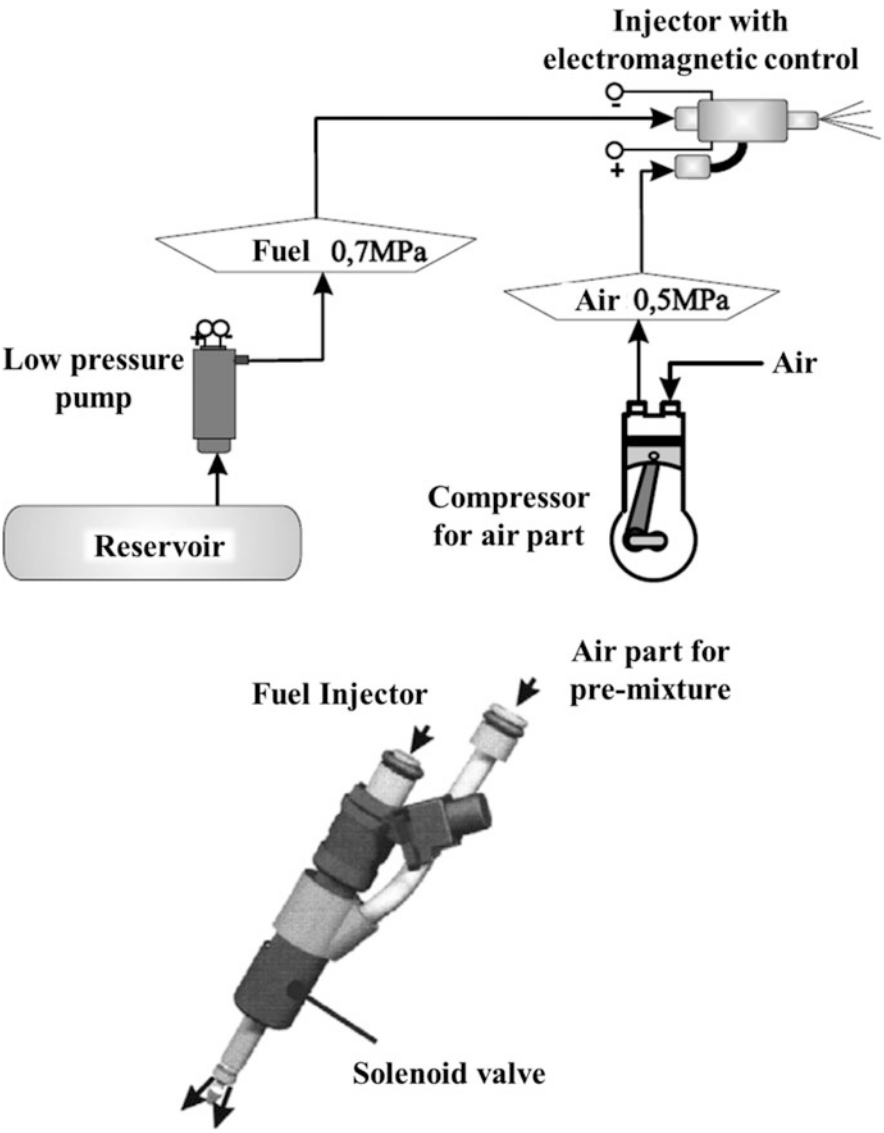

Fig. 2.48 Direct injection of a partially formed mixture (ORBITAL System)

piezoelectrically controlled injector. Variation of the injected mass corresponding to the required load is given by the duration of opening of the injector.

Injection of an emulsion has the advantage of fast vaporization and distribution within the combustion chamber; furthermore, the relatively low injection pressure leads to a decrease in the spray length. Combustion is favored both by the fast mixture formation resulting from good vaporization and distribution and by the

walls. However, this method has limitations in high load engines, because of the relatively high fuel mass to be injected in a very short time, which is impeded by the low injection pressure.

The direct injection of liquid fuel into SI engines occurs at a pressure that is orders of magnitude higher (10–30 MPa instead of 0.5–0.6 MPa) than the emulsion injection. The high pressure of the fuel can be maintained at the maximum level or formed as a wave with well-defined amplitude and duration. In both concepts, which form the basis for a multitude of injection system variations, the generated pressure (if constant at a maximum value or as a pressure wave) remains independent of the engine speed. The direct injection of liquid fuel at constant maximum pressure (common rail) in SI engines is based on the fuel boost at 10–30 MPa using a mechanical pump with one or more plungers. The configuration of such a system is illustrated in Fig. 2.49.

The constant pressure of the fuel is realized by accumulation of the boosted fuel in a rail that is common for all injectors that are connected to the cylinders of the engine. Injection starts at the opening of an injector by means of an electromagnetic or piezoelectric actuator. Similar to the described concept for emulsion injection,

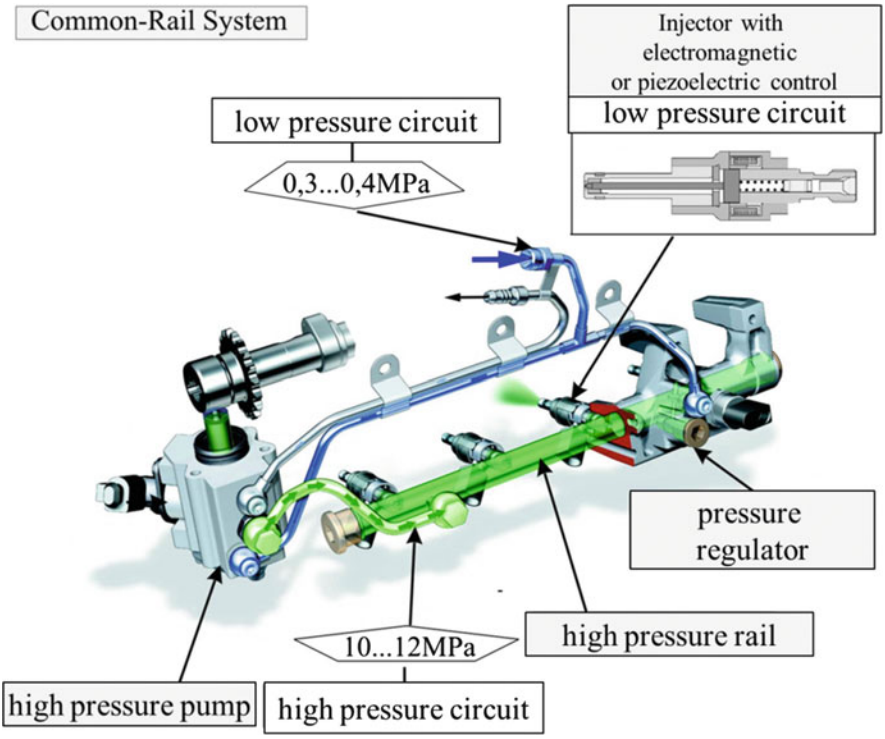

Fig. 2.49 Direct injection of liquid fuel at constant high pressure: BOSCH Common-Rail System (Source: Bosch)

the injected mass can be varied for different loads by controlling the opening duration of the injector.

The described system configuration corresponds to those for low pressure injection in intake ducts. Using piezoelectric control of the injector, the inertia of the injector needle lift during opening is extremely small. This allows the injection mass to be split into many portions, thus modulating the injection rate, which is beneficial for mixture formation at different combinations of load and speed.

Piezoelectric or electromagnetic control of the injector imposed in the case of common rail systems, and of emulsion injection systems because of the constant pressure level, could cause location problems in advanced, very compact engine heads.

Relocation of the actuation module out of the critical area is possible by stretching the injector needle, as shown in Fig. 2.49 (upper right). However, in this case, the inertial force increases and must be compressed by a supplementary electromagnetic or piezoelectric force at the actuator. The direct injection of liquid fuel with high pressure modulation (pressure pulse) is based on the hydrodynamic generation of a pressure wave with well-controlled amplitude and duration within the fuel column in a pipe. The load-dependent fuel dosage is obtained by varying the amplitude of the wave at unchanged wave duration. A basic characteristic of this concept is the actuation of the injector needle by the pressure wave itself. Therefore, separate actuation by electromagnetic or piezoelectric forces is not necessary in this case. Such a high-pressure wave can be generated by applying the water hammer effect. The function and control of such a system are illustrated in Fig. 2.50.

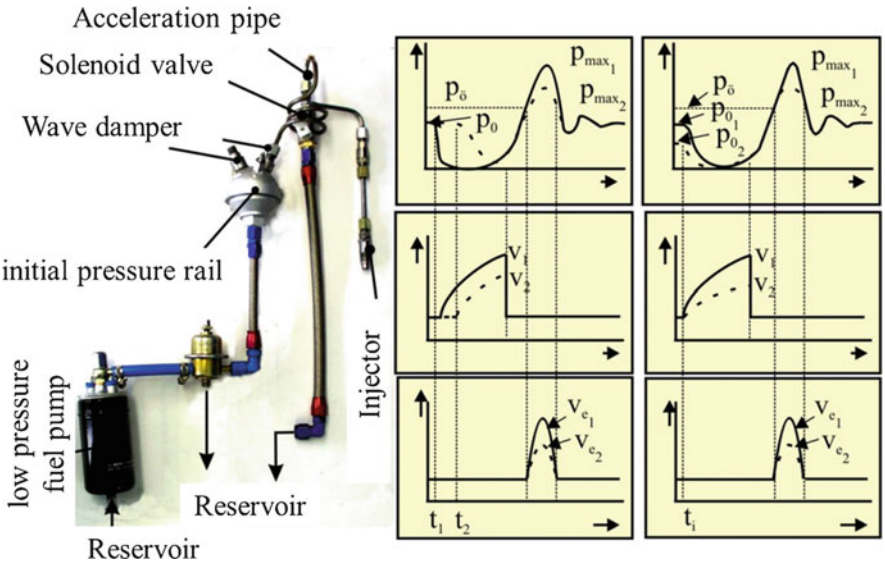

Fig. 2.50 Main modules and process sequences within a direct injection system with high pressure modulation for liquid fuel (Zwickau pressure pulse)

The system consists of a low pressure fuel pump ensuring an initial pressure p_o, a fuel acceleration pipe, a wave damper, a solenoid valve, and a fuel injector. When the solenoid valve opens, the fuel with the initial pressure in the pipe flows through a return tube back to the reservoir. During valve opening, the fuel in the pipe is accelerated up to a velocity v_1, which corresponds to the pressure difference between pipe and reservoir. The sudden closing of the electromagnetic valve provokes impact of the accelerating fuel column on the valve and subsequent weak fuel compression. This compression of a liquid generates a steep pressure rise, at a maximum amplitude that is 10–15 times higher than the initial pressure. This pressure wave propagates with sound velocity through the acceleration pipe against the still-flowing fluid, back to the wave damper. In this module, the amplitude of the wave is damped down to the value of the initial pressure. The reflected wave at this amplitude propagates forward to the electromagnetic valve, which is still closed. In this mode, a high-pressure wave with well-defined duration is obtained at the valve. This wave is captured close to the valve in an injector. The injector needle is controlled by a spring. The amplitude of the pressure wave, which determines the injection rate modulation, can be adjusted in two different ways: by the duration of fuel acceleration t_i and by the level of the initial pressure p_0. As shown in Fig. 2.50, a reduction in the duration of valve opening from t_1 to t_2 at constant initial pressure p_0 or a initial pressure decrement from p_{01} to p_{02} at constant valve opening duration t_1 have the same effect: the velocity before impact decreases from p_{01} to p_{02}, involving a decrease in the high pressure amplitude from p_{max1} to p_{max2}. Consequently, the injection volume derived from the pressure wave amplitude at constant duration decreases from v_{e1} to v_{e2}. The pressure and, therefore, the injection rate are unchanged at every frequency of the process and, thus, at any engine speed. In this manner, the fuel spray characteristics such as penetration length, droplet size, and droplet velocity remain at constant values for the entire operation range of the engine.

For application in compact engines, integration of the function modules in a unique part connected to the initial pressure supply is more effective. The initial pressure is commonly generated with electrically driven fuel pumps such as those for low pressure injector systems for intake ducts. For application in high-performances engines, requiring very small injectors, an integrated system design is not favorable. Furthermore, the very high amplitudes in very short duration require a relatively high initial pressure, which is better obtainable with mechanically driven pumps. Both variants of the system are presented in Fig. 2.51.

The pressure curves for high-performance direct injection systems are illustrated in Fig. 2.52 at 6000 min^{-1} and 18,000 min^{-1}. With such a gasoline direct injector system, a maximum pressure of 46 MPa at a wave duration of 1 ms has been achieved. The modulation and control of injection rate can be optimized in a very effective manner for a certain injection system by numerical simulation of the processes in each system module.

Figure 2.53 shows such an example, based on a simulation with the AMESim code [4]. The beginning and the duration of a direct injection event can present some difficulties for application in high-speed gasoline engines, independent of the

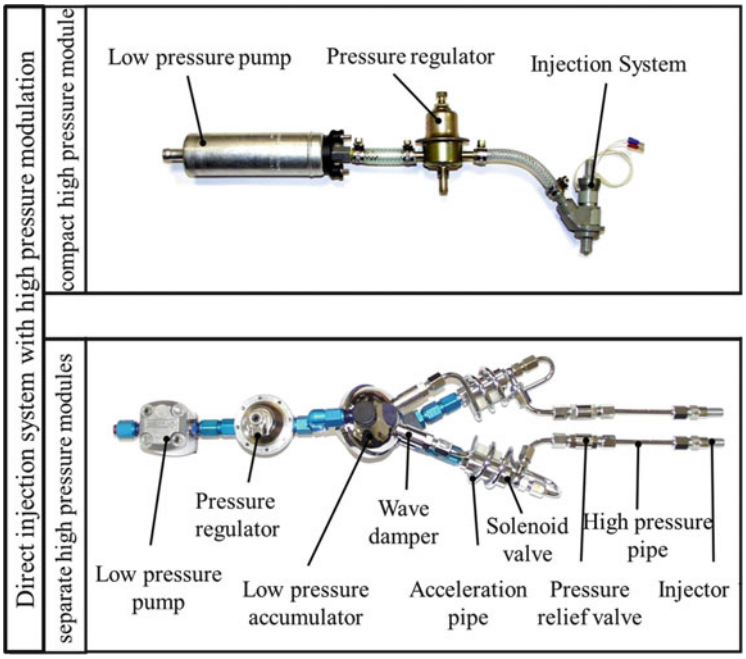

Fig. 2.51 Direct injection system with high pressure modulation for liquid fuel (Zwickau pressure pulse): system variants for compact and high performance engines

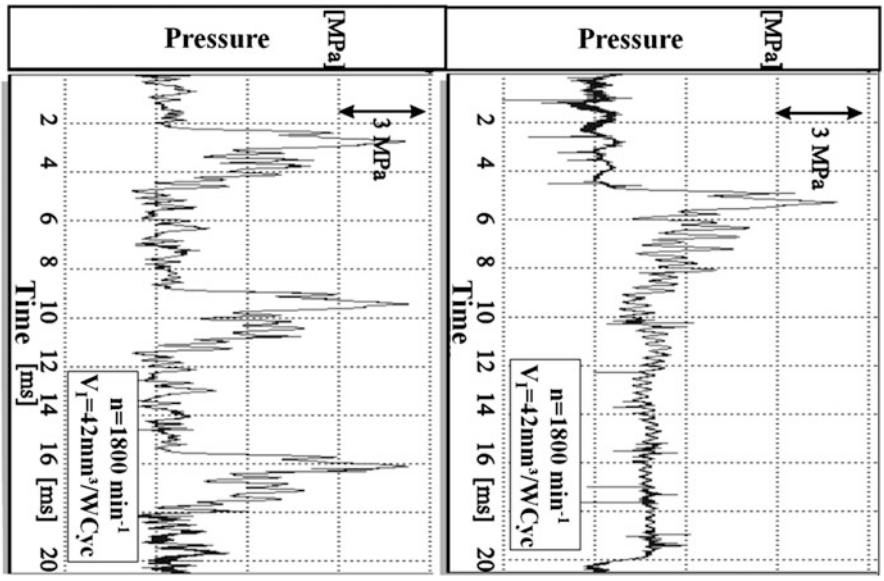

Fig. 2.52 Pressure history within a Zwickau pressure pulse system for two different experimental speed values

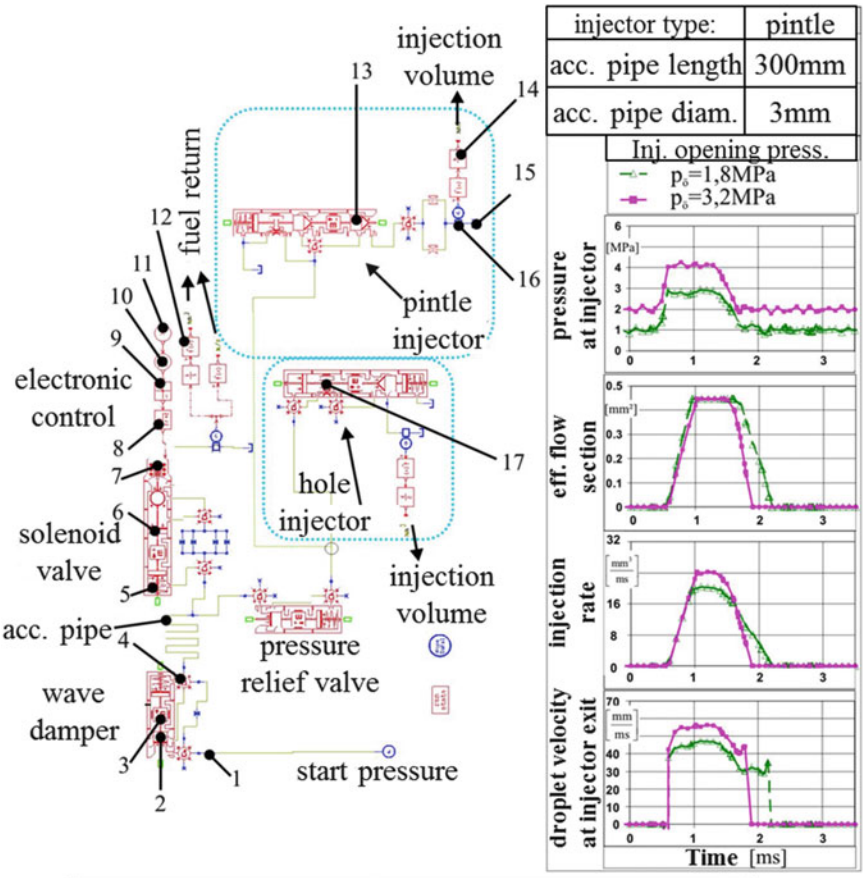

Model Configuration with 1D AMESim

1. throttle
2. pintle
3. mass with friction and lift stop
4. hydraulic volume
5. needle with spring
6. shaft
7. solenoid
8. press. converter
9. saturation element
10. pulse signal
11. constant signal
12. userdef. function
13. needle with conical seat
14. integration module
15. reservoir
16. flow signal
17. leak

Fig. 2.53 Configuration of the function modules of a direct injection system with high-pressure modulation and the resulting injection characteristics

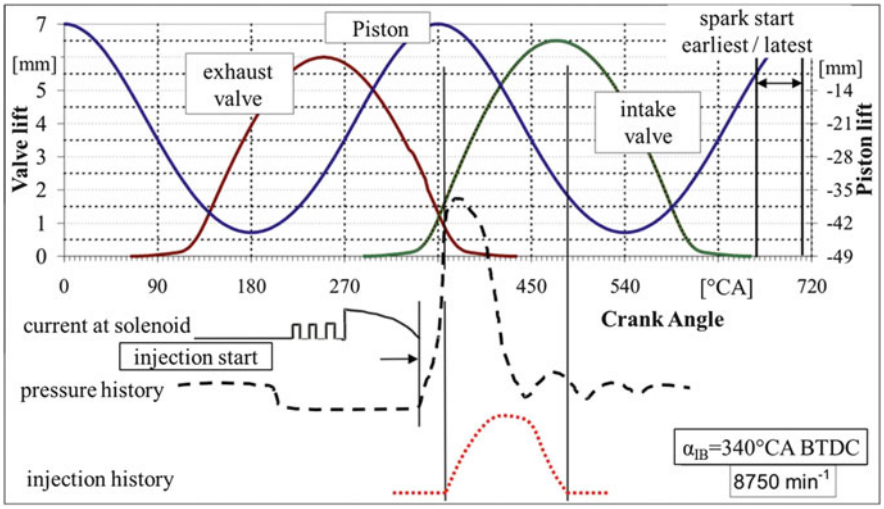

Fig. 2.54 Movement of intake/exhaust valve, piston, and injection spray within a SI engine (direct injection with high pressure modulation) at 8750 rpm

type of injection system, injectors, or mixture formation strategy (spray-guided, wall-guided, or air-guided). Figure 2.54 explains this relationship, based on the curves for the movement of the piston and intake and exhaust valves for an engine at 8750 min^{-1}.

There is a trade-off between a fuel spray with a wide angle for good distribution and the movement of the piston and valves. In high-speed engines, the duration of injection and mixture formation imposes an injection start during the opening phase of the intake valves, as shown in Fig. 2.45. A wide spray angle causes droplet impact on valve plates, impairing mixture formation. On the other hand, injection after closure of the intake valves, near top dead center (TDC), provokes impact of the spray on the piston surface. An ideal start of injection would be at closed intake valves and a piston position near bottom dead center (BDC). As shown in Fig. 2.54, this point corresponds to 600° CA and, thus, 120° CA before TDC at the working stroke. However, at 8750 min^{-1}, 120° CA corresponds to 2.28 ms. With a spark ignition start at 20° CA before TDC, the injection, mixture formation, and fuel vaporization have only 1.9 ms.

Figure 2.55 shows as an example the difference between the duration of injection and the duration of fuel vaporization when using a gasoline direct injection system with high-pressure modulation and a maximum fuel pressure of 12 MPa. The whole vaporization process is five times longer than fuel injection. Consequently, the injection start must occur earlier, but in this case the intake valves are still open and the piston is in a segment between TDC and BDC.

A reduction in spray angle and spray penetration are possible, as mentioned, if two injectors are used (Figs. 2.43, 2.44, and 2.45). Analysis of the complexity of internal mixture formation by direct fuel injection in SI engines requires numerous

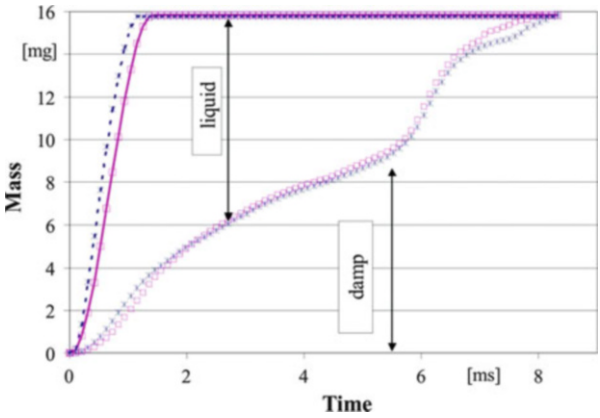

Fig. 2.55 Damp fraction during gasoline direct injection for two shapes of the injection rate (direct injection with high pressure modulation)

experiments and complex numerical analyses, combining 1D and 3D codes [5]. Figure 2.56 illustrates, as an example, a sequence of internal mixture formation and the most interesting aspects of this process.

The spray characteristics, injector location, geometry of the combustion chamber, and the start and duration of injection and ignition can be optimized in this way for all interesting combinations of load and speed. For such a complex process as internal mixture formation by direct fuel injection, simplified models such as the two-zone combustion model are no longer valid [6].

As shown in Fig. 2.57, the sequences of internal mixture formation by direct fuel injection with subsequent combustion broadly overlap. This leads to a heat exchange between different components and phases: burned gas–fuel, air–fuel, flame front–mixture, and flame front–combustion chamber walls.

As an example of such interaction, fuel vaporization requires enthalpy from the surrounding air or burned gas. The optimization of internal mixture formation in SI engines is at an advanced stage, allowing large-scale series application of gasoline direct injection. In diesel engines, direct fuel injection has been the state of the art for many years, and is therefore not the subject of analysis for alternative propulsion systems. However, a short overview should serve for its comparison with internal mixture formation in SI engines and, moreover, for analysis of controlled autoignition. In this way, the future convergence of SI and CI processes can be better evaluated.

Figure 2.58 shows, similar to the aspects presented for internal mixture formation in SI engines (Fig. 2.40), the main parameters influencing internal mixture formation in CI engines. Except for the spark, the parameters are the same as for the application of gasoline direct injection. In diesel engines for automobiles, only spray-guided mixture formation is used. Previous methods are shown in addition to spray-guided direct injection in Fig. 2.59. They show some apparent similarities to

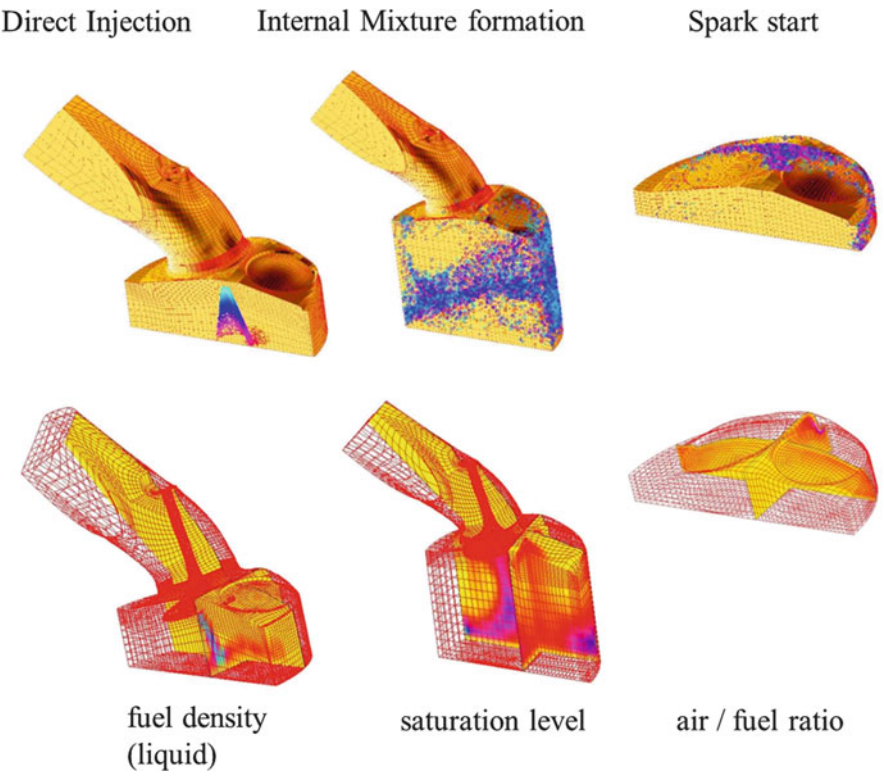

Fig. 2.56 Main characteristics for the analysis of internal mixture formation and combustion

recent approaches for gasoline direct injection, although the pressure droplet velocity and vaporization and the chamber wall temperatures are very different.

Spray-guided direct injection in actual CI engines is carried out with multihole injectors with 7–12 holes each and hole diameters in the range of 0.08 mm and less. Actuation of the injectors occurs electromagnetically or piezoelectrically, as shown in Fig. 2.60.

Piezoelectric control is up to five times faster than electromagnetic control, allowing multiple injection shots per cycle and, thus, modulation of the injection rate in relation to load and speed. For example, at full load two initial shots, a main injection volume, and two post shots are usual. Force transmission from the piezoelectric unit to the needle is made hydraulically. In the newest concepts, the needle is moved by the piezoelectric unit across a lever, as shown in Fig. 2.61.

Quartz crystal distention is proportional to the voltage (which can achieve 160 V), meaning that the needle course can be varied by changing the voltage. Using this variable needle course, multiple injection is no longer a necessary condition for injection rate modulation.

Up to the year 2008, there were two concepts regarding direct injection systems for CI car engines : common rails and pump-injector units. After 2008, the common

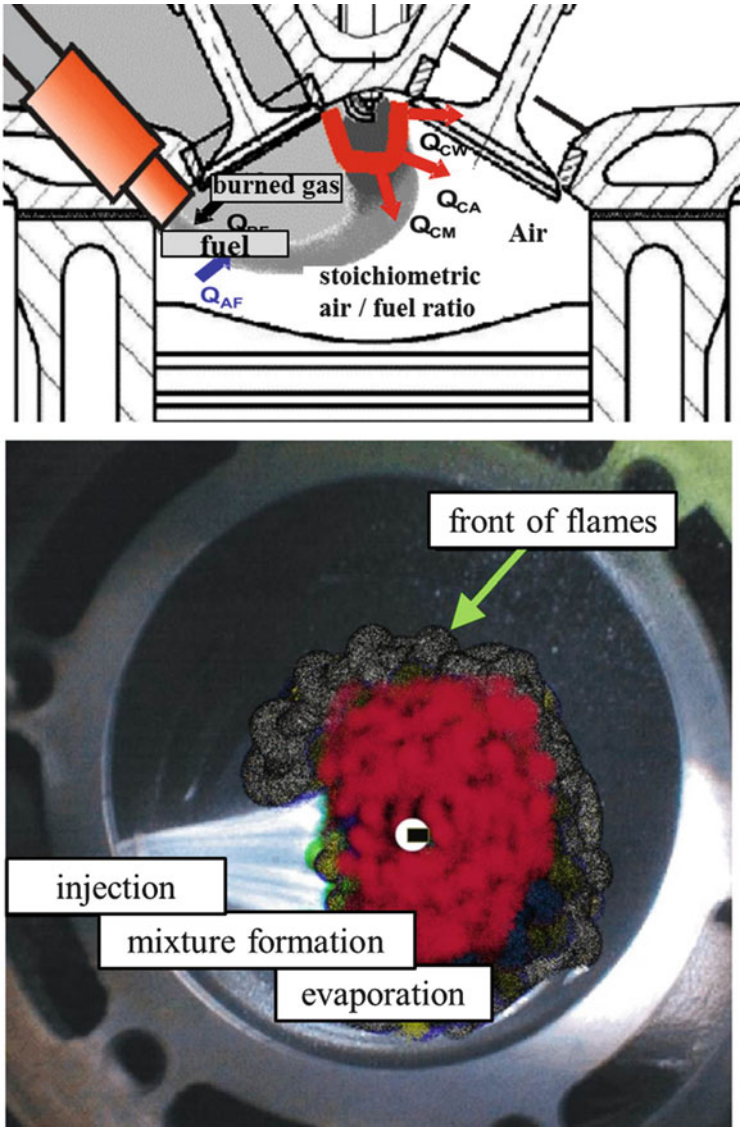

Fig. 2.57 Overlapping of process sequences within the combustion chamber of a piston engine with direct fuel injection

rail remained the only player in this field. In common rail systems for direct fuel injection in CI engines (see Fig. 2.62), the pressure can reach 160–250 MPa. The system configuration is generally the same as used for the common rail systems in SI engines.

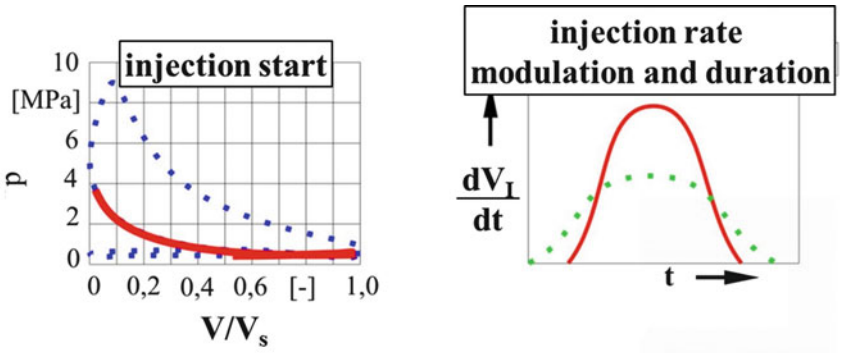

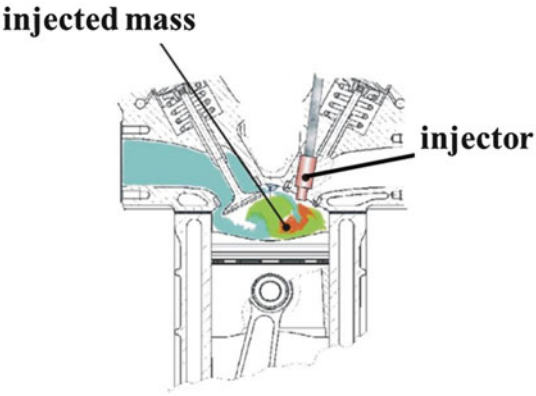

fuel

- injection modulation (Ⓚ)
- injector position / spray form
- injection start and duration (Ⓚ)

air

- intake pipe → air flow (Ⓚ)
- valves opening duration (Ⓚ)

design

- combustion chamber

Ⓚ Correlation depending on:

- load
- speed
- accel. / decel.
- atm. conditions

Fig. 2.58 Correlation of parameters for optimization of internal mixture formation in a CI engine

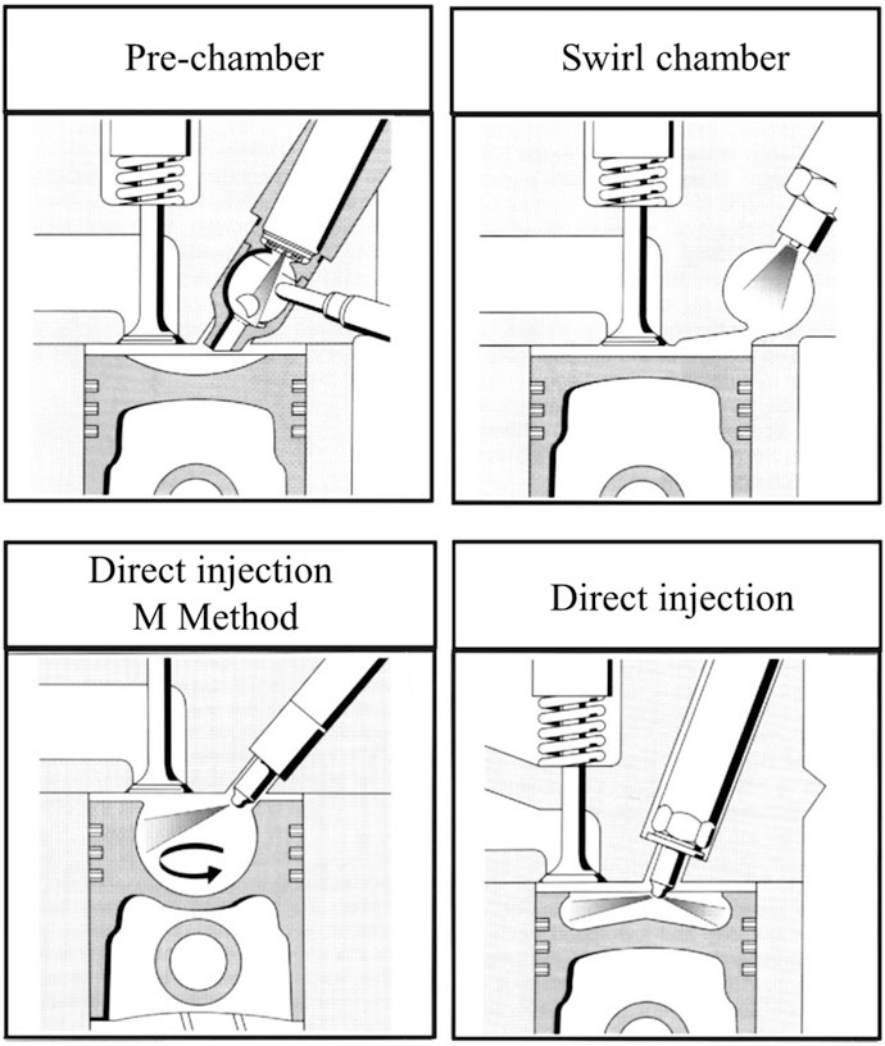

Fig. 2.59 Mixture formation methods in CI engines

The pump-injector units, as shown in Fig. 2.63, integrate both the pumping plunger and injector in the same housing; therefore, the fuel volume to be pressurized is much lower than in common rail systems, allowing pressure values of around 220 MPa. The reason for the higher pressure is the more effective compression work in a reduced fluid volume and the reduced deformation volumes of the fuel pipes or rail, which have a given elasticity.

On the other hand, higher pressure requires more precise fitting of pumping plunger and injector needle and, therefore, a more precise and expensive

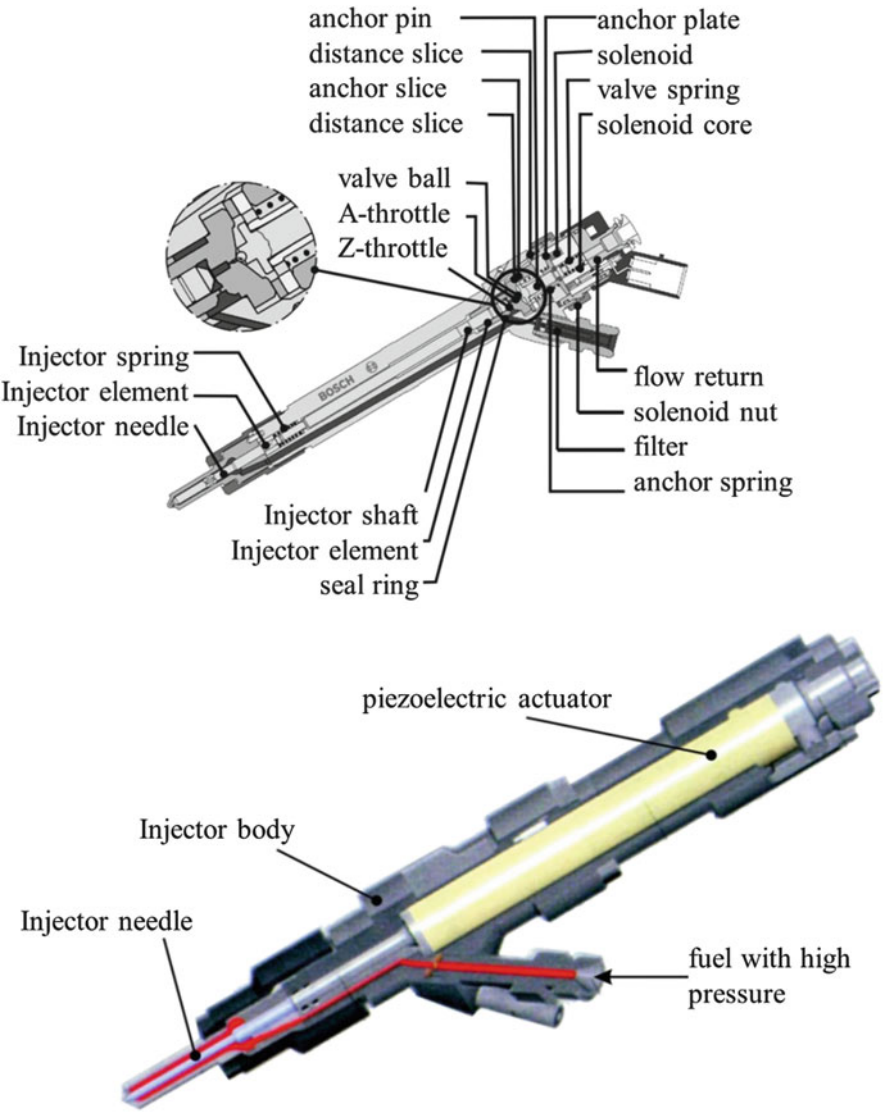

Fig. 2.60 Injectors with electromagnetic and piezoelectric/hydraulic actuation for direct injection systems in CI engines

manufacturing process than for common rail parts. Moreover, a pump-injector unit for each cylinder also leads to higher costs. A higher pressure has definite benefits in terms of fuel atomization and vaporization, influencing both fuel consumption and emission of pollutants. Nevertheless, modulation of injection rate as a function of load and speed (e.g., with five injection shots as for common rail systems) is not feasible because of pressure generation as a function of the driving cam profile,

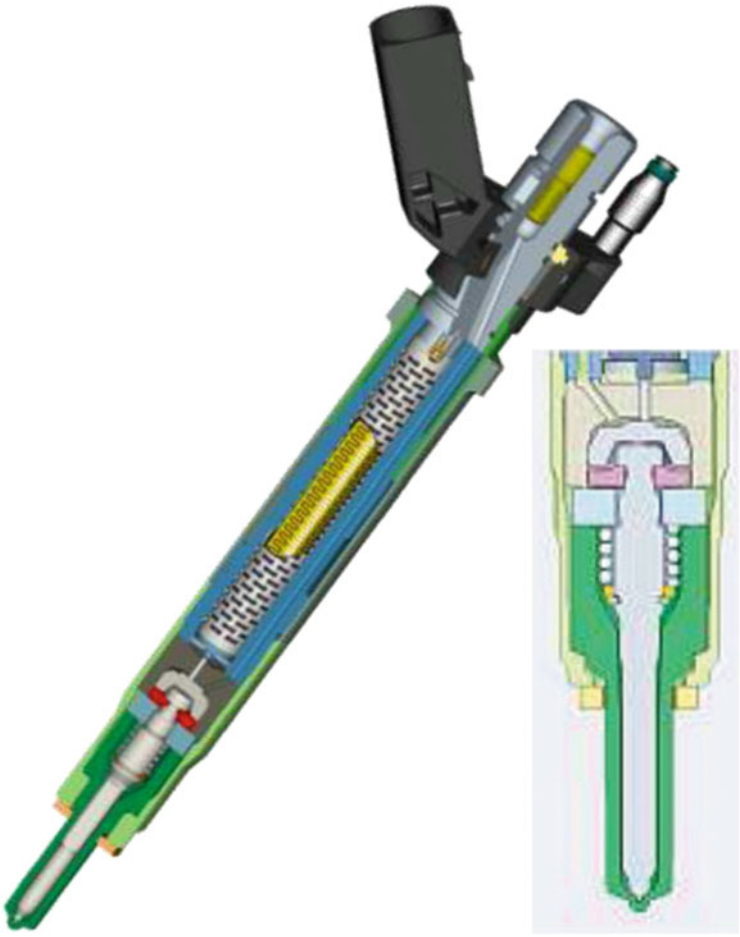

Fig. 2.61 Injector with direct mechanical contact between the stack of piezoelements and the injector needle (Continental) (Source: VDI)

which is geometrically given. However, the newly imposed limits on pollutant emissions worldwide require exact control of the combustion process by means of injection rate modulation. Therefore, in automobile diesel engines, the pump-injector unit concept has been completely replaced by common rail systems.

Adjustment of the momentary fuel/air ratio to load variation can improve the quality of mixture formation and combustion:

- In SI engines with low pressure injection in the intake duct, a steep load increase is obtained by rapid opening of the throttle. The difference between the densities of gasoline and air (in the range of 600:1) and the difference in the flow characteristics of fuel droplets and air cause inhomogeneities of the mixture

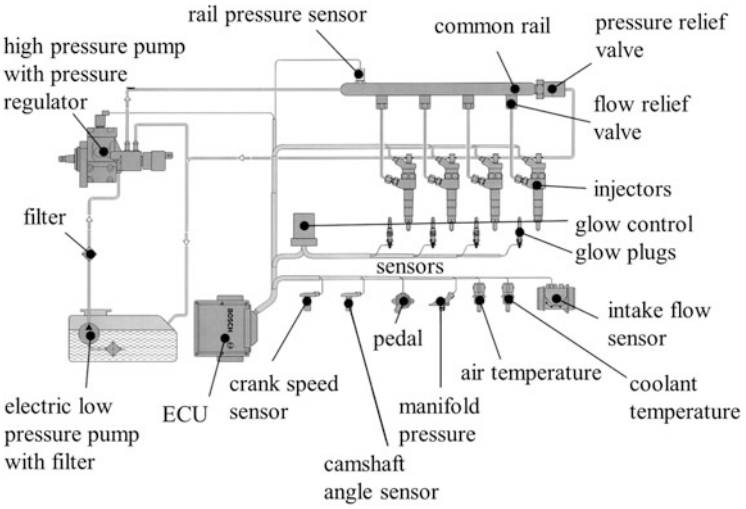

Fig. 2.62 Direct injection system with constant high pressure for CI engines (Common-Rail)

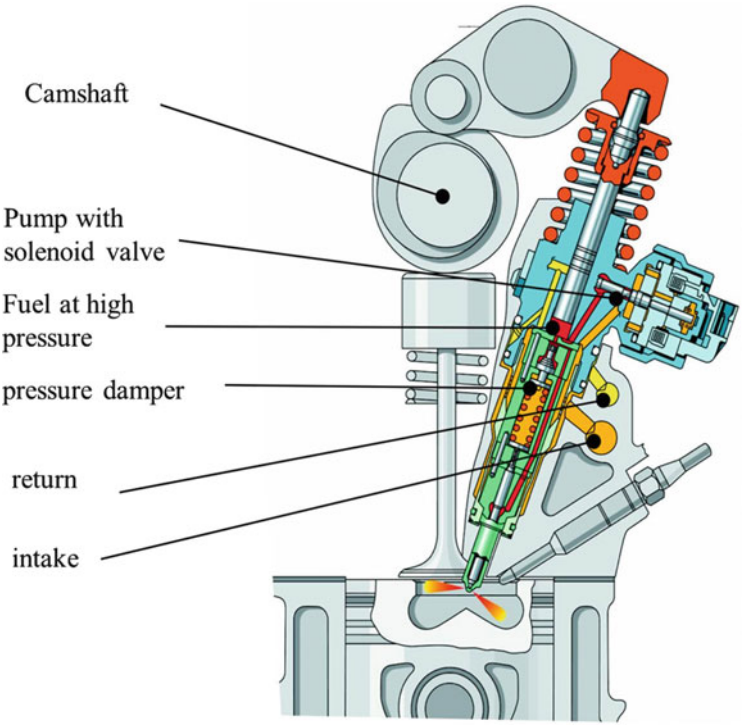

Fig. 2.63 Pump-injector unit

when the pressure between intake duct and cylinder is changed abruptly. In SI engines with gasoline direct injection and air throttling, this effect is accentuated. The increase in air mass entering the cylinder at steep throttle opening is moderate, because of the poor pressure difference between duct and cylinder. On the other hand, the fuel mass can be changed from minimum to maximum from one crankshaft revolution to the next. Consequently, the fuel mass must be adjusted during load variation controlled by the throttle as a function of the air flow.

- In CI engines and new SI engines with direct fuel injection without air throttling, the air mass in the cylinder remains constant, at a given speed, for every load. A rapid variation in load caused by changes in fuel mass from one cycle to the next is, like digestion, much more salubrious if the fuel is injected in small portions during an event. In diesel engines, five or more shots per cycle are usual. The relationship between injected mass, injection duration, and injection rate modulation must be optimized in terms of acceleration behavior, acoustics, pollutant emissions, and thermal efficiency.

Exhaust gas recirculation is realized in SI and CI engines as 5–70 % of the fresh charge mass. The recirculated burned gas mass is generally greater in the case of CI engines. Burned gas mass kept or recirculated to the cylinder separately from the fresh charge has advantages from different points of view:

- In SI engines at partial load, when the fuel mass is reduced, throttling of the aspirated air is required to obtain an inflammable mixture. A burned gas mass in a part of the cylinder volume leads to an increase in pressure within the cylinder during aspiration, improving scavenging work and, thus, thermal efficiency. Two-stroke engines with intake and exhaust port scavenging have such an advantage, whereby burned gas mass remains in the cylinder when the fresh mixture mass is throttled as a natural pressure balance when both intake and exhaust ports are opened.
- Burned gas mass within the cylinder partially impedes flame propagation in both CI and new SI engines with direct injection, as a measure to decrease the maximum combustion temperature, especially in very active exothermic centers where dissociation of combustion products into NO and NO_2 is very probable.
- Zones with hot burned gas in cylinders of CI and SI engines generate controllable self-ignition. Such zones activate exothermic centers to give fast combustion, avoiding dissociation and the formation of NO and NO_2. These mechanics are explained in the following section.

Exhaust gas recirculation is carried out via an external circuit, using backflow valves with redirection of exhaust gas into the intake ducts. Partial internal exhaust gas recirculation or, better, retention of partial burned gas within the combustion chamber can be obtained by the appropriate timing of exhaust and intake valves during scavenging, similar to the overlapping of exhaust and intake ducts in

two-stroke engines. Retention of partial burned gas is a very effective measure for reducing fuel consumption and pollutant emission.

2.2.1.5 Control of the Combustion Process in SI and CI Engines by Self-Ignition Techniques

The control of combustion by self-ignition shows advantages with respect to thermal efficiency, NO_x reduction, and process stability in both SI and CI engines [7]. As the main stage of energy conversion in an engine, the combustion process and its control play a determining role in the chain of process sequences. New self-ignition concepts are replacing the conventional forms of initiation and propagation of combustion in SI and CI engines. Figure 2.64 gives an overview of the applied methods.

Various self-ignition methods such as retention of burned gas, recirculation of exhaust gas, fuel additives, and heated intake pipes have been successfully applied at partial load operation of different engines. To qualify the effectiveness and controllability of various self-ignition methods, thermodynamic analysis followed by experimental validation is necessary.

Initiation of combustion in SI engines by external energy (e.g., by a spark) is succeeded by chain-like branching and propagation of the reaction within the fuel–air mixture, which is more or less homogeneous and isotropic. Each propagation from a single initiation center into a medium with homogeneous properties occurs as a diffusing front, and in combustion as a flame front. The high density of exothermic centers in such a thin front (as shown in Fig. 2.65) blocks heat transfer to the surrounding part with the same temperature level; thus, the heat is canalized

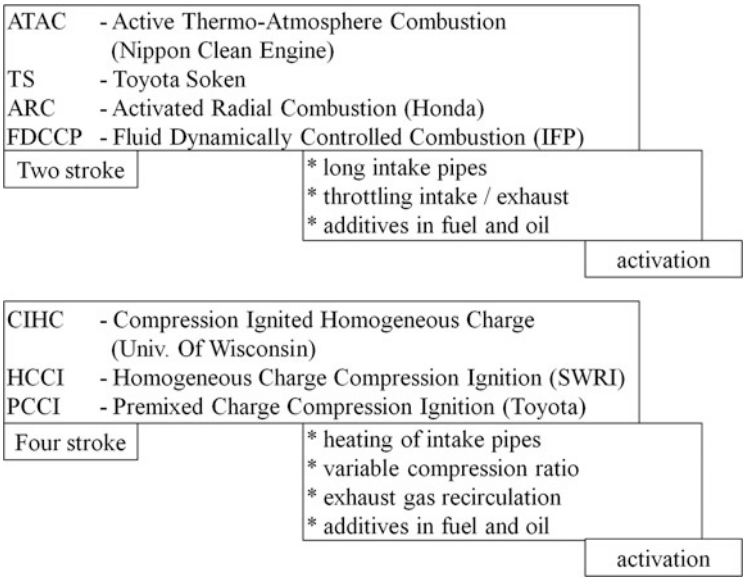

Fig. 2.64 Controlled self-ignition: most frequent methods

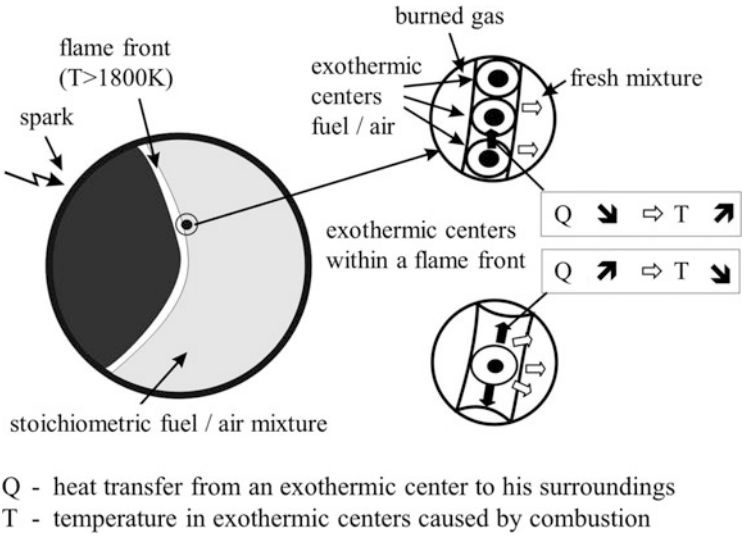

Fig. 2.65 Flame propagation into an isotropic, stoichiometric fuel–air mixture

to the fresh mixture, causing a steep temperature increase in the flame front. The corresponding increase in internal energy, representing the kinetic energy of molecules, occasionally leads to the disruption of molecules resulting from combustion; thus, the main products can form dissociation radicals, which are the seeds for new molecules such as NO or NO_2.

Therefore, a certain distance between exothermic centers for a fuel–air mixture, as shown in Fig. 2.65, is beneficial for the heat transfer of each center in its proximate vicinity. The temperature generated by combustion in such a relaxed front can remain under the dissociation level. Nevertheless, each solved problem often generates a new problem: the internal energy of the flame front, which leads partially to dissociation, is also the source of reaction initiation in further exothermic centers as a form of transmission of the spark energy.

Increasing the distance between exothermic centers leads to a decrease in heat transfer intensity from one center to the next, because of the low temperature of the medium between centers. Therefore, an ideal support for the combustion process is obtained when the temperature of the medium between the centers is high enough to transport heat from one center to the next, but low enough to avoid dissociation. Obviously, the lower limit is given when using a fuel with additives. In other cases, media that can transfer the heat for reaction are dispersed homogeneously within the combustion chamber. Some examples are given in Fig. 2.66.

A basic possibility is filling the volume between exothermic centers with already burned gas, at a temperature high enough for chain-like propagation of the reaction, generally over 1000 K. Such methods have been developed under different names, as cited in Fig. 2.64.

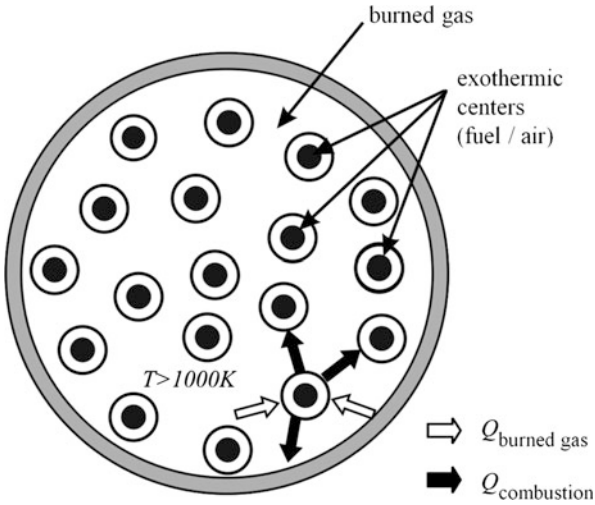

Fig. 2.66 Control of combustion by self-ignition in exothermic centers distributed isotropically within a burned gas volume

Combustion by self-ignition without diffusion and without propagation of the flame front is based on the same physical and chemical processes but at very different levels of pressure and temperature. Homogeneous charge compression ignition (HCCI) is a very popular method, but not very exact if applied to the CI process in diesel engines. The method consists of the distribution of exothermic centers within a mass of burned gas, and not in the generation of a homogeneous charge. Moreover, compression ignition is not given as a process per se; thus, a better designation of this method could be "ignition of exothermic centers that are isotropically dispersed by burned gas," as illustrated in Fig. 2.66. However, such designation seems to be too long, but is also restrictive because the burned gas is not the only reaction transmitter that can be used. Therefore, the designation "control of combustion by self-ignition" is more realistic, taking into account other process possibilities. The ignition of stochastically dispersed exothermic centers (in an ideal form, isotropically dispersed) using burned gas is generally applicable in both SI and CI engines.

An alternative method for the ignition of dispersed exothermic centers involves injection of a small amount of light flammable fuel into the compressed fuel–air mixture, instead of the use of burned gas [8]. This method is sometimes named "pilot injection," as for the injection of a shot of diesel fuel into a mixture of methane and air (see Fig. 2.67).

This approach confirms the benefits of combustion control by self-ignition, such as a remarkable decrease in NO_x emission. The hot walls of the combustion chamber, as created by roughness, combustion chamber design, or material combustion, also form large ignition areas. At a comparable temperature at combustion initiation, a spatial distribution of ignition sources around exothermic centers (such as created with burned gas or by pilot combustion) is more effective than

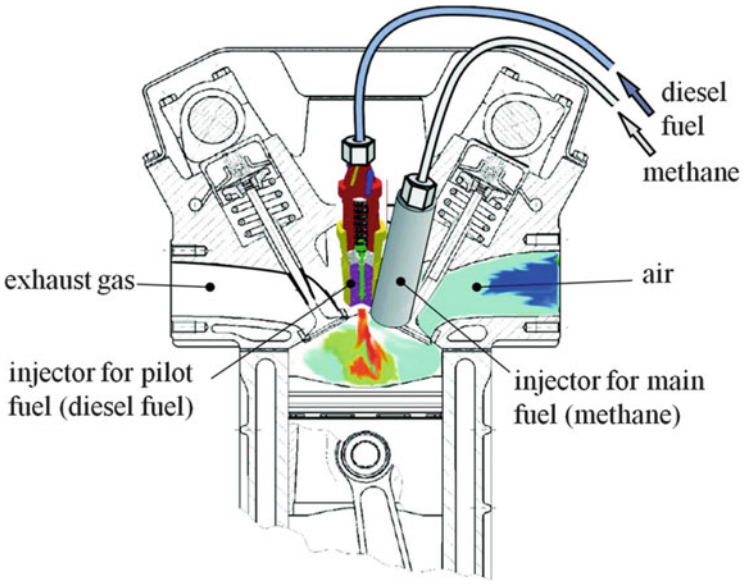

Fig. 2.67 Pilot injection of diesel fuel into a mixture of methane and air

propagation involving peripheral contact with exothermic centers. On the other hand, it is not a disadvantage when combining both forms.

The classic form of self-ignition is the enveloping of exothermic centers in hot air, as during compression in diesel engines. The temperature of compressed air is lower than the temperature of the alternatively used burned gas, which impairs the combustion process, leading to soot formation or unburned HC emission. On the other hand, the use of compressed hot air is restricted in SI engines by the knock limit.

In all the discussed forms, turbulence of the medium between the exothermic centers, but without disturbance of the isotropic distribution, is advantageous for the combustion process. However, self-ignition in exothermic centers seems to be disadvantageous, at least for SI engines, in terms of heat release, compared with propagation of a flame front from a spark source. This behavior is illustrated in Fig. 2.68.

The initiation of combustion in exothermic centers by heat transfer (e.g., from the surrounding burned gas) occurs at a lower temperature than if using an external spark source, resulting in lower velocity of the thermochemical reaction. The difference between the classic processes of spark ignition and compression ignition in gasoline and diesel engines is a good example of this.

A low gradient of heat release leads to deviation of the transformation of state from the isochoric limit to the isobaric limit. The effect of this deviation, under comparable conditions of ambient pressure, temperature and humidity, compression ratio, and engine speed, is a decrease in thermal efficiency. On the other hand,

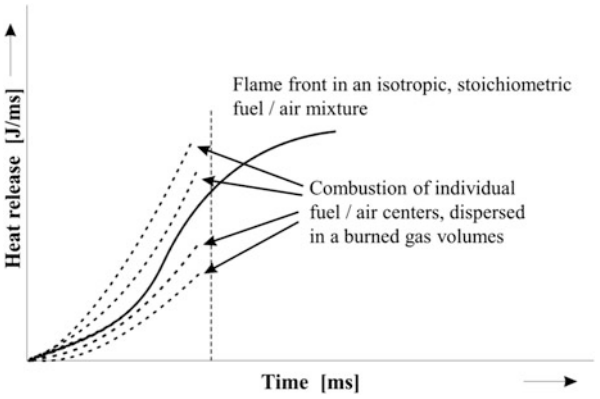

Fig. 2.68 Comparison of time-related heat release for combustion with flame front and by self-ignition of individual exothermic centers

considering that the initiation energy appears concomitantly in each of the exothermic centers, the global transformation of state is different to that in each center. The time-related heat release in each center is obviously slower than the reaction in a flame front, but occurs at the same time in all centers, as shown in Fig. 2.68. The reaction in each center takes place over a short distance and short time. Superposition of the curves from each center leads to the global time-related heat release, which tends to an isochore. The thermal efficiency is higher for concomitant combustion in each center than for combustion with a flame front. Moreover, the greater distance between exothermic centers, separated for example by previously burned gas, leads to heat transfer in that it amortizes the steep temperature increase during combustion. Combustion with steep time-related heat release, with the amortization of combustion temperature, results in a similar or higher pressure peak than for combustion with a flame front but at smaller specific volume (see Fig. 2.69). A comparable specific cycle work is thus obtainable with a lower value of maximum temperature, as a measure to avoid dissociation.

The control of combustion by self-ignition not only has the benefit of avoiding dissociation, but also gives a stable combustion process, without cyclic fluctuations. This can be explained by the high probability of a large contact surface with a hot medium, in comparison with the point contact obtained with a spark.

Contact of the fresh fuel–air mixture with the spark point can be lost by variation of load and speed. In the case of gasoline direct injection at partial load, controlled self-ignition is a net benefit. For this configuration with initially separate flows of air and fuel, it is difficult to obtain (in the first stage) sufficient mixture formation in a zone of the combustion chamber, and (in the second phase) to transport this mixture to a far point on the chamber wall, where the spark occurs.

A limit to self-ignition by burned gas appears at the transition from partial load to full load, when the fresh air mass increases and the burned gas mass decreases. The zero point is given at full load, which requires the maximum mass of fresh air. Nevertheless, there is the possibility of pilot injection of another fuel, generating

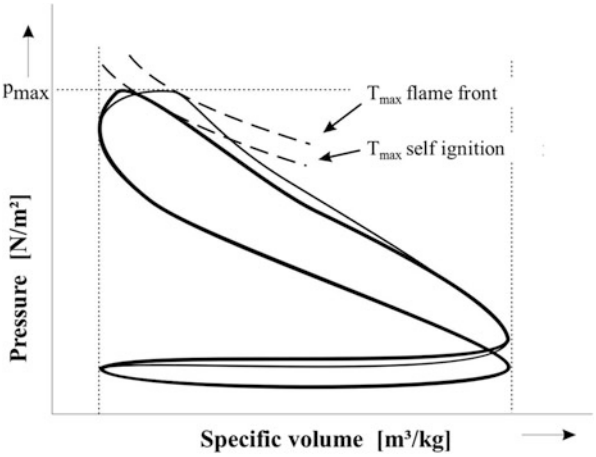

Fig. 2.69 Comparison of the thermodynamic cycles for an engine with combustion with flame front and by self-ignition

combustion in a zone of the cylinder and its contact with the fresh mixture. Self-ignition using burned gas at partial load is exemplified in Fig. 2.70.

In the classic process in an SI engine, the decrease in fuel mass corresponding to the level of partial load to be obtained imposes a proportional decrease in air mass for a constant fuel/air ratio. The air mass is generally reduced by throttling in the intake duct. A lower mass entering the same cylinder volume leads to a decrease in density. Thus, the distance between exothermic centers increases, as illustrated in Fig. 2.70a. The effect is a deceleration of the burning rate. This disadvantage can be avoided by keeping a mass of burned gas within the cylinder, effected by throttling in the exhaust duct. In this mode, only a partial volume for fresh air mass remains within the cylinder. Thus, the fresh charge density can be kept at a high level and the propagation of combustion is not impaired. The more the burned gas mass increases, the larger is the contact area with the fresh mass, stimulating self-ignition. An interesting alternative consists of the aspiration of fresh charge in the form of traces that penetrate the burned gas within the cylinder, giving a maximum contact area, as shown in Fig. 2.70c. This configuration has experimentally shown a good potential for optimization.

Fuels with high oxygen content, such as dimethylether (DME) and alcohols (methanol, ethanol) are very suitable for controlled self-ignition. Moreover, a high compression ratio and high engine speed both favor controlled self-ignition, the latter because of the lower heat transfer to the combustion chamber walls during the shorter time of mixture formation. The influence of burning gas mass on controlled self-ignition is the subject of extended 3D simulations and experimental analysis using fuels such as hydrogen, methane, heptane, iso-octane, and ethanol [9]. Controlled self-ignition favors thermodynamic processes in SI and CI engines, in terms of high efficiency and reduced NO_x formation.

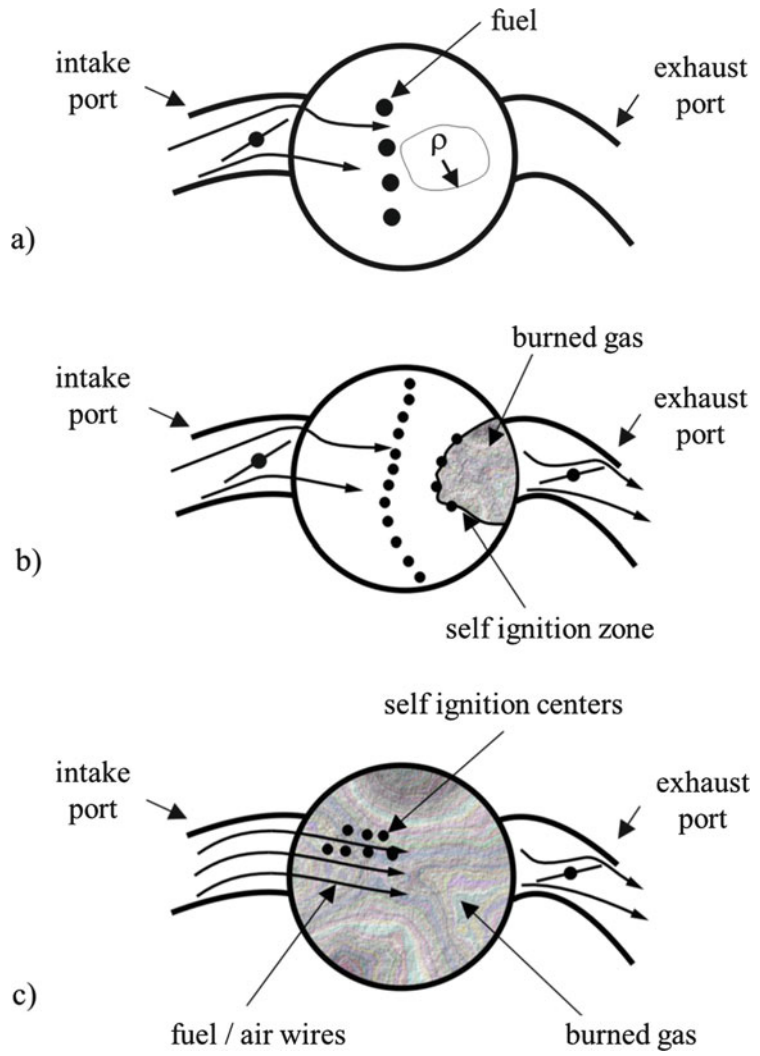

Fig. 2.70 Mixture formation at partial load: (**a**) throttling of fresh mixture, (**b**) retaining burned gas by exhaust port throttling, (**c**) intrusion of fuel–air wires into a burned gas volume

2.2.1.6 Increase in Compression Ratio

The advantages of increasing the compression ratio, especially for SI engines, were discussed from the point of view of the thermodynamic cycle in Sect. 2.1, and their realization, favored by direct fuel injection, was argued in Sect. 2.2. It was also mentioned, that the tendency to increase engine speed leads to an increase in the bore/stroke ratio, a situation that limits the increase in compression ratio. In SI engines, an increase in compression ratio at partial load leads to a decrease in combustion chamber volume, which is a means of maintaining a fresh mixture

density more or less at the level corresponding to full load, when the air is throttled. Such a solution is presented in Fig. 2.71.

A tilting device moves the cylinder block, including the engine head. For the same piston course, resulting from the invariable crank mechanism, the height of combustion chamber varies with the inclination of the block. This solution is shown in Fig. 2.72. Other solutions provide displacement of the crankshaft position in the main stock location, for a fixed cylinder block. Irrespective of such complicated mechanical solutions, the high density of the fresh mixture at partial load is obtained by increasing the burned gas mass within the cylinder, as discussed.

2.2.1.7 Management of Engine Cooling

It is generally considered that only a third of the heat input into a piston engine is transformed into work, another third is ejected as burned gas, and the last third is lost as heat transfer through the cooling circuit.

The improvement measures discussed in this section are related to the first third, the transformation of heat into work, and to the second third, utilization of exhaust gas in turbines. The loss of heat by cooling has been more or less neglected until now. Management between engine and cooling circuit has appeared recently in the opposite direction: water in the cooling system is occasionally heated by an external combustion system to warm the engine at start. The advantages are noticeable: increased torque, reduced consumption and pollutant emissions, and reduced friction of the moving parts. After reaching operating temperature, the engine gives about a third of the generated heat to the surroundings through the cooling system. A simple example shows the magnitude of this loss. Using a water pump of 60 l/min at a water density of 1 kg/l, a temperature drop of 10 °C at a specific heat value of the water of $c_p = 4.19$ kJ/kg K leads to a power loss as follows:

$$P = \dot{V} \cdot \rho \cdot c_p \cdot \Delta T = \frac{60}{60} \cdot 1 \cdot 4.19 \cdot 10$$

$$[\mathrm{KW}] \quad \left[\frac{\mathrm{l}}{\mathrm{s}}\right] \left[\frac{\mathrm{kg}}{\mathrm{l}}\right] \left[\frac{\mathrm{kJ}}{\mathrm{kgK}}\right] [\mathrm{K}] \tag{2.18}$$

$$P = 41.9 \ \mathrm{kW}$$

Furthermore, a considerable problem is actuation of the water pump by the engine itself, as a function of engine speed. Therefore, the volume flow of the coolant is strongly speed dependent; a load-dependent adjustment is very limited. A better alternative is actuation of the pump electrically, with speed control as a function of the momentary load–speed combination, for optimum operation between cooling effect and engine efficiency. Such applications are increasingly being introduced in series production of advanced four- and six-cylinder engines. The necessary electric power is 200–400 W. In addition to the benefit of reduced heat losses by cooling, electric control of the pump leads to a decrease in power input of up to 90 %. On the other hand, utilization of the enthalpy of the heated

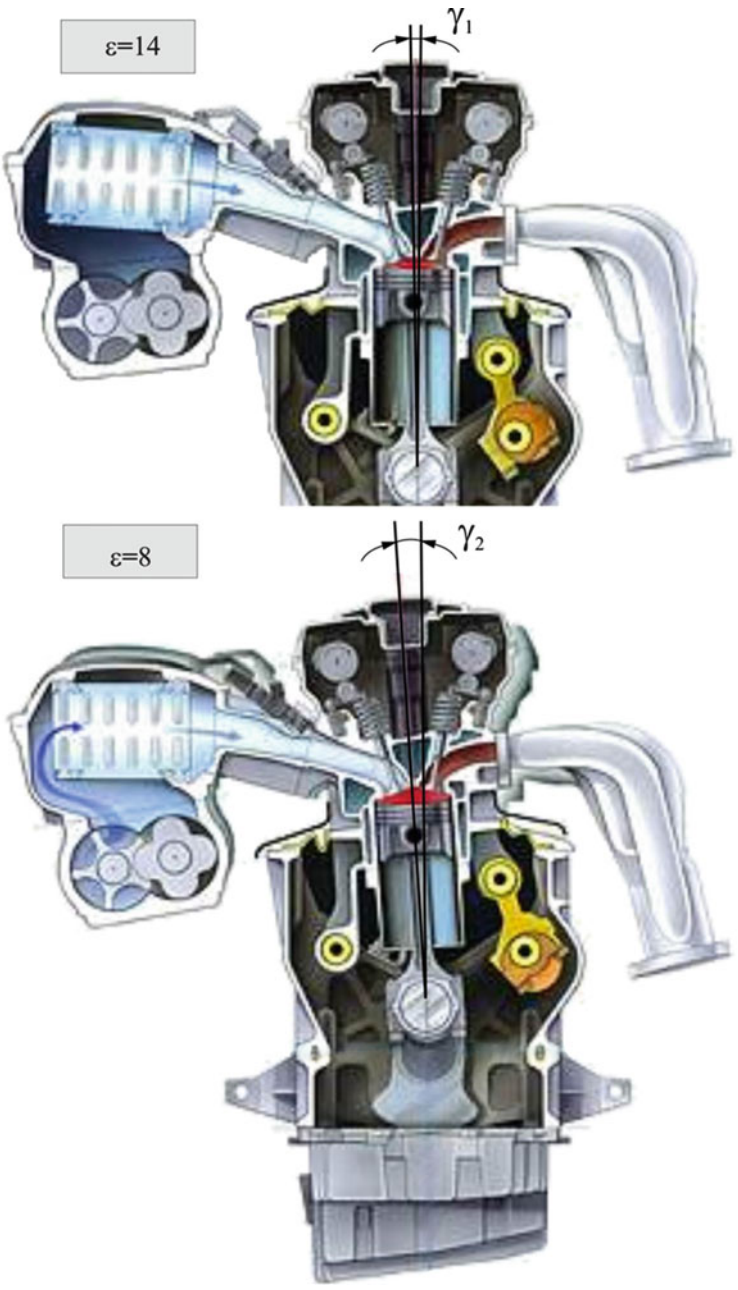

Fig. 2.71 Variable compression ratio, SVC (Saab variable compression)-cross section

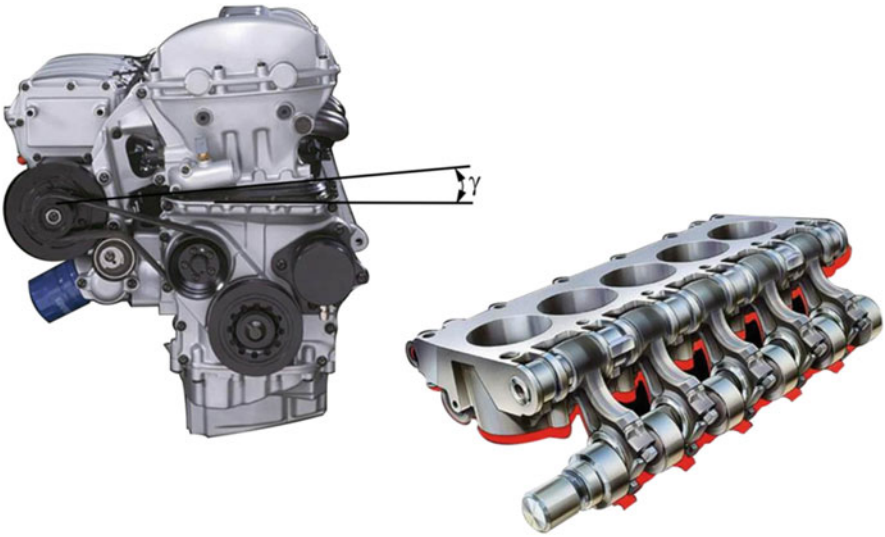

Fig. 2.72 Variable compression ratio, SVC (Saab variable compression)-view

coolant in the heat exchanger of a secondary power circuit can improve the total efficiency of the system.

The presented measures for the optimization of process sequences in SI and CI engines and for their adjustment to variable combinations of load and speed have the potential for fuel economy of around 50 %.

2.2.2 Convergence of Processes in SI and CI Engines

SI and CI engines have as common development targets an increase in the power-to-volume ratio, with a significant decrease in specific fuel consumption and pollutant emission. However, these targets are not a priori the reason for a convergence of the SI and CI processes: the advantageous speed characteristic of a SI engine meets the advantageous torque characteristic of a CI engine, as two excellent paths to the same power. However, a choice is imposed: quietness or fuel economy and HC or NO_x and particulate emissions. Such characteristic behavior is the reason for the polarization of acceptance for one or both. On the other hand, each innovation in the field of engines takes place with or without scientific comparison between both species. Super- or turbocharging, direct fuel injection, exhaust gas recirculation, and controlled self-ignition are representative examples in this sense. In this way, there is not only an improvement in separate process sequences, there also seem to be interrelations that influence the quality of the whole process [10]. The dynamic of innovations in the field of technical solutions and methods strongly recommends analysis of the generated thermodynamic behavior, following the process phases of scavenging, fuel injection, mixture formation, and combustion. Some of the seminal solutions are illustrated in Fig. 2.73.

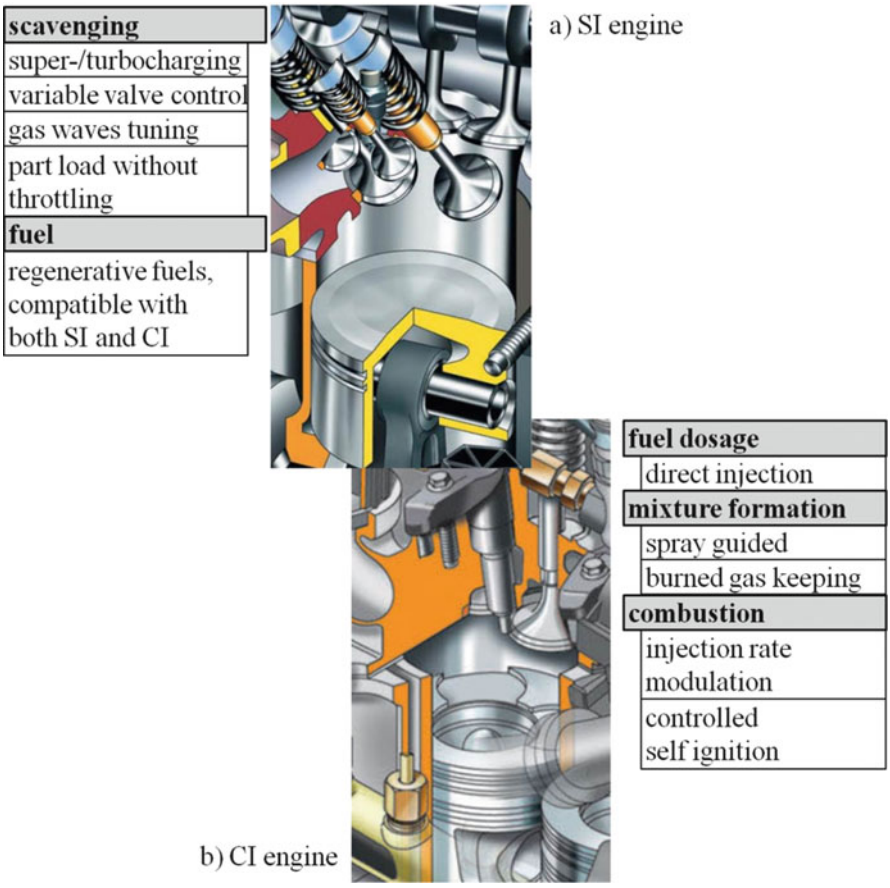

Fig. 2.73 Criteria for convergence of SI and CI processes

A representative example of transferable functions between SI and CI engines is the coupling of air mass charging and direct fuel injection. For diesel engines, turbocharging was the state of the art for a longer time; however, after a hesitant start this technique has now been successfully introduced for gasoline engines. Direct fuel injection in SI engines , has the aim of avoiding throttling, which is similar to its application in CI engines. The effect of such measures, as a causal chain, is an increasing similarity of the thermodynamic processes of both species, which promises interesting development potential.

An ideal SI cycle with a compression ratio of 13.8 and a CI cycle with a compression ratio of 22 have, as calculated in Sect. 2.1, the same thermal efficiency. Advanced concepts for internal mixture formation with mixture stratification and controlled self-ignition allow such an increment in the compression ratio for SI engines, whereas a value of 22 is now old for CI engines. The reduction in

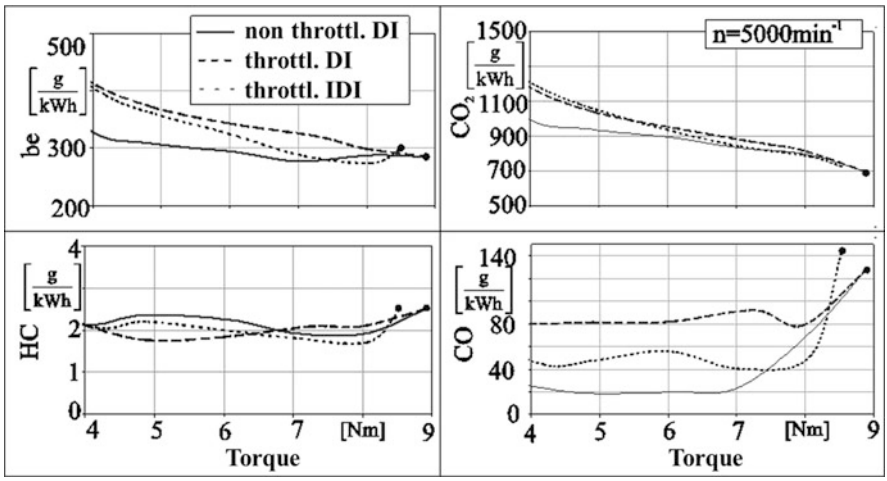

Fig. 2.74 bsfc, CO_2, CO, and HC for constant speed and different loads in SI engines with compression ratios of 15.4:1(direct injection, *DI*) and 11.5:1 (intake duct injection, *IDI*)

NO_x emissions imposes, for the moment, values of 15.5, to the detriment of thermal efficiency.

Figure 2.74 shows the curves for bsfc, CO_2, CO, and HC for an SI engine with direct injection compared with those for injection into the intake duct [10]. The direct injection is configured for stable mixture stratification, which allows an increase in compression ratio from 11.5 (intake duct injection) to 15.4. At such a high level of compression, the thermal efficiency converges to that of a diesel engine, as a result of the steep pressure rise caused by faster combustion.

A classic disadvantage in the cycle of a SI engine results from air throttling in the intake duct at partial load, leading to an increase in scavenging work; furthermore, the mixture density in a cylinder with constant volume decreases with lower mixture mass, impairing the flame front velocity and, consequently, the cycle work. This relationship is presented in Fig. 2.75.

The impairment in thermal efficiency as a result of throttling is mainly caused by downgraded combustion rather than by increased scavenging work, as shown in Fig. 2.75. Magnification of the scavenging cycle shows an increase in the surface corresponding to the scavenging work when throttling for partial load. On the other hand, the representation of the dependence of specific work on crank angle shows that the scavenging work is negligible in comparison with the work generated by combustion, at 20–30° CA after TDC, when changing the load. The sequence at 20° CA after TDC from full load to partial load shows the slow-down of combustion within the mixture with lower density, causing a flattening of the work curve.

Figure 2.75 also shows that air throttling also impairs the performance if the intake duct injection is replaced by direct injection. In this case, the impairment is provoked by the difficulties in obtaining a homogeneous mixture. On the other hand, throttling is a disadvantage for acceleration, which requires a steep torque

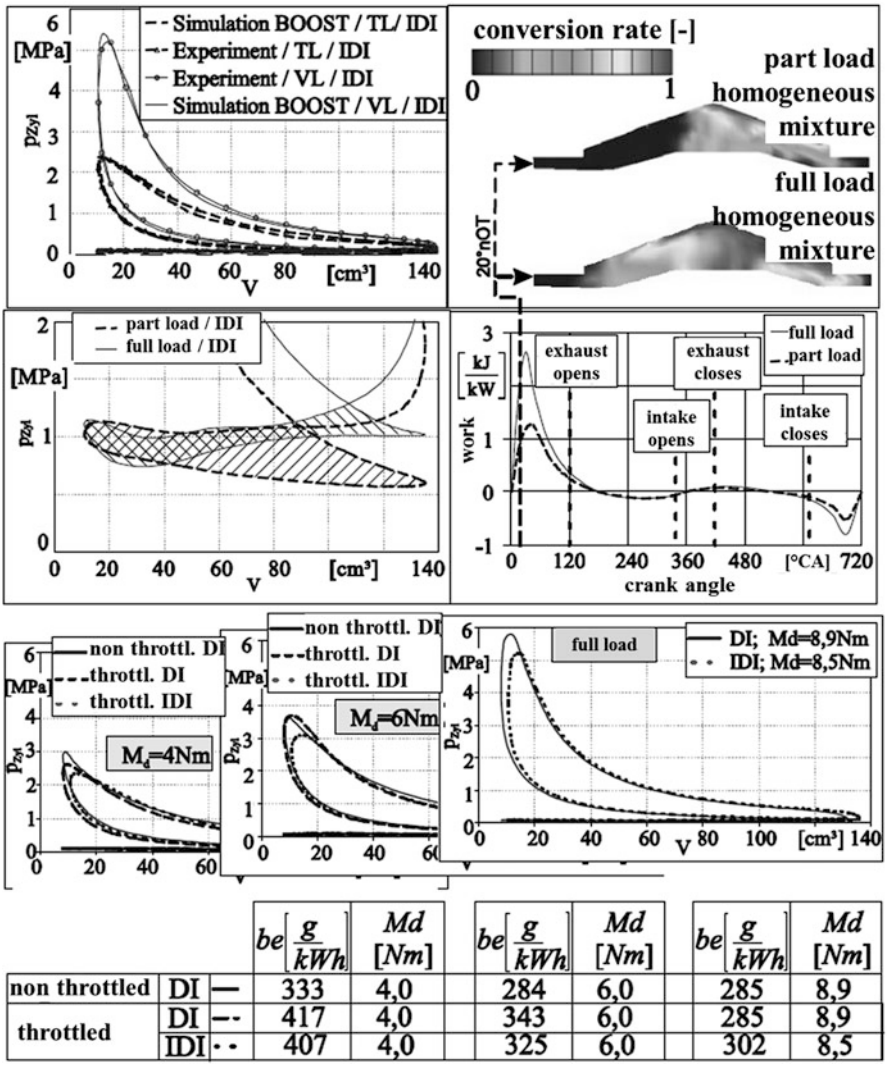

			be [g/kWh]	Md [Nm]	be [g/kWh]	Md [Nm]	be [g/kWh]	Md [Nm]
non throttled	DI	—	333	4,0	284	6,0	285	8,9
throttled	DI	– –	417	4,0	343	6,0	285	8,9
	IDI	· ·	407	4,0	325	6,0	302	8,5

Fig. 2.75 Impairment of the thermal efficiency of an SI engine provoked by throttling from full to partial load, deduced from the measured work during combustion and scavenging

increase: the necessary increase in air mass flow occurs only after a number of crank rotations, because of the very small difference in pressure between the air in the intake duct and in the cylinder during aspiration. The superposition of throttling also impairs this process in comparison with non-throttled aspiration at full and partial load, such as in CI engines. This also explains the difficulties in adjusting turbocharging to an SI engine, in comparison with this adaptation for CI engines:

the slower load increase when opening the throttle leads to a slower build-up of turbine enthalpy, which is necessary for actuating the compressor.

The availability of a constant maximum air mass within the cylinder at a given speed for every load leads to a shorter delay between part and full load: the amount of fuel injected into the combustion chamber can be varied from minimum to maximum between two consecutive crank rotations, which results from the high fuel pressure at direct injection. The elimination of throttling can be realized in SI engines with direct injection if mixture stratification can be generated and controlled at every load and speed combination.

Figure 2.74 illustrates some results from applying direct fuel injection in an SI engine without throttling (as shown in Fig. 2.45). For both SI and CI engines, turbocharging, as platform for downsizing, leads to an additional increase in thermal efficiency. The technical features are similar for both species. However, the application of turbocharging together with direct injection requires a load- and speed-dependent control of intake and exhausts valves for both SI and CI engines. This is an additional point of convergence. Furthermore, both SI and CI engines utilize similar direct injection systems, despite the different pressure levels until now, and similar techniques of internal mixture formation, based mostly on spray-guidance.

Generating a constant pressure at maximum level for all cylinders in a common rail (as shown in Fig. 2.49) means that control of the injected mass is possible only by varying the injection duration. This requires separate actuation of the injector, other than by the fuel pressure itself. There are both electromagnetic and piezoelectric devices for this. All parts and components of such a direct injection system are similar for application in both SI and CI engines, despite the different pressure levels. For generate a fuel high-pressure wave that is not dependent on engine speed, as shown in Figs. 2.50 and 2.51, the duration of the pressure mass is given by the pressure amplitude. The fuel atomization depends mainly on the pressure rise and not on the pressure amplitude; therefore, control of the injected mass by pressure amplitude is not disadvantageous for the fuel spray characteristics. On the other hand, a constant injection duration, resulting from a constant pressure wave duration when changing the load, is very advantageous for mixture formation. The injector opening and closing is actuated in this case by the pressure wave, making electromagnetic or piezoelectric devices superfluous. The other modules of the injection system are similar for both SI and CI engines. In CI engines, the combustion process is generally optimized between bsfc and NO_x. The injection rate modulation and control of exhaust gas recirculation as a function of load and speed are effective measures in this sense. The development of direct injection for SI engines follows a similar path. Controlled self-ignition or HCCI has been transferred in the opposite direction from SI to CI engines for a similar reason, NO_x reduction. The ignition of an exothermic center consisting of fuel with an air envelope, by its peripheral contact with a hot gas, has been initially introduced in CI engines, the hot gas being compressed air in this case. The fact that the global air/fuel ratio is much higher in this case than in the exothermic centers is a good base for developing direct injection techniques for SI engines; mixture stratification

is no longer necessary. On the other hand, the contact of a homogeneous, stoichiometric fuel–air mixture with the spark plug at every load and speed combination is essential.

Ignition in exothermic centers within the combustion chamber using burned gas enthalpy is the basis for three points of convergence for SI and CI cycles at partial load:

- Initiation of combustion without external spark sources (glow plugs are favored in both processes)
- Similar behavior of the burning rate, resulting from a similar injection rate modulation and from the combustion within exothermic centers, without flame front.
- Control of inducted heat solely by the fuel mass, without throttling of the air mass, independent of the load.

At full load, combustion can be initiated for both SI and CI processes by injection of a small amount of an additional fuel, similar to the process of diesel pilot injection in gas engines; this accelerates the combustion and leads to a remarkable reduction in NO_x. The chemical structures of the hydrocarbons used as gasoline and diesel fuel are similar, independent of their viscosity, density, or boiling point.

The new methods of mixture formation and combustion require new consideration of cetane and octane numbers, describing the ignitable state and the knock. Synthetic fuels such as SunFuel can be designed with a well-defined molecular structure, determining all properties from density and viscosity to knock resistance.

The first stage of such fuel design is the production of SunFuel from natural gas using the gas-to-liquid method. Experiments with SunFuel show a drastic decrease in HC, CO, and particulate emissions in comparison with the utilization of classic fuel. The next stage is the production of SunFuel from regenerative energy resources and from waste from the wood and paper industry. The intermediate stage is a synthetic gas, which is the basis for design of the molecular structure of the resulting fuel. This is a strong argument for the convergence of SI and CI processes. Both SI and CI engines must achieve the same performances, from the power-to-volume ratio and bsfc to the reduction in pollutant emission. Thus, a convergence of functions and modules would be beneficial.

Nevertheless, standardization of a universal piston engine for all car types and classes cannot be expected for the next few years, because of the remaining differences regarding torque characteristics, price, and consumption in traffic. In the last few decades diesel engines have been twice the price of gasoline engines for the same power. The maximum torque of a diesel engine is available at lower engine speed than in gasoline engines, the difference being roughly 2000 min^{-1} against 4000 min^{-1}. An expensive and heavy diesel engine with high torque just after idle is suitable for heavy and expensive limousines; sufficient acceleration in urban areas and on highways is available at moderate fuel consumption.

About 20 years ago, diesel engines were more or less associated with tractors, not with cars in the luxury class. On the other hand, cheap and light cars require compact and cheap SI engines; the maximum torque at higher engine speed is not a serious impediment at a low car mass. A standardized engine combining the advantages of SI and CI species has wide application for the middle class of cars. A future scenario could be as follows:

- For the upper class of cars: CI engines with a swept volume of about 2.5 l and four cylinders
- For the middle class of cars: standardized engines with SI and CI elements, with a swept volume of about 1.5 l and three cylinders
- For compact and cheap cars: SI engines with a swept volume of about 0.8 l and two cylinders

2.3 Alternative Thermal Engines

2.3.1 Two-stroke Engines

The power-to-volume ratio of a piston engine can be augmented by the energy density (brake mean effective pressure, bmep) or by the engine speed. However, there is a third way, consisting of the number of working strokes per cylinder, as follows:

- in two-stroke engines, $\frac{T_U}{T_A} = \frac{2}{2}$

$$\frac{P_\mathrm{e}}{V_H} = w_\mathrm{e} \cdot n \cdot \frac{T_U}{T_A} \tag{2.9}$$

- in four-stroke engines, $\frac{T_U}{T_A} = \frac{2}{4}$

The change from four-stroke to two-stroke engines in principle leads to twice the power-to-volume ratio at same energy density and speed. A comparison between 201 four-stroke engines and 99 two-stroke engines for series two-wheelers of the last three decades shows the following situation:

- The speed range of four- and two-stroke engines is very similar.
- In two-stroke engines for such applications, the bmep is at maximum torque, but is 20–30 % lower at maximum power.

The comparison shows:

$$\left(\frac{P_\mathrm{e}}{V_H}\right)_{2T} = (0.7 - .0.8) w_{\mathrm{e}4T} \cdot n \qquad \left(\frac{P_\mathrm{e}}{V_H}\right)_{4T} = (0.5) w_{\mathrm{e}4T} \cdot n \tag{2.19}$$

$$\left(\frac{P_e}{V_H}\right)_{2T} = (1.4 - 1.6)\left(\frac{P_e}{V_H}\right)_{4T} \tag{2.20}$$

The advantage of a power-to-volume ratio that is 40–60 % higher for two-stroke engines is the reason for their use in bikes, scooters, outboard applications, and hand-held devices such as chain-saws. The main disadvantage of two-stroke engines in this domain is the much higher scavenging losses than in four-stroke engines, which explains the lower bmep. In low-speed diesel engines with large swept volume, as generally used in ships, the scavenging losses are practically no higher than in four-stroke engines.

High scavenging losses are a basic disadvantage of two-stroke engines if the mixture of fuel and air is formed before scavenging, in the intake duct, by the carburetor or by low-pressure fuel injection. In this case, the scavenging losses contain not only air but also unburned fuel, causing HC emissions above the limits. This disadvantage can be completely avoided if the fuel and air mixture is formed after scavenging, within the cylinder, by direct fuel injection.

For scavenging in two-stroke engines, there are three main methods [11, 12]:

- Scavenging is along the cylinder axis, with intake valves in the cylinder head and exhaust ports at the bottom of the cylinder or, inversely, with intake ports and exhaust valves. A special form is given in two-stroke engines with two opposite pistons in the same cylinder, with ports for intake and exhaust.
- Cross-scavenging, with intake and exhaust ports.
- Loop scavenging (or Schnuerle scavenging, according to the name of its inventor) is largely applied for two-wheeler, outboard and chain-saw engines. This is very interesting in combination with direct fuel injection for on-board current generation in automobiles with electric propulsion. The principle of loop scavenging is shown in Fig. 2.76. The fresh charge is directed to the cylinder through laterally disposed transfer ports.

The exhaust stroke and aspiration stroke in four-stroke engines are replaced by the following scavenging method:

– The exhaust port opens during piston expansion, provoking a drop in pressure of the burned gas, as illustrated in the scavenging diagram in Fig. 2.76.
– The fresh charge subsequently entering the cylinder must push out the burned gas through the exhaust port with an appropriate pressure. This fresh charge pressure can be generated by an external compressor, but in simple two-stroke engines such a solution is too expensive. Instead, the volume under the piston, in the crankcase, serves to pump the gas. A cross-section through a classic two-stroke engine for a motorcycle with loop scavenging and crankcase pump is shown in Fig. 2.77

The transfer ports are oriented to the engine head, leading the fresh charge flow to the top, where the flow front meets the volume of burned gas, pushing it down,

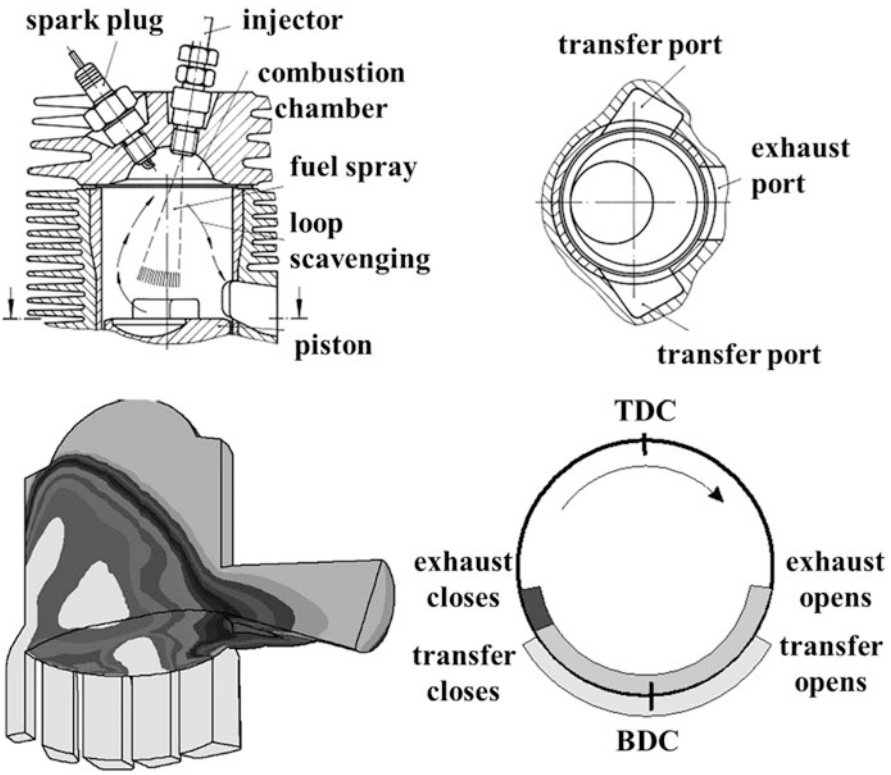

Fig. 2.76 Principle of loop scavenging in two-stroke engines with transfer and exhaust ports

on the opposite side, to the exhaust port. The looping should avoid a short circuit of the fresh mixture in a cross-flow between intake and exhaust ports. The other benefit of the loop is the transport of fresh charge to the combustion chamber. At partial load, the fresh charge mass is reduced by throttling within the intake duct. Consequently, more burned gas remains within the cylinder. This is advantageous for controlled self-ignition, as mentioned in Sect. 2.2. On the other hand, at the aspiration of fresh charge there is under-pressure in the cylinder (such as occurs in two-stroke engines) because of the burned gas mass, which increases with decreasing fresh gas mass. In this mode, the piston is charged with pressure up to the BDC, supporting the pumping work in the crankcase. The balance of these processes during scavenging results in good thermal efficiency compared with a four-stroke process during scavenging at partial load. However, a possible disadvantage of loop scavenging control by intake and exhaust ports is the required symmetry of opening and closing port valves, as shown in Fig. 2.76. After the closing of intake ports, the exhaust ports remain open for the given angle difference during fresh charge compression. An escape of fresh mixture through this window is damped by reflected, positive pressure waves from the exhaust pipe, which is similar to the

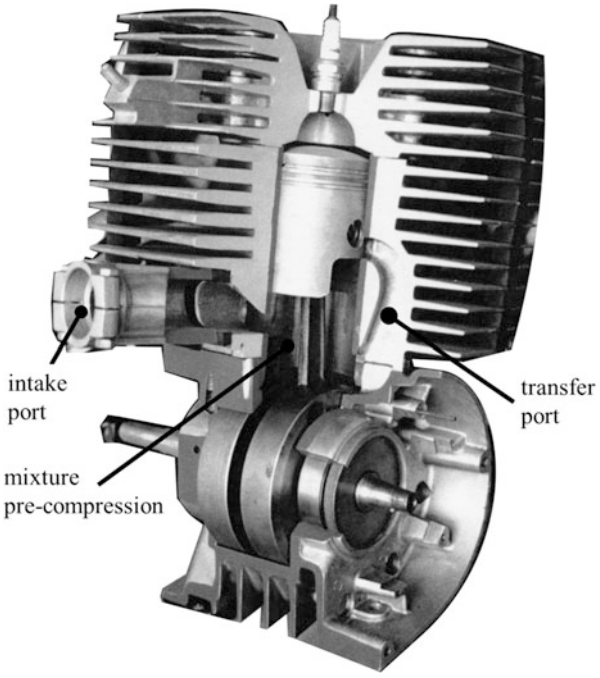

Fig. 2.77 Two-stroke engine with loop scavenging: section

process described in Sect. 2.2.1 (Fig. 2.22) in the case of waves in intake ducts. A closure of this window in every cycle by an obturator would be beneficial, but different solutions have so far not been successful. However, effective compensation is obtained by partial closure at low engine speed, when the time for a fresh mixture short circuit is longer. Figure 2.78 shows a solution consisting of a flat obturator.

The engine shown in Fig. 2.78 also has a one-way membrane in the intake duct to block the backflow of fresh mixture during its compression in the crank case. If such measures of scavenging improvement are completed by direct fuel injection into the cylinder after scavenging, the resulting bsfc and emissions compare favorably with those of four-stroke engines, but retain the advantages in terms of power-to-volume ratio. Direct fuel injection in two-stroke engines with loop scavenging has been very successfully applied for both liquid fuel injection and with fuel–air emulsion injection, as presented in Sect. 2.2.1, Figs. 2.48 and 2.51. Figure 2.79 shows the configuration of a direct injection system for a fuel–air emulsion (Orbital) in a two-stroke engine. The solution was adopted in the 1990s, showing remarkable success in Ford three-cylinder car engines in a large fleet test.

Figure 2.80 shows a scooter two-stroke engine with liquid fuel direct injection, using a system with fuel high-pressure modulation (Zwickau pressure pulse), as illustrated in Fig. 2.51. This solution was developed for Peugeot motorcycles and is shown in comparison with a basic two-stroke engine equipped with a carburetor following improvements: maximum torque increase of 10 %, bsfc decrease of

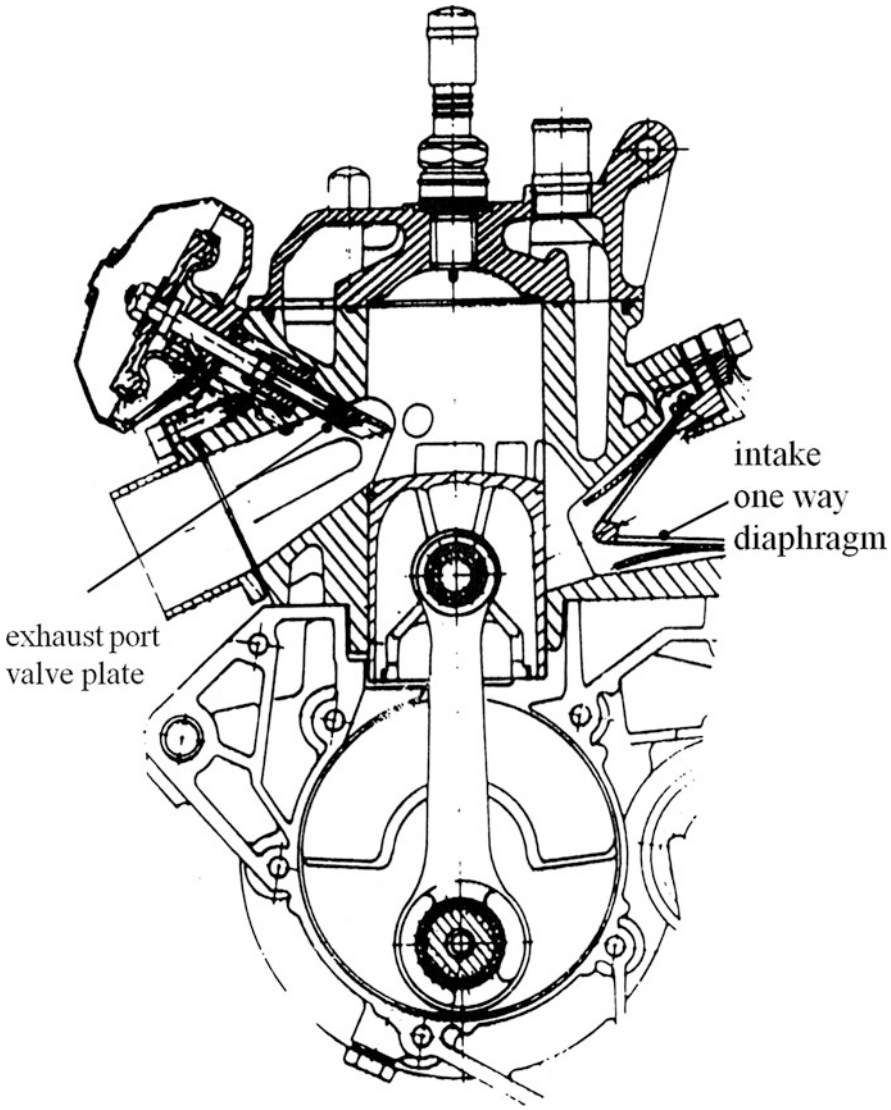

Fig. 2.78 Two-stroke engine with loop scavenging, intake one-way diaphragm, and exhaust port valve plate

35–45 %, HC emission reduction of 94 %, and CO emission reduction of 90 %. Expressed in absolute values, the minimum bsfc was 308 g/kW h, the minimum HC 13 g/kW h, and the minimum CO emission 10 g/kW h, values that are under those of four-stroke engines in the same class, with a swept volume of 50 cm^3 but with 60 % more power!

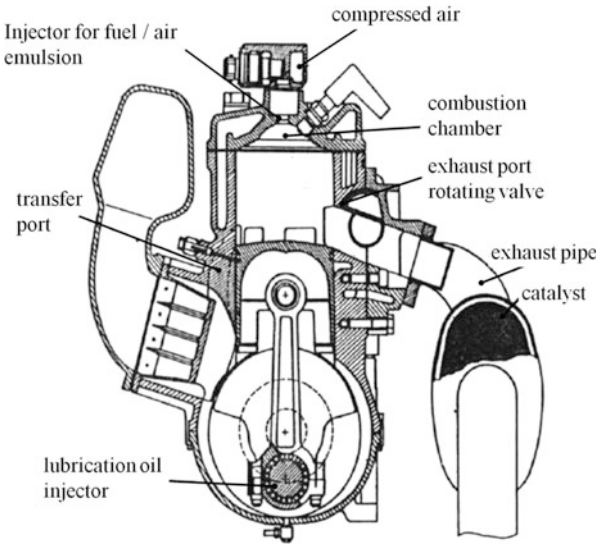

Fig. 2.79 Two-stroke engine with direct injection of a fuel–air emulsion (orbital method)

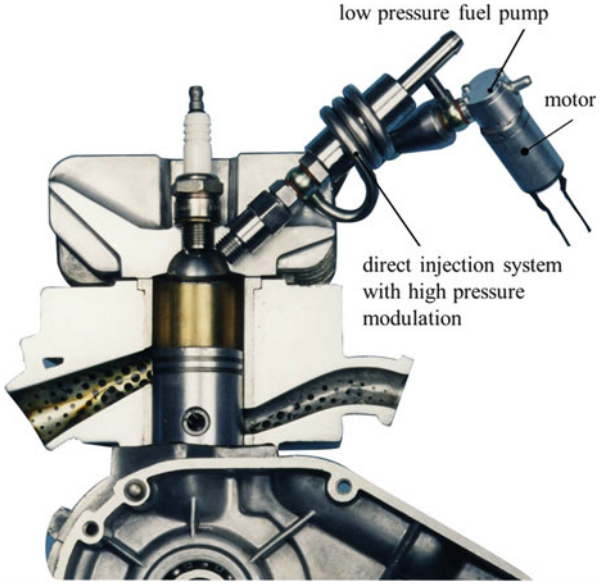

Fig. 2.80 Two-stroke engine with direct fuel injection by high pressure modulation (Zwickau pressure pulse)

A similar Zwickau pressure pulse direct injection system was applied to a gasoline two-stroke engine with opposite cylinders, with a swept volume of 200 cm^3, provided as current generator in cars with electric propulsion. This solution is presented in Chap. 5 in the frame of hybrid concepts.

Despite such excellent results with direct fuel injection in two-stroke engines for two-wheelers and in outboard engines, with many variants of injection systems and

engines, two-stroke engines have not been introduced in automobiles; moreover, they are disappearing more and more from two-wheelers and outboard applications. The reasons are various:

- With direct injection systems and parts for scavenging adjustment, two-stroke engines are no longer a cheap solution.
- The intake and exhaust ports in the cylinder liner provoke non-uniform thermal stresses, leading to liner deformation. Moreover, the piston rings run upon the edges of these ports. Both effects diminish the reliability and lifetime of two-stroke engines with ports.
- The induction of fresh charge (in the case of direct fuel injection, this is pure air) through the crankcase impedes oil lubrication with systems that are applied in four-stroke engines. The oil is injected to the bearings with small injectors in the crankcase, but the fresh air flow partially deviates the sprays. Slide bearings are not recommended in this case; most two-stroke engines simply have rolling bearings, with low reliability and typical two-stroke noise. The disadvantage of lubrication of the crank mechanism can be avoided, as shown in Fig. 2.81, if the entering fresh air is directed to an external compressor instead of to the crankcase

In this case, the lubrication and bearing can be made similar to the solution for four-stroke engines.

A next step is the replacement of intake and exhausts ports by intake and exhaust valves, avoiding both liner deformation and the symmetry of scavenging. Moreover, a variable valve control, as presented in Sect. 2.2.1 for four-stroke engines, becomes feasible. Such a solution is shown in Fig. 2.82.

The crankcase pumping is replaced by a supercharger, and the intake and exhaust ports by valves. The cross-section in Fig. 2.82 shows an engine that is

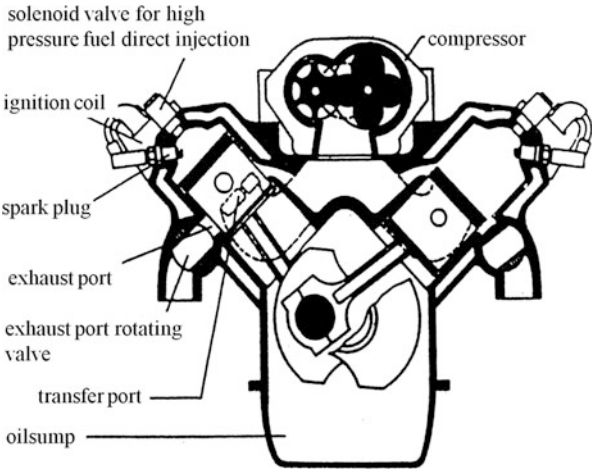

Fig. 2.81 Two-stroke engine with cylinder scavenging by a separate compressor instead of crankcase pump

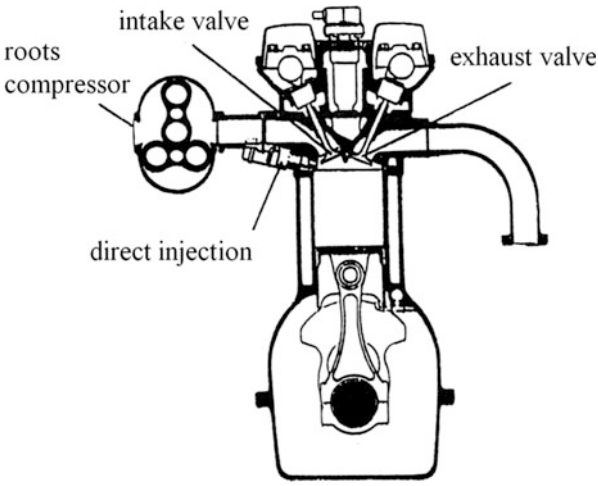

Fig. 2.82 Two-stroke engine with separate compressor and scavenging control by intake and exhaust valves

apparently an advanced four-stroke engine. The only difference is the form and the overlapping of the cams for the intake and exhaust valves, which should generate typical two-stroke scavenging angles, but without the symmetry leading to short circuit of the fresh air.

The process sequences are shown in Fig. 2.83. This solution was conceived as loop scavenging in the opposite direction, with flow inversion over the piston instead of looping under the engine head. Nevertheless, there seems to be a short circuit of the mixture between intake and exhaust valves, but not an inverse looping. The trapping efficiency of fresh air is very low, diminishing the power-to-volume ratio to an impractical level. Solutions with scavenging along the cylinder axis, using combinations of valves and ports for intake or exhaust, avoid such phenomena.

An alternative solution is an engine with two opposite pistons in the same cylinder. In this case, the lubrication is similar to that in four-stroke engines, the scavenging diagram is nonsymmetrical, and a swirl of the air between the cylinders can be generated by tangential intake and exhaust ducts. Such an engine is shown in Fig. 2.84.

It is not easy to predict whether such advanced two-stroke concepts, with evident advantages, will be introduced for automobile propulsion. Nevertheless, their application in hybrid configurations, as stationary working machines for generation of current, can have remarkable advantages in comparison with the use of four-stroke engines for such a function.

2.3.2 Wankel Engines

Wankel engines celebrated 50 years before their promising entry into the automotive industry: The NSU mid-class car Ro 80 (1967) was equipped with 115 PS

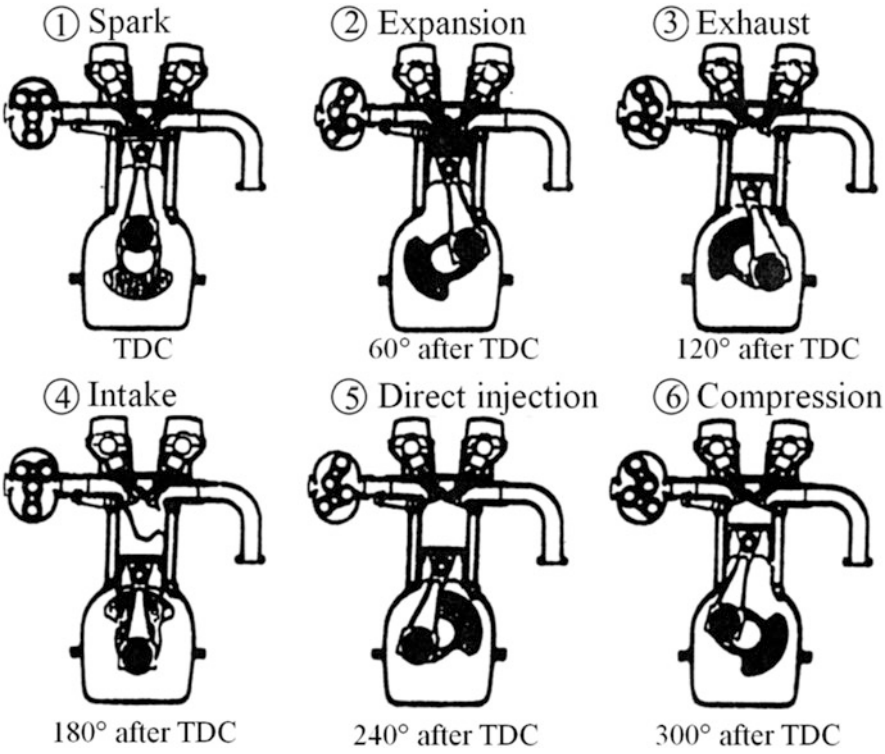

Fig. 2.83 Process sequences in the two-stroke engine, as shown in Fig. 2.82

(84.6 kW) at 5500 min^{-1}. This engine is shown in Fig. 2.85. The development of similar concepts for other automobiles and motorcycles was stopped after few years. At present, only one car maker worldwide is producing Wankel engines—Mazda, which developed its RX series. The working principle of a Wankel engine is illustrated in Fig. 2.86.

The eccentrically running rotary piston, together with the inner contour of its housing, forms three separate chambers that change their volume and position during piston rotation. Thus, concomitant multiple processes are feasible , allowing a compact engine design.

The fresh charge mass flows through intake ducts and ports into a first chamber, which becomes smaller by piston rotation, compressing the charge. In the piston position corresponding to a minimum volume and, thus, to the end of the compression, the combustion chamber contains one or two spark plugs for ignition. During subsequent rotation of the piston, the burned gas expands in an increasing volume. In the next position, there are exhaust ports and ducts. The cycle starts again when an edge of the piston reaches the intake ports. A better design for the scavenging

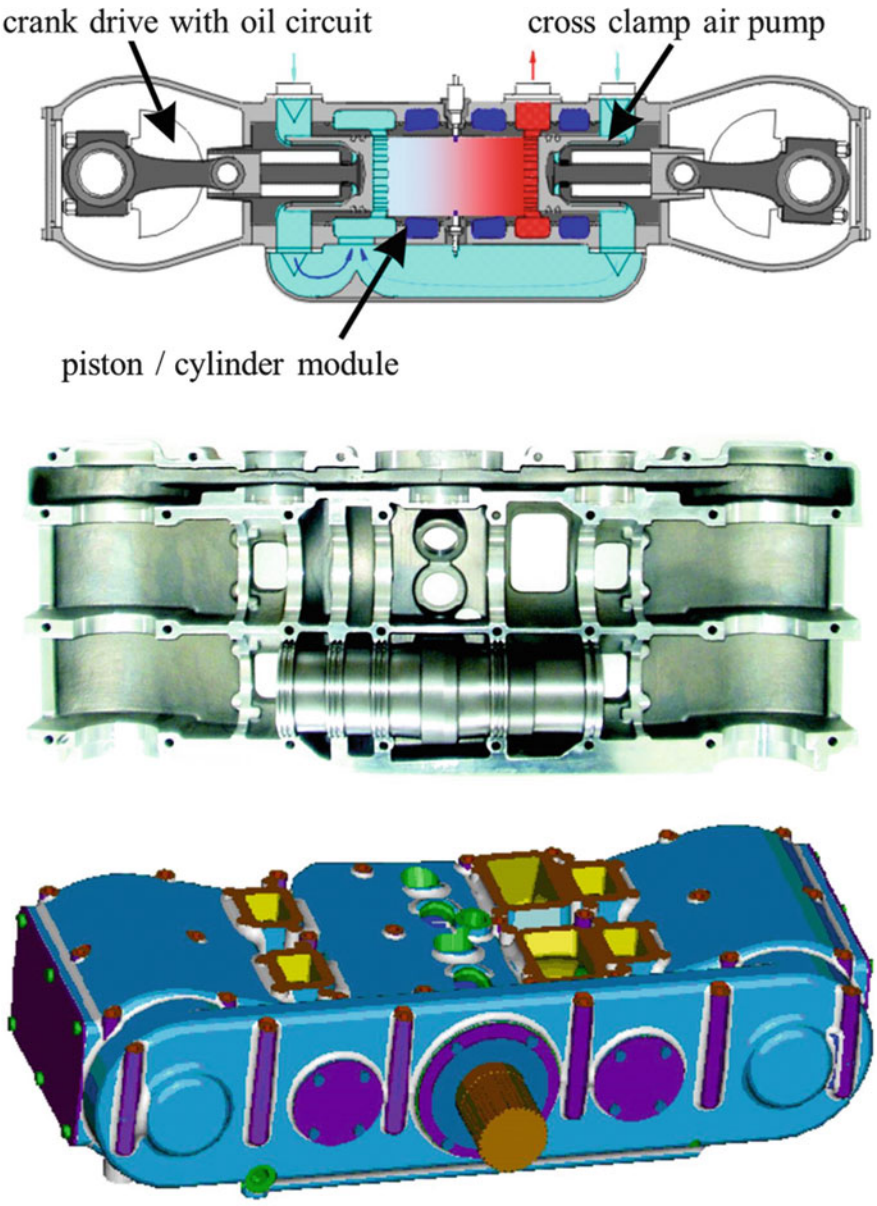

Fig. 2.84 Two-stroke engine with opposite pistons (Golle method)

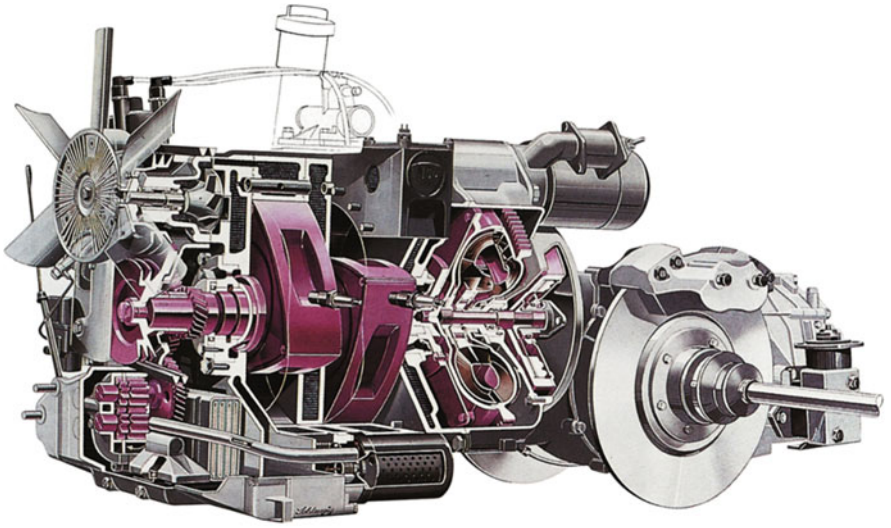

Fig. 2.85 NSU Ro 80 Wankel engine (two rotary pistons), 1967

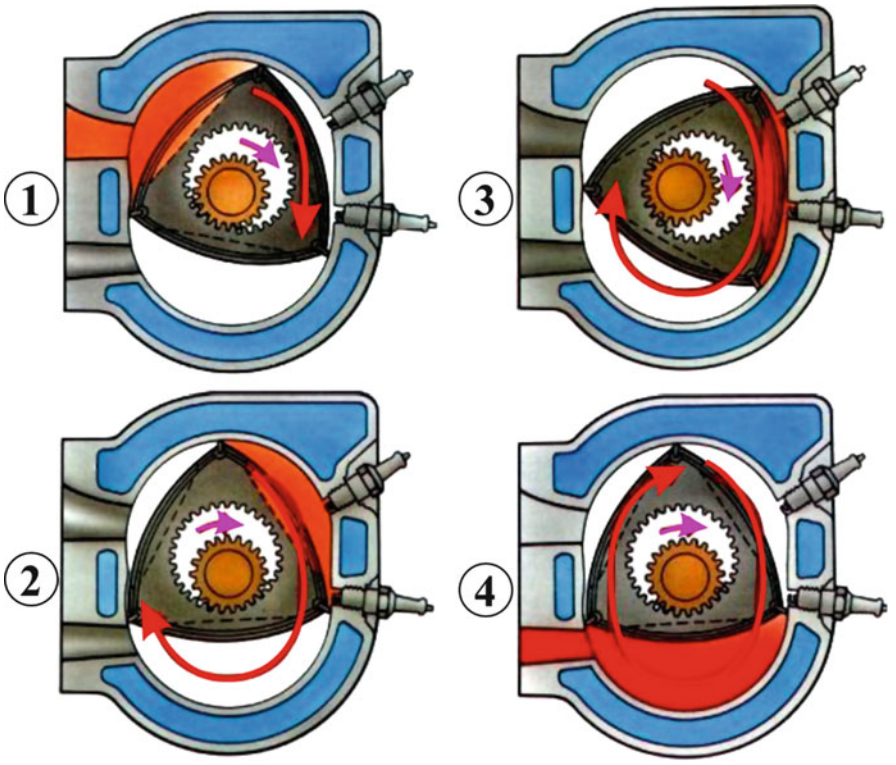

Fig. 2.86 Process sequences in a Wankel engine:(*1*) intake, (*2*) compression, (*3*) combustion, (*4*) expansion and exhaust

Fig. 2.87 Wankel engine with frontal intake and exhaust ports (Source: Mazda)

system is given when the intake and exhaust ports are disposed laterally, as shown in Fig. 2.87 for Mazda RX8, engine type 16xRENESIS.

This form is more advantageous for the design of ducts and ports. On the other hand, impact of piston rings at the port edges(similar to those in two-stroke engines) is avoided because the lateral sealing is less difficult. The advantage of compactness as a result of the concomitant process in three chambers is completed by the benefit of pure rotation of the piston, which is different from the crank mechanisms in two-stroke and four-stroke engines. This influences the inertia, bearing, and speed range. A known disadvantage of earlier Wankel engines was the sealing at the piston edges. This problem now seems to be generally solved. However, there remain some functional disadvantages that impede further development of this engine type. Scavenging occurs via intake and exhaust ports, similar to those in two-stroke engines. Fully variable control of intake and exhaust timing, in relation

to different load/speed combinations is similarly not possible. However, a more important problem is the form of combustion chamber, which allows neither mixture turbulence nor direct fuel injection with any kind of spray length. Furthermore, the surface-to-volume ratio is very high, leading to contact of the fuel droplets with walls, impairing bsfc and emissions of HC and CO.

Nevertheless, the Wankel engine is very interesting for on-board current generation in automobiles. At constant engine speed, both scavenging and combustion can be well tuned. In 2010, Mazda presented a Wankel engine, as shown in Fig. 2.87, running at constant speed, with hydrogen injection into the compression sequence. Up to combustion, the hydrogen is entirely gaseous; thus, there are no incomplete reactions on the combustion chamber walls.

2.3.3 Thermal Turbomachines (Gas Turbines)

Gas turbines are characterized by the pure rotation of moving parts, but without the eccentricity of Wankel engines. A basic functional advantage is that all the process sequences (compression, combustion, expansion, scavenging) occur concomitantly (as in Wankel engines). However, in this case every process sequence takes place in its own separate module, which is developed and optimized just for the one function of compressor, combustion chamber, turbine, aspirating diffuser, or exhaust gas duct. By contrast, the piston/liner unit of a piston engine is a compressor in the first sequence, then combustion chamber, expanding machine, and finally scavenging system; therefore compromises are necessary.

The function of a gas turbine that can be utilized in an automobile is based on the ideal Joule cycle. Figures 2.88 and 2.89 show such turbomachinery with axial compressor and turbine. Figures 2.90 and 2.91 illustrate a variant with radial compressor and turbine.

Axial compressors and turbines are usually applied in aircraft engines. Radial compressors and turbines are utilized on a large scale as turbochargers for piston

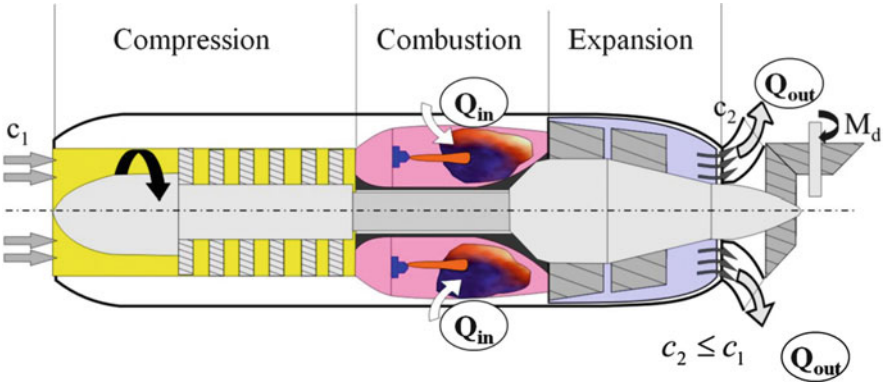

Fig. 2.88 Gas turbine with axial compressor and turbine

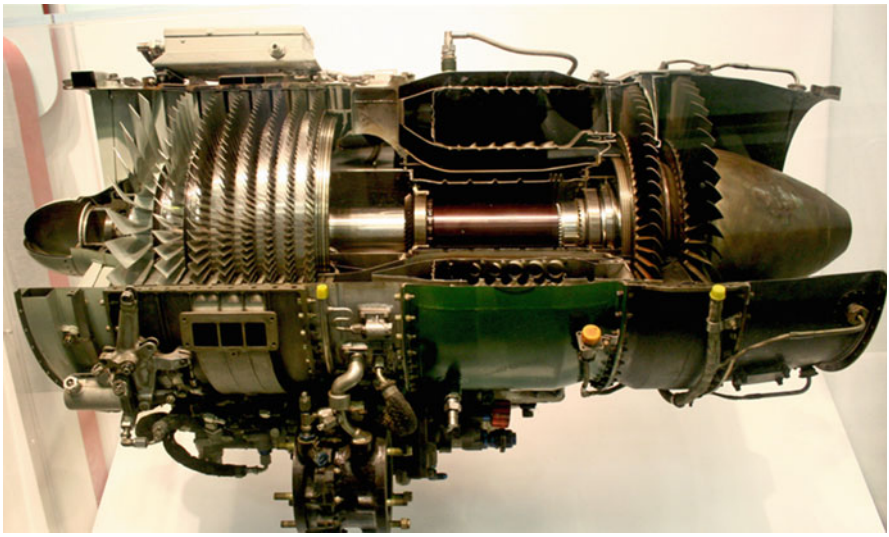

Fig. 2.89 Gas turbine with axial compressor and turbine (cross-section)

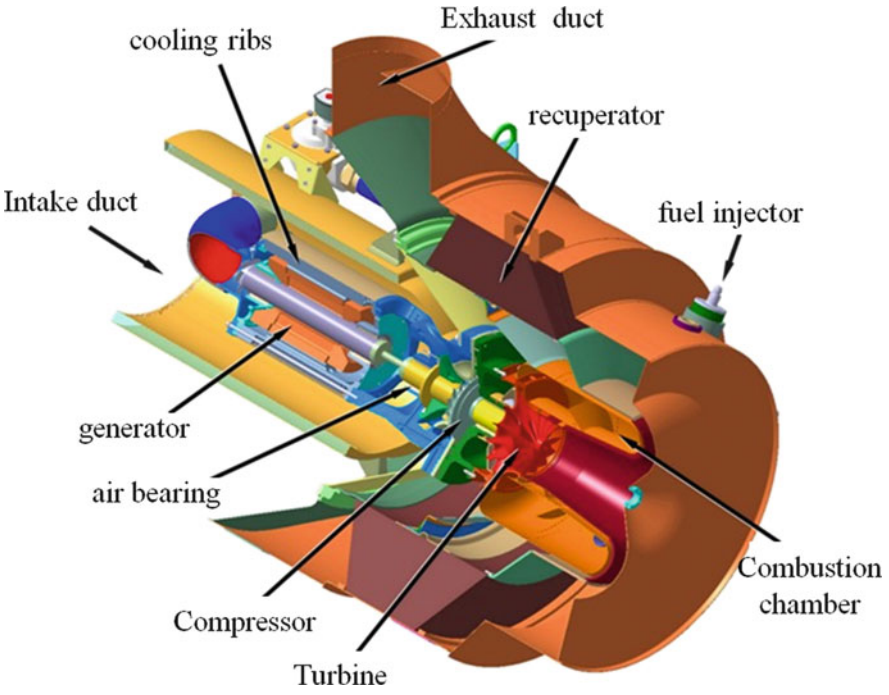

Fig. 2.90 Gas turbine with radial compressor and turbine (Source: Capstone)

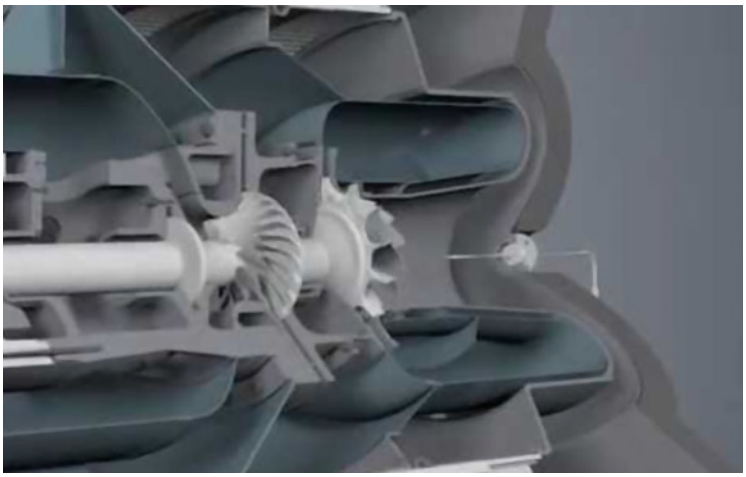

Fig. 2.91 Gas turbine with radial compressor and turbine (cross section) (Source: Capstone)

engines. Completion of such a turbocharger with a combustion chamber gives a very interesting on-board current generator.

Compression is realized with axial compressors, as shown in Fig. 2.88 in serially disposed compressor units that consist of rotor and stator. Basically, this compression can be considered isentropic. The combustion of continuously streaming masses of fuel and air is isobaric. The advantages for fuel–air mixture formation and combustion in comparison with such processes in piston engines are evident: the injector is open (i.e., without opening and closing needle) and the inner form of the injector allows a controllable fuel flow swirl, leading to sufficient atomization. The spray penetration length has practically no importance in an open chamber without length restriction. Contact of the fuel spray with the enveloping air can be optimized for different conditions. For example, the mostly cylindrical shell of the combustion chamber is enveloped by a secondary air flow coming from the same compressor as the main air flow. This air envelope diminishes the thermal stress and radial heat losses. Moreover, the shell contains holes for the suction of secondary air only in the zones where the local maximum temperature within the burning mixture is very high (at the limit of dissociation and, therefore, of NO_x formation). Expansion is realized in turbines with more stages: in the first stage or first group of stages the work for the compressor is generated, which is transmitted by an axial shaft. The second stage or group of stages transforms the remaining enthalpy of burned gas into effective work, which corresponds to the effective cycle work in a Joule process. This effective work can be used, by means of a gear, for the direct propulsion of an automobile or for current generation on board. Such an application as a generator is illustrated in Fig. 2.90. In this mode, the burned gas expands down to the surrounding pressure but (corresponding to the Joule cycle) at a higher temperature than that of atmospheric air. This temperature difference is considered

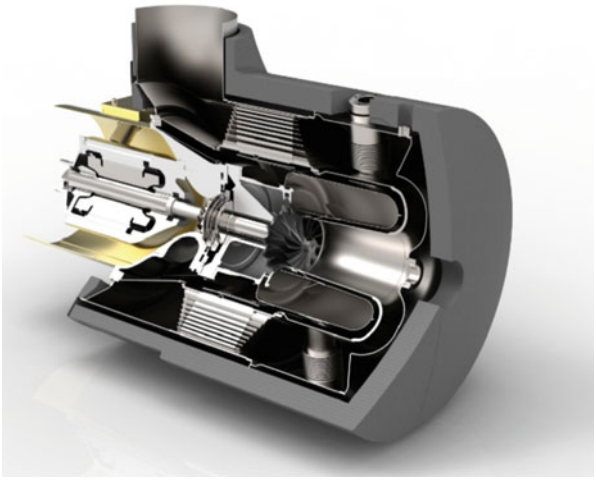

Fig. 2.92 Gas turbine as a current generator (Source: Capstone)

as giving exhaust heat at constant pressure in the Joule cycle. This exhaust heat can be recuperated in a heat exchanger, as illustrated in Fig. 2.92.

This solution can be explained further on the basis of Figs. 2.95 and 2.96. The gas turbine shown in Fig. 2.90 works on the basis of the Joule process, having radial compressor and turbine.

The energy balance for open systems (first law of thermodynamics) gives:

$$q_{12} - w_{12} = h_2^* - h_1^* \tag{2.21}$$

q_{12}	$\left[\frac{\text{kJ}}{\text{kg}}\right]$	Specific heat
w_{12}	$\left[\frac{\text{kJ}}{\text{kg}}\right]$	Specific work
h^*	$\left[\frac{\text{kJ}}{\text{kg}}\right]$	Specific total enthalpy

The compression is considered isentropic, $q_{12} = 0$. The air compression needs enthalpy, thus:

$$h_2^* > h_1^* \quad \text{for} \quad w_{12} < 0$$

With the specific total enthalpy:

$$h^* = u + \frac{p}{\rho} + \frac{c^2}{2} \tag{2.22}$$

u	$\left[\frac{\text{kJ}}{\text{kg}}\right]$	Specific internal energy
p	$\left[\frac{\text{N}}{\text{m}^2}\right]$	Pressure
ρ	$\left[\frac{kg}{m^3}\right]$	Density
$\frac{c^2}{2}$	$\left[\frac{\text{kJ}}{\text{kg}}\right]$	Specific kinetic energy
c	$\left[\frac{\text{m}}{\text{s}}\right]$	Flow velocity

The function of an axial or radial compressor can be explained as follows: The increase in specific total enthalpy generated in the rotor, by augmentation of the specific kinetic energy, corresponds to $c^2/2$. In the following stator stage, the specific total enthalpy from the rotor has no variation, because there is no exchange of heat or work. Equation (2.21) gives:

$$h_3^* = h_2^* \quad \text{for} \quad q_{23} = 0, w_{23} = 0$$

However, variation in cross-section for the air flow (in subsonic flows, a cross-section enlargement) gives the specific kinetic energy $c^2/2$ in Eq. (2.22), which was generated in the rotor and is transformed into the specific pump energy p/ρ:

– In axial compressors, the increase in velocity $\vec{c}$ is a result of a deviation in relative flow velocity $\vec{w}$ between rotor blades, which is given by the form of the blades. Taking into account the tangential velocity of the rotor $\vec{u}$, addition of the velocity vectors leads to:

$$\vec{c} = \vec{w} + \vec{u}$$

Thus, the deviation of the vector ($\vec{w}$) to another direction influences the projection and thereby the length of the vector, as illustrated in Fig. 2.93:

$$\vec{c} = \vec{w} + \vec{u}$$

In this mode, in every stage that is formed by a rotor and a stator a pressure is generated in the range:

$$\frac{p_{\text{Outlet}}}{p_{\text{Inlet}}} = 1.15...1.35$$

The total pressure results from the connection of a number of stages.

– In radial compressors, the flow deviation is radial and provokes a centrifugal force:

$dF = dm \cdot r \cdot \omega^2$	F	[N]	Centrifugal force
$dm = \rho \cdot dA \cdot dr$	m	[kg]	Mass
$c = r\omega$	ρ	$\left[\frac{\text{kg}}{\text{m}^3}\right]$	Density
	ω	$\left[\text{s}^{-1}\right]$	Angular velocity
	A	$\left[\text{m}^2\right]$	Flow cross-section
	c	$\left[\frac{\text{m}}{\text{s}}\right]$	Velocity

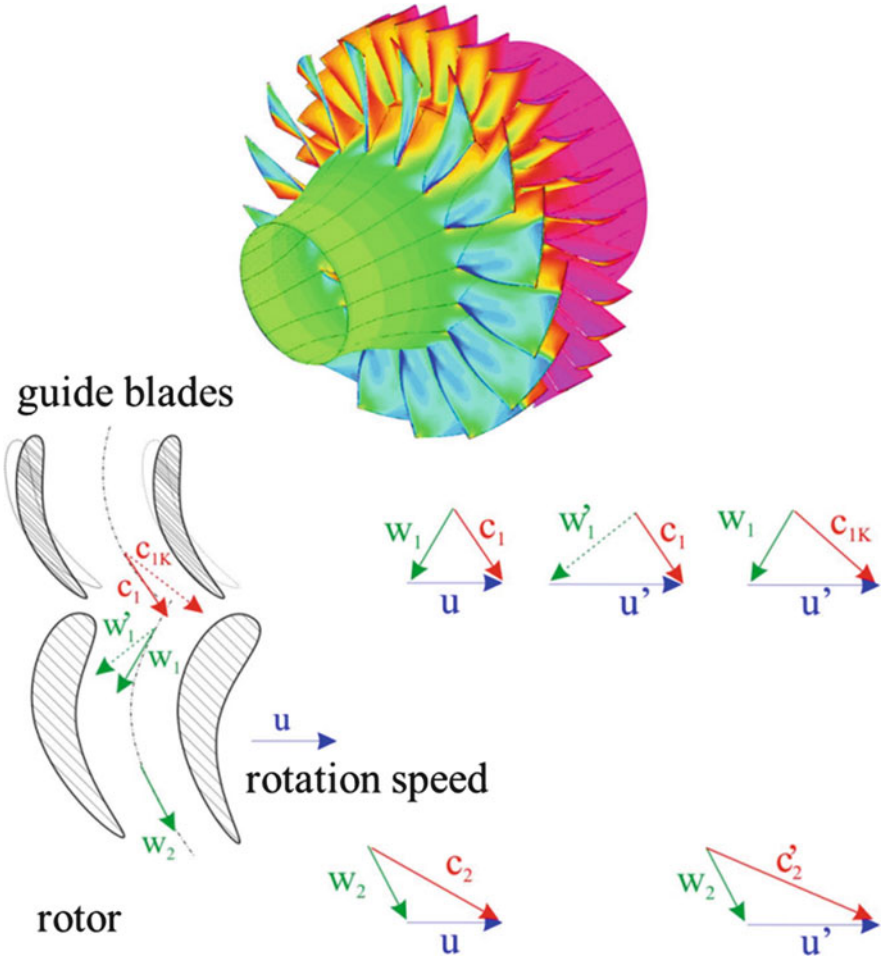

Fig. 2.93 Velocity vectors in guide blades and rotor blades in an axial compressor and compensation form for variable rotation speed (u) by the inclination of the guide blades

The generated velocity c leads to an increase in the specific total enthalpy in the rotor. Transformation of the specific kinetic energy into specific pump energy in the stator occurs in a similar manner as in the case of axial compressors:

$$\frac{c^2}{2} \rightarrow \frac{p}{\rho}$$

The pressure generated in the rotor/stator stage of a radial compressor is in the range:

$$\frac{p_{\text{Outlet}}}{p_{\text{Inlet}}} = 4.5...4.8$$

The connection of a number of stages gives the total pressure, as in axial compressors.

This overview is centered on the application of gas turbines in automobiles (especially as current generators), therefore calculation of the blade profiles in axial and radial compressors is not included. The following example illustrates the relationship of the velocity vectors $\vec{c}$, $\vec{w}$ $\vec{u}$ in the case of an axial compressor.

As shown in Fig. 2.93, the relative velocity $\vec{w}$ is deviated between the blades. Adjusting the direction of the intake blades and the entry angle of the rotor blades, the combination of the generated vector $\vec{c}_1$ and the tangential velocity u corresponding to a rotational speed n and radius r up to the analyzed cross-section leads to a relative flow velocity w_1, which follows the median curve between two blades. This curve between the blades leads to the relative velocity w_2 and, thus, to an increase in absolute velocity c_2, as previously explained.

However, an increase in engine speed (n') provokes a higher angular speed (w') and, thus, a higher tangential speed (u'), where $u' > u$. Consequently, the direction of the relative velocity $w_1{}'$ is no longer oriented along the medium curve between the blades (as shown in Fig. 2.93), causing impact of the flow on a blade wall and consequent backflow and pulsations. A compensation of this effect by engine speed variation is possible by changing the orientation of the intake blades, which leads to correction of the absolute flow velocity entering the rotor:

$$\vec{c}_1 \rightarrow \vec{c}_{1K}$$

In combination with the new tangential velocity $\vec{u}'$, this correction leads to the initial value of relative speed $\vec{w}_1$ and then to $\vec{w}_2$ at exit; however, the problem is:

$$\vec{w}_2 + \vec{u}' = \vec{c}_2{}' \; and \; \vec{c}_2{}' > \vec{c}_2$$

The intake angle of this new absolute velocity $\vec{c}_2$ should also be compensated for by an angle adjustment in the next stage and in the following rotor/stator stages. Such adjustment would be technically too complex. This problem is similar for radical compressors and turbines. Thus, adjustment of intake blades only at entry in compressors and turbines is not sufficient, making the efficiency of gas turbines strongly dependent on speed.

Energy transformation in axial and radial turbines occurs in the opposite direction to that in compressors. The specific total enthalpy is constant in the stator:

$$h^* = u + \frac{p}{\rho} + \frac{c^2}{2} \tag{2.22}$$

However, the variation in flow cross-section between the stator blades generates a transformation of energy form within this enthalpy:

$$\frac{p}{\rho} \rightarrow \frac{c^2}{2}$$

leading to decompression.

The augmented velocity enters the rotor, causing the blades to rotate; thus, a part of the specific total enthalpy is transformed into work:

$$q_{12} - w_{12} = h_2^* - h_1^*$$
$$q_{12} = 0;\ w_{12} > 0 \rightarrow h_2^* < h_1^*$$

Squeezing the cross-section between the rotor blades as well the decompression continues in the rotor. The two types of turbines are with constant pressure in the rotor and with decompression in the rotor.

The required flow profiles changes the angle along the blades, because of the variation in tangential velocity with the radius of the rotors in both compressors and turbines. The complicated profiles, measures for adjustment to variable speed, and the high speed level of gas turbines lead to a complex design and to a high level of manufacturing, making such gas turbines for automotive applications more expensive at this time than piston engines. Nevertheless, the stationary operation of gas turbines for on-board current generation would simplify their function. Figure 2.94 shows a gas turbine of 70 kW for current generation in a Jaguar C-X75 prototype.

A model of a gas turbine for current generation in automobiles, with a lower technical complexity, is shown in Figs. 2.95 and 2.96. In the example shown in Fig. 2.96, in a compressor with a pressure ratio of 3:1, the temperature increase is from 39 °C to 182 °C. After the compressor, the gas enters a heat exchanger and becomes the first heat input (in this example the temperature increases from 182 °C to 540 °C). A second heat input is generated by catalytic combustion in a burner, giving a temperature rise up to 816 °C. Thermal efficiency is not best at such a

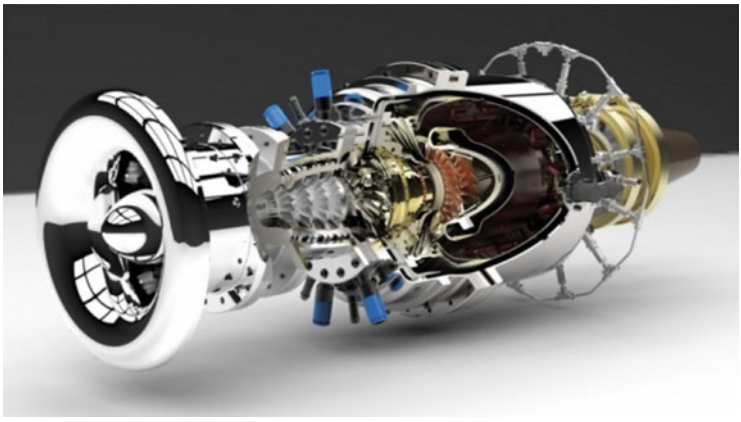

Fig. 2.94 Gas turbine for current generation in a hybrid with electric propulsion (Source: Bladon Jets)

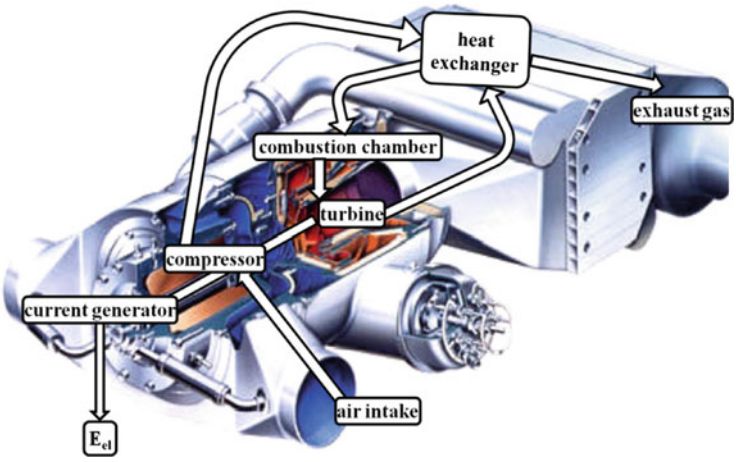

Fig. 2.95 Gas turbine for current generation in a hybrid with electric propulsion

temperature, but a NO_x emission is not expected and the technical complexity is very moderate.

The burned gas expands in the turbine down to 603 °C, the flow being directed at this temperature to the heat exchanger, which gives, as explained, the first heat input to the gas after the compressor. At the exit, the burned gas has in this example a temperature of 245 °C. This machine achieves a power of 24 kW at 96,000 min^{-1} and works with any kind of fuel, from natural gas or propane to gasoline or methanol. Its dimensions are very compact and the mass is only 41 kg, recommending such a solution as an efficient on-board current generator for automobiles.

2.3.4 Stirling Engines

The Stirling cycle consists of two isochoric and on two isothermic processes; a heat exchange (input or output) occurs on each isochore/isotherm pair. The entering heat is not generated by internal combustion; thus, the working fluid in the engine must be not changed by scavenging and its chemical structure is not transformed . The heat can be generated by external combustion, with advantages in terms of design of the combustion chamber, use of different fuels (in solid, liquid, or gaseous state), and high process efficiency. Between 1960 and 1970, Stirling engines were introduced for the propulsion of General Motors buses. Ford developed Stirling engines for automobiles with a power of 125 kW [13]. The working fluid was hydrogen, heated at 750 °C and then cooled down to 64 °C. The thermal efficiency was 38 %. Between 1971 and 1976, Philips and DAF together developed the prototype of a DAF bus (SB 200) powered by a Philips 4-235 Stirling engine with automatic gears. The same engine was utilized for propulsion of a bus of type MAN-MWM 4-658. The engine speed was 1550 min^{-1} and the maximum power 147 kW at 2400 min^{-1}.

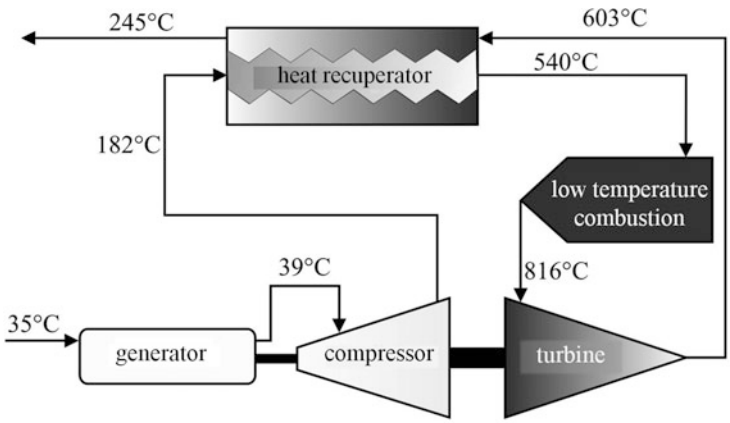

Power:	24 kW		fuels:	
Speed:	96000 min^{-1}		- nat. gas, propane, butane	
Compression ratio:	3:1		- gasoline, methanol, ethanol	
efficiency:	- compressor	79,6%	dimensions:	
	- turbine	85,0%	- length: 91 cm	
	- generator	96,0%	- diameter : 41 cm	
	- recuperator	85,0%	- mass: 41 kg	

Fig. 2.96 Principle of function of a NoMac gas turbine

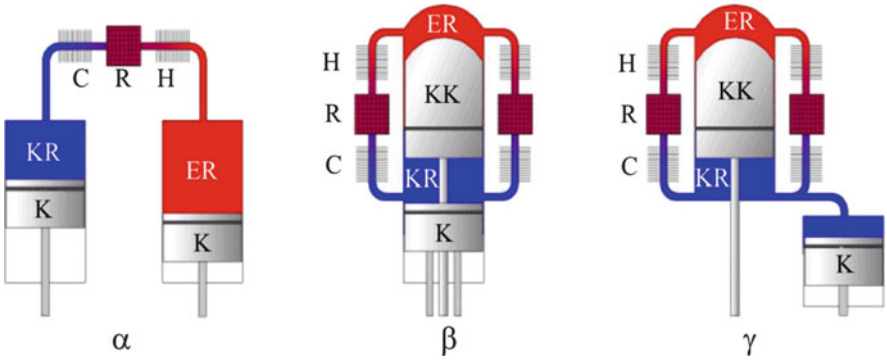

Fig. 2.97 Configurations of Stirling engines

These programs have since been discontinued. A disadvantage, as a matter of principle, is heat transfer from external combustion, which requires both large exchange surfaces and a relatively long duration in comparison with heat release by internal combustion. Hence, a high speed or fast variations in speed are not possible. However, operation at constant load and speed for current generation does not give such problems. In 1967, General Motors introduced an Opel Kadett with a Stirling engine of type GPU3 as a current generator in a hybrid system. The working fluid was in this case helium. The power was 7 kW. Stirling engines were developed in three different configurations (α, β, γ) as shown in Fig. 2.97.

KR compression volume
ER expansion volume
H heat intake
C heat exhaust
R heat recuperator
K piston
KK coaxial pistons (β and γ configuration)

The main functional modules are similar in all categories. Independent of the configuration, the process sequences are the same, as illustrated in Fig. 2.2:

– Isothermal compression with heat release
  Compression starts at the maximum volume of the compression space KR on the cool side C, and minimum volume of the expansion space ER on the hot side H. The KR volume decreases, whereas the volume ER remains small (DA in Fig. 2.2).
– Isochoric heat input
  The working fluid is displaced during the KR volume decrease through the zone of heat recuperator R from the cool side C to the hot side H, whereas the KR volume increases. Consequently, the working fluid remains between KR and ER at a constant volume (AB in Fig. 2.2).
– Isothermal expansion with heat input
  The heated working fluid on the hot side expands in the increasing volume ER, whereas the volume KR remains constant (BC in Fig. 2.2).
– Isochoric heat release
  The expanded working fluid moves from the hot to the cool side through the zone of the heat recuperator. The piston movement causes a decrease in the volume ER and an increase in the volume KR. Consequently, the working fluid remains at a constant volume (CD in Fig. 2.2).

The volume proportions during the four process sequences are realized in all configurations of Stirling engines (α, β, γ) by movement of the two pistons accordingly. The temperature of the hot side is approximately 800 °C in most of the produced Stirling engines. However, a Stirling engine is able to run even if the temperature difference between the hot and cold sides is only 0.5 °C! [14].

A potential of 70–80 °C between the hot and the cold sides seems to be feasible. This corresponds to the difference between the temperature of the water in the cooling circuit of a piston engine and that of the surroundings. A compact, steadily working Stirling engine could recuperate a part of the cooling losses of a piston engine for on-board generation of current in an automobile. This was calculated as 41.9 kW in the example in Sect. 2.2. Figure 2.98 shows a Stirling engine working in a series plant for cogeneration of heat and power.

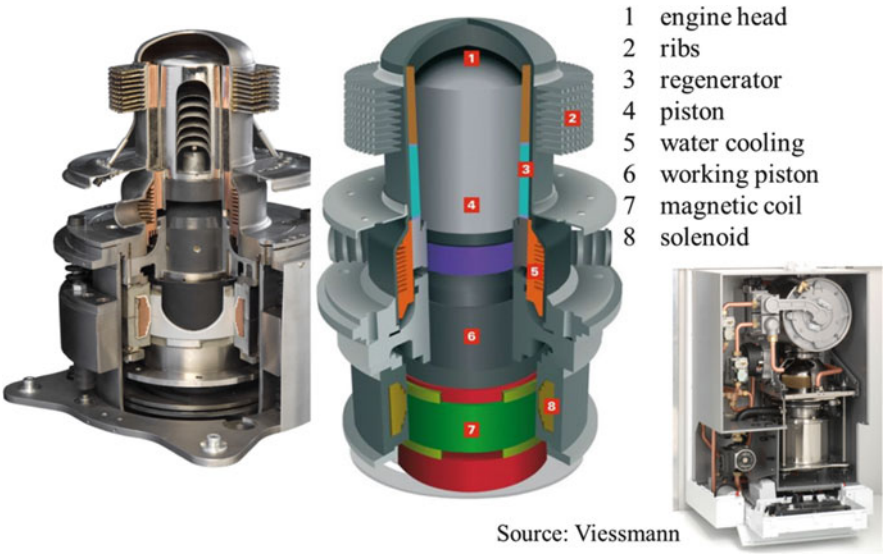

Fig. 2.98 Micro power station for heat and current (Viessmann) (Source: Viesmann)

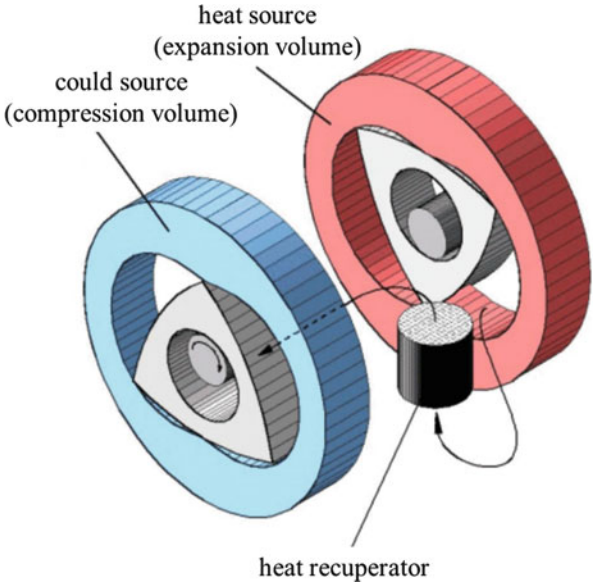

Fig. 2.99 Stirling process by means of a double-chamber Wankel engine with shifted rotary pistons

The numerous possibilities for combination of process sequences and function modules that are feasible with the same outlay as for piston engines is a reason for conceiving new forms of energy management in thermal engines for the future. A

revealing example in this sense is illustrated in Fig. 2.99. A Stirling cycle is generated by movement of the rotors of two Wankel modules with shifted position, combined with a heat recuperator.

From the presented examples, a clear tendency is recognizable: for about 110 years the machine design has determined the processes generated inside; however, the enormous potential of process design is increasingly dominating the machine layout.

Alternative Fuels

3

3.1 Energy Sources: Resources, Potential, and Properties

Transformation of the chemical energy of a fuel with the general structure $C_mH_nO_p$ is possible in two ways:

- In thermal engines, chemical energy is converted into heat and subsequently into work for direct car propulsion or for on-board current generation. In the same way, the conversion energy—heat—work occurs during the generation of electric energy in power plants, and so for the batteries of electric cars.
- In fuel cells, chemical energy is converted into electric energy as a result of proton exchange from hydrogen to oxygen. The hydrogen can be obtained on board from any available fuel with the structure $C_mH_nO_p$.

From this perspective, every combustion of propulsion units, energy accumulators, and energy conversion devices on board of an automobile, as shown in Sect. 1.3 (Fig. 1.26), uses the same energy sources. Note that the direct transformation of sun and wind energy into forms that are usable in automobiles is not included in this analysis.

Figure 3.1 gives an overview of the most interesting energy sources and the obtainable energy forms that can be stored on board automobiles. The fossil sources are shown in the lower part of Fig. 3.1 and the regenerative sources at the top. When one of these resources (whether fossil or regenerative) contains carbon in its molecule, any chemical reaction for an energy transformation into heat or electric energy leads, independent of other products, to CO_2. The difference between fossil and regenerative sources lies in the partial CO_2 recycling in nature. When using regenerative sources, plant nourishment is regulated by photosynthesis, with CO_2 absorption from the surroundings. The basic chemical reaction is:

C. Stan, *Alternative Propulsion for Automobiles*,
DOI 10.1007/978-3-319-31930-8_3

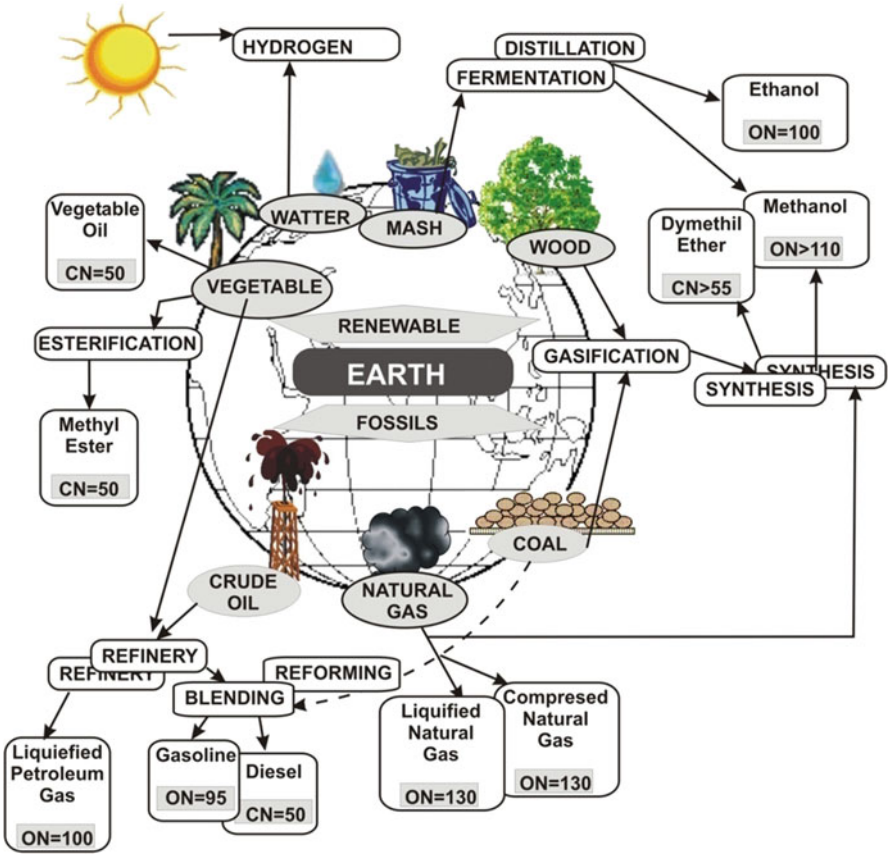

Fig. 3.1 Energy sources and fuels

$$6CO_2 + 6H_2O \overset{\text{LIGHT}}{\rightarrow} C_6H_{12}O_6 + 6O_2 \tag{3.1}$$

However, photosynthesis is a complex chain of intermediate reactions, with two main stages:

- During the light reaction phase, chlorophyll in the plant is activated by light absorption, generating adenosine triphosphate (ATP) and a form of triphosphopyridine nucleotide (TPN) accompanied by dissociation of water for the generation of hydrogen, which is necessary in this process.
- During the dark reaction phase, the ATP and TPN components provide energy for CO_2 absorption and its transformation into carbon hydrate (i.e., glucose) as nourishment for the plant.

The amount of CO_2 that is absorbed by plants and transformed into energy is, at this time, lower than CO_2 emissions from agricultural machines and combustion in car engines. In Brazil, for example, CO_2 recycling between sugar cane cultivation and the emission from combustion in car engines is estimated at 60 %. Even this is a net advantage in comparison with fossil fuels. This percentage will increase when all the machines in the entire chain between plant cultivation, fuel production, and fuel combustion in engines are adapted to work with the same regenerative fuel. The other, essential advantage is the unlimited, timeless availability of these regenerative energy sources, which are sufficient for the increasing mobility demands expected in the future.

The Food and Agriculture Organization of the United Nations (FAO) estimates for the year 2030 a total worldwide energy consumption of 720 exajoule (1 EJ = 10^{18} J) per year (430 EJ/year in 2000).The agrarian surface area used for production of bioenergy (sugar cane, sugar beet, rape) is estimated to increase up to 580×10^6 ha, giving 1031 EJ/year. There are different studies affirming, for example, that ethanol is not a fuel solution for Germany because the area for beet cultivation is not sufficient. Such opinions ignore the fact that the dependence on imported crude oil, necessary for thermal engines and machinery in Germany, is nearly 100 %. The transition from fossil to regenerative energy sources has some crucial aspects:

- Intensified introduction of oils and alcohols from plants, biomass, and waste from the wood, paper, and cellulose industries is expected, independent of the shortage of fossil energy resources. In May 2011, the US Congress adopted a law, the Open Fuel Standard Act, fixing that 50 % of the cars produced in the USA in 2014 must use fuels other than those obtained from crude oil (i.e., alcohols, natural gas, hydrogen, biodiesel). This percentage should rapidly increase to 80 % (2016) and then to 95 % (2017). Worldwide, in 2010 there were 22.6 million automobiles with engines functioning on variable mixtures of ethanol and gasoline (flex fuel), most of them in Brazil and the USA.
- Most prognoses show without doubt that thermal engines using regenerative fuels will be a larger part of future development, much more than other scenarios such as electric mobility (as shown in Fig. 3.2 for the year 2025).

The highest sale of electric cars (2 million) is predicted for Asia, as well as the highest sale of cars with thermal engines (32.6 million). A similar prognosis for Europe shows a ratio of 0.7:22.4 million. The types of automobile in use in Germany in January 2015 are shown in the following table – (in millions):

Gasoline	Diesel	Liquefied petroleum gas (bivalent)	Compressed natural gas (bivalent)	Electric	Hybrid	Total
29.8	13.9	0.5	0.08	0.019	0.1	44.4

A prediction for similar types of cars in the USA for 2040 show a similar configuration:

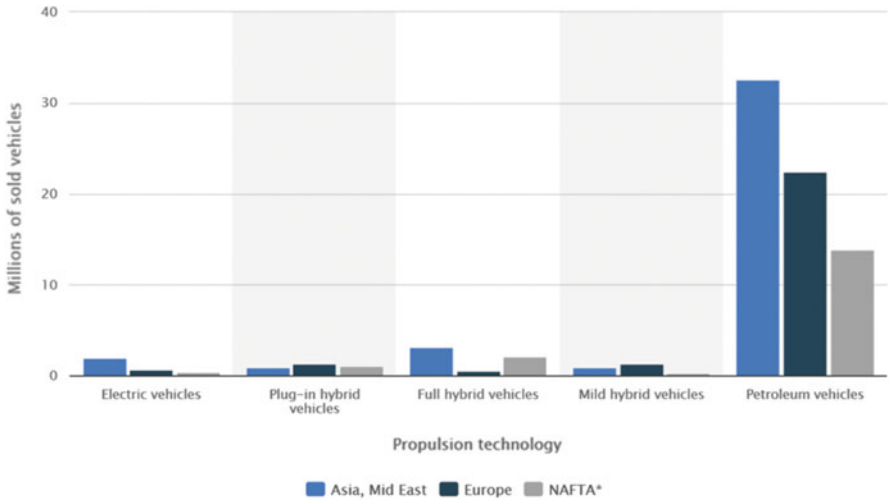

Fig. 3.2 Forecast for the worldwide selling of cars with conventional and alternative propulsion systems in 2015 (Source: www.statista.com, July 2015)

Year	Gasoline (%)	Diesel (%)	Ethanol (%)	Liquefied petroleum gas (bivalent) (%)	Compressed natural gas (bivalent) (%)	Electric (%)
2015	83	2	13	1	1	3
2040	78	4	11	1	1	6

A study by the International Energy Agency describes the possible share of alternative fuels in global transportation as a forecast for 2050, as shown in Fig. 3.3:

- Similar to the introduction of natural gas as a crude oil–based fuel in the automotive industry, the first step toward the use of other fuels will be bivalent on-board systems; this is a pragmatic reaction to the need for a supply infrastructure. There now are bivalent systems in use, such as compressed natural gas (CNG)/gasoline and liquid petroleum gas (LPG)/gasoline, with separate reservoirs and injection systems. Such bivalent systems are not required for alcohols and oils. Methanol and ethanol have properties that are similar to those of gasoline, allowing their storage (as a mixture) in the same reservoir, and their dosage with the same injection system. Engine operation with variable mixtures of gasoline, ethanol, and methanol is currently being explored. Vegetable oils and diesel fuel have similar properties. However, oils must generally be esterified because of possible cooking during combustion and the tendency for mucilage production in the storage system. This explains why the processing of mixtures of diesel fuel and oil is tending to be moved from the reservoir to the refinery; in this way, hydrocarbon fuels with unitary molecular structures are obtainable.

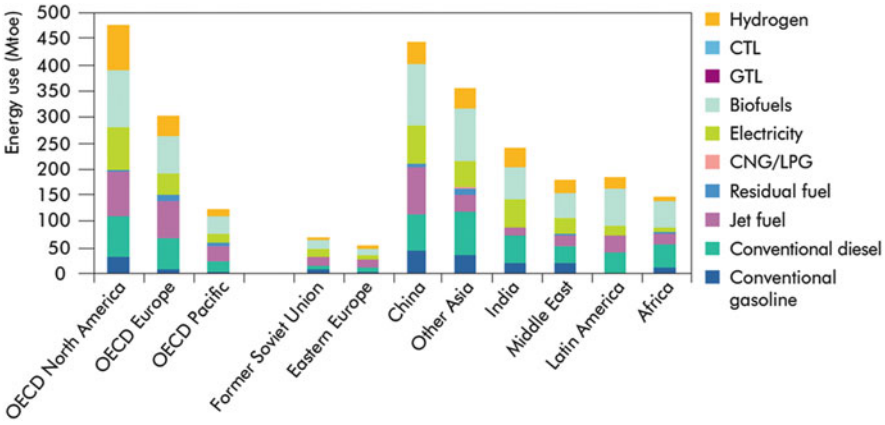

Fig. 3.3 Forecast for share of alternative fuels in global transportation in 2050 (Source: International Energy Agency, July 2015)

The utilization of alternative fuels depends on resources, environment impact, and the technical and technological base, but even more so on their properties on board. Table 3.1 shows the properties of fuels that are of special interest, in relation to the engine and the car itself. The most important correlations between fuel, engine, and car are described as follows:

- *Molecular structure of the fuel*: The fuel structure ($C_mH_nO_p$) has an influence on both the structure and concentration of the combustion products, which depend on the mass proportion of carbon and hydrogen in the combustion reaction. As extreme examples, the combustion of carbon ($C_1H_0O_0$) leads to the maximum concentration of CO_2; on the other hand, the combustion of hydrogen ($C_0H_1O_0$) results in pure water, without CO_2.
- *Fuel density*: The volume and mass of the entire system formed by fuel and storage devices (reservoir, ducts, valves) are determined by the fuel density at a necessary pressure and temperature. As shown in Table 3.1, gasoline, diesel, methanol, ethanol, and oil esters have similar densities at ambient pressure and temperature. This allows utilization of current reservoirs of low thickness and made from light materials.

  LPG is stored on board automobiles generally at a pressure level of 0.5–1.0 MPa, which is possible and sufficient for storage of petroleum gas in the liquid phase.

  Natural gas has, under ambient conditions, a density that does not permit its use in cars in this form. At 20 MPa and ambient temperature, the density of natural gas is one fifth of the density of gasoline, allowing storage on board as CNG. At −150 °C and 0.1 MPa natural gas becomes liquid (LNG), with half the density of gasoline. Hydrogen storage on board an automobile remains a problem:

Table 3.1 Properties of conventional and alternative fuels for automobiles

FUEL	STRUCTURE	DENSITY $[kg/dm^3]$	VISCOSITY (KIN.) $[cSt]$	FUEL ENTHALPY $[MJ/kg]$	STOICH. AIR-FUEL RATIO $[kgA/kg\ Fuel]$	MIXTURE ENTHALPY $[MJ/kg\ Mix]$	OCTAN NO / CETAN NO	VAPORIZATION ENTHALPIE $[KJ/kg]$ (25°C/0.1 MPa-LIQUID) (ts/0.1MPa-GAS)
HYDROCARBONS								
GASOLINE	C_mH_n ($<C_8H_{18}$)	0.72 - 0.78	0.6 - 0.75	44	14.6-14.7	3.9	91 - 99	350
DIESEL	C_mH_n ($<C_8H_{18}$)	0.78 - 0.84	3.5 - 3.9	43.2	14.5	3.8	50 - 54	270
NATURAL GAS (85-95% METHAN)	CH_4	0.141 (0°C/20MPa) 0.409 (-150°C/0.1MPa) 0.00079 (0°C/0.1MPa)	...	45	14.5	4.0	approx. 120	0.51 (GAS)
LPG 50% PROPAN; 50% BUTAN	C_3H_8/C_4H_{10}	0.00235 (GAS) (0°C/0.1MPa) approx. 0.5 (LIQUID) (0°C/0.5–1.0MPa)	...	46	15.5	3.8	98	386
ALCOHOLS METHANOL	CH_3-OH	0.792	0.75	20	6.47	3.5	106	1103
ETHANOL	C_2H_5-OH	0.785	1.5	26	9.00	3.5	107	840
HYDROGEN	H_2	0.009 (GAS) (-200°C/0.1MPa) 0.071 (LIQUID) (-253°C/0.1MPa)	-	120	34.3	3.0	-	436
VEGETABLE OILS RAPSED OIL	$C_mH_nO_pR_i$	0.92	68 - 75	35 - 39	12.4	3.5	38 - 44	...
RAPSED OIL METHYLESTHER	$C_mH_nO_pR_i$	0.86 - 0.9	6 - 8	37.2	12.5	3.5	51 - 58	...
DIMETHYLETHER	CH_3OCH_3	0.00197 (GAS) (15°C/0.1MPa) 0.67 (LIQUID) (20°C/0.5MPa)	0.12 - 0.15 (20°C/0.5MPa)	28 (GAS) 27 (LIQUID)	9.0	3.5	55 - 60	400 (GAS)
INFLUENCE ON	**exhaust gas components**	**storage on board**	**lubrication / coking**	**range**	**fuel dosage**	**torque**	**knock / flammability**	**cold start / mixture cooling / mass of air**

$$pV = mRT \rightarrow m_L = \frac{pV}{RT_L} \tag{3.2}$$

$$R = \frac{\overline{R}}{\overline{M}} \rightarrow R = \frac{8314}{2} = 4157 \left[\frac{\mathrm{J}}{\mathrm{kgK}}\right] \tag{3.3}$$

m	[kg]	Mass
p	$\left[\frac{\mathrm{N}}{\mathrm{m}^2}\right]$	Pressure
V	$[\mathrm{m}^3]$	Volume
R	$\left[\frac{\mathrm{J}}{\mathrm{kgK}}\right]$	Specific gas constant
$\overline{R}$	$\left[\frac{\mathrm{J}}{\mathrm{kmolK}}\right]$	Universal gas constant
$\overline{M}$	$\left[\frac{\mathrm{kg}}{\mathrm{kmol}}\right]$	Mass per kilomole

At the same pressure and temperature, in a reservoir with a given volume there would be 14.5 times less hydrogen than air! More mass is obtainable by increasing the pressure or decreasing the temperature. Table 3.1 shows the result of one of these methods, cryogenic hydrogen storage at 20 K and 0.1 MPa. Under such conditions, the hydrogen changes from gaseous to liquid phase, but its density remains only a tenth of that of gasoline. On the other hand, an increase in pressure requires special techniques and materials. Hydrogen is the smallest of all molecules and can permeate a reservoir wall if the difference in pressure between the reservoir and the surroundings is high, and if the wall material structure is conventional, such as a single layer of metal or plastic.

- *Viscosity of the fuel*: The fuel viscosity influences both the characteristics of the injection system and the combustion process. As an example, the pressure level achieved with diesel fuel in a common rail system is not obtainable with gasoline because of liquid leakage in pumping plungers and injector needles. However, gasoline, ethanol, and methanol have similar viscosity values, allowing use of the same injection system. Oils have viscosity values that are 20 times higher than that of diesel fuel, thus their direct use in engines is possible only in particular cases. Transesterification leads to shorter molecules, but the viscosity remains twice as high as that of diesel. On the other hand, viscosity (as an effect of long and branched molecules) influences the combustion process because of a local lack of oxygen for the numerous oil droplets. This is the reason why coking occurs when operating diesel engines with pure plant oil.
- *Heat value of the fuel*: The heat obtainable from the exothermal chemical reaction during combustion of 1 kg fuel is dependent on the mass fraction of carbon, hydrogen, and oxygen in its molecules. The higher the heat value of the fuel, the lower the fuel mass for a comparable energy output in an engine; this can be expressed as a power profile for a determined duration. Therefore, for the

same mass of fuel in a given reservoir and for the same power profile required by the car, the heat value of the fuel determines the operation range or the car autonomy. For a better view, compare Table 3.1 with Fig. 3.4.

With the same mass of stored fuel on board the same car, with the same power profile, the autonomy would increase threefold by replacing gasoline by hydrogen. Alternatively, replacing gasoline by methanol would decrease the autonomy by 50%. This last example is more realistic: gasoline and methanol have comparable densities and can be stored in a reservoir at the same ambient conditions. Generally, such comparisons should be made for the same volume of reservoir, not for the same stored fuel mass. From this point of view, the situation changes dramatically. The heat value of hydrogen is, as mentioned, three times higher than the heat value of gasoline, but the density of liquid hydrogen at 20 K is a tenth of the density of gasoline. Thus, replacing gasoline by hydrogen in a reservoir of the same volume causes a decrease in the autonomy of the car by one third.

- *Stoichiometric air-to-fuel ratio*: The air requirement depends, similar to the heat value, on the fuel structure. Hydrogen needs the most air mass for a stoichiometric reaction. Alcohols contain a fraction of oxygen, meaning that the requirement for air from the surroundings is proportionally reduced. In stationary engines, the mass flow of air can be adjusted to the injected fuel mass. However, in piston engines the air mass is given geometrically:

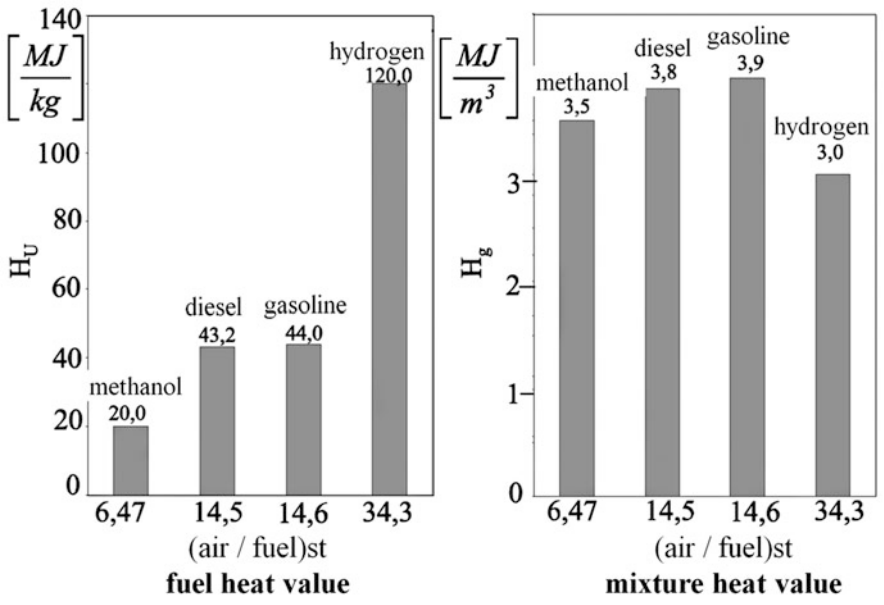

Fig. 3.4 Comparison of the heat values of fuel and fuel–air mixtures for different fuels

$$m_L = \frac{pV}{RT_L} \tag{3.2}$$

In this case, the fuel mass has to be adjusted according to the stoichiometric air/fuel ratio: the lower the stoichiometric air requirement, the greater the fuel mass. If replacing gasoline by methanol, the fuel mass must be 2.2 times higher. This amount can be adjusted by the fuel pressure, opening duration of injectors, and flow cross-areas at injection (e.g., by increasing the number of injectors). If replacing gasoline by hydrogen, the fuel mass must be reduced by a factor of 0.42.

- *Heat value of the fuel–air mixture*: A reduction in the injected mass of a fuel with high heat value leads to a decrease in its energetic effect as a result of the high air/fuel ratio. Values are given in Table 3.1 and Fig. 3.4 for fuels currently utilized in car engines. The heat value of hydrogen is much higher than the heat value of all other fuels, so there is more heat input in the cylinder and a greater power-to-volume ratio. However, the heat value of the fuel–air mixture is somewhat lower than for other fuels, because of the very high stoichiometric air/fuel ratio. Consequently, replacing gasoline by hydrogen in a piston engine results in lower torque, despite the higher combustion efficiency.
- *Octane and cetane number*: The knock resistance of spark ignition (SI) engines, as expressed by the cetane number and by octane number and ignitability in compression ignition (CI) engines, depends on the molecular structure and the volatility of the fuel and is strongly variable for different fuels. From this point of view, methane and alcohols are more advantageous than gasoline: a higher knock resistance allows higher thermal efficiency and lower brake-specific fuel consumption (bsfc). In CI engines, the ignitability of dimethyl ether (DME) is noticeable, resulting from its high volatility and the oxygen content in its molecule. On the other hand, pure, non-esterified oils have low ignitability because of their long molecules; the effect of transesterification on ignitability is remarkable, as shown in Table 3.1.
- *Enthalpy of vaporization*. Fuel vaporization is an important criterion for the quality of a fuel–air mixture and, thus, for combustion efficiency when using both fuel injection into the intake duct and direct fuel injection: the smaller the fuel droplets and the higher the vapor percentage, the more efficient the combustion process. The enthalpy for fuel vaporization is extracted, in an adiabatic mixture formation process, from the aspirated air; therefore, the internal energy of the air, expressed by its temperature, decreases. If the ambient temperature is low, there can be freezing of fuel nozzles, especially when injecting methanol into intake ducts. This effect is not found for direct fuel injection, where the higher air temperature through compression and radiation from walls leads to faster fuel vaporization. Furthermore, the air cooling effect within the cylinder as a result of fuel vaporization allows a higher compression ratio. Because of the high vaporization enthalpy, which leads to air cooling and fast vaporization, methanol and ethanol are highly appropriate fuels for direct injection in engines. At intake duct injection, the temperature difference between air and fuel is lower

than for direct injection, but the time and the space needed for mixture formation are larger. By cooling the intake air, the air mass that is aspirated into the cylinder increases, allowing an increase in fuel mass, leading to an increase in the power-to-volume ratio. This effect is of particular importance for high-speed engines, especially when using direct injection. In this case, the higher temperature difference between air and fuel (if direct injection begins during aspiration) leads to better filling of the cylinder with air.

The characteristics of alternative fuels strongly influence the performance of engines, allowing improvement of involved processes such as air aspiration, fuel atomization and vaporization, formation of the fuel–air mixture, and heat release during combustion.

3.2 Compressed Natural Gas

3.2.1 Properties

Natural gas contains 85–95 % methane. The heat value, stoichiometric air/fuel ratio, and heat value of the fuel–air mixture are similar to those of gasoline. Therefore, changing a car to run on methane from gasoline is not difficult. The higher octane number of methane is promising, allowing augmentation of the compression ratio to 12–14. Nevertheless, the infrastructure for natural gas does not allow such an increase in compression ratio because of the bivalent configuration of cars for both natural gas and gasoline using the same engine.

3.2.2 Storage on Board

On-board storage is the main disadvantage of using natural gas for car propulsion. Table 3.1 shows the gas density for different combinations of storage pressure and temperature. Current common practice is storage at 20 MPa at a rather low density, but using large and heavy tanks in comparison with other fuels, as shown in Fig. 1.17.

In addition to storage of natural gas as a gas under pressure (CNG), it is also stored as a liquid (LNG) at 123 K and 0.1 MPa. In this form, the density is three times higher than in the gaseous phase, but the cryogenic technique is more complex. An alternative method is the use of absorbed natural gas (ANG), whereby gas is absorbed into an activated carbon matrix at 4–7 MPa. The LNG and ANG methods are now under development and promise substitution of gasoline by natural gas on a large scale. Figure 3.5 shows the increase in the number of CNG filling stations in Germany between 2001 and 2014. In the same period, the number of gasoline and/or diesel fuel filling stations was 15,981 (2001) and 14,209 (2014), which means proportions of 78:1 (2001) and 16:1 (2014). Figure 3.6 shows the number of CNG cars in different countries of the world in 2015.

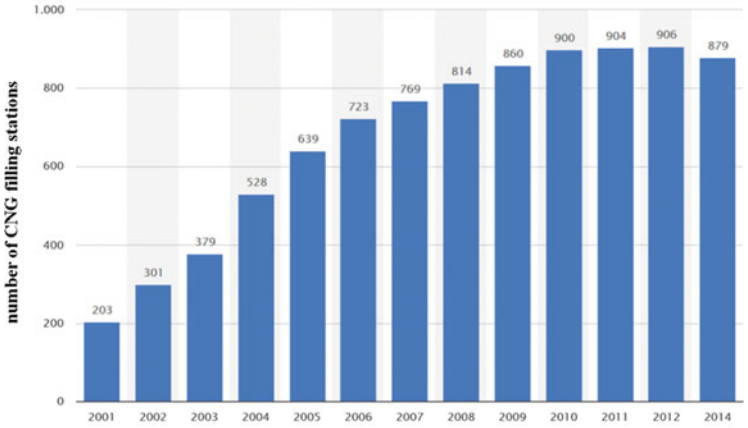

Fig. 3.5 Number of CNG filling stations in Germany between 2001 and 2014 (Source: www.statista.com, July2015)

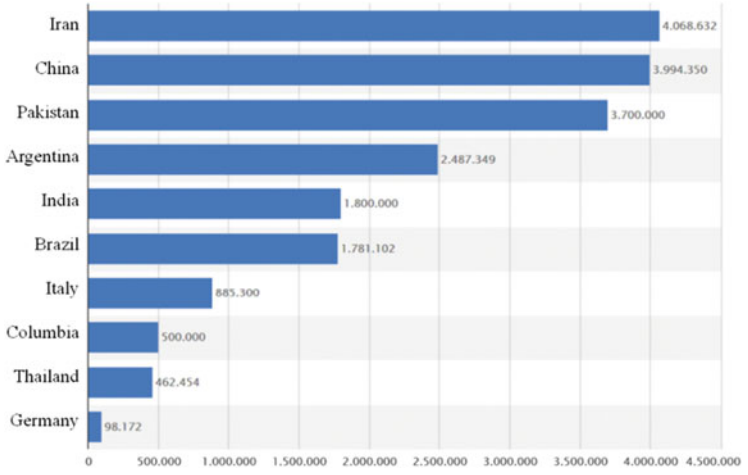

Fig. 3.6 Number of CNG cars (2015) in different countries (Source: www.statista.com, July 2015)

A comparison of the economic efficiency of gasoline, diesel fuel, and CNG for the same car type is illustrated in Table 3.2. The following facts are remarkable:

– A change from gasoline to CNG leads to a power decrease of the engine from 57 kW to 51 kW
– The operation range decreases when using CNG instead of gasoline from 714 km to 310 km.

Table 3.2 Comparison of costs (car and fuel) for CNG, gasoline, and diesel

Fiat Punto (2011)					
Parameter		CNG multipoint		SI multipoint	CI CR + ATL
Swept volume	[cm^3]	1368		1368	1248
Car weight	[kg]	1245		1100	1165
Power	[kW]	51	57[a]	57	55
Compression ratio	–	11.1:1		11.0:1	16.8:1
Tank volume for CNG or gasoline	[l] or [kg]	13	45[a]	45	45
Fuel consumption/100 km	[l] or [kg]	4.2	6.3[a]	5.7	4.1
Range	[km]	310	714[a]	790	1,098
Car price	[€]	16,150		13,950	15,550
Fuel price	[€/l] or [€/kg]	1.00	1.60[a]	1.60	1.45
Fuel price/100 km	[€/100 km]	4.2	10.08[a]	9.12	5.94
Tax	[€]	86		86	123
CNG system service	[€]	75		–	–

[a]with gasoline (Source: Fiat)
CR – Common Rail Direct Injection
ATL – Turbocharger

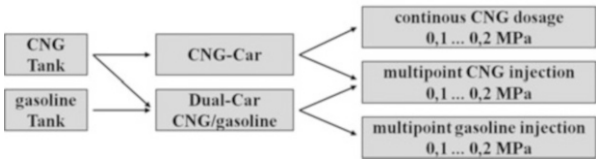

Fig. 3.7 CNG: mixture formation methods

– A car with both fuel systems and tanks on board has a higher consumption when operated with gasoline, 6.3 l/100 km instead of 5.7 l/100 km, and a lower operation range of 714 km instead of 790 km.
– A car with diesel fuel clearly has the lowest fuel consumption and the longest operation range at a power that is roughly similar to that of a car with a gasoline engine. The price of a diesel car is lower than the price of a bivalent car, but the working expenses are a bit higher, as shown in Table 3.2.

3.2.3 Mixture Formation

The technique of fuel dosage for natural gas follows the history of gasoline: it began with the carburetor, was succeeded by continuous injection into the intake duct, multipoint injection, sequential injection, and finally direct injection. Figure 3.7 shows a scheme of current injection techniques for CNG and for CNG/gasoline in dual-fuel cars.

Multipoint gas injection is characterized by a higher pressure than a similar gasoline injection, because of the lower gas density. Apart from that, the injection technique as well as the actuators and sensors are similar to those for gasoline injection (as shown in Figs. 3.8 and 3.9). This simplifies the switch from gas to gasoline in a bivalent car configuration.

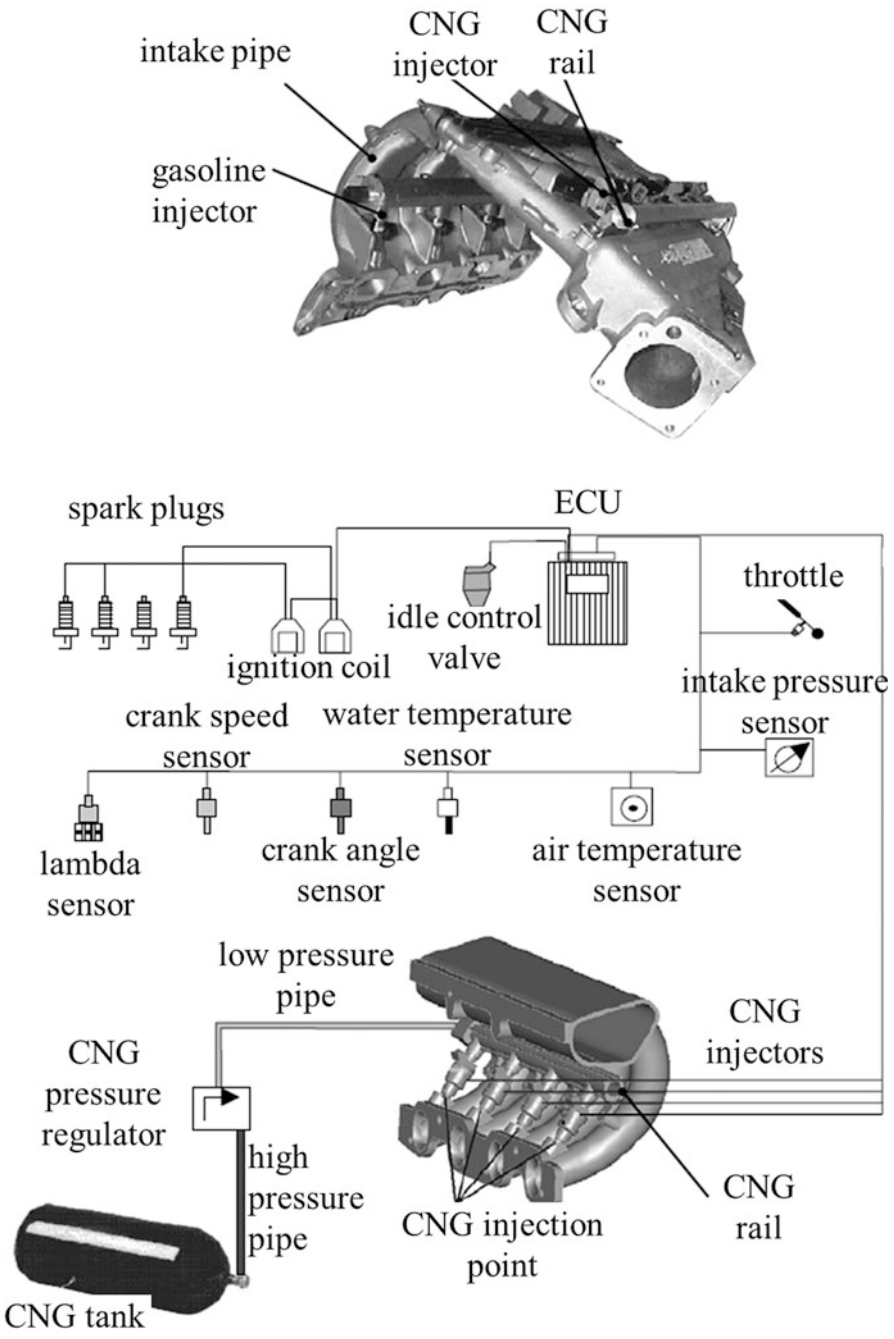

Fig. 3.8 CNG: mixture formation system

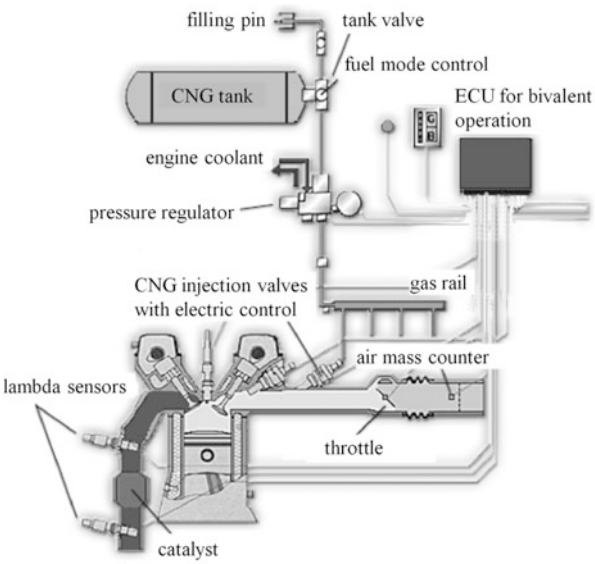

Fig. 3.9 CNG mixture formation: system components

After the successful introduction of direct injection of gasoline in SI engines, the direct injection of natural gas (as shown in Fig. 3.10) became the subject of intensive research [15]. The advantages are similar to those obtained from gasoline direct injection. Additionally, the potential of a higher compression ratio because of the higher knock resistance should result in a bsfc in the range of diesel engines, but with a better emission spectrum. Such an engine with gas direct injection can be operated without air throttling at partial load. Combustion is assisted by a glow plug, similar to that in diesel engines.

Direct injection systems for natural gas have elements in common with direct injection systems for gasoline. The difference is that the high-pressure gas is not generated in the system itself, but guided to the system from a tank, as shown in Fig. 3.10. For pressure compensation, necessary because of the decrease in gas mass in the tank during injection, the system is provided with a gas compressor. The injectors are actuated electromagnetically or piezoelectrically, similar to the control in gasoline direct injection systems.

3.2.4 Applications and Results

Figure 3.11 shows a cross-section through a bus diesel engine that was converted into a gas SI engine; the differences in term of power, torque, and bsfc in the speed range of the engine are also shown. Despite the higher combustion efficiency of natural gas at the same heat value as diesel fuel, the bsfc is higher because of the much lower compression ratio in SI mode. On the other hand, conversion of a diesel

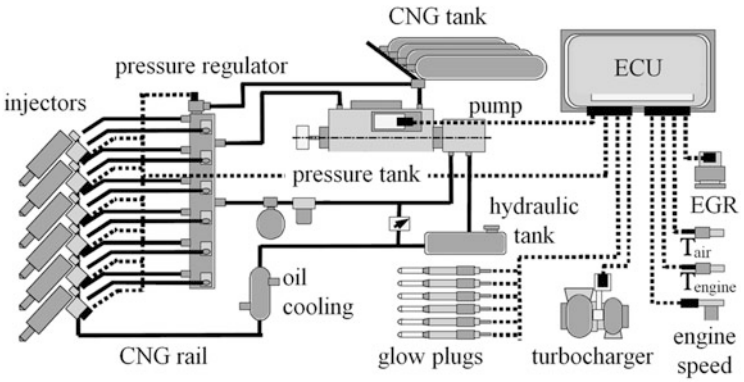

Fig. 3.10 CNG direct injection

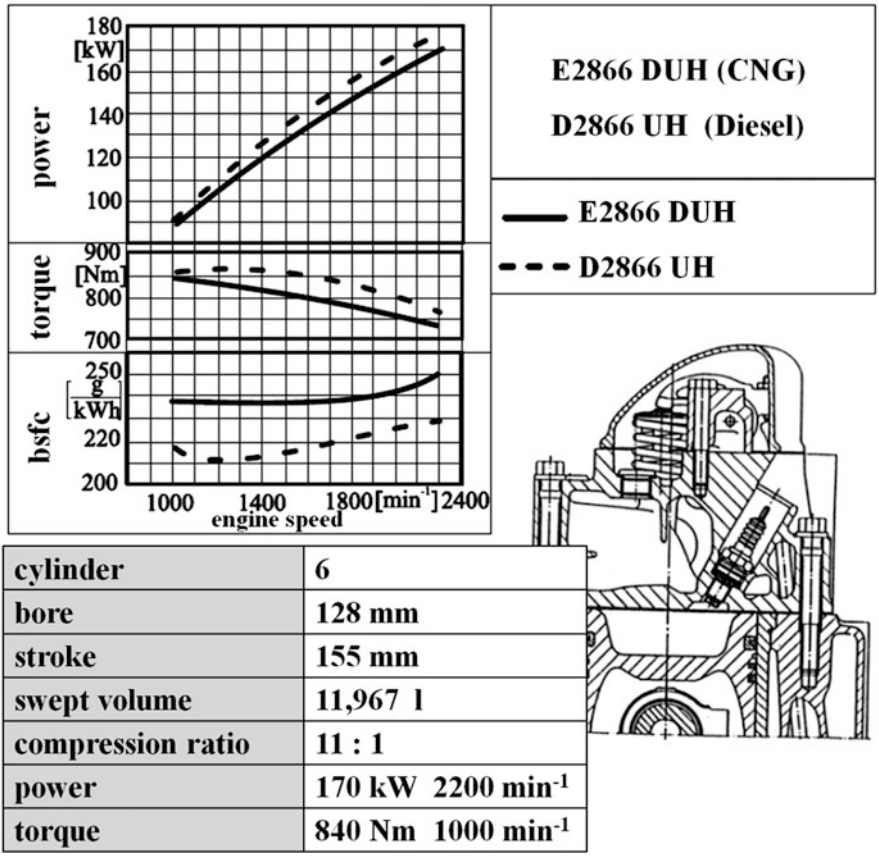

cylinder	6
bore	128 mm
stroke	155 mm
swept volume	11,967 l
compression ratio	11 : 1
power	170 kW 2200 min^{-1}
torque	840 Nm 1000 min^{-1}

Fig. 3.11 Comparison of performances between a CNG engine and its basic diesel variant (shown in cross-section)

engine into an SI engine is easily feasible, using a piston with a deeper bowl and spark plugs instead of glow plugs.

Figure 3.12 shows a series car with bivalent operation using CNG/gasoline (Fiat Panda), which has the same fuel dosage system and the same engine as presented for the car in Table 3.2 (Fiat Punto). The shift from gasoline to the gas injection system is made by a simple switch. Figures. 3.13 and 3.14 show two other examples, with the gas tanks in the luggage compartment instead in the vehicle floor, as shown in Fig. 3.12.

3.3 Liquefied Petroleum Gas

3.3.1 Production

LPG is a 50:50 mixture of propane and butane and is produced during the refining of crude oil, but also from natural gas. In the Netherlands, LPG for vehicles has been produced since the 1950s. Currently, crude oil refining produces 63 % gasoline, 23 % diesel fuel, and 14 % LPG. The target for the future is to obtain the same fractions of gasoline, diesel fuel, and LPG from the refining of crude oil.

3.3.2 Properties

The properties of LPG are broadly similar to those of gasoline, except for the C/H ratio and the density. The heat value, fuel/air ratio, heat value of the mixture, octane number, and vaporization enthalpy have similar values for both fuels, promising similar engine performances.

3.3.3 Storage on Board

In the gaseous phase at ambient pressure and temperature, a propane–butane mixture is not recommended for vehicle application because of the low density, as presented in Table 3.1. The liquid phase is obtainable under relatively simple conditions: 273 K and 0.5–1.0 MPa. Under such conditions, the density of LPG is 68 % of the density of gasoline. Therefore, operation with LPG using the same tank volume as for gasoline guarantees sufficient car autonomy. However, according to customer acceptance, the tanks of cars operating with LPG are 1.6–1.7 times larger than normal gasoline tanks.

Figure 3.15 shows the increase in the number of LPG filling stations in Germany between 2004 and 2012. The proportion of gasoline and/or diesel fuel filling stations compared with LPG filling stations is 2.3: 1 (2012). On the other hand,

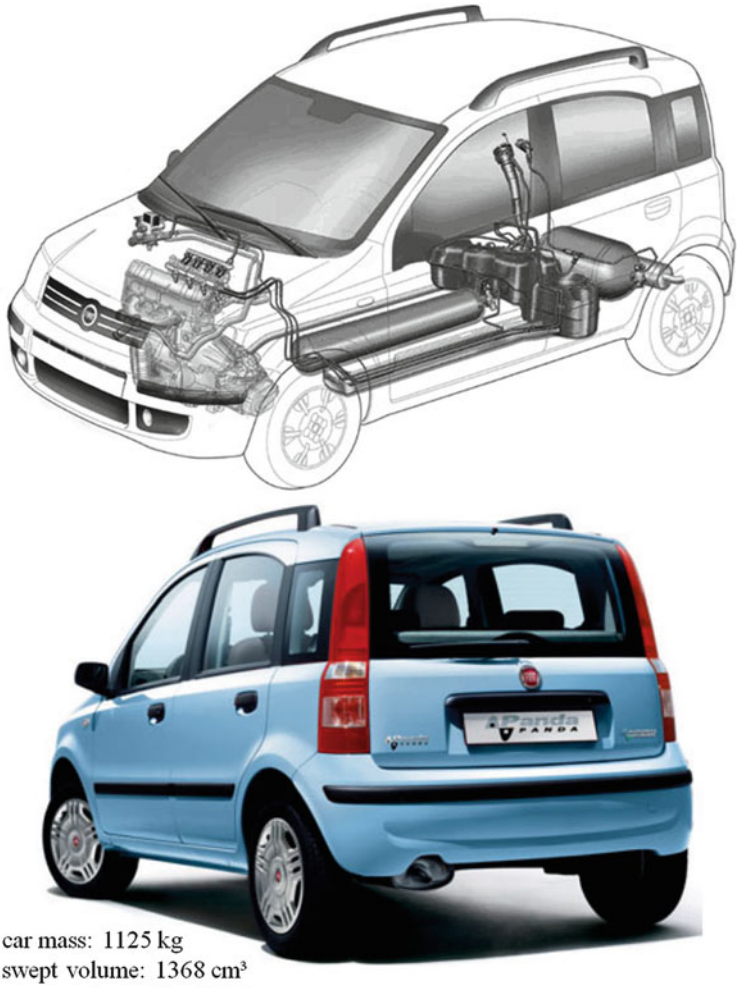

Fig. 3.12 Example of CNG series car: Fiat Panda, bifuel (Source: Fiat)

the proportion of LPG to CNG filling stations in the same year was 7.2: 1. Worldwide, there are more than 17 million vehicles operating with LPG from 57,000 filling stations (2010). It is expected that the sale of LPG cars will achieve 1.4 million units by 2020.

Fig. 3.13 Example of a bivalent car: Skoda Octavia (Source: Skoda)

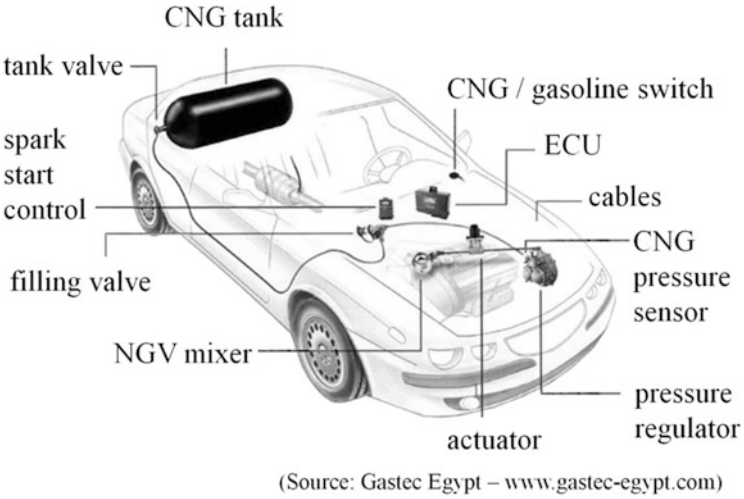

Fig. 3.14 Additional components for bivalent operation using CNG and gasoline

3.3.4 Mixture Formation

Figure 3.16 presents a scheme of a single-point injection system for LPG, which is maintained at a pressure of 0.5 MPa above the pressure in the tank by means of a pump, to avoid vaporization. The injection occurs through two injectors for each intake duct. Dosage is made by varying the opening duration of the injectors.

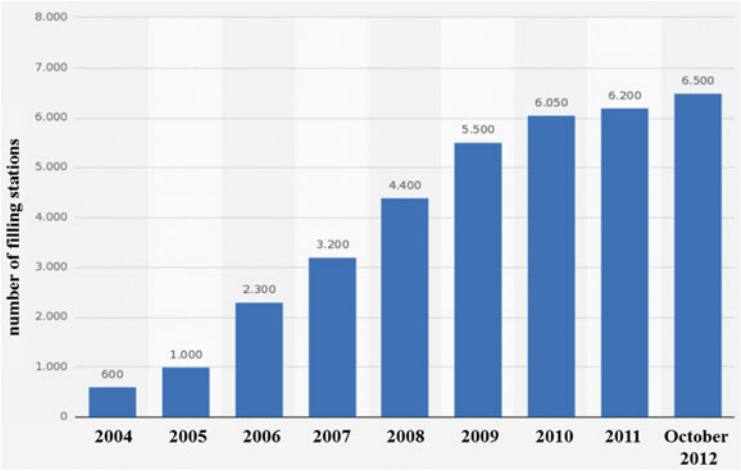

Fig. 3.15 LPG filling stations in Germany 2004–2012 (Source: www.statista.com, July 2015)

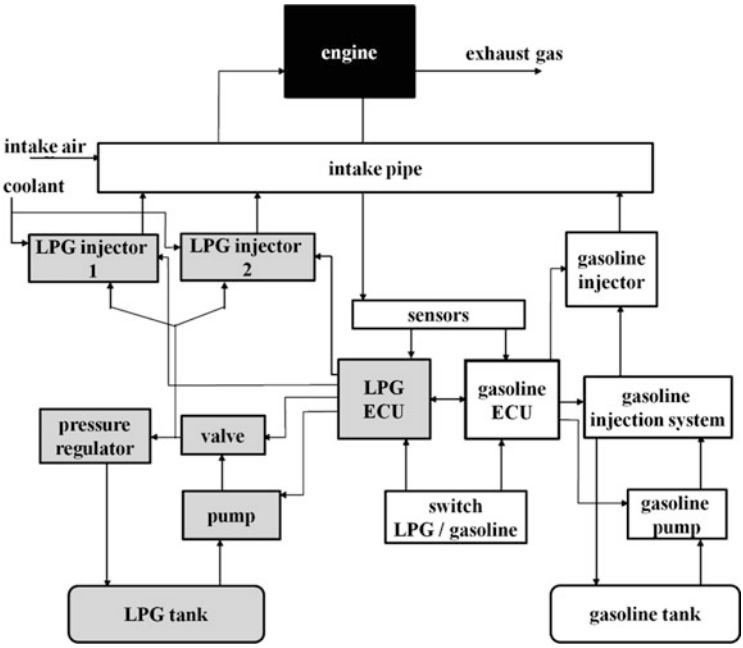

Fig. 3.16 Mixture formation system for bivalent operation using LPG and gasoline

Another variant of such a technique, the multipoint injection system, is shown in Fig. 3.17. Notable in this case are the measures for avoidance or separation of damp in the injection system, which can be a problem at LPG injection.

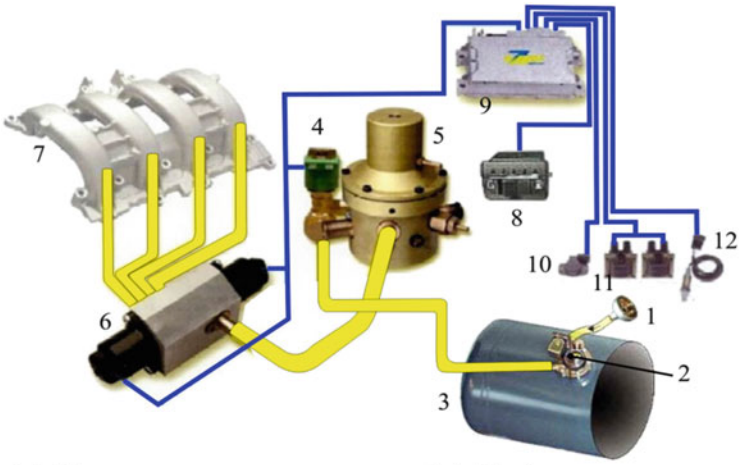

Fig. 3.17 Multipoint injection system for LPG

3.3.5 Applications and Results

The power of an LPG engine remains generally at 5 % under the power of the same engine operating with gasoline. The emissions of HC, CO, and NO_x are similar for both LPG and gasoline combustion. The CO_2 emission is 10 % lower when using LPG, because of the lower C/H ratio in the molecules of propane and butane compared with molecules of octane and heptane in gasoline. Figure 3.18 shows a car with bivalent operation using LPG or gasoline

3.4 Alcohols: Methanol and Ethanol

3.4.1 Production

Nikolaus August Otto utilized ethanol in his engine prototypes as early as 1860; Henry Ford used bioethanol between 1908 and 1927 in series cars and declared it to be the fuel of the future. Ethanol and methanol are obtained from two types of resources:

- Starch and sugar from plants and plant waste, especially sugar cane molasses in Brazil, corn in North America, sugar beet in Europe, and cassava in Asia

Fig. 3.18 VW Polo bifuel with bivalent operation using LPG and gasoline (Source: Volkswagen)

- Algae and cellulose from waste from the paper and wood-processing industries or from non-edible plants

The availability of such resources and the effects of their utilization as energy for mobility on the natural and human world are as follows:

- Sugar cane has been cultivated in Brazil since 1532. Ethanol from sugar cane was being used there as a fuel for car engines between 1925 and 1935. Since 1975, after the first worldwide oil crisis, the Brazilian government has been implementing the national program "Pro Alcohol" with the aim of replacing fossil fuels by alcohols. The first car operating with 100 % ethanol was a Fiat 147 (1979). Ten years later, four million vehicles using 100 % ethanol fuel could be found in the traffic of Brazil. The inversion of this tendency back to gasoline had economic and political causes created outside of Brazil. However, this situation was surmounted within a relatively short time. In 2003, the Brazilian VW Golf 1.6 Total Flex was introduced, with an engine that allowed the use of a variable mixture of ethanol and gasoline, in proportions varying between 0 % and 100 %. Seven years later, other cars with flex fuel engines (Chevrolet, Fiat, Ford, Peugeot, Renault, Volkswagen, Honda, Mitsubishi, Toyota, Nissan, and Kia) appeared on the Brazilian market, achieving a proportion of 94 % of new car registrations.

  By October 2013 the number of flex fuel cars had increased to 23 million. This intensive utilization of sugar cane ethanol could generate a problem of availability. Brazil has 355×10^6 ha of cultivable surface, but only 72×10^6 ha is cultivated. Sugar cane occupies only 2 % of the cultivable surface and 55 % of

the sugar cane crop is transformed into ethanol. Brazilian scientists estimate that sugar cane production can be 30 times greater without influencing the environment or food production. The productivity achieved is 8000 l ethanol/ha (2008) at a price of 22 US cents per liter. The obtained energy, as stored in ethanol, is ten times higher than the energy consumed from sugar cane cultivation up to the point of ethanol distillation. About 99.7 % of sugar cane plantations are situated on plains in the region of Sao Paolo, at least 2000 km from the Amazon tropical rain forest, where the climate is not favorable for sugar cane plantations.

- In the USA, ethanol is obtained mostly from corn, cropped from 10×10^6 ha, which corresponds to 3.7 % of the cultivable surface. The productivity is 4000 l ethanol/ha (2008), which is half the level of productivity in Brazil. The balance between the obtained energy as ethanol and the consumed energy for plant cultivation and fuel distillation is only 1.3–1.6, a very low value compared with 10 in Brazil. The price of production is higher than for production from sugar cane, 35 US cents per liter compared with 22 US cents per liter. Ford, Chrysler, and GM produce flex fuel cars for their whole range of car types, from sedans and SUVs to off-road vehicles. In the USA there are more than 10 million flex fuel vehicles. A current government program stipulates the production of cellulose-ethanol, obtained from agricultural and domestic waste.

Not only sugar cane, corn, sugar beet, and cassava are utilizable for alcohol production; algae also have a remarkable potential as a resource for alcohol production. Algae are beings that live in water and produce their nourishment by photosynthesis. The earnings per surface, if cultivated in reactors, are much higher than for biomass production in agriculture: 15 times higher than rapeseed and 10 times higher than corn. Research and development activities in the field of production and utilization of algae as fuel are very intensive at this time; Boeing and Exxon are good examples in this sense.

Alcohol can be obtained in two different ways:

– Distillation of fermented biomass
– Synthesis, after gasification of organic waste and reaction assisted by cyanobacteria and enzymes

Alcohol was distillated for the first time in 925 by the Persian doctor Abu al-Razi from wine, according to historical records. The natural genesis of alcohol as a result of fermentation of fruits with high sugar content was observed by people much earlier, as mentioned in ancient scripts from Mesopotamia and Egypt, and also in the Bible. The production of alcohol from biomass is similar to the distillation of brandy, rum, whisky, vodka, or sake (as representatives of all continents of the world) or from fruits or vegetables. Sake was produced in Japan some 2300 years ago, brandy from litchi, and plum wine in Anatolia some 1000 years ago. The

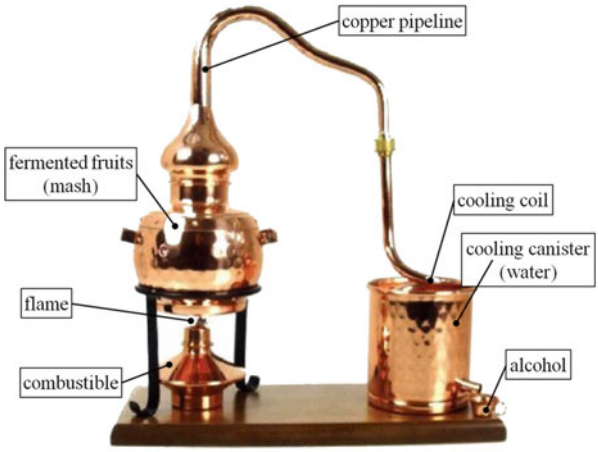

Fig. 3.19 Compact brandy still

overproduction of grain in England in the middle of the 18th century resulted in large-scale production of gin. Figure 3.19 shows a typical compact brandy still.

The simplest form of alcohol production is the boiling of fruits that have been left to ferment during a few weeks of storage under atmospheric conditions, followed by condensation of the generated steam by external cooling of the steam pipe (e.g., with a cold water flow) and collection of the resulting liquid in a vessel. This simple description underlines the fact that the technology of alcohol distillation is both easy and controllable. It can be applied worldwide in industrial plants but also in small, local distilleries. In industrial plants, the fermented biomass, which already contains about 10 % alcohol, is distilled to a concentration of 95 % alcohol. A very interesting method is the production of alcohol from waste that contains hydrocarbons, such as used tires, plastic bottles, or domestic trash. The treatment, which was developed by Coskata (Illinois, USA), is illustrated in Fig. 3.20.

Hydrocarbon structures in the waste are transformed by cracking into a synthesis gas. Part of the chemical energy contained in the $CO_2$and hydrogen is consumed by microorganisms within a bioreactor, producing ethanol. The microorganisms are permissive to impurities that would impede the classic chemical transformation of CO_2. General Motors, responsible for the project, reported that the cost of ethanol production using this procedure remains under US$1 per gallon, which is less than half the production cost for gasoline. The production of a gallon of ethanol in this way involves the consumption of one gallon of water; this is one third of the water consumption used for production of most other biofuels. In the year 2011, Coskata planned the production of 50–100 million gallons of ethanol in an industrial plant. By the year 2020, 18 % of the crude oil demand in the USA could be replaced by ethanol produced with this method. The efficiency chain between the energy resource and the moving wheel of a car, taking into account CO_2 recycling in nature, could lead to a decrease in CO_2 emission of 84 % in comparison with gasoline utilization.

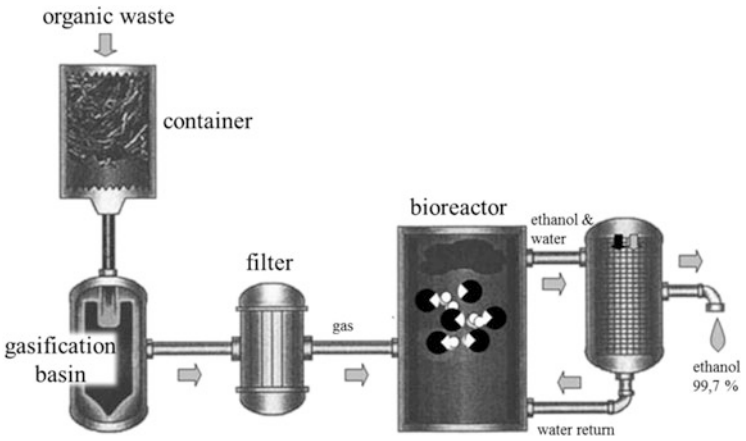

Fig. 3.20 Ethanol production from organic waste

3.4.2 Properties

Methanol and ethanol have lower heat values than gasoline (Table 3.1, Fig. 3.4), impairing car autonomy at comparable tank volumes. On the other hand, the lower air/fuel ratio leads to an increase in fuel mass in a mixture for the same air mass within a combustion chamber. Therefore, the heat value of the mixture remains in the range of air–gasoline mixtures. The octane numbers of ethanol and methanol are remarkably higher, allowing an increase in the compression ratio for monovalent engine operation. The vaporization enthalpy is 2.4 times higher than that of gasoline for methanol and 3.1 times higher for ethanol. This could be an impediment for injection in intake ducts. For direct injection, this high vaporization enthalpy is a net advantage because of the cooling of the compressed air.

3.4.3 Storage on Board

Methanol and ethanol have the same density at ambient pressure and temperature as diesel fuel and can be stored in the same kind of reservoir.

3.4.4 Mixture Formation and Combustion

The replacement of gasoline by methanol and ethanol in SI engines with injection in intake ducts was demonstrated in the 1970s, with remarkable success. Porsche tested a fuel containing 85 % methanol and 15 % gasoline, using two fuel pumps instead of one for gasoline, injectors with larger orifices, methanol-resistant materials for all fuel ducts, and methanol-compatible oil. The maximum energy density increased from 1.08 MPa to 1.22 MPa at 5000 min^{-1}, with 13 % effective

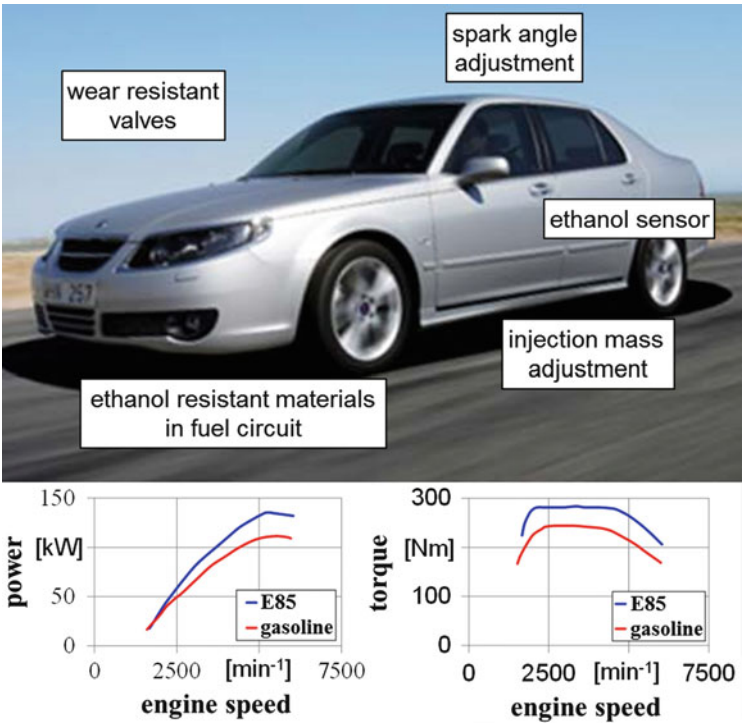

Fig. 3.21 Automobile with SI engine using variable ethanol–gasoline mixtures (flex fuel)

efficiency; the effective efficiency also increased, with 5.6 % at 2400 min^{-1} and 17.7 % at 5000 min^{-1}. Figure 3.21 shows, as an example, a current flex fuel automobile with similar adaptations for ethanol.

The benefits of using a mixture of 85 % ethanol and 15 % gasoline instead of 100 % gasoline are illustrated in Fig. 3.21 in terms of torque and power increase; a torque increase of 14 % is noticeable. All car manufacturers that have tested or introduced ethanol fuels have reported a torque increase in the range of 10–15 %. The reason for such an increase is an increase in specific cycle work when the combustion occurs faster, with the tendency to an isochoric process as an effect of the fast vaporization of ethanol and the fast combustion because of the oxygen content in ethanol molecules. An additional reason is the lower temperature of air during aspiration, as a consequence of the high vaporization enthalpy of ethanol during injection into the intake duct, leading to an increased air mass. Because of the lower heat value of ethanol (26 MJ/kg) compared with that of gasoline (44 MJ/kg), as shown in Table 3.1, and the lower stoichiometric air/fuel ratio (9 instead 14.7), the mass of ethanol injected into a cylinder with the same swept volume has to be increased. Under stoichiometric conditions, taking into account the densities of gasoline and ethanol, 1 l of gasoline must be replaced by 1.568 l of ethanol.

Adjustment of the injection system to the injected mass is feasible using different methods:

- Variation of the opening duration of the injector
- Variation of the flow cross-section through injectors, usually by doubling the number of injectors
- Variation of the fuel pressure, usually by using two pumps or a larger pump

Adjustment of the injection mass by one of these three measures can be described by following equation:

$$V_{\text{inj.}} = \int_{t_o}^{t_c} \mu A \cdot \sqrt{\frac{2}{\rho_{\text{fuel}}} \left(p_{\text{inj.}} - p_{\text{air}}\right)} \cdot dt \tag{3.4}$$

$V_{\text{inj.}}$	[mm^3]	Injected fuel volume
$t_c - t_o$	[ms]	Injected duration as the difference between opening and closing times
μA	[mm^2]	Effective flow cross-section
ρ_{fuel}	$\left[\frac{\text{kg}}{\text{m}^3}\right]$	Fuel density
$p_{\text{inj.}}$	$\left[\frac{\text{N}}{\text{m}^2}\right]$	Actual injection pressure
p_{air}	$\left[\frac{\text{N}}{\text{m}^2}\right]$	Air pressure in cylinder during compression at direct injection or in intake duct at intake duct injection
t	[s]	Time

Because of the steeper heat release when using ethanol instead of gasoline, both the specific cycle work and the thermal efficiency increase. A higher thermal efficiency leads to a lower bsfc; therefore, the ethanol/gasoline mass ratio remains under the stoichiometrically determined value, approximately 1.4 instead of the mentioned value of 1.568. The different molecular structures of ethanol and gasoline lead, for a stoichiometric complete combustion with the same air mass (corresponding to the cylinder swept volume), to following combustion products:

Combustion product	From 1.568 l ethanol [kg]	From 1 l gasoline [kg]
CO_2	2.356	2.285
H_2O	1.44	1.013
N_2	8.452	8.45

Despite the higher ethanol mass, CO_2 emission is roughly the same as from gasoline combustion, which is explainable by the lower C/H ratio in the ethanol molecule. For the same reason, the resulting water mass is higher.

An interesting concept is the direct injection of a mixture formed by gasoline, ethanol, and methanol in variable proportions depending on the momentary availability. The strongly different air/fuel ratios of the three fuels require noticeable adjustment of the injection mass for the same combination of load and speed,

depending on the actual mixture proportion. In this context, two problems need to be solved:

- Adaptation and controllability of the direct injection system for variable mixtures of gasoline, ethanol, and methanol
- Adaptation of the mixture formation and combustion technique to the variable injection rate and injection spray characteristics. At full load, a homogeneous mixture with air is required, whereas at partial load mixture stratification seems to be very beneficial.

At the same air mass within a cylinder, the complete substitution of gasoline by methanol in stoichiometric conditions would lead to an increase in injected mass of 2.2:1; a substitution with ethanol would give 1.6:1. Therefore, such an adjustment has to fulfill certain well-defined criteria [16–18].

3.4.4.1 Technical Feasibility and Engine Parameters

Detection of the momentary proportion of gasoline, ethanol, and methanol in the mixture up to the adjustment of injection mass, the start of injection, and the spark angle are solved problems in series engines with flex fuel injection into the intake ducts. Adaptation of such parameters for direct injection into the combustion chamber can be made with similar sensors and actuators.

3.4.4.2 Adaptation of the Injection System

The adaptation of a direct injection system to variable mixtures of gasoline, ethanol, and methanol must take into account the following aspects:

- Influence of the different properties of gasoline, ethanol, and methanol (e.g., density, viscosity, elasticity, and saturation limit) on the processes within the injection system (e.g., pressure course, pressure wave amortization, and injection rate modulation)
- Combination of parameters within the injection system, which depend on the momentary gasoline, ethanol, and methanol mixture to achieve optimum injection rate modulation at the given injection mass

3.4.4.3 Adaptation of the Mixture Formation

Modulation of the injection rate strongly depends on the injection mass for the mixture of gasoline, ethanol, and methanol. The characteristics of the fuel spray are determined by the properties of each component within the mixture.

If the amount of alcohol in the fuel is increased, the injected mass has to be augmented by a longer injection duration or a higher injection rate per time unit. Longer injection duration is limited by the engine speed of modern automobiles (doubling the injection duration when completely replacing gasoline by methanol does not seem to be feasible). For the same duration, there remains an increase in pressure at the injector input. This generates a higher flow velocity, higher droplet velocity in the fuel spray, and consequently longer spray penetration. However, this

theoretical additional spray length when injecting a fuel with increased alcohol fraction is damped by the faster vaporization of the alcohol droplets. Under such conditions, optimization between injection duration and injection pressure seems to be a reasonable method.

3.4.5 Applications and Results

Figure 3.22 shows the velocity and pressure curves for the direct injection of gasoline, ethanol, and methanol using a direct injection system with high pressure modulation (Zwickau pressure pulse system). The opening of an impact valve within a fuel acceleration pipe under an initial fuel pressure of 0.8 MPa generates an acceleration of the fuel column at the concomitant drop in pressure.

By closing the impact valve at a determined fuel velocity during acceleration (in this example 7 m/s), the steep pressure rise reaches 4 MPa, provoking fuel injection. For a higher injection mass, the initial pressure can be increased from 0.8 MPa (at 100 % gasoline) to 1.15 MPa (at 100 % ethanol) or 1.5 MPa (at 100 % methanol). For the same opening duration of the impact valve, the fuel velocity before impact increases from 7 m/s (gasoline) to 10.7 m/s (ethanol) or 12.6 m/s (methanol), generating a pressure rise from 4 MPa (gasoline) to 5.4 MPa (ethanol) or 5.8 MPa (methanol). In all these cases, the duration of the pressure wave is constant, corresponding to the length of acceleration pipe and the duration of

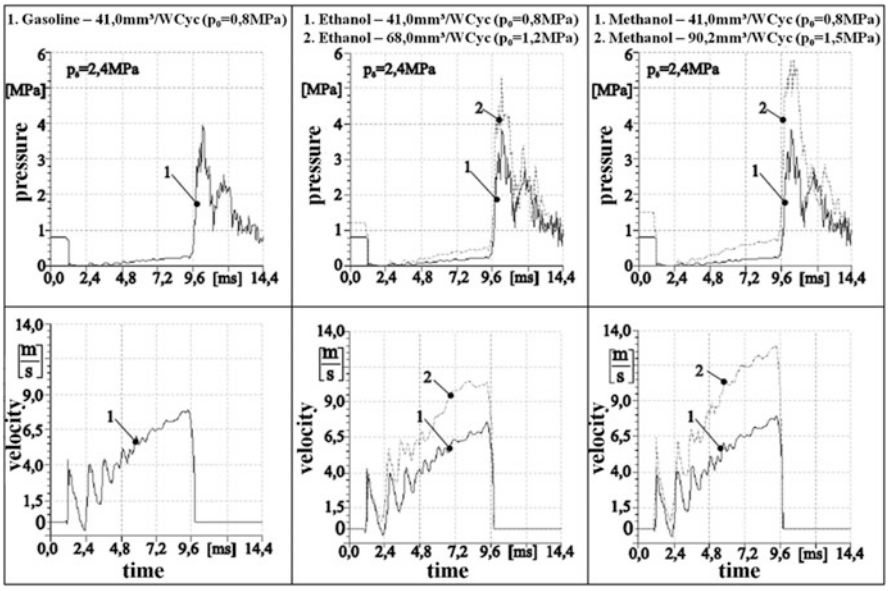

Fig. 3.22 Pressure and velocity history for direct injection of gasoline, ethanol, and methanol using high-pressure modulation (Zwickau pressure pulse): simulation

closure of the impact valve. The system was developed and optimized by simulation and experiments. Figure 3.23 shows the experimentally obtained pressure curves for the described cases. In this system configuration, the maximum injection volume (directly related to injection mass) was 22 mm^3 (for 100 % gasoline), 35.8 mm^3 (for 100 % ethanol), or 44.8 mm^3 (for 100 % methanol), obtained by augmenting the initial pressure at the values shown in Fig. 3.24, which illustrates the form of fuel dosage using gasoline, ethanol, and methanol.

The curves show a good proportionally from minimum to maximum injected amount. As shown in Fig. 3.22, an increase in the injected amount of ethanol or methanol is also obtainable by increasing the duration of acceleration of the fuel column, by the opening duration of the impact valve. However, increasing the fuel mass by increasing the initial pressure has the noticeable advantage of similar opening durations of the impact valve for all three fuels, simplifying electronic control. All curves for blends with different content of gasoline, ethanol, and methanol remain included between those for 100 % gasoline and 100 % methanol, as shown in Fig. 3.24. The increase in injected fuel mass with the alcohol content of the fuel, involving, as shown, a pressure increase at injector input, leads to an increase in fuel droplet velocity at exit. The consequence is a longer spray, which is partially compensated for by the faster vaporization of the alcohol fractions. This relationship between the time- and space-related spray characteristics at different alcohol content of the fuel blends is of importance for mixture formation and combustion when using direct fuel injection. Experimental analysis of the spray characteristics of the presented system with high pressure modulation was made using laser Doppler anemometry (LDA), laser sheet (LS) visualization, and charge-coupled device (CCD) camera and stroboscope. The LDA measurements give information about the distribution of droplet size and velocity within the spray and about their vaporization with time. The LS method allows analysis of droplet vaporization and distribution in every cross-section of the spray as well as visualization of the time- and space-related spray penetration. Using an Nd-Yag laser with a pulse of 5 ns, the spray can be cut in a particular cross-section and the image captured by a CCD camera. The droplet distribution is determined after measuring approximately 1300 injections for every fuel mass. In the first stage of analysis, the influence of an increased fuel mass (when blending gasoline with ethanol and methanol) on the spray length is determinable with sufficient accuracy by lateral spray visualization. The most interesting configurations can be analyzed in a second stage by the LS method and then by LDA. For the compact and clear information required in this overview, Figures 3.25, 3.26, 3.27, and 3.28 present results obtained from lateral spray visualization.

Figure 3.25 shows the time-related spray development during gasoline injection through a hole injector and through a pintle injector, for the same injection parameters, in terms of injection mass and injector opening pressure. From the fuel distribution around a pintle, the spray seems more homogeneous and shorter. Therefore, only the results for pintle nozzles are shown in Figs. 3.26 and 3.27. A comparison of the fuel spray during the direct injection of gasoline, ethanol, methanol, and a blend of all three fuels in the same proportion is shown in

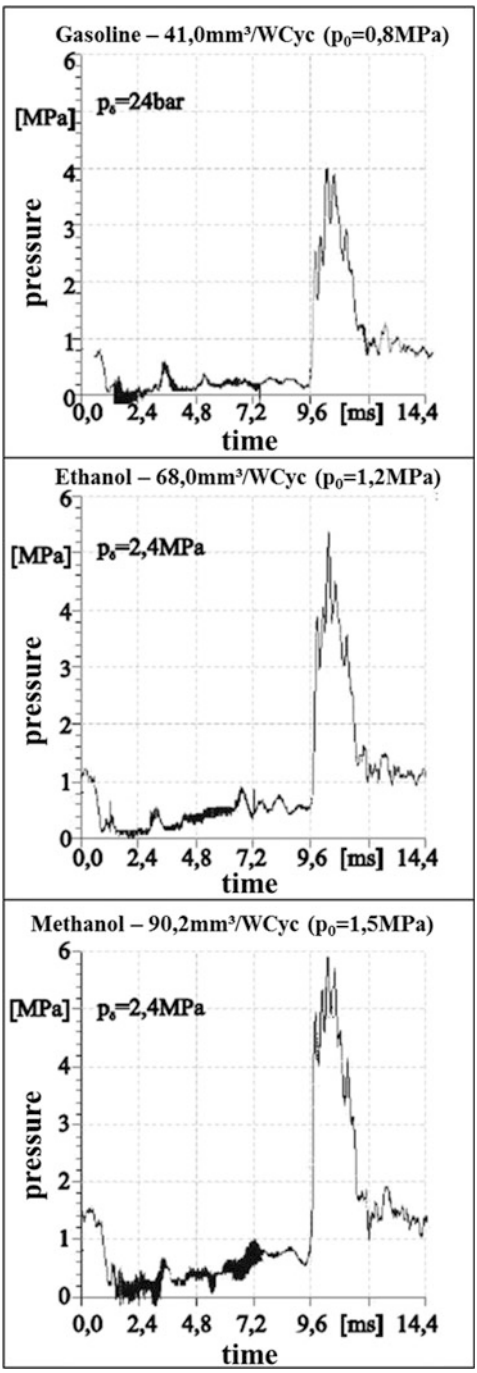

Fig. 3.23 Pressure history for direct injection of gasoline, ethanol, and methanol using high-pressure modulation (Zwickau pressure pulse): experimental

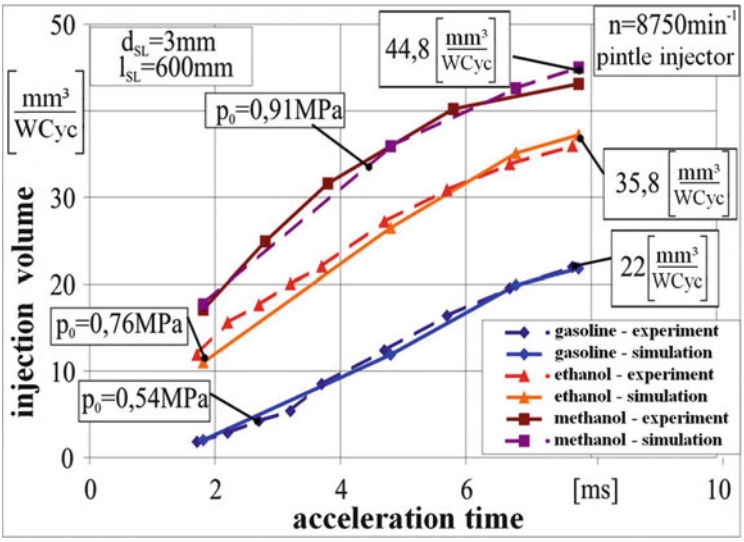

Fig. 3.24 Injection volume as a function of initial pressure and fuel acceleration time for gasoline, ethanol, and methanol: comparison of simulation and experimental results

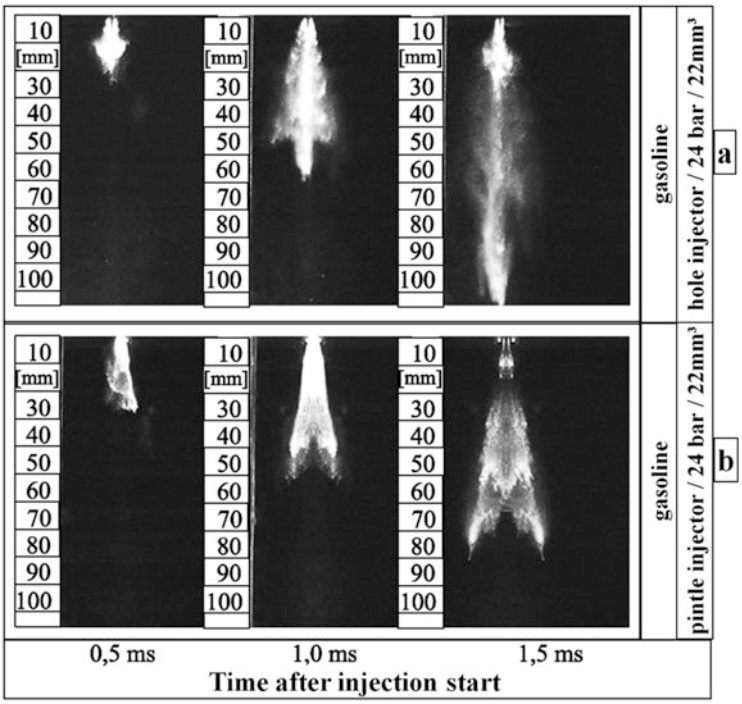

Fig. 3.25 Time-related spray development during gasoline injection through a two-hole injector (**a**) and a pintle needle injector (**b**)

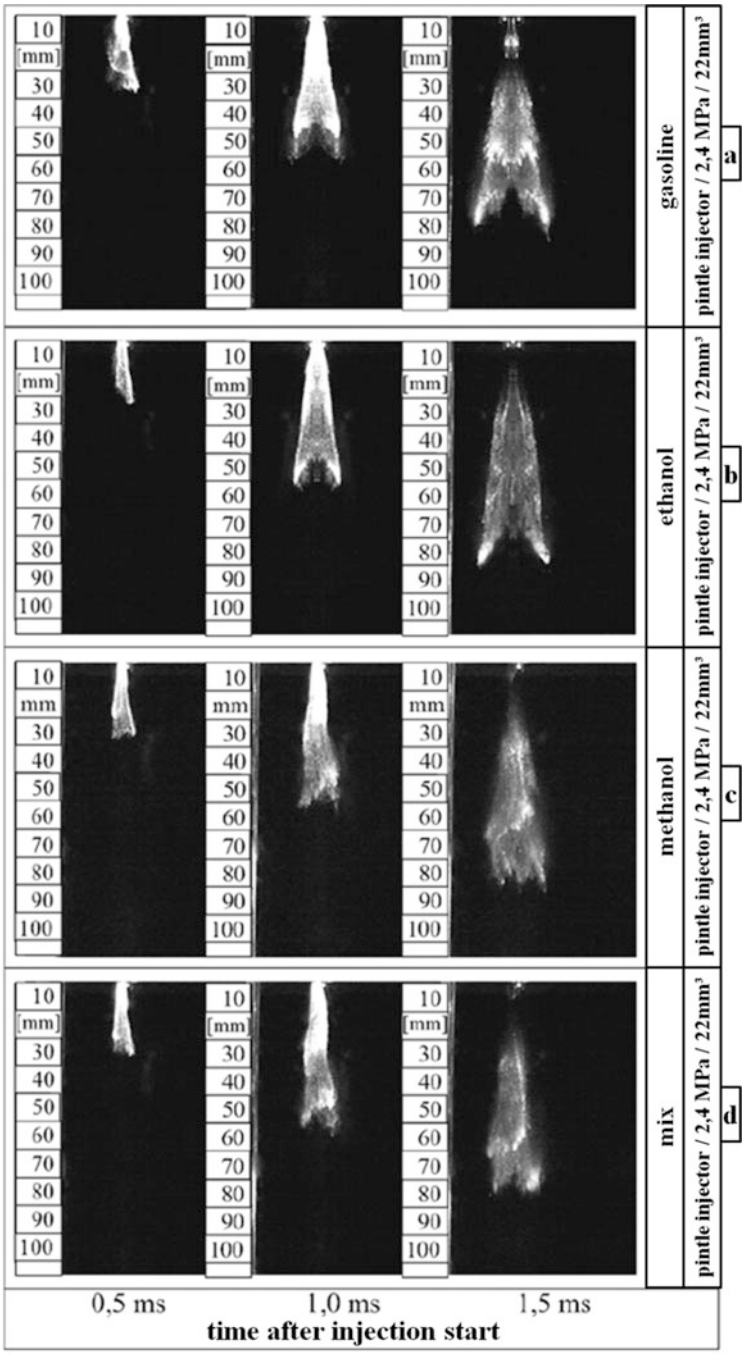

Fig. 3.26 Time-related spray development during injection of (**a**) gasoline, (**b**) ethanol, (**c**) methanol, and (**d**) a mix of all three fuels in equal parts, using the same injection mass

Fig. 3.26. For this first analyzed case, the injected volume as the same, 22 mm^3, for all four fuels. For comparison, Fig. 3.26a is identical with Fig. 3.25b. Using this method, there are no differences in the fuel distribution and vaporization, except for more accentuated liquid plumes when injecting gasoline. The time-related spray penetration length does not seem to be influenced by the fuel type, in this case with the same injection mass.

Figure 3.27 shows similar cases as in Fig. 3.26 but with the stoichiometrically required fuel mass at same air mass: 22 mm^3 for gasoline, 35.8 mm^3 for ethanol, 44.8 mm^3 for methanol, and 35.2 mm^3 for a blend of the three. In this case, the different concentrations of liquid kernel can be well recognized. At 1 ms after the start of injection, the liquid concentration in the ethanol spray is less strong than in the gasoline spray, despite the higher injected mass (1.63:1), as a result of faster vaporization. Comparison of the gasoline spray with the methanol spray at the same time sequence shows a similar situation. The opposite effects of injection mass and vaporization duration for the alcohol fraction lead to similar spray penetration lengths.

Figure 3.28 shows this relationship in terms of spray penetration length for all analyzed fuels. The increase in spray length between gasoline (80 mm), ethanol (95 mm), and methanol (100 mm) does not correspond to the increase in fuel mass for the same injection duration, from gasoline (22 mm^3) and ethanol (35.8 mm^3) to methanol (44.8 mm^3). This effect offers beneficial conditions for internal mixture formation by direct fuel injection when using blended fuels in different proportions.

The effects of vaporization during direct injection of blended gasoline have also been analyzed by numerical simulation [17]. The following directions of study can be mentioned:

- Calculation and representation of fuel concentration as the mass of liquid droplets in relation to the mass of the total gaseous phase formed by fuel and air.
- Calculation and representation of fuel concentration as the mass of liquid fuel in relation to the mass of air. However, by excluding the gaseous phase of the fuel, calculation of combustion in the next step is no longer possible. This form of calculation has the benefit of having a base (the constant mass of air) that is not variable with the injected fuel amount. Thus, such a representation is utilizable when analyzing the conditions of mixture formation.

Despite an increased mass in comparison with gasoline, ethanol and methanol have the advantage of a lower concentration of liquid droplets at every time during an injection event, as well as better distribution in air than gasoline. Such effects have been noted for every combination of injection mass, start of injection, and injection frequency corresponding to the engine speed. These results show that the direct injection of gasoline, ethanol, and methanol blends in variable proportions has no disadvantages compared with direct injection of pure gasoline.

The system configuration presented in Figs. 3.22, 3.23, 3.24, 3.25, 3.26, 3.27, and 3.28 served as the basis for experimental analysis at a test bench of a four-stroke, four-valve, single-cylinder engine of 125 cm^3 at a compression ratio of 11:1.

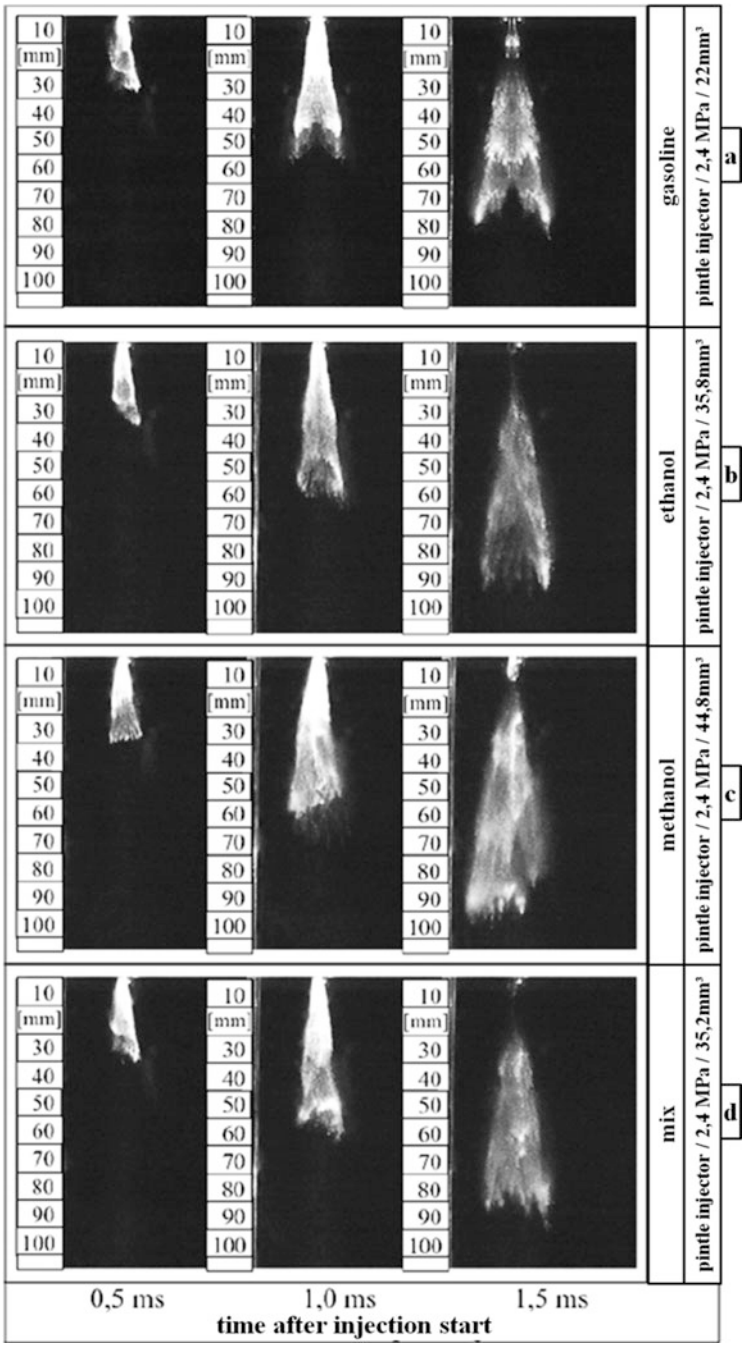

Fig. 3.27 Time-related spray development during injection of (**a**) gasoline, (**b**) ethanol, (**c**) methanol, and (**d**) a mix of all three fuels in equal parts, using a stoichiometric injection ratio

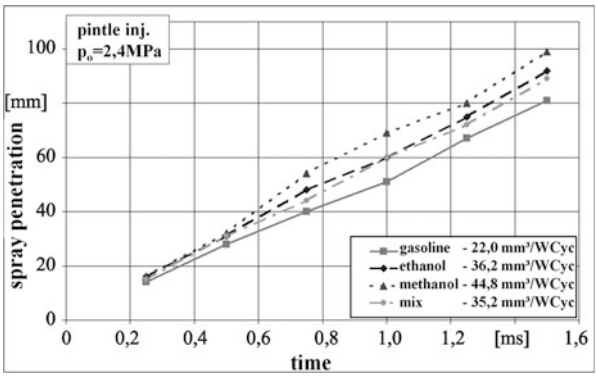

Fig. 3.28 Time-related spray penetration length for gasoline, ethanol, methanol, and a mix of all three, using a pintle injector and stoichiometric fuel/air ratio

Table 3.3 Performance comparison for stoichiometric gasoline/air and ethanol/air mixtures: experimental results

		Fuel		
Parameter		Gasoline	Ethanol	**Difference**
Specific work	$\left[\frac{kJ}{m^3}\right]$	900	750	−16 %
bsfc	$\left[\frac{g}{kWh}\right]$	450	800	+77 %
HC emission	[ppm]	7000	7000	–
CO emission	[%]	6	3.9	−35 %

The maximum effective power was achieved at 9500 min^{-1}, which imposed a very low stroke-to-bore ratio of 0.73. Such a compact volume, with a disadvantageous combustion chamber design resulting from the low stroke-to-bore ratio and at an engine speed that involves a high injection frequency, seems to be a good challenge for the injection system. The pintle-type injector was oriented from the engine head to the piston surface. A comparison of results for application of direct injection of gasoline and ethanol at 8750 min^{-1}, corresponding to the maximum torque of the tested engine, is shown in Table 3.3.

The specific work is 16 % lower for ethanol. Between the better heat release and the lower heat value for ethanol, this result gives a reason for further adjustment of the injection parameters. The bsfc increase of 77 % corresponds to the decrease in specific work. HC and CO emissions are equal and lower than for gasoline direct injection.

3.4.6 Applications and Potentialities

Worldwide there are 38.8 million flex fuel cars (October 2013) on the road, most of them in Brazil (23 million), USA (15 million), Canada (0.6 million), and Sweden (0.23 million). An overview of the yearly production of flex fuel cars in Brazil (2010) is shown in Table 3.4. The rapid increase in the number of flex fuel cars in Brazil is demonstrated in Table 3.5. In the USA, 216,000 flex fuel cars were

Table 3.4 Yearly production of flex fuel cars in Brazil (2010)

Manufacturer	Flex fuel cars (annual production)
VW	46,393
Fiat	41,581
GM	39,177
Ford	22,135
Renault	11,813
Honda	8136
Toyota	4536
PSA	3982

Table 3.5 Yearly production of flex fuel cars in Brazil for different years

Year	Flex fuel cars	Percentage of total produced cars
2003	49,264	2.9 %
2006	1,392,055	56.4 %
2012	2,701,781	83.4 %

produced in 1998 and 11 times more (2.47 million) in 2012. The 15.11 million flex fuel cars operating at this time demonstrates, more than all government programs, the customer acceptance of such a solution.

Figure 3.29 shows, as an example, a flex fuel car of type VW Golf 1.0 and the values for power and torque when operating with pure gasoline and with pure ethanol. As expected, the torque is 10 % higher when injecting ethanol, which implies a proportionally higher power.

The utilization of blends of gasoline and biomass alcohols for direct injection in SI engines has a noticeable potential for future application. The advantages are convincing: renewable energy sources, recycling of CO_2 emission after combustion in the plant cycle, decrease in fuel consumption by direct injection, and utilization of the existing fuel filling infrastructure by variable fuel blends, according to availability.

On the far horizon is the utilization of alcohols without gasoline content and the use of alcohol in the production chain as power source, comparable with hydrogen obtained by electrolysis using solar energy. The main energy sources and the process chain are similar in both cases, only the energy transporter is different:

- The energy of solar radiation is used for propulsion on the basis of CO_2, which is emitted by combustion and then absorbed by plants that act as natural reactors and break down the CO_2. Thus, the CO_2 in nature becomes the transporter of the energy conversion.
- The energy of solar radiation is used for propulsion on the basis of water, which is emitted by the reaction in a fuel cell or by combustion in an engine, and then broken down in a non-natural reactor (an electrolysis plant powered by solar energy). Thus, the water in nature becomes the transporter of the energy conversion.

	Torque [Nm]	Power [kW]	0-100 km/h [s]	v_{max} [km/h]
Gasoline (100 %)	97	53	13,5	165
Ethanol (100 %)	106	56	13	165,4

Fig. 3.29 Example of a flex fuel car: VW Golf 1.0 (Source: Volkswagen)

The only difference between both circuits is the process used for recycling of the molecules of CO_2 or H_2O: natural photosynthesis versus industrial electrolysis.

3.5 Hydrogen

3.5.1 Production

Hydrogen is the subject of numerous ideal scenarios about the propulsion of the future:

- Production of hydrogen is theoretically possible using solar energy, by electrolysis from water, without pollutants.
- Utilization of hydrogen by combustion in an engine or by proton exchange for current generation in a fuel cell results in production of water, provided the high combustion temperature in an engine does not provoke NO_x emission.

The dissociation of water in a stationary plant and its re-formation in an on-board device in a car seems to be an ideal form of energy transmission, with storage of an intermediate product (in this case hydrogen). However, the problem is storage. The gas constant of hydrogen has the highest value of all elements, corresponding to the lowest molecule mass of all elements. Thus, for storage of a sufficient mass, a very high pressure or a very low temperature is required, according to Eq. (3.5):

$$pV = mRT \text{ and } m = \frac{pV}{RT} \tag{3.5}$$

p	$\left[\frac{\text{N}}{\text{m}^2}\right]$	Pressure of the stored gas (hydrogen)
V	[m^3]	Volume of the stored gas (hydrogen)
m	[kg]	Mass of the stored gas (hydrogen)
R	$\left[\frac{\text{J}}{\text{kgK}}\right]$	Gas constant of the stored gas (hydrogen)
T	[K]	Temperature of the stored gas (hydrogen)

In a reservoir with volume V at pressure p and temperature T, the mass of the stored medium depends on its gas constant R, and on its molecular mass $\overline{M}$:

$$R = \frac{\overline{R}}{\overline{M}}$$

$\overline{R}$ [J] universal gas constant (joules/kilomole per degree Kelvin)
$\overline{M}$ [kg] molecular mass of a substance (kilograms/kilomole)
R [J] gas constant of a substance (joules/kilogram per degree Kelvin)

with
$\overline{R} = 8314$ J/kmol K and $\overline{M}_{H_2} = 2 \times 1.00794$ kg H_2/kmol
it follows that $R = 4124.25$ J/kg K.

Under ambient conditions, for example, at $p = 1 \times 10^5$ N/m^2 and $T = (273.15 + 20)$ K, an 80 l reservoir ($V = 0.08$ m^3) would contain the following mass:

$$m = \frac{pV}{RT} \rightarrow m = \frac{1 \times 10^5 \times 0.08}{4124.25\,(273.15 + 20)} \rightarrow m = 6.6 \ g \ H_2$$

Air has a specific gas constant of 287.04 J/kg K, which is 14.4 times lower than that of hydrogen. Therefore, in the above example, the mass of air in a reservoir of 80 l is 95 g. The same reservoir would contain, under same pressure and temperature conditions, 60 kg gasoline with a density of 0.75 kg/l. The heat value of hydrogen is 120 MJ/kg and of gasoline 44 MJ/kg (see Table 3.1); thus, 22 kg hydrogen would contain the same energy as 60 kg gasoline. But, this reservoir contains only 7 g of hydrogen!

Hydrogen can be stored at −253 °C in liquid phase; another possibility is to increase the pressure, and values of 90 MPa have been achieved. This physical

Table 3.6 Energy sources for the production of hydrogen

Energy source	Percentage (%)
Natural gas	38
Heavy oil	24
Gasoline	18
Ethylene	6.6
Other chemical products	1.4
Electrolysis	2
Coal gas–	10

relationship is independent of the technical progress of storage systems. Moreover, the production of hydrogen corresponds to the ideal scenario with clean water dissociation and hydrogen storage at only a percentage of 2 %! About 98 % of the yearly produced 500×10^9 Nm^3 (normal cubic meters) of hydrogen is from fossil energy sources, causing emission of CO_2 or coal gas.

– The re-forming reaction when using natural gas for hydrogen generation is:

$$CH_4 + 2H_2O \rightarrow CO_2 + 4H_2 \tag{3.6}$$

– The cracking reaction for the same energy source is:

$$CH_4 \rightarrow C + 2H_2 \tag{3.7}$$

The yearly production of the mentioned 500×10^9 Nm^3 of hydrogen is based on the energy sources shown in Table 3.6. The hydrogen obtained in this form has been utilized for many years in different industries for the production of fertilizer, colorants, solvents, and synthetic materials, but also for the improvement of fuel structures.

3.5.2 Properties

One of the main problems regarding the utilization of hydrogen on board automobiles is its storage on board. In the liquid phase, obtained as mentioned at −253 °C, the density of hydrogen is only a third of the gasoline density at ambient conditions. Generation of the liquid phase requires a third of the hydrogen energy content of the produced quantity. An alternative is to increase the pressure to 35–90 MPa, still in gaseous phase. However, in this case, the difference from ambient pressure generates a flow potential: the molecule of hydrogen is the smallest of all elements and can penetrate most material structures. Therefore, a hydrogen reservoir must have a wall structure composed of many layers, with high resistance to the high pressure. However, leakage is not avoidable, even from a structure with many layers. The most optimistic information indicates 1 % leakage

per day. Even though such an amount seems negligible, there is a float within the hollows spaces of the car body. On the other hand, hydrogen is inflammable at 4–77 % concentration in a mixture with air; the flame velocity is very high and the flame is invisible; the result can be dangerous detonation. The absorption of hydrogen clouds in car bodies by pumps increases the technical complexity.

3.5.3 Storage

The storage of hydrogen in the liquid phase, at −253 °C, requires cryogenic reservoirs with appreciably increased volume in comparison with gasoline tanks for same stored energy. Isolation between the wall layers of the reservoir is made by vacuum. A problem is that, although given by the connecting elements between layers, the thermal conductivity of a gas is in the range of 0.01–0.02 W/m K, whereas the thermal conductivity of a metal achieve values of 50 W/m K. Some reservoir models are characterized by a floating of the concentric layers, generated by magnetic forces. Figure 3.30 shows a cryogenic hydrogen tank for an automobile with bivalent operation (hydrogen and gasoline). Two layers are separated in this device by a gas layer, where gaseous hydrogen can be collected.

Cryogenic storage requires a cooling circuit with own heat exchanger.

Figure 3.31 shows more details of this storage technique, indicating the wall layer materials. Figure 3.32 shows the tanks for gasoline and for hydrogen in a car for bivalent operation [19].

The storage of hydrogen in filling stations and the filling itself necessitate additional technical support, despite the fact that the production and transport of hydrogen has a long tradition. Figure 3.33 shows a filling station for automobiles using hydrogen propulsion.

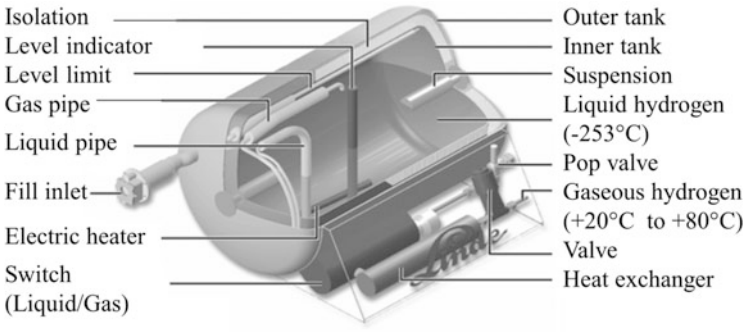

Fig. 3.30 Cryogenic hydrogen tank for automobiles

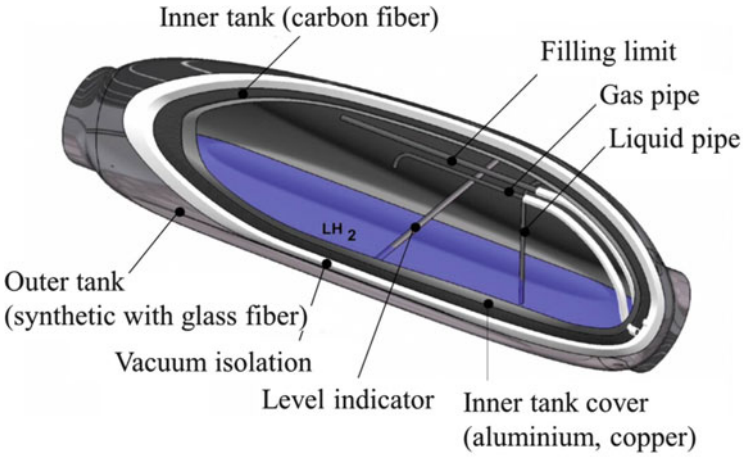

Fig. 3.31 Cross-section through a cryogenic hydrogen tank for automobiles

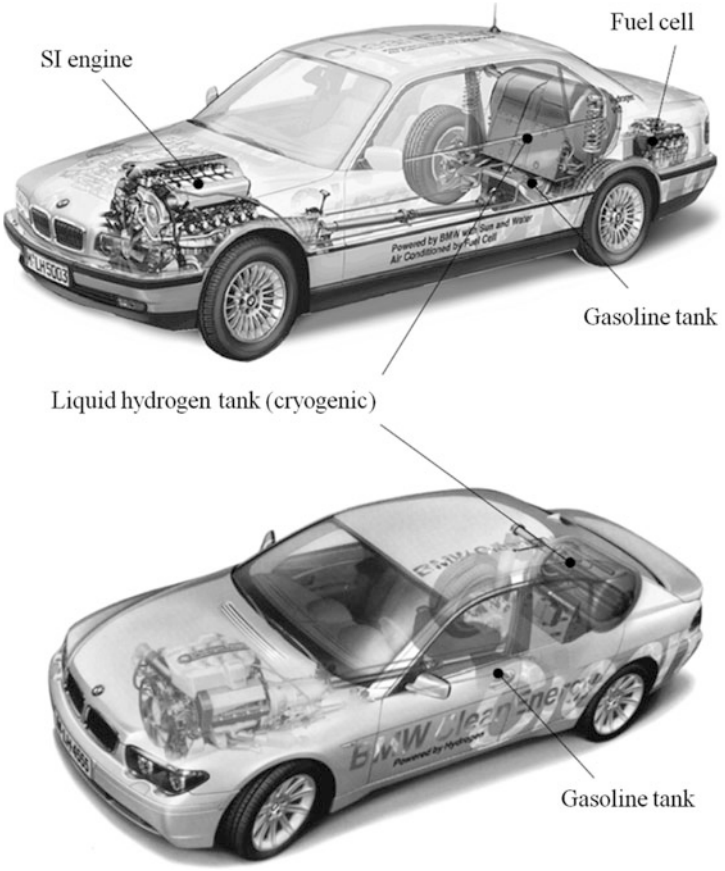

Fig. 3.32 Automobile with hydrogen SI engine (Source: BMW)

Fig. 3.33 Hydrogen filling station for automobiles (Source: BMW)

3.5.4 Mixture Formation

For the operation of SI engines with hydrogen, both techniques for mixture formation are utilized—direct injection into the combustion chamber and injection into the intake duct [28]. An interesting variant is the combination of both concepts, concomitant injection into the combustion chamber and into the intake duct. Figure 3.34 shows these variations for mixture formation. External mixture formation is similar to the methane dosage in SI engines (see Sect. 3.2, Fig. 3.8). Using cryogenic hydrogen storage, the complete system from the tank, pipes, and injection system to the injectors has to be thermally isolated to avoid gasification of the liquid phase of hydrogen. For this, the pressure within the system is additionally increased. Injection into the intake duct allows (similar to the injection of methane or gasoline) good homogenization of the mixture as a result of the longer route and time in comparison with direct injection. A special problem when injecting hydrogen into intake ducts is given by the low density of 0.071 kg/dm^3 in comparison with that of methane (0.141 kg/dm^3) or gasoline (0.736 kg/dm^3). In comparison with gasoline, the hydrogen to be injected has a volume that, for the same injected mass, is ten times higher (0.736 versus 0.071). On the other hand, the heating value of hydrogen is much higher than that of gasoline (120 versus 44 MJ/kg) and also the

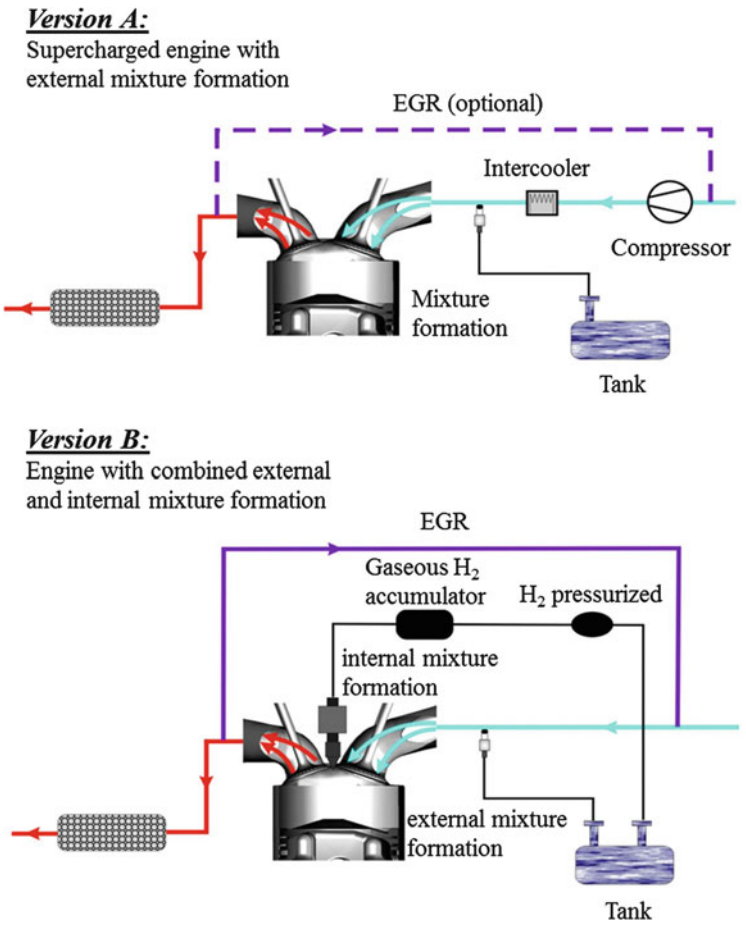

Fig. 3.34 Two versions of mixture formation in hydrogen SI engines (Source: BMW)

air/fuel ratio (34.3 versus 14.7 kg_{air}/kg_{fuel}) . Therefore, at stoichiometric complete combustion the hydrogen mass is only 14.7:34.3 = 0.429 of the gasoline mass. However, at a tenth of the density, the hydrogen volume to be injected is four times higher.

On the other hand, the air density within the intake duct (e.g., without super-/turbocharging and intercooling at 0.1 MPa and 273 K) is 0.0012 kg/dm^3; the injected hydrogen changes within the intake duct, at the given pressure and temperature, from liquid to gaseous phase. At the same pressure and temperature, the density of hydrogen is 13.4 times lower than the air density, corresponding to the gas constants of both substances (3851.21 and 287.04 J/kg K). The lower hydrogen density provokes (more than at methane injection) a decrease in air volume transferred from the intake duct to the cylinder, because of the hydrogen volume

within the duct. Less air within the cylinder means less injected hydrogen to remain at stoichiometric ratio. The heat value of the mixture decreases, resulting in a decrease in torque. A compensation of this effect is possible by supercharging and intercooling, as shown in Fig. 3.34, version A.

In this mode, the air mass increases. On the other hand, the low temperature damps the change of phase of hydrogen from liquid to gas. A better alternative would be hydrogen direct injection into the combustion chamber, after complete cylinder filling with air. The mixture turbulence generated by hydrogen direct injection and modulation of the injection rate for optimum heat release are, as presented in Sect. 2.2.2, additional advantages. Nevertheless, hydrogen direct injection has two major disadvantages in comparison with gasoline direct injection:

- Injection of a fuel volume that is four times higher than a gasoline volume requires a notable increase in injection pressure or a strong prolongation of the injection duration. The possibilities in either direction are very limited.
- Contact of the injector with the combustion chamber requires much more sophisticated thermal isolation than in the case of injection into the intake duct. The injector coat reaches a temperature of about 200 °C instead of 15–20 °C in the intake duct. In such conditions it is very difficult to maintain the hydrogen temperature at −253 °C until fuel exit from the injector.

A compromise, as shown in Fig. 3.34 version B, involves the combination of direct injection and duct injection.

3.5.5 Application and Results

Currently, approximately 600 automobiles with hydrogen engines are operating worldwide. The pioneer work in research and development of automobiles with hydrogen engines was performed by BMW [19].

The first hydrogen car from BMW was conceived in 1979. The four-cylinder engine achieved a power of 60 kW. Concomitantly with the development of hydrogen cars, BMW together with Solar Wasserstoff Bayern GmbH and other partners developed a method for the production of hydrogen by electrolysis using solar energy. As mentioned in Chap. 1 (Fig. 1.26) combined propulsion and on-board current generation with the same fuel is very favorable when using hydrogen. BMW developed a compact fuel cell for this application, as shown in Fig. 3.35, with an electric power of 5 kW at a tension of 42 V. Figure 3.36 shows the engine specifications and performance when operated with hydrogen and with gasoline. The twelve-cylinder engine has a swept volume of 5.38 dm^3 and a compression ratio of 10.

As deducible from the lower heat value of the air–hydrogen mixture, in comparison with the air–gasoline mixture, the torque decreases from 490 N m with gasoline to 300 N m with hydrogen. The power decrease is partially compensated

Fig. 3.35 Fuel cell with hydrogen for on-board current generation for an automobile with hydrogen SI engine (Source: BMW)

for by a higher engine speed: 240 kW at 5000 min^{-1} with gasoline and 150 kW at 5800 min^{-1} with hydrogen.

The utilization of hydrogen in fuel cells for propulsion or for on-board current generation is presented in Chap. 4.

Considering the future progress in production and storage of hydrogen on board automobiles, water as an energy source and reaction product is an ideal support for energy transformation. Nevertheless, an exciting alternative is CO_2, which in nature acts as a similar form of support for energy transformation from biomass through combustion to the next plant. The production of alcohol from biomass and its easy storage leads to beneficial competition between the two scenarios, the winner being mobility.

3.6 Vegetable Oils

3.6.1 Production

The variety of plants from which oil can be obtained provides considerable potential for nourishment and also for fuel; examples are rapeseed, beets, sunflowers, flax, olive trees, coconut palms, peanuts, soy, castor-oil plant, cocoa, and cotton. The extraction of oil using a mechanical press is well disseminated and not expensive. Generally, pressing is followed by refinement in stages to eliminate secondary substances. In the next stage, phosphates and slimes, and then free fatty acids are removed. As shown in Table 3.1 one of the characteristics of oil, its

Engine		BMW 12 Cylinder SI engine Super ROZ 95	BMW 12 Cylinder SI engine hydrogen
Swept volume	[cm³]	5,379	5,379
Stroke/ bore	[mm]	85/ 79	85/ 79
Compression ratio	[-]	10:1	10:1
Power at speed	[kW] [min^{-1}]	240 5,000	150[1)] 5,800[1)]
Torque at speed	[Nm] [min^{-1}]	490 3,900	300[1)] 3,000[1)]

[1)] With hydrogen

Fig. 3.36 Engine characteristics of an SI engine operating with gasoline and with hydrogen (Source: BMW)

viscosity, generally impedes the utilization of oils that are produced in this manner. The long and branched oil molecules, which are the cause of this high viscosity, impair the combustion process by preventing oxygen atoms from the air from reaching the carbon atoms. This leads to coking of the injector holes, valves, and piston rings, causing impairment of operation or engine damage. A basic solution to this problem is to shorten the branched molecules, which can be accomplished by the procedure known as transesterification. A schematic is presented in Fig. 3.37.

Transesterification is a chemical reaction between an oil and methanol, resulting in methyl ester and glycerin. As shown in Table 3.1, this process leads to a decrease in viscosity to a tenth of the value of a pressed oil, a level that is close to the viscosity of diesel fuel. Concomitantly, the ignitability increases. However, the transesterification procedure is expensive, its cost per liter ester being about that of 1 l of pressed oil or 1 l of diesel fuel. Furthermore, the energy required by this procedure is high, 360 kJ/l.

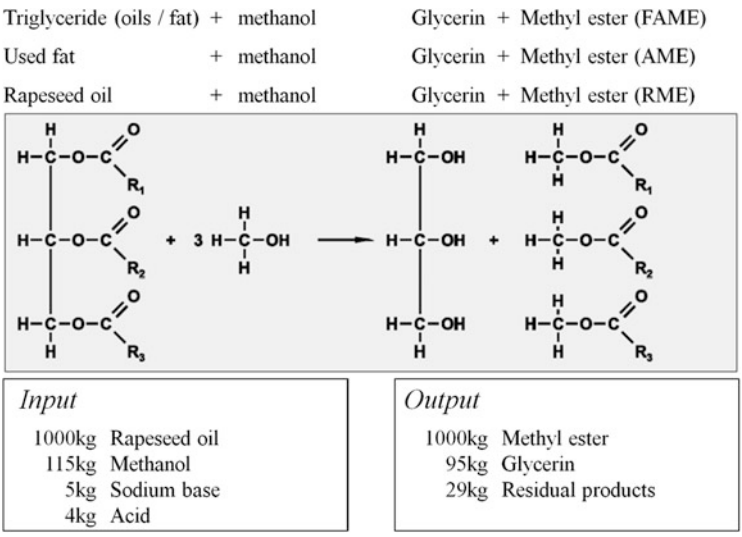

Fig. 3.37 Transesterification of oils

Biomass fuel 1: Generation

In Germany, such fuel is obtained from 80 % rapeseed and 20 % soy and is named FAME (fatty acid methyl ester), corresponding to the German standard DIN EN 14214. Its main characteristics are as follows:

- Density: $\rho = 0.88$ kg/dm^3
- Heat value: $H_u = 37.1$ MJ/kg
- Ignitability: CZ = 54–58

Biomass fuel 2: Generation

Biomass-to-Liquid (BtL), Next-Generation Biomass-to-Liquid (NexBtL)

Such fuels are generally produced from biomass waste such as wood scrap, straw, and plant residues after taking the fruits for nourishment. The main characteristics are as follows:

- Density: $\rho = 0.76$–0.79 kg/dm^3
- Heat value: $H_u = 43.9$ MJ/kg
- Ignitability: CZ > 70

The procedures for fuel production are generally the Fischer–Tropsch process, hydrogenation, and pyrolysis:

- The Fischer–Tropsch procedure (BtL) involves gasification of the biomass in a reactor at a certain pressure, with a heat input and with involvement of oxygen. The process consists of three stages:

  - Gasification at low temperature: The biomass with a water content of 15–20 %, partially oxidized with air or directly with oxygen, is carbonized at temperatures between 400 and 500 °C, resulting in a coal tar gas.
  - Substoichiometric oxidation of the coal tar gas over the dripping point, in a combustion chamber.
  - Injection of biocoke powder in the gasification medium: A synthetic raw gas is generated in an endothermic reaction. The gas is composed of CO_2, CO, and H_2. The subsequent Fischer–Tropsch synthesis produces so-called Sun Diesel, which has similar molecules to diesel fuel, from the synthesis gas (CO, H_2) using a catalyst based on iron, magnesium oxide, thorium oxide, or cobalt . The energy content per surface is three times higher than that of biomass fuel 1. Generation is based on rapeseed. A modern automobile with a diesel engine can achieve about 64,000 km, at a consumption of approximately 6 l/100 km, using the Sun Diesel that is obtained from 1 ha.
- Hydrogenation (NexBtL): A vegetable oil is treated with phosphoric acid and caustic soda (H_3PO_4, NaOH) and subsequently hydrogenated at a temperature of 320–360 °C and a pressure of 8 MPa. Such hydrogenation can be carried out in a typical refinery. The resulting fuel has, similar to that obtained with the Fischer–Tropsch procedure, the characteristics of a diesel fuel, but better ignitability of CZ = 84–99.
- Pyrolysis: The biomass is heated at 475 °C without oxygen. The products of pyrolysis are then cooled and condense. The heat value of the obtained fuel is half the heat value of a conventional diesel fuel.

3.6.2 Properties

Biofuels of the second generation (BtL, NexBtL) are broadly similar to classic diesel fuel. Oils obtained by transesterification (biofuels of the first generation) are less similar to diesel fuel: The oxygen content in the molecules of oils and oil esters lead to lower heat values and also to a lower stoichiometric air requirement, as shown in Table 3.1. In terms of the heat value of the mixture, the lower heat value is compensated for by a lower stoichiometric air requirement, which leads to a higher fuel participation in the mixture. However, an oil–air mixture cannot achieve the heat values of a diesel fuel–air mixture. This leads to a decrease in specific work within the cycle and, therefore, to a decrease in torque when powering the same diesel engine, as shown in Fig. 3.38.

However, using rapeseed oil or oil esters, the torque and power of a diesel engine is more or less achievable. This can be explained by the combustion behavior of such oil esters. After a first combustion phase at low velocity, caused by slow vaporization of the oil droplets, the oxygen atoms within the oil ester molecules provoke a high concentration of free OH radicals, which accelerate combustion.

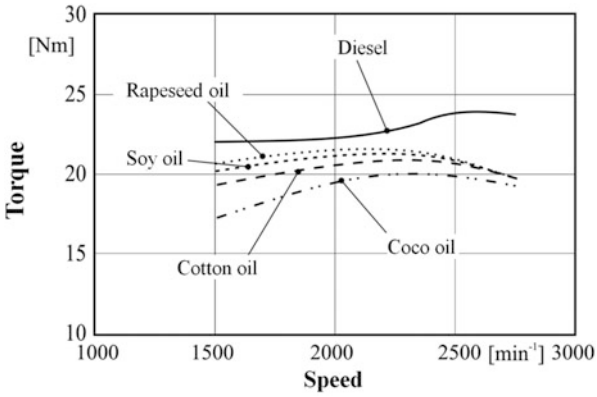

Fig. 3.38 Comparison of maximum torque obtained using different fuels

3.6.3 Storage

Oils and oil esters can be stored in a similar way to diesel fuels because of their similar density under ambient conditions. Non-esterified oils have a higher viscosity at low ambient temperature, which impedes normal engine operation. In some variants of storage and dosage systems, the oil is treated to diminishing the viscosity. An additional problem when using non-esterified oils is the formation of fungi and slime in the complete fuel system, including filters. Just 15 % rapeseed oil content in diesel fuel is sufficient for such formation. The storage of oil esters is similar to that of diesel fuel.

3.6.4 Mixture Formation

Piston engines working in a Diesel cycle, with large or small swept volume of between 1.6 and 12 dm^3, with all configurations for mixture formation from pre-chamber to direct injection, with aspiration, or with super-/turbocharging, have been operated with oils and oil esters.

Taking into account that direct injection is the only valid alternative to mixture formation in future diesel engines, as explained in Sect. 2.2, non-esterified oils have no future in this area for the following reasons:

- The usual pressure level of 180–220 MPa in common rail systems requires very small tolerances for plungers or pumping elements. The high viscosity of oil can impede free movement.
- Coking of injector holes, which in modern injection systems can have diameters of 0.08 mm, can disturb the injection process. Figure 3.39 shows deposits of coke around the holes of an injector after operating for a long duration with non-esterified oil.
- During the production of oil esters, non-negligible differences in properties are unavoidable, increasing the risk of high viscosity and coking.

Fig. 3.39 Coke at an injector for CI engines with direct injection after using pure rapeseed oil

3.6.5 Applications and Results

The power and consumption of engines powered with non-esterified rapeseed oil and alternatively with diesel fuel are identical in all tested types. However, long operation with such pure oil is possible only in engines with a large swept volume equipped with a swirl chamber. In automobile engines with relatively small swept volumes and with direct injection, the utilization of non-esterified oils is not recommended. The pollutant emission when using such oils is disadvantageous in comparison with the utilization of diesel fuel. Operation with an ester (e.g. rapeseed methyl ester, RME, from rapeseed oil) shows results comparable with those for diesel fuel, with small power differences, as shown in Fig. 3.40 for an engine with a swept volume of 1.6 dm^3.

A reason for the power difference is the lower heat value of the RME–air mixture. The increase in power difference at higher speed is explainable by the higher viscosity of RME, impairing flow through the nozzle holes. The pollutant emissions from RME and from diesel fuel show some differences:

- The smoke and particulate emission is lower for RME because of the oxygen content in the molecules, leading to more efficient combustion; the emission of aromatics is also lower.
- SO_2 emissions from RME were not observed.

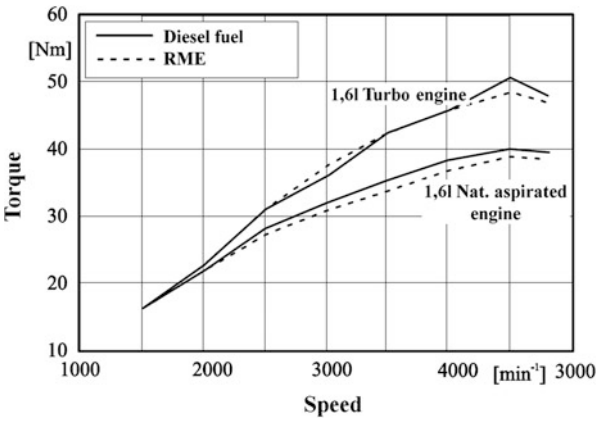

Fig. 3.40 Comparison of torque obtained for a CI engine using diesel fuel or RME

– Organic substances in the exhaust gas from RME and diesel fuel have different structures. The mass of organic substances in the exhaust gas is higher from RME combustion.
– The NO_x emission is higher from RME combustion.

The utilization of oil esters in diesel engines for automobiles is possible, but the price of transesterification limits its large scale application in the future. More interesting is the blending of crude oil with vegetable oils during refining. The resulting molecular structure is not different from the structure of diesel fuel.

3.7 Dimethylether

3.7.1 Production

Dimethylether (DME) is an interesting alternative to diesel fuel. It is obtainable from coal and from natural gas, but also from wood trash. Using wood trash, the procedure is similar to the production of methanol (i.e., gasification and synthesis). The availability of this resource and the resulting CO_2 recycling, as in the case of alcohol, are accompanied by additional benefits:

– The high oxygen content of 35 % mass allows, as for oil esters, efficient combustion and, therefore, low emission of soot and particulates.
– The low inflammation temperature of 235 °C (i.e., high inflammability) favors the combustion process, allowing an improvement in thermal efficiency.

3.7.2 Properties

DME in the liquid phase has a density that is only 15 % less than the density of diesel fuel. The viscosity is much lower than that of diesel fuel, creating problems within the injection system. However, in comparison with oils, lubrication of moving parts within the injection system is not possible with such a fuel. Because of the similar percentages of C, H, and O to those in a molecule of methanol, the heating value, stoichiometric air requirement, and mixture heat value are almost identical for both DME and ethanol. Thus, the mixture heat value is slightly lower than that of the diesel fuel–air mixture. Nevertheless, the better vaporization and combustion of RME compensates for this disadvantage.

3.7.3 Storage

Liquid DME is storable at 20 °C and 0.5 MPa. Liquid gases are characterized by a relatively high compressibility. Under the damp pressure limit, the formation of vapor bubbles is very probable, indicating a disturbance of function within the injection system. Therefore, such a system comprises a supplementary pump for maintaining the RME pressure over the damp limit. On the other hand, leakages in the modules of the injector system have a similar effect. In this case, the gaseous RME phase from such places is conducted to a separate purge tank and pumped at higher pressure, becoming liquid, before returning to the main tank. Such a layout of an injection circuit is shown in Fig. 3.41.

3.7.4 Mixture Formation

An injection system in which high pressure generation occurs only during the injection event, like a pressure wave, is not applicable for DME because of its compressibility. The only solution in this case is storage of DME at constant high pressure, in a common rail [2]. An initial pressure pump included in the tank maintains the fuel at a pressure corresponding to its liquid phase, before entering the high-pressure pump, which ensures a strong flow recirculation because of the compressibility of DME. The fuel contains additives for pump lubrication. Maintenance of the fuel in liquid phase can be additionally supported by a cooling, as illustrated in Fig. 3.42.

3.7.5 Applications and Results

Tests with DME in diesel engines with swept volumes of 1 dm^3 and 2 dm^3 per cylinder show excellent results. The ultra-low emission vehicle (ULEV) norm is achievable for larger engines without a catalyst, and for smaller engines with an oxidation catalyst [2]. The thermal efficiencies of the engines operated with DME

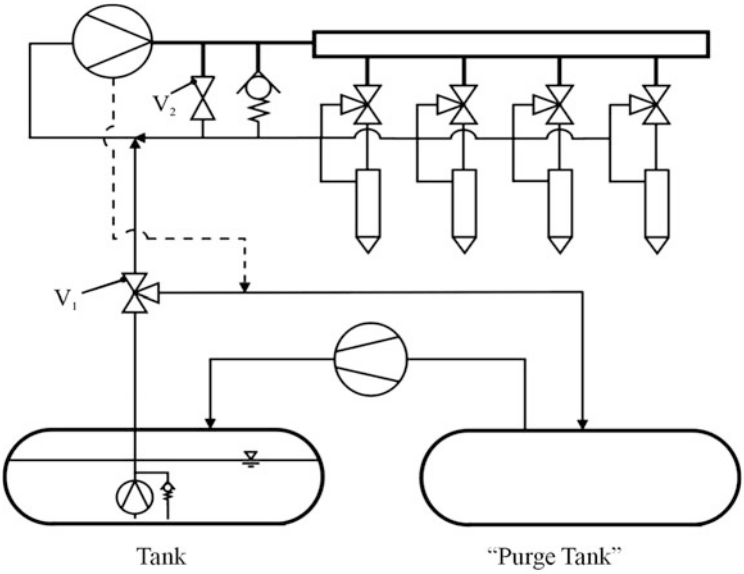

Fig. 3.41 Direct injection system for liquefied gases

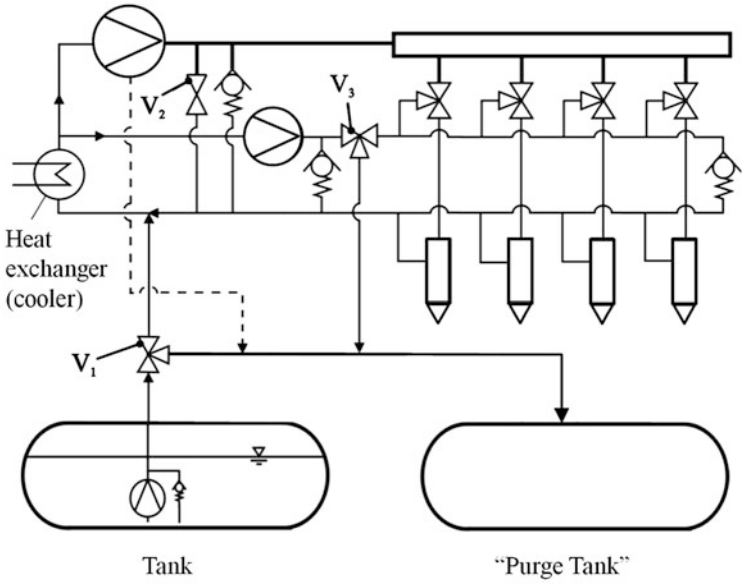

Fig. 3.42 Direct injection system with additional low pressure circuit for vapor collection from injectors

and with gasoline are identical, whereas the noise is remarkably reduced for DME. Alcohols, hydrogen, oil esters, and DME are true alternatives as fuels for thermal engines, being renewable and environmentally compatible.

3.8 Synthetic Fuels

Synfuel or designer fuel with well-calculated and composed molecular structures is increasingly becoming the expression of a new trend in the research and development of new energy sources. The vast and long experience of refining, distillation, gas synthesis, transesterification, pyrolysis, electrolysis, and other thermal and chemical procedures has led to new and very effective combination possibilities that open the door to the controllable formation of molecular structure. The requirement for on-board fuel storage at a high energy density under conditions that are not far from the ambient pressure and temperature has forced the development of structures such as BtL and GtL as intermediate steps. The main criteria for the development of synthetic fuels are as follows:

- Obtainable from renewable, unlimited resources in nature, such as inedible plants or plant waste and waste resulting from the wood, food, and cellulose industries, following efficient recycling logistics
- Produced with low energetic and technical investment and, thus, with low costs
- Adaptable for specific utilization in fuel cells or in internal combustion engines
- Transformable by chemical reaction in fuel cells or by combustion in internal combustion engines into products that are compatible with the environment

Exothermal reactions in thermal engines occur in general using fuels with molecular structures of the type $C_mH_nO_p$ in combination with oxygen from atmospheric air. Structures of the type $C_mH_nO_pN_r$ that also react with air, for example hydrazine ($H_2N–NH_2$), are not recommended at the usual temperatures during combustion because the formation of NO and NO_2 is very probable and the reaction becomes endothermic. A $C_mH_nO_p$ fuel has to accomplish the following main conditions for utilization in thermal engines:

- The proportion of hydrogen in the molecule should be as high as possible compared with carbon (i.e., low C/H ratio). In this case, combustion results in more H_2O and less CO_2 but also produces more exothermic energy (heat).
- When the molecule contains carbon atoms, they should be directly connected to oxygen atoms for a fast and efficient initiation of combustion. For many of the usual fuels, the oxygen from the air in the mixture does not penetrate the dense and branched fuel molecules, provoking incomplete combustion and production of soot and particulates.
- The molecular structure should allow a liquid phase with a density comparable with that of gasoline or diesel fuel at ambient conditions. In this mode, the fuel could be stored on board at high energy density in relatively simple tanks. The

liquid phase should not be close to the vapor limit to avoid gas bubble formation or compression in the injection system. The superficial tension of the droplets and the viscosity should be low to permit rapid vaporization. The lubrication of moving parts within the injections system can be ensured by using additives in the fuel to lower the viscosity.

– The heat value H_u (megajoules/kilogram fuel) corresponds to the participation of C, H, and O within the molecules; therefore, a high percentage of H can be beneficial.
– The stoichiometric air requirement $\left(\frac{L}{K}\right)_{st}$ (kilograms air/kilogram fuel) also depends on the C/H/O proportion. A high mixture heat value means a low stoichiometric air requirement, despite the fact that the fuel mass in the mixture increases. At direct injection of the fuel, the mixture heat value is calculated as:

$$H_g = \frac{H_u}{\lambda \left(\frac{L}{K}\right)_{st}} \cdot \rho_{Air} \tag{3.8}$$

Where λ is the air ratio and ρ_{Air} is the air density (kilograms/cubic meter).

Certainly, the hydrogen content provokes an increase in the stoichiometric air requirement:

$$\left(\frac{L}{K}\right)_{st} = 4.31(2.664c + 7.937h - o) \ \text{kg air/kg fuel} \tag{3.9}$$

c	Carbon part (kg C/kg fuel)
h	Hydrogen part (kg H_2/kg fuel)
o	Oxygen part (kg O_2/kg fuel)

This increase in stoichiometric air requirement can be partially compensated for by higher oxygen participation. On the other hand, more oxygen leads to a lower heat value of the fuel. In conclusion, the structure of a $C_mH_nO_p$ molecule should be optimized for all the mentioned requirements.

– An optimum combustion process requires additional properties of the fuel:
  The ignitability should be high to enable controllable self-ignition, especially with regard to the convergence of SI and CI processes in the future.
  The knock resistance should be high, allowing a high compression ratio without uncontrollable combustion reactions.
  Fast vaporization but high vaporization enthalpy are required to decrease the internal energy of air within the cylinder and, therefore, lower the air temperature. In this mode, the maximum temperature of the cycle could be kept under the temperature of dissociation to inhibit NO_x formation.

Ethanol and DME accomplish most of the conditions developed for a virtual, synthetic fuel. Recycling of the resulting CO_2 in the natural cycle without any other energy or device is another major advantage of these fuels. A synthetic fuel with

such properties should be obtainable with less energy and less technical complexity of the production plant, if possible from industrial and agricultural waste.

For fuel cell use, such a fuel should additionally allow fast detachment of the hydrogen before reaching the surface, where the protons should change from the anode to the cathode (the function of fuel cells is described in Sect. 4.3). A molecular structure of type $C_mH_nO_p$ is in this case not the optimal solution; instead, the hydrogen should be held in a matrix structure, in liquid phase, being delivered along the proton exchange membrane without chemical transformation of the matrix. This process is analogous to the transport of glucose from blood to the muscles by insulin in animals. Section 2.1 presents the most promising thermal cycles, and Sects. 2.2 and 2.3 describes appropriate thermal engines for performing such processes in steady-state, as on-board current generators for automobiles.

One example is of special interest: a stationary working Stirling engine requires a heat source, created by external combustion under steady fluid-dynamic and thermodynamic conditions. Such a process can be generated in a similar mode in a gas turbine if the combustion chamber is replaced by a heat exchanger, coupled to a device for external combustion. This concept gains new potential through the use of metallic powder for combustion. The burning of aluminum at high temperature is known from welding technology. The ignition of magnesium in air at 500 °C delayed the casting of magnesium components for a long time, but this disadvantage becomes an advantage in this context. A similar reaction is known for iron powder in contact with oxygen in the air. Mixtures of such solid powders, generally with aluminum content, are utilized in advanced rocket techniques because of their high energy density. Mixtures of metallic powders with defined percentages can be considered as synthetic fuels; their composition is, however, easier to control than in the case of liquid fuels. From this point of view, alternative thermal engines with external combustion for on-board current generation have a remarkable potential for future applications.

Electric Propulsion Systems

4

4.1 Electric Mobility

Taking into account traffic flow, the greenhouse effect, pollutant emission, and noise emission, it seems that electric mobility is the best alternative for transport in urban areas. Nevertheless, as shown in Chap. 1, these unique characteristics are prejudiced by severe disadvantages regarding the sources of electric energy (Fig. 1.4) and its storage on board vehicles (Fig. 1.17).

Generally, technical progress and the polarization of certain development paths can lead to solutions for complex problems. However, it should be mentioned that electric mobility is now in its third stage of development. The first two stages are illustrated in Fig. 4.1 with some representative examples.

It is interesting that, after the introduction of electric locomotives (1851) and batteries (1860), mobility in the USA was dominated by electric vehicles and steam engines, despite the fact that vehicles with combustion engines were being developed at the same time with the same intensity. In 1900, 34,000 electric vehicles were registered in the USA . The autonomy was on average 100 km. In 1882, Germany already had urban electric vehicles. As shown in Fig. 4.2, energy storage on board was not a problem at that time. A few years later, series cars with electric propulsion were running in Germany, as illustrated in Fig. 4.3.

The successful enhancement of internal combustion engines, the low price of crude oil, and its efficient conversion into fuel for mobility led to the temporary cessation of electric automobile production, because of the perpetual problem of insufficient on-board energy.

After the first oil crisis (1973), the industrial nations attempted a new orientation of energy politics to alternative energy sources. The second oil crisis (1979) accentuated this tendency. In 1990, the second Gulf war began, provoked by Kuwait annexation by Iraq. The two biggest crude oil exporters of the world were involved in this war. Thus, a third oil crisis was expected, provoking serious changes in energy management worldwide. There was no crisis, but the second stage of electric mobility began (1992–2005). The most representative electric cars

C. Stan, *Alternative Propulsion for Automobiles*,
DOI 10.1007/978-3-319-31930-8_4

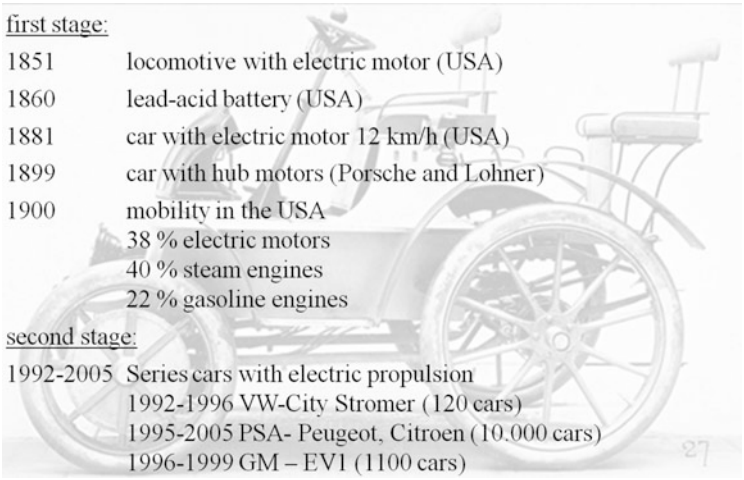

Fig. 4.1 Development of electric mobility: the first and second stages

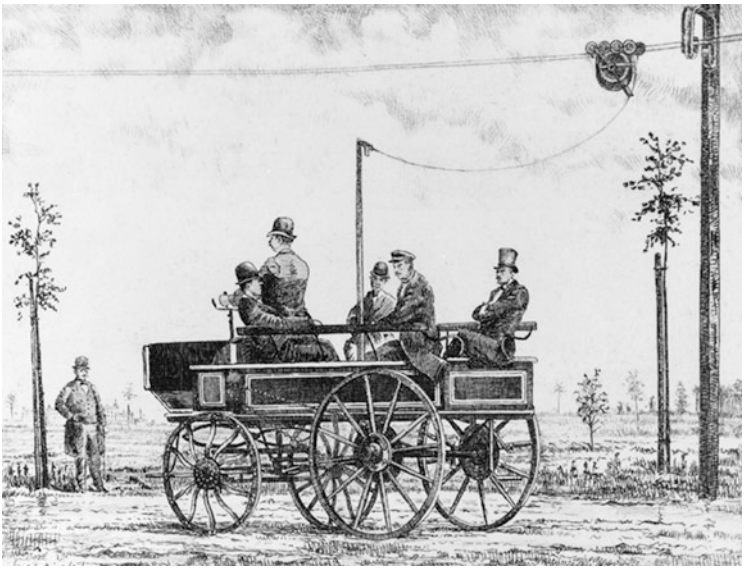

Fig. 4.2 First trolleybus by Werner von Siemens, Berlin-Kurfürstendamm (1882)

in series production at this time are listed in Fig. 4.1. In France, most of the electric cars produced were allocated to the administrative authorities, which explains the relatively large number of such cars. However, general acceptance remained low because of the restricted operation range.

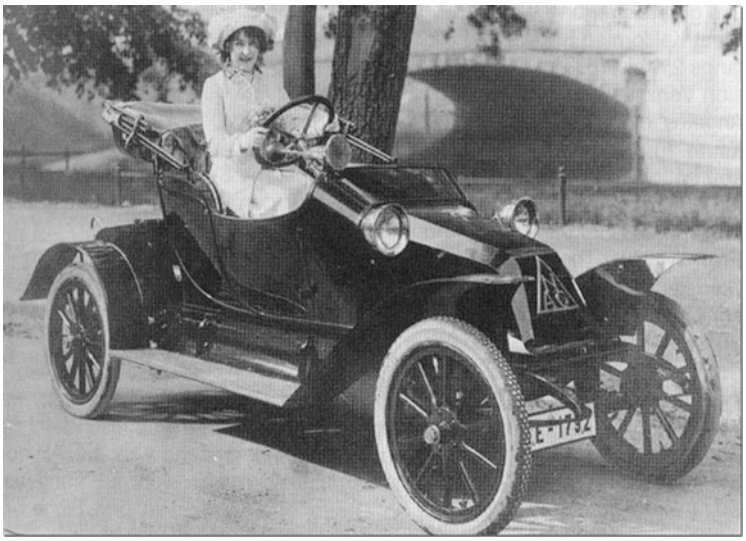

Fig. 4.3 Electric car from NAG (Neue Automobilgesellschaft mbH, 1903)

The third and current stage of development of electric cars was mainly induced by the severe limitations on CO_2 emissions into the atmosphere. The development is focused on motors, batteries for energy storage, and fuel cells for on-board energy conversion.

4.2 Motors

Motors have some major advantages as propulsion systems for automobiles:

- The torque characteristic is nearly ideal; maximum torque is available from the first revolution of the rotor. Acceleration of the car from a standstill is better than the values obtained with large engines or with super-/turbocharged engines.
- A gearbox and clutch are generally not necessary for such torque characteristics.
- Hub motors for front or rear wheels allow optimal connection for four- or two-wheel propulsion. All known stability programs are realizable at justifiable technical complexity.

Table 4.1 Motors for automobile propulsion

Car type	Power [kW]	Torque [N m]
DC motor ($n \leq 7000$ rev/min)		
Jinan Baoya Vehicle BY5000EV-1A	7	100
AC motor (asynchronous) ($n \leq 14{,}000$ rev/min)		
Fiat 500	93.15	215
AC motor (synchronous)		
BMW i3	125	250
Mitsubishi i-MiEV	35	180
Nissan Leaf	80	280
Renault Kangoo Z.E.	44	226
Tesla Roadster Sport	310	600
Mercedes Benz Vito E-Cell	60	280
Reluctance motor		
Prototype, University of Munich	30	110 N m at 0–2600 rev/min
		180 N m at 2600–9600 rev/min

The requirements for a propulsion motor are similar to those for propulsion engines: high power-to-volume ratio, high power-to-weight ratio, high efficiency, low technical complexity, and low cost.

All types of motors work on the basis of electrically generated electromagnetic fields, which induce magnetic forces. A magnetic field can keep the same position (in direct current motors) or rotate (in polyphase motors). For automobile propulsion, different variants were and are utilized, depending on the power, speed, and efficiency required. Table 4.1 shows some current examples.

The main features of such motors are shown in Fig. 4.4 for a general overview and not for analysis of their development potential. Figure 4.5 shows the types of direct current (DC) motors and their utilization in automobiles.

Commutation of the anchor for the adjustment of current sense to the field direction is realized by collectors [20]. The collectors have mechanical contact with the anchor by means of brushes. The abrasion of brushes is no longer a problem at the present stage of development; their lifetime is as long as the lifetime of the motor itself. However, this principle of collector function limits the maximum speed of a DC motor to approximately 7000 min^{-1}. The stator of a DC motor is built with a pole system, which consists of an exciter and a commutating pole

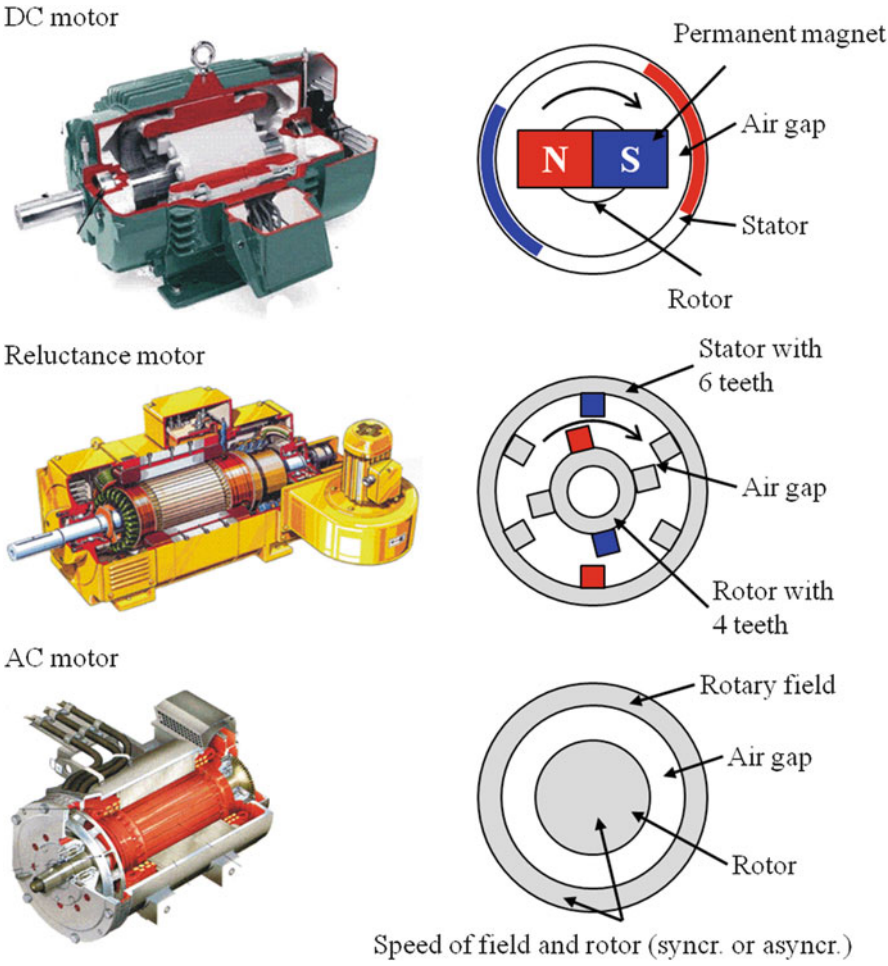

Fig. 4.4 Types of motor for use in car propulsion

with relatively high mass and volume [20]. Permanently excited rotating field motors have multiphase windings in the stator and are commuted by an electronic shifter, avoiding brush contact.

Figure 4.6 shows the function of polyphase motors and some characteristics of synchronous and asynchronous variants. Asynchronous motors are not too complex

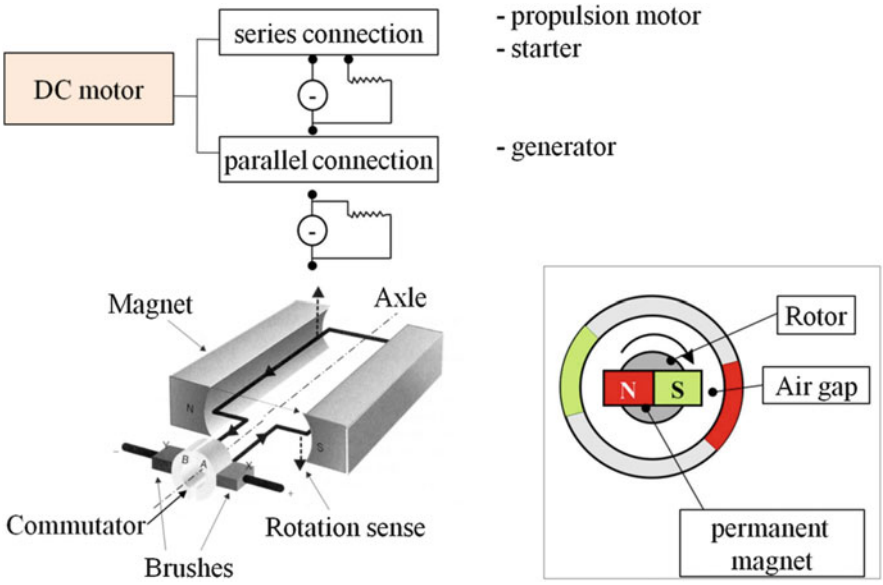

Fig. 4.5 DC motor

and therefore are producible at relatively acceptable cost. The design of the rotor permits a lower weight than in the case of DC motors, achieving speed values up to 14,000 min^{-1}, as shown in Table 4.1.

Synchronous motors are more complex than asynchronous variants because of the necessary electric excitation, but the synchronous phase of current and tension allows a higher efficiency to be achieved. Figure 4.7 shows the synchronous motor of a Nissan Leaf, with a power of 80 kW and torque of 280 N m.

A reluctance motor has a discontinuous magnetic field. Figure 4.8 presents a scheme of such a motor. The substantial advantage of this motor is its high efficiency for a broad field of operation.

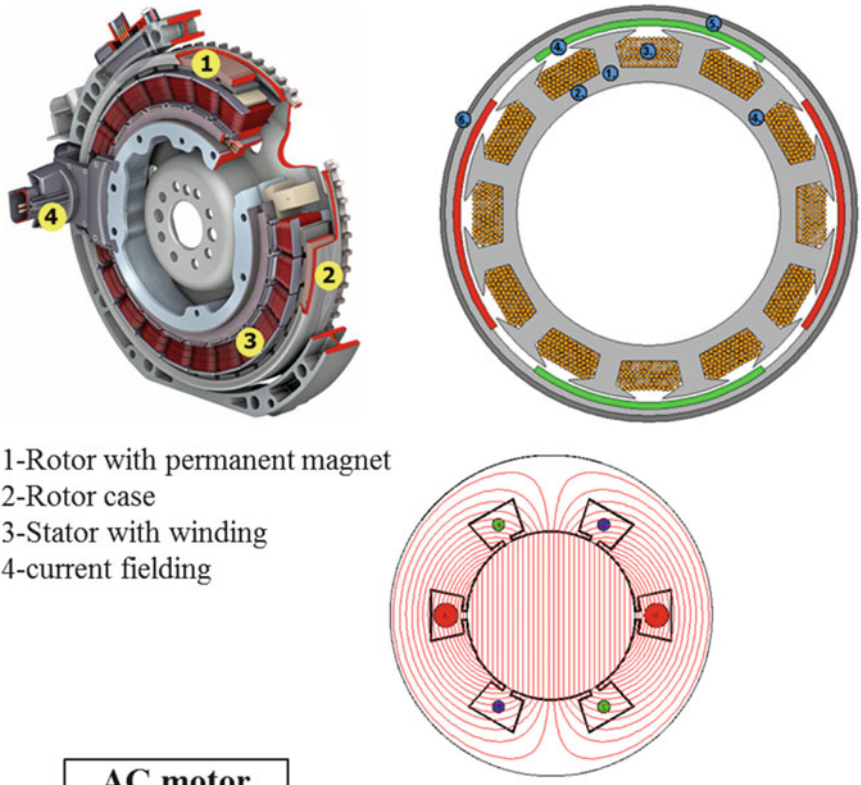

Fig. 4.6 AC motor

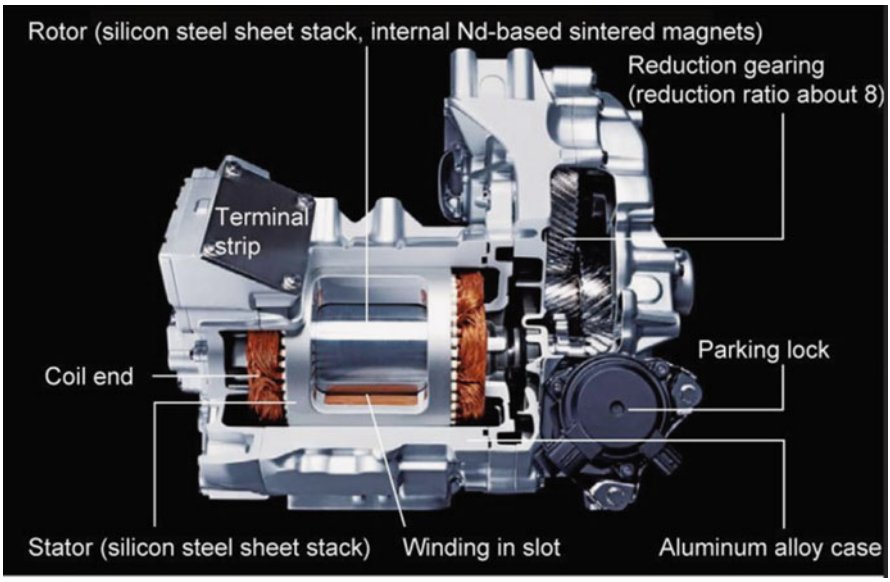

Fig. 4.7 Synchronous propulsion motor of Nissan Leaf (Source: Nissan)

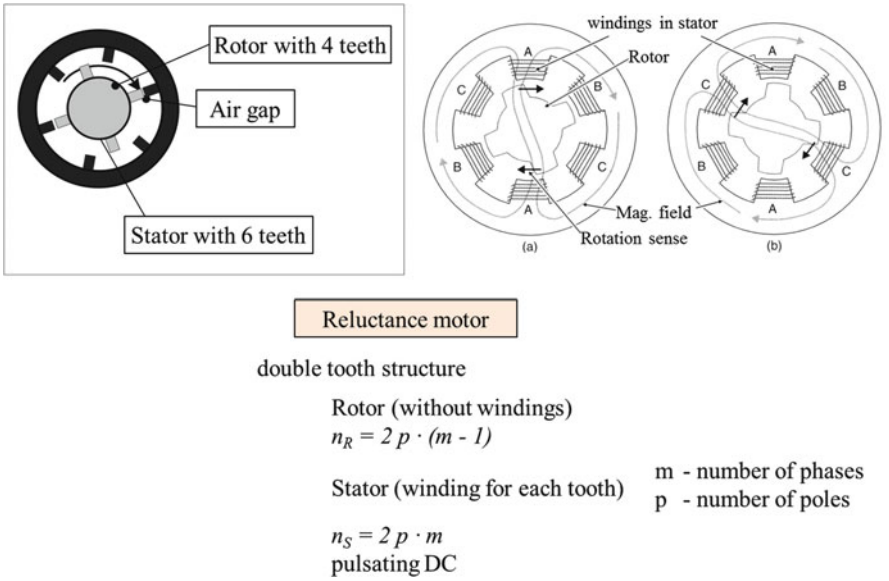

Fig. 4.8 Reluctance motor

4.3 Accumulators of Electrical Energy: Batteries

The storage of electrical energy on board an automobile in batteries was and is still the reason for the moderate presence of electric vehicles on the market. Table 4.2 gives the most relevant characteristics of some classic and advanced batteries: operation temperature, energy density for discharging in less than 2 h, and cell tension. Regarding the operation temperature, there are two forms of batteries: "cold" types and those with liquid electrolytes, which require a high temperature. For safety reasons, batteries with high temperatures are not used in the automobile industry, despite numerous tests in the 1990s. The main disadvantage of batteries as energy accumulators is their low energy density in comparison with liquid fuels. The theoretical values for energy density in batteries at very slow discharging are much higher than for discharging in less than 2 h, but only this discharging duration is realistic for use in automobiles.

An example is representative for the comparison of energy densities of batteries and fuels: Advanced lithium-ion batteries, such as in the BMWi3, Citroen c-zero, Mitsubishi iMiEV, Ford Focus Electric, Mercedes Vito E-Cell, Nissan Leaf, and Renault Zoe, have energy densities of around 80 W h/kg, which is four times higher than lead-acid batteries (Pb-PbO_2). However, the difference in cost shows the same proportion, but inversed: approximately €750/kW h for Li-ion and €150/kW h for Pb-PbO_2. At an energy density of 80 W h/kg for a drive requiring a mean power of 20 kW and an estimated achievable distance of 100–150 km in 1 h, the battery mass would be:

$$m = \frac{20\,kW \cdot 1\,h}{80\,\frac{kWh}{ton}} = 250\,kg \tag{4.1}$$

For the same application, a lead-acid battery would have a mass of 1000 kg, which is as much as the weight of a compact car.

Figure 4.9 shows the structure of an advanced lithium-ion battery for electric cars and Fig. 4.10 shows its configuration.

New developments such as lithium-metal-polymer batteries (especially lithium-cobalt dioxide), zinc-oxygen, zinc-air, and lithium-air can give an expected increase in energy density up to 200 W h/kg at costs that could be comparable with those of lead-acid batteries, if produced in large series.

The principle of function of a zinc-air battery and the most significant chemical reactions for tension generation are illustrated in Fig. 4.11. The anode consists of zinc powder. The cathode is formed by an air flow containing the necessary oxygen. The electrolyte is composed of caustic potash and the catalyst by graphite, in the form of a slab, powder, or grid. Air is introduced through minuscule holes, where the oxidation of zinc occurs, as shown in the reaction given in Fig. 4.11.

For a drive with 20 kW lasting 1 h, as in the above-mentioned example, a battery of this type could weigh only 100 kg. Nevertheless, comparison with an automobile with a diesel engine powered by diesel fuel is quite sobering: 100 kg can be expressed as 125 l diesel fuel, as deduced from the fuel density mentioned in

Table 4.2 Main characteristics of various battery types

System	Pb-PbO_2	Ni-Cd	Ni-MH	Zn-Br_2	Na-$NiCl_2$	Na-S	Li-ion
Function temp. [°C]	0–45	−20–50	−40–50	20–40	300–350	300–350	−40–60
Energy density for 2 h discharge [W h/kg]	20–30	40–55	50–80	50–70	80–100	90–120	90–140
Cell tension U_0 [V]	2.1	1.35	1.35	1.79	2.58	2.08	3.6

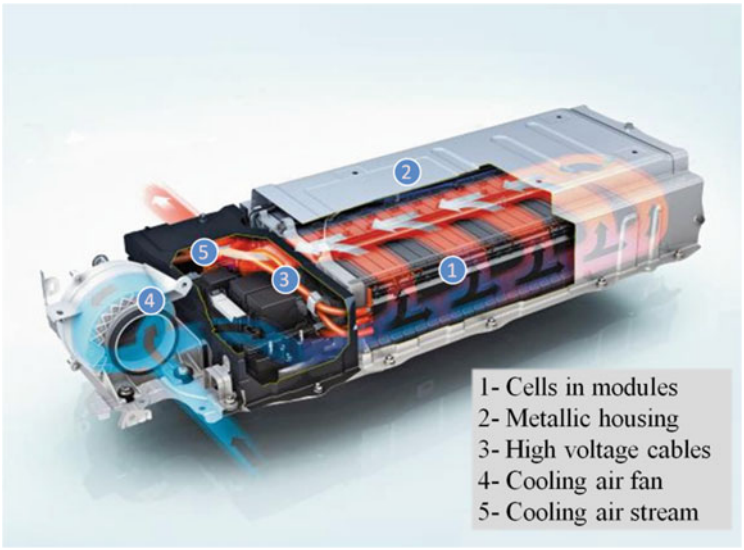

Fig. 4.9 Advanced Li-ion battery with cooling system for use in electric cars

Fig. 4.10 Li-ion battery for use in electric cars (Source: Audi)

Table 3.1. Considering the mean fuel consumption of a heavy limousine such as a Mercedes E Class 250 CDI, 7 l/100 km, with a mean power that is considerably higher than 20 kW, the range would not be 80 km but 1785 km! Such a comparison shows that batteries, even though becoming more developed, cannot be real alternatives to liquid fuel as on-board energy storage for an acceptable operation

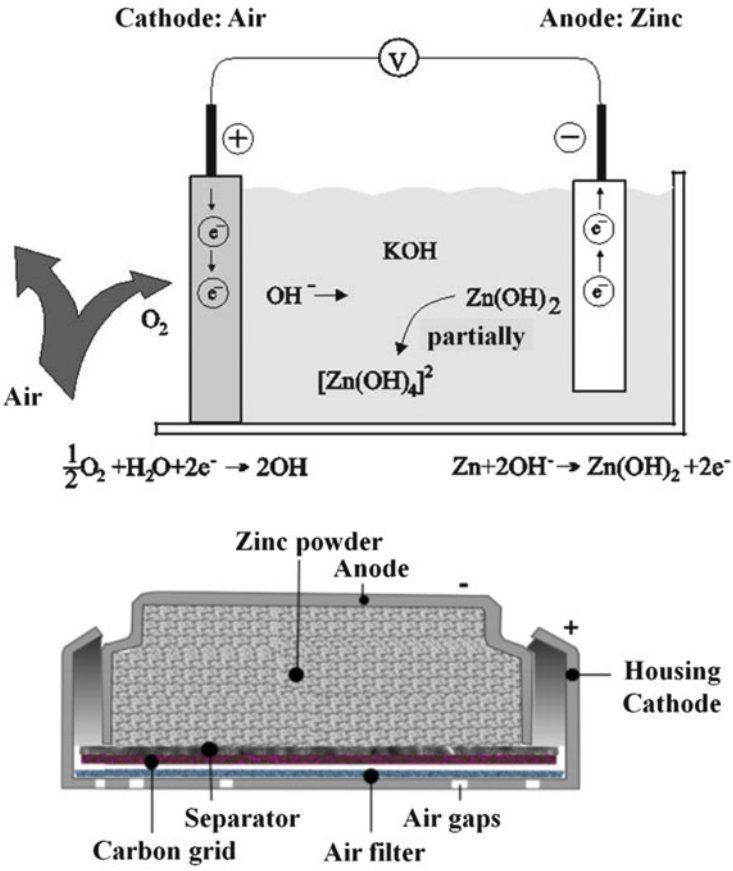

Fig. 4.11 Zinc–air battery: principle of function

range. On the other hand, an advanced battery is an uncontested on-board energy buffer between the current generator and the propulsion motor for cars with hybrid propulsion. Moreover, such a modern battery is an ideal solution for compact urban cars with electric propulsion. Figures 4.12 and 4.13 show examples of the configuration of batteries and motor in a compact automobile and in a transporter with a body frame.

The mean cruising range of urban cars is statistically under 50 km, so a very promising scenario including batteries of low capacity has been developed for urban electric cars in France, in the frame of the "Tulip" program. This scenario is illustrated in Fig. 4.14. The cars are supplied with electric energy, contactless, by induction. Such charging areas could be created in public parking garages and in car rental stations.

This concept is very compatible with car sharing or rental car systems: the parking garage or rental station could be detected from the car by GPS, the parking

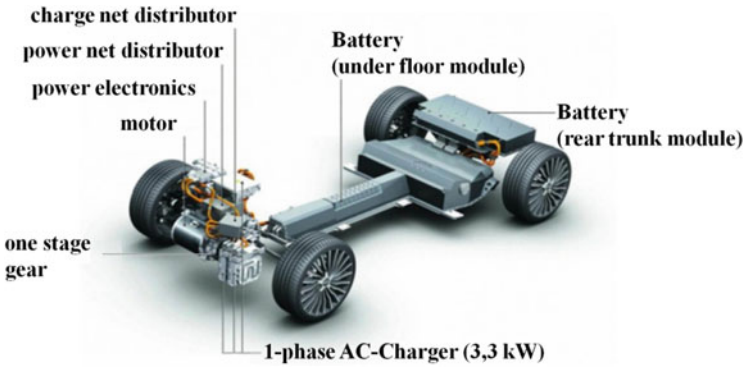

Fig. 4.12 Motor and battery topology in an automobile (Source: Audi)

Fig. 4.13 Motor and battery topology in a heavy duty vehicle (Source: Daimler)

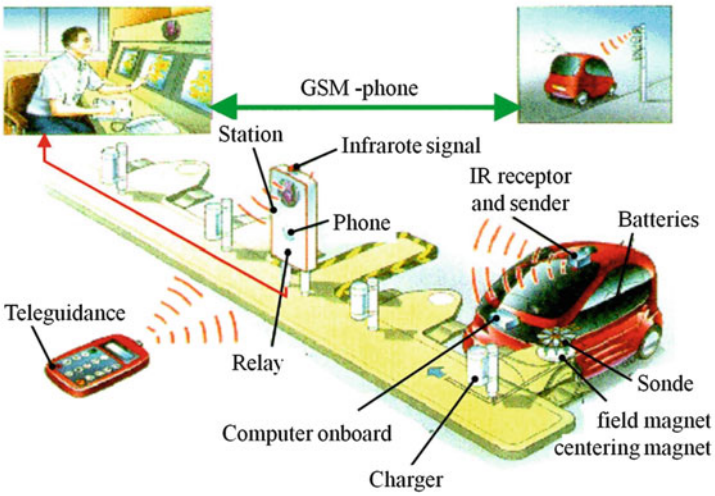

Fig. 4.14 Park-and-charge system for automobiles with electric propulsion

place also serves as the contactless charging point, and payment by credit card or SMS corresponds to the consumed energy [kW h]. The problem remains the electric energy supply of the parking garage. In France, most of the energy is produced in nuclear power plants, without CO_2 or pollutant emissions.

Some time ago, another concept was tested in Denmark and Israel, where the potential to use wind and solar energy is very high. The concept involves the exchange of an empty battery with a full battery in a specially developed exchange station. Battery exchange in a few minutes, from a pit under the car, could be a good idea, but the car body must be designed for such use. This would influence the kinematic and dynamic car behavior, the vibration spectrum, and the car stiffness. The complexity of the required technical adjustments, resulting in appreciable costs, has hampered the introduction of such a solution on the market. Car exchange seems to be simpler and more effective than battery exchange.

4.4 Electric Energy Conversion on Board: Fuel Cells

The storage of electric energy on board an automobile in batteries can be combined with the conversion of other energy forms, which can be stored at lower mass, volume, and cost. Such a conversion in a fuel cell was tested in 1839 by the British physician Sir William Robert Grove, as an "inversed electrolysis." The electrodes of this primal hybrid between battery and fuel cell were made of platinum strips, which were treated with acid water before being introduced into hydrogen, and then into oxygen. The principle of function of this first fuel cell is illustrated in Fig. 4.15.

In a second step, Grove used sulfuric acid as an electrolyte. The hydrogen was obtained on-site from the reaction of the acid with zinc. Oxygen was taken from the air flow. This is remarkably analogous to the newest zinc-air battery concepts and to the advanced fuel cell concepts of today. As often happens in engineering, many new concepts are based on previous physical experiments. In this context, the zinc-air battery is the functional chain link between batteries (with storage of the components) and fuel cells (with continuous feeding of the components as mass flow). A breakthrough was forced by the need for current generation in aeronautics, resulting in a fuel cell supplied with pure hydrogen and oxygen flows over light catalyst electrodes, in dilute alkali. The functional principle of a fuel cell is illustrated in Fig. 4.16.

The flows of hydrogen and oxygen are separated by electrolytes, which act together with a catalyst to generate proton transfer from hydrogen to oxygen. The chemical reaction is as follows:

$$\text{Anode}: H_2 \rightleftarrows 2H^+ + 2e^- \tag{4.2}$$

$$\text{Cathode}: 2H^+ + \frac{1}{2}O_2 + 2e^- \rightleftarrows H_2O \tag{4.3}$$

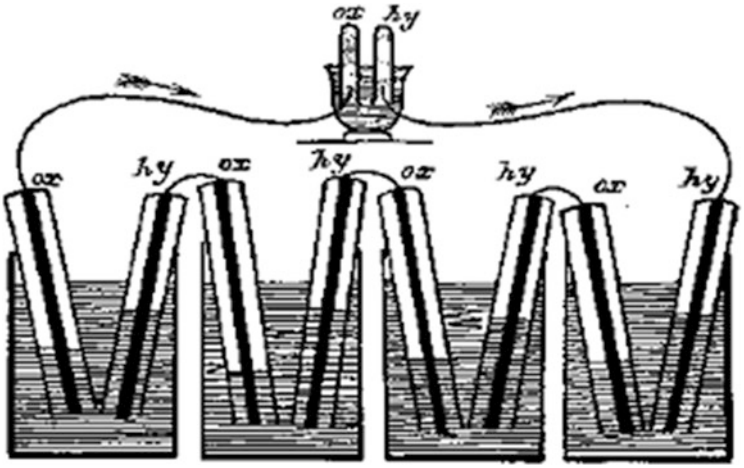

Fig. 4.15 Principle of function of the first fuel cell (1839)

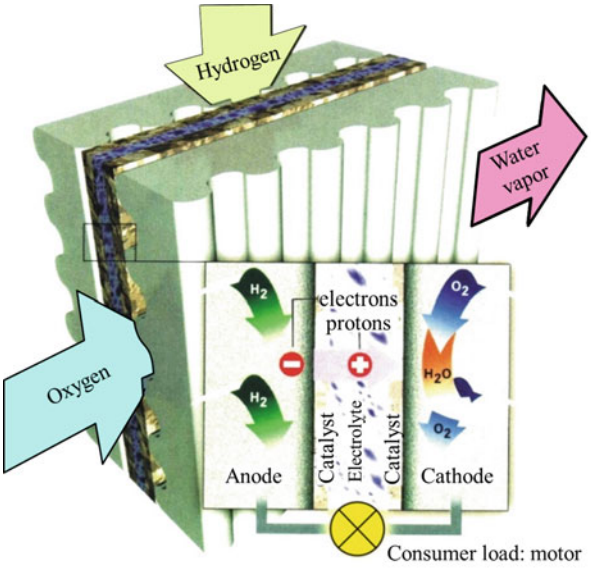

Fig. 4.16 Energy conversion in a fuel cell

$$H_2 + \frac{1}{2} O_2 \rightleftarrows H_2O \tag{4.4}$$

Table 4.3 gives an overview of the developed, tested, and produced fuel cells listed below.

Table 4.3 Electrolytes for fuel cells and their application fields

Type	Electrolyte	Temperature	Notes	Applications
AFC alkaline fuel cell	Dilute caustic potash	60–120 °C	Only with H_2/O_2	Spaceflight, military technology
DMFC direct-menthol fuel cell	Proton-conducting membrane	50–120 °C	Only with CH_3-OH	Small cars, military technology
HT-PEMFC high-temperature proton exchange membrane fuel cell	Proton-conducting membrane	120–200 °C	Without water circuit	House energy plant
NT-PEMFC low temperature proton exchange membrane fuel cell	Proton-conducting membrane	20–120 °C	Very flexible	Cars, current generation, heat/power generation
PAFC phosphoric acid fuel cell	Phosphoric acid	160–220 °C	Corrosion	Current generation, heat/power generation
MCFC molten carbonate	Molten carbonate	600–650 °C	Corrosion	Heat/power generation
SOFC solid oxide fuel cell	Solid oxide	850–1000 °C	Power directly from natural gas	Heat/power generation

- **Alkaline fuel cells (AFC):** The electrolyte is caustic potash, having the highest efficiency of all mentioned variants. This electrolyte only functions with pure oxygen and hydrogen, therefore this type is very appropriate for use in rockets.
- **Direct methanol fuel cells (DMFC**): These fuel cells are able to operate with pure methanol. Thus, hydrogen production on board from stored methanol can be avoided. The working temperature range is 50–120 °C. Their use in automobiles has been tested and applied very successful.
- **High-temperature proton exchange membrane fuel cells (HT-PEMFC**): These fuel cells can operate without additional water in the system. The newly developed polybenzimidazol membrane allows the use of phosphoric acid as a charge carrier for proton exchange.
- **Low-temperature proton exchange membrane fuel cells (PEM**): A very high energy density is obtained at a working temperature range of 20–120 °C. Their flexible operation and the ability to use oxygen from the air are reasons for their utilization in automobiles.
- **Phosphoric acid fuel cells (PAFC**): The working temperature of 180–220 °C is higher than for AFC and PEM, but these cells have a rather limited efficiency and suffer from corrosion problems. They are mainly used in units for cogeneration of heat and power in the range of 200 kW.
- **Molten carbonate fuel cells (MCFC**): These fuel cells work at high temperature, around 650 °C. Despite the complexity of the process and the corrosion

phenomena, they are intensively used for local energy supply because of their ability to operate with coal gas.
– **Solid oxide fuel cells**: The working temperature of 850–1000 °C is higher than that of the other fuel cells. The solid electrolyte consists of zirconium oxide. The high efficiency when working directly with natural gas justifies their use in heat and power generators.

The reaction between hydrogen and oxygen leads to the formation of new molecules; when operating with pure hydrogen and oxygen the product is water and this reaction is exothermic. The similarity to the kinetics of combustion reactions [1] can be expressed by the energetic balance:

$$\overline{G} = \overline{H} - T\overline{S} \tag{4.5}$$

$\overline{G}$ molar free reaction enthalpy of a component (kilojoules/kilomole)
$\overline{H}$ molar enthalpy of a component (kilojoules/kilomole)
T temperature of reaction (degrees Kelvin)
$\overline{S}$ molar entropy (kilojoules/kilomole per degree Kelvin)

The three reaction enthalpies of the components $\overline{G}_{H_2}$, $\overline{G}_{O_2}$, and $\overline{G}_{H_2O}$, as well as of other components when operating with substances other than hydrogen and oxygen, are dependent on the reaction temperature. Their values can be found in property tables. For the complete chemical reaction, the total free enthalpy $\left(\Delta\overline{G}_R\right)$ can be calculated as follows:

$$\Delta\overline{G}_R = \overline{G}_{H_2O} - \left(\overline{G}_{H_2} + \frac{1}{2}\overline{G}_{O_2}\right) \tag{4.6}$$

corresponding to the chemical reaction:

$$H_2O \overrightarrow{\leftarrow} H_2 + \frac{1}{2}O_2 \tag{4.7}$$

When the process is considered as ideal and reversible, the free enthalpy is the base for calculation of cell tension within the fuel cell:

$$\Delta\overline{G}_R = -n \cdot U_{\text{rev}} \cdot F \tag{4.8}$$

n number of changed electrons
U_{rev} reversible cell tension in the fuel cell (volts)
F Faraday constant, $F = 96.5$ C/kmol

In a reaction without heat exchange (cold reaction), the total free enthalpy would be transformed into electric energy with the given cell tension. For example, at 25 °C the cell tension would be $U_K = 1.23$ V. A reaction with heat exchange provokes a change in the real cell tension (U_z):

$$\dot{q} = (U_K - U_Z) \cdot \frac{I}{A} \tag{4.9}$$

$\dot{q}$ heat flow density (watts/square meter)
I current (amps)
A cross-section of the current (square meters)

The calculated heat flow density $\dot{q}$ is diminished by the specific evaporation enthalpy of the formed water, similar to calculation of the heat value of the fuel:

$$\dot{q} = (U_K - U_Z - \dot{m}\, h_{H_2O}) \cdot \frac{I}{A} \tag{4.10}$$

$\dot{m}$ mass flow of water (kilograms/second)
h_{H_2o} specific evaporation enthalpy of water (joules/kilogram)

Similar to combustion processes, components other than hydrogen and oxygen can also react in fuel cells. For example, hydrocarbons (gasoline, diesel fuel) and alcohols (methanol, ethanol) can react because of their hydrogen content. Thus, direct comparison of the reactions and processes in fuel cells and in engine combustion chambers is possible. The similarities and differences between these processes are summarized in Fig. 4.17.

At first glance, the process within a fuel cell seems to show better promise for efficient development. On the other hand, a basic condition for a combustion reaction is direct contact of fuel and air in a mixture, the contact surface being

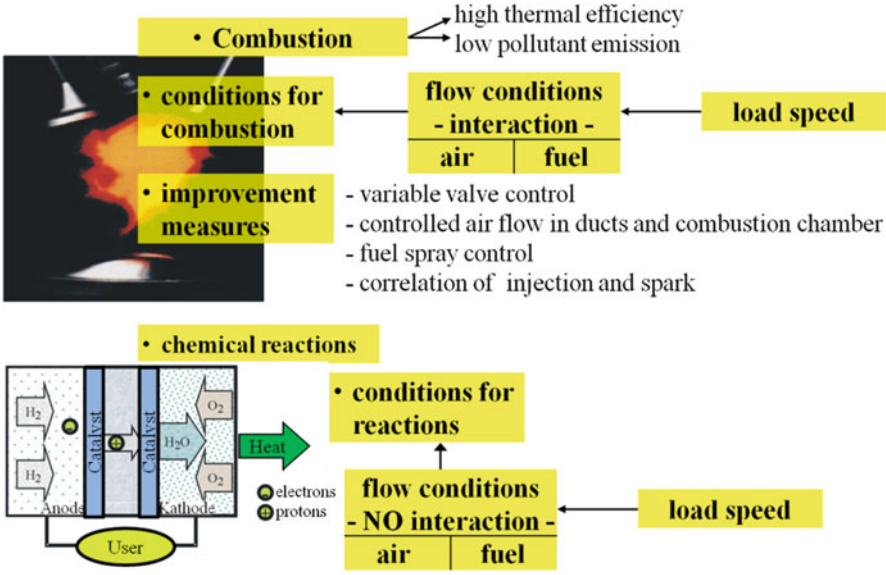

Fig. 4.17 Differences between the process of combustion within a piston engine and the reaction within a fuel cell

strongly enlarged by turbulence. The stoichiometric and homogeneous distribution of fuel and air within the combustion chamber and the control of their movements are possible only at exactly given flow conditions; thus, under real conditions, with strong variations in load and speed, such distribution and control are disturbed. There are, of course, numerous possibilities for adjusting and optimizing the parameters of mixture formation and combustion, ranging from variable valve control to modulation of the injection rate, as presented in Sect. 2.2 and shown in Fig. 4.17. From this point of view, the process in a fuel cell seems to be better controllable: the reaction partners have no direct contact with each other, which allows direct control of their mass flow along the membrane. The flows are generally one-dimensional. However, the exchanging surface must be enlarged if the power demand increases. The most frequent way of achieving this is to use a sandwich design for the fuel cell, with labyrinths and many strata. There is a remarkable analogy with a heat exchanger. Similarly, the frequent flow reversions in such channels within the fuel cells lead to turbulence, pulsations, and local cavitations. Moreover, rapid acceleration or deceleration of the flow, corresponding to the momentary required power, also disturbs the flow. During the process within a fuel cell, a higher efficiency than in an engine is only achievable under steady conditions, at low power requirements. Figure 4.18 compares the efficiencies of a hydrogen-air fuel cell and a diesel engine, demonstrating the efficiency advantage at low load.

The structure of a fuel cell module with a proton exchange membrane is shown in Fig. 4.19. This is the usual configuration of hydrogen-air fuel cells for automobiles. The air pressure of 0.2–0.3 MPa is ensured by a compressor. The current density can achieve 1 A/cm^2 and the tension 0.5–1 V. The power density is 0.7 kW/kg, which is much higher than the power densities in batteries. The configuration of a stack and the other elements of a fuel cell system in a compact car are illustrated in Fig. 4.20.

The functional elements are disposed as a modular platform. Similar to the hydrogen piston engine, as presented in Sect. 3.5 (Fig. 3.36), one of the most

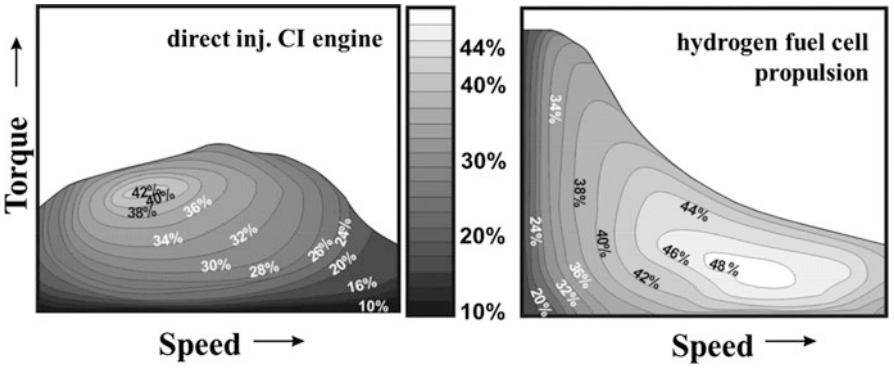

Fig. 4.18 Comparison of efficiency: CI engine and fuel cell with hydrogen

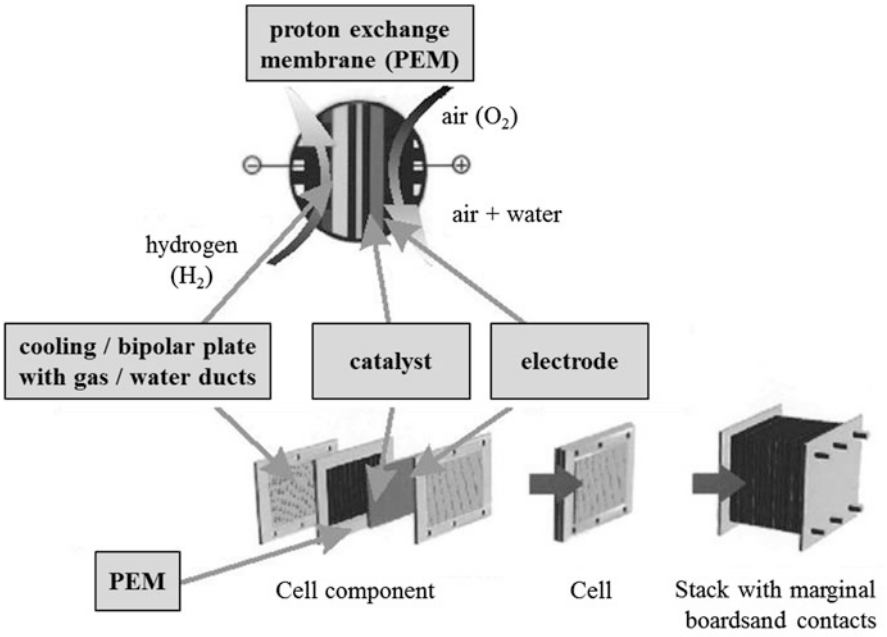

Parameters of a PEM fuel cell:	
Temp. of function	80[°C]
Pressure of function	0,2-0,3[MPa]
Current density	0-1,0[A/cm³]
Cell tension	1,0-0,5[V]
Energy density	
mass related	0,7[kW/kg]
volume related	1,0[kW/dm³]

Fig. 4.19 Stack of a fuel cell

important problems for fuel cells is on-board storage of hydrogen. Examples of on-board hydrogen tanks for fuel cell cars are presented in Fig. 4.20 and Fig. 4.21.

An inversion of roles, following the paths in Fig. 1.26, seems feasible. If a piston engine can operate with the energy source of a fuel cell (i.e., hydrogen), a fuel cell could work with the fuel for piston engines (i.e., gasoline, natural gas, diesel fuel, methanol, ethanol). The condition for such a function is the extraction of hydrogen from molecules of C_mH_n or $C_mH_nO_p$ in a pre-reaction. The advantage of such concept is the easy storage of the given high energy density fuel under ambient conditions. A disadvantage is the integration of a new module, a reactor for hydrogen production on board. However, the most important disadvantage is the CO_2 emission resulting from the following reactions:

– The reaction for the generation of hydrogen from methanol is:

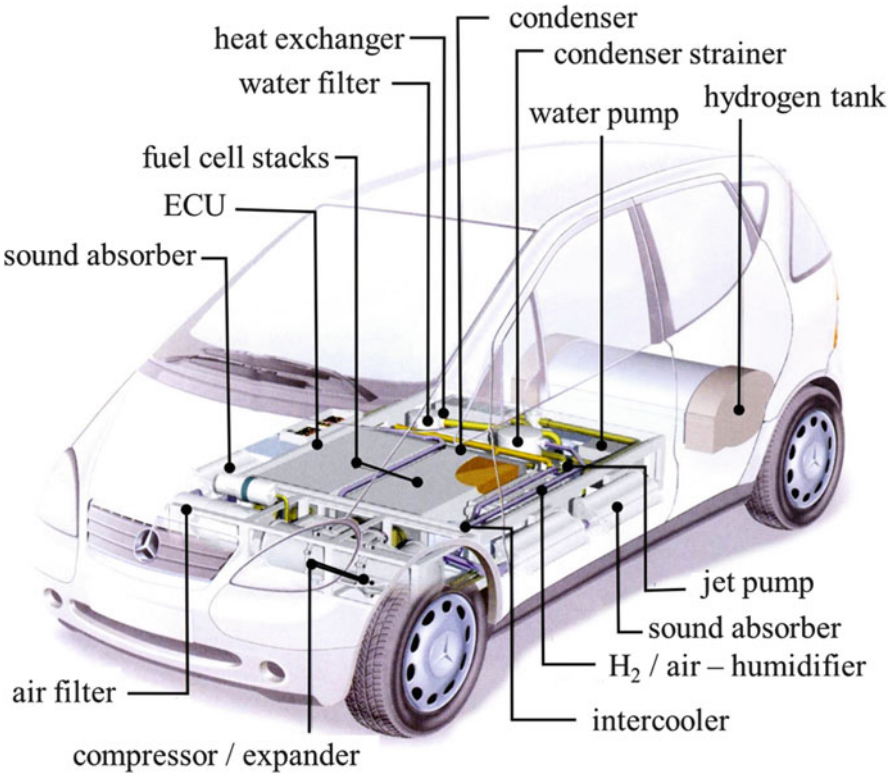

Fig. 4.20 Configuration of modules in an automobile using a hydrogen fuel cell (Source: Daimler)

$$CH_3OH + H_2O \rightleftharpoons CO_2 + 3H_2 \tag{4.11}$$

The water is introduced as a vapor stream at 300 °C

– The reaction for the generation of hydrogen from a hydrocarbon (gasoline or diesel fuel) is exemplified with octane:

$$2C_8H_{18} + 17O_2 \rightleftharpoons 16CO + 18H_2O \tag{4.12}$$

$$16CO + 16H_2O \rightleftharpoons 16H_2 + 16CO_2 \tag{4.13}$$

Water is introduced for the transformation of CO into CO_2 as a vapor stream at a temperature of 900 °C.

The comparison of fuel cells with internal combustion engines shows that the same fuel leads to the same reaction products:

– From hydrogen and air → water
– From gasoline/diesel fuel/ethanol/methanol and air → water and CO_2

Fig. 4.21 Automobile with electric propulsion using a hydrogen fuel cell (Source: Toyota)

These relationships are shown in Fig. 4.22.

As previously mentioned, the reaction in a fuel cell results not only in chemical products but also in heat, which reduces the proportion of electric energy. The formation of pollutants in incomplete reactions is similar in both fuel cells and combustion chambers, as shown in the following example. The reaction of methanol and water to CO_2 and hydrogen is an ideal form:

$$CH_3OH + H_2O \rightleftharpoons CO_2 + 3H_2 \tag{4.14}$$

Under real conditions, the reaction stages are as follows:

$$CH_3OH \rightleftharpoons CO + 2H_2 (exothermic) \tag{4.15}$$

$$CO + H_2O \rightleftharpoons CO_2 + H_2 (endothermic) \tag{4.16}$$

The exothermic reaction of methanol dissociation determines the whole process. In another reaction form, partial methanol oxidation is possible:

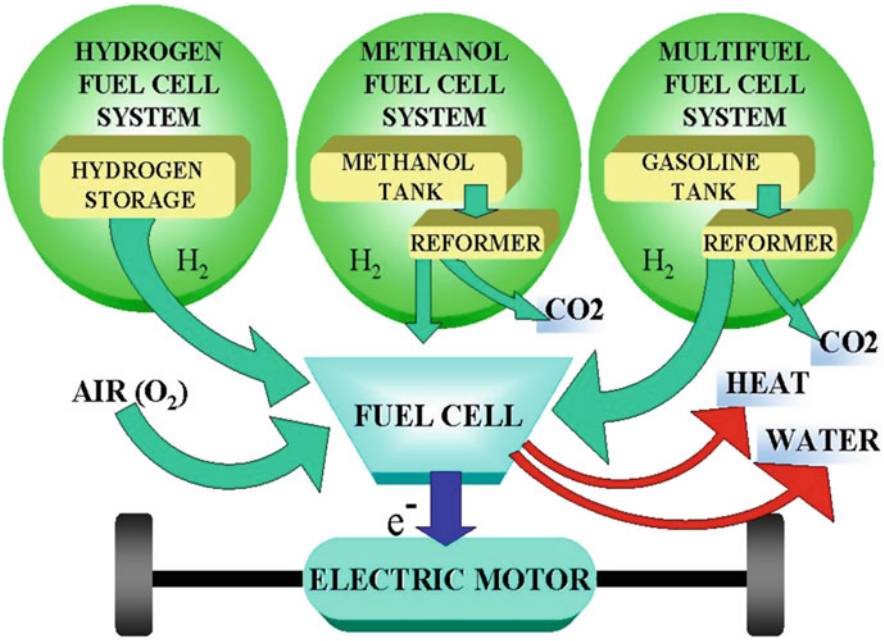

Fig. 4.22 Reaction products from fuel cells using the same fuel as piston engines

$$CH_3OH + \frac{1}{2}O_2 \rightleftarrows CO_2 + 2H_2(endothermic) \tag{4.17}$$

as the result of partial reactions as follows:

$$CH_3OH \rightleftarrows \frac{1}{2}O_2 \leftrightarrow CO + 2H_2 + H_2O \tag{4.18}$$

$$CO + H_2O \rightleftarrows CO_2 + H_2 \tag{4.19}$$

The reaction conditions within the reactor and the process duration determine the formation of intermediate products and pollutants, which is similar for the dissociation sequences during combustion in piston engines. The following examples are notable:

$$CO + 3H_2 \rightleftarrows CH_4 + H_2O(endothermic) \tag{4.20}$$

$$CO_2 + 4H_2 \rightleftarrows CH_4 + 2H_2O\,(endothermic) \tag{4.21}$$

$$2CO \rightleftarrows C^1 + CO_2(endothermic) \tag{4.22}$$

$$CO + H_2 \rightleftarrows C^1 + H_2O(endothermic) \tag{4.23}$$

$$CH_4 \rightleftarrows C^1 + 2H_2(exothermic) \tag{4.24}$$

$$CH_3OH \rightleftarrows CH_2O^2 + H_2(exothermic) \tag{4.25}$$

$$CH_2O + H_2O \rightleftarrows CHO_2H^3 + H_2(exothermic) \tag{4.26}$$

$$2CH_3OH \rightleftarrows CH_3OCH_3^4 + H_2O(exothermic) \tag{4.27}$$

$$CH_3OH + H_2O \rightleftarrows CH_3O_2H^5 + H_2(exothermic) \tag{4.28}$$

where the superscripts refer to:

1. Carbon in solid form (soot)
2. Formaldehyde
3. Formic acid
4. Dimethyl ether
5. Methyl formate

The formation of undesirable products can be reduced by control of process pressure and temperature; the analogy with similar measures in piston engines is remarkable. During an incomplete combustion reaction caused by freezing of a flame front, reaction on a cold combustion chamber wall, or by liquid fuel kernels the result is (for example):

$$2C_8H_{18} + 25O_2 \rightleftarrows 16CO + 18H_2O + 8O_2 \tag{4.29}$$

The same conditions, especially the presence of liquid kernels, can lead to the formation of soot. At combustion temperatures over 1500 °C, the probability of a water-gas shift reaction increases, similar to the transformation of methanol into hydrogen in Eq. (4.16):

$$CO + H_2O \rightleftarrows CO_2 + H_2(endothermic) \tag{4.30}$$

Other dissociation reactions with high probability in the combustion chambers of piston engines are [1]:

$$\begin{aligned} CO + \frac{1}{2}O_2 &\rightleftarrows CO_2 & H + H &\rightleftarrows H_2 \\ OH + \frac{1}{2}H_2 &\rightleftarrows H_2O & O + O &\rightleftarrows O_2 \\ H_2 + \frac{1}{2}O_2 &\rightleftarrows H_2O & NO &\rightleftarrows \frac{1}{2}N_2 + \frac{1}{2}O_2 \end{aligned} \tag{4.31}$$

Equilibrium in the formation of final or initial products during these reactions is determined by the free enthalpy at the given temperature.

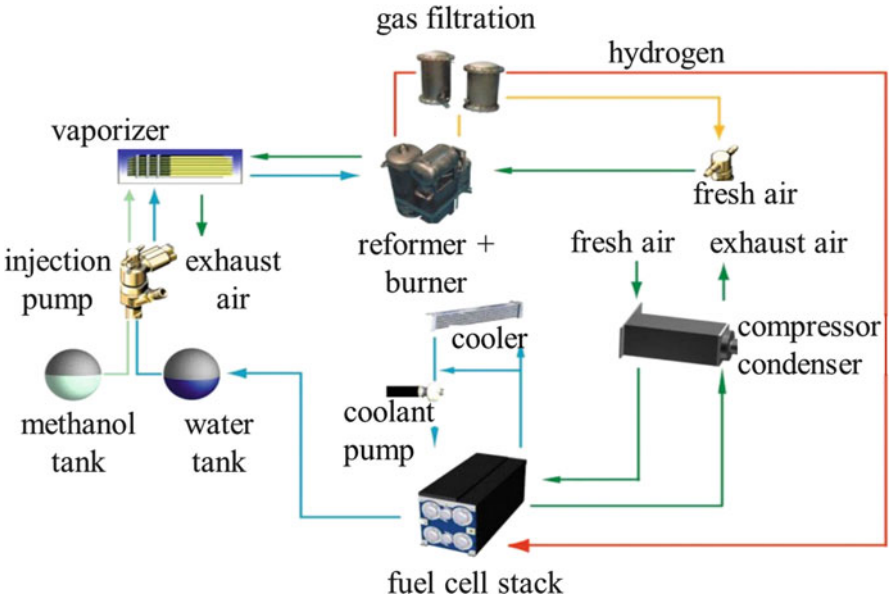

Fig. 4.23 Configuration of a methanol fuel cell

This similarity of relationships during the chemical reactions shows that the processes in fuel cells have no basic advantages compared with processes in the combustion chambers of piston engines. Thus, specific advantages can be exploited by improving the design of parts and parameter combinations. The technical complexity of one or other system, the achievable energy density, and the price are the determining factors in the choice of concept.

The technical complexity of a fuel cell with methanol is illustrated in Fig. 4.23. The configuration shown is similar to that of a supercharged SI engine with direct injection of methanol. Methanol injection into the fuel cell has the same provenience. Figure 4.24 shows the dosage curve for methanol in a fuel cell using a Zwickau pressure pulse injection system, as shown in Fig. 2.50 and Fig. 2.51. Figure 4.25 presents the functional modules of a methanol fuel cell on the platform of an automobile.

Fuel cell systems powered by hydrogen and by methanol, for utilization in automobiles, have been developed in the last two decades by different original equipment manufacturer consortia such as:

- Ballard Power Systems: Daimler, Ford, Honda, Mazda
- General Motors Hydrogenics
- United Technologies Fuel Cells: Renault, Nissan, Hyundai
- Toyota

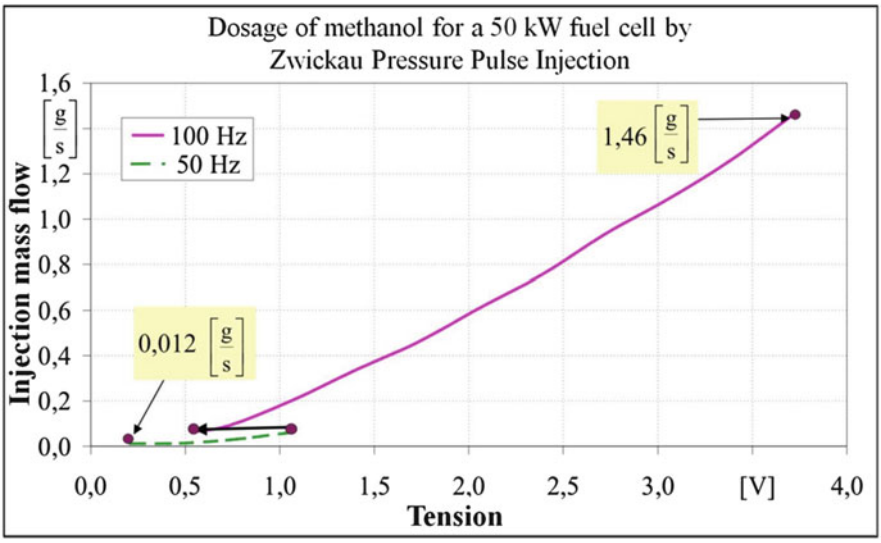

Fig. 4.24 Dosage curve for methanol in a fuel cell using a Zwickau pressure pulse injection system

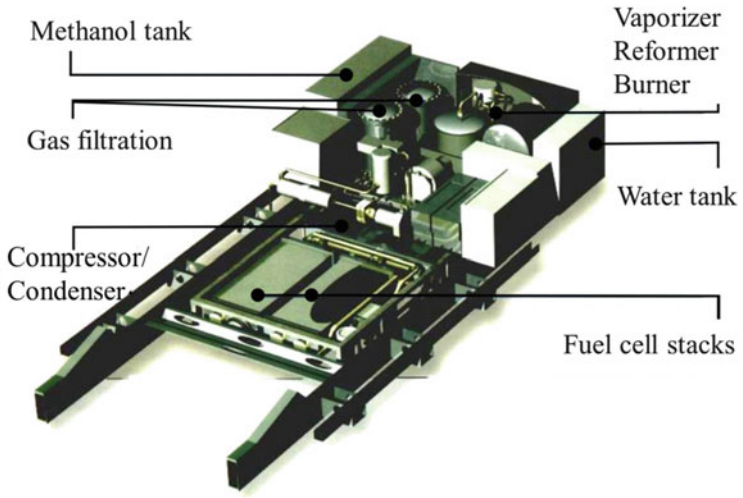

Fig. 4.25 Function modules of a methanol fuel cell in an automobile

Toyota FCHV (fuel cell hybrid vehicle) utilizes a hydrogen fuel cell, which is stored at a pressure of 34.5 MPa. A nickel-metal hydride battery with 274 V is provided as energy accumulator; the name of the system is “fuel cell hybrid.” The three-phase propulsion motor has a power of 80 kW and torque of 260 N m. The car

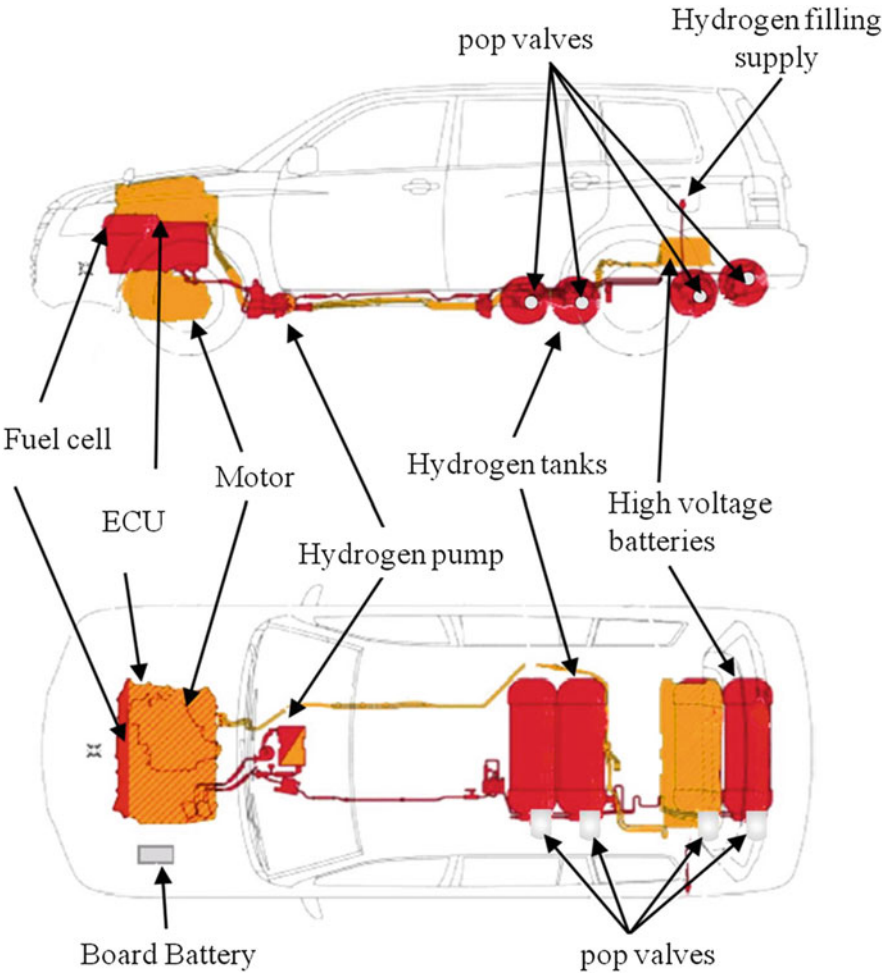

Fig. 4.26 Toyota FCHV: propulsion by motor, current generation by fuel cell, and storage by battery (Source: Toyota)

weight is 1860 kg and the operation range is given as 300 km. The layout of the modules in the car is shown in Fig. 4.26.

Ford FCEV (fuel cell electric vehicle) is based on a similar concept. The hydrogen is stored in a tank of 178 l at a pressure of 35 MPa. Under these conditions, the stored hydrogen mass is 4 kg. A Ballard fuel cell is combined in this system with a nickel-metal hydride battery of 216 V. The three-phase propulsion motor has a power of 68 kW and torque of 230 N m. With a limitation of the vehicle speed to 128 km/h, the range is 300 km. Figure 4.27 shows some Daimler prototypes as examples of the variants and concepts that have been developed during the last two decades. The achieved power is acceptable, but the range is

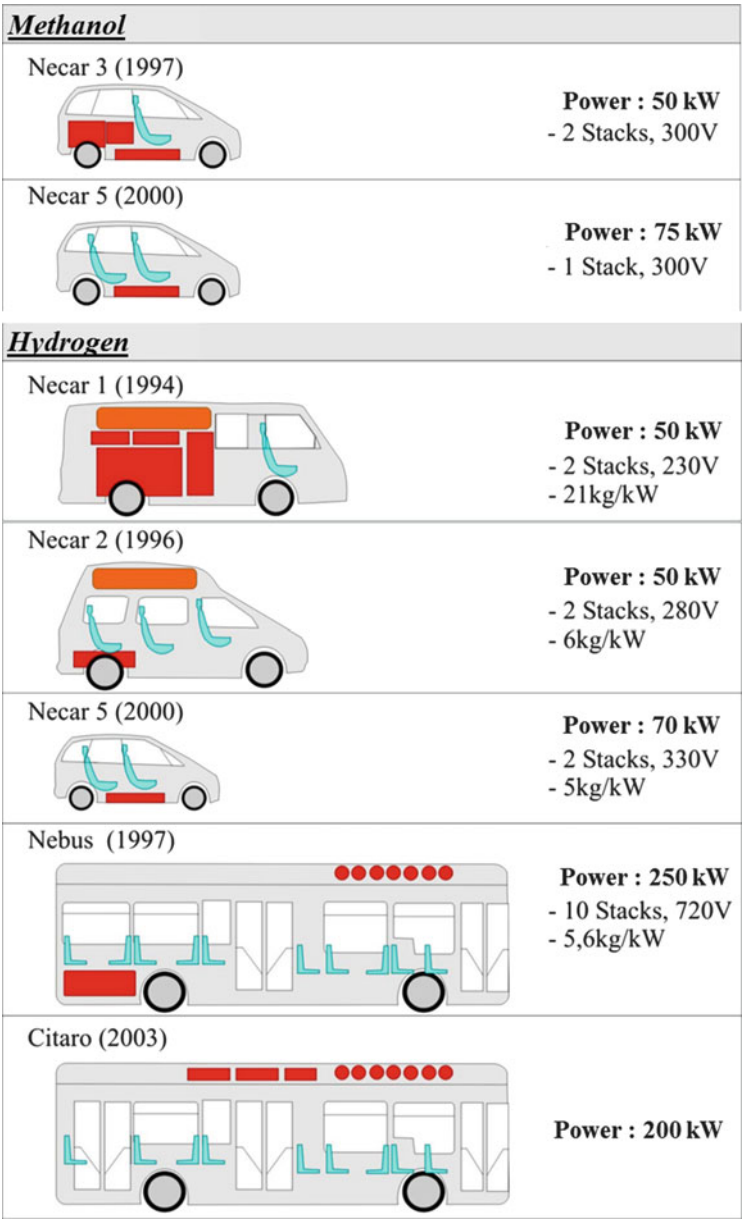

Fig. 4.27 Types of vehicles with fuel cells using methanol and hydrogen for electric propulsion (Source: Daimler)

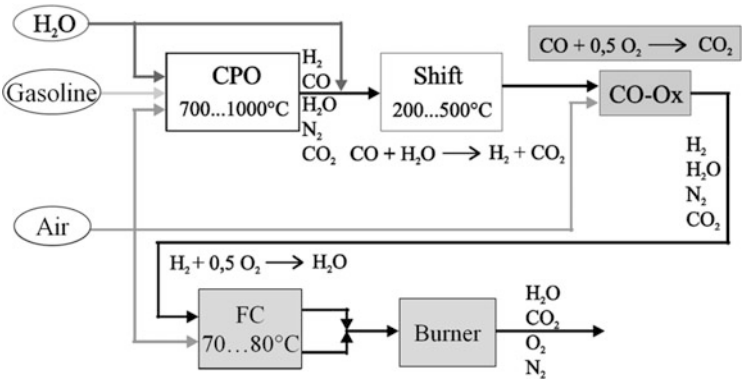

Fig. 4.28 Function modules of a gasoline fuel cell

still low because of the hydrogen storage problem and the modest efficiency. The very high price is hindering the introduction of fuel cells in large series.

Nevertheless, fuel cells have clear advantages at low load and steady function, being able to produce electric energy on board, independent of the propulsion motor, for numerous consumers such as climate control, lighting, telematics, seat heating and positioning, all in a power spectrum of 4–10 kW. Such electric power cannot be ensured by batteries or an alternator. A compact, low price fuel cell with steady function is a better alternative. An example has already been given in Sect. 3.5 (Fig. 3.32) of an automobile with hydrogen propulsion by an SI engine and current generation by a fuel cell, with hydrogen from the same reservoir.

A fuel cell can operate with gasoline, diesel fuel, methanol, or ethanol, which widens the scope of the above scenario to all engines with propulsion by SI or CI engines [21]. Figure 4.28 shows the process sequences, the main chemical reactions, and the functional modules of a fuel cell powered by gasoline.

Figure 4.29 presents the modules of a fuel cell for gasoline or diesel fuel with their respective process temperatures. The fuel dosage within the mixer is made using a high precision using a Zwickeu pressure pulse injection system. Figure 4.30 shows the dosage curve for diesel fuel when using such a system. The whole supply is very compact, and Figure 4.31 presents the main features of such a diesel fuel cell.

Propulsion by a piston engine and production of electric energy on board by a fuel cell using the same fuel in the reservoir is a very efficient scenario, which gives the fuel cell more development possibilities than as an energy supplier for car propulsion.

The storage of electric energy on board in batteries (Sect. 4.3) and conversion of the chemical energy of substances into electric energy on board by fuel cells (Sect. 4.4) are both reliable scenarios. However, combustion achieves a higher energy density: the turbulence of the mixture increases the contact surface of the reacting substances, and the very high temperature and, thus, very high internal energy of the molecules are very favorable for their chemical reaction.

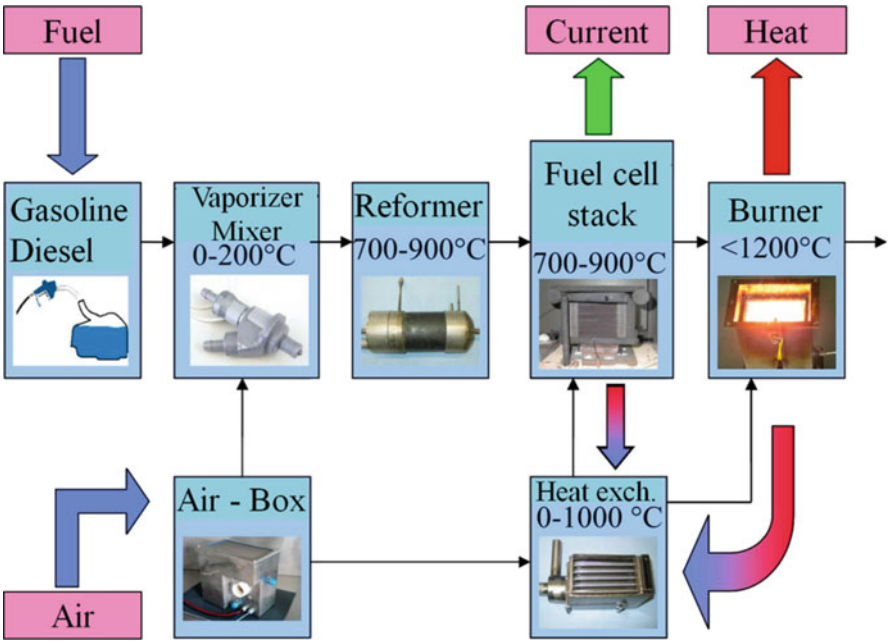

Fig. 4.29 Fuel cell using gasoline or diesel for current generation on board an automobile [21]

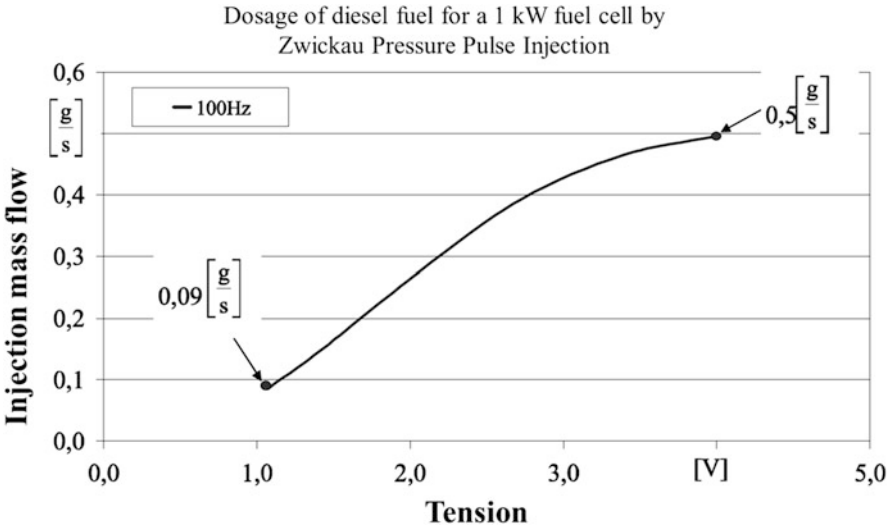

Fig. 4.30 Dosage curve for diesel fuel in a fuel cell using a Zwickau pressure pulse injection system

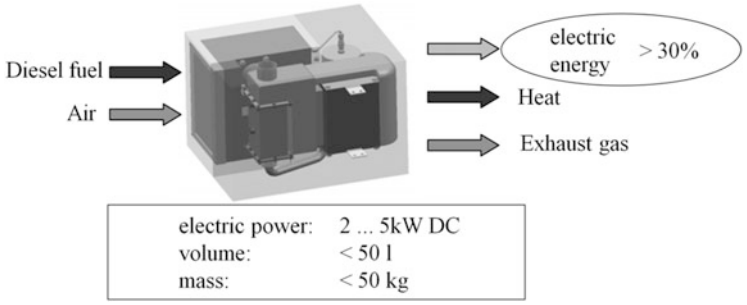

Fig. 4.31 Fuel cell using diesel fuel, with fuel dosage as shown in Fig. 4.29 [21]

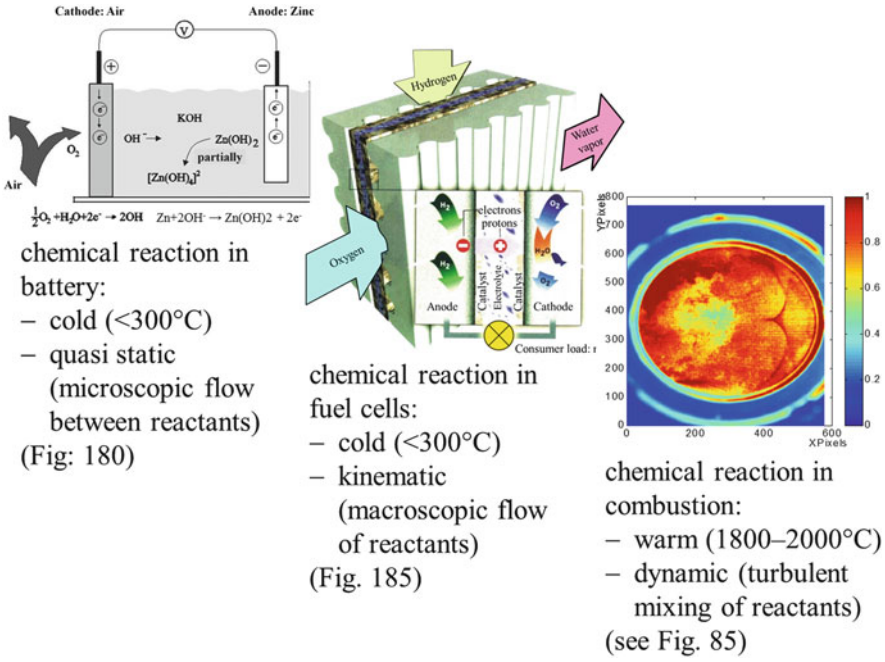

Fig. 4.32 Energy from chemical reactions

Figure 4.32 presents a comparison of the three process forms, corresponding to Figs. 4.11, 4.16, and 2.56.

4.5 Automobiles with Electric Propulsion

Table 4.4 presents a selection of series automobiles with electric propulsion and storage of the electric energy in batteries. The main characteristics of these vehicles have been classified in four categories:

Table 4.4 Selection of electric cars and their characteristics

Car			Motor			Energy storage		Performance		
Type	Mass [kg]	Production	Type	Power [kW]	Torque [N m]	Battery	Energy [kW h]	Range [km]	Consumption [kW h/ 100 km]	Maximum velocity [km/h]
Aixam MEGA e-City	750	Series	Asynchr.	8	30–45	LiFePO4	9	60–80	11.25–15	64
Aptera 2e	682	Series	–	22.8	112	LiFePO4	13	160	8.13	137
Alvarez Eco-E	549	Series	–	3.1	–	AGM	3.1	48.3–64.4	4.81–6.42	40.25
Artega SE	1400	Concept	–	280	–	Li-ion	37	200–300	12.33–18.5	250
Audi R8 e-tron	1780	Concept	Synchr.	280	820	Li-ion	48.6	215	22.60	200
BAIC C71 EV	1880	Series	Synchr.	63	160	LiFePO4	22	150	14.67	160
BAIC BE701 EV	1790	Series	Synchr.	110	300	–	–	200	–	160
BAIC C30 EV	1000	Series	–	47	82	Li-poly	31	200	15.5	160
Baoya Vehicle Bhc-BY02-1 / 2-1/ 3-3/ 4-4	790–880	Series	–	10	–	Lead-gel	–	130–160	–	70–95
Beijing Auto E150 EV	1370	Series	Synchr.	45	144	Li-ion	22	120–150	14.67–18.33	125
Bellier e-Jade	690	Series	–	–	–	Li-poly	–	200	–	75
BMW Mini E	2009	Series	Synchr.	150	220	Li-ion	35	160	21.88	153
BMW i3	1195	Series	Synchr.	125	250	Li-ion	21.6	130–160	13.5–16.62	150
Bomobil	1000	Series	Synchr.	10	300	–	27	150	18	130
Brabus 4WD	2190	Concept	Synchr.	320	3200	Li-ion	56	350	16.00	220
Brabus smart	–	Series	Synchr.	60	135	Li-ion	17.6	145	12.14	60
BYD e6	2295	Series	Synchr.	75	450	LiFePO4	60	300	20	185
BYD K9	14300	Series	Synchr.	90	550	LiFePO4	324	250	129.6	96

Cadillac Converj	–	Concept	Synchr.	120	370	Li-ion	16	–	–	160
Centric AutoMotive ThoRR	755	Series	Induction	200	450	Li-poly	29	200	14.5	180
Chang'an E30 EV	1610	Series	–	85	280	LiFePO4	29.1	180–210	13.86–16.17	120
Chery QQ3 EV	1100	Series	Synchr.	12	72	Li-ion	–	120	–	60
Chery Riich M1 EV	1060	Series	Synchr.	40	–	LiFePO4	–	120	–	150
Citys ax (Chevrolet-Matiz conversion)	910–1250	Series	–	16–26	96	Li-poly	7–13	120	5.83–10.83	130
Chevrolet Spark EV	1360	Series	Synchr.	105	443	Li-ion	21	132	15.91	145
Citroën Berlingo First Electrique	1315	Series	Asynchr.	42	175	Li-ion	23.5	120	19.58	110
Citroen c-Zero, Peugeot iOn	1120	Series	Synchr.	47	180	Li-ion	16	160	10	130
Citroën-C1-Umbau (Electric Car Corporation C1 ev'ie)	890	Series	–	30	–	–	–	95–120	–	100
CT&T e-Zone Plus	806	Series	–	–	90	Li-poly	–	100	–	68
Detroit Electric	1242	Series	–	150	380	Li-poly	25	320	7.81	192
Dodge ZEO	–	Concept	–	200	–	Li-ion	64	402	15.92	96

(continued)

Table 4.4 (continued)

Car		Production	Motor			Energy storage		Performance		
Type	Mass [kg]		Type	Power [kW]	Torque [N m]	Battery	Energy [kW h]	Range [km]	Consumption [kW h/ 100 km]	Maximum velocity [km/h]
Electric Cars Europe Qbee (Geely-GlobalEagle-EK-2-conversion)	–	Series	–	–	–	LiFePO4	–	180	–	150
Electro Vehicles Europe StartLab Open elettrica	490	Series	–	4	–	Lead-gel/ lithium	ca.7	50–80	14	45/65–75
EMC Electric Wagon E36	–	Series	Asynchr.	–	–	NiCl2	24	320	7.5	120
Estrima Birò	330	Series	–	4	–	Lead-gel	7.56	50	15.12	45
e-Twen	930	Series	–	5	–	Lead-gel	15	100–125	12–15	70
EVC S7electric (Škoda)	–	Series	Asynchr.	65	190	LiFePO4	30	200	15	130
e-Wolf ALPHA · 1 SRF	970	Series	Synchr.	30	800	Li-ion	41.5	105–300	13.83–39.52	110–230
FFW-Cars eMK6	865	Series	–	15	–	–	12–16	75	16–21.33	85
Fiat-500-Umbau Kamoo 500	1100	Series	Asynchr.	93.25	215	Li-ion	23.79	110–200	11.89–21.63	110–130

Fiat Palio Weekend EV	–	Series	–	14.71	–	NiCd	–	120	–	100
Fine Mobile Twike Easy	250	Series	Asynchr.	5	–	Li-ion	–	200	–	85
Flybo YM-E10	820	Series	–	5	76	Lead-gel	12	100–150	8–12	55
Ford Focus Electric	1675	Series	–	92	246	Li-ion	23	170	13.53	136
Foton Midi EV	-	Series	–	80	280	LiFePO4	24	150	16	160
Fribest FC6500E	960	Series	Asynchr.	6.5–8.5		Lead-fleece	–	80	–	80
Fuxing Fulaiwo Cl	875	Series	–	–	–	Lead-gel	–	150	–	45–60
Geely EK-2	1200	Series	Synchr.	90	177	LiFePO4	136	180	7.56	150
German E-Cars Stromos (Suzuki-Splash-/Opel-Agila-conversion)	1300	Series	–	56	140	Li-ion	15–20	70–100	20–21.43	120
GM EV1	1321	Series	Induktion	102	150	NiMH	26.4	105	25.14	113
Great Wall Haval M3 EV	1196	Series	Synchr.	56	150	LiFePO4	19.2	160	12	130
Great Wall Voleex C20 EV	–	Series	–	56	150	Li-ion	19.2	160	12	130
GreenGo Tek Cozmo NEV	500	Series	–	20		Lead-fleece	–	>90	–	40
GreenWheel Jimma GW12-A06L38-01	1055	Series	Asynchr.	7.5	80	Li-ion	10.8	160–200	5.4–6.75	110

(continued)

Table 4.4 (continued)

Car		Production	Motor			Energy storage		Performance		
Type	Mass [kg]		Type	Power [kW]	Torque [N m]	Battery	Energy [kW h]	Range [km]	Consumption [kW h/ 100 km]	Maximum velocity [km/h]
Hainan Mazd/ Freema EV	1549	Series	–	40	–	LiFePO4	–	160	–	90
Impact SAM EV II	500	Series	Synchr.	28	78	Li-poly	8	80	10	95
Infiniti LE Concept	–	Concept	–	100	325	Li-ion	24	–	–	–
Innovech MyCar	710	Series	DC	5	–	Lead-gel	9.6	115	8.35	66
JAC Tojoy EV	1200	Series	Synchr.	27	200	LiFePO4	15	150	10	95
Jetcar 2.5 Elektro	1150	Series	Synchr.	60	–	Li-ion	31.2	200–250	12.48–15.6	160
Jinan Baoya BY5000EV-1A	750	Series	DC	5	100	Lead-gel	–	100	–	65
Kandi KD-5010	980	Series	–	7.5	–	Lead-gel	86.4	80	108	70
Kia Ray EV	1185	Series	–	50	167	Li-poly	16.4	140	11.71	130
Land Rover Electric Defender	2055–2162	Concept	–	–	330	Li-ion	27	80	33.75	–
Lifan 620 EV	1350	Series	Synchr.	30–60	–	LiFePO4	24	150–320	7.5–16	120
Little Little4 Base Vintage	–	Series	–	–	–	Lead-gel	–	100	–	50
Longwise EVL050V	1280	Series	DC	8.5	–	Li-ion	14.4	160	9	78

LUIS 4U green	1830	Series	Synchr.	27.5	240	LiFePO4	35	150–200	17.5–23.33	95
Luxgen 7 MPV EV+	–	Series	Synchr.	176	265	Li-ion	40	350	11.43	145
Luxgen Neora EV	1600	Concept	Induction	180	245	Li-ion	48	400	12	150
Mahindra e2o	813	Series	Induction	14.8	53.9	Lead-gel	–	80–100	–	104
Mazda-2-five-door-conversion Energetique evMe Subcompact	1300	Series	–	89	ca.200	Li-poly	17	180	9.44	130
Mercedes-Benz SLS AMG Coupé Electric Drive	2110	Series	Synchr.	552	1000	Li-ion	60	ca.250	24	250
Mercedes Benz Vito E-Cell	2150	Series	–	60	280	Li-ion	36	150	24	130
MI C7-é Roadster	–	Series	–	–	–	LiFePO4	–	150–170	–	135
Microcar M.Go electric	540	Series	–	7.5	–	LiFePO4	–	80–140	–	60
Mitsuoka LIKE	306–328	Series	–	5.6	36	Li-ion	–	150	–	130
Mitsubishi i-MiEV	1185	Series	Synchr.	35	180	Li-ion	16	150	10.67	130
Movitron Teener	830	Series	DC	4	–	Lead-gel	–	70	–	45
My Electric Vehicle (Mini-) Daytona	–	Series	DC	–	–	Lead-gel	–	60	–	40

(continued)

Table 4.4 (continued)

Car		Production	Motor			Energy storage		Performance		
Type	Mass [kg]		Type	Power [kW]	Torque [N m]	Battery	Energy [kW h]	Range [km]	Consumption [kW h/ 100 km]	Maximum velocity [km/h]
Myers Motors NmG	612	Series	DC	20	–	–	–	50	–	122
Nissan Leaf	1545	Series	Synchr.	80	280	Li-ion	24	160	15	145
Opel-Corsa-Umbau German E-Cars Cetos	–	Series	–	60	182	Li-ion	15–20	120	12.5–16.67	130
Oka NEV ZEV (VAZ-1111-Oka-conversion)	698	Series	–	–	–	Lead-gel	–	32	–	40.2/56.3
PG Elektrus	860	Series	–	200	350	Li-ion	–	350	–	300
PMMC Greenrunner EP 1500	–	Series	–	–	–	LiFePO4	–	80–140	–	60
Porsche-911-conversionu eRuf Roadster Greenster	–	Series	Synchr.	250	–	Li-ion	37	200	18.5	250
Pure Mobility Buddy	650	Series	–	13	–	NiMh	14.4	60–100	14.4–24	80
Quadix e-Buggy	–	Series	–	25	–	Li-poly	6.5	90	7.22	100
Renault Fluence Z.E.	1610	Series	Synchr.	70	226	Li-ion	22	185	11.89	135

Renault Kangoo Z.E.	1410	Series	Synchr.	44	226	Li-ion	22	170	12.94	130
Renault Zoe	1460	Series	–	60	220	Li-ion	–	160	–	140
Renault Twizy Urban	450	Series	–	15	33	Li-ion	7	100	7	80
Roewe E50	1080	Series	Synchr.	47	155	Li-ion	18	180	10	130
Saab 9-3 ePower	–	Series	–	135	–	Li-ion	35.5	200	17.75	150
SAIC Roewe 350 EV	–	Series	Synchr.	75	190	LiFePO4	25	200	12.5	150
SAIC Roewe E1	1040	Series	Synchr.	47	–	LiFePO4	16	135	11.85	120
Sanifer Mini-Car L7e	–	Series	–	15	–	Li-poly	–	120	–	100
Shandong Huoyun HY-B22120	960	Series	Synchr.	8.5		Lead-fleece	–	80	–	80
Shandong Jindalu FL5000ZK-1	–	Series	–	5	71.4	Lead-gel	18	100–125	14.4–18	70
Shanghai-GM Sail Springo EV	1385	Series	Synchr.	85	510	Li-ion	21.4	130	16.46	130
Shelby Aero EV	1341	Series	–	750	1088	Li-ion	36–48	241	14.94–19.92	334
Smart ED	854	Series	Synchr.	30	88	Li-ion	16.5	137	12.04	121
Stevens ZeCar	–	Series	Induction	52.2	217	LiFePO4	–	160	–	90
Takayanagi Miluira Retro EV	–	Series	Asynchr.	3.5	–	Lead-gel	ca.5	35	14.29	60

(continued)

Table 4.4 (continued)

Car		Production	Motor			Energy storage		Performance		
Type	Mass [kg]		Type	Power [kW]	Torque [N m]	Battery	Energy [kW h]	Range [km]	Consumption [kW h/ 100 km]	Maximum velocity [km/h]
Tara Tiny EV	ca.850	Series	–	3	–	Lead-gel	12	120	10	50
Tazzari Zero	542	Series	–	15	150	Li-ion	12.3	140	8.79	100
Tesla Model S	2100	Series	Induction	225–310	440–600	Li-ion	60–85	370–480		190–210
Tesla Motors Roadster	1235	Series	Induction	215	400	Li-ion	53	395	13.42	201
TGMY EV Himiko	1640	Series	–	25	140	Li-poly	62.4	450–550	11.35–13.87	120–160
TGS Xtreme Buggy EV	620	Series	Asynchr.	10.5	–	Li-ion	16	145	11.03	75
Th!nk City	1038	Series	Induction	47	90	Li-ion	23	180	12.78	100
TommyKaira ZZ EV	850	Concept	DC	225	415	Li-ion	–	120	–	150
Toyota COMS	400–420	Series	–	5	250	Li-ion	3.7	50	7.4	60
Toyota RAV 4 EV	1564	Series	–	50	226	Li-ion	27.4	203	13.50	127
Toyota TMG EV	970	Concept	–	280	800	LiCe	41.5	–	–	260
Town Life Helektra	550–600	Series	–	4	–	Lead-gel	8.6	90	9.56	45/80
Venturi Fétish	1225	Series	–	220	380	Li-ion	54	350	15.43	250
Volteis X4 VS2	681–740	Series	Synchr.	4–8	–	Lead-gel	11.5	60	19.17	70
Volvo C30 DRIVe Electric	1600	Series	–	82	240	Li-ion	24	150	16	130
Volkswagen E-Bugster	–	Concept	–	147	–	–	28.3	–	–	–

Volkawagen E-up!	1214	Series	Synchr.	60	210	Li-ion	18.7	160	11.69	130
Vromos Kiwi	3500	Series	DC	10	–	Lead-gel	9.6	150	6.4	85
Wheego Whip LiFe	1282.76	Series	Induction	14.7	128.8	LiFePO4	30	100	30	113
Yogomo MA4 EV	550	Series	–	3–5	–	Lead-gel	7.68–9.72	50–100	9.72–15.36	60
Zenn Electric Car	635	Series	Synchr.	22.37	57	Lead-gel	–	56	–	40
Zotye Lerio EV	1350	Series	Synchr.	11	200	LiFePO4	32	ca.160	20	110
Zotye M300 EV	1705	Series	Synchr.	30	250	LiFePO4	35.2	ca.160	22	120
Zytel Gorila EV	–	Series	DC	30	–	Lead-gel	10	80	12.5	8

Source: Information from the manufacturers

- Vehicle mass, including batteries
- Propulsion: motor type, power, torque
- Energy storage: battery type, energy content
- Performance: range, energy consumption, maximum speed

In the second stage of vehicle electrification (1992–2005) the motors were mainly asynchronous, whereas in the present third stage, synchronous motors, with their high efficiency, have practically no competitors. As presented in Sect. 1.1 (Fig. 1.5), the electric energy content of batteries on board determines not only the obtainable power and torque, but also the vehicle weight. A Renault Twizy Urban (Table 4.4) has a battery of 7 kW h, allowing only a moderate power of 15 kW and a low torque of 33 N m. For the required autonomy of 100 km, the car mass must be limited to 450 kg, thus the safety and comfort functions are reduced. Nevertheless, this configuration is acceptable for a city vehicle. For most of the vehicles that are listed in Table 4.4, the battery capacity is in the range of 25 kW h, meaning that 25 kW is available for 1 h. An interesting exception is the Chinese bus BYDK9, with a battery capacity of 324 kW h; the vehicle weight is 14,300 kg, the power 90 kW, and the torque 550 N m. The high torque at low power indicates a low speed, which is sufficient for an urban bus.

The range of the cars listed in Table 4.4 is on average 120–150 km. From the data in Table 4.4, one can deduce a relationship between torque, power, vehicle mass, and battery capacity, as presented in Fig. 4.33. Most of the vehicles have a torque in the range of 150–300 N m. The motor power seems more heterogeneous, with a mean of 50–60 kW. This discrepancy between torque and power is explainable by the speed range. For vehicles in urban use or for vehicles with motors equipped with more than one gear level, a high torque at low power is not a disadvantage. The weight of the listed cars is in the range of 1000–2000 kg, similar to that for vehicles powered by piston engines.

Figures 4.34, 4.35, 4.36, 4.37, and 4.38 show some examples of automobiles with propulsion by motor and electric energy storage in batteries. The variety of configuration is impressive. The Nissan Leaf, BMWi3, and Renault Zoe are compact cars. A comparison of power and torque between the Nissan and BMW shows more power for the BMW but more torque for the Nissan. The reason is the envisaged driving profiles: predominantly urban cycles for the Nissan, with many start–stop situations, and urban cycles for the BMW, but with considerable motorway use. The mentioned energy consumption for 100 km shows a net advantage for the BMW, which is explainable by the low car mass, achieved with a carbon fiber body. The difference in car mass between the BMWi3 and Renault Zoe is also the reason for the unequal energy consumption of these two vehicles. Therefore, the BMW reaches the same range as the Renault Zoe, but with more power and less battery capacity. On the other hand, the price of a light car body is reasonable. In the class of small cars such as the Mitsubishi i-MieV, a low motor power in the range of 35 kW is sufficient, whereas in the compact class the required power range is 65–125 kW. Nevertheless, the torque in both classes is comparable: 180 N m in the

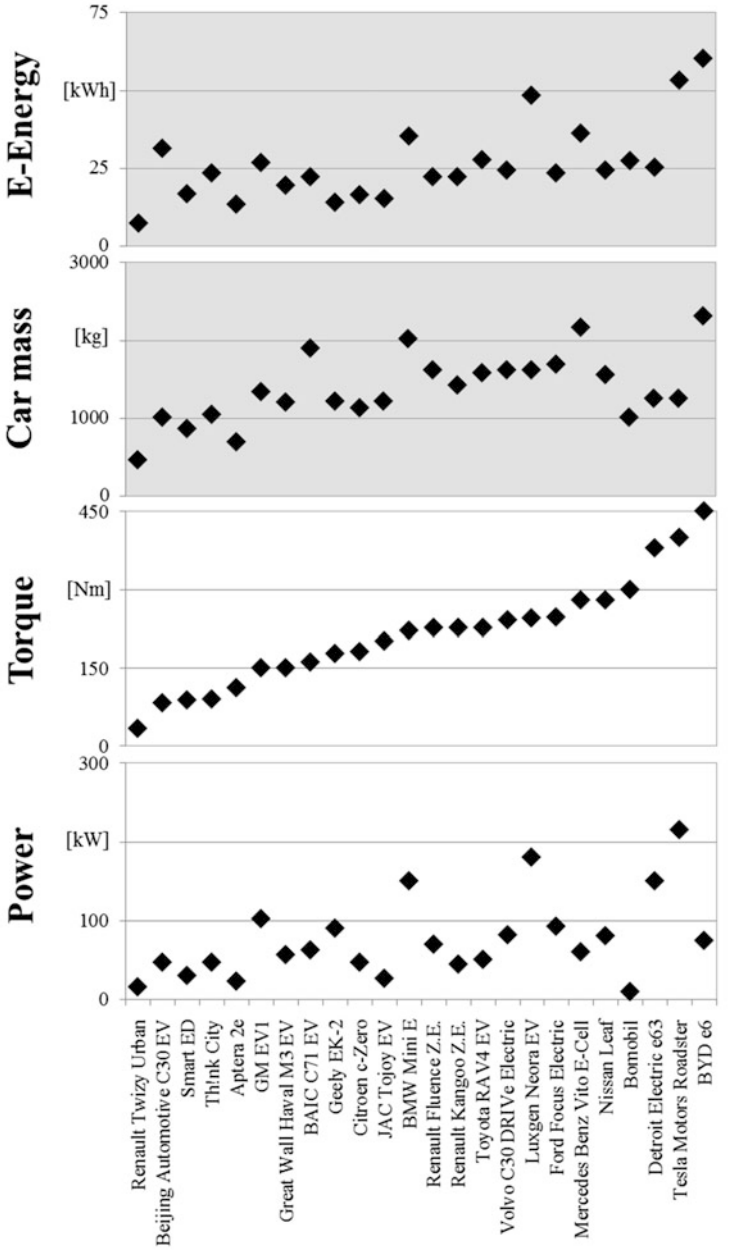

Fig. 4.33 Relationship between power, torque, and car mass and the electric energy stored on board for a selection of electric cars

power:	80	[kW]
torque:	280	[Nm]
car masse:	1545	[kg]
Energy in battery:	15	[kWh]
Energy consumption:	24	[kWh/100km]
range:	160	[km]

Fig. 4.34 Electric car: Nissan Leaf (Source: Nissan)

power:	125	[kW]
torque:	250	[Nm]
car masse:	1195	[kg]
Energy in battery:	18,8	[kWh]
Energy consumption:	13,5	[kWh/100km]
range:	160	[km]

Fig. 4.35 Electric car: BMW i3 (Source: BMW)

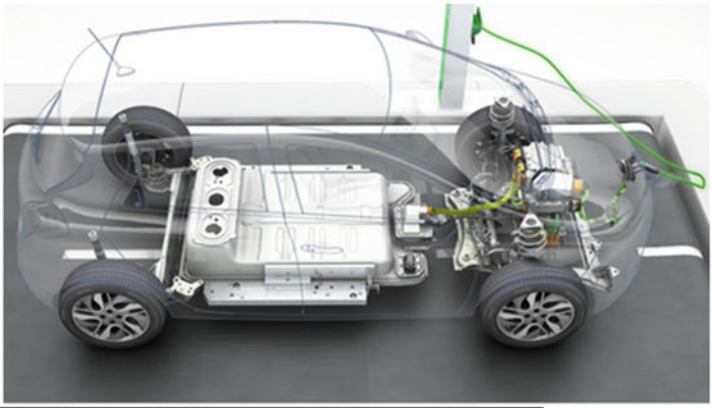

power:	65	[kW]
torque:	220	[Nm]
car masse:	1460	[kg]
Energy in battery:	22	[kWh]
Energy consumption:	-	[kWh/100km]
range:	160	[km]

Fig. 4.36 Electric car: Renault Zoe (Source: Renault)

power:	35	[kW]
torque:	180	[Nm]
car masse:	11850	[kg]
Energy in battery:	16	[kWh]
Energy consumption:	11	[kWh/100km]
range:	150	[km]

Fig. 4.37 Electric car: Mitsubishi i-MiEV (Source: Mitsubishi)

power:	60	[kW]
torque:	280	[Nm]
car masse:	2150	[kg]
Energy in battery:	36	[kWh]
Energy consumption:	25	[kWh/100km]
range:	150	[km]

Fig. 4.38 Electric car: —Mercedes Vito E-Cell (Source: Mercedes)

small class versus 220–280 N m in the compact class. The vehicle mass in the small class is comparable with that of the BMWi3 in the compact class.

The Mercedes Vito E-Cell is a transporter with higher weight (twice that of the BMWi3 and Mitsubishi iMiEv) and a power that corresponds to that of electric vehicles in the middle class of cars, which is sufficient for the driving profile of a transporter. The higher vehicle mass requires more consumption of electric energy and, thus, more battery capacity, requiring higher battery mass and volume. All these examples have a common point, vehicle autonomy in the range of 150–160 km.

A central problem with respect to electric vehicles is the CO_2 emission, which is comparable on a well-to-wheel basis with vehicles powered by internal combustion engines. A large-scale analysis made by the Technical University of Vienna [35] compared the CO_2 emissions of four electric cars:

- Nissan Leaf
- Mitsubishi i-MiEV
- Smart For Two Electric Drive
- Mercedes Benz A Class E-Cell

Data were compared with those of a car with a diesel engine, the Volkswagen Polo Blue Motion. The data for the electric cars are given in Table 4.4. The

Volkswagen Polo Blue Motion has a weight of 1150 kg (similar to the BMWi3 and Mitsubishi i-MiEV) and is equipped with a diesel engine of 1.2 dm^3, reaching a power of 55 kW.

In comparing the real energy requirement and real CO_2 emissions, the atmospheric temperature profiles in Austria and in the European Union were considered, requiring the function of climate and heating on board for a range of −20 °C to +30 °C. The driving cycle was in the city, country, and on motorways; the road inclination was in the range of −2 % to +2 %; and energy production (for fuel and for electric energy) was taken into account. Some results, which are representative for Europe, are summarized as follows:

– Mean energy requirement with/without energy production (kilowatt hours/100 kilometers)

Type	City	Country
Diesel car	42.8/48.8	42.0/47.5
Electric car	22.8/64.2	24.2/68.1

The CO_2 emission resulting from the electric energy production corresponds to the utilized sources (coal, natural gas, wind, water, nuclear), as mentioned in Chap. 1 (Fig. 1.4). This leads to the following CO_2 emissions (grams/100 kilometers):

Type	City	Country
Diesel car	132	129
Electric car	109	116

Climatization of the car over the year was taken into account. Figure 4.39 shows the influence of climatization at 22 °C, for surrounding temperatures ranging

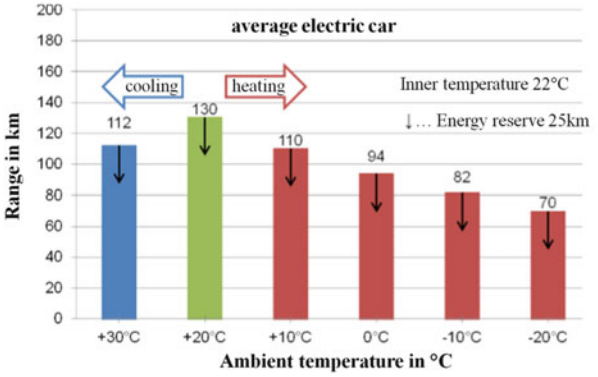

Fig. 4.39 Range of electric cars (average) as a function of ambient temperature in an Eco-test (road inclination ±2 %) [35]

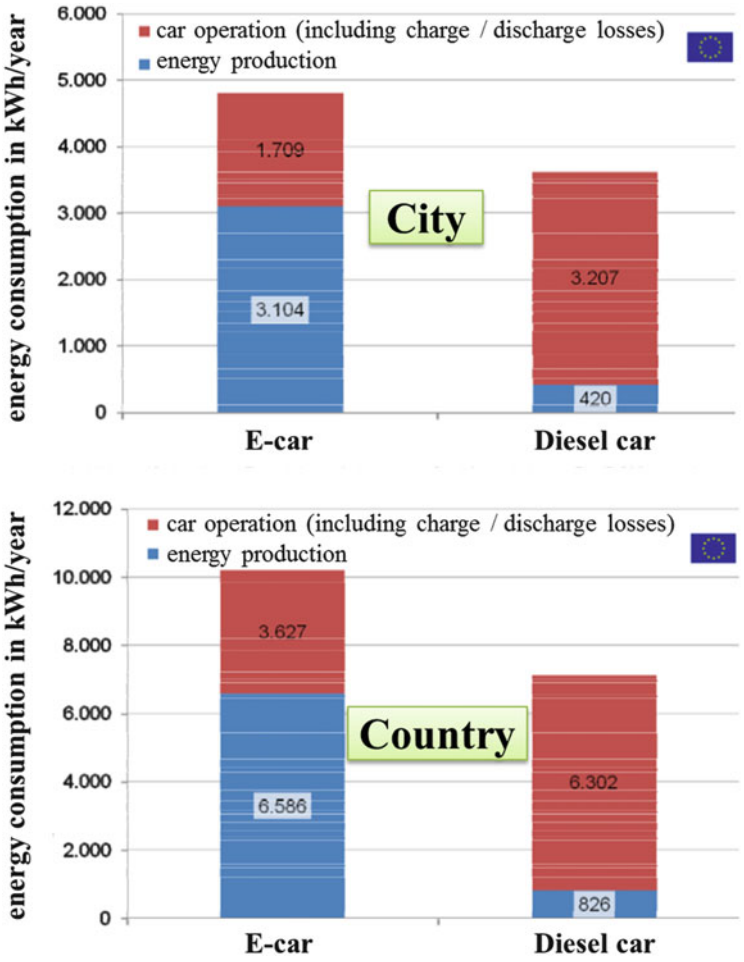

Fig. 4.40 Yearly energy demands for city and country driving [35]

between −20 °C and +30 °C, on average vehicle autonomy for the four analyzed electric cars. The decrease in vehicle autonomy to 54 % at −20 °C is considerable. Car climatization (cooling in summer and heating in winter) could be accomplished for such short distances before driving, during contact with the power source.

The yearly energy requirement for all the analyzed driving profiles, including all energy consumers on board is shown in Fig. 4.40. Figure 4.41 presents the CO_2 balance under the same conditions as for Fig. 4.40.

The energy consumption of electric cars is higher than that of diesel cars for both an urban cycle (7500 km/year) and a country cycle (15,000 km/year)! The reason for this surprising result is not the energy consumption by the car itself, but the energy production. This situation is not repeated for CO_2 emissions. In this respect, electric vehicles show a marginal advantage because of the type of electric energy

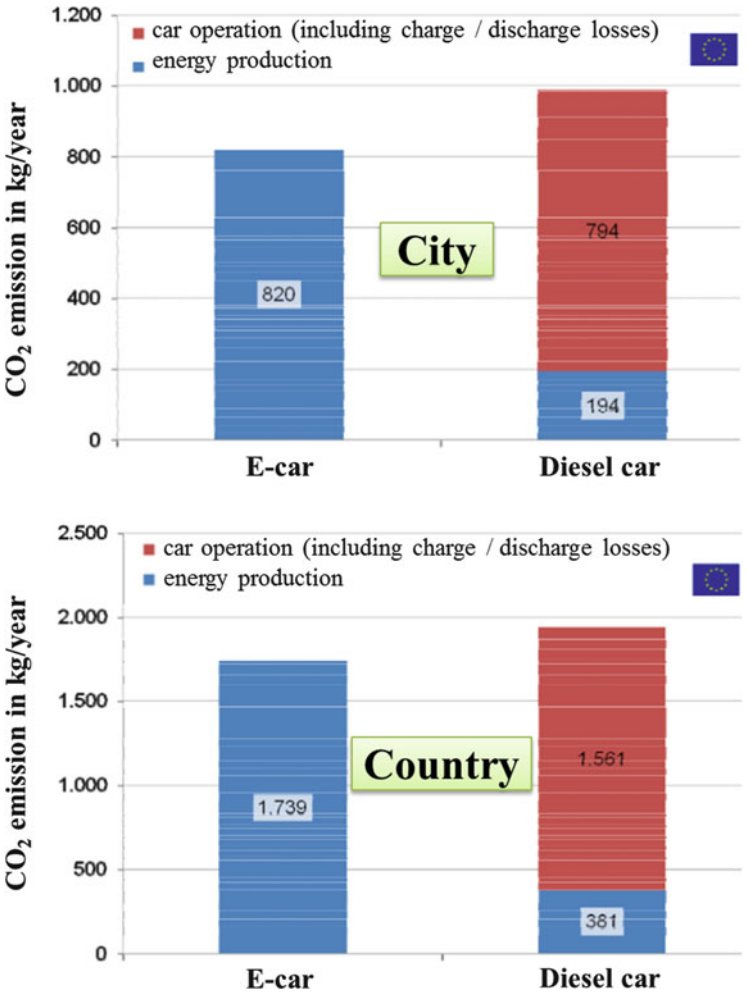

Fig. 4.41 Yearly CO_2 emissions for city and country driving [35]

production in the EU, with 76 % from nuclear plants in France and 98.5 % from hydraulic plants in Norway. However, worldwide, 41 % of electric energy is produced from coal as the main source.

A compact electric car with batteries is a real alternative for transportation in urban areas, where a drastic limitation of CO_2 emissions is expected. The request for local emission-free driving with light, compact cars at low electric energy consumption will push the development of such vehicles. However, a city car of this type will be centered on a certain customer profile, because it is not the cheapest solution. On the other hand, car rental, car sharing, and car leasing are concepts with numerous advantages and could facilitate the introduction of electric urban cars on a large scale.

Combinations of Propulsion Systems, Energy Sources, Energy Converters, and Storage

5

5.1 Configuration of the Propulsion System

The assessment of propulsion systems for automobiles in terms of energy demand and energy source, as well as in relation to ecological, technical, and economic criteria, leads to the awareness that a universal configuration is not realistic. The specific benefits of different functional modules are arguments for their effective combination. Development trends are mainly determined by the following aspects:

- The emission of pollutants and CO_2 will be drastically reduced. Zero-emission vehicles are a stringent necessity for congested urban areas and for protected landscapes.
- The requirement for comfort, including car climatization in summer and winter, and for power and torque are important criteria of acceptance.
- The strong development of electronic systems recommends the integration of propulsion control into the whole system.

From these aspects, as well as from the examples of combinations presented in Chap. 1 (Figs. 1.26 and 1.27), the following categories of propulsion system are possible:

- Propulsion by motor with energy conversion on board via a thermal engine (piston engine, Wankel engine, gas turbine, Stirling engine) using liquid or gaseous fuel, working in a limited domain of load and speed, as a current generator in combination with electric energy storage in a battery.
- Propulsion by motor with energy conversion on board via a fuel cell using liquid or gaseous fuel, in combination with storage of electric energy in a battery.
- Propulsion by motor with storage of electric energy in a battery.
- Propulsion by a combination of internal combustion spark-ignition (SI) or compression-ignition (CI) engines (as a parallel hybrid), using liquid or gaseous fuel and one or more motors, with energy stored in batteries.

C. Stan, *Alternative Propulsion for Automobiles*,
DOI 10.1007/978-3-319-31930-8_5

– Propulsion by shiftable modules formed by engines and motors, using liquid or gaseous fuel for the engines and batteries for the motors.
– Propulsion by an SI or CI engine, using liquid or gaseous fuel and generation of electric energy on board by a fuel cell working with the same fuel as the engine.

Such concepts are by no means new, similar to electric cars with hub motors or to fuel cells. In Belgium in 1900, Henri Pieper conceived a car with a gasoline engine under the hood and a motor under the driver's seat. This configuration, shown in Fig. 5.1, was presented in 1905.

The engine was utilized at constant cruise and load as a current generator for charging the battery, and propulsion was achieved by motor only. At a higher load, required for acceleration or for ascending slopes, both engine and motor were coupled for traction. The Belgian company Auto Mixte manufactured series cars of this type between 1906 and 1912.

The choice of a configuration corresponding to the required utilization depends on technical and economic aspects and on customer acceptance.

5.2 Propulsion by Motor, With a Thermal Engine as Current Generator: Serial Hybrids

There is a basic difference between propulsion by motor and by thermal engine in terms of torque, as described in Sect. 1.2:

– The maximum torque of a motor is given from standing and remains constant at this level in the lower speed range.
– The maximum torque of an engine is achieved only at a certain engine speed, which is lower for CI engines than for SI engines.

Thus, propulsion by motor is very advantageous in urban situations because of the speedy run-up and operation without changing gears. This propulsion form, which was tested many years ago by Ferdinand Porsche, has the disadvantage of an insufficient on-board energy supply if using batteries, as shown in Chap. 4. Fuel cells offer a certain enhancement, but they are not a clear alternative for large series applications because of the high technical complexity of both the fuel cell system and the hydrogen storage system, which leads to a high price but does not improve the operation range sufficiently.

Nevertheless, propulsion by motor or motors offers remarkable advantages in terms of vehicle dynamics, vehicle stability, and freedom of movement. Traditional motors situated on the front and rear axle could be replaced by newly developed hub motors integrated into the wheels, which could radically change propulsion concepts. Such hub motors are shown in Fig. 5.2.

A hub motor of this type usually achieves 20 kW power and 200 N m torque. If sufficient electric energy can be provided, a hub motor can be placed in every wheel. The classic vehicle axles are in this case no longer indispensable. This gives

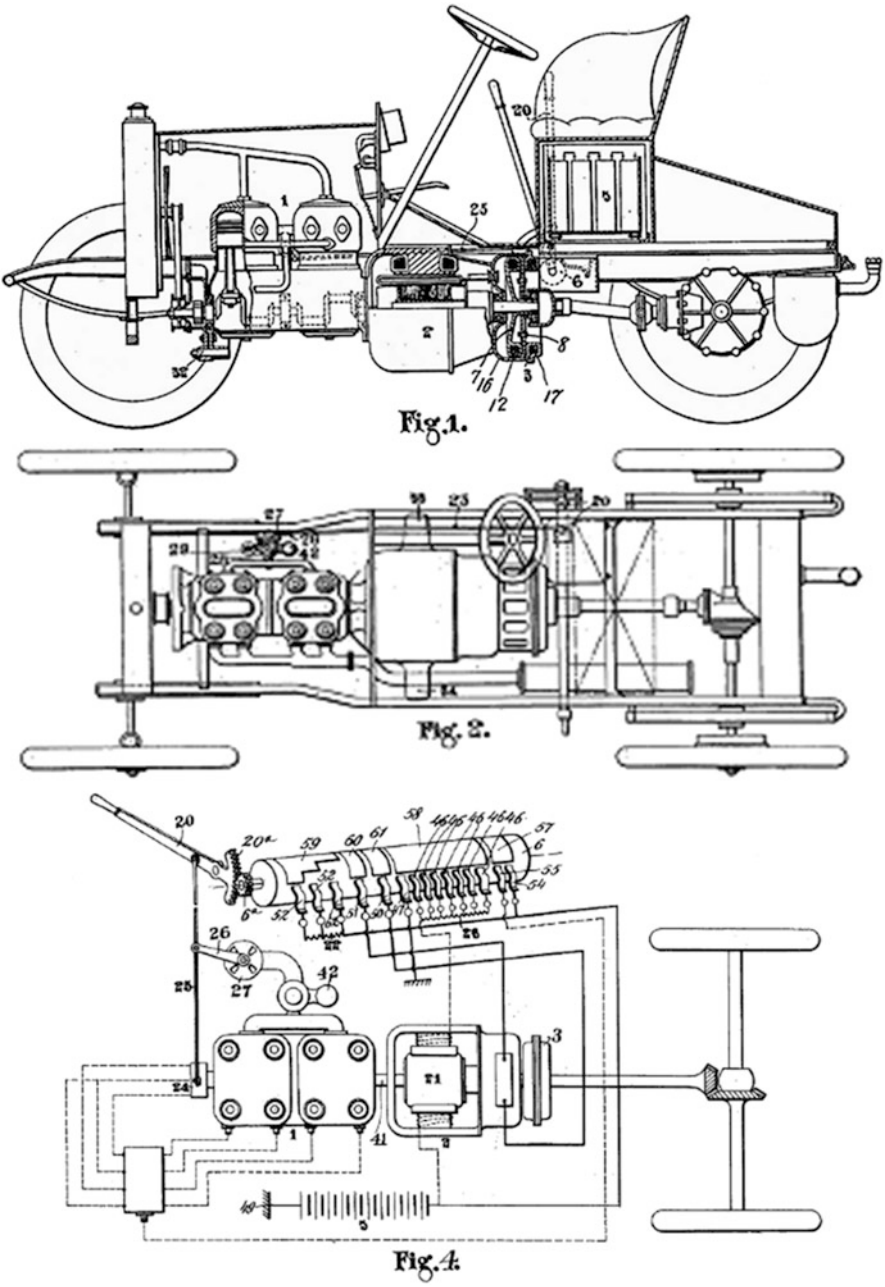

Fig. 5.1 Hybrid car from Henri Pieper: patent request from 1905

Fig. 5.2 Hub motors for car propulsion: Mitsubishi (*left*), Michelin (*center*), Honda (*right*) (Sources: Mitsubishi, Michelin, Honda)

new degrees of freedom for wheel movement. Similar orientation of the front and the rear wheels is no longer a condition. There are notable advantages regarding the kinematics and dynamics of the vehicle, as demonstrated by the following examples:

- Four-wheel and two-wheel propulsion (front or rear) can be activated by simply switching between different electric circuits. In the same mode, functions such as an electronic stability program (ESP), antislip regulation (ASR), or anti-lock braking system (ABS) are easily realizable.
- Parking and turning become light exercises, enabling lateral entry into a parking space and turning around the car's own axis in a small turning cycle, as shown in Fig. 1.3. Such maneuvers are notably advantageous in urban traffic.
- Driving stability on curves can be increased by appropriate orientation of the front and rear wheel pairs, as shown in Fig. 1.3.

Criticism of hub motors for vehicles is polarized on the nonamortized vibration of the wheels, which is provoked by the motor mass under the spring. A concept such as "eCorner" developed by Siemens/Continental is a convincing argument against such objections [24]. The eCorner system turns the wheel into an intelligent robot. The wheel position is defined by means of the six degrees of freedom within a system of coordinates. Exchange of information with the electronic control unit is realized by controller area network, local interconnected network, and Flex Ray bus systems in real time. The development plan stipulates the integration of steering, damping, and braking into the wheel with a hub motor. Similar hub motors have been developed by Volvo and are being tested in the Volvo C30 with serial hybrid propulsion.

For intelligent wheel robots, a supply of on-board electric energy is imperative. A solution with basic advantages is the use of thermal engines as on-board current generators instead of fuel cells, which have a higher technical complexity for the same efficiency. The addition of an energy storage module (e.g., a nickel–metal hydride battery) to such a generator allows valuable energy management. Such concepts are increasingly becoming the subject of development.

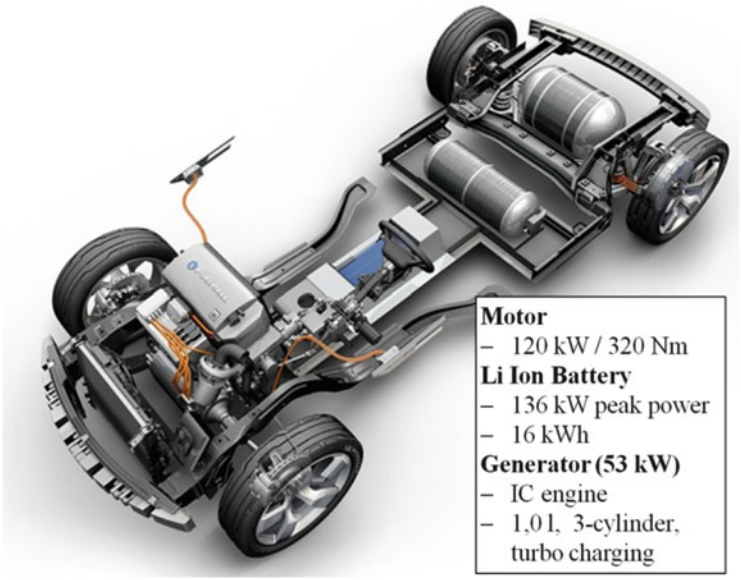

Fig. 5.3 Chevrolet E Flex Volt prototype (Source: General Motors)

Figure 5.3 shows a basic prototype from General Motors, the Chevrolet E Flex Volt. The propulsion motor has a power of 120 kW and torque of 120 N m. Current generation is ensured by a three-cylinder SI engine with a turbocharger with a swept volume of 1 l, developing a power of 53 kW. The system is completed with a lithium-ion battery with a capacity of 16 kW h and a momentary peak power of 136 kW.

This concept was initially planned for the Opel Ampera as well. Nevertheless, the configuration was redrafted for series application and marketed for a short time. A four-cylinder SI engine without a turbocharger, but with a larger swept volume of 1.4 l, replaced the turbocharged three-cylinder engine and gained the supplementary role of providing direct propulsion at high vehicle velocity, together with the motor. The configuration of the Opel Ampera is illustrated in Fig. 5.4.

The motor had a power of 111 kW and torque of 370 N m; the lithium-ion battery had a capacity of 16 kW h. The operation range with only motor and battery achieved 40–80 km. With the engine as a range extender and a gasoline tank of 35 l, the autonomy increased to 500 km. Volvo developed a serial hybrid with the same concept for the C30 model. The SI engine as a current generator with 1.6 l was replaced by a CI engine with the same swept volume, developing a power of 80 kW. The engine was set up to start when the battery capacity fell below 70 %. However, there was also an option for manual operation, for driving in urban areas where zero pollutant emission was imposed.

There have also recently appeared prototypes of serial hybrid propulsion systems with similar power and torque levels, as developed by GM and Opel, but with gas

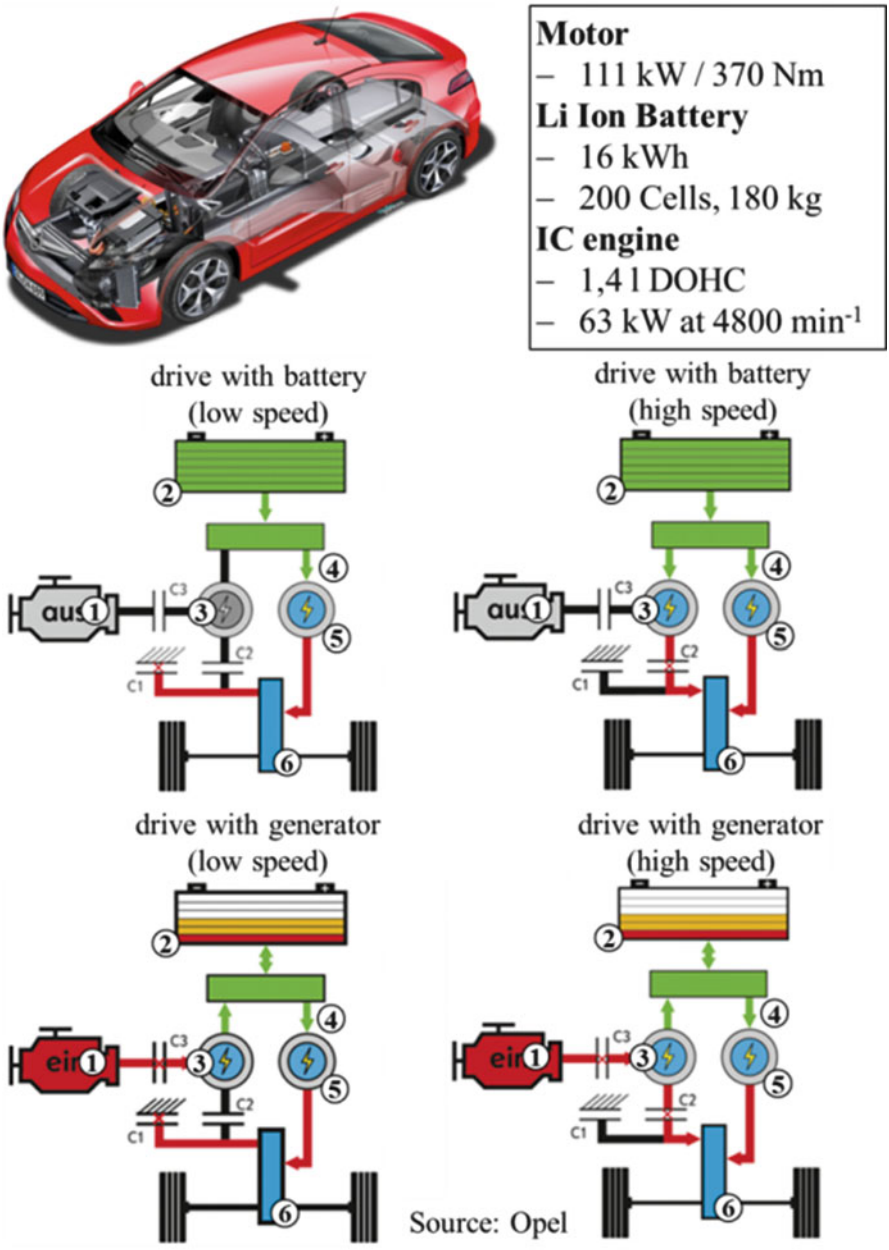

Fig. 5.4 Opel Ampera: propulsion features and function modes (Source: Opel)

Manufacturer	Car	Propulsion	
Capstone	CMT-380	C30 (30 kW_{el})	
Jaguar	C-X75	Bladon Jets (2 x 75 kW_{el})	
LPEngineering	Whisper ECO-Logic	C30 (30 kW_{el})	
ETVMotors	Toyota Prius Conversion	in house development (8 kW_{el})	
DesignLine	ECOSaver IV	C65 (65 kW_{el})	
Velozzi	Supercar	C65 (65 kW_{el})	
Velozzi	Solo Crossover	C30 (30 kW_{el})	

Fig. 5.5 Prototypes of cars with gas turbines as on-board current generators (Source: Deutsches Zentrum für Luft- und Raumfahrt)

turbines instead of piston engines as on-board current generators. Figure 5.5 shows a selection of such prototypes, working with Capstone and Bladon Jets gas turbines (see also Sect. 2.3.3). Some examples are representative:

- Volvo ECC (Environmental Concept Car) (Fig. 5.6): A gas turbine providing 41 kW at 90,000 min^{-1} is provided on the same axle as the current generator of 39 kW. The system is completed by a nickel-cadmium battery with a capacity of 16.8 kW h. The propulsion motor has a maximum power of 70 kW, and a continuous power rating of 56 kW. The performance of this system was convincing.

Maximum speed	175 km/h
Diesel fuel consumption	6 l/100 km in urban cycle
	5.2 l/100 km in combined cycle
Pollutant emission	NO_x 0.11 g/km
	CO 0.08 g/km
Autonomy	670 km with 35-l diesel fuel tank
Vehicle weight	1580 kg

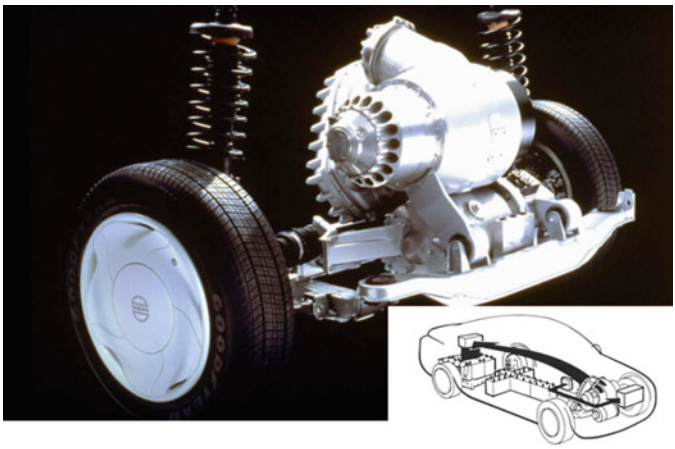

Fig. 5.6 Volvo Environmental Concept Car (ECC)

- Peugeot 406 Hybrid: The configuration of functional modules is similar to that of the Volvo ECC. The gas turbine has a power of 37 kW, also working with diesel fuel. The propulsion motor works up to a speed of 6500 min^{-1} and achieves a power of 45 kW and maximum torque of 260 N m in a speed range between 0 and 1600 min^{-1}.
- Jaguar C-X75: This concept is characterized by one hub motor of 45 kW and 400 N m for every wheel. Two gas turbines serve as current generators, each developing a power of 70 kW. The system battery has a capacity of 19.6 kW h. The vehicle achieves a speed of 330 km/h and an acceleration of 3.4 s from standing to 100 km/h. The CO_2 emission is given at 99 g/100 km. The compactness of the gas turbines at such power and the possibility of operating with various fuels are convincing arguments for the further development of such concepts, despite their high price at the moment. The NoMac gas turbine described in Sect. 2.3 (Fig. 2.95) is a low price alternative with high efficiency.

An efficient concept with very moderate price has been developed for the Citroen Saxo. Low power generation is sufficient for current generation in a compact car with electric propulsion, but the dimensions, weight, and price also have to be very moderate. On the other hand, for current generation only, the engine function can be limited to a narrow load/speed range. Thus, a simple engine with low fuel consumption and low pollutant emission is required. In this context, two-stroke engines seem to be advantageous as a matter of principle: the power-to-volume ratio of two-stroke engines is 40–60 % higher than that of four-stroke engines, as shown in Sect. 2.3.1, Eqs. (2.19) and (2.20). The power-to-weight ratio is accordingly higher for two-stroke than for four stroke-engines. The disadvantages of two-stroke engines regarding specific fuel consumption and pollutant emission are not intrinsic to the two-stroke cycle, but connected to the kind of fuel introduction into the cylinder. Different concepts for direct injection in

two-stroke engines have been successfully developed and applied over the last 30 years and demonstrate this potential in a remarkable manner [2].

For such a function range of an engine working as a current generator, the scavenging can be very well tuned. The following configuration has been developed:

- Activation of the current-generating two-stroke engine at a previously adjusted level of low battery tension
- Deactivation of the two-stroke engine in urban cycles, which is detected from the wheel velocity profile
- Activation of the two-stroke engine for continuous current supply of the propulsion motor when a previously adjusted level of speed (higher than the speed in urban areas) is exceeded

This concept can be described as follows:

5.2.1 System Configuration

The basic propulsion motor and the battery pack were proven modules from a series vehicle with motor propulsion and energy stored in a battery. The two-stroke engine was developed for a determined load/speed operation range, the main stages being tuning of the scavenging, adjustment of direct injection, and optimization of the combustion process. The conceived Citroen Saxo Electrique [23] had a DC motor with a power of 20 kW in a speed range of 1600–5500 min^{-1} and a torque of 127 N m at 1600 min^{-1}. The battery was formed by 20 Ni-Cd modules. The module for current generation, a two-stroke engine with gasoline tank and current generator, was integrated into the vehicle as illustrated in Fig. 5.7. The functions are described by the schematic in Fig. 5.8.

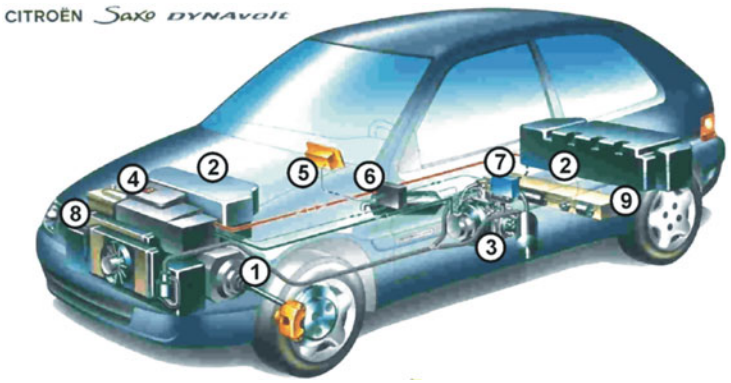

Fig. 5.7 Configuration of function modules (denoted in Fig. 5.8) within a serial hybrid system for a compact car

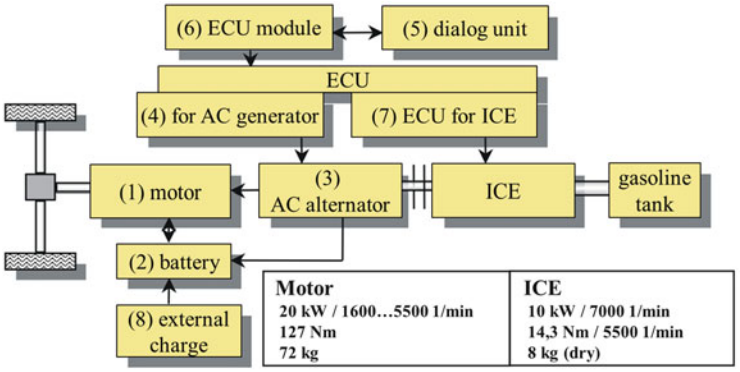

Fig. 5.8 Scheme of the function modules corresponding to Fig. 5.7; *ECU* electronic control unit, *ICE* internal combustion engine

The two-stroke engine was designed with two horizontally opposed cylinders with a swept volume of 2×100 cm^3, weight of 8 kg (dry), and dimensions of $0.3 \times 0.3 \times 0.25$ m. The effective power achieved was 10 kW. Engine and tank were placed under the back seat. The weight, dimensions, and placement of this current generation unit did not disturb the configuration of the functions of the basic series vehicle. On the other hand, the vehicle autonomy was increased fivefold!

A compact car with motor propulsion is very comfortable to use in urban traffic, with very fast acceleration, without gear shifting. To complement this, current generation on board offers a sufficient operation range. A developed two-cylinder two-stroke engine with loop scavenging, such as described in Sect. 2.3.1, is shown in Fig. 5.9. The extremely reduced stroke-to-bore ratio of 0.655 is justified by the compact dimensions and by the mean piston velocity at such a high engine speed.

However, such a compact engine poses challenges for every direct injection technique:

- The duration of fuel injection, vaporization, and mixture formation with air must be extremely short, because of the shorter interval between scavenging and spark than in four-stroke engines.
- Control of the fuel spray orientation must be very accurate, because of the extremely compact combustion chamber and the pulsations of the air column at loop scavenging in two-stroke engines.

Continuous correlation of the injection rate modulation, injection start, and spark start is necessary. The main requirements for the injection system are described in Fig. 5.10.

As discussed in Sect. 2.2, there are two main techniques for direct injection:

- Injection of liquid fuel at high pressure (Figs. 2.49, 2.50, and 2.51)
- Injection of a fuel–air emulsion at relatively low pressure (Fig. 2.48)

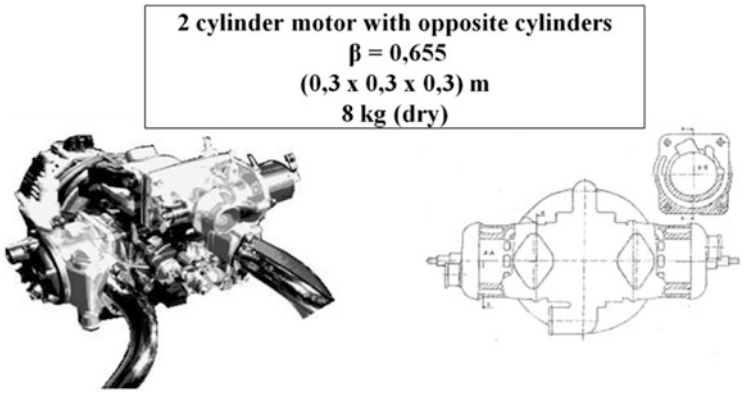

Fig. 5.9 Two-stroke two-cylinder engine with gasoline direct injection and integrated AC generator

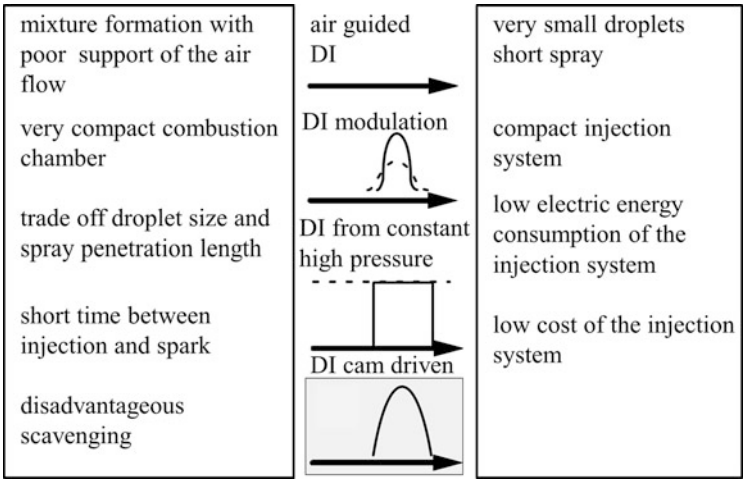

Fig. 5.10 Specific requirements of direct injection systems for compact two-stroke engines working as current generators for cars with hybrid electric propulsion

For a given application, the injection of liquid fuel in a simple and very compact two-stroke engine working as a current generator is less complex than injection of emulsion, which requires an air compressor, a mixing chamber, and an additional injector. On the other hand, a system for direct injection of liquid fuel with high pressure modulation is more advantageous than a common rail system, which requires more power than is available in such a compact engine.

A system with high-pressure modulation (Zwickau pressure pulse injection system) has been developed and adjusted for this application based on the following criteria:

– The spray length must be extremely reduced, because of the very compact combustion chamber.
– The high pressure module of the system, consisting of injector, electromagnetic valve, acceleration pipe, and wave damper should be integrated into a unit with very compact dimensions, as shown in Fig. 2.51.
– Electric power for actuation of the injection system must remain under 2 % of the effective engine power.
– The price of an engine incorporating the direct injection system should be extremely reduced, allowing its implementation in existing series vehicles with propulsion by motor and electric energy stored in a battery.

A benefit of the Zwickau pressure pulse direct injection system is that the high pressure course and, thereby, the injection rate modulation are not dependent on the engine speed. The system can be tuned for short fuel atomization, allowing fast vaporization and mixture formation. The injection system is shown in Fig. 5.11.

Acceleration of the fuel before impact is generated by the difference between the initial fuel pressure and the ambient pressure in a return pipe to the tank. The initial fuel pressure is produced in a module consisting of a low-pressure fuel pump, filter, and pressure control valve, the whole module being integrated in the tank. The initial pressure is fitted at values between 0.4–0.5 MPa. In the high-pressure module, the sudden closing of an electromagnetic valve at the end of the acceleration pipe provokes a high-pressure wave, with a peak that is 10–15 times higher than the initial pressure. The duration of this wave depends on the length of the acceleration pipe and the duration of closure of the electromagnetic valve, usually

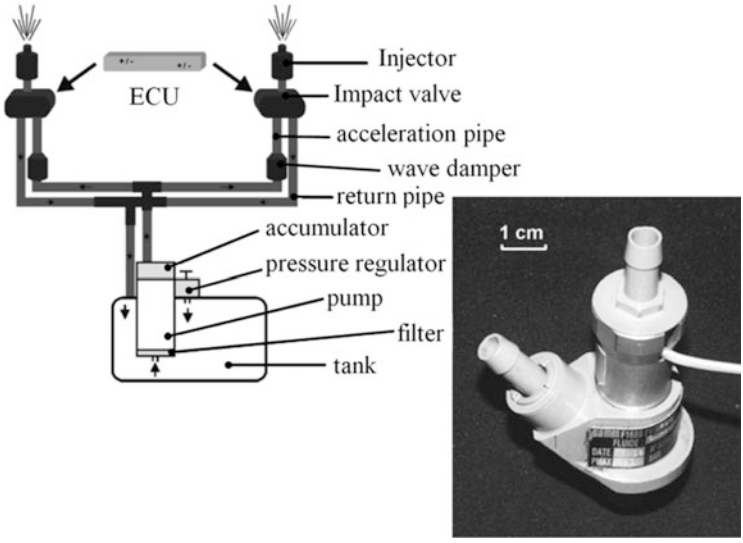

Fig. 5.11 Configuration of the direct injection system with high-pressure modulation (*left*) and view of the compact high-pressure module (*right*)

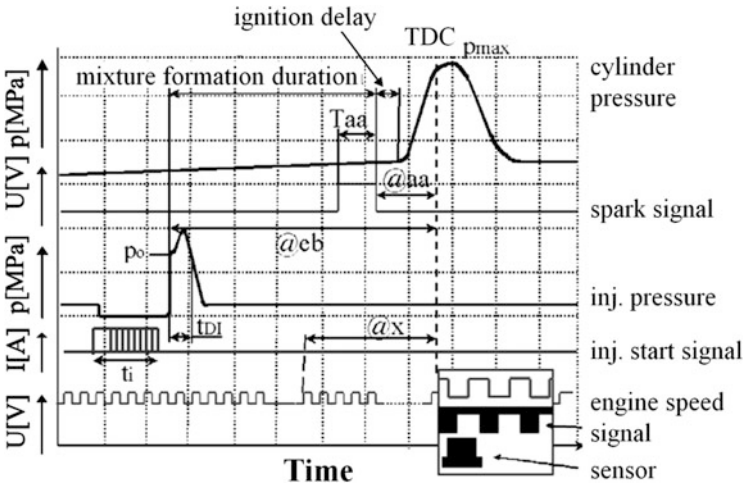

Fig. 5.12 Time-related history of injection and ignition delay in a direct injection system with high-pressure modulation

0.5–0.8 ms. This wave is available at the input of an injector, which is placed close to the electromagnetic valve. The injector consists of a needle with a spring and a body. By adjusting the spring, the opening pressure of the injector can be set to values required for this utilization (i.e., 1.8–2.5 MPa). The injected mass is controlled by the opening duration of the electromagnetic valve, which determines the velocity of the accelerated fuel before impact on the closing valve. The start of an injection event is the start of opening of the electromagnetic valve, which provokes fuel acceleration. This opening start is easily controllable by the current. The relationship is shown in Fig. 5.12.

The longer the opening duration of the electromagnetic valve, the higher the velocity of the accelerated fuel before impact and, thus, the higher the pressure peak, which determines the injected mass. After a duration that corresponds to the mixture formation time at the given load and speed, the spark is initiated by the same electronic control unit (ECU). The main functions of the ECU are illustrated in Fig. 5.13.

For better adjustment of the injection system to the engine at the lowest energy consumption, both the opening duration of the electromagnetic valve and the initial pressure can be varied and correlated with each other for every load and speed point. The measured injection volume for an injector opening pressure of 1.8 MPa at combined adjustment of the valve opening duration and initial pressure is shown in Fig. 5.14.

Internal mixture formation by direct injection was optimized by 3D simulation, combined with experimental analysis. Figure 5.15 shows an example of the simulated and measured events. The determined droplet velocity and size for every injection mass and engine speed, at different time sequences during injection, demonstrates that the engine speed has no influence on the spray characteristics.

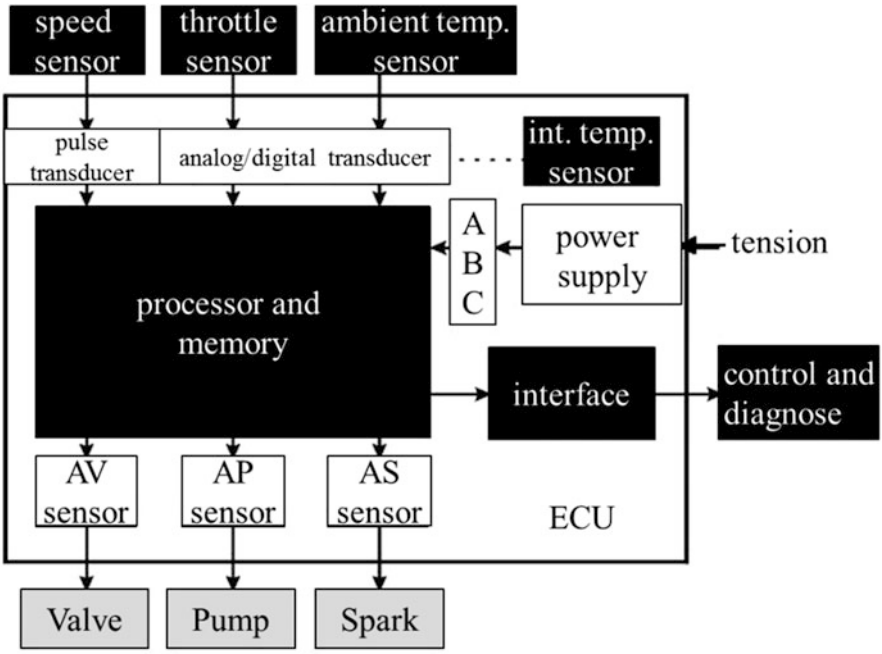

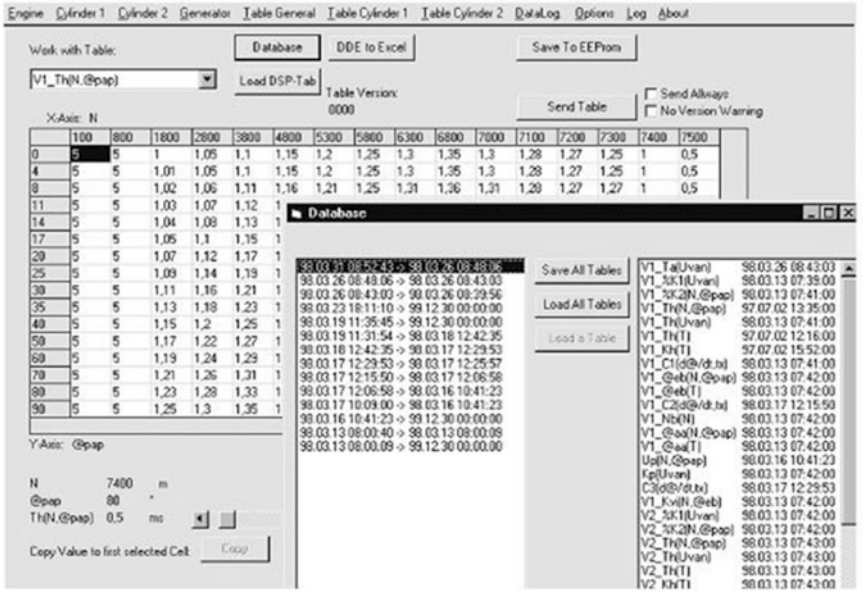

Fig. 5.13 Electronic control and data map for a direct injection system with high-pressure modulation

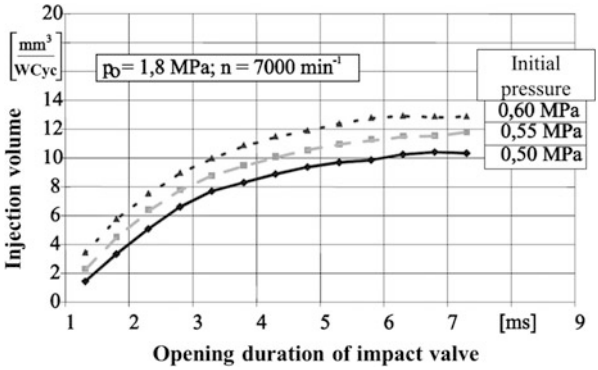

Fig. 5.14 Injection volume as a function of the opening duration of the impact valve and the initial pressure in a direct injection system with high-pressure modulation

On the other hand, variation of the injection mass has no influence on the droplet size. This is typical of the water hammer effect in the pressure pulse injection system: atomization of the fuel is mainly determined by the steep pressure rise and not by the pressure peak itself. This behavior is very favorable for mixture formation in an extremely short time in a compact combustion chamber. The combustion chamber design and the positions of the injector and spark plug have been optimized by 3D simulation and experiment and tested on the engine test bench. For each configuration, the injection and spark start and the injection rate modulation were analyzed. The compression ratio was also adjusted to obtain minimum pollutant emission. The compression ratio achieved a value of 12.13:1. A major problem was design of the exhaust pipes, which determines the scavenging of a two-stroke engine. The vehicle configuration did not permit placement of two exhaust pipes of identical length. The results of two different pipes in terms of torque and bsfc are illustrated in Fig. 5.16. To avoid such differences, the injection event in each cylinder was adjusted to obtain the same performance. The adjusted values were registered in separate function maps for electronic control of injection in each cylinder.

An additional potential of this type of direct injection is the variability of the global air/fuel ratio within the cylinder, resulting from mixture stratification. Thus, an excess of air (such as in diesel engines) is possible, improving the thermal efficiency. The effects of such operation without air throttling are shown in Fig. 5.17.

The global air/fuel ratio in the given operation range was 1.11–1.54, leading to torque that varied between 14.4 N m and 7 N m. The CO and HC emissions are also shown in Fig. 5.17, demonstrating an optimum at an air/fuel ratio of 1.26–1.4. This behavior is explainable by the difference between start of injection and start of spark, which corresponds to the duration of mixture formation. This is shown in Fig. 5.18 for the given range of torque and speed.

As can be deduced from Fig. 5.18, the duration of mixture formation mainly depends on the engine speed and almost not at all on the load. On the other hand, the speed does not influence the spray characteristics. A Citroen Saxo Dynavolt with

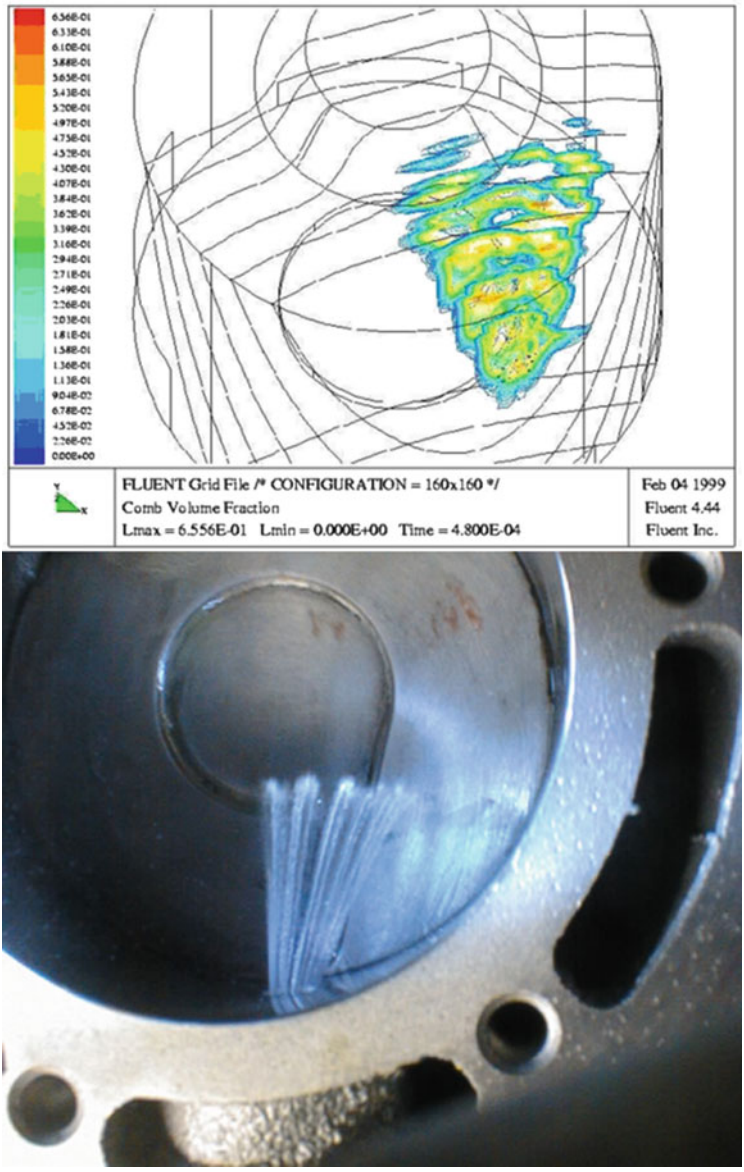

Fig. 5.15 Internal mixture formation within a compact two-stroke engine: simulated (*top*) and measured (*bottom*)

such configuration was tested in France on a route of 1100 km between Clermont-Ferrand and Paris, in different cycles and on different roads, including the circuit of Magny Cours [23]. The additional weight caused by the range extender (consisting of a two-stroke engine with a fuel tank of 15 l and the current generator) was

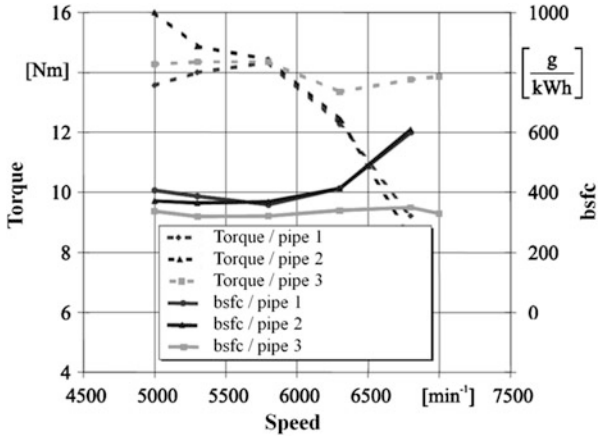

Fig. 5.16 Torque and bsfc as a function of engine speed at full load, for three different exhaust pipe designs

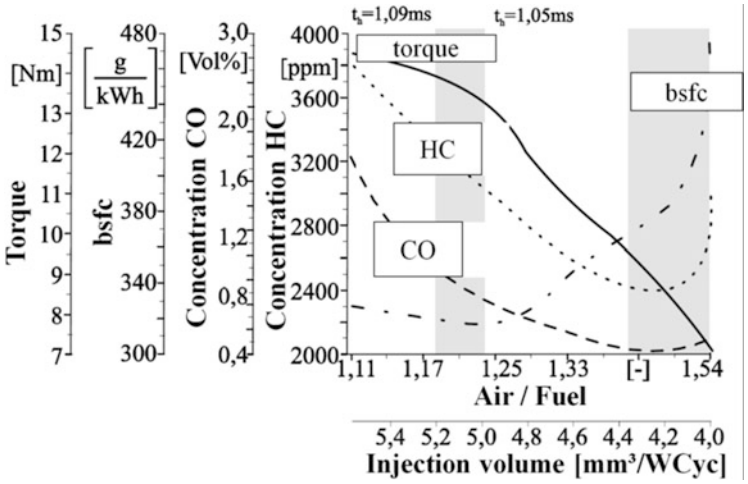

Fig. 5.17 Engine characteristics for unthrottled SI engine from full to part load

completely eliminated by changes to the car body, without endangering car safety. The car weight was 1050 kg, the maximum speed 110 km/h, and the operation range 340 km instead of 80 km for the same car with battery only.

The CO_2 emission was reduced to 60 g/km, which is a third of the emission of a Citroen Saxo with propulsion by SI engine. This emission corresponds to a fuel combustion of 2.4 l/100 km. These results demonstrate that a serial hybrid could be a very advantageous solution for compact cars in urban traffic. Many tests in the metropolitan area of Paris, confirmed by the author of this book, show that a motor

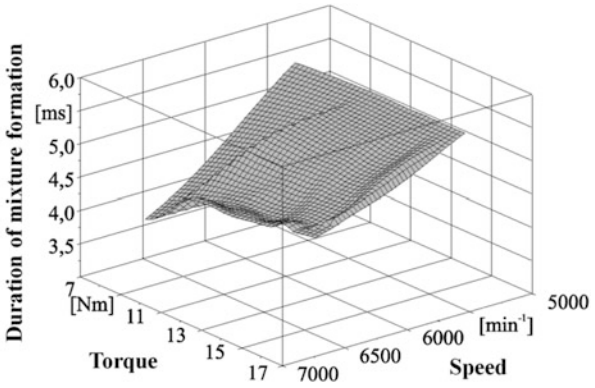

Fig. 5.18 Duration of mixture formation as a function of load and speed

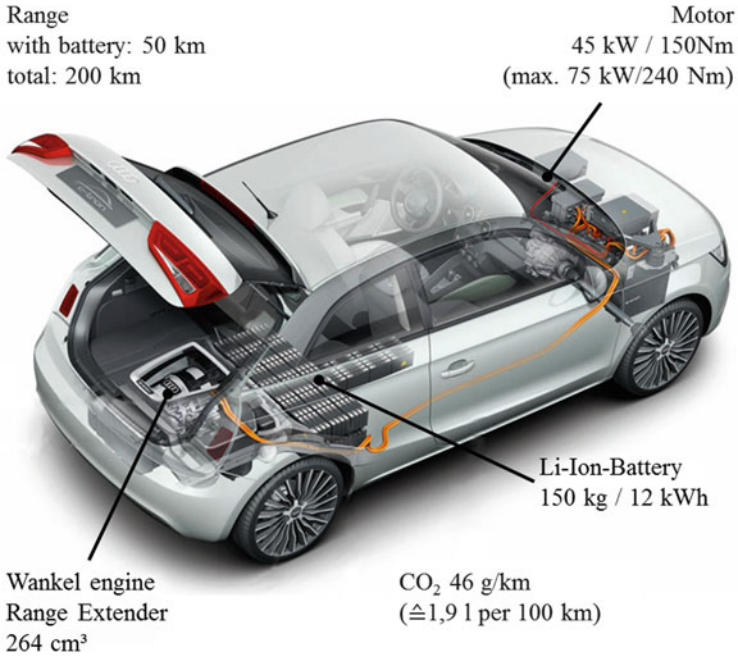

Fig. 5.19 Audi A1 e-tron with electric propulsion and range extension by means of a Wankel engine (Source: Audi)

power of 20 kW is sufficient for speedy accordance with very dynamic traffic. The utilization of a simple two-stroke engine with direct fuel injection contributes to the reduction in cost, size, and weight, achieving the imposed limits on fuel combustion and pollutant emissions.

Stirling and Wankel engines used as current generators have a similar potential. Figure 5.19 shows a recently developed configuration using a Wankel engine. The

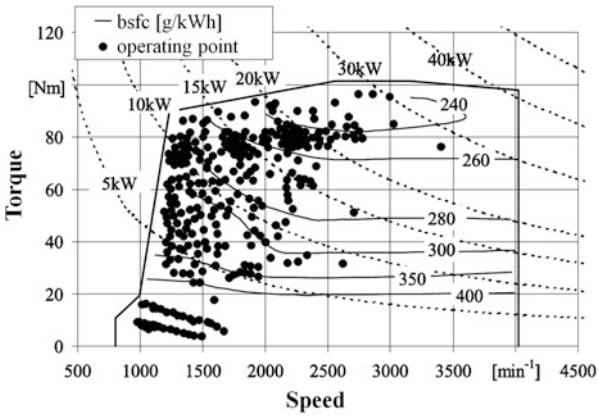

Fig. 5.20 Torque–speed maps for Toyota Prius operating on country roads

propulsion motor has a power of 45 kW and a maximum torque of 240 N m. A Wankel engine of 264 cm^3 has, in the role as range extender, a gasoline combustion of 1.9 l/100 km. The system is completed by a battery with a capacity of 12 kW h. The autonomy is given at 200 km.

The probability of operating load/speed combinations in the most frequent cruising situations (urban traffic, country, and motorway) is a convincing argument for the utilization of serial hybrids in compact cars. Such probabilities, as a result of long-term studies by Toyota, are shown in Figs. 5.20, 5.21, and 5.22. The most frequent operation points are represented in torque versus speed maps, which also contain the curves for constant bsfc of the given Toyota engine. Hyperbolae are also shown for constant power values, which are independent of the given engine, being obtained from the product of torque and speed values on the axles ($P = M \times 2\pi n$, where P is power, M is torque, and n is engine speed).

The differences between the driving situations in urban areas and in the country are mainly expressed by the engine speed, calculated from the given vehicle speed in these situations. Therefore, at comparable torque levels, the power requirement in urban traffic is considerably lower than for country driving. The differences between driving in normal city traffic and congested city traffic are more significant:

- On country roads, the torque is relatively high and the speed range is broad, as shown in Fig. 5.20. The most frequent power range is 10–25 kW h.
- In city traffic, the power becomes lower, as shown in Fig. 5.21.
- In congested city driving, which is characteristic for New York and most of the cities in Europe, Central and South America, China, and India, the torque/speed range is very restricted, as shown in Fig. 5.22. A power of 5–10 kW at speeds of 1000–1500 min^{-1} is realizable with normal motors at the required torque with high efficiency. In such a field of operation, common automobile piston engines have the lowest efficiency, demonstrated by the highest bsfc (as illustrated in Fig. 5.22).

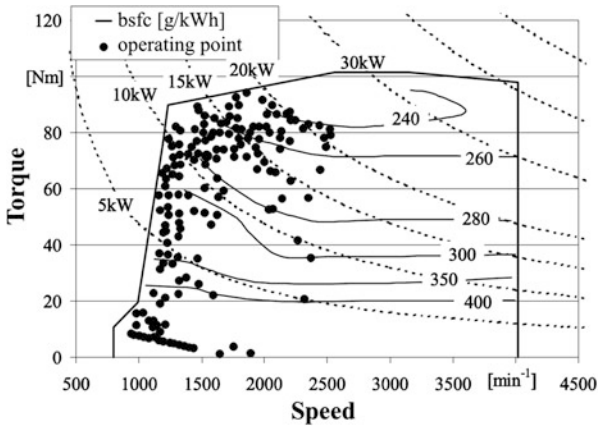

Fig. 5.21 Torque–speed maps for Toyota Prius operating in the city

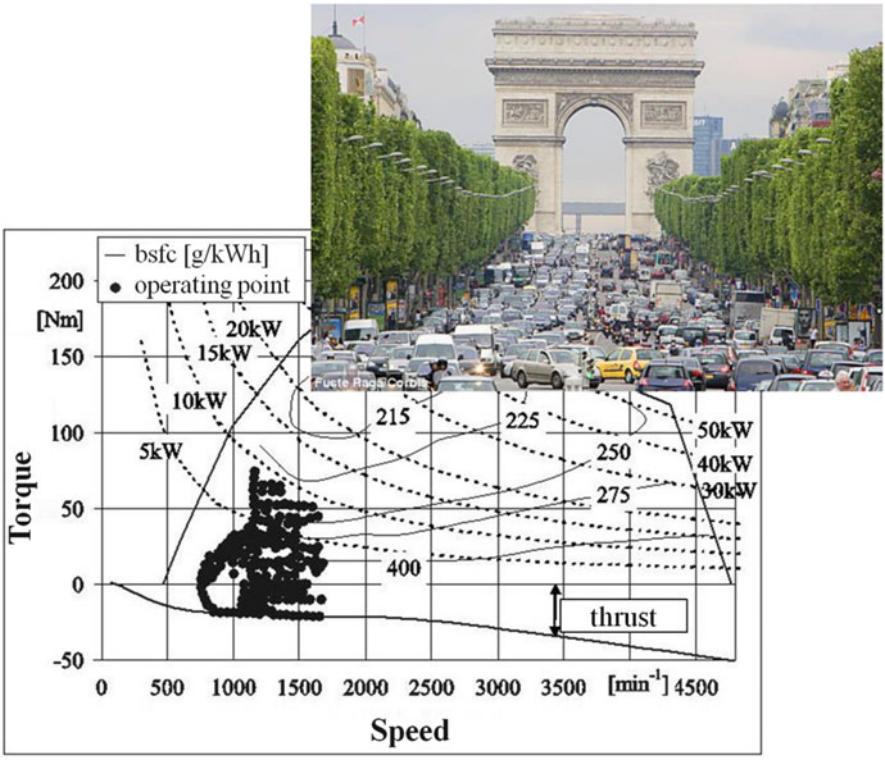

Fig. 5.22 Torque–speed maps for Toyota Prius operating in congested city traffic

Compact, middle and upper classes of automobiles should be adapted for the most probable utilization in a given traffic situation, and have the most appropriate form of propulsion system.

About 80 % of the population of Europe, as an example, lives in urban areas. Some 50 % of their inhabitants drive in their own car less than 5 km per day. More interesting is the fact that 80 % of the inhabitants of European cities drive less than 50 km per day. For such utilization, a compact car with an acceleration profile that corresponds to the most frequent city driving cycle is the best alternative. Moreover, such a car should have zero emission of CO_2, pollutants, and noise in the city centers. Thus, propulsion by motor seems to be the best form under such conditions. Out of the city center, electric energy for the motor can be produced on board in fuel cells or in thermal engines at steady operation (gas turbines, Stirling engines, Wankel, or two-stroke engines) as discussed in Sect. 2.3, the energy being stored in batteries. However, fuel cells are more complex than thermal engines, necessitating more room on board; last but not least they are much more expensive than simple engines for current generation.

An optimum balance between the power of the generator module, power of the propulsion motor, battery capacity, and the achievable range can be deduced from the imposed price, weight, and dimensions of the car. This relationship is illustrated in Fig. 5.23.

For a compact car, a serial hybrid with motor for propulsion and engine for current generation, as shown in Fig. 5.24, is more advantageous than a parallel hybrid. Variable power addition from motor and engine, the latter also having the role of current generator, is more efficient for the middle class of cars.

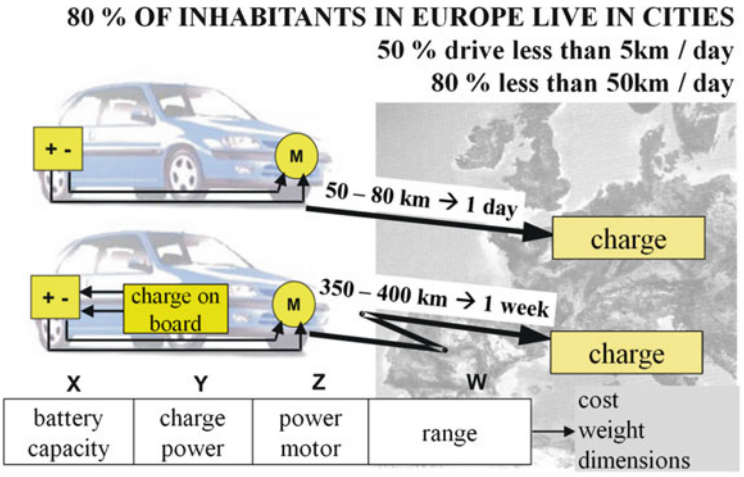

Fig. 5.23 Parameter optimization of a serial hybrid system for compact city cars

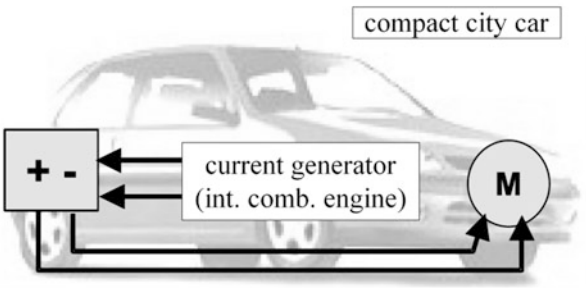

Fig. 5.24 The city car of the future: development options

5.3 Propulsion by Internal Combustion and/or Motor: Parallel and Mixed Hybrids

5.3.1 Hybrid Classes

The involvement of engines and motors for propulsion has been tested in numerous configurations. The common classifications of such hybrid configurations are made on the basis of the relative or absolute electric power part of the entire propulsion.

$$Hr = \frac{motor\ \ power}{motor\ \ power + engine\ \ power} \cdot 100\%$$

Consideration of the absolute form (P_{EM}) is more frequent, because of its simplicity. On this basis, parallel and mixed hybrids can be classified into the following categories:

Micro-Hybrids: $P_{EM} < 6$ kW

In such a configuration, a motor is not provided for direct propulsion but only for engine start at a power demand by the driver and for engine stop after a given idle period (start/stop function). Such motors, generally, operate at 12 V. The price of this additional start/stop function is between €300 and €800. The advantage of this solution is a reduction in fuel consumption of 3–6 %

Mild Hybrids: $P_{EM} = (6–20)$ kW

Such motors not only provide a start/stop function, but are also involved in propulsion during acceleration. On the other hand, the motor serves as a generator for the recuperation of braking energy, which is transformed into electric energy and stored in the battery. Such motors operate with a tension of 42 V or 144 V. This form of completion of the propulsion system costs between 1000 and €2000 . The potential decrease in combustion is 10–20 %.

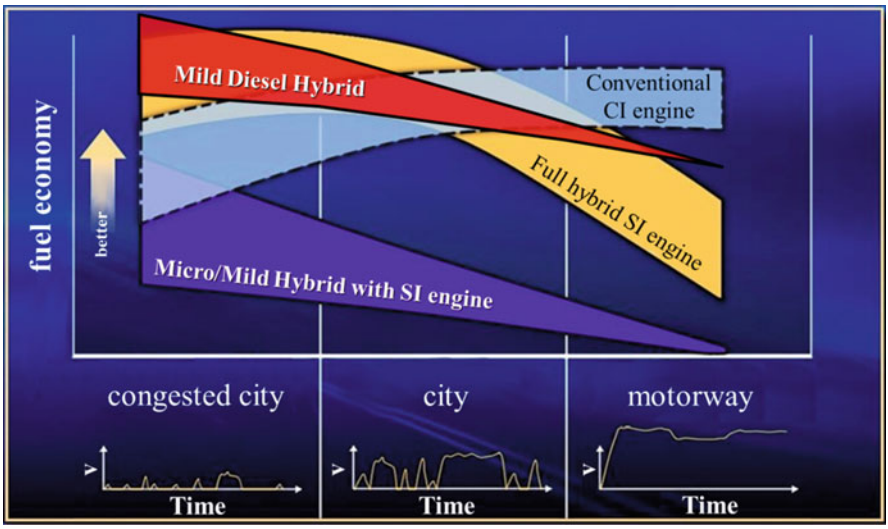

Fig. 5.25 Influence of driving cycle on fuel economy when using micro-, mild and full hybrids, in comparison with a conventional diesel engine

Full Hybrids: $P_{EM} > 40$ kW

In this category there are two application concepts:

- With only one motor, which ensures propulsion together with the internal combustion engine (the classic form of a parallel hybrid).
- With more than one motor in addition to the internal combustion engine (a "power split" or mixed hybrid). In some situations, one of the motors can ensure vehicle propulsion by itself, with the engine decoupled.

The voltage in such configurations is 250 V. The additional price of such a solution, compared with an engine only, is in the range of €4000–€8000, depending on the features. The potential decrease in fuel consumption is 30–40 %. However, the reduction in fuel consumption when using micro-, mild or full hybrids is strongly dependent on the driving cycle. Figure 5.25 [25] illustrates this relationship.

As shown in Fig. 5.25, micro- and mild hybrids are very advantageous for urban driving but their efficiency is impaired on country roads, and especially on motorways. Full hybrids are very efficient in urban traffic, being more advantageous than the other hybrid forms and propulsion by diesel engine. However, in urban traffic, the differences between the cycles in the USA, Europe, and Japan should be taken into account. On country roads, a full hybrid has practically no advantages in comparison with a diesel engine. On motorways, the diesel engine is clearly the best alternative.

	1989 Audi 100 duo	1991 Audi 100 duo	1997 Audi A4 duo
Piston engine	2,3 l 5 Cylinder	2,0 l 4 Cylinder	1,9l 4 Cylinder TDI
	100 kW	not specified	66 kW
	Propulsion front	Propulsion front + rear	Propulsion front
Motor	AC	AC	AC
	9 kW	21 kW	21 kW
	Propulsion rear	Propulsion rear	Propulsion front
Battery	Ni-Cd	Ni-Cd	Lead-acid

Fig. 5.26 Full hybrid variants from Audi (Source: Audi)

There are many configurations and solutions for full hybrid propulsion systems. The variety of brands and the number of configurations are remarkable. Audi is the true worldwide pioneer of the full hybrid technique, developing three basic variants between 1989 and 1997, as shown in Fig. 5.26 and described below:

- The first variant (1989) involved propulsion of the front axle, using a five-cylinder piston engine of 100 kW, combined with propulsion of the rear axle with a low power motor of 9 kW.
- The second variant (1991) used four-wheel propulsion by a piston engine, combined with additional electric propulsion of the rear axle.
- The third variant (1997) combined propulsion of the front axle by a diesel engine of 66 kW and a motor of 21 kW. To reduce the price, the nickel-cadmium battery utilized in the first two variants was replaced by a common lead-acid battery. This third propulsion variant (Audi A4 duo) was introduced in series applications in 1997 and was produced for some months. However, the limited advantages in comparison with propulsion by a diesel engine alone, at a much higher price, stopped the series production of this system.

5.3.2 Parallel Full Hybrid with One Piston Engine and One Motor, Interconnected by Means of a Planetary Gear: Toyota Prius, Honda Insight

The Toyota Prius was introduced in series production in 1997, a short time after the interruption of production of the Audi A4 duo, but with an essential difference: a gasoline engine instead of a diesel engine. After introduction in Japan, this car was launched in 2000 onto the USA and European markets. The engine is coupled by a planetary gear to a synchronous motor and to a generator. The main function modules are shown in Fig. 5.27. The braking energy is recuperated and stored as electric energy.

The configuration of the function modules is shown in Fig. 5.28. The module for power addition for propulsion and for power supply of the current generator plays a central role. This module consists of a planetary gear, as shown in Fig. 5.29. The functions are optimized according to an energy management program, as illustrated by the following examples:

- *Start and low–middle load/speed*: Propulsion is ensured by the motor to avoid the low efficiency domains of the SI engine.
- *Middle load/speed:* Propulsion is generated by both motor and engine, with part of the total power being directed to the current generator, which splits the produced current between battery and motor. In this mode, the engine works most of the time at a relatively high load and high efficiency.
- *Strong acceleration*: Both engine and motor work at high load; the generator mode is not functioning, with current coming only from the battery.

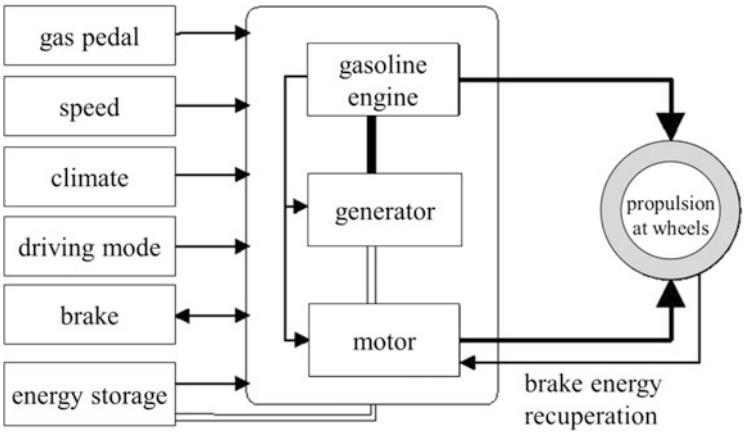

Fig. 5.27 Function modules of the parallel hybrid propulsion system (gasoline engine plus motor) in a Toyota Prius (Source: Toyota)

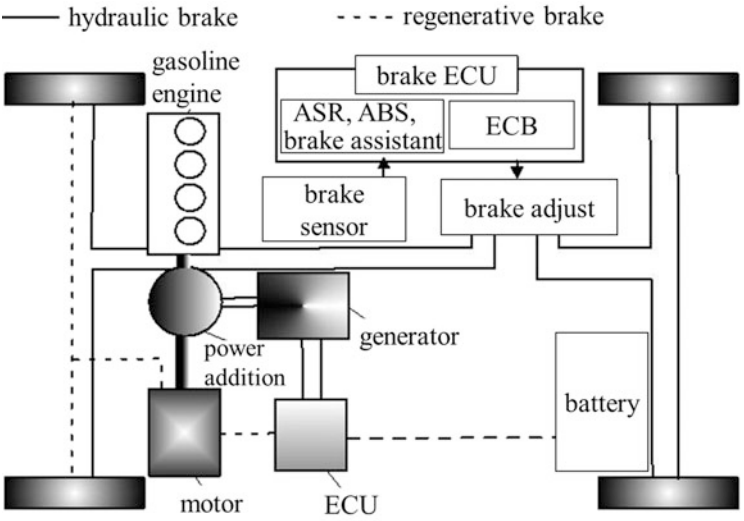

Fig. 5.28 Configuration of the function modules of the parallel hybrid propulsion system (gasoline engine plus motor) on board a Toyota Prius, 2nd generation (Source: Toyota)

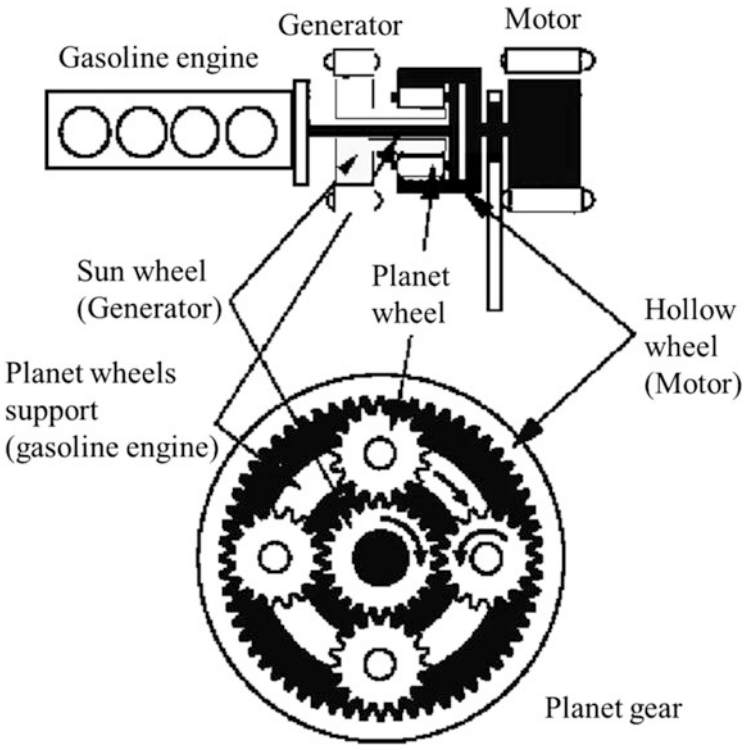

Fig. 5.29 Planet gear for power addition in a parallel hybrid propulsion system (gasoline engine plus motor) (Source: Toyota)

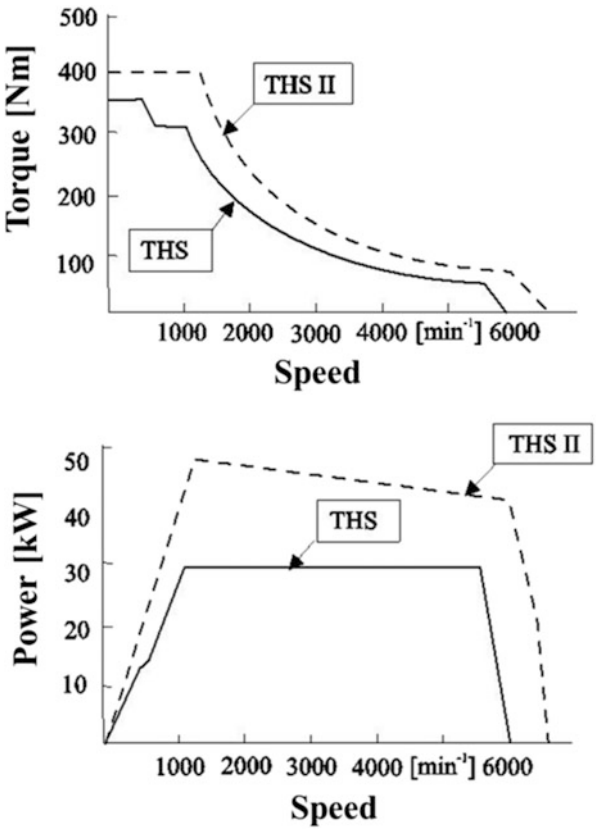

Fig. 5.30 Torque and power characteristics of the motor in the hybrid propulsion system (gasoline engine plus motor) of the Toyota Prius, 1st and 2nd generation; *THS* Toyota hybrid system (Source: Toyota)

- *Braking*: The motor works as a current generator, being powered by the moving wheels. The produced current power is stored in the battery.

The propulsion motor is of synchronous type, having permanent magnets in a V form for the improvement of torque and power. The difference between the performances of motors of the first and second generation of Toyota Prius full hybrid cars is demonstrated by the curves for torque and power in Fig. 5.30. Figure 5.31 shows a cross-section and Fig. 5.32 a part section through the complete hybrid system. Table 5.1 shows the main characteristics of the three generations of Toyota Prius to date.

Figure 5.33 shows the configuration of the propulsion system in the newest form of Toyota Prius. In additional to the values given in Table 5.1, the following performances of this type are notable:

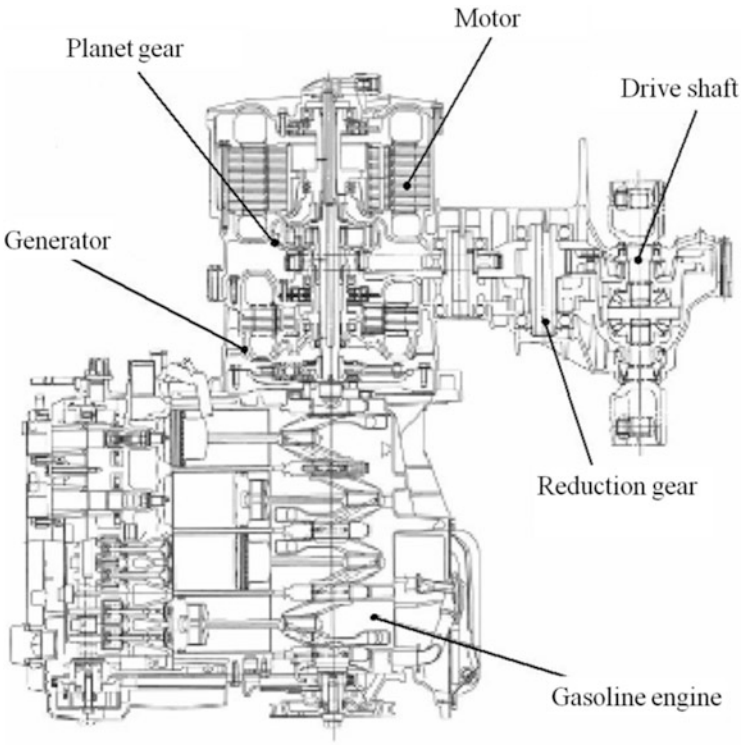

Fig. 5.31 Cross-section through the hybrid propulsion system (gasoline engine and motor) in a Toyota Prius, 2nd generation (Source: Toyota)

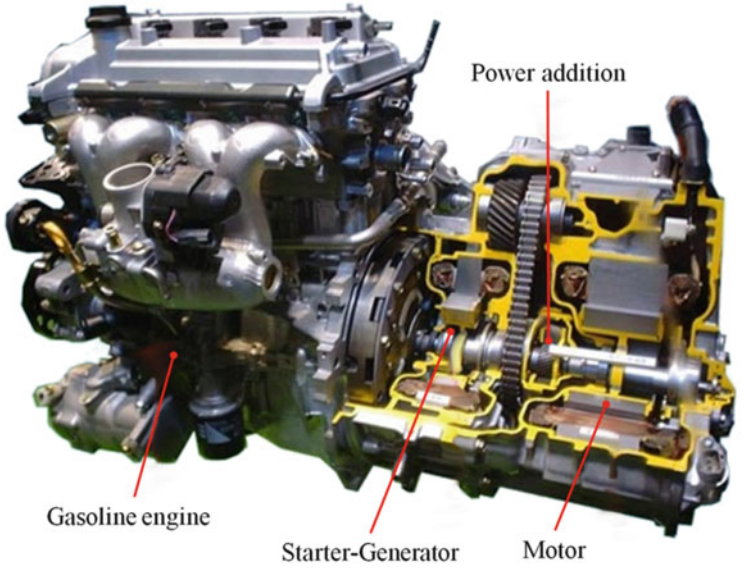

Fig. 5.32 Partial section through the hybrid propulsion system (gasoline engine plus motor) of a Toyota Prius, 2nd generation (Source: Toyota)

Table 5.1 Dynamics of development of Toyota Prius

		1st generation	2nd generation	3rd generation
Year of production	–	1997–1999	2000–2003	2004–
Power, engine	[kW]	43	52	73
Max. torque, engine	[N m]	4000	4500	5000
Power, motor	[kW]	30	33	60
Max. speed, motor	[min^{-1}]	225	258	255
0–96 km/h (60 mph)	[s]	14.1	12.5	10.1
Battery energy	[W/kg]	600	900	1250
Battery weight	[kg]	57	52	45
System tension	[V]	288	273.6	500

Fig. 5.33 Toyota Prius HSD (Hybrid Synergy Drive)

– Total maximum power: 100 kW at 5200 min^{-1}
– Maximum vehicle speed: 180 km/h
– Gasoline consumption: 3.8–4.4 l/100 km (combined city and country)

Another form of combining the powers of engine and motor within a hybrid system was conceived for the Honda Insight. The curves for torque and power are illustrated in Fig. 5.34. The gasoline engine works in this case over the whole

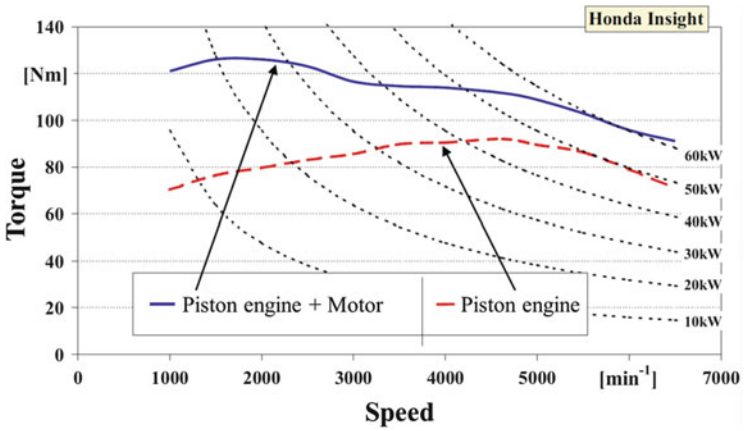

Fig. 5.34 Addition of torque of engine and motor in a parallel hybrid

operation range, up to the maximum power. The power of the motor is provided as an addition to the maximum engine power. This function is beneficial, especially at low engine speed, ensuring more torque at acceleration from standing.

5.3.3 Parallel Full Hybrid with One Piston Engine and One Motor, Coupled by a Planetary Gear, with an Additional, Separate Propulsion Motor: Lexus RX400 h

For powerful sport utility vehicles (SUVs), especially for the US market, the solution described in Sect. 5.3.2 was completed with a motor on the rear axle. Between the front and the rear axle there is no torque transmission in any way. The V6 engine on the front axle has a power of 183 kW at a swept volume of 3.5 dm^3 and is coupled by a planetary gear to a synchronous motor of 123 kW and with a generator. The rear motor has a power of 50 kW. The main modules for their configuration on board are shown in Fig. 5.35. The propulsion scenario was developed for very dynamic driving.

When accelerating from standing, first the rear motor is activated, then the front motor, and then (if still accelerating) the engine. When the load decreases, the power modules are decoupled in inverted succession, engine, then front motor. The acceleration from standing to 100 km/h occurs in 7.8 s, for moving a vehicle mass of 2185 kg. The gasoline consumption is 6.3 l/100 km. The main data are summarized in Fig. 5.36.

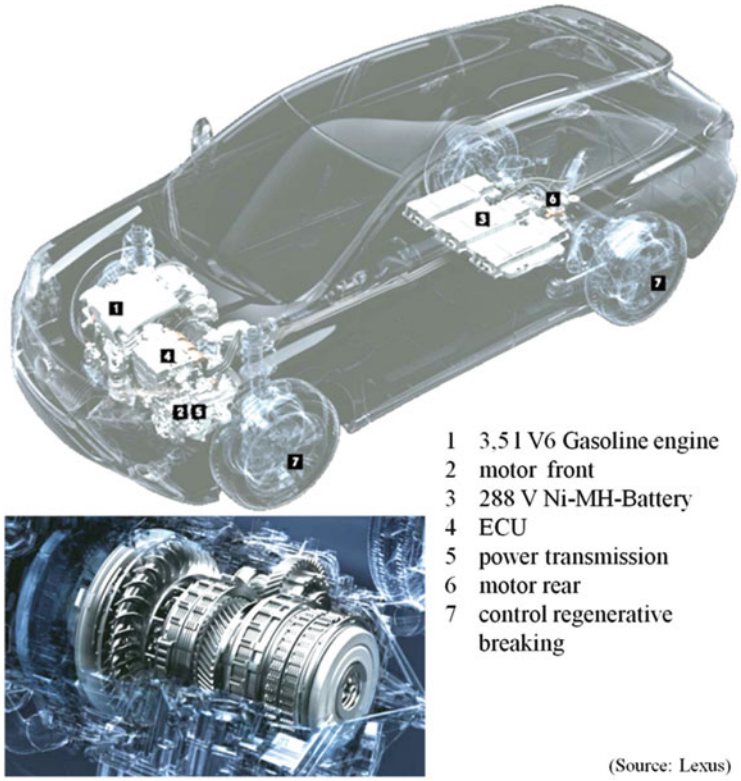

Fig. 5.35 Configuration of main modules in an automobile with parallel and full hybrid propulsion system and, additional, separate motor propulsion

Type	Lexus RX 450h
Hybrid type	Full
Mass	2185 kg
Engine	3,5 l V6
	183 kW, 317 Nm
motor front	123 kW, 335 Nm
motor rear	50 kW, 139 Nm
fuel consumption	6,3 l / 100 km
CO_2 emission	145 g / km
0-100 km/h	7,8 s
price	59950 €

Fig. 5.36 Characteristics of an automobile with hybrid propulsion corresponding to Fig. 5.35 (Source: Lexus)

5.3.4 Full Hybrid with One Piston Engine and One Motor along a Propulsion Axle: Porsche

The Porsche Panamera S Hybrid is provided with a propulsion system consisting of one engine and one motor, coupled along the same rotation axle by a clutch. This configuration is represented in Fig. 5.37. Figure 5.38 shows the hybrid module with the motor and the clutch.

Fig. 5.37 Porsche Panamera S Hybrid (Source: Porsche)

Fig. 5.38 Hybrid module with motor and clutch (Source: Porsche)

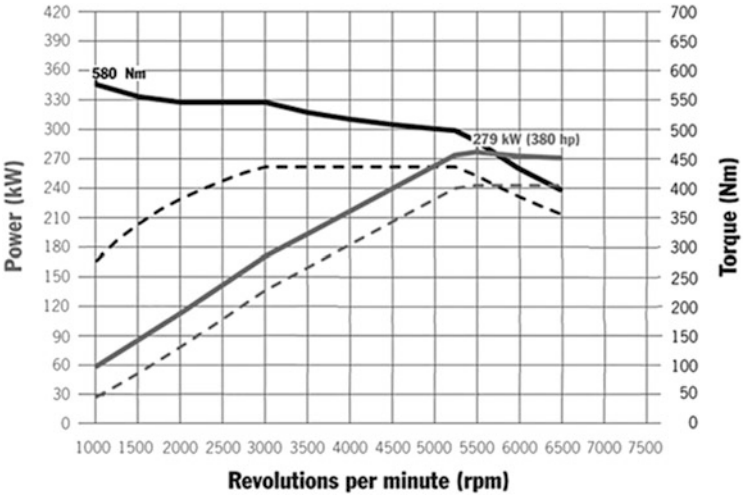

Fig. 5.39 Power and torque curves of a Porsche Cayenne S Hybrid

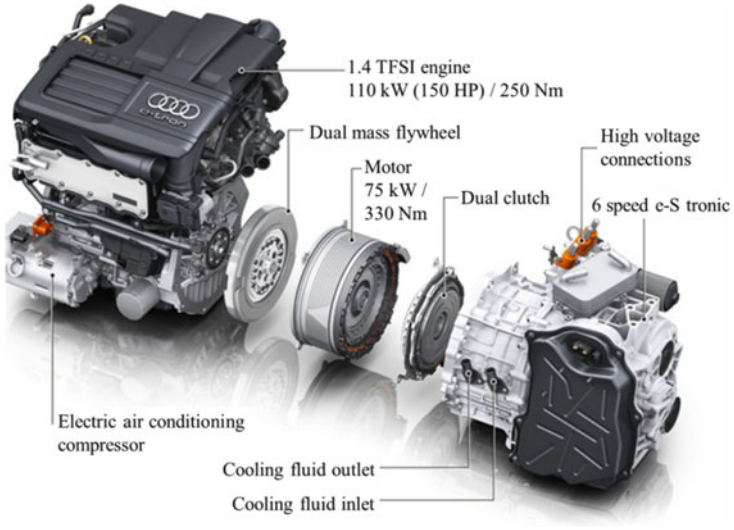

Fig. 5.40 Audi A3 e-tron (Source: Audi)

As illustrated in Fig. 5.39, the motor is mainly responsible for increasing the total torque of the propulsion system, especially at low speed. For the acceleration of a heavy automobile such as the Porsche Cayenne with 2240 kg or the Porsche Panamera with 1980 kg, especially in urban traffic conditions, this behavior becomes very advantageous, as demonstrated by the fuel consumptions of 8.7 l/100 km for the Cayenne and 7.6 l/100 km for the Panamera. Figures 5.40, 5.41, and

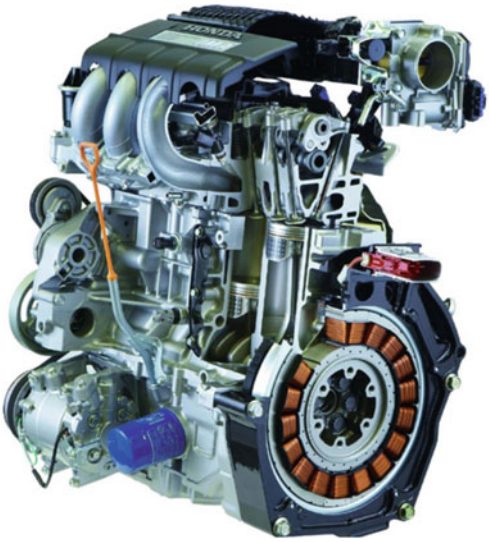

Fig. 5.41 Hybrid propulsion system of Honda (Source: Honda)

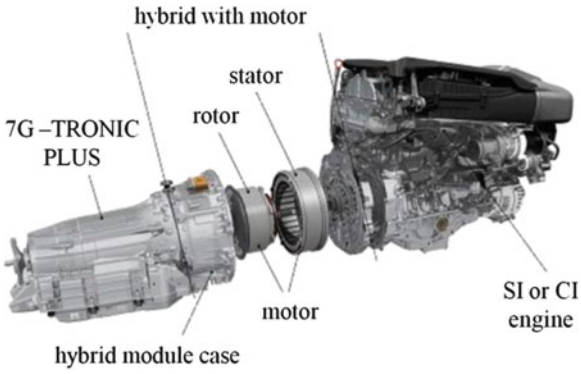

Fig. 5.42 E-300 Blue Tec Hybrid (Source: Daimler)

5.42 show examples of similar configurations of the propulsion system, developed by Audi, Honda, and Daimler, respectively.

5.3.5 Full Hybrid with One Piston Engine and Two Motors along a Propulsion Axle: Daimler

A different concept for high power has been developed by Daimler based on an eight-cylinder CDI diesel engine with a maximum power of 191 kW and maximum torque of 560 N m, coupled to two motors with a total power of 50 kW. This configuration is shown in Fig. 5.43.

The system includes a nickel-metal hydride battery with a capacity of 1.9 kW h. The acceleration is well supported by the motors; the engine start is actuated by

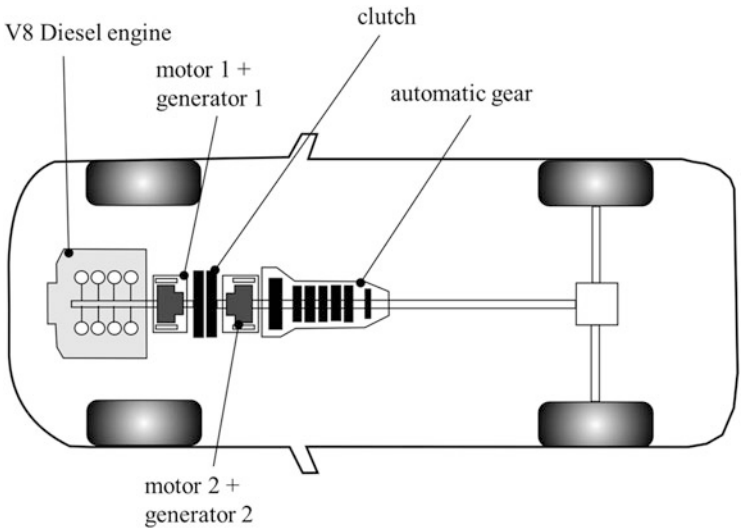

Fig. 5.43 Parallel hybrid propulsion system (diesel and motor) for high power Daimler (Source: Daimler)

motor 2, as illustrated in Fig. 5.43. During driving, the battery is charged by means of the engine power. Additional electric energy is generated by braking. The propulsion power is transmitted by a seven-stage automatic gear. In this configuration, the fuel consumption can be decreased by 15–25 %, depending on the given driving cycle, achieving an average of 7 l/100 km. The acceleration from standing to 100 km/h is 7.6 s.

General Motors is developing a hybrid system for delivering higher power, especially for SUVs with four-wheel drive [22]. Four configurations have been found very advantageous. One configuration is based on an eight-cylinder gasoline engine with a maximum power of 203 kW and maximum torque of 427 N m. Additionally, the system is provided with two motors of 72.33 kW and 271 N m. The vehicle has a weight of 2751 kg. Simulation results show a possible decrease in fuel consumption of between 19 % and 26 % in comparison with the series vehicle equipped only with the gasoline engine.

5.3.6 Full Hybrid with Motors Within the Gear of the Piston Engine (Two-Mode Hybrid): BMW, Daimler, GM

This full hybrid configuration is centered on optimization of total efficiency for every driving situation (urban cycle, stop-and-go, country road, motorway) by adequate coupling of engine and motors. Basically, propulsion is possible only by motor, only by engine, or by coupling all these propulsion modules [26]. The concept is based on an electrically assisted variable transmission (EVT), which is

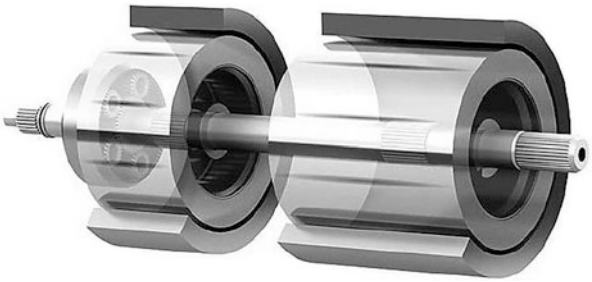

Fig. 5.44 Main components of the electrically supported, continuously variable gear with one power split (one-mode EVT)

similar to continuously variable transmission (CVT). A remarkable additional function of EVT in comparison with CVT is continuous regenerative braking, using the kinetic energy of the decelerating vehicle for generation of electric energy, which is then stored in the battery. Using conventional gears with electrically assisted, continuously variable ratio, an important part of the engine power is transmitted through the electric branch. At high vehicle speed (on country roads or motorways), this becomes a major disadvantage, because of the rapid decrease in torque at motor speeds over about 2200 min^{-1}. The advantages of a two-mode hybrid are derived from the development of automatic gears and one-mode hybrids with EVT. An automatic gear with six or seven stages has a torque converter with coupling by more than one planetary gear and with hydraulic coupling elements. There are many gear ratios, which can be varied. For a continuously variable gear ratio, variation can be accomplished by motors, as for example in EVT. The main components of such a system are shown in Fig. 5.44. Similar solutions were developed in the USA in the 1920s.

The main components of a series gear of this type are a planetary wheel set and two motors. There are no clutches. The engine power is guided to the planetary wheel set and distributed to electric and mechanical branches. One of the motors plays the role of a generator, the current being led to the second motor (for propulsion) or to the battery. This configuration is shown in Fig. 5.45.

The ratio between the electric and mechanical power flows is crucial because the efficiency of the electric branch (approximately 70 %) is lower than the mechanical branch (approximately 90 %). The electric power flow depends on the engine speed, gear ratio within the planetary gear, and vehicle speed. In the case of a one-mode EVT, the electric power flow is high, requiring large motors. Hence, the total power of the motors is generally higher than the engine power, reducing general efficiency, increasing costs, and causing an increase in dimensions. A disadvantageous power ratio between the mechanical and the electric power flows is caused by the fixed gear ratio for the transmission of engine power to the wheels. At this gear ratio (often named the "mechanical point"), the speed of the first motor is zero. At all

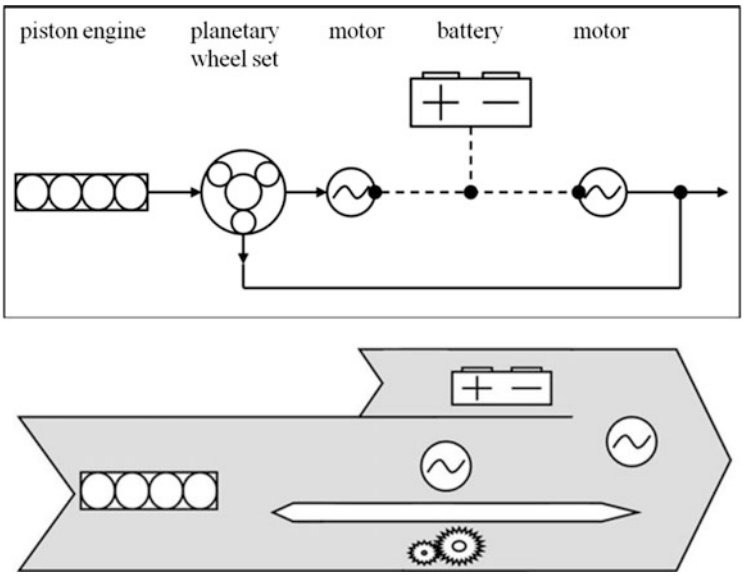

Fig. 5.45 Energy flow in one-mode EVT

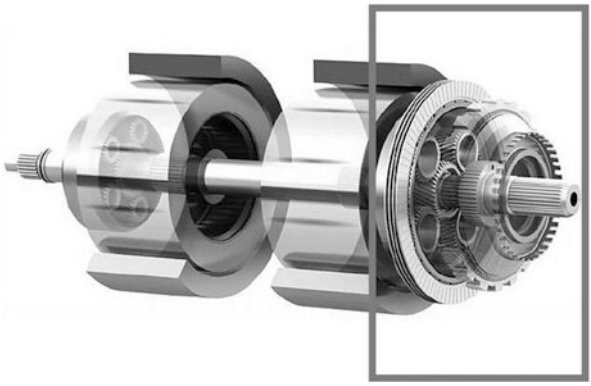

Fig. 5.46 Main components of the electrically supported, continuously variable gear with two-stage gear

other gear ratios, the electric power flow is higher and the efficiency is lower, especially at high load and speed. Therefore, a one-mode EVT is more recommended for compact cars. To reduce the size of the motors, at least a second gear ratio is required. A solution is the one-mode hybrid with a two-stage gear. As shown in Fig. 5.46, the propulsion motor at gear exit is provided with a two-stage gear, but this requires an additional clutch and also an additional gear set.

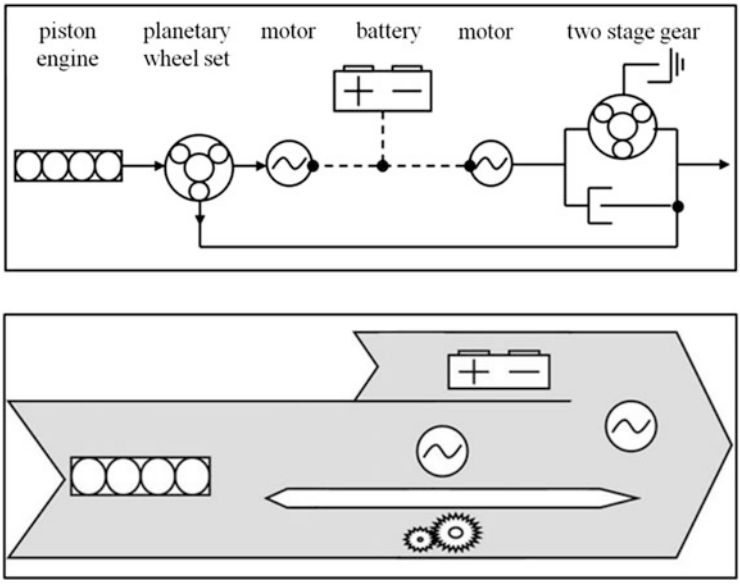

Fig. 5.47 Energy flow in one-mode hybrid with two-stage gear

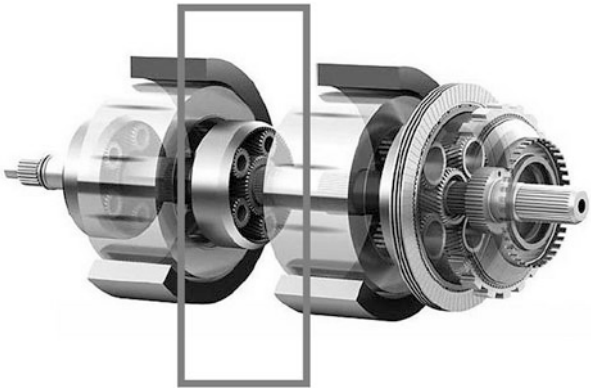

Fig. 5.48 Main components of a two-mode hybrid system

The function of the one-mode hybrid is not modified by this measure, there remains only one gear ratio between engine and gear exit. However, the maximum power and torque of the motor can be reduced. The switch in the two-stage gear is generally activated close to the mechanical point. The motor speed changes very abruptly at gear switching. The principle is shown in Fig. 5.47.

The described disadvantages regarding the electric and mechanical power flows can be avoided by completing the system with an additional planetary wheel set. In this mode, a two-branched EVT is formed. The main components are shown in Fig. 5.48.

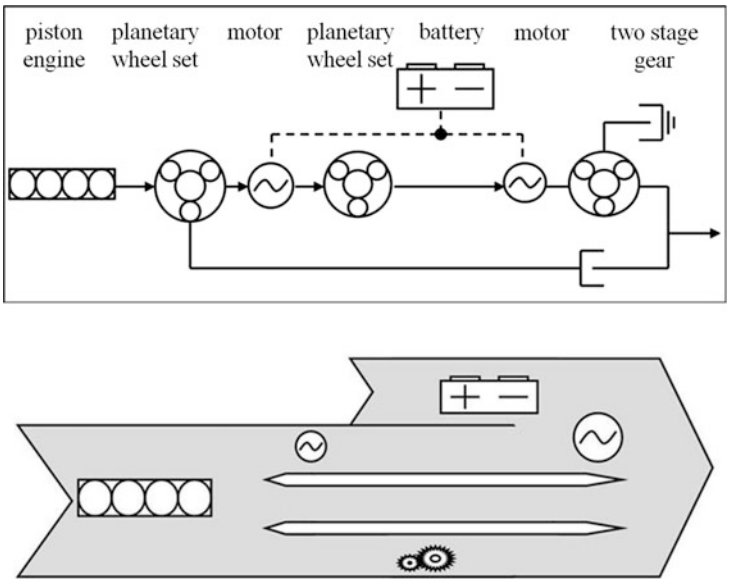

Fig. 5.49 Energy flow in a two-mode hybrid system

Using two clutches within the system, the energy flow is changed, improving the efficiency of the motor, especially at low speed. The flow scheme is illustrated in Fig. 5.49. The electric energy flow can be considerably reduced in this mode, in comparison with a one-mode EVT. This leads to net advantages regarding total efficiency, dimensions of the motor, and cost of the system.

The combination of two power-split modes allows a broad range of gear ratios at a relatively low motor power. The three resulting mechanical points can be utilized in different modes: the first for increasing the acceleration capability, and the others for maintaining the efficiency at a high level on country roads and motorways. An extension of the two-mode hybrid system consists of a gear module with four stages with fixed gear ratios, which allow parallel function. The motors are activated during acceleration and deceleration or braking. This parallel function can be connected by two additional clutches. The main components of this system are shown in Fig. 5.50.

When the system is operated, for example, in the fourth fixed gear, at high speed, as a parallel system, one of the motors can be decoupled. The second motor serves as a current generator for the electric energy consumers on board. Switching to other fixed gears couples or decouples the two motors, which can be done to obtain the lowest energy consumption. In first and third gear, both motors operate up to maximum power, whereas in second gear only one motor is working.

This configuration permits six modes of operation:

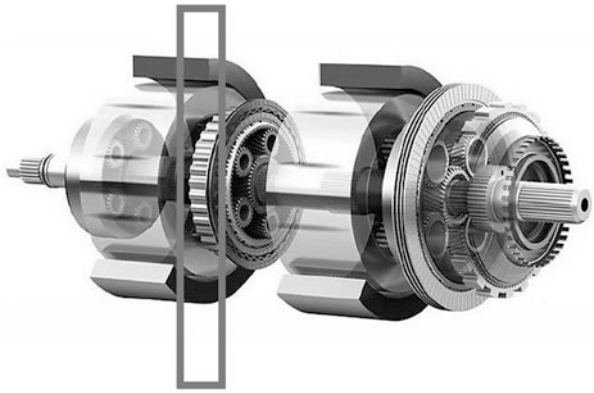

Fig. 5.50 Main components of a two-mode hybrid system with two EVT ranges and four gear stages with fixed transmission ratio

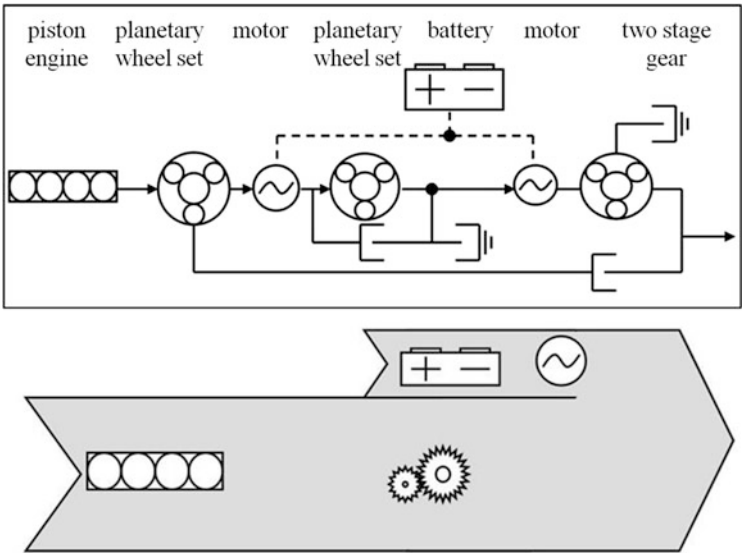

Fig. 5.51 Energy flow in a two-mode hybrid system with two EVT ranges and four gear stages with fixed transmission ratio

1. EVT with one power split, stageless
2. EVT with double power split, stageless
3. 1st gear with fixed gear ratio and two operating motors (acceleration assistance, braking energy recuperation)
4. 2nd gear with fixed gear ratio and one operating motor (acceleration assistance, braking energy recuperation)

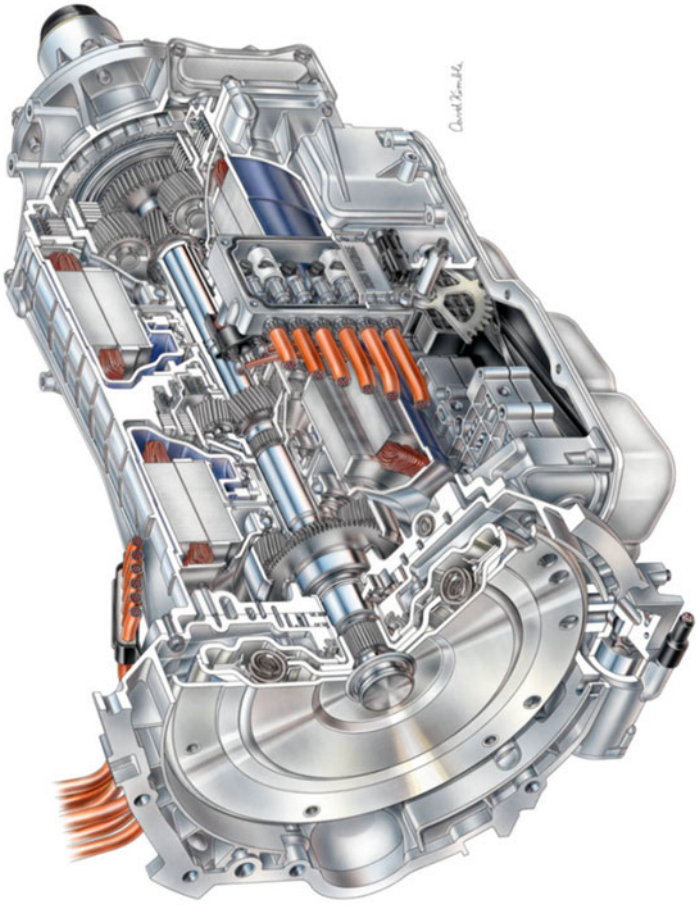

Fig. 5.52 Partial section of a two-mode hybrid system (Source: GM)

5. 3rd gear with fixed gear ratio and two operating motors (acceleration assistance, braking energy recuperation)
6. 4th gear with fixed gear ratio and one operating motor (acceleration assistance, braking energy recuperation).

Figure 5.51 shows the flow scheme for this configuration. Numerous possibilities for combination of gear ratios and the optional use of one or two motors allow adjustment of the system for all load and speed situations.

Figure 5.52 shows a partial section through a two-mode hybrid system. Figures 5.53 and 5.54 illustrate some applications of this system in the BMW Active Hybrid X6 and in the Dodge Ram.

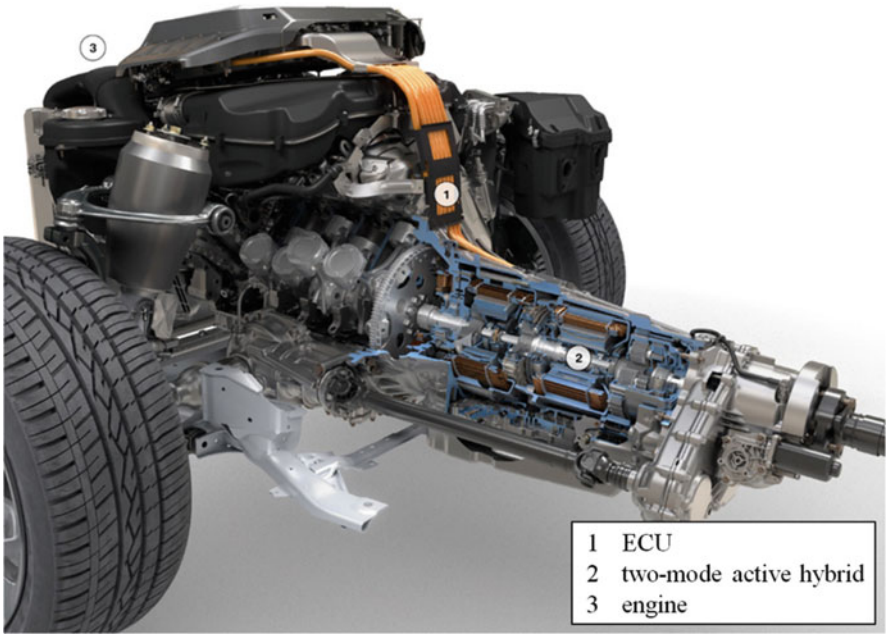

Fig. 5.53 Two-mode active hybrid: BMW Active Hybrid X6 (Source: BMW)

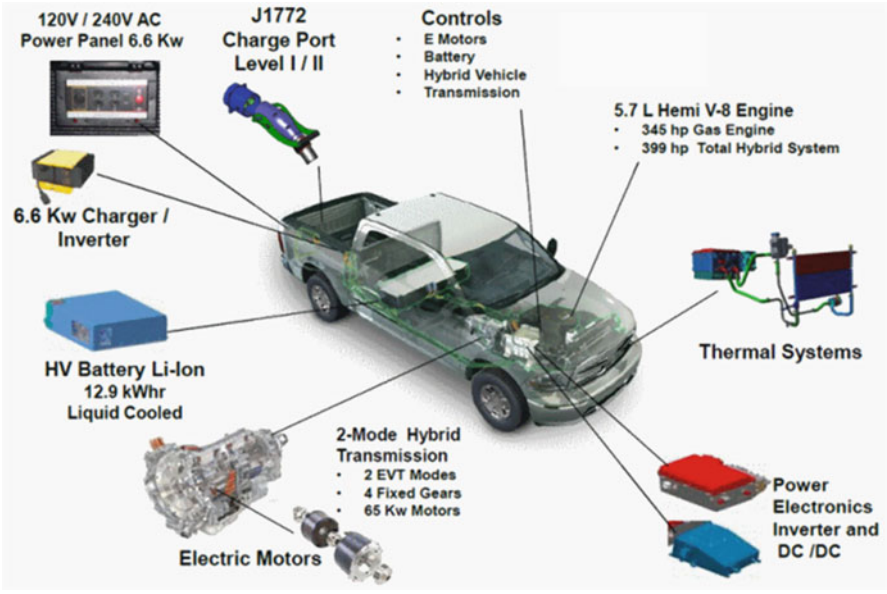

Fig. 5.54 Function modules of a fuel cell hybrid: Dodge Ram (Source: GM)

5.3.7 Hybrid with Propulsion of One Vehicle Axle by an Engine and of the Second Axle by a Motor, Without Mechanical Coupling on Either: Peugeot

Such a configuration corresponds to the first full hybrid variant by Audi (Audi 100 duo, 1989), presented in Fig. 5.26. In the Peugeot 3008 Hybrid4, which was introduced in series production, front axle propulsion is by a diesel engine and rear axle propulsion by a motor, which allows electric-only driving for 3–4 km. This configuration is presented in Fig. 5.55.

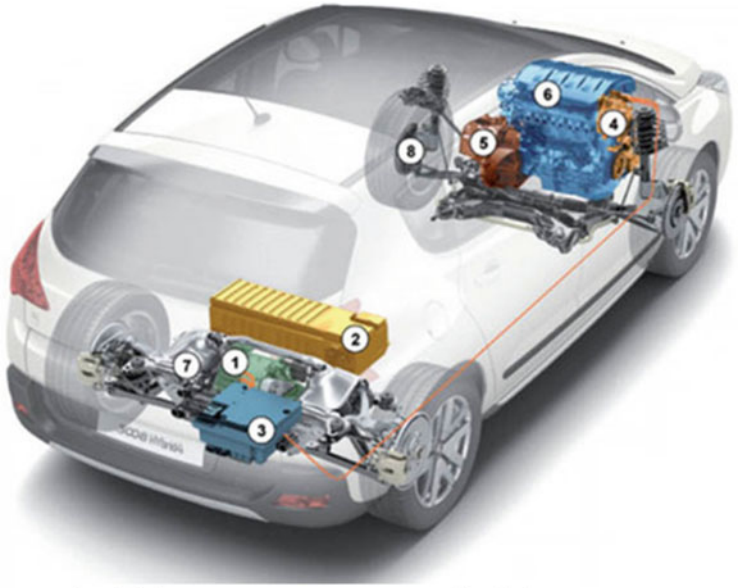

Fig. 5.55 Hybrid automobile: Peugeot 3008 Hybrid (Source: PSA)

5.3.8 Overview of the Present Parallel and Mixed Hybrid Propulsion Systems

A selection of representative hybrid systems of these types is shown in Table 5.2. Based on the given data for vehicles and propulsion systems, their characteristics can be divided into four categories:

- Vehicle weight: including hybrid propulsion system and batteries
- Propulsion features: engine and motor types, power and torque (separate and combined for engines and motors)
- Electric energy storage: batteries and their capacities
- Fuel consumption: corresponding to the US Federal Testing Procedure (FTP).

The following remarks, based on these data, refer to the parallel and mixed hybrids:

- Vehicle weight is generally 10–12 % higher than the weight of vehicles equipped with the basic engines, which means 100–260 kg.
- Gasoline engines are generally used for hybridization.
- The main aim of hybridization of systems with gasoline engines is to reduce fuel consumption in the range of automobiles with diesel engines, which do not have high acceptance in the USA, China, and Japan.
- The motors are generally synchronous, similar to those of electric vehicles with batteries (Table 5.1).
- General power is in the range of 73–360 kW and torque 167–780 N m. The general power and torque are not remarkable, because they are related to the vehicle type. Much more interesting are the percentage contributions of engines and motors to the general power and torque.

Concepts cars:

- Audi: A6, A8, Q5, Q7
- BMW: Vision Efficient Dynamics, X3, X5
- Citröen: C-Cactus, C5 Airscape Urban Hybrid, C-Métisse, C4 Hdi
- Daihatsu: HVS, UFE-III
- Ferrari: 599 HY KERS
- Honda: CR-Z, Small Hybrid Sport Concept
- Jaguar: C-X75
- Kia: Rio Hybrid
- Land Rover: Diesel-Hybrid ERAD, LRX, Land_e
- Lexus: LF-Ch, LF-XH
- Mercedes: F 500 Mind, F 700, F 800 Style, GLK Bluetec Hybrid, S 350 Direct Hybrid
- Nissan: HEV
- Opel: Flextreme, Corsa Hybrid, Astra GTC Diesel Hybrid
- Peugeot: SxC, HR1, RCZ Hybrid4, Prologue HYmotion4
- Porsche: 918 RSR, 918 Spyder

Table 5.2 Selection of hybrid systems and their characteristics

Car		Performance								Energy storage		Consumption[b]	
	Mass	Propulsion		Power [kW]			Torque [N m]				E_{el}	City	Country
Type	[kg]	ICE	Motor	ICE	Motor	Comb.	ICE	Motor	Comb.	Battery	[kW h]	[l/100 km]	[l/100 km]
BMW ActiveHybrid 7	2175	Otto	Syn.	328	15	342	480	210	–	Li-ion	0.8	13.9[a]	9.1[a]
BMW ActiveHybrid X6	2615	Otto	Syn.	300	67	357	600	280	780	Ni-MH	2.4	13.9[a]	12.4[a]
BYD F3DM (PHEV)	1560	Otto	Syn.	50	50	125	–	–	–	LiFePO	16	–	–
Cadillac Escalade Hybrid[c]	2667	Otto	Syn.	–	60	248	–	320	498	Ni-MH	2.1	11.8	10.2
Chevrolet Malibu[f]	1619	Otto	–	122	3.7	122	216	–	–	Ni-MH	–	9.1	6.9
Chevrolet Silverado[c]	2747	Otto	Syn.	–	–	248	–	–	498	Ni-MH	2.1	11.8	10.2
Chevrolet Tahoe Hybrid[c]	2580	Otto	Syn.	–	–	248	–	–	498	Ni-MH	2.1	11.8	10.2
Chevrolet Volt (PHEV)	1715	Otto	Syn.	60	112	–	122	370	–	Li-ion	16	2.5/6.7[d]	2.6/5.9[d]
Dodge Durango	2389	Otto	Syn.	257	65	287	515	319	–	Ni-MH	–	12.4	11.8
Fisker Karma (PHEV)	1950	Otto	Syn.	194	352	–	353	1300	–	Li-ion	20	7.1	6.2
Ford Escape Hybrid	1664	Otto	Syn.	116	70	132	–	–	184	Ni-MH	1.8	7.6	6.9
Ford Fusion Hybrid	1690	Otto	Syn.	116	–	142	184	–	338	Ni-MH	1.3	13.1	8.7
GMC Sierra Hybrid[c]	2658	Otto	Syn.	–	60	248	–	320	498	Ni-MH	2.1	11.8	10.2

(continued)

Table 5.2 (continued)

Car		Performance								Energy storage		Consumption[b]	
	Mass	Propulsion		Power [kW]			Torque [N m]				E_{el}	City	Country
Type	[kg]	ICE	Motor	ICE	Motor	Comb.	ICE	Motor	Comb.	Battery	[kW h]	[l/100 km]	[l/100 km]
GMC Yukon Hybrid[c]	2561	Otto	Syn.	–	–	248	–	–	498	Ni-MH	2.1	11.8	10.2
Honda Accord Hybrid	1593	Otto	Syn.	189	12	–	315	136	–	Ni-MH	13.8	8.4	6.7
Honda Civic Hybrid	1294	Otto	Syn.	–	17	82	–	106	172	Li-ion	–	5.4	5.4
Honda Civic Hybrid	1294	Otto	Syn.	–	17	82	–	106	172	Li-ion	–	5.4	5.4
Honda CR-Z Hybrid	1196	Otto	Syn.	84	10	91	145	79	167	Ni-MH	–	7.6	6.4
Honda FCX Clarity	1624	H_2 F Cell	Syn.	100	100	100	–	256	256	Li-ion	–	1.0[e]	1.0[e]
Honda Insight Hybrid	1196	Otto	Syn.	–	10	73	–	79	167	Ni-MH	0.58–	5.9	5.5
Honda Jazz/Fit Hybrid	1234	Otto	Syn.	65	10	73	121	78	–	Ni-MH	0.58	6.4	4.4
Hyundai Elantra LPI Hybrid	1335	Otto	–.	85	15	99	150	105	–	Li-Pol	–	–	–
Hyundai Sonata Hybrid	1568	Otto	Syn.	123	30	154	209	205	262	Li-ion	1.4	6.7	5.9
Infiniti M35 Hybrid	1882	Otto	Syn.	225	50	268	350	270	–	Li-ion	1.4	8.7	7.4
Kia Optima Hybrid	1583	Otto	Syn.	124	30	154	209	205	265	Li-ion	1.4	6.7	5.9
Lexus CT 200 h	1420	Otto	Syn	73	60	100	182	207	–	Ni-MH	1.6	5.5	5.9
Lexus GS 450 h	1875	Otto	Syn.	221	147	254	368	203	–	Ni-MH	1.9	10.7	9.4

Lexus HS 250 h	1710	Otto	Syn.	110	105	140	187	270	–	Ni-MH	1.6	6.7	6.9
Lexus LS 600 h	2360	Otto	Syn.	291	165	360	382	220	–	Ni-MH	1.9	12.4	10.2
Lexus RX 450 h	2050	Otto	Syn.	182	125	220	317	350	–	Ni-MH	1.9	7.8	8.4
Lincoln MKZ Hybrid	1702	Otto	Syn.	116	70	142	184	225	–	Ni-MH	1.4	5.7	6.5
Mazda Tribute	1656	Otto	Syn.	99	52	116	167	–	–	Ni-MH	–	6.9	7.8
Mercedes ML 450 Hybrid	2381	Otto	Syn.	205	60	246	350	260	517	Ni-MH	2.4	11.2[a]	9.8[a]
Mercedes S400 BlueHybrid	1955	Otto	Syn.	205	15	220	350	160	385	Li-ion	0.9	10.7[a]	6.3[a]
Mercury Milan Hybrid[f]	1717	Otto	Syn.	116	–	142	184	–	338	Ni-MH	1.3	13.1	8.7
Mercury Mariner Hybrid[f]	1660	Otto	Syn.	116	70	132	–	–	184	Ni-MH	1.8	7.8	6.9
Nissan Altima Hybrid	1584	Otto	Syn.	138	105	148	220	270	–	Ni-MH	–	4.7	4.9
Peugeot 3008 Hybrid4	1701	CI	Syn.	120	27	147	300	200	500	Ni-MH	–	3.9[a]	3.7[a]
Porsche Cayenne S Hybrid	2240	Otto	Syn.	245	34	279	440	300	580	Ni-MH	1.7	8.7[a]	7.9[a]
Porsche Panamera S Hybrid	1980	Otto	Syn.	245	34	279	440	300	580	Ni-MH	1.7	7.6[a]	6.8[a]
Saturn Aura Green Line[f]	1601	Otto	–	122	3.7	122	216	–	–	Ni-MH	–	8.4	6.7
Suzuki Twin[h]	703	Otto	Syn.	32	5	–	57	33	–	–	–	–	–
Toyota Auris Hybrid	1455	Otto	Syn.	73	60	100	142	207	–	Ni-MH	1.3	3.8[a]	3.8[a]

(continued)

Table 5.2 (continued)

Car		Performance								Energy storage		Consumption[b]	
	Mass	Propulsion		Power [kW]			Torque [N m]				E_{el}	City	Country
Type	[kg]	ICE	Motor	ICE	Motor	Comb.	ICE	Motor	Comb.	Battery	[kW h]	[l/100 km]	[l/100 km]
Toyota Camry Hybrid	1480	Otto	Syn.	110	105	140	187	270	–	Ni-MH	–	10.7	7.1
Toyota Prius	1380	Otto	Syn.	73	60	100	142	207	–	Ni-MH	–	3.8[a]	4.0[a]
VW Touareg Hybrid	2329	Otto	Syn.	248	34	290	441	580	576	Ni-MH	1.7	8.7[a]	7.9[a]
Volvo V60 Plug-in Hybrid	–	CI	–	158	52	-	440	200	–	Li-ion	12	–	–

Sources: Car manufacturers
[a]NEDC
[b]US Environmental Protection Agency Federal Test Procedure (EPA FTP)
[c]Propulsion GM
[d]Equivalent, as range extender only
[e]kg/100 km until 2009
[f]Mercury (GM) and Saturn (Ford) are no longer brands
[h]Until 2005, after 10,000 sold cars

– Seat: IBX, Leon TwinDrive
– SsangYong: C200 Eco
– Subaru: B5-TPH
– Toyota: FT-CH, 1/X, A-BAT, Hybrid X, FT-HS Concept
– Volkswagen: XL1, L1, Gold TwinDrive, Touran EcoPower II
– Volvo: ReCharge Concept

Figure 5.56 shows the contribution of engines and motors to the general power and torque for some representative models. The main points are noted below:

- The electric power is generally rather low, at values of approximately 30 kW, except for some brands. In pure electric vehicles, the range of motor power is 90 kW, as shown in Fig. 4.33. Power from the engine is 180–220 kW, six times higher than the electric power. On the other hand, there are no significant torque differences between engines and motors for the same propulsion system. However, it should be noted that the maximum torque of motors is available from standing to 2000–2200 min^{-1}, at which point the torque of engines begins to increase. Thus, a high torque is ensured for a large speed range of the hybrid.
- Electric energy is stored mainly in Ni–metal hydride batteries and less often in Li-ion batteries, which are more expensive.
- Pure electric vehicles have batteries with a capacity of about 25 kW h (Fig. 4.33). In parallel and mixed hybrids, the battery capacity is only a tenth of this value (Fig. 5.56).
- Fuel consumption can be evaluated only in relation to vehicle weight and the acceleration behavior in a reference driving cycle. The consumption of some vehicles of the same type (based on the values in Table 5.2) are compared in Table 5.3. All vehicles were fitted with gasoline engines and had similar values for weight, power, and torque, in the same new European driving cycle (NEDC). The main points to note are the following:
  – The total weight of the BMW Active Hybrid 7 is 100 kg more than that of the BMW 750i , and the power of the engine is 28 kW greater; the total power, including the motor, in this mode is 42 kW more. Nevertheless, the fuel consumption of the Active Hybrid 7 is 3.8 l/100 km lower for the urban cycle, going from 16.4 to 12.6 l/100 km for the hybrid. On country roads this difference is 0.9 l/100 km.
  – The BMW Active Hybrid X6 weighs 260 kg more than the BMW X6 xDrive 50i with gasoline engine, at same engine power but with additional electric power of 57 kW. This hybrid configuration leads to a reduction in fuel consumption of 6.7 l/100 km for the urban cycle. On country roads the consumption is somewhat higher than that of the BMW X6 xDrive 50i.
  – Comparing the Porsche Cayenne S Hybrid with the Cayenne S, and the Porsche Panamera S Hybrid with the Porsche Panamera S, the weight of the hybrids is higher (175 and 210 kg, respectively). The engine power is reduced by 49 kW, the additional motor has 34 kW, and the total power is 15 kW less than those of the basic variants with gasoline engine only. However, the acceleration is not impaired, because of the high torque of the motor at low

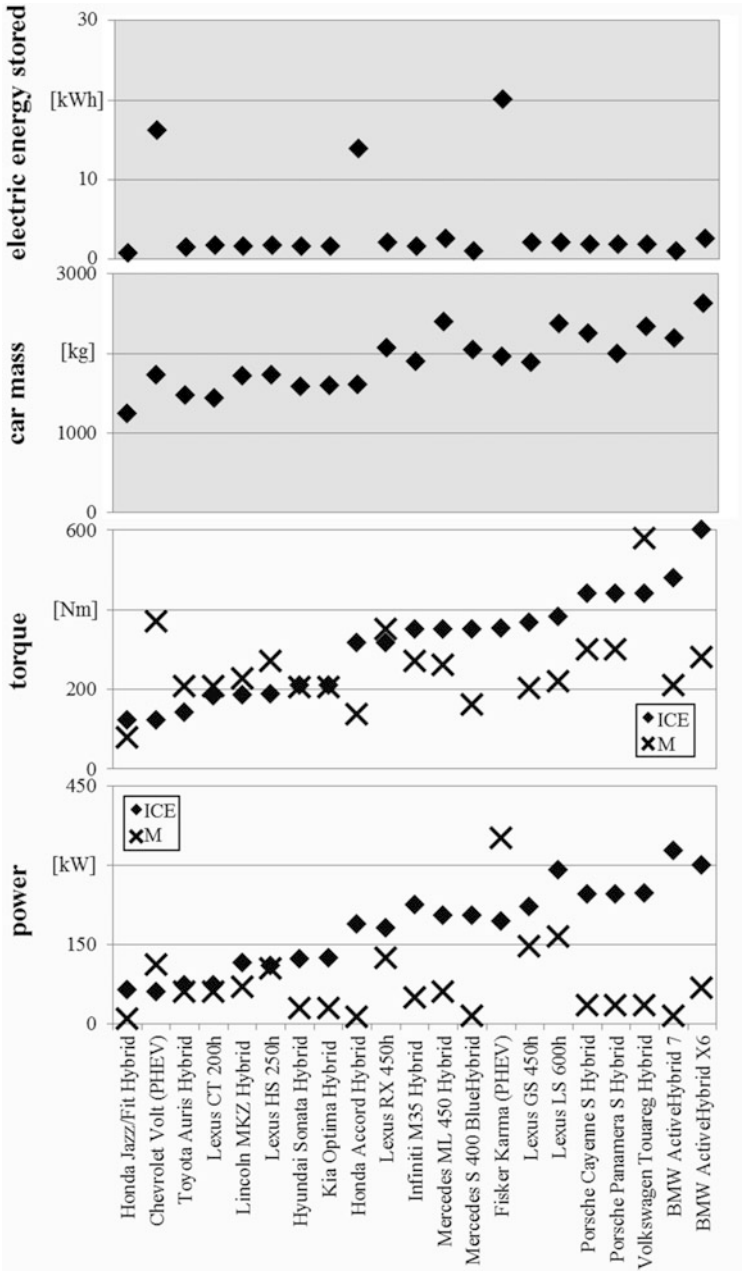

Fig. 5.56 Relationship between power, torque, car mass, and stored electric energy on board for a selection of hybrid cars

Table 5.3 Comparison of hybrid and gasoline engines in same car type

Car		Propulsion								Consumption[a]		
	Mass	Propulsion		Power [kW]			Torque [N m]			City	Country	Combined
Type	[kg]	ICE	Motor	ICE	Motor	Comb.	ICE	Motor	Comb.	[l/100 km]	[l/100 km]	[l/100 km]
BMW ActiveHybrid 7	2120	Otto	Syn.	328	15	342	480	210	–	12.6	7.6	
BMW 750i	2020	Otto	–	300	–	300	600	–	–	16.4	8.5	
Difference	+100	–	–	+28	–	+42	–	–	–	−3.8	−0.9	
BMW ActiveHybrid X6	2525	Otto	Syn.	300	67	357	600	280	780	10.8	9.4	
BMW x6 xDrive 50i	2265	Otto	–	300	–	300	600	–	–	17.5	9.6	
Difference	+260	–	–	±0	–	+57	–	–	–	−6.7	+0.2	
Mercedes ML 450 Hybrid	2381	Otto	Syn.	205	60	246	350	260	517	11.8	9.8[a,b]	–
Mercedes ML350 4MATIC	2130	Otto	–	225	–	225	350	–	–	11.8	9.4[b]	–
Difference	+251	–	–	−20	–	+21	–	–	–	±0	+0.4	–
Mercedes S400 BlueHybrid	1955	Otto	Syn.	205	15	220	350	160	385	10.7	6.3	
Mercedes S350 Blue Efficiency	1910	Otto	–	225	–	225	370	–	–	10.2	6.0	
Difference	+45	–	–	−20	–	−5	–	–	–	+0.5	+0.3	
Porsche Cayenne S Hybrid	2240	Otto	Syn.	245	34	279	440	300	580	8.7	7.9	
Porsche Cayenne S	2065	Otto	–	294	–	294	500	–	–	14.4	8.2	
Difference	+175	–	–	−49	–	−15	–	–	–	−5.7	−0.3	
Porsche Panamera S Hybrid	1980	Otto	Syn.	245	34	279	440	300	580	7.6	6.8	
Porsche Panamera S Automatic	1770	Otto	–	294	–	294	500	–	–	15.3	7.8	
Difference	+210	–	–	−49	–	−15	–	–	–	−7.7	−1.0	
VW Touareg Hybrid	2329	Otto	Syn.	245	34	290	440	580	576	8.7	7.9	8.2

(continued)

Table 5.3 (continued)

Car		Propulsion								Consumption[a]		
	Mass	Propulsion		Power [kW]			Torque [N m]			City	Country	Combined
Type	[kg]	ICE	Motor	ICE	Motor	Comb.	ICE	Motor	Comb.	[l/100 km]	[l/100 km]	[l/100 km]
VW Touareg 3.6 V6	2103	Otto	–	206	–	206	360	–	–	13.2	8.0	9.9
Difference	+226	–	–	+42	–	+84	–	–	–	−4.5	−0.1	−1.7

[a]NEDC
[b]FTP

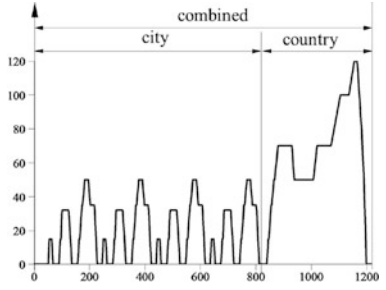

speed. The fuel economies are 5.7 and 7.7 l/100 km, respectively, in urban cycles. Out of the city, the hybrids have an advantage of 0.3 and 1.0 l/100 km, respectively.

- The VW Touareg Hybrid weighs an additional 226 kg in comparison with the Touareg 3.6 V6. The power of the engine in the hybrid is 42 kW higher and is completed by a motor power of 34 kW, resulting in a total power that is 84 kW more than with the basic gasoline engine. Despite the noticeable increase in weight and total power, fuel consumption in the urban cycle is 4.5 l/100 km less. Out of the urban cycle, the fuel consumption remains similar for both vehicles.
- The Mercedes ML 450 Hybrid has only 25 kg more weight than the ML 350 4 Matic. Comparison of these two different engines in the same car type is motivated by the power: the hybrid has a gasoline engine with 20 kW less power than the ML350; however, with the motor, the total power increases to 21 kW. The fuel consumption is equal in all situations.
- The Mercedes S400 Blue Hybrid has only 45 kg more weight than the S350 Blue, but less power. The engine power is lower by 20 kW and the total power by 5 kW. The fuel consumption increases by 0.5 l/100 km for the hybrid in urban areas, and by 0.3 l/100 km on country roads.

In conclusion, in heavy automobiles of the upper class with gasoline engines, an additional propulsion motor is very advantageous, if the torque characteristics of motor and engine are adjusted for the given operation profile. The increase in weight, dimensions, and price is not very significant for this vehicle class.

It is a different situation for vehicles of a lower class, where price and weight play very important roles. On the other hand, high power is not an essential criterion in this case. As already mentioned, in the USA, China, and Japan the acceptance for vehicles with diesel engines is rather low. Hybrid systems consisting of gasoline engine and motor have the advantage of considerably lower fuel consumption compared with propulsion by gasoline engine only.

Another comparison of vehicles of the same class and similar power, but with diesel engines, seems to be justified. Table 5.4 shows the results of this comparison between three series automobiles with diesel engines (VW, Citroen and Fiat), and a very successful hybrid, the Toyota Prius.

- The Toyota Prius weighs 100 kg more than the Citroen C4HDi90, 66 kg more than the VW Golf VI 1.6 TDI, but 15 kg less than the Fiat Bravo 1.6 16 V Multijet. The power differences between the three vehicles with diesel engines and the Toyota Prius are irrelevant (−4, +5 kW), this being the base of this comparison. The Toyota Prius has a motor of 60 kW in addition to the gasoline engine, but the torque characteristics of both are very different; therefore, the total power is only 23–32 kW higher than that of the diesel engines.
- In the NEDC, the hybrid shows a reduced fuel consumption of 0.9–2.0 l/100 km compared with the three diesel vehicles. In the rural cycle, the consumption is higher, as shown in Fig. 5.25. A comparison of the basic prices (October 2010) of the four vehicle types shows the advantage of the diesel variants, the difference being in the range of €3600–€7360.

Table 5.4 Comparison of Toyota Prius Hybrid and series diesel cars at the same power level

Car		Propulsion								Consumption[a]		
	Mass	Propulsion		Power [kW]			Torque [N m]			City	Country	Combined
Type	[kg]	ICE	Motor	ICE	Motor	Comb.	ICE	Motor	Comb.	[l/100 km]	[l/100 km]	[l/100 km]
Toyota Prius	1380	Otto	Syn.	73	60	100	142	207	–	3.8	4.0	4.0
Citroen C4 HDi 90	1280	Diesel	–	68	–	68	230	–	–	5.2	3.6	4.2
Difference	+100		–	+5	–	+32	–	–	–	−1.4	+0.4	−0.2
Toyota Prius	1380	Otto	Syn.	73	60	100	142	207	–	3.8	4.0	4.0
Fiat Bravo1.6 16 V Multijet	1395	Diesel	–	77	–	77	290	–	–	5.8	3.8	4.5
Difference	−15		–	−4	–	+23	–	–	–	−2.0	+0.2	−0.5
Toyota Prius	1380	Otto	Syn.	73	60	100	142	207	–	3.8	4.0	4.0
VW Golf 6 1,6 bluemotion	1314	Diesel	–	77	–	77	250	–	–	4.7	3.4	3.8
Difference	+66		–	−4		+23	–	–	–	−0.9	+0.6	+0.2

[a]NEDC

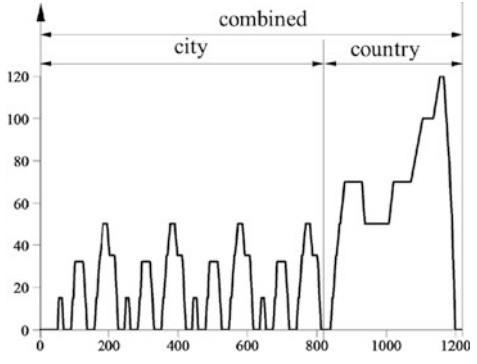

This consideration of parallel and mixed hybrid systems again confirms that the various operating conditions impose various combinations of functional modules (engines, motors, and batteries).

5.4 Plug-In Hybrid Propulsion

An extension of the hybrid propulsion systems appeared recently in the form of the plug-in configuration. This configuration offers an additional degree of freedom because the battery of a full hybrid can be charged from outside. In this form, a range extension is achievable only for electric propulsion . This presupposes a higher battery capacity, at values between those for pure electric vehicles and full hybrid batteries.

For the Toyota Prius plug-in hybrid, the operation range in electric mode becomes 20 km. The propulsion is ensured by an engine with a swept volume of 1.8 dm^3, developing a power of 73 kw and a torque of 142 N m in combination with a motor of 60 kW power and 207 N m torque. The maximum total power is 100 kW. The cobalt-lithium battery has a capacity of 5.2 kW h at 346 V. The additional cost of this version in comparison with a classic Toyota Prius is €9750. Figure 5.57 shows the configuration of such a system. A new variant provides contactless battery charge, as shown in Fig. 5.58.

In the Audi Q7 e-tron 3.0 TDI Quattro [36], propulsion is ensured by a diesel engine with a swept volume of 3.0 dm^3 in combination with a synchronous motor. Figure 5.59 illustrates the configuration of this system. Figure 5.60 shows the six-cylinder diesel engine that is the main module of this system. The maximum

Fig. 5.57 Toyota Prius plug-in hybrid (Source: Toyota)

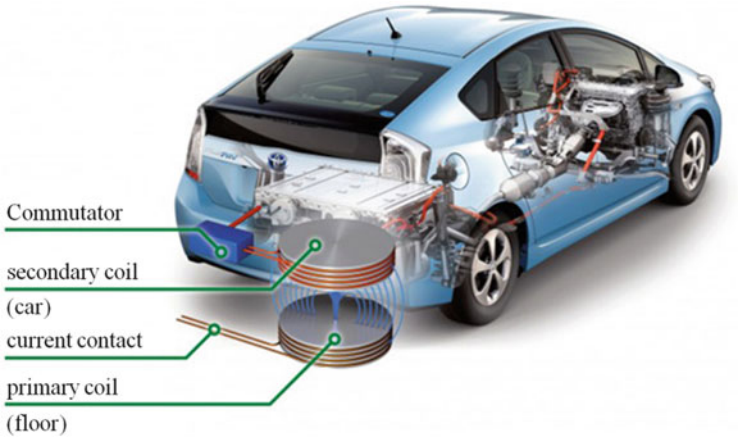

Fig. 5.58 Toyota Prius plug-in hybrid with contactless, inductive charging (Source: Toyota)

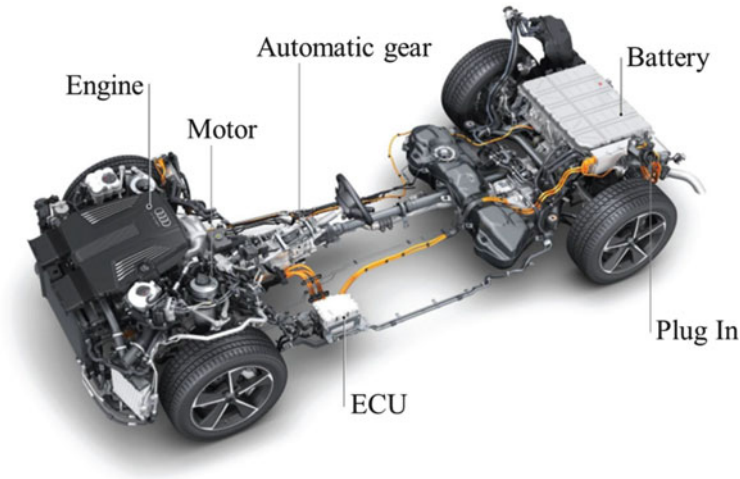

Fig. 5.59 Audi Q7 e-tron 3.0 TDI quattro plug-in hybrid (Source: Audi)

power of the engine is 190 kW and the maximum torque 600 N m in a speed range of 1200–3000 min^{-1}, as shown in Fig. 5.61.

The motor is integrated in the eight-stage automatic gear, as illustrated in Fig. 5.62. The rotor with permanent magnets encircles the stator, which is provided with coils. The maximum power of the motor is 94 kW and the maximum torque is 348 N m from standing to 2000 min^{-1}, as shown in Fig. 5.63. The total power of the hybrid system achieves 275 kW and the maximum torque reaches 700 N m in a speed range between 1200 and 3800 min^{-1}, as illustrated in Fig. 5.64.

The system contains a Li-ion battery with 14 cell modules, achieving a capacity of 17.3 kW h. This battery is shown in Fig. 5.65.

Fig. 5.60 Audi Q7 e-tron 3.0 TDI quattro plug-in hybrid with diesel engine (Source: Audi)

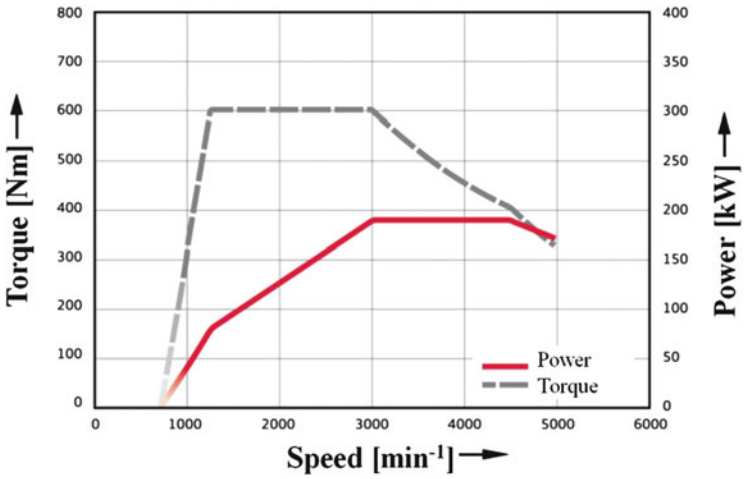

Fig. 5.61 Audi Q7 e-tron 3.0 TDI quattro plug-in hybrid with diesel engine: torque and power curves at full load

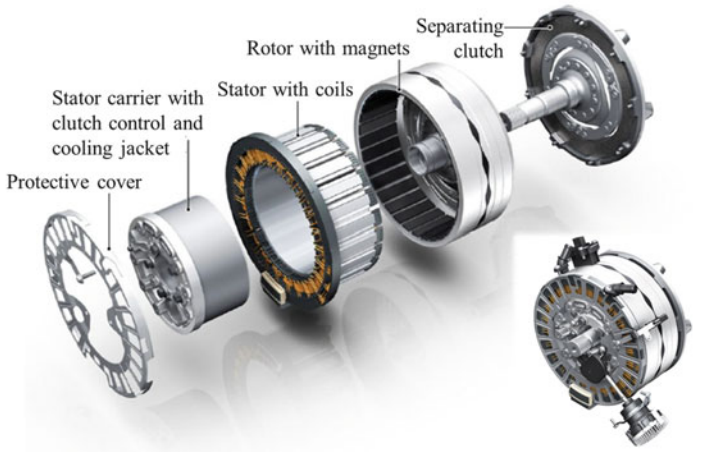

Fig. 5.62 Audi Q7 e-tron 3.0 TDI quattro plug-in hybrid with motor

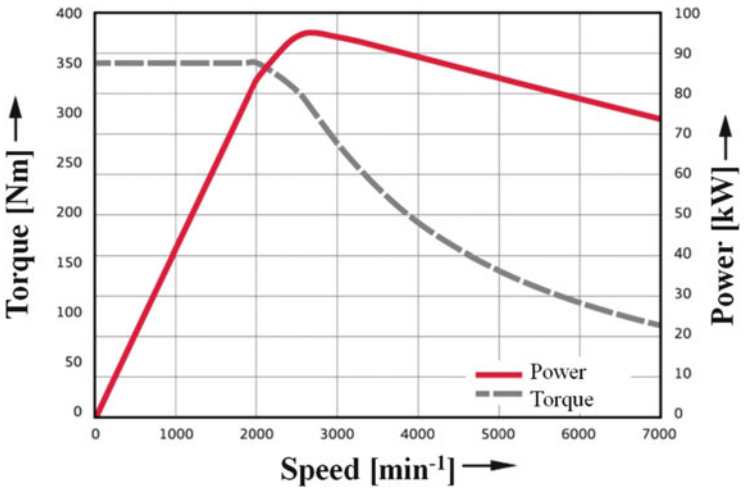

Fig. 5.63 Audi Q7 e-tron 3.0 TDI quattro plug-in hybrid with motor: torque and power curves at full load

Evaluation of this concept, with its high costs and weight, is needed for comparison with the same vehicle equipped with a diesel engine only. Certainly, serious evaluation is only possible after long-term tests. However, two observations could be of use:

- The total torque increase by hybridization is 100 N m in comparison with the torque of the basic diesel engine, at the same speed, as deduced from Fig. 5.64. However, the benefit of 100 N m is paid for by 400 kg more weight. An advantage in terms of acceleration is therefore not evident.

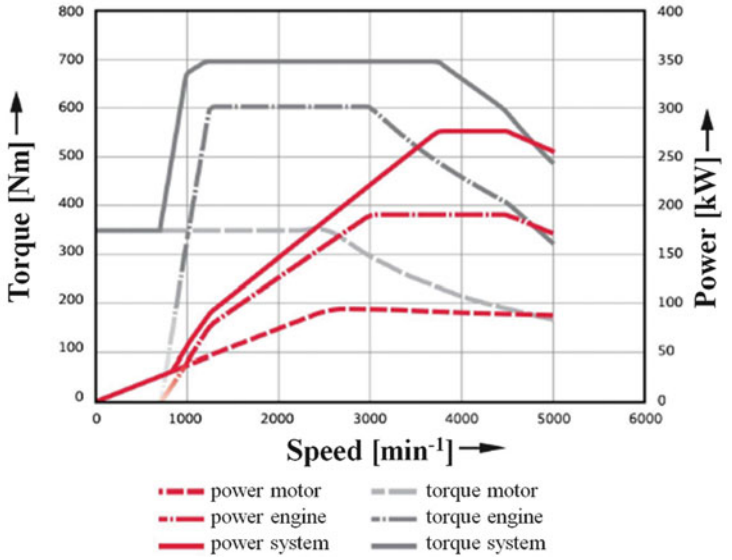

Fig. 5.64 Audi Q7 e-tron 3.0 TDI quattro plug-in hybrid with diesel engine plus motor: torque and power curves of the whole system at full load

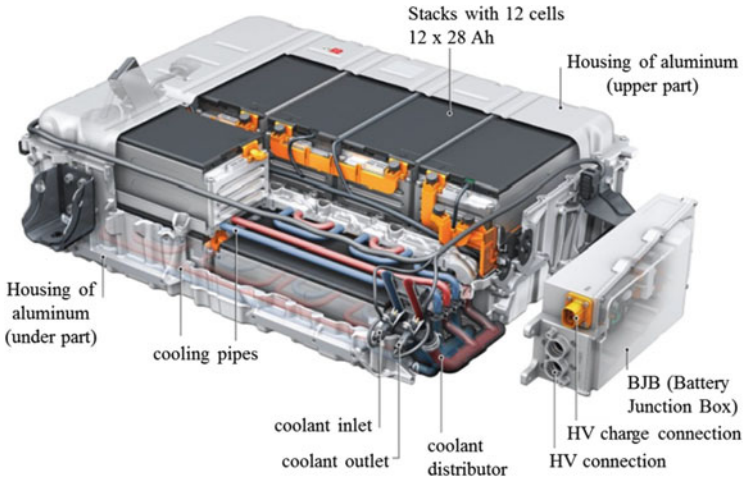

Fig. 5.65 Audi Q7 e-tron 3.0 TDI quattro plug-in hybrid: Li-ion battery (Source: Audi)

- Before the diesel engine can reach maximum torque, the motor has already achieved maximum torque. Thus, a total torque of 348 N m is available from standing. This total torque shows a steep increase to between 800 and 1000 N m, in a range where the diesel engine achieves only 100–200 N m at full load. The advantage is the low fuel consumption of the diesel engine when accelerating

Fig. 5.66 BMW X5 eDrive plug-in hybrid (Source: BMW)

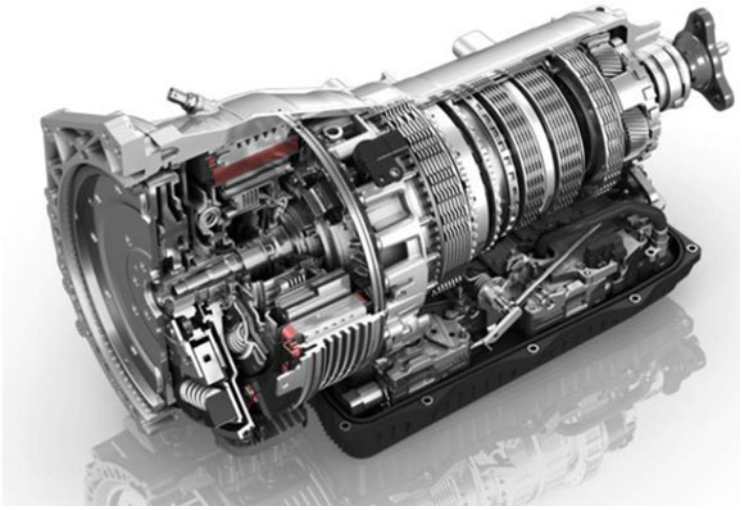

Fig. 5.67 BMW X5 eDrive plug-in hybrid: motor within automatic gear with eight stages (Source: BMW)

from standing or from a low speed. In a cycle with frequent variation of load and speed, such an advantage becomes more explicit. For the plug-in configuration in the Audi Q7, the fuel consumption is only 1.7 l/100 km and the CO_2 emission 50 g/km [36].

The propulsion system of the BMW X5 eDrive plug-in hybrid is similar to the above example. Figure 5.66 illustrates the configuration of this system. The gasoline engine of this system, with 180 kW is combined with a motor of 70 kW, which is integrated in the with eight-stage automatic gear system [37]. The gear is shown in Fig. 5.67. The total power of the hybrid reaches 230 kW, and the torque achieves

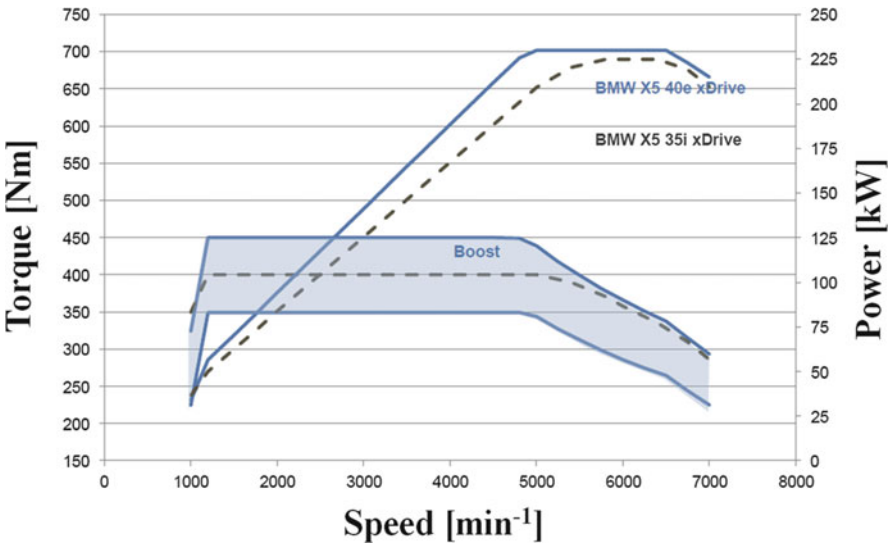

Fig. 5.68 BMW X5 eDrive plug-in hybrid with gasoline engine plus motor: torque and power at full load (Source: BMW)

Fig. 5.69 BMW X5 eDrive plug-in hybrid: Li-ion battery (Source: BMW)

450 N m, as demonstrated in Fig. 5.68. The battery, shown in Fig. 5.69, consists of 6 cell modules with 16 prismatic cells in each module and has a capacity of 9 kW h.

Another example of plug-in configuration is shown in Fig. 5.70. The BMW i8 has a gasoline engine with a swept volume of 1.5 dm^3, developing 170 kW and 320 N m, and a motor with 96 kW and 250 N m. The gasoline engine ensures propulsion on the rear axle, whereas the motor provides power to the front axle. The total power is 266 kW. The lithium-polymer battery has a capacity of 5.2 kW h.

A plug in concept with the aim of minimum fuel consumption is the VW XL1, which is illustrated in Fig. 5.71. The propulsion system consists of a diesel engine

Fig. 5.70 BMW i8 Plug-in hybrid (Source: BMW)

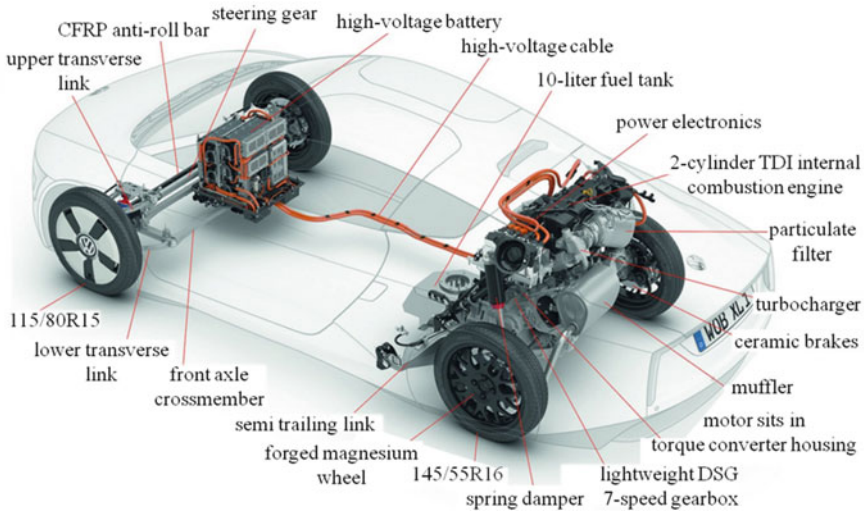

Fig. 5.71 VW XL1 plug-in hybrid (Source: VW)

with a swept volume of 0.8 dm^3, reaching a power of 35 kW. The engine works in combination with a motor of 20 kW. The whole vehicle has a weight of 795 kg.

The plug-in concepts demonstrate wide diversity in terms of the utilized engines and motors and in the composition of the torque from both modules. Figure 5.72 shows a variant with an engine and two motors, one per vehicle axle. The four-cylinder diesel engine has 140 kW, the motor at the front axle 40 kW and 180 N m,

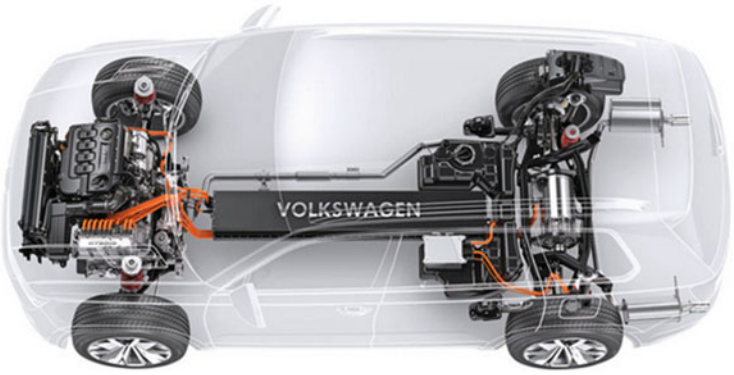

Fig. 5.72 VW Cross Blue plug-in hybrid (Source: VW)

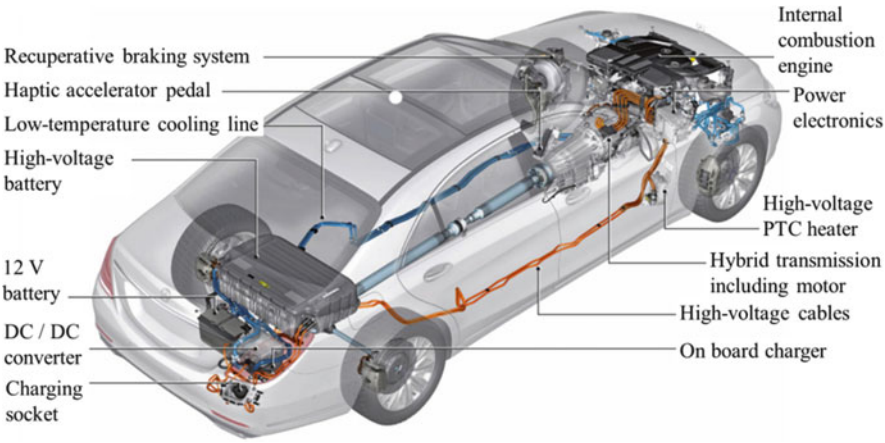

Fig. 5.73 Mercedes S 500 plug-in hybrid (Source: Daimler)

and the motor at the rear axle 85 kW power and 270 N m torque. The total power achieved is 224 kW and the total torque 700 N m. The Li-ion battery has a capacity of 9.8 kW h.

The Mercedes S 500 plug-in hybrid, illustrated in Fig. 5.73, has a propulsion system formed by the combination of a six-cylinder gasoline engine with a motor. The engine has a maximum power of 245 kW, whereas the motor achieves a power of 85 kW. The total power reaches 325 kW and the maximum torque 650 N m. The Li-ion battery has a capacity of 8.7 kW h. The additional weight by hybridization is 200 kg.

The described plug-in concepts show no major differences from the hybrid solutions presented in Sect. 5.3. The main differences are the higher battery capacity and the possibility of external battery charging. In comparison with pure

hybrids, the plug-in system has two advantages resulting from the increased battery capacity, if fully charged from an external source:

- More autonomy in electric driving mode, as required in urban areas for emission-free traffic
- More frequent involvement of the motor in the propulsion at acceleration or for ascending slopes, improving the fuel consumption of the engine. On the other hand, the increased battery capacity is beneficial for electric energy storage during braking or downhill driving.

Energy Management in the Automobile as a Complex System

6

The exemplary development of propulsion systems for automobiles, from increased power to decreased pollutant emission, is based on a massive innovation potential directed by requirements, limitations, and acceptance criteria. The true highlight of future automobiles is the management of energy during propulsion and of the energy supply on board. Propulsion forms, energy sources, and modules for energy conversion and storage are combined in different configurations for this aim. An all-purpose and generally accepted automobile is in contradiction to the usual development rules and to natural, economic, technical, and social conditions. The modularization of functional components allows more effective diversification of car types and classes. This diversification follows three principal directions, as illustrated in Fig. 6.1:

1. In relation to size, special features, and price: upper class, middle class, compact class, low-price multipurpose class
2. In relation to regional, geographic, economic, and ecological conditions: from low-price pick-ups for country areas in South America to luxury electric cars with zero emissions for the urban areas of industrial countries
3. In relation to objective and subjective customer preferences: sport utility vehicle (SUV), coupe, sedan, convertible

The result of this diversification of car types is a large variety of propulsion systems; thus, an all-purpose propulsion concept is not realistic in this context. Nevertheless, a focus on the propulsion systems used for the different car classes can be useful.

C. Stan, *Alternative Propulsion for Automobiles*,
DOI 10.1007/978-3-319-31930-8_6

Fig. 6.1 The variety of cars, classified according to customer preference, regional conditions, and class

6.1 Upper Class of Cars, SUVs

For the upper class of cars and SUVs, such as illustrated in Fig. 6.2, a polarization between parallel and mixed hybrids with one engine and one or two motors, as well as for plug-in hybrids, is expected. Such solutions are very efficient in these classes because of the required driving characteristics and profiles. The additional costs of between €4000 and €8000 in comparison with propulsion by engine only becomes relative in regard to the vehicle costs (at €80,000, the additional costs would be 5–10 %).

6.2 Middle Class of Cars

For the middle class of cars, the most probable perspective for the coming decades is an advanced piston engine with an operation mode combining SI and CI processes. Accurate shaping of the thermodynamic process stages and their adjustment to momentary torque/speed combinations, transient conditions (acceleration, deceleration), and environmental conditions (temperature, pressure, humidity) allow a remarkable increase in efficiency, giving serious challenge to fuel cell

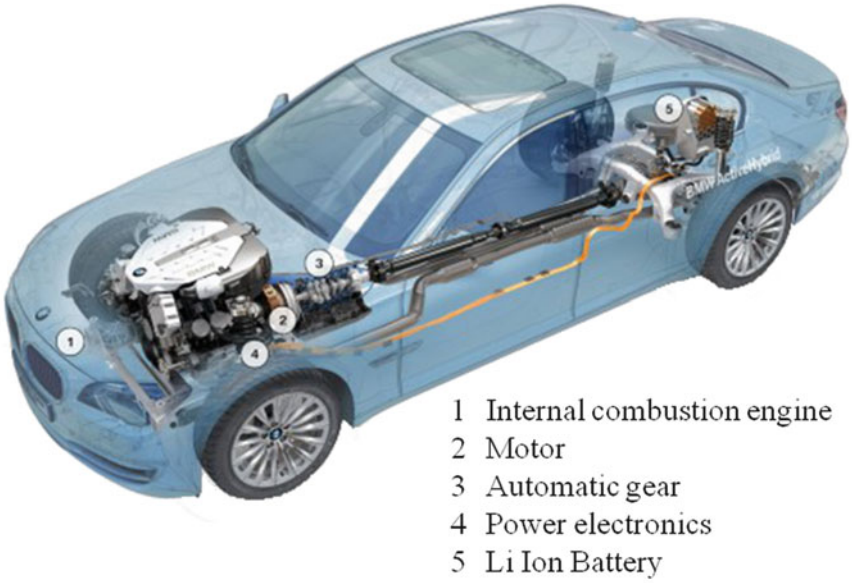

Fig. 6.2 Upper class/SUV full hybrid: BMW Active Hybrid 7

systems. Technical support for such process shaping and adjustment is complex: double super-/turbocharging, fully variable intake and exhaust valve control, direct fuel injection and mixture stratification, controlled self-ignition based on burned gas kernel within the combustion chamber, and different catalytic stages. The expected decrease in fuel consumption and pollutant emission through applying such measures, of course, has its price. In such a scenario, the role of the fuel cell will change from being a competitor to a concurrent module. With steady function at relatively low power, the fuel cell has a remarkable efficiency. Operating with the same fuel on board as the propulsion engine, such a fuel cell can ensure the supply of electric energy on board for numerous consumers, at a level of 5–10 kW. A system with a propulsion engine and full cell as current generator is shown in Fig. 6.3.

Further potential for an increase in total efficiency of the engine plus fuel cell system is given by their coupling. The electric energy from the fuel cell can be also utilized by the engine itself for the supercharger, valves, injection pumps, and water pumps, based on specific maps.

6.3 Compact Class, City Cars

The rapid development of megacities, as shown in Fig. 1.1, requires the future adoption of protected urban zones that are free of CO_2, pollutants, and noise emissions. An alternative to electric vehicles in public transportation such as

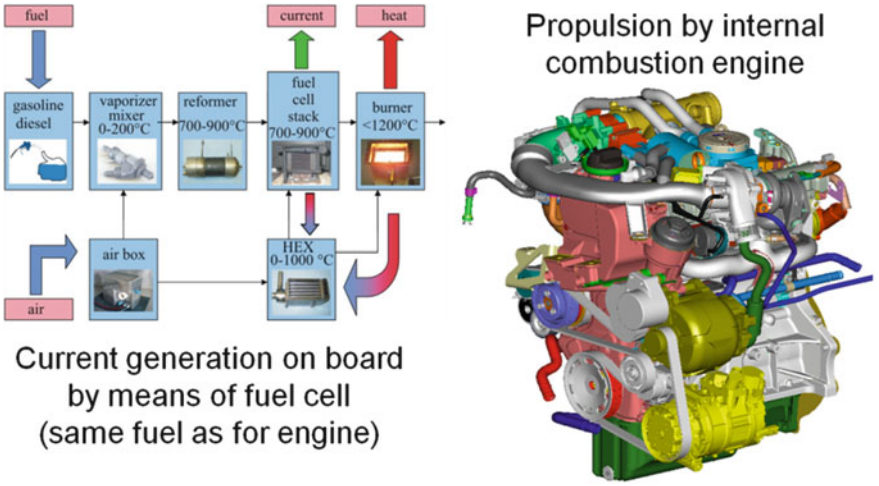

Fig. 6.3 Middle class of car with propulsion by internal combustion engine, and current generation on board by means of a fuel cell using the same fuel as the engine

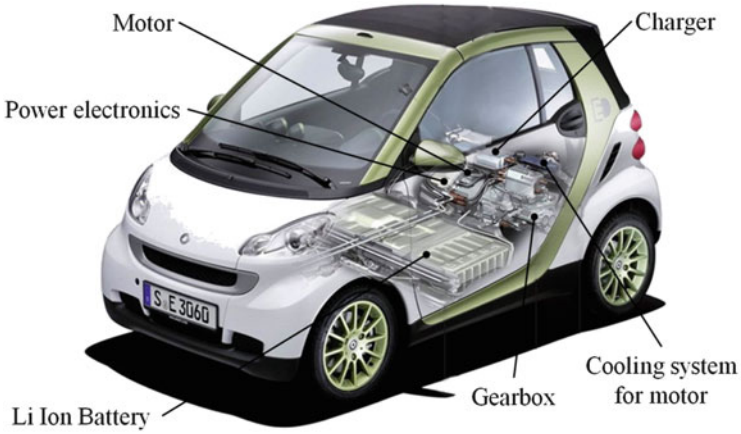

Fig. 6.4 Compact city car with propulsion by motor, and electric power from a battery on board (Source: Daimler)

buses and trams or trains is the purely electric car, with motor propulsion and electric energy stored in a battery, as illustrated in Fig. 6.4.

A compact car design would be very useful in dense city traffic. The car-sharing model has increasing importance in this context. Park-houses with rental cars are a beneficial infrastructure for battery charging. The low operation range of electric cars with batteries is, under these conditions, no longer an impediment.

6.4 City Cars with Range Extender

Purely electric propulsion with energy from a battery is advantageous in compact cars and recommendable in urban areas, but not outside of these because of the limited range of operation. An extension of range for suburban areas or for intercity traffic is feasible in two modes:

- Switching the propulsion from the electric mode to the engine mode (i.e., from the battery to a fuel)
- Keeping the electric propulsion, but switching the energy source from the battery to a fuel

Vehicles operating in the first mode are currently being introduced into the market, for example the Peugeot 3008 Hybrid shown in Fig. 5.55, with a motor and an engine that are not coupled. Vehicles working in the second mode are now in advanced development, for example, cars with electric propulsion and energy generated on board in a fuel cell, as shown in Fig. 4.21.

Electric propulsion offers noticeable advantages:

- Driving dynamics are excellent, because of the torque characteristic of motors, with a maximum from standing to 2000 min^{-1}.
- Emission of pollutants and noise can be avoided in urban areas by using the stored electric energy; energy generation in an engine or fuel cell is decoupled in such zones.
- The degrees of freedom of the wheels allows intelligent driver-assistance systems to be incorporated. Parking and turning are much easier when based on the six offered degrees of freedom.
- Electric energy can be generated on board in thermal engines working at fixed points, with electric energy storage in batteries or super-caps. The steady function of such engines allows the utilization of two-stroke, Stirling, and Wankel engines or of gas turbines at relatively low combustion temperatures but high efficiency. Such examples are illustrated in Fig. 6.5.
- Electric energy can be generated on board by means of fuel cells, with storage in batteries or in super-caps. Using a hydrocarbon as an energy source for the fuel cell (gasoline, diesel, ethanol, or methanol) means that the technical complexity and the price is higher than in the case of a thermal engine operating with the same role and with the same fuel. Hydrogen allows emission-free operation in urban areas. But, the emission-free, regenerative production of hydrogen, its storage on board, and its inflammability are still unsolved problems.

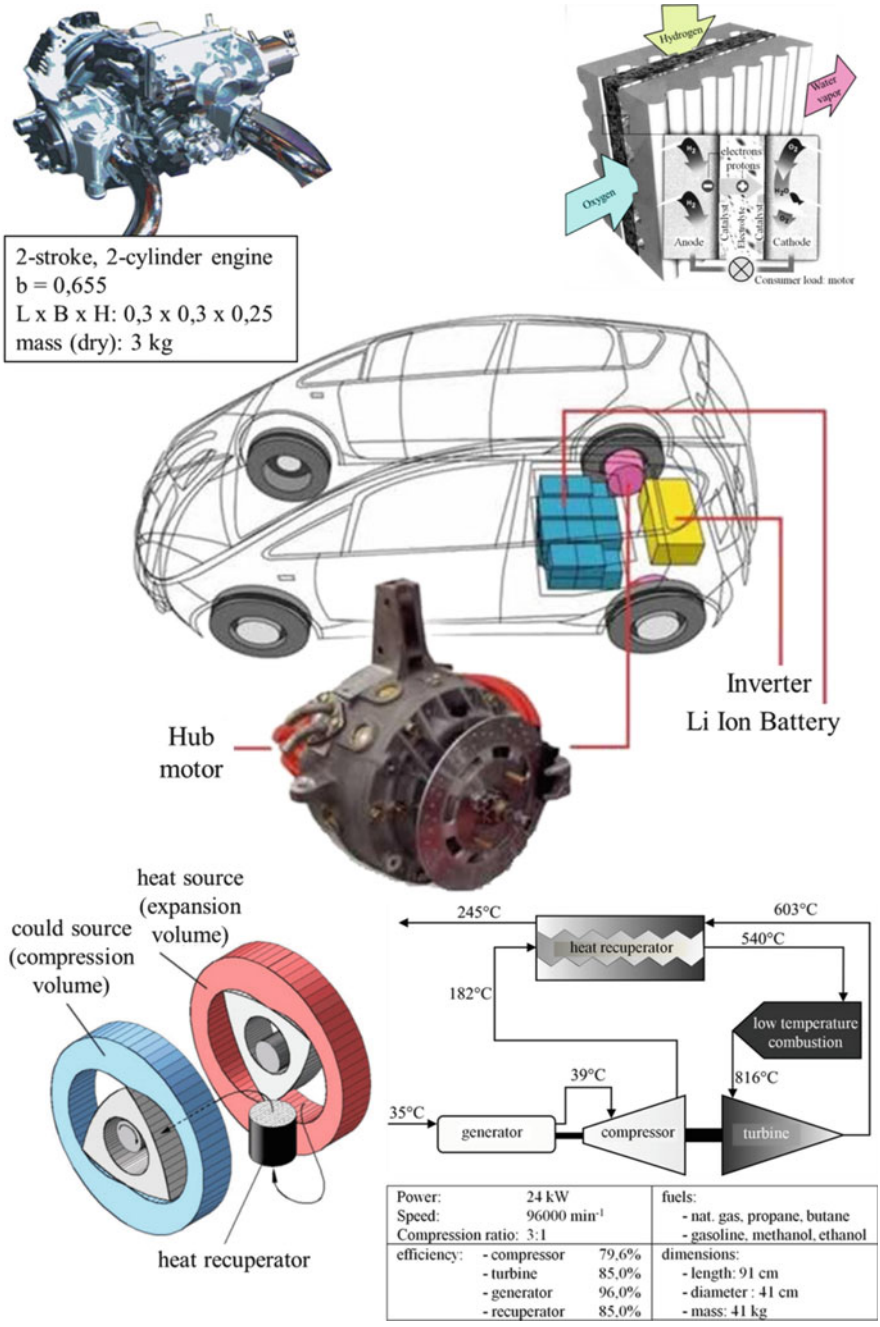

Fig. 6.5 City car with range extender. Propulsion is by motors, and electric power is generated by means of a fuel cell or by combustion (piston engine, Wankel, Stirling, or gas turbine)

Fig. 6.6 Cheap all-rounder with conventional propulsion (Source: Dacia)

6.5 Low-Price Multipurpose Cars

Low-price cars are often produced as the compact variant of a successful series bestseller car. These cars are not only small, but also reduced to the basic functions and features. However, in Brazil, India, and Eastern Europe such small and limited cars are not the real demand. Customers are looking for large and cheap cars that can transport couples with children and parents, cartons of food, and all kinds of luggage, in rough terrains, in hot summer, and in icy winter. Figure 6.6 shows the successful implementation of such a concept. A high-tech propulsion system is not reasonable from the point of view of price, nor regarding service. A simple two- or three-cylinder engine with injection of an alcohol from biomass is a better solution in this case.

6.6 Automotive Engineering and Manufacturing

Actual developments confirm the tendency for polarization of car types in relation to regional, geographical, economic, ecological, and social conditions. This complex structure of the energy management between propulsion and energy supply on board an automobile has now received a new dimension, caused by globalization of the development and production of automobiles. The main aspects of this complex structure are illustrated in Fig. 6.7.

The demand for specific propulsion systems for specific automobile classes and regional characteristics marks the discussed development trends, the very concrete interpretation of "demand" being the purchase behavior.

The resources of energy and raw materials are another independent factor to consider during development. The trend to transition from fossil to regenerative

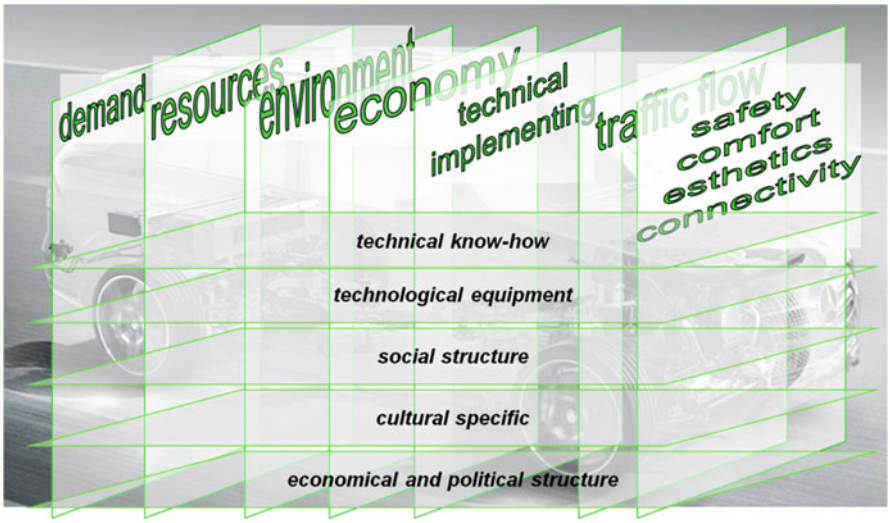

Fig. 6.7 Globalized automotive engineering and manufacturing: requirements and exigencies

energy sources is more developed than predicted a decade ago, whereas the consideration of hydrogen as the ideal fuel of the future is now much more moderate.

Compatibility with the environment traces the limits of development, independently of demand or resources. A drastic reduction in CO_2 emission (or its recycling in a natural cycle) and pollutant-free operation are conditions that remain paramount for every technical innovation.

Cost effectiveness does not always allow solutions that seem feasible from the point of view of demand, resources, or compatibility with the environment. A compact car with a fuel cell fed by hydrogen obtained from photovoltaic facilities would be an exemplary solution if considered in terms of demand, resources, and environment. Nevertheless, the obvious expense means that there is no chance of a large series production of such cars. An example confirms this fact: some time ago it was demonstrated in a very impressive manner that an automobile with fuel consumption of under 3 l/100 km is technically feasible. But, the price of this car corresponds to the price of a large luxury car; therefore, series production is not effective.

Technical feasibility is an additional challenge: a good example is, once again, the utilization of hydrogen. Even though production without emission of CO_2 and at moderate costs is possible, on-board storage remains a problem. Hydrogen has the smallest molecular mass and therefore the largest gas constant of all elements in nature. This results in the lowest density at comparable pressure and temperature, in the same volume of a tank. The penetration of such small hydrogen molecules through any wall structure at a given pressure potential and its inflammability in

ambient air at concentrations above 4 % remain physical problems, despite technical progress.

Traffic problems can affect any development plan, even if encouraged from the point of view of demand, resources, environment, economy, and technical feasibility. The Mayor of a European megacity remarked some time ago during a conference of specialists: "cars without emissions of pollutants and noise would be excellent for any city—but I have no more streets for them."

Safety, comfort, aesthetics, and communication are reliable functions of the automobile, partially imposed by law and partially required by customers. Obviously, the autonomy of an electric car with battery could be improved if the car mass were drastically reduced. Miniature vehicles with a weight of 250–300 kg are good testimonies of this. However, safety and comfort are also reduced; thus, such vehicles are more recommended for urban use.

The creation of automobiles with appropriate propulsion systems for different utilizations requires, especially in the given conditions of modular functions, taking into account globalized construction and production, which are complex, as illustrated in Fig. 6.7. Technical knowhow and a technological base are the first conditions that decide the destiny of a promising car or propulsion concept. Furthermore, the social structure, cultural specifics, and political and economic stability are intrinsic conditions for the planned development or production in a given region.

Efficient implementation of strong innovation for the functional components of automobiles also determines modification of the manufacturing structure, from car maker to manager of a modular, spatial networking, as shown in Figs. 6.8 and 6.9. Innovation can propagate with high velocity in the horizontal channels of globalization, supported by modern communication systems. The vertical net is also very interactive, but from another perspective: research, development, and production

Fig. 6.8 Horizontal and vertical network of automotive engineering and manufacturing

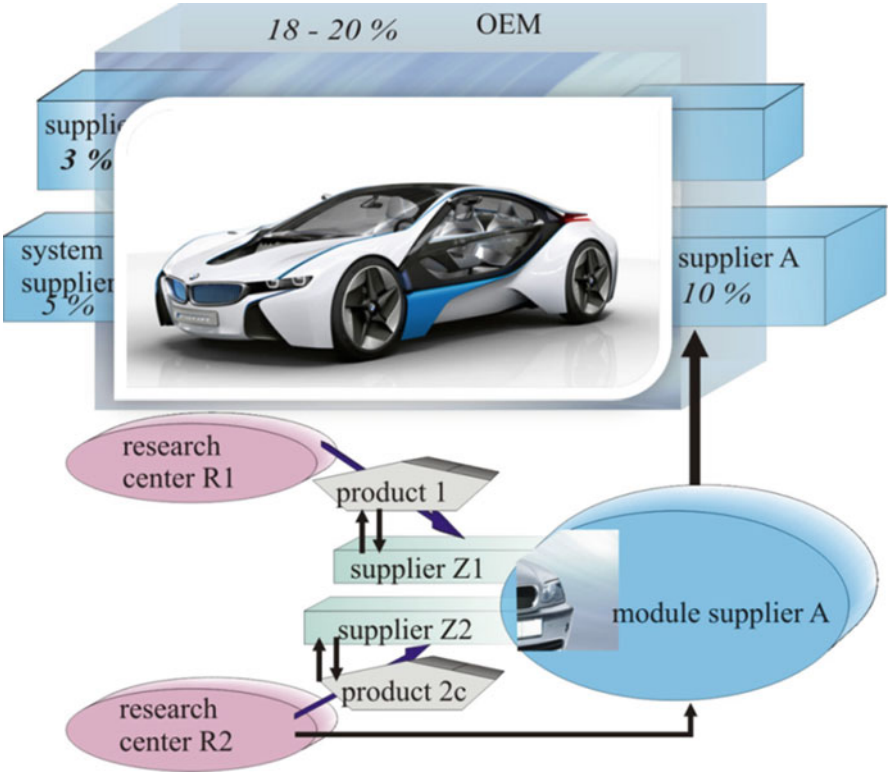

Fig. 6.9 Role allocation for creation of modular propulsion systems and modular automobiles: from research and manufacturing partners to supplier alliances

are necessary and well established in all structures from research centers and suppliers up to the OEMs, but in different proportions.

The research center has to focus on the scientific fundamentals of the target-product; in most cases this is based on many interdisciplinary connections. Another duty of the research center is to develop appropriate experimental machinery and to manufacture the basic prototypes. The supplier is very often the initiator of the innovative module, as a link between the theoretical and technical prototypes. The supplier is producer of the final module. The manufacturer is responsible for integration of the module into the new vehicle, which also requires research and development activities.

Figure 6.8 shows the propagation of innovation from research to development and on to manufacture, from the research center through the supplier to the manufacturer. The car manufacturer or the propulsion system manufacturer is in this scenario a link between horizontal and vertical degrees of freedom. The better use is made of the available degrees of freedom, the more successful the manufacturer. Adaptability to the dynamics of an innovative system requires classic virtues

such as quality, complying with due dates, and low price, but creativity and ability are also increasingly necessary.

The complexity of automobile systems, and especially combinable configurations, has led to a new distributions of roles:

- Participation of the OEM in car creation and production has diminished to under 20 % as a result of the required flexibility.
- The low-cost platform concept is gradually being replaced by the innovation-adapted modular concept. The supplier is increasingly becoming a system manufacturer.
- The new role of the supplier forces alliances to be formed with research centers and other suppliers; furthermore, the cost limits alliances with global partners.

This chain-linking provokes a backflow of development activities from the OEM to the supplier, especially in the field of alternative propulsion systems. It is thought that the OEM of the future will be purely a production manager. This would change the competence for creation of new automobiles from the OEM to the supplier, leading to less control over development paths. Such theories, which are published from time to time, are exaggerated, but they suggest the strong interaction of OEM, research centers, and suppliers at present. The new role distribution has specific attributes:

- Innovation is idea: This requires the formation and concentration of competences, leading to formation of mega-suppliers through interaction of satellites or by joint ventures with other suppliers.
- Innovation is time: This requires fast responses. Small companies are more adaptable and, thus, more effective in this relationship between OEM and supplier.

The more degrees of freedom are created by automobile propulsion, the more intense the innovation stream. The requirement for efficiency provokes displacement of innovative activity from the car maker to the supplier, which then becomes responsible not only for parts, but also for functions. Strong innovation flow also requires intensive interaction with the scientific community. The coordination of such networks and their adjustment in horizontal and vertical directions is a new form of management.

Triptolemos, the son of a king, cultivated cereals using a chariot with wings, a gift from the goddess Demeter, as illustrated in Fig. 6.10. Unfortunately, we have no information about the fuel, energy storage system, or energy conversion on board for such an elegant and highly innovative propulsion system. Nevertheless, this must be the true challenge for the numerous innovative spirits that are creating the alternative propulsion systems of the future.

Fig. 6.10 Triptolemos, son of King Celeus of Attika, cultivating cereals in a winged chariot: lekythos, approx. 490–480 BC, Archeological Museum of Syracuse

Bibliography

1. Stan, C.: Thermodynamik des Kraftfahrzeugs. Springer, Berlin (2004). ISBN 3-540-40611-5
2. Stan, C.: Direkteinspritzsysteme für Otto- und Dieselmotoren. Springer, Berlin (1999). ISBN 3-540-65287-6
3. Stan, C., Tröger, R., Stanciu, A.: Direkteinspritzsysteme für Hochleistungsmotoren—zwischen Rennsport und Serienanwendung. "Rennsport und Serie". Expert Verlag, Renningen (2003). ISBN 3-8169-2273-2
4. Stan, C., Stanciu, A., Tröger, R.: Influence of mixture formation on injection and combustion characteristics in a Compact GDI Engine. SAE Paper 2002-01-0833
5. Stanciu, A.: Gekoppelter Einsatz von Verfahren zur Berechnung von Einspritzhydraulik, Gemischbildung und Verbrennung von Ottomotoren mit Kraftstoff-Direkteinspritzung Dissertation, Technische Universität Berlin (2005)
6. Blair, G.P.: Design and simulation of four stroke engines. SAE International, Warrendale, PA (1999). ISBN 0-7680-0440-3
7. Stan, C.: Verbrennungssteuerung durch Selbstzündung—Thermodynamische Grundlagen Motortechnische Zeitschrift 1/2004. ISSN 0024-8525
8. Stan, C., Hilliger, E.: Pilot injection system for gas engines using electronically controlled ram tuned diesel injection 22. CIMAC Congress, Proceedings, Copenhagen, 04/1998
9. Guibert, P., Morin, C., Mokhtari, S.: Verbrennungssteuerung durch Selbstzündung—Experimentelle Analyse Motortechnische Zeitschrift 2/2004. ISSN 0024-8525
10. Stan, C.: Aspekte der zukünftigen Konvergenz von Otto- und Dieselmotoren Motortechnische Zeitschrift 6/2004. ISSN 0024-8525
11. Sher, E., Heywood, I.: The two-stroke cycle engine—its development, operation and design. Taylor and Francis, Philadelphia, PA (1999). SAE Order-No. R-267. ISBN 1-56032-831-2
12. Blair, G.P.: Design and simulation of two-stroke engines. SAE International, Warrendale, PA (1996). ISBN 1-56091-685-0
13. Stouffs, P.: Stirling engines—possibilities of automotive applications in "Alternative Automotive Propulsion Systems". Proceedings H030-10-007-0/Haus der Technik Essen (2000)
14. Senft, I.R.: An introduction to low temperature differential stirling engine. Moriya Press, River Falls, WI (1996). ISBN 0-9652455-1-9
15. Duda, U.: Entwicklungstendenzen der Erdgasbetriebenen Fahrzeuge in "Alternative Automotive Propulsion Systems". Proceedings H030-10007-0/Haus der Technik Essen (2000)
16. Stan, C., Tröger, R., Grimaldi, C.N., Postrioti, L.: Direct injection of variable gasolina/methanol mixtures: injection and spray charakteristics. SAE Paper 2001-01-0966
17. Stan, C., Tröger, R., Günther, S., Stanciu, A., Martorano, L., Tarantino, C., Lensi, R.: Internal mixture formation and combustion from gasoline to ethanol. SAE Paper 2001-01-1207
18. Stan, C., Tröger, R., Lensi, R., Martorano, L., Tarantino, C.: Potentialities of direct injection in spark ignition engines—from gasoline to ethanol. SAE Paper 2000-01-3270

C. Stan, *Alternative Propulsion for Automobiles*,
DOI 10.1007/978-3-319-31930-8

19. Freymann, R.: Highlights in hydrogen research within the BMW Group in "Entwicklungstendenzen im Automobilbau". Zschiesche Verlag, Wilkau-Haßlau (2004). ISBN 3-9808512-1-4
20. Kahlen, H.: Elektroantriebe für Straßenfahrzeuge—Ergänzung oder Konkurrenz zum Verbrennungsmotor in "Alternative Automotive Propulsion Systems". Proceedings H030-10-007-0/Haus der Technik Essen (2000)
21. Boltze, M., Wunderlich, C.: Energiemanagement im Fahrzeug mittels Auxiliary Power Unit in "Entwicklungstendenzen im Automobilbau". Zschiesche Verlag, Wilkau-Haßlau (2004). ISBN 3-9808512-1-4
22. Liao, G.Y., Weber, T.R., Pfaff, D.P.: Modelling and analysis of powertrain hybridization on all-wheel-drive sport utility vehicles. J. Automob. Eng. **218**(D 10), IMechE, London. (October 2004) ISSN 0954-4070
23. Stan, C., Personnaz, I.: Hybridantriebskonzept für Stadtwagen auf Basis eines kompakten Zweitaktmotors mit Ottodirekteinspritzung Automobiltechnische Zeitschrift 2/2000. ISSN 0001-2785
24. Gombert, B.: eCorner: Antrieb durch Radnabenmotoren in "Alternative Propulsion Systems for Automobiles". Expert Verlag, Renningen (2007). ISBN 978-3-8169-2752-5
25. Cipolla, G.: Hybrid automotive powertrains: the GM global approach in "Alternative Propulsion Systems for Automobiles". Expert Verlag, Renningen (2007). ISBN 978-3-8169-2752-5
26. Nitz, L., Truckenbrodt, A., Epple, W.: Das neue Two-Mode-Hybridsystem der Global Hybrid Cooperation, 27. Internationales Wiener Motorensymposium, VDI Verlag (2006). ISBN 3-18-362212-2
27. Stan, C.: Process improvement within an advanced car diesel engine in base on the variability of a concentric cam system, 10th International conference on engines and vehicles, SAE Paper 11ICE-0204
28. Eichlseder, H., Klell, M.: Wasserstoff in der Fahrzeugtechnik. Vieweg + Teubner (2010). ISBN 978-3-8348-1027-4
29. Stan, C., Cipolla, G.: Alternative Antriebe für Automobile I. Expert Verlag, Renningen (2007). ISBN 978-3-8169-2752-5
30. Stan, C.; Cipolla, G.: Alternative Antriebe für Automobile II. Expert Verlag, Renningen (2009). ISBN 978-3-8169-2835-5
31. Lenz, H.-P.: 31. Internationales Wiener Motorensymposium (Proceedings). VDI Verlag Düsseldorf 2010. ISBN 978-3-18-371612-8
32. Lenz, H.-P.: 32. Internationales Wiener Motorensymposium (Proceedings). VDI Verlag Düsseldorf 2011. ISBN 978-3-18-373512-9
33. Bargende, M., Reuss, H.-C., Wiedemann, J.: 10th Stuttgart International symposium (Proceedings). Vieweg + Teubner Verlag/Springer Fachmedien (2010). ISBN 978-3-8384-1301-5
34. Bargende, M., Reuss, H.-C., Wiedemann, J.: 11th Stuttgart International symposium (Proceedings). Vieweg + Teubner Verlag/Springer Fachmedien (2011). ISBN 978-3-8384-1561-3
35. Geringer,B., Tober, W.: Batterieelektrische Fahrzeuge in der Praxis—Studie des Österreichischen Vereins für Kraftfahrzeugtechnik, OEKV, Wien, Oktober 2012
36. Knirsch, S., Straßer, R., Schiele, G., Möhn, S., Binder, W., Enzinger, M.: Der Antriebsstrang des neuen AUDI Q7 e-tron 3.0 TDI quattro—36. Wiener Motorensymposium 2015—Proceedings
37. Ardey;Bollig; Jurasek; Klüting; Landerl: Plug and Drive—das neue Plug In System von BMW 36. Wiener Motorensymposium 2015, Proceedings

Supplementary Bibliographic Sources

autocarsnews.info
automagz.net
autos.yahoo.com
chinaautoweb.com
de.wikipedia.org
en.wikipedia.org/
green.autoblog.com
greenbigtruck.com
hybridcarspec.com
newsroom.saab.com
richmond-lexus-vancouver.com
www.7-forum.com
www.allcarselectric.com
www.altfuelprices.com
www.atz-online.de
www.autoblog.com
www.autoblog.com
www.autoexpress.co.uk
www.autogastanken.de
www.autoguide.com
www.automotiveonline.co.za
www.auto-motor-und-sport.de
www.autospectator.com
www.caranddriver.com
www.carnewschina.com
www.chinacartimes.com
www.ecvv.com
www.engadget.com
www.evsroll.com
www.evsroll.com
www.fhwa.dot.gov

C. Stan, *Alternative Propulsion for Automobiles*,
DOI 10.1007/978-3-319-31930-8

www.fiat.de
www.focus.de
www.ford.com
www.gps-data-team.com
www.greencarcongress.com
www.greenmotor.co.uk
www.hybrid-autos.info
www.hybridcars.com
www.hyundaiusa.com
www.iac.org.in
www.iangv.org
www.insideline.com
www.insideline.com
www.kia.com
www.lexus.com
www.lincoln.com
www.mazda.com
www.mbusa.com
www.mercedes.com
www.myperfectautomobile.com
www.netcarshow.com
www.nissanusa.com
www.peugeot.de
www.plugincars.com
www.porsche.com
www.roadandtrack.com
www.sueddeutsche.de
www.suyashgupta.com
www.telegraph.co.uk
www.thetorquereport.com
www.toyota.co.th
www.toyota.com
www.toyota.de
www.treehugger.com
www.volkswagen.com
www.volvocars.com
www.welt.de
www.worldcarfans.com
www.worldlpgas.com
www.zercustoms.com
zautos.com